From the Kinetic Investigation of Different Modifiers in the Carbanionic Copolymerization to Enteric Drug Coatings

Dissertation zur Erlangung des Grades

„Doktor der Naturwissenschaften“

Im Promotionsfach Chemie

Am Fachbereich Chemie, Pharmazie, Geographie und Geowissenschaften der

Johannes Gutenberg-Universität Mainz

vorgelegt von

Dominik Albrecht Hugo Fuchs

geboren in Ludwigshafen am Rhein

Mainz, Juni 2025

Die als Dissertation vorgelegte Arbeit wurde in der Zeit vom September 2021 bis Juni 2025 im Departement Chemie der Johannes Gutenberg-Universität Mainz angefertigt.

Dekanin:

1. Berichterstatter:
2. Berichterstatter:

Tag der mündlichen Prüfung: 30.07.2025

Eigenständigkeitserklärung

Hiermit erkläre ich, Dominik Albrecht Hugo Fuchs, dass ich die vorliegende Arbeit mit dem Titel:

„From the Kinetic Investigation of Different Modifiers in the Carbanionic Copolymerization to Enteric Drug Coatings“

selbstständig verfasst und keine anderen als die angegebenen Quellen und Hilfsmittel benutzt habe. Sämtliche wörtlichen oder sinngemäßen Übernahmen und Zitate sind kenntlich gemacht und nachgewiesen. Ich versichere, dass ich keine Hilfsmittel verwendet habe, deren Nutzung die Prüferin oder der Prüfer explizit ausgeschlossen hat. Folgende KI-Tools habe ich wie entsprechend beschrieben verwendet:

KI-Tool	Genutzt für	Warum	Wann
Microsoft Word	Rechtschreibkorrektur, Grammatikprüfung, Formulierungsvorschläge	Sprachliche Korrektheit, Verständnis	Über die gesamte Arbeit hinweg
ChatGPT	Neuformulierung meiner Textentwürfe, Bereitstellung von Synonymen, Grammatikkorrektur, Übersetzung von Englischem ins Deutsche	Sprachliche Korrektheit, Verständnis, bessere Lesbarkeit	Über die gesamte Arbeit hinweg
DeepL Translate	Übersetzung von Deutsch zu Englisch	Sprachliche Korrektheit, Verständnis, bessere Lesbarkeit	Über die gesamte Arbeit hinweg

Mit Abgabe der vorliegenden Leistung übernehme ich die Verantwortung für das eingereichte Gesamtprodukt. Ich verantworte damit auch jegliche KI-generierten Inhalte,

die ich in meine Arbeit übernommen habe. Die Richtigkeit übernommener (KI-generierter) Aussagen und Inhalte habe ich nach bestem Wissen und Gewissen geprüft.

Mir ist bekannt, dass ein Verstoß gegen die genannten Punkte prüfungsrechtliche Konsequenzen hat und insbesondere dazu führen kann, dass die Promotionsleistung als mit „nicht bestanden“ bewertet wird. Die Einschreibung kann für bis zu zwei Jahre widerrufen werden, wenn Studierende zweimal oder häufiger bei Prüfungsleistungen täuschen (§ 69 Abs. 4 und 5 HochSchG).

Hiermit versichere ich gemäß §10 Abs. 3 der Promotionsordnung vom 24. Juli 2007 in der Fassung vom 22. August 2012:

Ich habe die jetzt als Dissertation vorgelegte Arbeit selbst angefertigt und alle benutzten Hilfsmittel (Literatur, Apparaturen, Material, KI-Tools) in der Arbeit angegeben. Ich habe oder hatte die jetzt als Dissertation vorgelegte Arbeit nicht als Prüfungsarbeit für eine andere staatliche oder andere wissenschaftliche Prüfung eingereicht. Ich hatte weder die jetzt als Dissertation vorgelegte Arbeit noch Teile davon bei einer anderen Fakultät bzw. einem anderen Fachbereich als Dissertation eingereicht.

Mainz, 3.06.2025 _____

Dominik A. H. Fuchs

Für meine Familie

“Throughout history, it has been the inaction of those who could have acted;

the indifference of those who should have known better;

the silence of the voice of justice when it mattered most;

that has made it possible for evil to triumph.”

Haile Selassie I.

Danksagung

Author Contributions

Colleagues and collaborators provided essential scientific input that supported the content of the individual chapters.

Chapter 1: The introduction was written by Dominik Fuchs. [redacted] and [redacted] helped with discussions and corrections.

Chapter 2: The experimental part, data interpretation and writing was performed by Dominik Fuchs. [redacted] supplied the monomer TMSS, [redacted] and [redacted] helped with discussions and corrections.

Chapter 3: D. A. H. Fuchs, [redacted] and [redacted] primarily conceptualized the article. All synthetic work was carried out by D. A. H. Fuchs. The manuscript was primarily written by D.A.H. Fuchs and finalized by contribution of all authors. [redacted] and [redacted] supervised the entire project.

Chapter 4: Monomer and polymer synthesis and characterization was mainly performed by Dominik Fuchs. [redacted] supervised the low molar mass polymerizations, the pharmaceutical evaluation (acid uptake and time dependent drug release) was performed by [redacted] and [redacted] and supervised by [redacted] and [redacted]. The scale up synthesis was performed by [redacted]. The manuscript was written mainly by Dominik Fuchs and [redacted]. [redacted] helped with discussions and corrections.

Chapter 6: Monomer and polymer synthesis and characterization was performed by Dominik Fuchs. The pharmaceutical evaluation (acid uptake and time dependent drug release) was executed by [redacted]. The manuscript was written by Dominik Fuchs. [redacted] helped with discussions and corrections.

Appendix chapters

Chapter A1: [redacted], [redacted] and [redacted] primarily conceptualized the article. All synthetic work concerning the homopolymerization of isoprene and *β*-farnesene, *in situ* ^{1}H NMR kinetics and half-life determination was carried out by [redacted]. D. A. H. Fuchs contributed all copolymerization kinetics of isoprene and styrene using *in situ* NIR kinetics. The manuscript was primarily written by [redacted] and finalized by contribution of all authors. [redacted] and [redacted] supervised the entire project.

Chapter A2: The experimental part and writing was mainly performed by [redacted]. The investigated polymers were synthesized and characterized by Dominik Fuchs. [redacted] and [redacted] helped with discussions and corrections.

Table of Contents

Motivation and Objectives

Motivation and Objectives

This thesis is divided into two parts that cover different fields related to copolymerization: the first part focuses on the in-depth live kinetic investigations of the copolymerization of styrene and diene derivates in the presence of different Lewis acids and bases, while the second part addresses a synthetic strategy to improve the dissolution behavior of enteric drug coatings based on acrylate- and methacrylate copolymers.

I. Copolymerization of styrene and diene derivates

Human history has often been defined by the materials developed during specific periods, stone, bronze and iron. Today, with the discovery and identification of polymers by Hermann Staudinger in 1920, we are living in what can be described as the plastic age.[1,2] This classification is well justified, as plastics have transformed both the surface of our planet and every facet of modern life. From densely populated cities to remote islands, from mountain peaks to ocean floors, plastics are everywhere. And they are integral to nearly every industry, including transportation, medicine, sanitation, electronics, construction, packaging and even clothing.[3,4]

One of the first technological applications of polymers was the vulcanization of natural rubber by Charles Goodyear in 1839 for tire production.[5] Remarkably, this process was developed long before Staudinger introduced the concept and understanding of polymers and is still used to this day. Over the decades, petroleum based polymer materials such as polyethylene, polypropylene, polystyrene, polyvinyl chloride and many more were developed and commercialized. But none of these polymers was able to fully reproduce the material properties of the biobased caoutchouc homopolymer (*cis*-1,4-polyisoprene). This became an issue in the 20th century due to increased demand for tires and the limited scalability of its natural source, the rubber tree *hevea brasiliensis*, which only thrives in specific tropical climates.

This scarcity of natural rubber prompted the search for synthetic alternatives. A key breakthrough came in 1926, when W. Bock and E. Tschunkur developed a styrene-

butadiene rubber (SBR) called “Buna”, which relies on a random copolymerization of butadiene with styrene to improve certain properties of the materials, such as abrasion resistance.[6] However, the resulting copolymer still requires vulcanization to achieve the desired mechanical properties for car tires. Vulcanization introduces irreversible covalent crosslinks between polymer chains, hindering reprocessing and recycling, an increasing problem in light of the global rubber production volume, which exceeds 29 million tons annually.[7] In contrast, many elastomeric applications, such as shoe soles or car interiors, do not require the same level of abrasion resistance and thermal stability. For these, alternatives to chemical crosslinking sought to improve recyclability and enable processing via injection molding.

This alternative, a physical crosslinking, was found with the discovery of the living anionic polymerization by Szwarc, followed by the development of organolithium initiators. This enabled the synthesis of high *cis*-1,4 polyisoprene, which is like its natural counterpart a viscous, sticky liquid.[8–11] However, due to its living chain end, sequential monomer additions to synthesize well defined architectures became possible for the first time.[12–14] While the material properties of the previously mentioned homopolymers are mainly determined by their molar mass, copolymerization made it possible to combine properties that were previously impossible to combine. And already the combination of just two monomers opened nearly limitless possibilities for tailoring material properties.[15] By adding styrene to a living, difunctional diene polymer a stable and processable thermoplastic material was formed.

For such materials to exhibit rubber-like behavior, it is essential that the individual polymer blocks are thermodynamically immiscible and undergo microphase separation. To achieve elastomeric properties, one block (polydiene) must have a glass transition temperature (T_g) below the service temperature, while the other (polystyrene) must have a T_g above it. The high T_g polystyrene domains serve as physical crosslinking points upon cooling and vitrification, in analogy to the sulfur crosslinks in vulcanized rubber.[16] To replicate rubber like materials, with the advantage of processibility and recyclability, it is necessary to synthesize copolymers with at least two of these crosslinking points (ABA-triblock structure) to obtain elastomeric properties.[17] These materials are called thermoplastic elastomers (TPEs) and combine the elastic properties of rubber with the

melt processability of thermoplastics, which enables processibility via high speed extrusion.[18]

However, the stepwise addition of monomers required to synthesize the desired ABA structures presents a significant challenge. The highly reactive living anionic chain ends are prone to termination reactions. Additionally, for the resulting materials the strong phase separation of the different blocks prepared by sequential monomer addition results in a high order-disorder transition temperature (T_{ODT}) close to the degradation temperature and an increased melt viscosity, which is generally undesirable for melt extrusion.[18–21]

A solution lies in the statistical copolymerization, leading to the formation of so called "tapered" block copolymers. Unlike traditional block copolymers, which feature abrupt transitions between blocks, tapered block copolymers exhibit a gradual transition, either steep or flat, depending on the reactivity ratios of the monomers. With a steep gradient they retain the phase-separated characteristics of block copolymers, but offer multiple advantages. Fewer monomer addition steps reduce the risk of termination, and the gradient enhances compatibility between blocks. This results in lower T_{ODT}, reduced melt viscosity and therefore improved processibility even with higher molar masses. Additionally, the material properties can be tailored by adjusting the shape and slope of the tapered region.[22]

In the statistical copolymerization of dienes with styrene, the diene typically polymerizes preferentially, resulting in block-like structures with a tapered transition. This tapered transition, however, can be precisely tuned through the addition of so-called modifiers, which influence the reactivity ratios of the monomers through different mechanisms. As an example, Lewis bases such as ethers (THF) can be utilized to alter reactivity ratios by accelerating the styrene polymerization considerably more than the diene. In contrast, Lewis acids like lithium alkoxides also alter the reactivity ratios, but by slowing down the diene polymerization to a greater extent than styrene, resulting in a preferred styrene incorporating as well.[23–25] To fully leverage these advantages, precise understanding of copolymerization kinetics is essential. Earlier publications investigated the effect of different monomer pairs, temperature and solvents, but systematic studies regarding the kinetics, microstructures and thermal properties are rare.[23,25,26] Therefore, the first part of

this thesis is dedicated to the influence of different Lewis acids (different alkoxides) and bases (THF and MTBE) on the copolymerization kinetics of styrene and diene derivates, as well as their impact on the resulting microstructure of the diene. These kinetics information will help to synthesize specialized polymer architectures with specifically tailored material properties.

II. Improving the pH-responsiveness of enteric drug coatings

Chapters 4 and 5 explore a different class of copolymers and polymerization techniques aimed at developing improved enteric drug coatings. Specifically, these chapters focus on copolymers derived from poly(methacrylic acid), synthesized via free radical polymerization.

Stimuli-responsive polymers that respond to triggers such as temperature,[27] mechanical force,[28] electric/magnetic fields[29] and pH[30] are widely used in biomedical applications.[31–33] One of the most established uses is in enteric drug coatings for controlled drug release. In these systems, the polymer coating of a tablet or capsule acts as a protective barrier, shielding the drug from the acidic environment of the stomach, preventing hydrolysis, oxidation or deamination of an acid labile drug.[34,35] Besides, this coating also protects the stomach from potential harmful drugs.

For this purpose, many different copolymers can be employed, depending on the preferred release site (stomach, duodenum and small intestine or colon). Most of these coatings are based on poly (meth) acrylates with different pH responsive functionalities for immediate, sustained or controlled release.[32] Commercially available enteric drug coatings known under their trademark Eudragit® (Evonik AG), are based on poly(methacrylic acid) copolymerized with different acrylates. Both chapters 4 and 5 focus on the improvement of these enteric drug coatings.

To qualify as an enteric drug coating, a polymer must meet two critical requirements: (i) it must be stable and insoluble under the acidic conditions of the stomach, and (ii) it must dissolve rapidly once the drug passes into the more neutral environment of the small intestine. This pose a challenge, as gastric pH typically ranges from 1 to 3, but can occasionally even rise to 6,[34,36] while the pH of the small intestine typically ranges from 5.1 to 7.8.[37] Therefore, poly(methacrylic acid), with a pK_a value of 4.65, is ideally suited for

this application. It remains insoluble in the stomach and dissolves at the higher pH of the small intestine.[38] By copolymerizing with different comonomers such as methyl methacrylate or ethyl acrylate in different monomer ratios, the dissolution profile of these drug coatings can be tailored. For example, poly(methyl-methacrylic-acid-*co*-ethyl-acrylate) (Eudragit® L-100-55) dissolves above a pH level of 5.5, targeting a drug release in the duodenum, while poly(methyl-methacrylic-acid-*co*-methyl-methacrylate) (Eudragit® L-100) dissolves above a pH level of 6, targets the small intestine.[32] However, several *in vitro* studies have raised concerns whether this dissolution is rapid enough to ensure drug release in the duodenum.[39,40] This becomes even more concerning considering the fact that *in vitro* experiments often overestimate the *in vivo* drug release, due to incorrect assumptions about the buffer capacity and the liquid volume surrounding the tablet.[41–43] This delayed drug release can be particularly problematic for drugs that are preferably absorbed in the duodenum, such as iron containing drugs.[44,45] If the drug cannot be absorbed there, the bioavailability decreases, requiring higher drug doses, which is not only economically unfavored but also increases the risk of side effects.[46]

Thus, the objective of chapter 4 and 5 is to reduce the pK_a value of the copolymer to improve dissolution and drug release at lower pH levels. This is achieved by esterifying Eudragit® L-100 and L-100-55 copolymers with various α-hydroxy acids: glycolic- and lactic acid (chapter 4), and mandelic- and malic acid (chapter 5). Here, the electron withdrawing (-I) effect of the ester bonds reduces the pK_a value of the copolymer. The modified copolymers are synthesized either by free radical copolymerization or via post polymerization modifications of commercially available Eudragit® copolymers.

Chapter 4 focuses on the synthesis of glycolic and lactic acid modified copolymers, synthesized via free radical polymerization, as well as a scalable post-polymerization technique. Cloud point titrations and drug release studies using coated capsules confirmed the enhanced dissolution behavior. In addition, the acid stability and uptake under gastric conditions were tested. All modified copolymers proved to be stable, but the modifications increased acid uptake. Further pharmaceutical evaluation of these copolymers can be found in the Appendix.

Chapter 5 addresses the synthesis of mandelic and malic acid modified copolymers using free radical polymerization. Mandelic acid was chosen to increase the hydrophobicity of the copolymer through the phenyl side chain, which resulted in reduced acid uptake. We assume that this effect should aid obtaining uniform drug release profiles, not only across patient populations, but also for different gastric emptying times. Malic acid, with its second acid functionality with a higher pK_a value should increase the dissolution rate and was investigated with respect to its influence on the dissolution behavior.

References:

(1) Porta, R. Anthropocene, the Plastic Age and Future Perspectives. *FEBS Open Bio* **2021**, *11* (4), 948–953. https://doi.org/10.1002/2211-5463.13122.

(2) Staudinger, H. Über Polymerisation. *Berichte der deutschen chemischen Gesellschaft (A and B Series)* **1920**, *53* (6), 1073–1085. https://doi.org/10.1002/cber.19200530627.

(3) Koltzenburg, S.; Maskos, M.; Nuyken, O. *Polymere: Synthese, Eigenschaften Und Anwendungen*; Springer Berlin Heidelberg: Berlin, Heidelberg, 2014. https://doi.org/10.1007/978-3-642-34773-3.

(4) Teo, A. J. T.; Mishra, A.; Park, I.; Kim, Y.-J.; Park, W.-T.; Yoon, Y.-J. Polymeric Biomaterials for Medical Implants and Devices. *ACS Biomater Sci Eng* **2016**, *2* (4), 454–472. https://doi.org/10.1021/acsbiomaterials.5b00429.

(5) Hurley, P. E. History of Natural Rubber. *Journal of Macromolecular Science: Part A - Chemistry* **1981**, *15* (7), 1279–1287. https://doi.org/10.1080/00222338108056785.

(6) Marvel, C. S.; Bailey, W. J.; Inskeep, G. E. Sodium-catalyzed Copolymerization of 1,3-butadiene and Styrene. *Journal of Polymer Science* **1946**, *1* (4), 275–288. https://doi.org/10.1002/pol.1946.120010408.

(7) Pegoretti, A. Material Circularity in Rubber Products. *Express Polym Lett* **2023**, *17* (4), 352–352. https://doi.org/10.3144/expresspolymlett.2023.25.

(8) Hsieh, H.; Tobolsky, A. V. Polymerization of Isoprene by N-butyl Lithium. *Journal of Polymer Science* **1957**, *25* (109), 245–247. https://doi.org/10.1002/pol.1957.1202510918.

(9) Hsieh, H.; Kelley, D. J.; Tobolsky, A. V. Polymerization of Isoprene with Lithium Dispersions and Lithium Alkyls Using Tetrahydrofuran as Solvent. *Journal of Polymer Science* **1957**, *26* (113), 240–242. https://doi.org/10.1002/pol.1957.1202611315.

(10) Morita, H.; Tobolsky, A. V. Isoprene Polymerization by Organometallic Compounds. I. *J Am Chem Soc* **1957**, *79* (22), 5853–5855. https://doi.org/10.1021/ja01579a004.

(11) Szwarc, M. 'Living' Polymers. *Nature* **1956**, *178* (4543), 1168–1169. https://doi.org/10.1038/1781168a0.

(12) Porter; Milkovich, R.; Phillips Petroleum Co. GB888624A Block Polymers and Process for Preparation Thereof, 1959.

(13) Holden, G.; Milkovich, R. U.S. Patent 3265765, Block Polymers of Monovinyl Aromatic Hydrocarbons and Conjugated Dienes., 1962.

(14) Holden, G.; Milkovich, R. Block Polymers of Monovinyl Aromatic Hydrocarbons and Conjugated Dienes US3265765A, US3265765A to Shell Oil Company, 1966.

(15) Bates, F. S.; Hillmyer, M. A.; Lodge, T. P.; Bates, C. M.; Delaney, K. T.; Fredrickson, G. H. Multiblock Polymers: Panacea or Pandora's Box? *Science (1979)* **2012**, *336* (6080), 434–440. https://doi.org/10.1126/science.1215368.

(16) Politakos, N.; Kortaberria, G. Exploring the Self-Assembly Capabilities of ABA-Type SBS, SIS, and Their Analogous Hydrogenated Copolymers onto Different Nanostructures Using Atomic Force Microscopy. *Materials* **2018**, *11* (9). https://doi.org/10.3390/ma11091529.

(17) Qiao, L.; Leibig, C.; Hahn, S. F.; Winey, K. I. Isolating the Effects of Morphology and Chain Architecture on the Mechanical Properties of Triblock Copolymers. *Ind Eng Chem Res* **2006**, *45* (16), 5598–5602. https://doi.org/10.1021/ie0511940.

(18) Knoll, K.; Nießner, N. Styrolux+ and Styroflex+ - From Transparent High Impact Polystyrene to New Thermoplastic Elastomers: Syntheses, Applications and Blends with Other Styrene Based Polymers. *Macromol Symp* **1998**, *132*, 231–243. https://doi.org/10.1002/masy.19981320122.

(19) Gouinlock, E. V.; Porter, R. S. Linear Dynamic Mechanical Properties of an SBS Block Copolymer. *Polym Eng Sci* **1977**, *17* (8), 535–543. https://doi.org/10.1002/pen.760170809.

(20) Bernd, T. *Makromolekulare Chemie*; Wiley-VCH: Weinheim, 2014.

(21) Sinturel, C.; Bates, F. S.; Hillmyer, M. A. High χ–Low N Block Polymers: How Far Can We Go? *ACS Macro Lett* **2015**, *4* (9), 1044–1050. https://doi.org/10.1021/acsmacrolett.5b00472.

(22) Hodrokoukes, P.; Floudas, G.; Pispas, S.; Hadjichristidis, N. Microphase Separation in Normal and Inverse Tapered Block Copolymers of Polystyrene and Polyisoprene. 1. Phase State. *Macromolecules* **2001**, *34* (3), 650–657. https://doi.org/10.1021/ma001479i.

(23) Wofford, C. F.; Hsieh, H. L. Copolymerization of Butadiene and Styrene by Initiation with Alkyllithium and Alkali Metal *Tert*-Butoxides. *J Polym Sci A1* **1969**, *7* (2), 461–469. https://doi.org/10.1002/pol.1969.150070205.

(24) Fuchs, D. A. H.; Hübner, H.; Kraus, T.; Niebuur, B.-J.; Gallei, M.; Frey, H.; Müller, A. H. E. The Effect of THF and the Chelating Modifier DTHFP on the Copolymerisation of β-Myrcene and Styrene: Kinetics, Microstructures, Morphologies, and Mechanical Properties. *Polym Chem* **2021**, *12* (32), 4632–4642. https://doi.org/10.1039/D1PY00791B.

(25) Steube, M.; Johann, T.; Hübner, H.; Koch, M.; Dinh, T.; Gallei, M.; Floudas, G.; Frey, H.; Müller, A. H. E. Tetrahydrofuran: More than a "Randomizer" in the Living Anionic Copolymerization of Styrene and Isoprene: Kinetics, Microstructures, Morphologies, and Mechanical Properties. *Macromolecules* **2020**, *53* (13), 5512–5527. https://doi.org/10.1021/acs.macromol.0c01022.

(26) Steube, M.; Johann, T.; Plank, M.; Tjaberings, S.; Gröschel, A. H.; Gallei, M.; Frey, H.; Müller, A. H. E. Kinetics of Anionic Living Copolymerization of Isoprene and Styrene Using in Situ NIR

Spectroscopy: Temperature Effects on Monomer Sequence and Morphology. *Macromolecules* **2019**, *52* (23), 9299–9310. https://doi.org/10.1021/acs.macromol.9b01790.

(27) Heskins, M.; Guillet, J. E. Solution Properties of Poly(N-Isopropylacrylamide). *Journal of Macromolecular Science: Part A - Chemistry* **1968**, *2* (8), 1441–1455. https://doi.org/10.1080/10601326808051910.

(28) Davis, D. A.; Hamilton, A.; Yang, J.; Cremar, L. D.; Van Gough, D.; Potisek, S. L.; Ong, M. T.; Braun, P. V.; Martínez, T. J.; White, S. R.; Moore, J. S.; Sottos, N. R. Force-Induced Activation of Covalent Bonds in Mechanoresponsive Polymeric Materials. *Nature* **2009**, *459* (7243), 68–72. https://doi.org/10.1038/nature07970.

(29) Tanaka, T.; Nishio, I.; Sun, S.-T.; Ueno-Nishio, S. Collapse of Gels in an Electric Field. *Science (1979)* **1982**, *218* (4571), 467–469. https://doi.org/10.1126/science.218.4571.467.

(30) Dai, S.; Ravi, P.; Tam, K. C. PH-Responsive Polymers: Synthesis, Properties and Applications. *Soft Matter* **2008**, *4* (3), 435. https://doi.org/10.1039/b714741d.

(31) Wei, M.; Gao, Y.; Li, X.; Serpe, M. J. Stimuli-Responsive Polymers and Their Applications. *Polym Chem* **2017**, *8* (1), 127–143. https://doi.org/10.1039/C6PY01585A.

(32) Evonik Industries AG. *Functional polymers to take control of your release profile Versatility and reliability for oral solid dosage forms*. https://healthcare.evonik.com/en/drugdelivery/oral-drug-delivery/oral-excipients/eudragit-portfolio/attachment/149083?rev=fd91102acf8d769a56d0716b20544216.

(33) Hu, J.; Liu, S. Responsive Polymers for Detection and Sensing Applications: Current Status and Future Developments. *Macromolecules* **2010**, *43* (20), 8315–8330. https://doi.org/10.1021/ma1005815.

(34) Stamatopoulos, K.; O'Farrell, C.; Simmons, M.; Batchelor, H. In Vivo Models to Evaluate Ingestible Devices: Present Status and Current Trends. *Adv Drug Deliv Rev* **2021**, *177*, 113915. https://doi.org/10.1016/j.addr.2021.113915.

(35) McConnell, E. L.; Fadda, H. M.; Basit, A. W. Gut Instincts: Explorations in Intestinal Physiology and Drug Delivery. *Int J Pharm* **2008**, *364* (2), 213–226. https://doi.org/10.1016/j.ijpharm.2008.05.012.

(36) Beasley, D. E.; Koltz, A. M.; Lambert, J. E.; Fierer, N.; Dunn, R. R. The Evolution of Stomach Acidity and Its Relevance to the Human Microbiome. *PLoS One* **2015**, *10* (7), e0134116. https://doi.org/10.1371/journal.pone.0134116.

(37) Felber, A. E.; Dufresne, M.-H.; Leroux, J.-C. PH-Sensitive Vesicles, Polymeric Micelles, and Nanospheres Prepared with Polycarboxylates. *Adv Drug Deliv Rev* **2012**, *64* (11), 979–992. https://doi.org/10.1016/j.addr.2011.09.006.

(38) Ibarra-Montaño, E. L.; Rodríguez-Laguna, N.; Sánchez-Hernández, A.; Rojas-Hernández, A. Determination of PKa Values for Acrylic, Methacrylic and Itaconic Acids by 1H and 13C NMR in Deuterated Water. *Journal of Applied Solution Chemistry and Modeling* **2015**, *4* (1), 7–18. https://doi.org/10.6000/1929-5030.2015.04.01.2.

(39) Khan, M. Z. I.; Prebeg, Ž.; Kurjaković, N. A PH-Dependent Colon Targeted Oral Drug Delivery System Using Methacrylic Acid Copolymers. *Journal of Controlled Release* **1999**, *58* (2), 215–222. https://doi.org/10.1016/S0168-3659(98)00151-5.

(40) Cole, E. T.; Scott, R. A.; Connor, A. L.; Wilding, I. R.; Petereit, H. U.; Schminke, C.; Beckert, T.; Cadé, D. Enteric Coated HPMC Capsules Designed to Achieve Intestinal Targeting. *Int J Pharm* **2002**, *231* (1), 83–95. https://doi.org/10.1016/S0378-5173(01)00871-7.

(41) Al-Gousous, J.; Amidon, G. L.; Langguth, P. Toward Biopredictive Dissolution for Enteric Coated Dosage Forms. *Mol Pharm* **2016**, *13* (6), 1927–1936. https://doi.org/10.1021/acs.molpharmaceut.6b00077.

(42) Al-Gousous, J.; Ruan, H.; Blechar, J. A.; Sun, K. X.; Salehi, N.; Langguth, P.; Job, N. M.; Lipka, E.; Loebenberg, R.; Bermejo, M.; Amidon, G. E.; Amidon, G. L. Mechanistic Analysis and Experimental Verification of Bicarbonate-Controlled Enteric Coat Dissolution: Potential in Vivo Implications. *European Journal of Pharmaceutics and Biopharmaceutics* **2019**, *139*, 47–58. https://doi.org/10.1016/j.ejpb.2019.03.012.

(43) Blechar, J. A.; Al-Gousous, J.; Wilhelmy, C.; Postina, A. M.; Getto, M.; Langguth, P. Toward Mechanistic Design of Surrogate Buffers for Dissolution Testing of PH-Dependent Drug Delivery Systems. *Pharmaceutics* **2020**, *12* (12), 1197. https://doi.org/10.3390/pharmaceutics12121197.

(44) Rudinskas, L.; Paton, T. W.; Walker, S. E.; Dotten, D. A.; Cowan, D. H. Poor Clinical Response to Enteric-Coated Iron Preparations. *CMAJ* **1989**, *141* (6), 565–566.

(45) Walker, S. E.; Paton, T. W.; Cowan, D. H.; Manuel, M. A.; Dranitsaris, G. Bioavailability of Iron in Oral Ferrous Sulfate Preparations in Healthy Volunteers. *CMAJ* **1989**, *141* (6), 543–547.

(46) LaVan, D. A.; McGuire, T.; Langer, R. Small-Scale Systems for in Vivo Drug Delivery. *Nat Biotechnol* **2003**, *21* (10), 1184–1191. https://doi.org/10.1038/nbt876.

Abstract

This thesis is divided into two parts, that cover different fields related to copolymerization: anionic copolymerization kinetics and enteric drug coatings. The first part focuses on the kinetic investigation of the carbanionic copolymerization of styrene and diene derivates in the presence of Lewis acids or bases. Near-infrared (NIR) spectroscopy is used for live measurements of the copolymerization to calculate reactivity ratios, which are further translated into polymer composition diagrams. The synthesized copolymers are further characterized in terms of molar mass, dispersity, microstructure, thermal properties and blockiness. These data provided additional insight into the reaction mechanisms in presence of different Lewis modifiers. Chapter 2, 3 and A1 investigate the effects of different Lewis bases (THF and MTBE) and various alkoxides.

The second part is dedicated to the synthesis and characterization of enteric drug coatings based on acrylate- and methacrylate copolymers. Novel copolymers are synthesized by either free radical copolymerization or post polymerization modifications. To improve the dissolution behavior of the poly(methacrylic acid) based copolymers, they are modified with various α-hydroxy acids to lower the pK_a and accelerate drug release. Cloud point titration as well as further pharmaceutical experiments confirmed this concept. Chapter 4 focuses on the modification with glycolic and lactic acid and their scalability, while chapter 5 extends the concept to more complex α-hydroxy acids, mandelic and malic acid. The appendix chapter A2 addresses further pharmaceutical evaluations of the copolymers synthesized in chapter 4.

Chapter 1 is the introduction into the living carbanionic polymerization and enteric drug coatings. The first section covers the theoretical background, copolymerizations, reactivity ratios and modifier effects in the carbanionic polymerization. The second section introduces the history, applications and current limitations of enteric drug coatings.

Chapter 2 deals with the copolymerization of trimethylsilyl styrene (TMSS) and isoprene (I) in cyclohexane with THF as a modifier. The trimethylsilyl group has an electron withdrawing and donating effect, which is dominated by the withdrawing effect, explaining the increased reactivity of this monomer. This was confirmed for the system

TMSS/I in cyclohexane (r_I = 2.37; r_{TMSS} = 0.16), resulting in a gradient copolymer, while the traditional S/I system (r_S = 0.015 r_I = 10.03) results in a tapered copolymer. THF was used as a modifier to alter the reactivity ratios over the entire range and produce various copolymers. Already 0.5 equiv THF are sufficient to alter the reactivity ratios into a random copolymerization, compare to 6 equiv necessary for the styrene system. Additionally to the kinetic investigations are also thermal properties and the diene microstructure analyzed and the copolymers are proposed as potential gas separation membranes.

Chapter 3 investigates the impact of lithium, sodium and potassium amylates on S/I copolymerizations in cyclohexane via NIR spectroscopy. These modifiers have a similar impact on the reactivity ratios like previous investigated THF, but do this via a different mechanism. While Lewis bases reduce aggregation, the addition of alkoxides changes the polymer chain ends counterion. Lithium alkoxides retard the isoprene polymerization more than styrene; sodium accelerates both monomer consumptions but favors styrene, similar to Lewis bases, and potassium drastically accelerates the styrene polymerization while barely affecting isoprene. These very different behaviors can be explained by different polymerization mechanisms, which were further confirmed by additional NMR, DSC and degradation studies.

Chapter 4 focuses on the synthesis and characterization of new enteric drug coatings, based on established poly(methacrylic acid) copolymers. These are modified with α-hydroxy acids to reduce the pK_a of the copolymers and accelerate drug release. The new monomers are synthesized by a Steglich esterification of benzyl protected glycolic- or lactic acid with methacrylic acid. After successful copolymerization with methyl methacrylate or ethyl acrylate and subsequent deprotection of the acid functionalities, the pH responsiveness of the copolymers was investigated via cloud point titrations. All modified showed increased solubility at lower pH, while maintaining acid resistance. After the proof of concept was given, a scalable post polymerization modification was developed to produce high molecular weight copolymers and the drug release and acid uptake of these coated capsules was further tested.

Chapter 5 expands the concept of modifying enteric drug coatings with α-hydroxy acids towards mandelic and malic acid. These were specifically chosen due to the results obtained in the previous chapter. Since the modification with glycol and lactic acid

increased the acid uptake of coated capsules, mandelic acid was used to improve the hydrophobicity of the copolymer and therefore reduce the acid uptake. Malic acid was chosen as a new monomer due to its second acid functionality, to further improve the dissolution at lower pH. Unfortunately, the malic modification reduces the pK_a of the copolymer too much, so that the copolymer is no longer insoluble at a pH of two. The mandelic acid modification on the other hand decrease the acid uptake, while maintaining acid stability and improved the dissolution profile compared to the unmodified copolymers.

Chapter A1 investigates the possibility of using MTBE as a more stable and sustainable polar solvent in the carbanionic polymerization. The improved stability was confirmed by the 50 times longer half-life of *n*-butyl lithium in MTBE than in THF. MTBE has also the advantages of no peroxide formation, compatibility with bifunctional initiators and a moderate polarity between cyclohexane and THF. Besides the stability is the homopolymerization of different dienes in MTBE investigated, as well as the copolymerization of styrene and isoprene. The copolymerization is investigated with NIR-spectroscopy and reactivity ratios were adjusted over the entire range from tapered structures in pure cyclohexane to an inverted gradient (r_S = 1.82; r_I = 0.55). Compared to THF has MTBE a lesser influence on the copolymerization kinetics, but also on the diene microstructure.

Chapter A2 focuses on further pharmaceutical evaluations of the enteric drug coatings presented in Chapter 4. The high molar mass copolymers synthesized via post polymerization modifications are investigated towards their dissolution properties, long term stability and possible cytotoxicity. Further tests confirmed the accelerated dissolution and long term stability of these novel copolymers, as well as their non-toxicity.

Zusammenfassung

Diese Arbeit ist in zwei Teile gegliedert, die verschiedene Bereiche der Copolymerisation abdecken: (i) die kinetische Untersuchung der carbanionischen Copolymerisation und (ii) der Synthese und Charakterisierung von magensaftresistenten Tablettenüberzügen. Der erste Teil konzentriert sich hierbei auf die kinetischen Untersuchungen der Copolymerisation verschiedener Styrol und Dien Derivaten in Gegenwart von Lewis Säuren oder Basen. Hierfür wird die Nahe-Infrarot Spektroskopie genutzt, die es ermöglicht aus den Echtzeit Messungen Konzentrationen zu berechnen und aus diesen dann Copolymerisationsparameter. Diese werden anschließend genutzt um die Monomer Verteilung innerhalb der Polymerketten darzustellen. Zusätzlich wurden die Copolymere in Bezug zu ihrer Molmasse, Dispersität, Mikrostruktur, thermischen Eigenschaften und ihrer Blockiness charakterisiert. Kapitel 2 beschäftigt sich mit dem Modifier THF, Kapitel 3 mit verschiedenen Alkoxiden und Kapitel A1 mit dem Modifier MTBE.

Der zweite Teil dieser Arbeit widmet sich der Synthese und Charakterisierung von Polyacrylat- und Methacrylat Copolymeren für magensaftresistente Tablettenüberzüge. Diese werden entweder durch die freie radikalische Polymerisation von neuartigen Monomeren oder durch eine Modifikation bereits kommerzialisierter Tablettenüberzüge hergestellt. Eine Beschleunigung der Auflösungsgeschwindigkeit wird hierbei durch die Modifikation der Poly(Methacrylsäure) mittels einer α-Hydroxysäure erreicht, die den pK_s Wert des Copolymers senkt. Dieses Konzept konnte durch pH abhängige Trübungstitrationen, sowie weitere pharmazeutische Experimente bestätigt werden. Kapitel 4 behandelt die Modifikation mittels Glykol- und Milchsäure und deren Skalierbarkeit, während Kapitel 5 das Konzept auf komplexere α-Hydroxysäuren, Mandel- und Äpfelsäure, erweitert. Das Kapitel A2 im Anhang befasst sich mit weiteren pharmazeutischen Untersuchungen der im Kapitel 4 synthetisierten Copolymere.

Kapitel 1 ist eine Einführung in die lebende Carbanionische Polymerisation sowie in magensaftresistente Tablettenüberzüge. Der erste Abschnitt diese Kapitels befasst sich mit dem theoretischen Hintergrund, Copolymerisationen, Copolymerisationsparametern und den Auswirkungen verschiedener Modifier auf die Copolymerisation. Im zweiten

Abschnitt wird die Geschichte, Anwendung und die derzeitigen Probleme von magensaftresistenten Tablettenüberzügen erörtert.

Kapitel 2 befasst sich mit der Copolymerisation von Trimethylsilylstyrol (TMSS) und Isopren (I) in Cyclohexan in der Gegenwart von THF als Modifier. Die Trimethylsilyl Gruppe besitzt sowohl eine elektronenziehende als auch elektronenschiebende Wirkung, wobei die elektronenziehende überwiegt, was wiederum die erhöhte Reaktivität dieses Monomer erklärt. Dies wurde für das System TMSS/I bestätigt, indem in Cyclohexan ein Gradienten Copolymer (r_I = 2.37; r_{TMSS} = 0.16) entsteht, während in dem klassischen S/I System ein Tapered Copolymer (r_S = 0.015 r_I = 10.03) gebildet wird. THF wurde als Modifier der Copolymerisation untersucht, um die Reaktivitätsverhältnisse über den gesamten Bereich zu verändern und unterschiedliche Copolymere herzustellen. Bereits 0.5 Äquivalente THF, anstatt 6 für S/I, sind hierbei ausreichend um die Copolymerisationsparameter anzugleichen. Zusätzlich zu den kinetischen Untersuchungen wurde auch die thermischen Eigenschaften und die Mikrostruktur untersucht in Bezug zu möglichen Anwendungen als Gas Membranen.

Kapitel 3 untersucht den Einfluss von Lithium-, Natrium- und Kaliumamylaten auf S/I Copolymerisationen in Cyclohexan mittels NIR-Spektroskopie. Diese Modifier haben einen ähnlichen Einfluss auf die Copolymerisation wie THF, jedoch deutlich stärker und mittels eines anderen Mechanismus. Während Lewis Basen die Aggregation des Kettenendes reduzieren, verändert die Zugabe von Alkoxiden das Gegenion am Kettenende. Lithiumalkoxide verzögern die Isopren Polymerisation stärker als die Styrol Polymerisation; Natriumalkoxide beschleunigt beide Monomere, jedoch Styrol deutlich stärker als Isopren und Kaliumalkoxide beschleunigen die Styrol Polymerisation drastisch, während Isopren kaum beeinflusst wird. Diese sehr unterschiedlichen Ergebnisse lassen sich durch unterschiedliche Reaktionsmechanismen erklären, die durch zusätzliche NMR-, DSC- und Abbaustudien bestätigt wurden.

Kapitel 4 befasst sich mit der Synthese und Charakterisierung neuer magensaftresistenter Tablettenüberzügen auf Grundlage von bereits etablierten Poly(Methacrylsäure) Copolymeren. Diese wurden mit Glykol- und Milchsäure modifiziert um den pK_s Wert des Copolymers zu senken und die Wirkstofffreisetzung zu beschleunigen. Hierfür wurden die neuen Monomere in einer Steglich Veresterung von

Benzyl geschützten α-Hydroxysäuren mit Methacrylsäure hergestellt. Nach erfolgreicher Copolymerisation mit Methylmethacrylat oder Ethylacrylat wurde die Säurefunktion entschützt und das pH-abhängige Auflösungsvermögen mittels Trübungs-Titration untersucht. Alle modifizierten Copolymere zeigten eine erhöhte Löslichkeit bei niedrigerem pH Wert als die kommerziell erhältlichen Eudragit® Tablettenüberzüge, wobei die Säurebeständigkeit erhalten blieb. Nachdem das Konzept der verbesserten Löslichkeit bewiesen wurde, wurde eine skalierbare Modifikation der kommerziell erhältlichen Eudragit® Tablettenüberzüge entwickelt. Diese wurde in weiteren Experimenten hinsichtlich ihres Auflösungsverhaltens und ihrer Säureaufnahme untersucht.

In **Kapitel 5** wird das Konzept der Modifizierung magensaftresistenter Tablettenüberzüge auf die α-Hydroxysäuren Mandel- und Äpfelsäure ausgeweitet. Diese wurden speziell aufgrund der im vorherigen Kapitel erzielten Ergebnisse ausgewählt. Da die vorherigen Modifizierungen die Säureaufnahme der beschichteten Kapseln erhöhte, wurde Mandelsäure verwendet um durch die Phenyl Seitenkette die Hydrophobie des Copolymers zu erhöhen. Äpfelsäure wurde gewählt um durch die zweiten Säurefunktion die Auflösung zusätzlich zu beschleunigen. Dies war erfolgreich, aber zu Lasten der Säurestabilität. Die Äpfelsäure basierte Copolymere waren bereits ab einem pH Wert von 2 löslich, wodurch ihre Verwendung als magensaftresistenter Tablettenüberzug ausgeschlossen werden kann. Die Mandelsäure Modifikation hingegen ist säurebeständig, zeigte ein beschleunigtes Auflösungsverhalten und wie erwartet eine verringerte Säureaufnahme.

Kapitel A1 untersucht Methyl-*tert*-butylether (MTBE) als stabileres und nachhaltigeres polares Lösungsmittel in der carbanionischen Polymerisation. Die erhöhte Stabilität wurde durch eine 50 mal längere Halbwertszeit von *n*-Buthyllithium in MTBE gegenüber THF bestätigt. MTBE besitzt außerdem den Vorteil keiner Peroxidbildung und hat eine moderaten Polarität zwischen Cyclohexan und THF. Neben der Stabilität wurde der Einfluss von MTBE auf die Homopolymerisation verschiedener Diene mittels NMR-Spektroskopie, sowie MTBE als Modifier in der Copolymerisation von Styrol und Isopren mittels NIR-Spektroskopie untersucht. Durch Zugabe unterschiedlicher Äquivalente MTBE gelang es den Copolymergradienten über den gesamten Bereich, von tapered

Strukturen in reinem Cyclohexan bis hin zu umgekehrten Gradienten ($r_S = 1.82$; $r_I = 0.55$) in reinem MTBE einzustellen, wobei MTBE einen geringeren Einfluss auf die Dien Mikrostruktur als THF hatte.

Kapitel A2 konzentriert sich auf weitere pharmazeutische Tests der in Kapitel 4 vorgestellten magensaftresistenten Tablettenüberzügen. Die hochmolekularen Copolymere, die durch Modifikation nach der Polymerisation synthetisiert wurden, wurden auf ihre Auflösungseigenschaften, Langzeitstabilität und mögliche Zytotoxizität untersucht. Weitere Tests bestätigen die beschleunigte Auflösung und Langzeitstabilität dieser neuartigen Copolymere sowie ihre Ungiftigkeit.

Graphical Abstract

Chapter 2:

Effect of THF on the Anionic Copolymerization of 4-Trimethylsilylstyrene with Isoprene

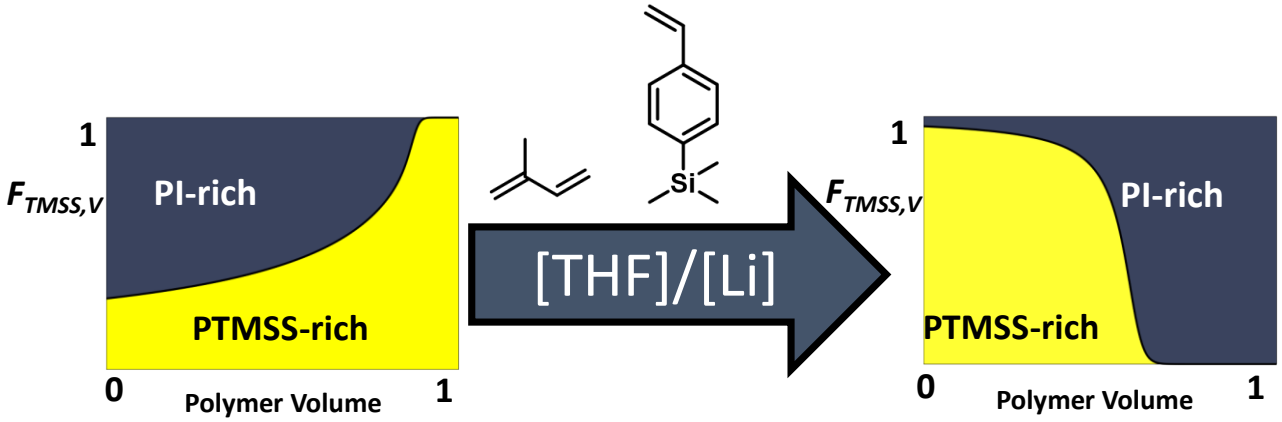

Chapter 3:

Dramatic Effect of Alkali Metal Alkoxides on the Anionic Copolymerization of Styrene and Isoprene

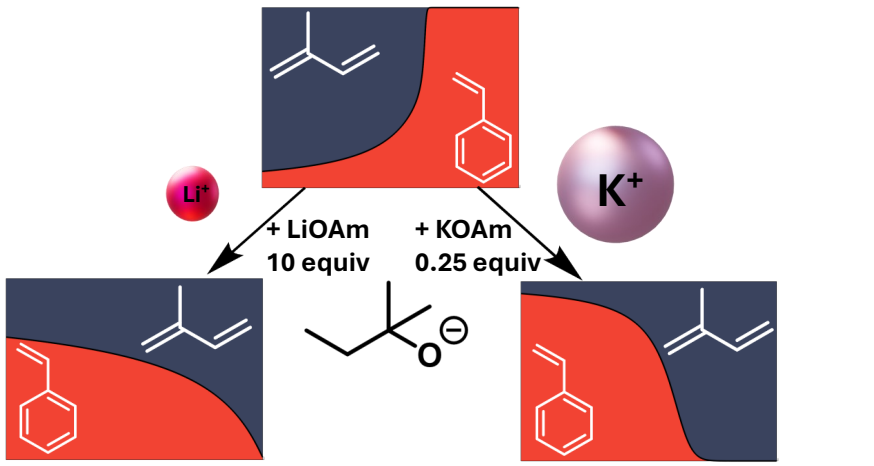

Styrene rate:↓
Isoprene rate:↓↓
Vinyl unsaturation:↑
T_g :↑

Styrene rate:↑↑
Isoprene rate:⟶
Vinyl unsaturation:⟶
T_g :↓

Chapter 4:

Enteric drug coatings: Synthesis and copolymerization of novel α-hydroxy acid monomers to adjust the pH for dissolution

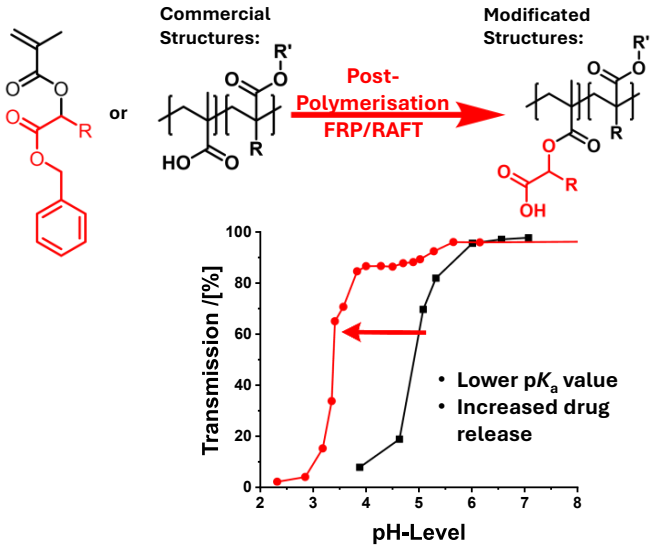

Chapter 5:

Enteric drug coatings: Synthesis and copolymerization of novel α-hydroxy acid monomers to adjust the pH for dissolution

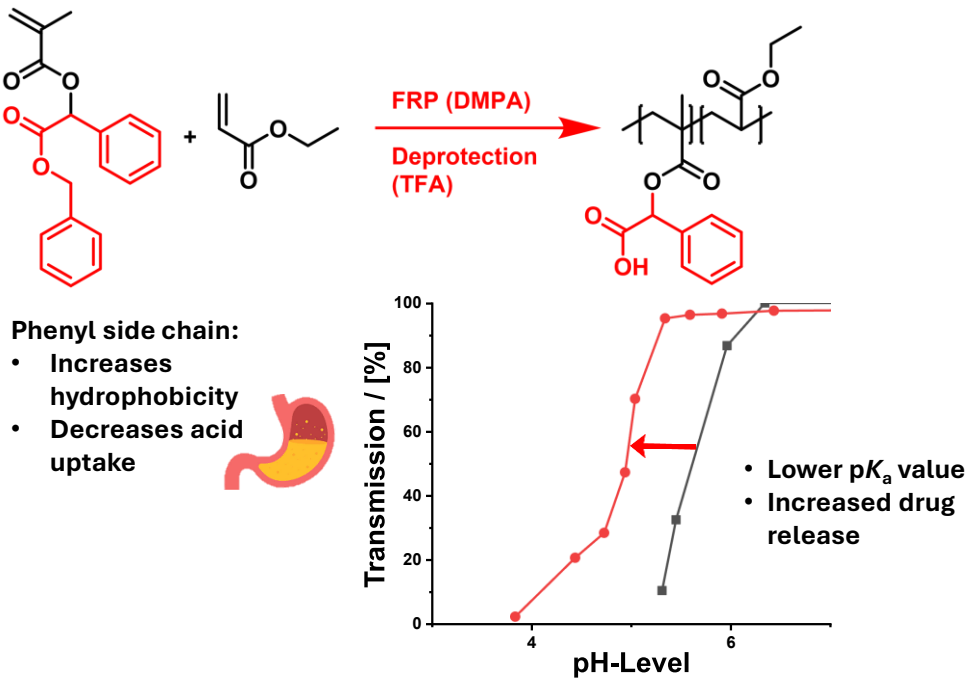

Chapter A1:

Spotlight on Methyl *tert*-Butyl Ether - Underrated or Overlooked? Unveiling Its Role for Living Anionic Polymerization

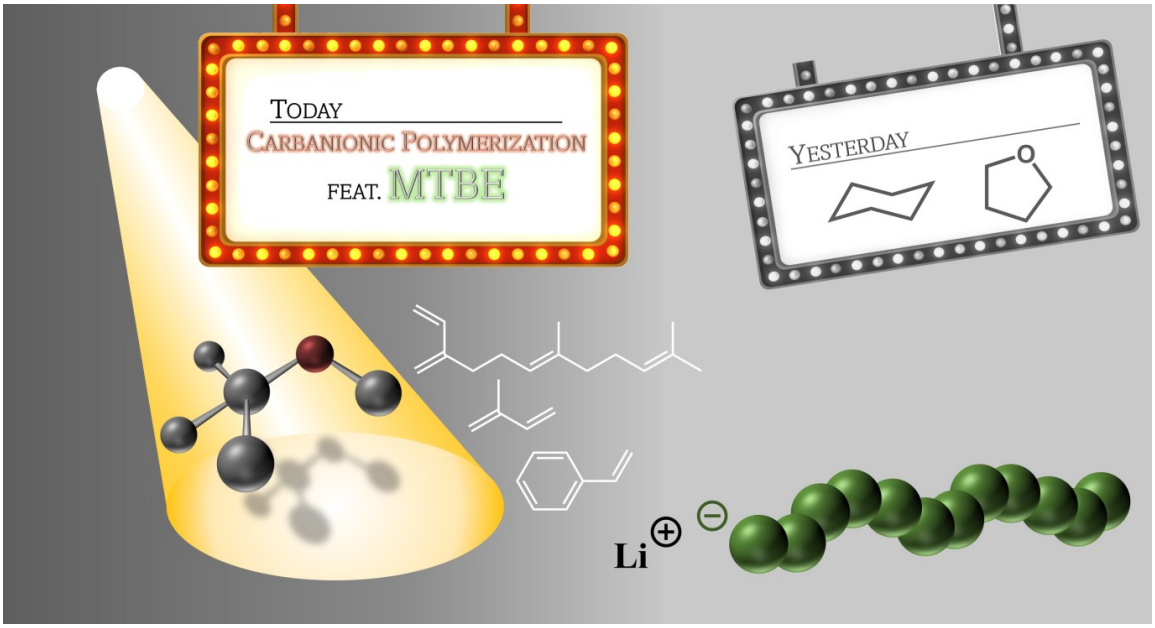

Chapter 1

Introduction

Over a century ago, Herrmann Staudinger introduced the concept of a new class of materials: polymers, a term derived from the Greek word meaning "many parts".[1,2] These materials are composed of small repeating units that form large macromolecules. However, long before the formal concept of macromolecules emerged, natural and synthetic (bio)polymers were already in use. From the rubber balls of ancient Mesoamerican ballgames to Goodyear's vulcanized rubber for tires, and the invention of Bakelite, used in countless applications, the history of polymers is deeply intertwined with human innovation. These developments marked the beginning of the "age of polymers", an impressive era characterized by inventiveness in which polymer materials have become indispensable due to their unique material properties and cost-effective synthesis. Today, polymers are found everywhere, from bitumen and footwear to automobiles, planes, electronics and medical devices, shaping nearly every aspect of modern life. However, their excessive production and consumption has also lead to some serious health and environmental problems.[3,4]

Polymers can be synthesized or extracted using various techniques. This introduction will focus primarily on the anionic polymerization of dienes and styrene derivates, while also briefly addressing the use of poly(meth)acrylates in enteric drug coatings.

Anionic polymerization

The first successful living anionic polymerization was reported by M. Szwarc in 1956, when he polymerized styrene using sodium naphthalene as a bifunctional initiator in tetrahydrofuran.[5] While this was not revolutionary in itself, given that radical (co)polymerization techniques had already been well established for decades, the advantages of this new method were unprecedented.[6] The key breakthrough separating it from the previous polymerization techniques is its living nature: initiation is significantly faster than propagation and no termination or chain transfer reactions occur.[7] This fundamental distinction sets it apart from conventional and even controlled polymerization techniques. This enabled, for the first time, the precise synthesis of (block)copolymers with well-defined block lengths and architectures.

Despite these benefits, living anionic polymerization comes with significant limitations. The highly reactive yet stable polymer chain anions do not tolerate any protic substances, many functional groups and often even not polar solvents or monomers, restricting the method's potential use. As a result, monomers are mostly hydrocarbon based, although some functionalized monomers, such as methyl methacrylate (MMA) can be tolerated under specific reaction conditions.[8–14] In contrast, the development of reversible deactivation radical polymerization (RDRP) methods such as RAFT,[15–18] ATRP,[19–21] and NMP[22–24] as well as techniques like ring-opening metathesis polymerizations (ROMP)[25–30] and organocatalytic polymerizations[27–30] introduced more tolerant "living" systems capable of handling functional groups as well as polar and protic solvents and monomers. Nonetheless, anionic polymerization remains unmatched in its precision and control.[31,32] It allows the synthesis of polymers with controllable molar masses, narrow dispersities and a wide range of complex polymer architectures, while maintaining a high compositional and molecular homogeneity.[7,32,33]

Carbanionic polymerization proceeds through three fundamental steps: initiation, propagation and termination.[7] Initiators (I) are radical anions (e.g. sodium naphthalene) or alkali organyl compounds, mostly based on lithium. In the case of radical anions, an electron is first transferred from an alkali metal to an electron-deficient aromatic hydrocarbon (e.g. naphthalene), forming a radical anion that can be reversibly transfer an electro to a monomer.[34] This results in another radical anion, which rapidly dimerizes to form a bifunctional initiator. During the initiation step, both radical anion-derived and alkyl lithium initiators perform a nucleophilic attack on the monomer, generating a new carbanion, which propagates the chain by continuously attacking and incorporating new monomer units until the monomer is fully consumed.[34] Because termination reactions are typically absent, unless a termination agent is added, the concentration of living chain ends remains equal to the initial initiator ($[I_0]$) concentration, resulting in a first order kinetic for monomer ($[M]$) consumption:

$$-\frac{\mathrm{dM}}{\mathrm{d}t} = k_\mathrm{p} \cdot [M] \cdot [P^-] = k_\mathrm{p} \cdot [M] \cdot [I_0] \quad (1)$$

This allows the degree of polymerization ($\overline{DP}_n$) to be calculated directly from the amount of monomer consumed; in a complete reaction (conversion (x_p) = 1), the monomer consumed corresponds to the starting monomer concentration.

$$\overline{DP}_n = \frac{[M_0]}{[I_0]} \cdot x_p \tag{2}$$

Because all chains initiate nearly simultaneously and grow with the same rate, their molar mass distribution follows a Poisson distribution, which narrows with increasing $\overline{DP}_n$, converging the dispersity (*Đ*) to one. [35,36]

$$Đ = \frac{\bar{M}_w}{\bar{M}_n} \approx 1 + \frac{1}{\overline{DP}_n} \tag{3}$$

In Szwarc's original first anionic polymerization sodium naphthalene in THF served as a bifunctional initiator for styrene. However, this system was incompatible to synthesize polyisoprene (PI) with a high *cis* 1,4 content, a key structural requirement for synthetic rubber alternatives, due to the requirements of using THF as a polar solvent for the formation of the initiator. Despite this limitation, the technique sparked considerable industrial and academic interest, leading to numerous patents and publications. [37–39]

The problem of the undesired PI microstructure was soon addressed with the introduction of butyllithium (BuLi) as an initiator. BuLi, soluble in apolar solvents such as benzene or *n*-heptane, enabled the synthesis of PI with a high *cis*-1,4-content. [40–42] This selectivity is attributed to a six-membered transition state between the propagating chain end and the incoming monomer, as depicted in Figure 1. [43,44] Beyond solvent effects, modifiers and counterions also significantly influence the resulting microstructure, topics which will be elaborated in the following chapters.

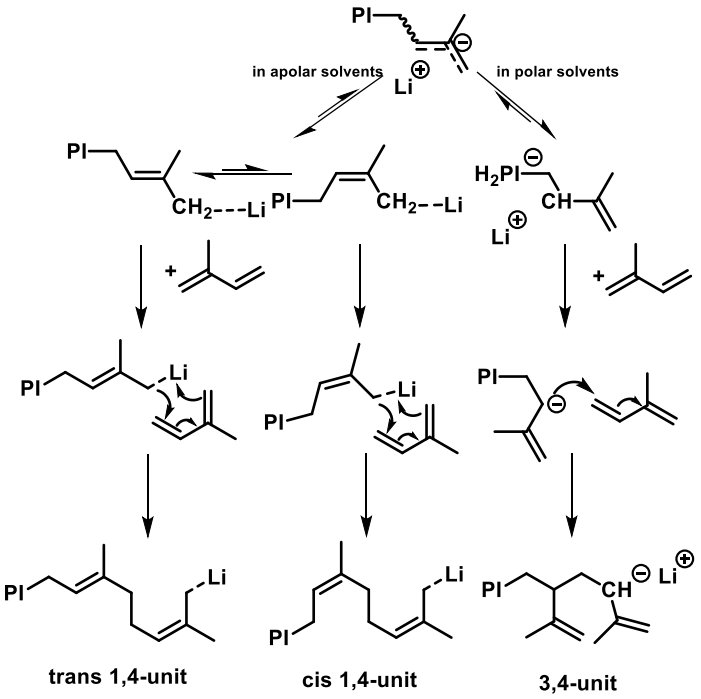

Figure 1: Proposed polymerization mechanism of isoprene in polar and apolar solvents with a lithium counterion.[43]

Once high *cis*-1,4 diene synthesis became feasible, companies such as Shell and Phillips petroleum began developing and patenting ABA-type multiblock copolymers, synthesized by sequential monomer additions.[39,45,46] These block copolymers gave rise to a novel material class: thermoplastic elastomers (TPEs). TPEs combine the elasticity of conventional rubbers at service temperature with the processability of thermoplastics when heated above their glass transition temperature. Their unique performance characteristics led to a production volume nearing 5 million tons in 2022.[47] TPEs can exhibit a variety of architectures: linear, branched, star-shaped, coupled or crosslinked (to different extents) to achieve different material properties. Besides the primary polymer architecture block length as well as block sequences can be additionally altered to further tune the material properties of the polymer.[48] In addition to stepwise monomer additions, copolymerization techniques can be employed to create tapered block copolymer, which will be discussed in subsequent sections.

Monomers

Due to the harsh conditions required for anionic polymerization, the range of suitable monomers, solvents and initiators is relatively limited. The previously mentioned sodium naphthalene used as a bifunctional initiator requires polar solvents such as THF, a solvent

particularly unfavorable for the polymerization of high 1,4-content dienes. This limitation was addressed by employing BuLi as a more effective initiator in apolar solvents, enabling the synthesis of polymers with very low dispersities (Đ < 1.1).[41] However, this polymerization technique has still some significant disadvantages, due to the extremely high nucleophilicity of *sec*-BuLi ($pK_b \approx -37$) and the resulting polymer chain ends, compatible solvents and monomers are quite restricted.[49] They must be aprotic and only limited functional groups are tolerated. The most commonly used monomers are styrene and its derivates (S), as well as various dienes (butadiene (B), isoprene (I), myrcene (M) and farnesene (F)), but also methyl methacrylate (MMA) is anionic polymerizable.[50] However, MMA having an ester functionality requires special conditions, such as low temperature, the use of polar modifiers (e.g. Lewis bases and/or acids) and less nucleophilic, sterically hindered initiators, in order to prevent termination via nucleophilic attack on the monomer's ester group.[8–14]

Beyond these commercially available monomers, various functionalized styrene derivates have also been explored in carbanionic polymerization, broadening the scope of this powerful yet demanding technique. However, even slightly acidic functional groups can induce termination or chain transfer, limiting the direct use of such derivates. To overcome these challenges, protective strategies have been developed, mostly based on bulky alkyl silyl functionalities. Hirao *et al.* demonstrated that functionalities such as alcohols, thiols and amines can be effectively protected using various sterically demanding groups such as *tert.* butyl or trialkyl silyl groups, enabling their polymerization under living anionic conditions to obtain of well-defined polymers with precise control over molar mass and low dispersity .[51–54] These polymers can subsequently be hydrolyzed and grafted onto inorganic substances such as silica or metal oxides, making them valuable precursors for organic-inorganic composite materials.[55]

In addition to serving as protective groups, silyl functionalities can also be integrated into the polymer backbone, leading to the synthesis of silicon containing polymers.[56,57] The incorporation of silicon atoms influences several key materials properties, including the glass transition temperature (T_g), Flory-Huggins interaction parameter (χ), hydrophobicity, etch resistance, and gas permeability and are used in different applications like photonics, lithography and gas separation.[58–64] Nagasaki et al. investigated a range of silyl-

functionalized styrene derivates for their gas separation properties. Their findings revealed that Si-C bonds significantly enhance oxygen permeability and that increased silicon content leads to higher O_2 solubility. Additionally, polymers with a higher T_g showed greater gas permeability, attributed to an increase in free volume.[65] Using positron annihilation spectroscopy, it was shown that trimethylsilyl styrene (TMSS) possesses the highest free volume among the polymers studied, approximately 19% greater than that of polystyrene (PS).[60,66] TMSS also exhibited a T_g of 135°C and the highest gas permeability in this study. Beyond its effect on material properties, the TMS group also influences the reactivity of the styrene derivate, due to a change in electron density in the vinyl group, which can be probed via the ^{13}C β-carbon shift. In general, electron-withdrawing groups reduce the electron density at the vinyl group, increasing polarity and monomer reactivity.[67] The TMS group has an +I effect, increasing electron density due to the difference in electronegativity between Si and C.[68,69] Besides this +I effect has the silicon another -M effect, due to the empty 3d orbitals of Si. As it is directly bound to the phenyl ring, the π-electrons can undergo a d_π-p_π interaction, drawing π-electrons from the ring.[70] These competing effects are analyzed in the downfield shift of the β-carbon from 113.36 ppm for styrene to 114.14 ppm for TMSS ($CDCl_3$), suggesting an increase in polarity and reactivity of the vinyl group.[58] This enhanced reactivity has already been investigated by Wadgaonkar *et al*. for the copolymerization of TMSS with I in cyclohexane (r_{TMSS} = 0.152 and r_I = 3.28).[58] These study indicate significant potential for tailoring copolymer compositions by utilizing polar modifiers to synthesize a variety of polymer compositions for potential applications in gas separation membranes.

In anionic polymerization, apolar solvents such as cyclohexane, benzene or various aliphatic hydrocarbons are commonly used. Although toluene is classified as apolar, it is unsuitable due to its slightly acidic methyl group, which can undergo chain transfer reactions, compromising the living nature of the polymerization.[71] Apolar solvents typically promote aggregation of the active chain ends. The addition of polar modifiers such as ethers or amines, prevents the aggregation by better solvating the cation.[34,72,73] Among these, tetrahydrofuran (THF) is most common, but the addition of such modifiers significantly influences the polymerization kinetics and the microstructure of diene-based monomers, often leading to a reduction in the desired low T_g 1,4-units in favor of less desirable 3,4 and 1,2-vinyl linkages. A further challenge arises from the chemical

instability of ethers, which often can undergo decomposition in the presence of alkyl lithium initiators or living chain ends, limiting its use in multiblock synthesis and polymerizations at elevated temperatures.[74] Moreover, the potential formation of explosive peroxides limits the use of most ethers in industrial scale synthesis.

To mitigate these issues, 2-methoxy-2-methylpropane (MTBE) was introduced as a more stable alternative solvent/modifier for carbanionic polymerizations.[75–79] This linear ether has the advantage of not forming peroxides and exhibits greater stability against nucleophilic attacks by both initiator and active chain ends.[78,80] Unfortunately, its higher polarity compared to cyclohexane also enhances vinyl unsaturation, although to a lesser extent than THF.[81–83]

In addition to the inherent limitations on monomers and solvents, special reaction conditions such as an inert gas atmosphere are essential for successful anionic polymerizations. Trace amounts of carbon dioxide or water will result in immediate termination of the growing chains, while oxygen couples them, effectively doubling the molar mass and terminating further polymerization. However, these termination reactions can also be exploited to introduce end-group functionality, as illustrated in Figure 2.[35,84]

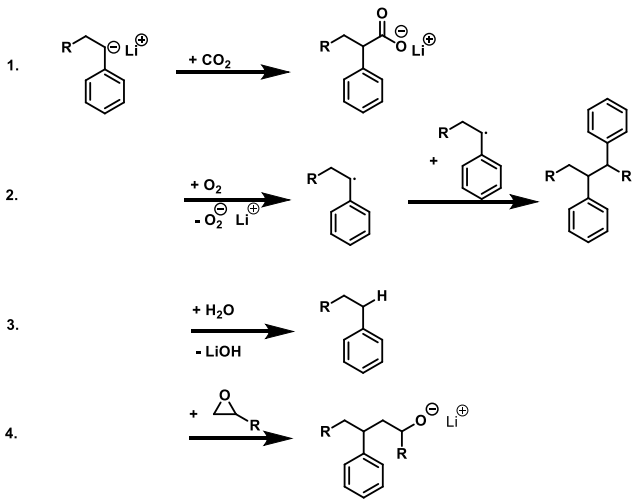

Figure 2: Possible termination reactions of the polystyryl anion with carbon dioxide, oxygen, water and epoxides.

The following chapters will focus on the most common monomers in the carbanionic polymerization: styrene (S) and isoprene (I), as well as trimethylsilylstyrene (TMSS), which

will be copolymerized in cyclohexane using various polar modifiers to investigate their influence on reactivity ratios and the resulting material properties.

Glass transition temperature

Every polymer can exhibit up to two thermal transition temperatures: the melting temperature (T_m) and the glass transition temperature (T_g), depending on the crystallinity of the polymer.[85] These temperatures correspond to transitions in the polymers crystalline and amorphous domains, respectively. As a result, semicrystalline polymers typically display both T_m and T_g, while totally amorphous polymers do not meet the necessary symmetry requirements for crystallization and therefore do not have a melting point. However, since the polymers discussed in the following chapters are entirely amorphous, we will focus in this chapter on the glass transition temperature.

The T_g is described as a transition of a polymer from a rigid, glassy state into a soft, viscous state. At this temperature the long-range segmental motion of the polymer chain ceases, rotational freedom is hindered and the free volume decreases resulting in a noticeable change in the heat capacity. Unlike a first-order transition such as melting, the glass transition is a gradual transition. Therefore, the T_g is not a fixed point, but has a softening/solidification range and depends on the determination method.[85] The most used method to determine the T_g is the differential scanning calorimetry (DSC), which is also used in the following chapters. Other methods include dilatometry, thermal analysis, dynamic mechanical analysis and NMR spectroscopy.[86] In the DSC experiment the heat capacity of the polymer is measured as a function of temperature, with the T_g appearing as a step change in heat capacity.[85]

The T_g is influenced by molecular symmetry, structural rigidity and secondary attractive forces (e.g. van der Waals forces, hydrogen bonding or π-π stacking) of the polymer chains. These factors reduce chain mobility and typically result in a higher T_g. Polymers with bulky side groups such as phenyl rings in polystyrene or multiple substituents per monomer unit such as in poly(methyl methacrylate) (PMMA) exhibit increased rigidity and therefore higher T_g's. Several examples of polymers utilized in the following chapters are shown in Figure 3.

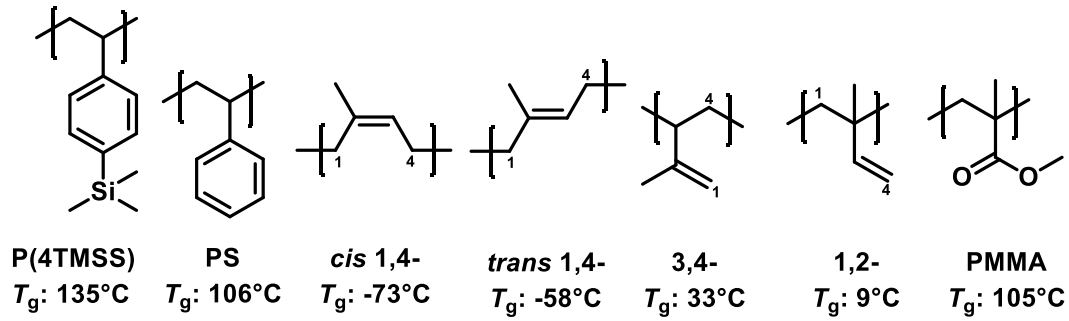

P(4TMSS)	PS	*cis* 1,4-	*trans* 1,4-	3,4-	1,2-	PMMA
T_g: 135°C	T_g: 106°C	T_g: -73°C	T_g: -58°C	T_g: 33°C	T_g: 9°C	T_g: 105°C

Figure 3: Structures of various polymers and their corresponding glass transition temperatures.[66,85,87]

In addition to molecular structure and intermolecular interactions, the T_g is also dependent on molar mass, as described in the Flory-Fox equation.[88] Although material properties such as viscosity and Young's modulus change significantly at the T_g the chemical structure of the polymer remains unaltered.[89] Therefore, the T_g is a critical parameter not only in polymer processing and production, but also in determining the temperature application window of the material. Above the T_g, polymers exhibit viscous, soft, flexible behavior, losing mechanical properties, while below the T_g they become glassy, stiff and brittle.

Another key factor for material properties is the entanglement molar mass, which refers to the minimum molar mass at which chain entanglements begin to influence mechanical properties.[90] As molar mass increases, so does the possibility of mechanical interlocks between polymer chains (see Figure 4), leading to an increased melt viscosity and enhanced mechanical properties of the polymer.[91]

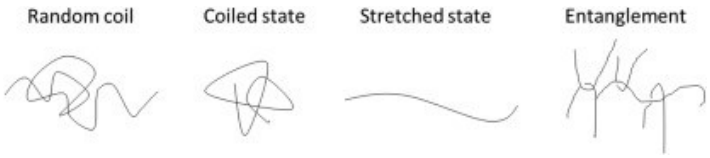

Figure 4: Schematic comparison of different polymer states.

These entanglements are not chemically crosslinked, but rather physical interlocks due to the increased chain length.

Copolymerization

Besides the previously discussed sequential monomer additions to synthesize block copolymers, statistical copolymerizations can also be used to synthesize various polymer architectures. When two or more monomers are copolymerized, differences in their reactivity often lead to non-random polymer compositions. For a system involving

two different monomers, four possible reactions can occur during copolymerization, as illustrated in Figure 5, and the monomer consumption can be described by the two differential equations (4) + (5).[92]

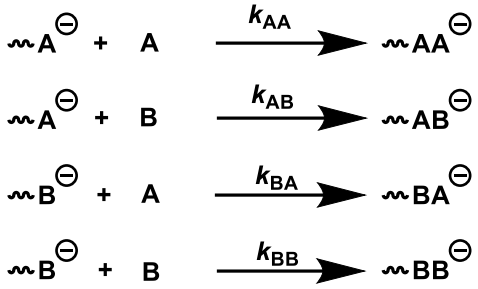

Figure 5: Possible copolymerization reactions between monomers A and B.

$$-\frac{\mathrm{d}A}{\mathrm{d}t} = k_{\mathrm{AA}} \cdot [A] \cdot [A^-] + k_{\mathrm{BA}} \cdot [A] \cdot [B^-] \quad (4)$$

$$-\frac{\mathrm{d}B}{\mathrm{d}t} = k_{\mathrm{BB}} \cdot [B] \cdot [B^-] + k_{\mathrm{AB}} \cdot [B] \cdot [A^-] \quad (5)$$

Here k_{AA} and k_{BB} represent the homopolymerization rate constants for monomers A and B, respectively, while k_{AB} and k_{BA} represent the cross-over rates. [*A*] and [*B*] represent the concentration of monomer A and B, while [A^-] and [B^-] the concentration of active polymer chain ends with A or B as the last unit. Therefore, the reactivity of each monomer can be characterized by its reactivity ratio, defined as:

$$\frac{k_{\mathrm{AA}}}{k_{\mathrm{AB}}} = r_{\mathrm{A}} \qquad \frac{k_{\mathrm{BB}}}{k_{\mathrm{BA}}} = r_{\mathrm{B}} \quad (6)$$

These reactivity ratios provide a description of the monomer preferences during copolymerization and can be used to describe the resulting polymer composition:

Table 1: Polymer composition depending on the reactivity ratios.[35]

Typ of copolymer	r_A	r_B
Tapered copolymer	>>1	~0
Gradient copolymer	>1	<1
Random copolymer	1	1
Alternating copolymer	0	0

These reactivity ratios can be determined by kinetic experiments or by analyzing the resulting polymer at various conversions, and depend on monomers, the polymerization technique and the solvent used. Especially in anionic polymerization, the reactivity ratios can be altered by introducing so called polar modifiers, as can be seen in the following

chapters.[34] Significant changes in the reactivity ratios for the same combination of monomers can lead to completely different material properties.[93,94]

The copolymerization of styrene and dienes in apolar solvents was investigated by several groups, which determined strongly varying reactivity ratios: $r_S = 0.05$; $r_B = 15$ and $r_S = 0.013$; $r_I = 10.1$ for the S/B[95,96] and S/I[97] system resulting in strong gradient copolymers.[39,45] These differences in reactivity ratio are explained by the favored cross-over from styrene to isoprene and the unfavored cross-over reaction from isoprene to styrene ($k_{SI} >> k_{IS}$), even though the homopolymerization of styrene is faster than the of isoprene ($k_{SS} >> k_{II}$).[93,97,98]

Gradient copolymers are described by a continuous change of the polymer composition along the copolymer chain, as shown in the following Fig. 6. Here every continuous transition from one monomer to the other is considered a gradient copolymer, while every copolymer with a steep transition and a pure endblock, exhibiting block copolymer properties, is considered a tapered copolymer.

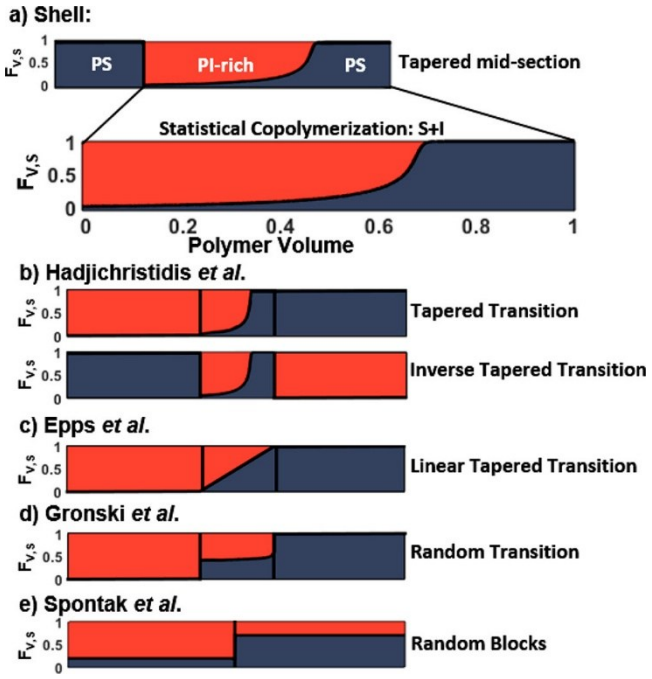

Figure 6: Overview of different tapered block copolymers, based on the styrene volume incorporation.[45,93,99–102] Reprinted with permission from Steube, M., Johann, T., Hübner, H., Koch, M., Dinh, T., Gallei, M., Floudas, G., Frey, H., & Müller, A. H. E. (2020). Macromolecules, 53(13), 5512–5527. Copyright 2020 American Chemical Society.

The presence of tapered regions in copolymers significantly influences their mechanical properties, morphology, domain spacing, glass transition temperature and order-disorder transition temperature (ODT), despite being composed of the same molar ratio and molar

mass. Therefore, the tapered region introduced a new tunable parameter that can be controlled either through the copolymerization of two monomers with adjustable reactivity ratios or by precisely regulating the monomer feed using automated pumps.[93,94,100] During the copolymerization of two monomers (i.e. isoprene (I) and styrene (S)), with differing reactivity ratios, the more reactive monomer (I) is initially preferred incorporated, forming a block that is contaminated with small units of the less reactive monomer (S). As the concentration of (I) decreases, the incorporation of (S) increases, resulting in the formation of a tapered gradient. Once (I) is fully consumed, (S) homopolymerizes forming a pure polystyrene end block.

When the reactivity ratios are significantly different, the tapered region is short and the resulting copolymer closely resembles a traditional block copolymer. However, it benefits from a lower ODT, which is beneficial for processing techniques such as extrusion.[99] Hereby, acts the tapered transition between the monomers as a compatibilizer between the different blocks, lowering the Flory-Huggins interaction parameter (χ) and therefore reducing phase separation. And this compatibilization effect can be finely tuned by adjusting length, slope and sequence of the tapered region.[99,103,104] By altering the interfacial compatibility, these gradients also influence the thermal behavior of the copolymer. In tapered block copolymers the T_g of the more reactive monomer phase is altered due to contamination by the other monomer, while the T_g of the latter is only slightly affected due to the enhanced compatibility from the tapered region. As the volume fraction of the tapered region increases, these effects become more pronounced, and in some cases, an *inverse* tapered transition (regarding the outer blocks; Figure 6b) provides greater benefits than a conventional tapered region.[105]

In contrast, when the reactivity ratios are similar, a longer and more gradual gradient is formed, resulting in polymers with distinct properties that diverge from their block copolymer analogs.[94] These random copolymers do not exhibit any phase separation and tend to exhibit a single, mixed T_g.

The following chapters will focus on the manipulation of reactivity ratios and therefore the tapered region by different polar modifiers (Lewis bases and acids).

Effect of polar modifiers

Lewis bases

As already mentioned, the choice of solvent has a great influence on the copolymerization kinetics, diene microstructure and ultimately the material properties of the resulting polymer. This is largely due to the degree of aggregation of the living polymer chain ends, which varies depending on the solvent environment. These different aggregated chain ends all exhibit different polymerization kinetics, see Figure 7.[92]

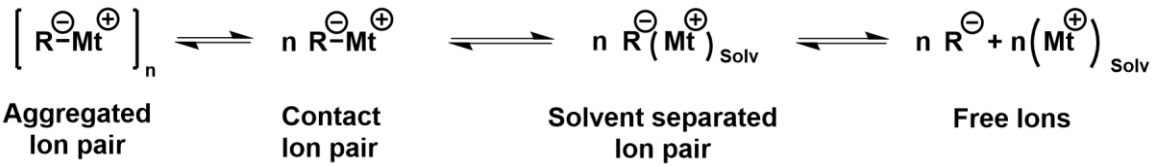

Figure 7: Equilibrium between the different ion pairs.[92]

In apolar solvents such as cyclohexane, the equilibrium is strongly on the side of the aggregated ion pairs, which do not participate in the polymerization. Polymerization only takes place at the non-aggregated contact ion pairs. With the addition of polar modifiers (e.g. ethers or amines), the equilibrium can shift towards solvated free ions, which differ in reactivity by several orders of magnitude.

This was investigated by Bywater and Fetters for the homopolymerization of styrene and isoprene using THF as a polar modifier in apolar solvents.[106,107] They observed that increasing THF content initially accelerates the polymerization rate of both monomers, reaching a maximum before further THF additions lead to a decrease in propagation rate. This is explained by the following equilibrium of the aggregated chain ends with the modifier THF.

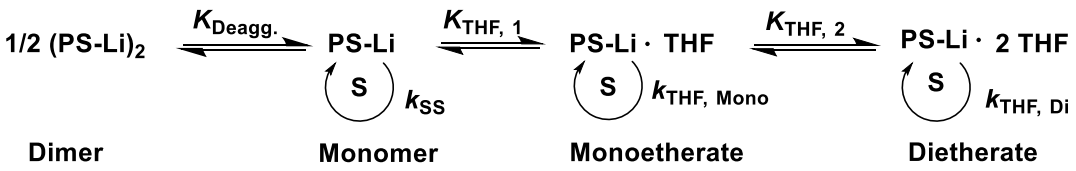

Figure 8: Aggregation behavior of polystyryllithium in apolar solvents and the effect of polar modifiers (THF).

In apolar solvents, polystyryllithium typically exists as an unreactive dimer, in equilibrium with a polymerization active unimer. Upon the addition of THF, this dimer is disrupted, forming mono- and dietherates, both more reactive than the unimer. However, excess THF

leads to a dominance of the dietherate, which is less reactive, thereby slowing the polymerization.[106,107] A similar aggregation behavior is observed for polydienyl chain ends, which form tetrameric and hexameric aggregates, which can be also broken apart by polar modifiers, enhancing reactivity.[34,72,73,108]

Since the reactivity change is different for every monomer, polar modifiers like THF can be used to alter reactivity ratios in a copolymerization. The system styrene/isoprene or styrene/myrcene have quite distinct reactivity ratios resulting in almost block like structures in cyclohexane r_S = 0.013; r_I = 10.1; r_S = 0.02; r_{Myr} = 40.6, but can be altered over the entire range up to r_S = 12.6; r_I = 0.15; r_S = 10.0; r_{Myr} = 0.1 with 2500 equiv of THF.[94,97] Besides this kinetic effect, polar modifiers also influence the microstructure and the T_g of the resulting polymer. For instance, polyisoprene synthesized in cyclohexane typically consisting of 95% 1,4- and 5% 3,4-units with a T_g of -64°C.[59,78,93,109–111] However, with 2500 equiv of THF, the microstructure shifts to 18% 1,4-; 57% 3,4- and 25% 1,2-units and an increased T_g of 2 °C.[93] This increase in vinyl content is attributed to a greater ionic character of the C-Mt bond in the presence of polar modifiers, due to the solvation of the counterion, facilitating π-electron delocalization.[34,112–114] Resulting in a different polymerization mechanism, see Figure 1.

Beyond THF, various other Lewis bases have been evaluated as polar modifiers, including ethers, amines and particularly bidentate ligands, which have proven highly effective in enhancing both polymerization kinetics and vinyl unsaturation.[94,115,116]

Lewis acids

In addition to the previously discussed ether-based modifiers, which reduce chain-end aggregation and thereby accelerate the homo- and copolymerization of styrene and dienes, certain Lewis acids, such as various alkali alkoxides, also affect polymerizations, but through a different mechanism, since they do not decrease aggregation.[117,118] Bywater et al. investigated the use of lithium *tert*-butoxide in the homopolymerization of styrene.[117] Unlike Lewis bases, this modifier does not reduce chain end aggregation; styrene consumption still depends on half the potency of active chain ends. Nevertheless, lithium alkoxides significantly alter both homo- and copolymerization rates as well as diene microstructure, despite the unchanged aggregation. Instead of accelerating like Lewis

bases, lithium alkoxides retard both homo- and copolymerization, depending on the monomer, modifier concentration and solvent.[117,119] Even though the homopolymerization of different monomers are slowed down differently, as well as retarding the copolymerization monomer incorporation seemed to be unaltered.[120,121] Moreover, lithium alkoxides increased vinyl unsaturation, an often undesirable feature in thermoplastic elastomers, but to which extent is not fully clarified. While Hsieh reported only a 10% vinyl unsaturation Makowski observed up to 40%, even under similar conditions.[120,122] The retardation is attributed to the formation of mixed aggregates, from reactive chain ends with lithium alkoxides, $(P\text{-}Li)_x(LiOR)_y$, reducing the concentration of unaggregated polymer chain ends. These mixed aggregates serve as new polymerization centers and are responsible for both the reduced polymerization rate and altered microstructure.[123,124]

Beyond lithium, researchers have studied alkoxides of heavier alkali metals (Na, K, Rb, Cs), as well as those from the alkaline earth and boron group.[114,117,119–121,125,126] However, the focus of the following studies will be placed on sodium and potassium alkoxides, since rubidium and cesium alkoxides do not offer any performance benefits and are commercially not available.[114,121] As a general trend: increasing the modifier amount and counterion size accelerates both styrene and diene polymerizations and styrene is being more effected than dienes.[114,127] This allows tuning of reactivity ratios across the whole range. For instance, already 0.2 equiv of a sodium alkoxide leads to an almost ideally random copolymerization, whereas the heavier potassium analogue required only 1/30 equiv.[33,121,128–130] Such behavior contradicts the assumption of homogeneous reaction centers typically associated with Lewis bases, as significantly less than one equivalent is sufficient to alter reactivity ratios. Given that polymer chains coordinated by potassium and lithium exhibit distinctly different reactivities, yet well-defined molar masses and low dispersities are achieved in homo- and copolymerizations, it can be assumed that counterion exchange must be rapid. Moreover, because the active centers can tautomerize the resulting polymers exhibit microsegment characteristics of each of the counterions, as can be seen in Figure 9.[121,131]

Besides this strong impact on copolymerization kinetics, exceeding the previously investigated Lewis bases, alkali alkoxides also affect the diene microstructure.[59,78,93,94]

Unlike lithium, which is typically localized at the α-position of the terminal monomer unit (favoring 1,4-addition), heavier alkoxides increase vinyl unsaturation. This phenomenon can be explained by two different theories:

1. Heavier alkoxides are considered as dissociated ion-pairs due to the larger ionic radius and the metal ions are π-bonded to the last units, favoring the formation of vinyl units.
2. The metal ion, free or complexed, coordinates the incoming monomer into a specific position before the nucleophilic attack, favoring 1,2- and 3,4-additions.[34,132]

Reports on the influence of different alkoxides on the polybutadiene microstructure vary greatly depending on the counterion, solvent and temperature. Especially for sodium modifiers vinyl unsaturation varies from 30–70%, depending on the used solvent.[125,133] This high vinyl microstructure corresponds to the microstructure when sodium initiators are used, indicating that sodium becomes the dominant polymerization center.[115,125,134] For potassium alkoxides, results are more consistent: vinyl unsaturation typically ranges from 35–50% for various solvents, indicating the high inherent ionic character of the potassium-carbon bond.[114,115,135] Hsieh used potassium *tert*-butoxide as a modifier in the homo- and copolymerization of butadiene and styrene. He could show that the microstructure increased sigmoidal up to 50% vinyl unsaturation, a microstructure that corresponds to the same as when metallic or organo potassium initiators were used.[114,115,136,137] The literature on rubidium- and cesium based alkoxides is limited. However, available studies indicate that they behave similarly to potassium alkoxides and show no unusual effects.[114,121] Compared to the other alkali alkoxides, sodium has the strongest influence on the microstructure, making it a preferred modifier for synthesizing polymers with high vinyl unsaturation, while potassium has the weakest effect on the diene microstructure, but shows the strongest influence on styrene propagation.[114,115,121,138,139]

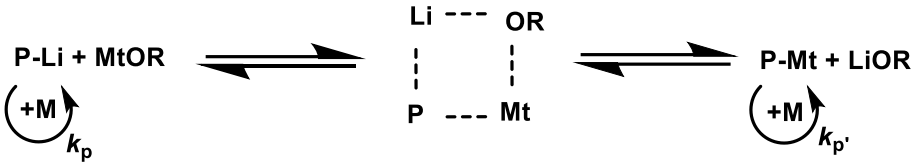

Figure 9: Illustration of the two-state polymerization model, involving a transition state complex, $k_{p'} >> k_p$.[114]

These observations can be explained by two different polymerization mechanisms, the associated mixed complex model and the two-state model. [126,131,140]

In the associated mixed complex mechanism has the reaction center not simply the chemical properties of a mixture of the components, but of an intermediated type with distinct chemical properties.[125,126,134,141–143] This mechanism is particularly relevant for sodium alkoxides, where the resulting microstructure suggests a predominant sodium reaction center, either by a complex or a metal exchange in the two-state equilibrium. Combining these findings with the report of Arest-Yakubovich that lithium alkoxides added to a sodium alkyl initiator can suppress chain transfer to toluene this supports the idea that both metal ions as well as the alkoxide participate in the polymerization by forming an associated complex.[134]

The other model the two-state polymerization was reported by many authors and is mostly considered for potassium modifiers in sub-stoichiometric concentrations, see Figure 9.[10,114,121,126,131,140] In this model, the different counterions are in an equilibrium and the polymerization proceeds at two different types of active centers: potassium (soft, big) containing chain ends favoring styrene (soft, delocalized) polymerization and lithium (hard, small) containing chain ends favoring diene (hard, localized) polymerization, resulting in a lithium dominated 1,4-microstructure. This can be summarized in the *hard and soft acids and bases* (*HSAB*) concept.[144]

The ability to achieve targeted molar mass and low dispersities implies that rapid exchange between lithium and the other counterions occurs during polymerization.[114,126,132,145–148] Despite these insights, the exact polymerization mechanism remains under debate. The scientific community is still divided on whether the active centers are best described as mixed aggregates or a two-state model.[10,143,149]

Methods to follow Polymerization Kinetics

In addition to the determination of polymer compositions at different conversions to estimate the comonomer sequence,[83,96,121,150–152] reactivity ratios (equation 1) can be used to fully describe the copolymerization of two different monomers. For this purpose, it is important to determine either the individual homo- and cross-over polymerization rates or the exact monomer concentrations during the copolymerization.[153,154] Highly accurate measurements are required for all approaches, as even small errors can lead to strong deviations. Since the first method requires several experiments at different conversions and/or with different concentrations, the focus will be on the determination of the individual monomer concentrations.

This approach was first introduced by Bywater and Worsfold in 1960 for the homopolymerization of styrene. They introduced a real-time monitoring method using glass reactors with ultraviolet optical cells to calculate the monomer concentration at any given time and therefore all rate constants.[155] This technique helped understanding carbanionic polymerization kinetics and was further improved and simplified by Quinebèche et al. using a mid-infrared (M-IR) probe for the system styrene and isoprene.[106,111,156–158] In addition to M-IR[158–160] spectroscopy, various analytical methods such as ^{1}H-NMR-,[78,161–166] UV-Vis,[158,167,168] and near-infrared (NIR)[59,78,93,94,97,169–174] spectroscopy are also possible for real-time kinetic measurements, which all have their different advantages and disadvantages. ^{1}H-NMR spectroscopy is routinely used in most chemical institutes and companies, but has the problem of insufficient time resolution of ~ 1 minute, which is too slow for the investigation of some of the experiments presented in the following chapters.[97] In addition to the time resolution problem, NMR experiments have other disadvantages: the temperature cannot be measured during the polymerization and the reaction heat may not be dissipated. As the reaction temperature increases, the polymerization rates and reactivity ratios change.[97] Also often reaction parameters have to be tailored for the NMR-experiment, such as the use of deuterated solvents and adjusted initiator and monomer concentrations, which are mostly not in the range of real word polymerizations and might have an unknown influence on polymerization kinetics. The limited reaction volume only leads to yields in the milligram scale, which makes further investigations of the material properties impossible. Furthermore, mixing in the NMR tube is limited to diffusion and no additional stirrer can be used. All of these problems can be solved by an *in situ* probe head for UV-Vis, mid-IR

or near infrared (NIR) spectroscopy. Since the reaction can now be performed inside a glass flask, the reaction volume is increased and material properties can be investigated on the very same batch as the kinetics. Additionally, the time resolution is improved, and magnetic stirrers can be used for mixing.

UV-Vis spectroscopy was introduced by Worsfold et al. in 1960 for the homo- and copolymerization of styrene, butadiene and isoprene.[106,111,157,158,175,176] Unfortunately, the overlapping of the absorption bands of poly butadienyl lithium, styrene and polystyrene made it very complicated to determine the individual monomer concentrations.[158,175]

Mid-IR spectroscopy solves this problem by tracking the well separated monomer peaks (1597 cm^{-1} (I) and 1630 cm^{-1} (S)) but has the disadvantage of needing an optic cable made out of crystalline AgCl or hollow waveguides, which are expensive, mechanical weak and would need a permanent installation.[158,177]

Therefore, the following chapters will rely on NIR spectroscopy, which only requires a flexible optical fiber cable, has a lower time resolution limit of > 0.1 seconds, uses nondeuterated solvents, has a temperature probe, a cryostat, a magnetic stirrer for mixing (Figure 10) and is used in a glass flask of 100–1000 ml. This allows the use of realistic concentrations to synthesize high molar mass polymers and achieve yields in the range of 10–100 grams, enabling us to perform every further experiment with the kinetically monitored polymer. However, interpretating NIR spectra is more complex than analyzing NMR spectra, where distinct signals provide clear molecular information. In the measured NIR region (5900–6250 cm^{-1}), the different monomers and polymers signals are broad and overlapping. Therefore, Long et al. used a combination of NIR and UV spectroscopy for their kinetic investigations.[170] To conduct these investigations solely using NIR spectroscopy, a deconvolution of the measured spectra with the calibration spectrum (Figure 11) of all individual monomers and resulting polymers must be performed. This was first introduced by our group (M. Steube and T. Johann) for the copolymerization of styrene and dienes in apolar solvents with the possibility to add polar modifiers.[93,97] Further improvements were achieved by adding a temperature probe to monitor the reaction temperature inside the flask and having a smaller flask to utilize monomers with limited availability.[59]

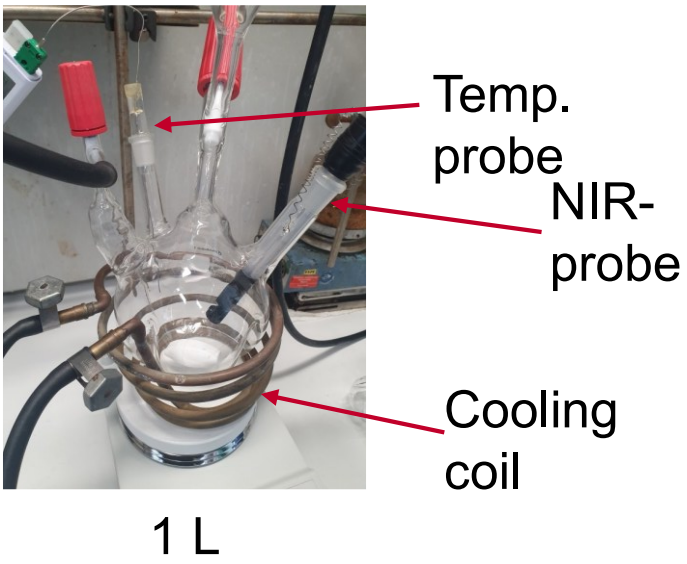

Figure 10: Illustration of the experimental setup: glass flask with temperature and NIR probe head, a cooling coil, which is normally immersed in a water bath, and argon inlets to maintain the argon atmosphere.

To calculate the concentration of all components that are present at any given time, a deconvolution of the measured spectra with the calibration spectra must be performed, see Figure 11. The spectra for polyisoprene synthesized in cyclohexane and in cyclohexane with 0.75 equiv of sodium amylate are quite different due to their different microstructure, which is a problem for the following deconvolution. To avoid this problem, the polyisoprene spectrum can be calculated by subtracting the polystyrene spectrum from the end spectrum.

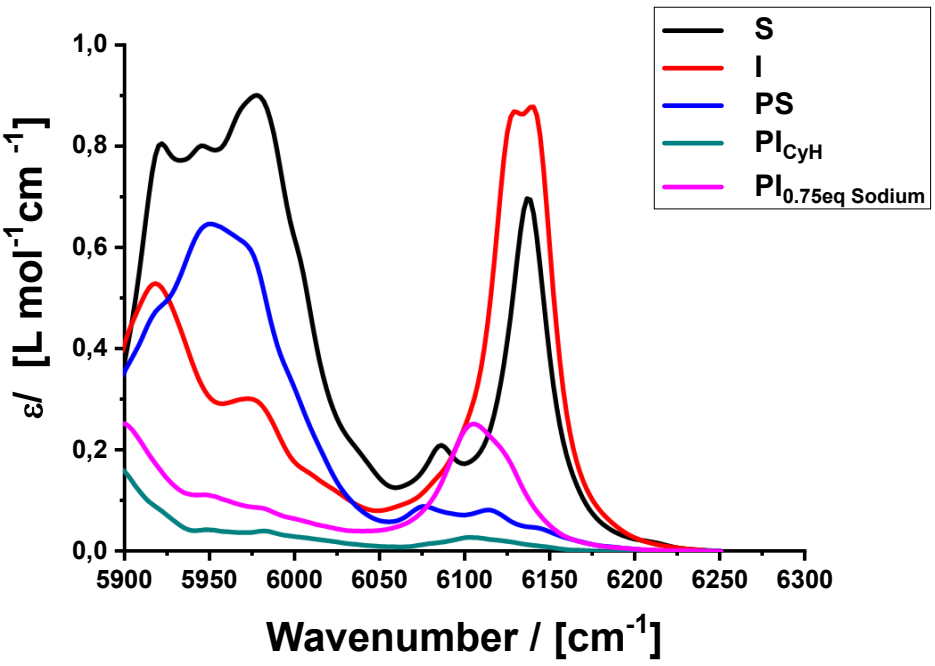

Figure 11: Calibration spectra of styrene (S), isoprene (I), polystyrene (PS), polyisoprene synthesized in cyclohexane (PI_{CyH}) and polyisoprene synthesized in cyclohexane in the presence of 0.75 equiv of sodium amylate.

After calculating the polyisoprene calibration spectrum, a deconvolution can be performed based on the linear equation system in (7)–(10), as described in previous publications.[97]

$$A(\tilde{\nu}) = A_{\mathrm{Monomer}}(\tilde{\nu}) + A_{\mathrm{Polymer}}(\tilde{\nu}) = [c_{\mathrm{I}} \cdot \varepsilon_{\mathrm{I}}(\tilde{\nu}) + c_{\mathrm{S}} \cdot \varepsilon_{\mathrm{S}}(\tilde{\nu})] + [c_{\mathrm{PI}} \cdot \varepsilon_{\mathrm{PI}}(\tilde{\nu}) + c_{\mathrm{PS}} \cdot \varepsilon_{\mathrm{PS}}(\tilde{\nu})] \quad (7)$$

$$c_{\mathrm{PI}} = c_{\mathrm{I},0} - c_I \quad (8)$$

$$c_{\mathrm{PS}} = c_{\mathrm{S},0} - c_{\mathrm{S}} \quad (9)$$

$$A(\tilde{\nu}) - c_{\mathrm{S},0} \cdot \varepsilon_{\mathrm{PS}}(\tilde{\nu}) - c_{\mathrm{I},0} \cdot \varepsilon_{\mathrm{PI}}(\tilde{\nu}) = c_{\mathrm{S}} \cdot [\varepsilon_{\mathrm{S}}(\tilde{\nu}) - \varepsilon_{\mathrm{PS}}(\tilde{\nu})] + c_I \cdot [\varepsilon_{\mathrm{I}}(\tilde{\nu}) - \varepsilon_{\mathrm{PI}}(\tilde{\nu})] \quad (10)$$

$A(\tilde{\nu})$ represents the total absorption of monomers and polymers at a certain wavelength, which depends on the concentration (c) and the extinction coefficient (ε) of the individual components, and since the polymer concentration depends on the initial monomer concentration, equation (7) can be simplified to equation (10). This means that only two (c_I, c_S) of the original four parameters (c_I, c_S, c_{PI}, c_{PS}) are relevant. For the deconvolution, 184 different equations are solved, which corresponds to a data interval of 1.9 cm^{-1}.

Determination of reactivity ratios

Differential fitting methods

To determine the reactivity ratios (equation (6)), various models can be used, which can be divided into an integral and differential fitting method. The differential method includes different models like the Mayo-Lewis-Non-Linear-Least-Square- (*Mayo-Lewis NLLS)*, Fineman-Ross- and Kelen-Tüdös-method, which will be presented shortly. These methods are based on the comparison of monomer feed with the polymer composition.

The necessary equations are shown in the following:[35]

$$f_1 = \frac{M_1}{M_1+M_2} \tag{11}$$

$$f_2 = 1 - f_1 \tag{12}$$

$$F_1 = \frac{\mathrm{d}M_1}{\mathrm{d}(M_1+M_2)} \tag{13}$$

$$X = 1 - \frac{M_1+M_2}{M_{1,0}+M_{2,0}} = 1 - \frac{M}{M_0} \tag{14}$$

Where *f* is the instantaneous monomer molar fraction, *F* the instantaneous monomer incorporation and *X* the total monomer conversion.

Since carbanionic polymerization is a living polymerization, characterized by the absence of termination and chain transfer reactions, equations (4) and (5) can be used to describe the consumption of monomer A and B. Since the concentration of active chain ends remains constant and the decrease in monomer concentration corresponds to the amount of monomer incorporated, the quotient of equations (4) and (5) can be used to calculate the composition of the resulting polymer at any conversion. The *Mayo-Lewis-NLLS* method is based on equation (15), where [*M*] represents the concentration of each monomer during the reaction. For the sake of simplicity, molar fractions can be used instead of concentrations (equation (16)). The reactivity ratios are determined by plotting *F* against the molar fraction f_1, using the least squares method.[153]

$$\frac{d[M_1]}{d[M_2]} = \frac{[M_1](r_1[M_1]+[M_2])}{[M_2](r_2[M_2]+[M_1])} \tag{15}$$

$$F_1 = \frac{r_1 f_1^2 + f_1 f_2}{r_1 f_1^2 + 2 f_1 f_2 + r_2 f_2^2} \tag{16}$$

Fineman-Ross used a linearized form of the Mayo-Lewis equation to calculate the reactivity ratios (equation 17). *G* and *H* must be calculated for every copolymerization,

and when they are plotted against each other, a straight line is obtained whose slope corresponds to r_1 and whose ordinate intercept corresponds to r_2.[178]

$$G = H \cdot r_1 - r_2 \tag{17}$$

$$G = \frac{f_1 \cdot (2F_1 - 1)}{(1 - f_1) \cdot F_1} \tag{18}$$

$$H = \frac{f_1^2 \cdot (1 - F_1)}{(1 - f_1)^2 \cdot F_1} \tag{19}$$

This method has the disadvantage that the experimental data are weighted unequally and that the calculated reactivity ratios depend on arbitrary factors, e.g. which monomer was selected as M_1.[179] Therefore, Kelen and Tüdös introduced a correction factor α (equation (20)), based on the highest and lowest value of H (equation (19)), to eliminate this arbitrariness.[180,181]

$$\alpha = (H_{min} \cdot H_{max})^{0.5} \tag{20}$$

$$\eta = \left[r_1 + \frac{r_2}{\alpha}\right] \mu - \frac{r_2}{\alpha} \tag{21}$$

$$\eta = \frac{G}{\alpha + H} \tag{22}$$

$$\mu = \frac{H}{\alpha + H} \tag{23}$$

All the differential fitting methods are based on the Mayo-Lewis equation (16), which is only valid for low conversions and assumes a constant monomer feed during the polymerization.[182] This restriction is only valid for a random copolymerization (r_1=r_2=1). In every non-random copolymerization, the reactivity differences between the monomers will cause a compositional drift towards the less reactive monomer as conversion increases.[85,182,183] By stopping the experiment at low conversions, $\frac{d[M_1]}{d[M_2]}$ can be approximated by the overall consumption $\frac{\Delta M_1}{\Delta M_2}$. The initial comonomer feed [M_1] and [M_2] is given by the molar ratio of monomers and $\frac{\Delta M_1}{\Delta M_2}$ can be determined after the experiment. However, these methods require conducting multiple low-conversion copolymerizations at different monomer feed ratios, a process that is experimentally intensive and prone to experimental errors.[184]

Integral fitting methods:

To overcome these problems, it is mandatory to integrate the Mayo-Lewis equation either analytically[185] or numerically.[184] These integral fitting methods can be divided into two

groups, the terminal and non-terminal model. The terminal model includes the direct numerical integration method (*DNI*), the Meyer-Lowry method (*Meyer-Lowry)* and the logarithmic Meyer-Lowry method (*Log Meyer-Lowry*), while the non-terminal model includes the Jaacks method (*Jaacks*), the Beckingham-Sanoja-Lynd method (*BSL*) and the ideal Meyer-Lowry method (*Meyer-Lowry ideal*). The non-terminal model assumes an chain-end independent copolymerization, resulting in $k_{12} = k_{22}$, $k_{21} = k_{11}$ and $r_1 * r_2 = 1$. Thus polymerizes the M_1 chain end as fast M_1 as the M_2 chain end polymerizes M_1 and vice versa. While the terminal model assumes a chain-end dependent copolymerization.

Terminal fitting models:

The Meyer-Lowry model is based on the analytical integration of the Mayo-Lewis equation and allows the determination of reactivity ratios for full conversions.[185] However, it is subject to some restrictions: polymerization must be isothermal, isochoric and the reactivity ratios must be constant for complete conversion, which is not always the case, especially for higher conversions. To describe the issue of composition drift, Meyer-Lowry solved the Skeist equation (24) analytically, and used it in the Meyer-Lowry equation (25).[184,185]

$$X_n = \frac{f_1 - f_{1,0}}{f_1 - \bar{F}_1} \tag{24}$$

X_n represents molar conversion, $f_{1,0}$ the molar fraction of monomer 1 at the beginning of the copolymerization and $\bar{F}_1$ the cumulative copolymer composition.

$$\frac{M}{M_0} = \left(\frac{f_1}{f_{1,0}}\right)^{\alpha} \left(\frac{f_2}{f_{2,0}}\right)^{\beta} \left(\frac{f_{1,0} - \delta}{f_1 - \delta}\right)^{\gamma} \tag{25}$$

$$\text{with} \quad \alpha = \frac{r_2}{1 - r_2};\ \beta = \frac{r_1}{1 - r_1};\ \gamma = \frac{1 - r_1 r_2}{(1 - r_1)(1 - r_2)};\ \delta = \frac{1 - r_2}{2 - r_1 - r_2}$$

The reactivity ratios are calculated by the method of least squares, by plotting $\frac{[M]}{[M_0]}$ against f_1.[185] This Meyer-Lowry equation (25) can also be written in a logarithmic way.[184]

$$log\left(\frac{[M_2]}{[M_{2,0}]}\right) = log\left(\frac{[M_{2,0}][M_1]}{[M_{1,0}][M_2]}\right) - \frac{1 - r_1 \cdot r_2}{(1 - r_1) \cdot (1 - r_2)} \cdot log\left(\frac{(r_1 - 1) \cdot \frac{[M_1]}{[M_2]} - r_2 + 1}{(r_1 - 1)\frac{[M_{1,0}]}{[M_{2,0}]} - r_2 + 1}\right) \tag{26}$$

Obviously, these equations have some restrictions, since they are numerical unstable for $r_1 = 1$; $r_2 = 1$; $f_1 = 0$ or 1 and $r_1 + r_2 = 2$.[184,185] In the case of an ideal copolymerization ($r_1 r_2 = 1$) the equation can be simplified to Walls equation (29).

Besides the Meyer-Lowry equation it is also possible to use numerical integration for the determination of reactivity ratios, by using and re-expressing the Skeist equation (24).

$$\bar{F_1} = \frac{f_{1,0} - f_1(1-X_n)}{X_n} \tag{27}$$

During the polymerization, while the molar conversion X_n changes, the mole fraction of unreacted monomer f_1 is calculated by a numerical solution of the differential equation (28), while the instantaneous monomer incorporation F_1 is given by Mayo-Lewis.[184]

$$\frac{df_1}{dX_n} = \frac{f_1 - F_1}{1-X_n} \tag{28}$$

Comparing the integral and differential fitting methods, the results are comparable for low conversions but significantly differ at higher conversions. Therefore, it can be assumed that the integral models are more accurate, as more data points are included in the determination.[184] In addition, the error range of the differential methods is significantly larger. Kazemi *et al*. were able to prove that the Meyer-Lowry method has convergence problems at high conversions, making it unsuitable for reliable use under such conditions.[184]

Non-terminal fitting methods

The nonterminal model includes the *Jaacks, Meyer-Lowry ideal* and *BSL* fitting methods. All of these calculate one reactivity ratio and the other from the relationship of an ideal copolymerization: $r_1 \cdot r_2 = 1$. This is based on the Wall model (equation (29)), which introduced a time-independent differential equation, that assumes a first-order copolymerization using relative rates.[186]

$$\frac{d[M_1]}{d[M_2]} = \varepsilon \frac{[M_1]}{[M_2]} \tag{29}$$

This equation can be integrated into the following equations:

$$\frac{[M_1]}{[M_{1,0}]} = \left(\frac{[M_2]}{[M_{2,0}]}\right)^{\varepsilon} \tag{20}$$

$$log\left(\frac{[M_1]}{[M_{1,0}]}\right) = \varepsilon \cdot log\left(\frac{[M_2]}{[M_{2,0}]}\right) \tag{31}$$

Here, ε represents the ratio of the polymerization rates. Jaacks proved that when there is a large excess of one monomer, the copolymerization is dominated by this monomer and the integrated equation (31) can be used to determine the reactivity ratio by the slope of

the fit.[187,188] The other reactivity ratio is then measured by an experiment with inverted monomer concentrations or calculated assuming an ideal copolymerization $\left(r_1 = \frac{1}{r_2};\ k_{11} = k_{21};\ k_{22} = k_{12}\right)$. In the non-terminal model, the polymerization is independent of the chain end and is controlled only by the monomer reactivity. Therefore, an M_1 chain end polymerizes M_1 as fast as an M_2 chain end polymerizes M_1. This independence of the chain end is typical for ionic polymerizations.[85,189–191] However, this method can only be used as long as the data points form a straight line.

The *Meyer-Lowry ideal* method (equation (32)) uses an integrated form of the Skeist equation for the non-terminal model of Wall. This allows the terminal model to be compared with the non-terminal model.[186,192]

$$X = 1 - \left(\frac{f_1}{f_{1,0}}\right)^{\frac{1}{r_1 - 1}} \cdot \left(\frac{1-f_1}{1-f_{1,0}}\right)^{\frac{r_1}{1-r_1}} \tag{32}$$

By plotting $X\,\frac{M}{M_0}$ against f_1, r_1 can be calculated by the method of least squares and r_2 follows due to the ideal copolymerization. Frey *et al*. investigated the robustness of this system, by introducing a systematic error into a simulated copolymerization.[192] The terminal Meyer-Lowry fit has an error of 60%, while the non-terminal methods have an error of less than 10%. Therefore, non-terminal methods should be preferred if an ideal copolymerization can be assumed, and only if it can be excluded to resort to the more complex terminal models.

2015 introduced Beckingham-Sanoja-Lynd (*BSL*) another method for the non-terminal model, which is based on the following equations:[191,193]

$$X = 1 - n_A \cdot (1 - p_A) - (1 - n_A) \cdot (1 - p_A)^{r_2} \tag{33}$$

$$X = 1 - n_A \cdot (1 - p_B)^{r_1} - (1 - n_A) \cdot (1 - p_B) \tag{34}$$

Here represents X the molar conversion, p_A the consumption of monomer A and n_A the starting mol fraction of monomer A. By plotting the molar conversion X against the individual monomer conversion $\left((1 - n_A) \cdot (1 - p_A)^{r_2}\right)$ reactivity ratios can be calculated.

The following chapters will focus on integral fitting methods, as they have a greater accuracy, a lower uncertainty in their implementation and require significantly less

experimental effort than the traditional linear differential methods.[184,193] The main advantage of the integral methods is their ability to calculate reactivity ratios across the full range of conversion. We will be focusing on the *Jaacks* method for the non-terminal model and the *Meyer-Lowry* method for the terminal model. Previous comparisons of the two models indicate that the non-terminal model is less error-prone than the terminal models.[192] Moreover, the *Meyer-Lowry* method tends to overfitting by adjusting irrelevant parameters to the background noise.[192,194] In accordance to Ockham's razor, which states that if there are several explanations for one and the same fact, the simplest theory is always preferable to the others,[195] we will always prefer the non-terminal model when ideal copolymerization can be assumed. The more complex terminal model will only be applied when experimental data rules out an ideal copolymerization and the *Jaacks* fit is nonlinear.[194,196]

Phase separation

The copolymers formed in the previously discussed chapters often exhibit block-like structures to varying degrees. If the reactivity ratios are dissimilar enough, the resulting copolymer can be assumed as two distinct homopolymers, covalently linked by a short transition region. As a result, the tapered copolymer exhibits a combination of the properties of both homopolymers, along with new characteristics arising from their covalent bond.

In block copolymers the different blocks are often immiscible and the system tries to minimize the interface between the incompatible phases. This results in the formation of various morphologies exhibiting domain spacing of 10 to 100 nm, which is called microphase separation.[197] That microphase separation occurs the Gibbs free energy of mixing (equation 35) must be positive.[197]

$$\Delta G_{\mathrm{m}} = \Delta H_{\mathrm{m}} - T\Delta S_{\mathrm{m}} \tag{35}$$

ΔG_m represents the change in Gibbs free energy, ΔH_m the mixing enthalpy and ΔS_m the mixing entropy. Since mixing is entropically always favored ($\Delta S_{\mathrm{m}} > 0$), higher temperatures generally favor mixing. However, for polymers the entropy term decreases with increasing degree of polymerization, making enthalpic interactions more dominant.

The mixing enthalpy describes the interactions of the different blocks and can be calculated by the following equation:

$$\Delta H_{\mathrm{m}} = \mathrm{R} \cdot T \cdot \chi \cdot \phi_{\mathrm{A}} \cdot \phi_{\mathrm{B}} \quad (36)$$

R represents the ideal gas constant, T the temperature, χ the Flory Huggins parameter and ϕ_A (ϕ_B) the volume fraction of monomer A (B). Hereby the Flory Huggins parameter describes the interactions of A and B monomer units and is defined as:

$$\chi = \frac{z}{k_B T} \cdot [\varepsilon_{AB} - 0.5 \cdot (\varepsilon_{AA} + \varepsilon_{BB})] \quad (37)$$

Z is the number of nearest monomers in a copolymer configuration cell (limited periodic space in the copolymer) k_B the Boltzmann constant and ε_{AB} represents the interaction energy of monomers A and B. Therefore, a positive Flory Huggins parameter indicates repulsive interactions and favors separation.[198] With an increasing temperature χ decreases, thus also favoring mixing. As a consequence, most polymers have a temperature at which the ordered state changes into a disordered state, which is called the order-disorder-transition temperature (T_{ODT}).

Leibler and Bates *et al*. investigated the phase separation theoretically as well as experimentally and proved that phase separation is dependent on the product of the Flory Huggins parameter, χ, the degree of polymerization, N, and the volume fraction of the one monomer, ϕ_A.[199,200] For a symmetric block copolymer ($\phi_A = \phi_B = 0.5$) phase separation occurs if the product of χ·N is ≥ 10.5. This phase separation leads to very different morphologies because of three competing effects:[201]

- Minimization of the interface of two immiscible blocks
- Homogeneous phases reduce entropy
- Localization of the connection points leads to further entropy lost

These entropic and enthalpic contributions force the system under energy minimizing to form a range of microphase separated structures (Fig. 12).[202–205]

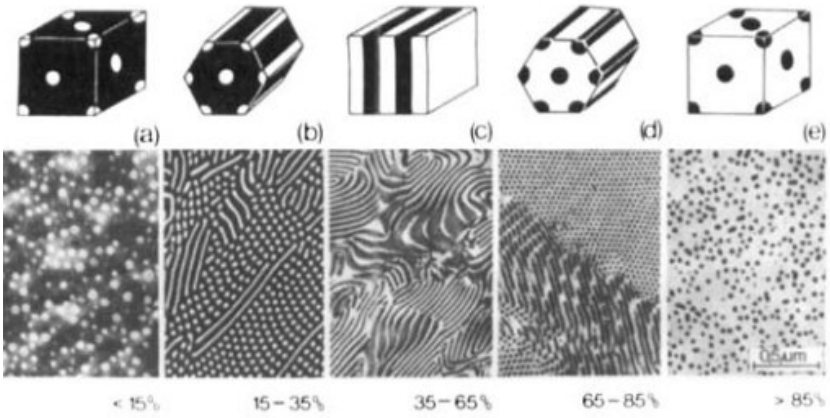

Figure 12: Morphologies for P(S-*b*-B) in dependence of the styrene content: a) PS-spheres in PB matrix; b) PS cylinders in PB matrix; c) PS and PB lamella; d) PB cylinders in PS matrix; e) PB spheres in PS matrix.[205] Reprinted with permission from Schmitt, B. J. (1979). Angewandte Chemie, 91(4), 286–309. Copyright 1979 Wiley & Sons Inc.

These can be summarized in Leibler's self-consistent mean-field theory (SCFT) and de Gennes random phase approximation, which allow the prediction of phases based on the polymer composition, degree of polymerization and the Flory-Huggins parameter.[200,206] Using these parameters Bates et al. determined a phase diagram for the diblock copolymer P(S-*b*-I), Fig. 13.[198]

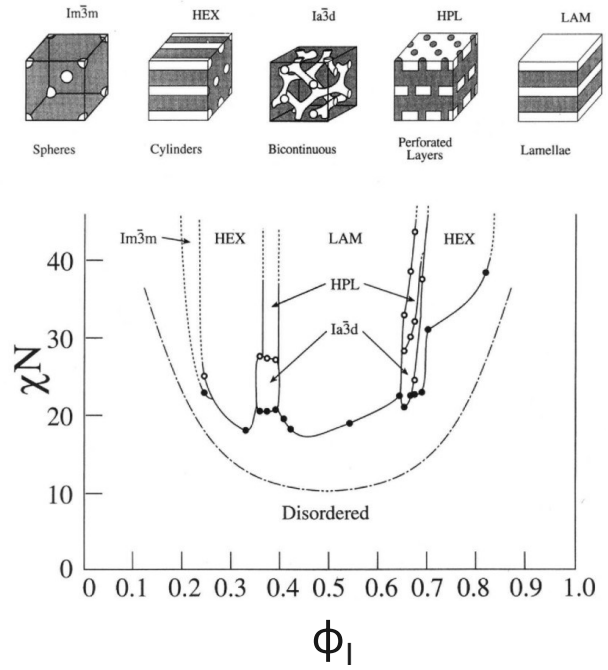

Figure 13: Phase diagram of P(S-*b*-I), depending on the product of $\chi \cdot N$ and the volume fraction of the polyisoprene phase (ϕ_I). Open and filled circles represent the order-order (OOT) and order-disorder (ODT) transition. Mean field predictions are shown as dashed-doted lines, and the five experimentally found morphologies are shown schematically above the phase diagram.[198] Reprinted with permission from

The asymmetry in the phase diagram of symmetric block copolymer, arises from differences in space-filling characteristics due to the unequal shape and densities of the monomers.[198,207] As a result, each unique comonomer pair has its own phase diagram, with varying boundaries, but same morphologies.

Since any change in polymer composition directly influences χ, as well as microphase separation and mechanical properties of the polymer. This proves as an effective lever to tailor the properties of the polymer. The Flory-Huggins parameter can be decreased using tapered copolymers, since the gradient increases miscibility between the different blocks and reduces χ to an effective Flory-Huggins parameter χ_{eff}.[208,209]

As a result, phase separation is weakened, mechanical properties are reduced and the T_{ODT} decreases, which is particularly favorable for industry. A lower T_{ODT} leads to lower melt viscosity, facilitating high-speed melt processing, such as extrusion.[33,210] Modifying χ, rather than the degree of polymerization, allows the processing of higher molar mass polymers, well above the entanglement molar mass, resulting in mechanically tough materials with accessible T_{ODT}.[87,211] Additionally, the gradient also affects the volume fraction, as there is now no longer a discrete transition and the first synthesized A block is partially contaminated by B units,[201] providing a simple way of customizing mechanical properties.[212]

Thermoplastic elastomers

Thermoplastic elastomers (TPE's) are a unique class of materials that combine previously incompatible properties such as thermoplastic and elastomeric properties. At service temperature, TPE's behave like traditional elastomers, while above their T_g, they exhibit thermoplastic behavior. This allows TPE's to be processed by extrusion and injection molding, as well as 3D printing.[33,213]

TPE's typically consist of at least three blocks (ABA), where the A block is a high T_g polymer phase and the B block a low T_g polymer phase, which phase separate to form microdomains, for the same fundamental thermodynamic reasons as AB blocks.[48,214,215] Hereby it is essential that the multiblock has at least two high T_g domains enabling

physical crosslinking between the hard domains, similar to the crosslinking in vulcanized rubber, but reversible, making TPE's recyclable.[216]

Most commercial TPE's are styrene based, with polystyrene as the hard- and dienes like butadiene or isoprene as the soft-domain. While the industry still heavily relies on petrol-based dienes, interest in bio-based alternatives is growing.[79,110,217] For example, Amyris Inc. and Kuraray Co. Ltd. commercialized a TPE based on farnese.[218,219] Nevertheless, petrochemical routes still remain dominant. Styrolux® and Styroflex®, both products of BASF, are synthesized by the copolymerization of styrene and butadiene in cyclohexane, sometimes in the presence of potassium alkoxides as modifier.[33] Even though these materials were already introduced in the 1950s, they are still the subject of research.[33,220–224] Commercially available are also alternative TPE's based on (meth)acrylates, which are sold by Kuraray, but need specific reaction conditions, which will not be discussed here.

Styrolux®, a transparent and tough polystyrene is synthesized by sequential anionic polymerization. First, a long polystyrene block is synthesized, which is extended by the addition of more styrene and BuLi to form additional shorter styrene segments. In the final step a styrene butadiene mixture is then added, leading to copolymerization and the formation of gradient copolymers with 70–80% styrene content. These long and short blocks are subsequently coupled to yield a four-arm star polymer, enhancing processability and compatibility with general purpose polystyrene for blending.[33]

Styroflex® is also based on styrene and butadiene but is a linear copolymer with a block composition of 15:70:15. The enlarged soft middle block is a random styrene butadiene polymer with a T_g of -30 °C, increasing flexibility comparable to plasticized PVC. Despite containing nearly 70% styrene, similar to Styrolux®, Styroflex® can achieve much higher molar masses (140 kg/mol vs 70 kg/mol) without compromising melt flow or viscosity.[33]

Compared to sequentially synthesized SBS block copolymers (e.g., Kraton D®), the gradient offers several advantages. The reduced T_{ODT} enables processibility at lower temperatures, while the higher styrene content reduces the diene need, beneficial for both thermal stability and cost. The gradient also enhances impact resistance and functions as a compatibilizer, although it weakens phase separation.

Overall copolymerization simplifies the synthesis and improves material properties. However, achieving the desired low T_g and thermal stability requires low vinyl unsaturation in the soft domain. Therefore, a selective modifier that influences copolymerization kinetics without altering the diene microstructure is needed. Chapter 2 will focus on the use of THF in the copolymerization of TMSS and I, while chapter 3 will focus on the use of different alkoxides as modifiers in the copolymerization of styrene and isoprene.

Enteric drug coatings for controlled release

Since this thesis is divided into two parts, the following section is about another class of copolymers, stimuli responsive copolymers suitable for enteric drug coatings.

Medicines can be administered in very different ways, including intravenously, pulmonary, orally, nasally or dermally. Regardless of the method, it is crucial that the drug is released in a controlled manner and can be absorbed at the right place, to achieve the desired therapeutical effect. Therefore, the drug must not only be pharmacologically active but must also reach the correct location in the right concentration.[225]

Historically, even without any understanding of pharmacokinetics, early civilizations achieved basic forms of drug delivery and controlled release by incorporating medicine into fatty substances to create cremes. As pharmaceutical science progressed, the need for controlled drug release became increasingly important, not only to enhance therapeutic outcomes but also to minimize undesirable side effects.[225]

Amon the various delivery routes, oral administration stands out for its simplicity, convenience and practicality, especially for chronic therapy. Tablets are easy to store, transport and are produced cost-effectively. They can be self-administered, even by children, and dosages can be easily adjusted.[226–228] Therefore, it is not surprising that already more than 60% of all marketed drugs are orally admitted.[227] The foundation of modern oral drug delivery began in 1867 with the discovery that pills coated with collodion could resist dissolution in the stomach. This concept was further improved by Unna in 1884 with the introduction of keratin coated tablets.[225]

With increasing insight into gastrointestinal physiology, it has become clear that certain drugs must be protected from the harsh acidic environment of the stomach (pH = 1–3), where they are susceptible to hydrolysis, oxidation or deamination.[229,230] While in other

cases, it is necessary to protect the stomach from the drug itself, to prevent side effects such as nausea, vomiting, loss of appetite or diarrhea.[227,231–234] Enteric coatings offer a solution to these challenges by providing a protective barrier that prevents premature drug release in the stomach. In addition to this primary function, enteric coatings enable targeted drug release in the small intestine (pH = 5.1–7.8), particularly to the duodenum, where drug absorption is more effective, improving the drug's bioavailability.[231] This targeted delivery allows lower dosages of the active pharmaceutical ingredient to achieve therapeutic efficacy, reducing potential side effects and lowering production cost, thus making this approach economically favorable. Moreover, enteric coatings improve the chemical and physical stability, mask unpleasant tastes, protect against moisture and can be used for immediate or delayed drug releases.[225]

To achieve these effects, a variety of polymers were synthesized and investigated towards their possible applications in drug coatings, illustrated in Figure 14. These polymers must meet several requirements:[225]

1. Stability and insolubility in the acidic environment of the stomach until gastric emptying
2. Impermeability to both gastric fluids and the drug
3. Rapid disintegration or dissolution in the more neutral pH of the small intestine
4. Physical and chemical stability
5. Nontoxicity
6. Applicability via scalable methods like spray drying
7. Cost-effectiveness and scalability for industrial production

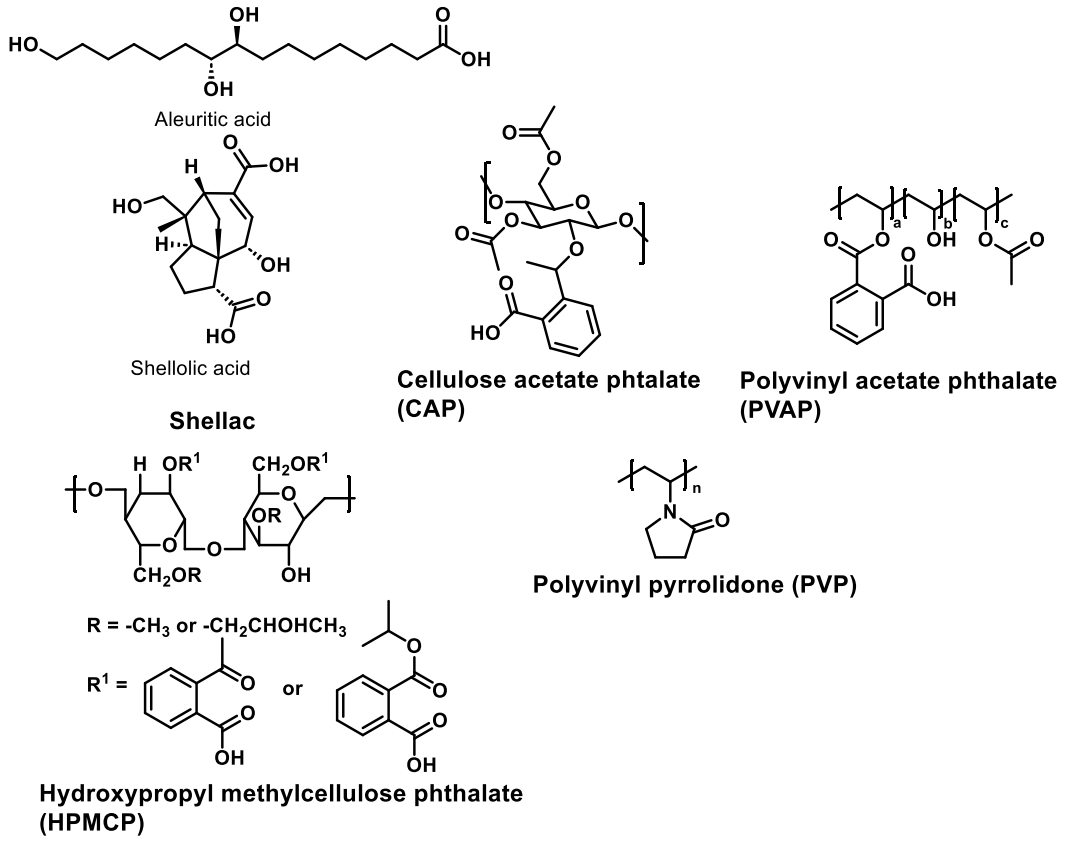

Figure 14 Illustration of different commercially available enteric drug coatings.[225]

To meet these criteria researchers have focused on stimuli-responsive polymers, particularly pH-responsive materials, which dissolve at a certain pH. These polymers have become central to the development of galenic coatings that enable precise control over drug release.[235]

Shellac was one of the earliest materials used for enteric drug coatings, with applications dating back to 1930. However, its usage was limited due to drawbacks such as stickiness, natural origin, poor long-term stability and insolubility at pH levels below 7.[236] This could result in shellac coated tablets passing the gastrointestinal tract without releasing their payload or a change in the release profile due to side reactions like polycondensations during storage. Despite these issues, shellac offers excellent humidity protection and has been recommended in combination with Hydroxypropyl methylcellulose phthalate (HPMCP) capsules.[237]

Cellulose acetate phthalate (CAP), introduced in 1940, is composed of cellulose with approximately half of its hydroxyl groups acetylated, a quarter esterified with phthalic acid and the remaining as free carboxylic acids. CAP demonstrated superior performance

to shellac in various studies, despite disagreements regarding its exact mechanism.[238,239] CAP is already soluble at a pH of 6, but permeable to water vapor, gastric fluids and some ionic substances, which makes it necessary to use an impermeable seal subcoat.

To further improve and accelerate the drug release poly(vinyl acetate phthalate) (PVAP) was introduced as enteric coating, offering solubility at a pH of 5.[225] PVAP is synthesized via esterification of partially hydrolyzed poly(vinyl acetate) with phthalic anhydride. While its acetyl content remains fixed, the phthalyl content can be modified to achieve the desired disintegration. In addition to the improved dissolution, PVAP is significantly less permeable to water vapor and gastric fluids than CAP and exhibits greater hydrolytic stability.[240]

HPMCP, another phthalate based polymer for enteric drug coatings, is synthesized by reacting phthalic anhydride with hydroxypropyl methylcellulose.[237] Like other phthalate containing enteric coatings, HPMCP is insoluble in acidic environments, but dissolves when the pH level increases due to deprotonation of the free carboxylic acid groups. Its dissolution characteristics can be tailored via the phthalate content. However, HPMCP shares CAP's permeability to water vapor and gastric fluids, a drawback that can be mitigated by combining it with shellac.[237] An additional challenge is its tendency to crack post-coating, which can be reduced with the right choice of solvent, plasticizer and using higher molar masses for improved material strenght.[237]

In addition to phthalate-based drug coatings, various amine-containing polymers are also utilized for controlled drug release. Poly(vinylpyrrolidone) (PVP) has been successfully employed either alone or in combination with HPMC to form solid dispersions that significantly enhance drug release.[241,242] Other amine base copolymers such as poly(dimethylaminoethylmethacrylate-*co*-butylmethacrylate-*co*-methylmethacrylate) (Eudragit® E100), are used for coatings designed to enable immediate drug release under the acidic conditions of the stomach.[243]

Currently, the most widely used materials for enteric coatings are methacrylic acid (MA)-based copolymers, synthesized through radical copolymerization with either methyl methacrylate (MMA) or ethyl acrylate (EA).[231,244,245] These copolymers are commercially available under the trademarks Eudragit® (Evonik AG) and Kollicoat® (BASF), and are

available in 1:1 or 1:2 (MA:comonomer) ratios to achieve dissolutions at pH levels ranging from 5.5 to 7. Due to their pH-sensitive solubility, polycarboxylates with transition pH values between 4 to 6 are considered ideal candidates for enteric drug coatings. Moreover, the transition pH and sharpness of the pH response can be finely tuned by utilizing different carboxylic acids, adjusting the molar mass or incorporating different comonomers.[231]

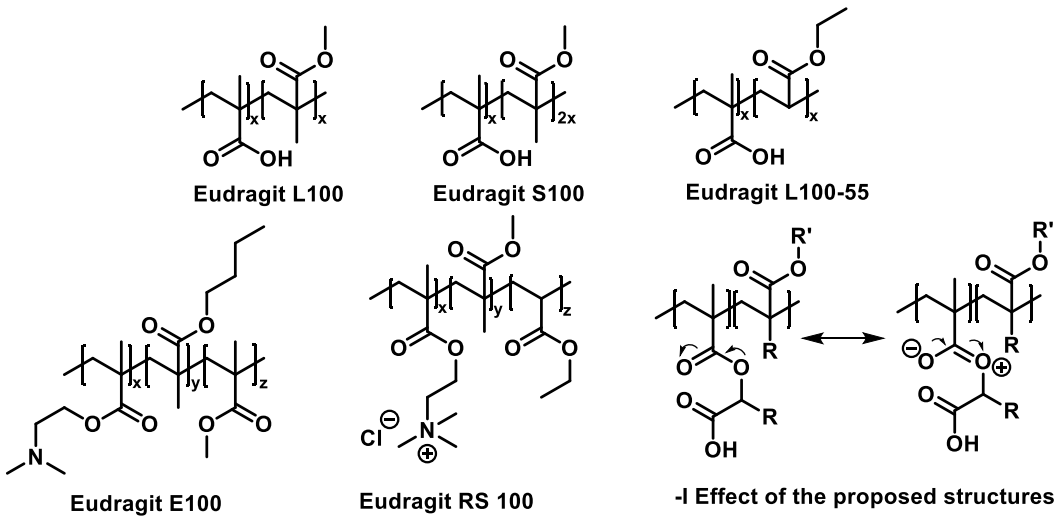

Figure 15: Illustration of several commercial Eudragit® structures, designed for immediate, delayed and controlled drug release, along with a structural modification aimed at lowering the pK_a value to accelerate dissolution.

Both Eudragit® S and L type polymers are soluble in polar organic solvents such as alcohols or acetone and can be processed as aqueous solutions for spray drying applications. These polymers are non-toxic, exhibit low permeability to water and gastric fluids, maintain long-term stability and are insoluble under acidic conditions. [225,246] Poly(methacrylic acid) (PMA), the component responsible for the pH responsiveness, has a pK_a value of approximately 5.5.[247,248] Under acidic conditions, PMA forms a collapsed polymer coil due to hydrophobic interactions. As the pH increases and the carboxylic acid groups are deprotonated, electrostatic repulsion between the negatively charged carboxylates causes the polymer to adapt an expanded, soluble conformation.

According to the manufacturer, Eudragit® L100-55 begins to dissolve at a pH ≥ 5.5; Eudragit® L100 at a pH ≥ 6.0 and Eudragit® S100 at a pH ≥ 7.0. Although the delayed dissolution of Eudragit® S100 may result in incomplete drug release in the small intestine, it is advantageous for targeting drug release in the colon. All Eudragit® structures are

neither absorbed nor degraded within the body, are excreted unchanged and are FDA-approved.[225] Therefore, they are ideal candidates for enteric drug coatings.

Nevertheless, several *in vivo* and *in vitro* studies have raised serious concerns about the consistency of their release profiles, particularly regarding reliable drug release in the duodenum.[249–253] Al-Gousous *et al*. was able to prove that the widespread misconception that enteric drug coatings dissolve rapidly after gastric emptying is not true. This is explained by an overloading of the buffer capacity in the vicinity of the enteric drug coating, which leads to a locally lower pH, resulting in a delay of the pharmacokinetic profile.[249,253,254] Consequently, *in vitro* experiments often overestimate the rate of drug release compared to *in vivo* conditions.[254]

Both Khan *et al*. and Cole *et al*. investigated the release behavior of Eudragit® L100-55 at slightly different pH levels.[250,251] In their studies, coated tablets were first subjected to an acidic stability test by immersion into a 0.1M hydrochloric acid (pH ~ 1) solution for 120 minutes, simulating the acidic conditions of the stomach. In both studies, the coatings remained intact, and no drug release was detected. After 120 minutes, the pH was raised using a phosphate buffer. Both studies observed a delay of approximately 20 minutes before drug release commenced. In Khan's study, about 80% of the drug was released within one hour at a pH 6.5, whereas Cole's study (Figure 16) reported only 50-60% drug release at a pH 6.8.

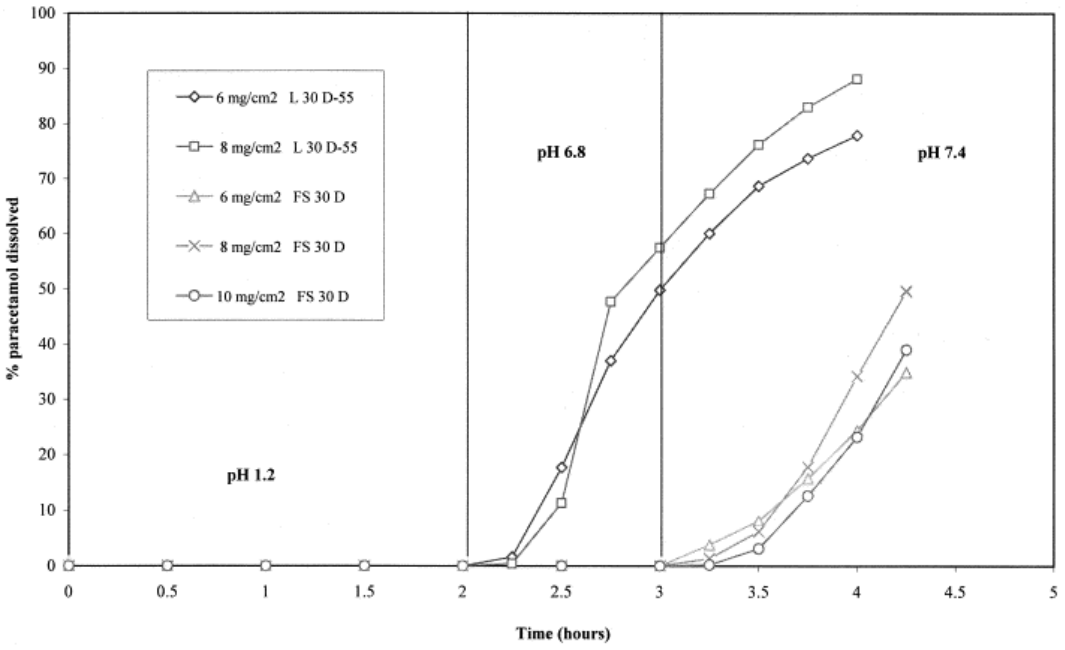

Figure 16: Dissolution of paracetamol from HPCM capsules coated with Eudragit® L30 D-55 (an aqueous dispersion of Eudragit® L100-55) and Eudragit® FS 30 D (an aqueous dispersion of Eudragit® FS100).[251] Reprinted with permission from Cole, E. T., Scott, R. A., Connor, A. L., Wilding, I. R., Petereit, H. U., Schminke, C., Beckert, T., & Cadé, D. (2002).. International Journal of Pharmaceutics, 231(1), 83–95. Copyright 2002 Elsevier.

Regardless of which study is considered, complete dissolution of the enteric coating requires more than one hour, in Cole's study even more than two hours. Given that the typical residence time in the small intestine ranges from 1–3 hours, and considering that *in vitro* experiments often overestimate release rates due to a too high buffer capacity, larger fluid volumes and an abrupt pH change compared to the gradual pH transition occurring *in vivo*, it can be reasonably doubted that complete dissolution occurs within the small intestine, particularly within the duodenum.[225]

The duodenum, the first and shortest segment of the small intestine (approximately 25 cm in length), is a critical site for drug absorption, especially for iron containing preparations, as iron uptake predominantly occurs in this compartment.[255,256] A prominent example of the limitations of enteric drug coatings is the low efficiency of acetylsalicylic acid in antiplatelet therapy, which is believed to result from delayed release and/or poor absorption.[257–259] When the bioavailability of the drug is reduced due to slow dissolution of its coating, higher doses may be required to achieve therapeutic effects, thereby increasing the risk of side effects, an issue that could be alleviated by enhancing the rate of dissolution.[260] If an enteric coating fails to release their content

within the small intestine, dissolution may instead occur in the colon, where absorption is significantly less efficient.[225] This is particularly problematic for enzyme based drugs such as acid labile pancreatin, which must be released promptly upon entry into the small intestines to prevent gastrointestinal issues caused by incomplete lipid digestion.[261]

To address this challenge of a to slow release, it is essential to accelerate the dissolution of the enteric coating by lowering its pK_a value, while preserving acid resistance, physical and chemical stability, non-toxicity, and compatibility with spray-drying processes, all while ensuring cost-effectiveness and scalability. Retaining the Eudragit® backbone structure helps maintaining these properties, while the pK_a can be reduced by introducing electron withdrawing groups (-I effect) through esterification of the methacrylic acid with α-hydroxy acids, as illustrated in Figure 15. The non-toxicity of the modified polymers is ensured by the choice of the α-hydroxy acid, such as glycolic-, lactic-, mandelic- and malic acid. Therefore, even if acidic hydrolysis of the ester bonds were to occur, it would regenerate the original Eudragit® polymer and release non-toxic α-hydroxy acids. Notably, glycolic acid is naturally produced by various edible plants, both lactic and malic acid are synthesized by the human body and Mandelic acid was clinically used for the treatment of urinary tract infections.[262] Chapter 4 will focus on the synthesis and scalability of glycol and lactide modified Eudragit® copolymers for an accelerated drug release, while Chapter 5 will focus on the synthesis of mandelic- and malic-acid modified Eudragit® copolymers, with the goal of further accelerating drug release and minimizing acid uptake.

References

(1) Staudinger, H. Über Polymerisation. *Berichte der deutschen chemischen Gesellschaft (A and B Series)* **1920**, *53* (6), 1073–1085. https://doi.org/10.1002/cber.19200530627.

(2) Frey, H.; Johann, T. Celebrating 100 Years of "Polymer Science": Hermann Staudinger's 1920 Manifesto. *Polym Chem* **2020**, *11* (1), 8–14. https://doi.org/10.1039/C9PY90161B.

(3) Guart, A.; Bono-Blay, F.; Borrell, A.; Lacorte, S. Migration of Plasticizersphthalates, Bisphenol A and Alkylphenols from Plastic Containers and Evaluation of Risk. *Food Additives & Contaminants: Part A* **2011**, *28* (5), 676–685. https://doi.org/10.1080/19440049.2011.555845.

(4) MacLeod, M.; Arp, H. P. H.; Tekman, M. B.; Jahnke, A. The Global Threat from Plastic Pollution. *Science (1979)* **2021**, *373* (6550), 61–65. https://doi.org/10.1126/science.abg5433.

(5) Szwarc, M. 'Living' Polymers. *Nature* **1956**, *178* (4543), 1168–1169. https://doi.org/10.1038/1781168a0.

(6) Bock, W.; Tschunkur, E. DE511145C Verfahren Zur Darstellung von Kuenstlichem Kautschuk, 1927.

(7) Müller, A. H. E.; Matyjaszewski, K. *Controlled and Living Polymerizations*; Wiley, 2009. https://doi.org/10.1002/9783527629091.

(8) Ntetsikas, K.; Ladelta, V.; Bhaumik, S.; Hadjichristidis, N. Quo Vadis Carbanionic Polymerization? *ACS Polymers Au* **2023**, *3* (2), 158–181. https://doi.org/10.1021/acspolymersau.2c00058.

(9) Hadjichristidis, N.; Pispas, S.; Floudas, G. *Block Copolymers*; Wiley, 2002. https://doi.org/10.1002/0471269808.

(10) Grovenstein, E. Jr. Cation Effects in Organoalkali Metal Chemistry. In *Recent Advances in Anionic Polymerization*; Hogen-Esch, T. E., Smid, J., Eds.; Springer Netherlands: Dordrecht, 1987; pp 3–21. https://doi.org/10.1007/978-94-009-3175-6.

(11) Wiles, D. M.; Bywater, S. Polymerization of Methyl Methacrylate Initiated by 1,1-Diphenyl-Hexyl Lithium. *Transactions of the Faraday Society* **1965**, *61* (8226), 150. https://doi.org/10.1039/tf9656100150.

(12) Nishioka, A.; Watanabe, H.; Abe, K.; Sono, Y. Grignard Reagent-Catalyzed Polymerization of Methyl Methacrylate. *Journal of Polymer Science* **1960**, *48* (150), 241–272. https://doi.org/10.1002/pol.1960.1204815024.

(13) Allen, R. D.; Long, T. E.; McGrath, J. E. Preparation of High Purity, Anionic Polymerization Grade Alkyl Methacrylate Monomers. *Polymer Bulletin* **1986**, *15* (2), 127–134. https://doi.org/10.1007/BF00263389.

(14) Hadjichristidis, N.; Iatrou, H.; Pispas, S.; Pitsikalis, M. Anionic Polymerization: High Vacuum Techniques. *J Polym Sci A Polym Chem* **2000**, *38* (18), 3211–3234. https://doi.org/10.1002/1099-0518(20000915)38:18<3211::AID-POLA10>3.0.CO;2-L.

(15) Perrier, S. *50th Anniversary Perspective* : RAFT Polymerization—A User Guide. *Macromolecules* **2017**, *50* (19), 7433–7447. https://doi.org/10.1021/acs.macromol.7b00767.

(16) Le, T. P.; Moad, G.; Rizzardo, E.; Thang, S. H. WO1998001478A1 Polymerization with Living Chatacteristics, 1998.

(17) Corpart, P.; Charmot, D.; Zard, S.; Franck, X.; Bouhadir, G. US6812291 Method for Block Polymer Synthesis by Controlled Radical Polymerizations from Dithiocarbamate Compounds, 2004.

(18) Chiefari, J.; Chong, Y. K. (Bill); Ercole, F.; Krstina, J.; Jeffery, J.; Le, T. P. T.; Mayadunne, R. T. A.; Meijs, G. F.; Moad, C. L.; Moad, G.; Rizzardo, E.; Thang, S. H. Living Free-Radical Polymerization by Reversible Addition−Fragmentation Chain Transfer: The RAFT Process. *Macromolecules* **1998**, *31* (16), 5559–5562. https://doi.org/10.1021/ma9804951.

(19) Kato, M.; Kamigaito, M.; Sawamoto, M.; Higashimura, T. Polymerization of Methyl Methacrylate with the Carbon Tetrachloride/Dichlorotris- (Triphenylphosphine)Ruthenium(II)/Methylaluminum Bis(2,6-Di-Tert-Butylphenoxide) Initiating System: Possibility of Living Radical Polymerization. *Macromolecules* **1995**, *28* (5), 1721–1723. https://doi.org/10.1021/ma00109a056.

(20) Wang, J.-S.; Matyjaszewski, K. Controlled/"living" Radical Polymerization. Atom Transfer Radical Polymerization in the Presence of Transition-Metal Complexes. *J Am Chem Soc* **1995**, *117* (20), 5614–5615. https://doi.org/10.1021/ja00125a035.

(21) Matyjaszewski, K.; Xia, J. Atom Transfer Radical Polymerization. *Chem Rev* **2001**, *101* (9), 2921–2990. https://doi.org/10.1021/cr940534g.

(22) Sciannamea, V.; Jérôme, R.; Detrembleur, C. In-Situ Nitroxide-Mediated Radical Polymerization (NMP) Processes: Their Understanding and Optimization. *Chem Rev* **2008**, *108* (3), 1104–1126. https://doi.org/10.1021/cr0680540.

(23) Solomon, D. H.; Waverley, G.; Cacioli, P.; Hill, W.; Waverley, G. US 4,681,429 Polymerization Process and Polymer Production Thereby, 1984.

(24) Georges, M. K.; Veregin, R. P. N.; Kazmaier, P. M.; Hamer, G. K. Narrow Molecular Weight Resins by a Free-Radical Polymerization Process. *Macromolecules* **1993**, *26* (11), 2987–2988. https://doi.org/10.1021/ma00063a054.

(25) Tebbe, F. N.; Parshall, G. W.; Reddy, G. S. Olefin Homologation with Titanium Methylene Compounds. *J Am Chem Soc* **1978**, *100* (11), 3611–3613. https://doi.org/10.1021/ja00479a061.

(26) Gilliom, L. R.; Grubbs, R. H. Titanacyclobutanes Derived from Strained, Cyclic Olefins: The Living Polymerization of Norbornene. *J Am Chem Soc* **1986**, *108* (4), 733–742. https://doi.org/10.1021/ja00264a027.

(27) MacMillan, D. W. C. The Advent and Development of Organocatalysis. *Nature* **2008**, *455* (7211), 304–308. https://doi.org/10.1038/nature07367.

(28) Bertelsen, S.; Jørgensen, K. A. Organocatalysis—after the Gold Rush. *Chem Soc Rev* **2009**, *38* (8), 2178. https://doi.org/10.1039/b903816g.

(29) Alemán, J.; Cabrera, S. Applications of Asymmetric Organocatalysis in Medicinal Chemistry. *Chem. Soc. Rev.* **2013**, *42* (2), 774–793. https://doi.org/10.1039/C2CS35380F.

(30) Qin, Y.; Zhu, L.; Luo, S. Organocatalysis in Inert C–H Bond Functionalization. *Chem Rev* **2017**, *117* (13), 9433–9520. https://doi.org/10.1021/acs.chemrev.6b00657.

(31) Hadjichristidis, N.; Iatrou, H.; Pitsikalis, M.; Mays, J. Macromolecular Architectures by Living and Controlled/Living Polymerizations. *Prog Polym Sci* **2006**, *31* (12), 1068–1132. https://doi.org/10.1016/j.progpolymsci.2006.07.002.

(32) Hirao, A.; Goseki, R.; Ishizone, T. Advances in Living Anionic Polymerization: From Functional Monomers, Polymerization Systems, to Macromolecular Architectures. *Macromolecules* **2014**, *47* (6), 1883–1905. https://doi.org/10.1021/ma401175m.

(33) Knoll, K.; Nießner, N. Styrolux+ and Styroflex+ - From Transparent High Impact Polystyrene to New Thermoplastic Elastomers: Syntheses, Applications and Blends with Other Styrene Based Polymers. *Macromol Symp* **1998**, *132*, 231–243. https://doi.org/10.1002/masy.19981320122.

(34) Hsieh, H.; Quirk, R. P. *Anionic Polymerization*; CRC Press, 1996. https://doi.org/10.1201/9780585139401.

(35) Koltzenburg, S.; Maskos, M.; Nuyken, O. *Polymere: Synthese, Eigenschaften Und Anwendungen*; Springer Berlin Heidelberg: Berlin, Heidelberg, 2014. https://doi.org/10.1007/978-3-642-34773-3.

(36) Gold, L. Statistics of Polymer Molecular Size Distribution for an Invariant Number of Propagating Chains. *J Chem Phys* **1958**, *28* (1), 91–99. https://doi.org/10.1063/1.1744088.

(37) Baskaran, D.; Müller, A. H. E. Anionic Vinyl Polymerization-50 Years after Michael Szwarc. *Progress in Polymer Science (Oxford)* **2007**, *32* (2), 173–219. https://doi.org/10.1016/j.progpolymsci.2007.01.003.

(38) Szwarc, M. *Living Polymers and Mechanisms of Anionic Polymerization*; Advances in Polymer Science; Springer Berlin Heidelberg: Berlin, Heidelberg, 1983; Vol. 49. https://doi.org/10.1007/3-540-12047-5.

(39) Porter; Milkovich, R.; Phillips Petroleum Co. GB888624A Block Polymers and Process for Preparation Thereof, 1959.

(40) Hsieh, H.; Tobolsky, A. V. Polymerization of Isoprene by N-butyl Lithium. *Journal of Polymer Science* **1957**, *25* (109), 245–247. https://doi.org/10.1002/pol.1957.1202510918.

(41) Hsieh, H.; Kelley, D. J.; Tobolsky, A. V. Polymerization of Isoprene with Lithium Dispersions and Lithium Alkyls Using Tetrahydrofuran as Solvent. *Journal of Polymer Science* **1957**, *26* (113), 240–242. https://doi.org/10.1002/pol.1957.1202611315.

(42) Morita, H.; Tobolsky, A. V. Isoprene Polymerization by Organometallic Compounds. I. *J Am Chem Soc* **1957**, *79* (22), 5853–5855. https://doi.org/10.1021/ja01579a004.

(43) Barent, R. D.; Wagner, M.; Frey, H. Geometric Requirements for Living Anionic Polymerization: Polymerization of Rotationally Constrained 1,3-Dienes. *Polym Chem* **2022**, *13* (38), 5478–5485. https://doi.org/10.1039/d2py00999d.

(44) Gebert, W.; Hinz, J.; Sinn, H. Umlagerungen Bei Der Durch Lithiumbutyl Initiierten Polyreaktion Der Diene Isopren Und Butadien. *Die Makromolekulare Chemie* **1971**, *144* (1), 97–115. https://doi.org/10.1002/macp.1971.021440109.

(45) Holden, G.; Milkovich, R. U.S. Patent 3265765, Block Polymers of Monovinyl Aromatic Hydrocarbons and Conjugated Dienes., 1962.

(46) Holden, G.; Milkovich, R. Block Polymers of Monovinyl Aromatic Hydrocarbons and Conjugated Dienes US3265765A, US3265765A to Shell Oil Company, 1966.

(47) *Thermoplastic elastomer (TPE) Market Analysis: Industry Market Size, Plant Capacity, Production, Operating Efficiency, Demand & Supply, Type, End-User Industries, Sales Channel, Regional Demand, Company Share, Manufacturing Process, 2015-2032*. https://www.chemanalyst.com/industry-report/thermoplastic-elastomers-market-567 (accessed 2025-05-01).

(48) Qiao, L.; Leibig, C.; Hahn, S. F.; Winey, K. I. Isolating the Effects of Morphology and Chain Architecture on the Mechanical Properties of Triblock Copolymers. *Ind Eng Chem Res* **2006**, *45* (16), 5598–5602. https://doi.org/10.1021/ie0511940.

(49) *pKa and pKb Reference Table*. https://www.aatbio.com/data-sets/pka-and-pkb-reference-table (accessed 2025-05-01).

(50) Varshney, S. K.; Jacobs, C.; Hautekeer, J. P.; Bayard, P.; Jerome, R.; Fayt, R.; Teyssie, P. Anionic Polymerization of Acrylic Monomers. 6. Synthesis, Characterization, and Modification of Poly(Methyl Methacrylate)-Poly(Tert-Butyl Acrylate) Di- and Triblock Copolymers. *Macromolecules* **1991**, *24* (18), 4997–5000. https://doi.org/10.1021/ma00018a003.

(51) Hirao, A.; Yamamoto, A.; Takenaka, K.; Yamaguchi, K.; Nakahama, S. Protection and Polymerization of Functional Monomers: 8. Anionic Living Polymerization of 4-[2-(Trialkyl)Silyloxyethyl]Styrene as Protected 4-(2-Hydroxyethyl)Styrene. *Polymer (Guildf)* **1987**, *28* (2), 303–310. https://doi.org/10.1016/0032-3861(87)90422-8.

(52) Hirao, A.; Nagawa, T.; Hatayama, T.; Yamaguchi, K.; Nakahama, S. Polymerization of Monomers Containing Functional Silyl Groups. 1. Anionic Living Polymerization of (4-Vinylphenyl)Dimethyl-2-Propoxysilane. *Macromolecules* **1985**, *18* (11), 2101–2105. https://doi.org/10.1021/ma00153a003.

(53) Taki, T.; Hirao, A.; Nakahama, S. Polymerization of Monomers Containing Functional Silyl Groups. 9. Anionic Living Polymerization of (4-Vinylphenyl)(N,N-Diethylamino)Dimethylsilane. *Macromolecules* **1991**, *24* (7), 1455–1458. https://doi.org/10.1021/ma00007a003.

(54) Hirao, A.; Takenaka, K.; Packirisamy, S.; Yamaguchi, K.; Nakahama, S. Polymerization of Monomers Containing Functional Groups Protected by Trialkylsilyl Groups, 4. Studies on Anionic Living Polymerization of 4-(*Tert* -butyldimethylsilyloxy)Styrene. *Die Makromolekulare Chemie* **1985**, *186* (6), 1157–1166. https://doi.org/10.1002/macp.1985.021860605.

(55) Laible, R.; Hamann, K. Formation of Chemically Bound Polymer Layers on Oxide Surfaces and Their Role in Colloidal Stability. *Adv Colloid Interface Sci* **1980**, *13* (1–2), 65–99. https://doi.org/10.1016/0001-8686(80)87002-3.

(56) Hirao, A.; Ando, Y.; Ishizone, T.; Nakahama, S. Anionic Polymerization of *p* -Pentamethyldisilyl-, *p* -Heptamethyltrisilyl-, and *p* -Nonamethyltetrasilylstyrenes. *Macromolecules* **2003**, *36* (14), 5081–5087. https://doi.org/10.1021/ma021742a.

(57) Hirao, A.; Nakahama, S. Anionic Living Polymerization of Monomers with Functional Silyl Groups. *Prog Polym Sci* **1992**, *17* (3), 283–317. https://doi.org/10.1016/0079-6700(92)90018-T.

(58) Wadgaonkar, S. P.; Schüttner, S.; Berger-Nicoletti, E.; Müller, A. H. E.; Frey, H. Anionic Copolymerization of 4-Trimethylsilylstyrene: From Kinetics to Gradient and Block Copolymers. *Macromolecules* **2022**, *55* (11), 4721–4732. https://doi.org/10.1021/acs.macromol.2c00570.

(59) Fuchs, D. A. H.; Wadgaonkar, S. P.; Müller, A. H. E.; Frey, H. Effect of <scp>tetrahydrofuran</Scp> on the Anionic Copolymerization of 4-trimethylsilylstyrene with Isoprene. *Polym Adv Technol* **2024**, *35* (6). https://doi.org/10.1002/pat.6478.

(60) Khotimskii, V. S.; Filippova, V. G.; Bryantseva, I. S.; Bondar, V. I.; Shantarovich, V. P.; Yampolskii, Y. P. Synthesis, Transport, and Sorption Properties and Free Volume of Polystyrene Derivatives Containing Si and F. *J Appl Polym Sci* **2000**, *78* (9), 1612–1620. https://doi.org/10.1002/1097-4628(20001128)78:9<1612::AID-APP60>3.0.CO;2-T.

(61) Maher, M. J.; Bates, C. M.; Blachut, G.; Sirard, S.; Self, J. L.; Carlson, M. C.; Dean, L. M.; Cushen, J. D.; Durand, W. J.; Hayes, C. O.; Ellison, C. J.; Willson, C. G. Interfacial Design for Block Copolymer Thin Films. *Chemistry of Materials* **2014**, *26* (3), 1471–1479. https://doi.org/10.1021/cm403813q.

(62) Sunday, D. F.; Maher, M. J.; Hannon, A. F.; Liman, C. D.; Tein, S.; Blachut, G.; Asano, Y.; Ellison, C. J.; Willson, C. G.; Kline, R. J. Characterizing the Interface Scaling of High χ Block Copolymers near the Order–Disorder Transition. *Macromolecules* **2018**, *51* (1), 173–180. https://doi.org/10.1021/acs.macromol.7b01982.

(63) Maher, M. J.; Rettner, C. T.; Bates, C. M.; Blachut, G.; Carlson, M. C.; Durand, W. J.; Ellison, C. J.; Sanders, D. P.; Cheng, J. Y.; Willson, C. G. Directed Self-Assembly of Silicon-Containing Block Copolymer Thin Films. *ACS Appl Mater Interfaces* **2015**, *7* (5), 3323–3328. https://doi.org/10.1021/am508197k.

(64) Kim, H.-C.; Park, S.-M.; Hinsberg, W. D. Block Copolymer Based Nanostructures: Materials, Processes, and Applications to Electronics. *Chem Rev* **2010**, *110* (1), 146–177. https://doi.org/10.1021/cr900159v.

(65) Nagasaki, Y.; Hashimoto, Y.; Kato, M.; Kimijima, T. Gas Permeation Properties of Organosilicon-Containing Polystyrenes. *J Memb Sci* **1996**, *110* (1), 91–97. https://doi.org/10.1016/0376-7388(95)00236-7.

(66) Kawakami, Y.; Karasawa, H.; Aoki, T.; Yamamura, Y.; Hisada, H.; Yamashita, Y. Polymers with Oligoorganosiloxane Side Chains as Material for Oxygen Permeable Membranes. *Polym J* **1985**, *17* (11), 1159–1172. https://doi.org/10.1295/polymj.17.1159.

(67) Ishizone, T.; Hirao, A.; Nakahama, S. Anionic Polymerization of Monomers Containing Functional Groups. 6. Anionic Block Copolymerization of Styrene Derivatives Para-Substituted with Electron-Withdrawing Groups. *Macromolecules* **1993**, *26* (25), 6964–6975. https://doi.org/10.1021/ma00077a039.

(68) Chernyshev, E. A.; Tolstikova, N. G. Hammett Constants of Some (Trialkylsilyl)Alkyl Groups. *Bulletin of the Academy of Sciences of the USSR Division of Chemical Science* **1961**, *10* (3), 419–423. https://doi.org/10.1007/BF01131058.

(69) Benkeser, R. A.; Krysiak, H. R. The Conjugative Ability of the Trimethylsilyl Group. *J Am Chem Soc* **1953**, *75* (10), 2421–2425. https://doi.org/10.1021/ja01106a043.

(70) Nagy, J.; Réffy, J. Quantum Chemical Calculations of Saturated, Unsaturated, and Aromatic Compounds of Silicon I. The Calculation of Dπ-Pπ Interaction and σ Bond Systems. *J Organomet Chem* **1970**, *22* (3), 565–572. https://doi.org/10.1016/S0022-328X(00)87710-4.

(71) Gatzke, A. L. Chain Transfer in Anionic Polymerization. Determination of Chain-transfer Constants by Using Carbon-14-labeled Chain Transfer Agents. *J Polym Sci A1* **1969**, *7* (8), 2281–2292. https://doi.org/10.1002/pol.1969.150070823.

(72) Bauer, W.; Winchester, W. R.; von Rague Schleyer, P. Monomeric Organolithium Compounds in Tetrahydrofuran: Tert-Butyllithium, Sec-Butyllithium, "Supermesityllithium", Mesityllithium, and Phenyllithium. Carbon-Lithium Coupling Constants and the Nature of Carbon-Lithium Bonding. *Organometallics* **1987**, *6* (11), 2371–2379. https://doi.org/10.1021/om00154a017.

(73) Morton, M.; Fetters, L. J. Anionic Polymerization of Vinyl Monomers. *Rubber Chemistry and Technology* **1975**, *48* (3), 359–409. https://doi.org/10.5254/1.3547458.

(74) Clayden, J.; Yasin, S. A. Pathways for Decomposition of THF by Organolithiums: The Role of HMPA. *New Journal of Chemistry* **2002**, *26* (2), 191–192. https://doi.org/10.1039/b109604d.

(75) Iovu, M.-C.; Mapolie, S.; Britchi, A. G. Styrene-Butadiene Rubber Synthesized by Anionic Polymerization. *Macromol Symp* **2001**, *165* (1), 55–62. https://doi.org/10.1002/1521-3900(200103)165:1<55::AID-MASY55>3.0.CO;2-N.

(76) Iovu, M.-C.; Buzdugan, E.; Ghioca, P.; Briţchi, A. G.; Mapolie, S. F.; Iovu, H. Random Anionic Copolymerization of Styrene with Butadiene Using Methyl Tert-Butyl Ether/n-Butyl Lithium as Initiator System. Reaction Mechanism and Kinetic Model. *Revue Roumaine de Chimie* **2003**, *48* (2), 163–171. https://doi.org/doi.org/10.1002/(SICI)1522-9505(19991101)271:1<18::AID-APMC18>3.0.CO;2-%23.

(77) Iovu, M. C.; Buzdugan, E.; Teodorescu, M.; Britchi, A. G.; Hubca, G.; Iovu, H. Copolymerization of Styrene with Butadiene Using Methyl Tert-Butyl Ether as Active Center Modifier. *Die Angewandte Makromolekulare Chemie* **1999**, *271* (1), 18–23. https://doi.org/10.1002/(SICI)1522-9505(19991101)271:1<18::AID-APMC18>3.0.CO;2-%23.

(78) Meier-Merziger, M.; Fuchs, D. A. H.; Frey, H.; Müller, A. H. E. Spotlight on Methyl *Tert* -Butyl Ether–Underrated or Overlooked? Unveiling Its Role for Living Anionic Polymerization. *Macromolecules* **2024**, *57* (16), 8154–8161. https://doi.org/10.1021/acs.macromol.4c01262.

(79) Meier-Merziger, M.; Fotaras, N.; Tzourtzouklis, I.; Allouch, C.; Wagner, M.; Müller, A. H. E.; Floudas, G.; Frey, H. One-Step Synthesis of Fully Biobased Two-Sided Tapered ABA-Type Thermoplastic Elastomers. *ACS Sustain Chem Eng* **2024**, *12* (26), 9922–9933. https://doi.org/10.1021/acssuschemeng.4c02530.

(80) Hamid, S. H.; Ali, M. A. EFFECT OF MTBE BLENDING ON THE PROPERTIES OF GASOLINE. *Fuel Science and Technology International* **1995**, *13* (5), 509–544. https://doi.org/10.1080/08843759508947692.

(81) Uraneck, C. A. Influence of Temperature on Microstructure of Anionic-initiated Polybutadiene. *J Polym Sci A1* **1971**, *9* (8), 2273–2281. https://doi.org/10.1002/pol.1971.150090814.

(82) Iovu, M. C.; Buzdugan, E.; Teodorescu, M.; Britchi, A. G.; Hubca, G.; Iovu, H. Copolymerization of Styrene with Butadiene Using Methyl Tert-Butyl Ether as Active Center Modifier. *Die Angewandte Makromolekulare Chemie* **1999**, *271* (1), 18–23. https://doi.org/10.1002/(SICI)1522-9505(19991101)271:1<18::AID-APMC18>3.0.CO;2-%23.

(83) Antkowiak, T. A.; Oberster, A. E.; Halasa, A. F.; Tate, D. P. Temperature and Concentration Effects on Polar-modified Alkyllithium Polymerizations and Copolymerizations. *J Polym Sci A1* **1972**, *10* (5), 1319–1334. https://doi.org/10.1002/pol.1972.150100504.

(84) Catala, J. M.; Boscato, J. F.; E., F.; Brossas, J. *Coupling Reactions of Carbanionic Polymers by Elemental Compounds Such as Oxygen and Sulfur*; 1981. https://doi.org/10.1021/bk-1981-0166.ch031.

(85) Odian, G. *Principles of Polymerization*; Wiley, 2004. https://doi.org/10.1002/047147875X.

(86) Kühn, K.-D.; Ege, W.; Maurer, H.; Tuchscherer, Ch.; Gopp, U. Die Glasübergangstemperatur – Kenngröße Zur Charakterisierung. *BIOmaterialien* **2001**, *2* (2–3). https://doi.org/10.1515/BIOMAT.2001.2.2-3.87.

(87) Mark, J. E. *Physical Properties of Polymers Handbook*; Mark, J. E., Ed.; Springer New York: New York, NY, 2007. https://doi.org/10.1007/978-0-387-69002-5.

(88) Fox, T. G.; Flory, P. J. Second-Order Transition Temperatures and Related Properties of Polystyrene. I. Influence of Molecular Weight. *J Appl Phys* **1950**, *21* (6), 581–591. https://doi.org/10.1063/1.1699711.

(89) Binder, K. Glass Formation in Polymers: Theory of Glass Transition. In *Encyclopedia of Materials: Science and Technology*; Elsevier, 2001; pp 3553–3559. https://doi.org/10.1016/B0-08-043152-6/00633-1.

(90) *Physical Properties of Polymers Handbook*; Mark, J. E., Ed.; Springer New York: New York, NY, 2007. https://doi.org/10.1007/978-0-387-69002-5.

(91) An, J. Polymer Materials for Additive Manufacturing. In *Digital Manufacturing*; Elsevier, 2022; pp 221–245. https://doi.org/10.1016/B978-0-323-95062-6.00011-5.

(92) Lechner, M. D.; Nordmeier, E. H.; Gehrke, K. *Makromolekulare Chemie*; Birkhäuser Basel: Basel, 2010. https://doi.org/10.1007/978-3-7643-8891-1.

(93) Steube, M.; Johann, T.; Hübner, H.; Koch, M.; Dinh, T.; Gallei, M.; Floudas, G.; Frey, H.; Müller, A. H. E. Tetrahydrofuran: More than a "Randomizer" in the Living Anionic Copolymerization of Styrene and Isoprene: Kinetics, Microstructures, Morphologies, and Mechanical Properties. *Macromolecules* **2020**, *53* (13), 5512–5527. https://doi.org/10.1021/acs.macromol.0c01022.

(94) Fuchs, D. A. H.; Hübner, H.; Kraus, T.; Niebuur, B.-J.; Gallei, M.; Frey, H.; Müller, A. H. E. The Effect of THF and the Chelating Modifier DTHFP on the Copolymerisation of β-Myrcene and Styrene: Kinetics, Microstructures, Morphologies, and Mechanical Properties. *Polym Chem* **2021**, *12* (32), 4632–4642. https://doi.org/10.1039/D1PY00791B.

(95) Korotkov, A. A.; Chesnokova, N. N. Catalytic Copolymerization of Styrene and Butadiene. *Polymer Science U.S.S.R.* **1961**, *2* (3), 284–298. https://doi.org/10.1016/0032-3950(61)90165-4.

(96) Kuntz, I. The Copolymerization of 1,3-butadiene with Styrene by Butyllithium Initiation. *Journal of Polymer Science* **1961**, *54* (160), 569–586. https://doi.org/10.1002/pol.1961.1205416020.

(97) Steube, M.; Johann, T.; Plank, M.; Tjaberings, S.; Gröschel, A. H.; Gallei, M.; Frey, H.; Müller, A. H. E. Kinetics of Anionic Living Copolymerization of Isoprene and Styrene Using in Situ NIR Spectroscopy: Temperature Effects on Monomer Sequence and Morphology. *Macromolecules* **2019**, *52* (23), 9299–9310. https://doi.org/10.1021/acs.macromol.9b01790.

(98) Szwarc, M.; Van Beylen, M. *Ionic Polymerization and Living Polymers*; Springer Netherlands: Dordrecht, 1993. https://doi.org/10.1007/978-94-011-1478-3.

(99) Hodrokoukes, P.; Floudas, G.; Pispas, S.; Hadjichristidis, N. Microphase Separation in Normal and Inverse Tapered Block Copolymers of Polystyrene and Polyisoprene. 1. Phase State. *Macromolecules* **2001**, *34* (3), 650–657. https://doi.org/10.1021/ma001479i.

(100) Singh, N.; Tureau, M. S.; Epps, T. H. Manipulating Ordering Transitions in Interfacially Modified Block Copolymers. *Soft Matter* **2009**, *5* (23), 4757–4762. https://doi.org/10.1039/b908739g.

(101) Annighöfer, F.; Gronski, W. Block Copolymers with Broad Interphase. Determination of Morphological Parameters and Interphase Width by Electron Microscopy and Small Angle X-ray Scattering. *Die Makromolekulare Chemie* **1984**, *185* (10), 2213–2231. https://doi.org/10.1002/macp.1984.021851016.

(102) Ashraf, A. R.; Ryan, J. J.; Satkowski, M. M.; Lee, B.; Smith, S. D.; Spontak, R. J. Bicomponent Block Copolymers Derived from One or More Random Copolymers as an Alternative Route to Controllable Phase Behavior. *Macromol Rapid Commun* **2017**, *38* (17), 1–7. https://doi.org/10.1002/marc.201700207.

(103) Seo, Y.; Brown, J. R.; Hall, L. M. Effect of Tapering on Morphology and Interfacial Behavior of Diblock Copolymers from Molecular Dynamics Simulations. *Macromolecules* **2015**, *48* (14), 4974–4982. https://doi.org/10.1021/ma502309h.

(104) Luo, M.; Brown, J. R.; Remy, R. A.; Scott, D. M.; Mackay, M. E.; Hall, L. M.; Epps, T. H. Determination of Interfacial Mixing in Tapered Block Polymer Thin Films: Experimental and Theoretical Investigations. *Macromolecules* **2016**, *49* (14), 5213–5222. https://doi.org/10.1021/acs.macromol.6b00946.

(105) Sigle, J. L.; Clough, A.; Zhou, J.; White, J. L. Controlling Macroscopic Properties by Tailoring Nanoscopic Interfaces in Tapered Copolymers. *Macromolecules* **2015**, *48* (16), 5714–5722. https://doi.org/10.1021/acs.macromol.5b01215.

(106) Bywater, S.; Worsfold, D. J. Anionic Polymerization of Styrene Effect of Tetrahydrofuran. *Can J Chem* **1962**, *40* (8), 1564–1570. https://doi.org/10.1139/v62-236.

(107) Morton, M.; Fetters, L. J. Homogeneous Anionic Polymerization. V. Association Phenomena in Organolithium Polymerization. *J Polym Sci A* **1964**, *2* (7), 3311–3326. https://doi.org/10.1002/pol.1964.100020726.

(108) Bywater, S. Polymerization Initiated by Lithium and Its Compounds. In *Adv. Polymer Sci*; 1965; Vol. 4, pp 66–110. https://doi.org/10.1007/BFb0050965.

(109) Steube, M.; Johann, T.; Plank, M.; Tjaberings, S.; Gröschel, A. H.; Gallei, M.; Frey, H.; Müller, A. H. E. Kinetics of Anionic Living Copolymerization of Isoprene and Styrene Using in Situ NIR Spectroscopy: Temperature Effects on Monomer Sequence and Morphology. *Macromolecules* **2019**, *52* (23), 9299–9310. https://doi.org/10.1021/acs.macromol.9b01790.

(110) Wahlen, C.; Blankenburg, J.; Von Tiedemann, P.; Ewald, J.; Sajkiewicz, P.; Müller, A. H. E.; Floudas, G.; Frey, H. Tapered Multiblock Copolymers Based on Farnesene and Styrene: Impact of Biobased Polydiene Architectures on Material Properties. *Macromolecules* **2020**, *53* (23), 10397–10408. https://doi.org/10.1021/acs.macromol.0c02118.

(111) Worsfold, D. J.; Bywater, S. Anionic Polymerization of Isoprene. *Can J Chem* **1964**, *42* (12), 2884–2892. https://doi.org/10.1139/v64-426.

(112) Hirao, N. H. *Anionic Polymerization Principles, Practice, Strength, Consequences and Applications*; Springer Japan: Tokyo, 2015. https://doi.org/10.1007/978-4-431-54186-8.

(113) Morton, M.; Bostick, E. E.; Livigni, R. A.; Fetters, L. J. Homogeneous Anionic Polymerization. IV. Kinetics of Butadiene and Isoprene Polymerization with Butyllithium. *J Polym Sci A* **1963**, *1* (5), 1735–1747. https://doi.org/10.1002/pol.1963.100010525.

(114) Hsieh, H. L.; Wofford, C. F. Alkyllithium and Alkali Metal *Tert*-Butoxide as Polymerization Initiator. *J Polym Sci A1* **1969**, *7* (2), 449–460. https://doi.org/10.1002/pol.1969.150070204.

(115) Forens, A.; Roos, K.; Dire, C.; Gadenne, B.; Carlotti, S. Accessible Microstructures of Polybutadiene by Anionic Polymerization. *Polymer (Guildf)* **2018**, *153*, 103–122. https://doi.org/10.1016/j.polymer.2018.07.071.

(116) Hesterwerth, D.; Beckelmann, D.; Bandermann, F. Classification of Polar Additives with Respect to Their Influence on the Microstructure in Anionic Polymerization of Butadiene with Butyllithium by Transition Energy Measurements. *J Appl Polym Sci* **1999**, *73* (8), 1521–1532. https://doi.org/10.1002/(SICI)1097-4628(19990822)73:8<1521::AID-APP21>3.0.CO;2-7.

(117) Roovers, J. E. L.; Bywater, S. Butyl Lithium-Initiated Polymerization of Styrene. Effect of Lithium Butoxide. *Transactions of the Faraday Society* **1966**, *62*, 1876. https://doi.org/10.1039/tf9666201876.

(118) Halaška, V.; Lochmann, L.; Lím, D. Association Degree of T-Butoxides of Alkali Metals in Aprotic Solvents. *Collect Czechoslov Chem Commun* **1968**, *33* (10), 3245–3253. https://doi.org/10.1135/cccc19683245.

(119) Roovers, J. E. L.; Bywater, S. The Polymerization of Isoprene with Sec-Butyllithium in Hexane. *Macromolecules* **1968**, *1* (4), 328–331.

(120) Hsieh, H. L. Effect of Lithium Alkoxide and Hydroxide on Polymerization Initiated with Alkyllithium. *J Polym Sci A1* **1970**, *8* (2), 533–543. https://doi.org/10.1002/pol.1970.150080223.

(121) Wofford, C. F.; Hsieh, H. L. Copolymerization of Butadiene and Styrene by Initiation with Alkyllithium and Alkali Metal *Tert*-Butoxides. *J Polym Sci A1* **1969**, *7* (2), 461–469. https://doi.org/10.1002/pol.1969.150070205.

(122) Makowski, H. S.; Lynn, M. Butyllithium Polymerization of Butadiene. III. Effect of Inactive Lithium Compounds. *Journal of Macromolecular Science: Part A - Chemistry* **1968**, *2* (4), 683–700. https://doi.org/10.1080/10601326808051434.

(123) Quirk, R. P.; Ma, J. -J. Dilithium Initiators Based on 1,3-bis(1- Phenylethenyl)Benzene. Tetrahydrofuran and Lithium Sec-butoxide Effects. *Polym Int* **1991**, *24* (4), 197–206. https://doi.org/10.1002/pi.4990240402.

(124) McGarrity, J. F.; Ogle, C. A. High-Field Proton NMR Study of the Aggregation and Complexation of n-Butyllithium in Tetrahydrofuran. *J Am Chem Soc* **1985**, *107* (7), 1805–1810. https://doi.org/10.1021/ja00293a001.

(125) Cheng, T. C.; Halasa, A. F. Anionic Polymerization. III. Polymerization of Butadiene with Alkali Metal Alkoxide-modified Alkali Metal System. *Journal of Polymer Science: Polymer Chemistry Edition* **1976**, *14* (3), 573–581. https://doi.org/10.1002/pol.1976.170140306.

(126) Nakhmanovich, B. I.; Zolotareva, I. V.; Arest-Yakubovich, A. A. Study on the Mechanism of Anionic Polymerization with Mixed RLi-R'OK Initiators, 1. Polymerization of Butadiene. *Macromol Chem Phys* **1999**, *200* (9), 2015–2021. https://doi.org/10.1002/(SICI)1521-3935(19990901)200:9<2015::AID-MACP2015>3.0.CO;2-I.

(127) Kirchevskaya, I. Yu.; Samotsvetov, A. R.; Seredina, N. P.; Urazov, N. I.; Shatalov, V. P. Relations between Polymerization of Hydrocarbon Monomers in the Presence of Lithium Alkyls Modified with Potassium Tert.Butylate. *Polymer Science U.S.S.R.* **1976**, *18* (8), 2111–2118. https://doi.org/10.1016/0032-3950(76)90398-1.

(128) Smith, S. D.; Ashraf, A.; Clarson, S. J. Styrene-Diene Random Copolymers, Blends and "Random-Diblock" Copolymers. *Prepr., Am. Chem. Soc. Div. Polym. Chem.* **1994**, *35* (2), 466–467.

(129) Ashraf, A.; Smith, S. D.; Clarson, S. J. Synthesis and Characterization of PS-PI and PS-PBD Random Copolymers and "Random-Block" Copolymers via Anionic Polymerizations. *Prepr., Am. Chem. Soc. Div. Polym. Chem.* **1993**, *34* (2), 672–673.

(130) Smith, S. D.; Ashraf, A.; Satkowski, M. M.; Spontak, R. J. Determination of the Phase Diagram for a New Class of Block Copolymers:"Random-Diblock" Copolymers. *Prepr., Am. Chem. Soc. Div. Polym. Chem.* **1994**, No. 35, 651–652.

(131) Litvinenko, G. I.; Arest-Yakubovich, A. A. Study on the Mechanism of Anionic Polymerization with Mixed RLi-R'OK Initiators, 2. Theoretical Study of Random Styrene-Butadiene Copolymerization. *Macromol Chem Phys* **2000**, *201* (17), 2417–2423. https://doi.org/10.1002/1521-3935(20001101)201:17<2417::AID-MACP2417>3.0.CO;2-T.

(132) Forens, A.; Roos, K.; Dire, C.; Gadenne, B.; Carlotti, S. Anionic Polymerization of Butadiene Using Lithium/Potassium Multi-Metallic Systems: Influence on Polymerization Control and Polybutadiene Microstructure. *Chinese Journal of Polymer Science (English Edition)* **2020**, *38* (4), 357–362. https://doi.org/10.1007/s10118-020-2355-4.

(133) Arest-Yakubovich, A. A.; Basova, R. V.; Nakhmanovich, B. I.; Kristalnyi, E. V. The Main Special Characteristics of Anionic Polymerization Initiated by Group II Metals. *Acta Polymerica* **1984**, *35* (1), 1–7. https://doi.org/10.1002/actp.1984.010350101.

(134) Pakuro, N. I.; Zolotareva, I. V.; Kitayner, A. G.; Rogozhkina, E. D.; Izyumnikov, A. L.; Arest-Yakubovich, A. A. Diene Polymerization by Mixed Sodium- and Lithiumalkyl Initiators in Hydrocarbon Medium. *Macromol Chem Phys* **1995**, *196* (1), 375–383. https://doi.org/10.1002/macp.1995.021960127.

(135) Patterson, D. B.; Halasa, A. F. Anionic Polymerization of 1,3-Butadiene to Highly Crystalline High Trans-1,4-Poly(Butadiene) with Potassium Catalysts Generated from an Alkyllithium and Potassium Tert-Amyloxide. *Macromolecules* **1991**, *24* (16), 4489–4494. https://doi.org/10.1021/ma00016a002.

(136) Salle, R.; Essel, A.; Gole, J.; Pham, Q. Polymérisation Anionique Des Diènes. III. Etude Thermodynamique de La Propagation Du Butadiène et de i'isoprène Par Les Organo-alcalins. *Journal of Polymer Science: Polymer Chemistry Edition* **1975**, *13* (8), 1855–1867. https://doi.org/10.1002/pol.1975.170130810.

(137) Hsieh, H. L. .; Quirk, R. P. . *Anionic Polymerization : Principles and Practical Applications*; CRC Press, an imprint of Taylor and Francis, 1996.

(138) Meyer, A. W.; Hampton, R. R.; Davison, J. A. Structure of Alkali Metal-Catalyzed Butadiene Polymers [1,2]. *J Am Chem Soc* **1952**, *74* (9), 2294–2296. https://doi.org/10.1021/ja01129a037.

(139) Kozak, R.; Matlengiewicz, M. Influence of Polar Modifiers on Microstructure of Polybutadiene Obtained by Anionic Polymerization. Part 5: Comparison of μ, σ, Σ+μ, and Σ−μ Complexes. *International Journal of Polymer Analysis and Characterization* **2017**, *22* (1), 51–61. https://doi.org/10.1080/1023666X.2016.1230264.

(140) Litvinenko, G. I.; Arest-Yakubovich, A. A. Chain Transfer to Solvent in Two-state Anionic Polymerization, 2. Slow Exchange between Propagating Species. *Macromol Theory Simul* **1995**, *4* (2), 357–366. https://doi.org/10.1002/mats.1995.040040210.

(141) Arest-Yakubovich, A. A.; Litvinenko, G. I.; Basova, R. V. Synthesis of High Vinyl Styrene-Butadiene Random Copolymers with a New Soluble Organosodium Initiators. *Prepr., Am. Chem. Soc. Div. Polym. Chem.* **1994**, *2* (35), 544–545.

(142) Arest-Yakubovich, A. A.; Pakuro, N. I.; Zolotareva, I. V.; Kristal'nyi, E. V.; Basova, R. V. Polymerization of Conjugated Dienes Initiated by Soluble Organosodium Compounds in Hydrocarbon Solvents. *Polym Int* **1995**, *37* (3), 165–169. https://doi.org/10.1002/pi.1995.210370303.

(143) Arest-Yakubovich, A. A. Role of Bimetallic Active Centres in Anionic Polymerization of Hydrocarbon Monomers. *Macromol Symp* **1994**, *85* (1), 279–294. https://doi.org/10.1002/masy.19940850121.

(144) Pearson, R. G. Hard and Soft Acids and Bases. *J Am Chem Soc* **1963**, *85* (22), 3533–3539. https://doi.org/10.1021/ja00905a001.

(145) Coleman, B. D.; Fox, T. G. A Multistate Mechanism for Homogeneous Ionic Polymerization. II. The Molecular Weight Distribution. *J Am Chem Soc* **1963**, *85* (9), 1241–1244. https://doi.org/10.1021/ja00892a007.

(146) Litvinenko, G.; Müller, A. H. E. General Kinetic Analysis and Comparison of Molecular Weight Distributions for Various Mechanisms of Activity Exchange in Living Polymerizations. *Macromolecules* **1997**, *30* (5), 1253–1266. https://doi.org/10.1021/ma960945u.

(147) Figini, V. R. V. Theoretische Analyse Der Bei Einem Zweiwegwachstumsmechanismus Auftretenden Molekulargewichtsverteilungen Und Ihre Anwendung Auf Die Anionische Polymerisation von Styrol. *Die Makromolekulare Chemie* **1967**, *107* (1), 170–187. https://doi.org/10.1002/macp.1967.021070117.

(148) Coleman, B. D.; Fox, T. G. Multistate Mechanism for Homogeneous Ionic Polymerization. I. The Diastereosequence Distribution. *J Chem Phys* **1963**, *38* (5), 1065–1075. https://doi.org/10.1063/1.1733803.

(149) Schlosser, M. Zur Aktivierung Lithiumorganischer Reagenzien. *J Organomet Chem* **1967**, *8* (1), 9–16. https://doi.org/10.1016/S0022-328X(00)84698-7.

(150) Kelley, D. J.; Tobolsky, A. V. Anionic Copolymerization of Isoprene and Styrene. I [1]. *J Am Chem Soc* **1959**, *81* (7), 1597–1600. https://doi.org/10.1021/ja01516a021.

(151) Tobolsky, A. V.; Rogers, C. E. Isoprene Polymerization by Organometallic Compounds. II. *Journal of Polymer Science* **1959**, *40* (136), 73–89. https://doi.org/10.1002/pol.1959.1204013605.

(152) Tobolsky, A. V.; Rogers, C. E. Anionic Polymerization of Isoprene: Effect of Ionic Character of the Growing Ion Pair on Polymer Structure. *Journal of Polymer Science* **1959**, *38* (133), 205–207. https://doi.org/10.1002/pol.1959.1203813317.

(153) Mayo, F. R.; Lewis, F. M. Copolymerization. I. A Basis for Comparing the Behavior of Monomers in Copolymerization; The Copolymerization of Styrene and Methyl Methacrylate. *J Am Chem Soc* **1944**, *66* (9), 1594–1601. https://doi.org/10.1021/ja01237a052.

(154) Wu, Z.; Liu, Y.; Wei, W.; Chen, F.; Qiu, G.; Xiong, H. Reaction Kinetics in Anionic Copolymerization: A Revisit on Mayo-Lewis Equation. *Chinese Journal of Polymer Science* **2016**, *34* (4), 431–438. https://doi.org/10.1007/s10118-016-1758-8.

(155) Worsfold, D. J.; Bywater, S. ANIONIC POLYMERIZATION OF STYRENE. *Can J Chem* **1960**, *38* (10), 1891–1900. https://doi.org/10.1139/v60-254.

(156) Worsfold, D. J. Anionic Copolymerization of Styrene and Isoprene in Cyclohexane. *J Polym Sci A1* **1967**, *5* (11), 2783–2789. https://doi.org/10.1002/pol.1967.150051106.

(157) Johnson, A. F.; Worsfold, D. J. Anionic Polymerization of Butadiene and Styrene. *J Polym Sci A* **1965**, *3* (2), 449–455. https://doi.org/10.1002/pol.1965.100030204.

(158) Quinebèche, S.; Navarro, C.; Gnanou, Y.; Fontanille, M. In Situ Mid-IR and UV-Visible Spectroscopies Applied to the Determination of Kinetic Parameters in the Anionic Copolymerization of Styrene and Isoprene. *Polymer (Guildf)* **2009**, *50* (6), 1351–1357. https://doi.org/10.1016/j.polymer.2009.01.041.

(159) Williamson, D. T.; Buchanan, T. D.; Elkins, C. L.; Long, T. E. Synthesis of Block Copolymers Based on the Alternating Anionic Copolymerization of Styrene and 1,3-Cyclohexadiene. *Macromolecules* **2004**, *37* (12), 4505–4511. https://doi.org/10.1021/ma035040c.

(160) Idelson, M.; Blout, E. R. Polypeptides. XV. Infrared Spectroscopy and the Kinetics of the Synthesis of Polypeptides: Primary Amine Initiated Reactions. *J Am Chem Soc* **1957**, *79* (15), 3948–3955. https://doi.org/10.1021/ja01572a002.

(161) Rauschenbach, M.; Stein, L.; Linden, G. M.; Barent, R.; Heinze, K.; Frey, H. Anionic Polymerization of Phenyl-Substituted Isoprene Derivatives: Polymerization Behaviour and Cyclization-Enabled Fluorescence. *Polym Chem* **2024**, *15* (31), 3204–3213. https://doi.org/10.1039/D4PY00601A.

(162) Herzberger, J.; Leibig, D.; Liermann, J. C.; Frey, H. Conventional Oxyanionic versus Monomer-Activated Anionic Copolymerization of Ethylene Oxide with Glycidyl Ethers: Striking Differences in Reactivity Ratios. *ACS Macro Lett* **2016**, *5* (11), 1206–1211. https://doi.org/10.1021/acsmacrolett.6b00701.

(163) Schüttner, S.; Linden, G. M.; Hoffmann, E. C.; Holzmüller, P.; Frey, H. Glycidyl Ethers from Acyclic Terpenes: A Versatile Toolbox for Multifunctional Poly(Ethylene Glycol)s with Modification Opportunities. *Polym Chem* **2025**, *16* (3), 374–385. https://doi.org/10.1039/D4PY01201A.

(164) Zhang, W.; Allgaier, J.; Zorn, R.; Willbold, S. Determination of the Compositional Profile for Tapered Copolymers of Ethylene Oxide and 1,2-Butylene Oxide by In-Situ-NMR. *Macromolecules* **2013**, *46* (10), 3931–3938. https://doi.org/10.1021/ma400166n.

(165) Natalello, A.; Alkan, A.; von Tiedemann, P.; Wurm, F. R.; Frey, H. Functional Group Distribution and Gradient Structure Resulting from the Living Anionic Copolymerization of Styrene and *Para* -But-3-Enyl Styrene. *ACS Macro Lett* **2014**, *3* (6), 560–564. https://doi.org/10.1021/mz500255h.

(166) Natalello, A.; Werre, M.; Alkan, A.; Frey, H. Monomer Sequence Distribution Monitoring in Living Carbanionic Copolymerization by Real-Time ^{1}H NMR Spectroscopy. *Macromolecules* **2013**, *46* (21), 8467–8471. https://doi.org/10.1021/ma401847y.

(167) Ariura, F.; Carlotti, S.; Deffieux, A. Selectivity in Polystyryllithium Chain Coupling Induced by Monobromoalkane Additives. *Macromol Rapid Commun* **2004**, *25* (18), 1595–1599. https://doi.org/10.1002/marc.200400251.

(168) Viola, G. T.; Bortolotti, M.; Zazzetta, A. Thermolytic Behavior of Polydienyllithium and Polystyryllithium. *J Polym Sci A Polym Chem* **1996**, *34* (1), 13–24. https://doi.org/10.1002/(SICI)1099-0518(19960115)34:1<13::AID-POLA1>3.0.CO;2-4.

(169) Rodriguez-Guadarrama, L. Investigating The Kinetics of Anionic Polymerization of Butadiene in Presence of 1,2-diethoxypropane Using Online Near-Infrared Spectroscopy. *Macromol React Eng* **2024**, *18* (2). https://doi.org/10.1002/mren.202300051.

(170) Long, T. E.; Liu, H. Y.; Schell, B. A.; Teegarden, D. M.; Uerz, D. S. Determination of Solution Polymerization Kinetics by Near-Infrared Spectroscopy. 1. Living Anionic Polymerization Processes. *Macromolecules* **1993**, *26* (23), 6237–6242. https://doi.org/10.1021/ma00075a018.

(171) Nees, F. W.; Buback, M. Untersuchung Der Hochdruckpolymerisation Des Äthylens Durch Spektroskopie Im Nahen Infrarot. *Berichte der Bunsengesellschaft für physikalische Chemie* **1976**, *80* (10), 1017–1023. https://doi.org/10.1002/bbpc.19760801017.

(172) André, X.; Benmohamed, K.; Yakimansky, A. V.; Litvinenko, G. I.; Müller, A. H. E. Anionic Polymerization and Block Copolymerization of N,N-Diethylacrylamide in the Presence of Triethylaluminum. Kinetic Investigation Using in-Line FT-NIR Spectroscopy. *Macromolecules* **2006**, *39* (8), 2773–2787. https://doi.org/10.1021/ma051506a.

(173) Schmalz, H.; Lanzendörfer, M. G.; Abetz, V.; Müller, A. H. E. Anionic Polymerization of Ethylene Oxide in the Presence of the Phosphazene Base ButP4 - Kinetic Investigations Using in-Situ FT-NIR Spectroscopy and MALDI-ToF MS. *Macromol Chem Phys* **2003**, *204* (8), 1056–1071. https://doi.org/10.1002/macp.200390077.

(174) Schilli, C.; Lanzendörfer, M. G.; Müller, A. H. E. Benzyl and Cumyl Dithiocarbamates as Chain Transfer Agents in the RAFT Polymerization of N-Isopropylacrylamide. In Situ FT-NIR and MALDI-TOF MS Investigation. *Macromolecules* **2002**, *35* (18), 6819–6827. https://doi.org/10.1021/ma0121159.

(175) Johnson, A. F.; Worsfold, D. J. Anionic Copolymerization of Styrene and Butadiene. *Die Makromolekulare Chemie* **1965**, *85* (1), 273–279. https://doi.org/10.1002/macp.1965.020850122.

(176) Worsfold, D. J.; Bywater, S. ANIONIC POLYMERIZATION OF STYRENE. *Can J Chem* **1960**, *38* (10), 1891–1900. https://doi.org/10.1139/v60-254.

(177) Artyushenko, V. Mid IR-Fiber Optics for Process Spectroscopy and Laser Power Delivery. *Advanced Photonics* **2014**, JTu3A.10. https://doi.org/10.1364/BGPP.2014.JTu3A.10.

(178) Fineman, M.; Ross, S. D. Linear Method for Determining Monomer Reactivity Ratios in Copolymerization. *Journal of Polymer Science* **1950**, *5* (2), 259–262. https://doi.org/10.1002/pol.1950.120050210.

(179) Tidwell, P. W.; Mortimer, G. A. An Improved Method of Calculating Copolymerization Reactivity Ratios. *J Polym Sci A* **1965**, *3* (1), 369–387. https://doi.org/10.1002/pol.1965.100030137.

(180) Kelen, T.; Tüdős, F. A New Improved Linear Graphical Method for Determing Copolymerization Reactivity Ratios. *Reaction Kinetics and Catalysis Letters* **1974**, *1* (4), 487–492. https://doi.org/10.1007/BF02074484.

(181) Kelen, T.; Tüdös, F.; Turcsányi, B. Confidence Intervals for Copolymerization Reactivity Ratios Determined by the Kelen-Tüdös Method. *Polymer Bulletin* **1980**, *2* (1), 71–76. https://doi.org/10.1007/BF00275556.

(182) Riahinezhad, M.; Kazemi, N.; McManus, N.; Penlidis, A. Optimal Estimation of Reactivity Ratios for Acrylamide/Acrylic Acid Copolymerization. *J Polym Sci A Polym Chem* **2013**, *51* (22), 4819–4827. https://doi.org/10.1002/pola.26906.

(183) Kim, J. M.; Chakrapani, S. B.; Beckingham, B. S. Tuning Compositional Drift in the Anionic Copolymerization of Styrene and Isoprene. *Macromolecules* **2020**, *53* (10), 3814–3821. https://doi.org/10.1021/acs.macromol.0c00526.

(184) Kazemi, N.; Duever, T. A.; Penlidis, A. Reactivity Ratio Estimation from Cumulative Copolymer Composition Data. *Macromol React Eng* **2011**, *5* (9–10), 385–403. https://doi.org/10.1002/mren.201100009.

(185) Meyer, V. E.; Lowry, G. G. Integral and Differential Binary Copolymerization Equations. *J Polym Sci A* **1965**, *3* (8), 2843–2851. https://doi.org/10.1002/pol.1965.100030811.

(186) Wall, F. T. The Structure of Vinyl Copolymers. *J Am Chem Soc* **1941**, *63* (7), 1862–1866. https://doi.org/10.1021/ja01852a016.

(187) Jaacks, V. A Novel Method of Determination of Reactivity Ratios in Binary and Ternary Copolymerizations. *Makromol Chem* **1972**, *161* (1), 161–172. https://doi.org/10.1002/macp.1972.021610110.

(188) Jaacks, V. Eine Neuartige Methode Zur Bestimmung von Copolymerisationsparametern. *Angewandte Chemie* **1967**, *79* (9), 419–419. https://doi.org/10.1002/ange.19670790927.

(189) Lee, B. F.; Wolffs, M.; Delaney, K. T.; Sprafke, J. K.; Leibfarth, F. A.; Hawker, C. J.; Lynd, N. A. Reactivity Ratios and Mechanistic Insight for Anionic Ring-Opening Copolymerization of Epoxides. *Macromolecules* **2012**, *45* (9), 3722–3731. https://doi.org/10.1021/ma300634d.

(190) Boileau, S.; Deffieux, A.; Lassalle, D.; Menezes, F.; Vidal, B. Reactivities of Anionic Species for the Ring Opening of Ethylene Oxide. *Tetrahedron Lett* **1978**, *19* (20), 1767–1770. https://doi.org/10.1016/0040-4039(78)80039-2.

(191) Beckingham, B. S.; Sanoja, G. E.; Lynd, N. A. Simple and Accurate Determination of Reactivity Ratios Using a Nonterminal Model of Chain Copolymerization. *Macromolecules* **2015**, *48* (19), 6922–6930. https://doi.org/10.1021/acs.macromol.5b01631.

(192) Blankenburg, J.; Kersten, E.; Maciol, K.; Wagner, M.; Zarbakhsh, S.; Frey, H. The Poly(Propylene Oxide-: Co -Ethylene Oxide) Gradient Is Controlled by the Polymerization Method: Determination

of Reactivity Ratios by Direct Comparison of Different Copolymerization Models. *Polym Chem* **2019**, *10* (22), 2863–2871. https://doi.org/10.1039/c9py00500e.

(193) Lynd, N. A.; Ferrier, R. C.; Beckingham, B. S. Recommendation for Accurate Experimental Determination of Reactivity Ratios in Chain Copolymerization. *Macromolecules* **2019**, *52* (6), 2277–2285. https://doi.org/10.1021/acs.macromol.8b01752.

(194) Hawkins, D. M. The Problem of Overfitting. *J Chem Inf Comput Sci* **2004**, *44* (1), 1–12. https://doi.org/10.1021/ci0342472.

(195) Hoffmann, R.; Minkin, V. I. Ockham's Razor and Chemistry. *International Journal for the Philosophy of Chemistry* **1996**, No. 3, 3–28.

(196) Blankenburg, J.; Kersten, E.; Maciol, K.; Wagner, M.; Zarbakhsh, S.; Frey, H. The Poly(Propylene Oxide- Co -Ethylene Oxide) Gradient Is Controlled by the Polymerization Method: Determination of Reactivity Ratios by Direct Comparison of Different Copolymerization Models. *Polym Chem* **2019**, *10* (22), 2863–2871. https://doi.org/10.1039/C9PY00500E.

(197) Strobl, G. The Physics of Polymers. *Polymer (Guildf)* **1974**, *15* (5), 258. https://doi.org/10.1016/0032-3861(74)90120-7.

(198) Khandpur, A. K.; Förster, S.; Bates, F. S.; Hamley, I. W.; Ryan, A. J.; Bras, W.; Almdal, K.; Mortensen, K. Polyisoprene-Polystyrene Diblock Copolymer Phase Diagram near the Order-Disorder Transition. *Macromolecules* **1995**, *28* (26), 8796–8806. https://doi.org/10.1021/ma00130a012.

(199) Bates, F. S.; Fredrickson, G. H. Block Copolymer Thermodynamics: Theory and Experiment. *Annu Rev Phys Chem* **1990**, *41* (1), 525–557. https://doi.org/10.1146/annurev.pc.41.100190.002521.

(200) Leibler, L. Theory of Microphase Separation in Block Copolymers. *Macromolecules* **1980**, *13* (6), 1602–1617. https://doi.org/10.1021/ma60078a047.

(201) Mai, Y.; Eisenberg, A. Self-Assembly of Block Copolymers. *Chem Soc Rev* **2012**, *41* (18), 5969–5985. https://doi.org/10.1039/c2cs35115c.

(202) Helfand, E.; Wasserman, Z. R. Block Copolymer Theory. 5. Spherical Domains. *Macromolecules* **1978**, *11* (5), 960–966. https://doi.org/10.1021/ma60065a023.

(203) Helfand, E.; Wasserman, Z. R. Block Copolymer Theory. 6. Cylindrical Domains. *Macromolecules* **1980**, *13* (4), 994–998. https://doi.org/10.1021/ma60076a045.

(204) Helfand, E.; Wasserman, Z. R. Block Copolymer Theory. 4. Narrow Interphase Approximation. *Macromolecules* **1976**, *9* (6), 879–888. https://doi.org/10.1021/ma60054a001.

(205) Schmitt, B. J. Polymerlegierungen – Struktur, Morphologie, Eigenschaften. *Angewandte Chemie* **1979**, *91* (4), 286–309. https://doi.org/10.1002/ange.19790910406.

(206) de Gennes, P. G. Theory of X-Ray Scattering by Liquid Macromolecules with Heavy Atom Labels. *Journal de Physique* **1970**, *31* (2–3), 235–238. https://doi.org/10.1051/jphys:01970003102-3023500.

(207) Bates, F. S.; Schulz, M. F.; Khandpur, A. K.; Förster, S.; Rosedale, J. H.; Almdal, K.; Mortensen, K. Fluctuations, Conformational Asymmetry and Block Copolymer Phase Behaviour. *Faraday Discuss.* **1994**, *98*, 7–18. https://doi.org/10.1039/FD9949800007.

(208) Kawai, H.; Tsukahara, Y.; Kawai, H. Structure and Properties of Tapered Block Polymers of Styrene and Isoprene 2. Dynamic Mechanical Responses and Their Structural Interpretations. *Polym J* **1983**, *15* (10), 699–711. https://doi.org/10.1295/polymj.15.699.

(209) Hashimoto, T.; Tsukahara, Y.; Kawai, H. Structure and Properties of Tapered Block Polymers of Styrene and Isoprene II. Dynamic Mechanical Responses and Their Structural Interpretations. *Polym J* **1983**, *15* (10), 699–711. https://doi.org/10.1295/polymj.15.699.

(210) Gouinlock, E. V.; Porter, R. S. Linear Dynamic Mechanical Properties of an SBS Block Copolymer. *Polym Eng Sci* **1977**, *17* (8), 535–543. https://doi.org/10.1002/pen.760170809.

(211) Steube, M.; Johann, T.; Galanos, E.; Appold, M.; Rüttiger, C.; Mezger, M.; Gallei, M.; Müller, A. H. E.; Floudas, G.; Frey, H. Isoprene/Styrene Tapered Multiblock Copolymers with up to Ten Blocks: Synthesis, Phase Behavior, Order, and Mechanical Properties. *Macromolecules* **2018**, *51* (24), 10246–10258. https://doi.org/10.1021/acs.macromol.8b01961.

(212) Storey, R. F.; Chisholm, B. J.; Choate, K. R. Synthesis and Characterization of PS-PIB-PS Triblock Copolymers. *Journal of Macromolecular Science, Part A* **1994**, *31* (8), 969–987. https://doi.org/10.1080/10601329409349773.

(213) Kumar, A.; Rana, D. K.; Pandey, P. M.; Sasmal, C.; Banerjee, S. S. Additive Manufacturing of Styrene-Isoprene-Styrene Block Copolymer Based Soft Thermoplastic Elastomeric Nanocomposites: Influence of Reduced Graphene Oxide on Microstructural, Mechanical and Functional Properties. *Macromol Chem Phys* **2025**. https://doi.org/10.1002/macp.202400409.

(214) Bates, C. M.; Bates, F. S. 50th Anniversary Perspective: Block Polymers-Pure Potential. *Macromolecules*. American Chemical Society January 10, 2017, pp 3–22. https://doi.org/10.1021/acs.macromol.6b02355.

(215) Fredrickson, G. H.; Bates, F. S. Dynamics of Block Copolymers: Theory and Experiment. *Annual Review of Materials Science* **1996**, *26* (1), 501–550. https://doi.org/10.1146/annurev.ms.26.080196.002441.

(216) Jiun, Y. L.; Tze, C. T.; Moosa, U.; Tawawneh, M. A. Effects of Recycling Cycle on Used Thermoplastic Polymer and Thermoplastic Elastomer Polymer. *Polymers and Polymer Composites* **2016**, *24* (9), 735–740. https://doi.org/10.1177/096739111602400909.

(217) Wahlen, C.; Frey, H. Anionic Polymerization of Terpene Monomers: New Options for Bio-Based Thermoplastic Elastomers. *Macromolecules*. American Chemical Society August 24, 2021, pp 7323–7336. https://doi.org/10.1021/acs.macromol.1c00770.

(218) Sasaki, H.; Uehara, Y.; Kato, M. US009752027B2 Thermoplastic Elastomer Composition and Molded Body, 2017.

(219) Mcphee, D. J.; Graham, M. J. EP 2 334 707 B1 Adhesive Compositions Comprising a Polyfarnesene, 2010.

(220) Siggel, L.; Knoll, K.; Hadickeb, E.; Brodea, S. Anionic Polymerization of Butadiene: A MNDO Study of the Potential Energy Surface of the Propagation Reaction in Polar and Non-Polar Media. *Makromol. Chem., Macromol. Symp* **1993**, *65*, 243–254.

(221) Niessner, N.; Jahnke, E.; Wagner, D.; Duerkheim, B.; Knoll, K. US 11,066,503 B2 Very Soft, Non-Sticky and Transparent Styrenic Thermoplastic Elastomer Composition, 2021.

(222) Knoll, K.; Gausepohl, H.; Niessner, N.; Naegele, P.; Fischer, W. EP0859803B1 Thermoplastische Formmasse, 1997.

(223) Niessner, N.; Knoll, K.; Bender, D.; Gottschalk, A.; Weber, M. WO9620248 Impact-Resistent, Thermoplastic Mixture of Elastomers and Thermoplastic Materials, 1996.

(224) Zelinski, R. P.; Hsieh, H. L. US 3,078,254 HIGH MOELECULAR POYMERS AND METHOD FOR THEIR PEREPARATION, 1963.

(225) Tarcha, P. J. *Polymers for Controlled Drug Delivery*; CRC Press: Boca Raton, 2023. https://doi.org/10.1201/9781003418252.

(226) Findlay, M.; von Minckwitz, G.; Wardley, A. Effective Oral Chemotherapy for Breast Cancer: Pillars of Strength. *Annals of Oncology* **2008**, *19* (2), 212–222. https://doi.org/10.1093/annonc/mdm285.

(227) Xu, W.; Ling, P.; Zhang, T. Polymeric Micelles, a Promising Drug Delivery System to Enhance Bioavailability of Poorly Water-Soluble Drugs. *J Drug Deliv* **2013**, *2013*, 1–15. https://doi.org/10.1155/2013/340315.

(228) De Portu, S.; Mantovani, L. G.; Ravaioli, A.; Tamburini, E.; Bollina, R.; Cozzi, C.; Grimaldi, A. M.; Testa, T. E.; Bianchessi, C.; Cartenì, G. Cost Analysis of Capecitabine vs 5-Fluorouracil-Based Treatment for Metastatic Colorectal Cancer Patients. *Journal of Chemotherapy* **2010**, *22* (2), 125–128. https://doi.org/10.1179/joc.2010.22.2.125.

(229) Stamatopoulos, K.; O'Farrell, C.; Simmons, M.; Batchelor, H. In Vivo Models to Evaluate Ingestible Devices: Present Status and Current Trends. *Adv Drug Deliv Rev* **2021**, *177*, 113915. https://doi.org/10.1016/j.addr.2021.113915.

(230) McConnell, E. L.; Fadda, H. M.; Basit, A. W. Gut Instincts: Explorations in Intestinal Physiology and Drug Delivery. *Int J Pharm* **2008**, *364* (2), 213–226. https://doi.org/10.1016/j.ijpharm.2008.05.012.

(231) Felber, A. E.; Dufresne, M.-H.; Leroux, J.-C. PH-Sensitive Vesicles, Polymeric Micelles, and Nanospheres Prepared with Polycarboxylates. *Adv Drug Deliv Rev* **2012**, *64* (11), 979–992. https://doi.org/10.1016/j.addr.2011.09.006.

(232) Sood, A.; Panchagnula, R. *Peroral* Route: An Opportunity for Protein and Peptide Drug Delivery. *Chem Rev* **2001**, *101* (11), 3275–3304. https://doi.org/10.1021/cr000700m.

(233) Harel, Z.; Harel, S.; Shah, P. S.; Wald, R.; Perl, J.; Bell, C. M. Gastrointestinal Adverse Events with Sodium Polystyrene Sulfonate (Kayexalate) Use: A Systematic Review. *Am J Med* **2013**, *126* (3), 264.e9-264.e24. https://doi.org/10.1016/j.amjmed.2012.08.016.

(234) Bytzer, P.; Connolly, S. J.; Yang, S.; Ezekowitz, M.; Formella, S.; Reilly, P. A.; Aisenberg, J. Analysis of Upper Gastrointestinal Adverse Events Among Patients Given Dabigatran in the RE-LY Trial. *Clinical Gastroenterology and Hepatology* **2013**, *11* (3), 246-252.e5. https://doi.org/10.1016/j.cgh.2012.10.021.

(235) Ting, J. M.; Porter, W. W.; Mecca, J. M.; Bates, F. S.; Reineke, T. M. Advances in Polymer Design for Enhancing Oral Drug Solubility and Delivery. *Bioconjugate Chemistry*. American Chemical Society April 18, 2018, pp 939–952. https://doi.org/10.1021/acs.bioconjchem.7b00646.

(236) Wruble, M. Enteric Coatings. *Am. J. Pharm.* **1930**, *102*, 318–318.

(237) Kuriyama, T.; Nobutoki, M.; Nakanishi, M. Permeability of Double-Layer Films I. *J Pharm Sci* **1970**, *59* (9), 1341–1344. https://doi.org/10.1002/jps.2600590928.

(238) Malm, C. J.; Emerson, J.; Hiait, G. D. Cellulose Acetate Phthalate as an Enteric Coating Material. *Journal of the American Pharmaceutical Association (Scientific ed.)* **1951**, *40* (10), 520–525. https://doi.org/10.1002/jps.3030401014.

(239) HODGE, H. C. THE CHRONIC TOXICITY OF CELLULOSE ACETATE PHTHALATE IN RATS AND DOGS. *J Pharmacol Exp Ther* **1944**, *80* (3), 250–255. https://doi.org/10.1016/S0022-3565(25)09088-3.

(240) PORTER, S. C.; RIDGWAY, K. The Permeability of Enteric Coatings and the Dissolution Rates of Coated Tablets. *Journal of Pharmacy and Pharmacology* **1982**, *34* (1), 5–8. https://doi.org/10.1111/j.2042-7158.1982.tb04667.x.

(241) Paradkar, A.; Ambike, A. A.; Jadhav, B. K.; Mahadik, K. R. Characterization of Curcumin–PVP Solid Dispersion Obtained by Spray Drying. *Int J Pharm* **2004**, *271* (1–2), 281–286. https://doi.org/10.1016/j.ijpharm.2003.11.014.

(242) KARAVAS, E.; GEORGARAKIS, E.; BIKIARIS, D. Felodipine Nanodispersions as Active Core for Predictable Pulsatile Chronotherapeutics Using PVP/HPMC Blends as Coating Layer. *Int J Pharm* **2006**, *313* (1–2), 189–197. https://doi.org/10.1016/j.ijpharm.2006.01.015.

(243) Evonik Industries AG. *Functional polymers to take control of your release profile Versatility and reliability for oral solid dosage forms*. https://healthcare.evonik.com/en/drugdelivery/oral-drug-delivery/oral-excipients/eudragit-portfolio/attachment/149083?rev=fd91102acf8d769a56d0716b20544216.

(244) Breitkreutz, J. Leakage of Enteric (Eudragit® L)-Coated Dosage Forms in Simulated Gastric Juice in the Presence of Poly(Ethylene Glycol). *Journal of Controlled Release* **2000**, *67* (1), 79–88. https://doi.org/10.1016/S0168-3659(00)00197-8.

(245) Nikam, A.; Sahoo, P. R.; Musale, S.; Pagar, R. R.; Paiva-Santos, A. C.; Giram, P. S. A Systematic Overview of Eudragit® Based Copolymer for Smart Healthcare. *Pharmaceutics* **2023**, *15* (2), 587. https://doi.org/10.3390/pharmaceutics15020587.

(246) Bettencourt, A.; Almeida, A. J. Poly(Methyl Methacrylate) Particulate Carriers in Drug Delivery. *Journal of Microencapsulation*. June 2012, pp 353–367. https://doi.org/10.3109/02652048.2011.651500.

(247) Ibarra-Montaño, E. L.; Rodríguez-Laguna, N.; Sánchez-Hernández, A.; Rojas-Hernández, A. Determination of PKa Values for Acrylic, Methacrylic and Itaconic Acids by 1H and 13C NMR in Deuterated Water. *Journal of Applied Solution Chemistry and Modeling* **2015**, *4* (1), 7–18. https://doi.org/10.6000/1929-5030.2015.04.01.2.

(248) Van Gheluwe, L.; Chourpa, I.; Gaigne, C.; Munnier, E. Polymer-Based Smart Drug Delivery Systems for Skin Application and Demonstration of Stimuli-Responsiveness. *Polymers (Basel)* **2021**, *13* (8), 1285. https://doi.org/10.3390/polym13081285.

(249) Al-Gousous, J.; Amidon, G. L.; Langguth, P. Toward Biopredictive Dissolution for Enteric Coated Dosage Forms. *Mol Pharm* **2016**, *13* (6), 1927–1936. https://doi.org/10.1021/acs.molpharmaceut.6b00077.

(250) Khan, M. Z. I.; Prebeg, Ž.; Kurjaković, N. A PH-Dependent Colon Targeted Oral Drug Delivery System Using Methacrylic Acid Copolymers. *Journal of Controlled Release* **1999**, *58* (2), 215–222. https://doi.org/10.1016/S0168-3659(98)00151-5.

(251) Cole, E. T.; Scott, R. A.; Connor, A. L.; Wilding, I. R.; Petereit, H. U.; Schminke, C.; Beckert, T.; Cadé, D. Enteric Coated HPMC Capsules Designed to Achieve Intestinal Targeting. *Int J Pharm* **2002**, *231* (1), 83–95. https://doi.org/10.1016/S0378-5173(01)00871-7.

(252) Liu, F.; Basit, A. W. A Paradigm Shift in Enteric Coating: Achieving Rapid Release in the Proximal Small Intestine of Man. *Journal of Controlled Release* **2010**, *147* (2), 242–245. https://doi.org/10.1016/j.jconrel.2010.07.105.

(253) Al-Gousous, J.; Ruan, H.; Blechar, J. A.; Sun, K. X.; Salehi, N.; Langguth, P.; Job, N. M.; Lipka, E.; Loebenberg, R.; Bermejo, M.; Amidon, G. E.; Amidon, G. L. Mechanistic Analysis and Experimental Verification of Bicarbonate-Controlled Enteric Coat Dissolution: Potential in Vivo Implications. *European Journal of Pharmaceutics and Biopharmaceutics* **2019**, *139*, 47–58. https://doi.org/10.1016/j.ejpb.2019.03.012.

(254) Blechar, J. A.; Al-Gousous, J.; Wilhelmy, C.; Postina, A. M.; Getto, M.; Langguth, P. Toward Mechanistic Design of Surrogate Buffers for Dissolution Testing of PH-Dependent Drug Delivery Systems. *Pharmaceutics* **2020**, *12* (12), 1197. https://doi.org/10.3390/pharmaceutics12121197.

(255) Rudinskas, L.; Paton, T. W.; Walker, S. E.; Dotten, D. A.; Cowan, D. H. Poor Clinical Response to Enteric-Coated Iron Preparations. *CMAJ* **1989**, *141* (6), 565–566.

(256) Walker, S. E.; Paton, T. W.; Cowan, D. H.; Manuel, M. A.; Dranitsaris, G. Bioavailability of Iron in Oral Ferrous Sulfate Preparations in Healthy Volunteers. *CMAJ* **1989**, *141* (6), 543–547.

(257) Haastrup, P. F.; Grønlykke, T.; Jarbøl, D. E. Enteric Coating Can Lead to Reduced Antiplatelet Effect of Low-Dose Acetylsalicylic Acid. *Basic Clin Pharmacol Toxicol* **2015**, *116* (3), 212–215. https://doi.org/10.1111/bcpt.12362.

(258) Grosser, T.; Fries, S.; Lawson, J. A.; Kapoor, S. C.; Grant, G. R.; FitzGerald, G. A. Drug Resistance and Pseudoresistance. *Circulation* **2013**, *127* (3), 377–385. https://doi.org/10.1161/CIRCULATIONAHA.112.117283.

(259) Haastrup, P. F.; Grønlykke, T.; Jarbøl, D. E. Enteric Coating Can Lead to Reduced Antiplatelet Effect of Low-Dose Acetylsalicylic Acid. *Basic Clin Pharmacol Toxicol* **2015**, *116* (3), 212–215. https://doi.org/10.1111/bcpt.12362.

(260) LaVan, D. A.; McGuire, T.; Langer, R. Small-Scale Systems for in Vivo Drug Delivery. *Nat Biotechnol* **2003**, *21* (10), 1184–1191. https://doi.org/10.1038/nbt876.

(261) Mössner, J.; Keim, V. Pancreatic Enzyme Therapy. *Dtsch Arztebl Int* **2011**, *108* (34–35), 578–582. https://doi.org/10.3238/arztebl.2011.0578.

(262) van Putten, P. L. Mandelic Acid and Urinary Tract Infections. *Antonie Van Leeuwenhoek* **1979**, *45* (4), 622–623. https://doi.org/10.1007/BF00403669.

Chapter 2

Effect of THF on the Anionic Copolymerization of 4-Trimethylsilylstyrene with Isoprene

Dominik A. H. Fuchs[a], [redacted]

[a] *Department of Chemistry, Johannes Gutenberg University, Duesbergweg 10-14, 55128 Mainz, Germany.*

[redacted]

Published in: *Polymers for Advanced Technologies*, **2024**, 35 (6), https://doi.org/10.1002/pat.6478

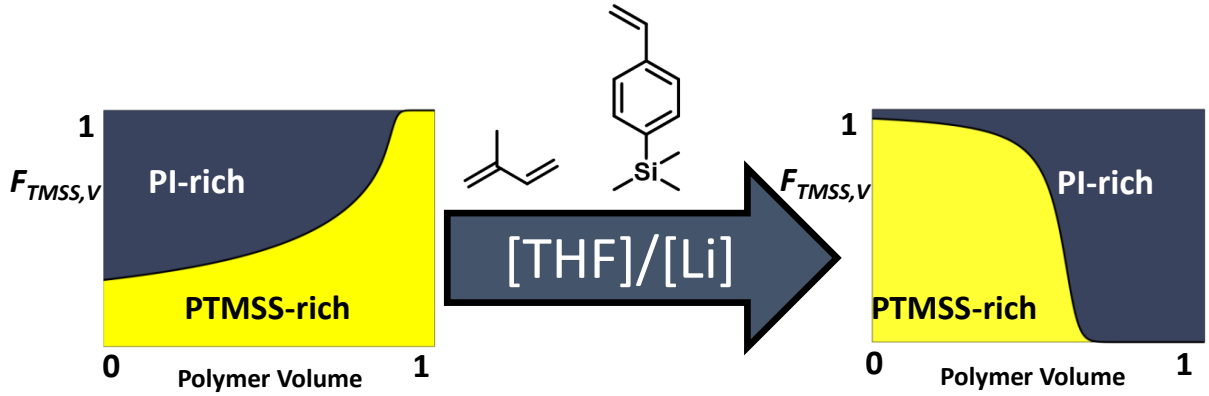

The following publication is adapted with permission from Fuchs, D. A. H. ; [redacted] Effect of THF on the Anionic Copolymerization of 4-Trimethylsilylstyrene with Isoprene, *Polymers for Advanced Technologies*, **2024**, 35 (6).

Abstract:

The statistical anionic copolymerization of 4-trimethylsilylstyrene (4TMSS) with isoprene (I) in cyclohexane was investigated using *in-situ* near-infrared (NIR) spectroscopy in the presence of various amounts of the polar modifier THF. Polymers with narrow molecular weight distribution of 85 - 138 kg/mol and dispersities of 1.09 - 1.22 were obtained. Increasing modifier content, the reactivity ratios can be adjusted over a wide range from $r_{TMSS} < r_I$ to $r_{TMSS} >> r_I$. Compared to the system styrene/isoprene (S/I) only a minute amount of modifier (0.5 eq THF relative to lithium) is sufficient to alter the reactivity ratios, resulting in a random copolymerization, which validates the higher reactivity of TMSS compared to styrene. Using these reactivity ratios, molar and volume composition gradients were calculated. Additionally, the glass transition temperature and microstructure of the PI units was investigated via DSC and ^{1}H-NMR. The results are encouraging for use of these materials in high-end applications like membranes.

Introduction

Since the discovery of living anionic polymerization in 1956, both industry and research have been using this technique to produce polymers with tailored properties, in particular block copolymers and other high-performance materials. [1–9] Most frequently, the products are based on styrene and diene monomers, which are polymerized under specific conditions to obtain nanophase separated multiblock structures, which are summarized as thermoplastic elastomers (TPE).

In the copolymerization of styrene (S) with isoprene (I) in apolar solvents, such as cyclohexane, the diene polymerizes first until almost all diene monomer is consumed, as can be seen from the disparate reactivity ratios: r_S = 0.015 r_I = 10.03.[10] This leads to a strong comonomer gradient in the chains and has been used to synthesize tapered block and multiblock copolymers.[11,12] By adding only small amounts of polar modifiers (Lewis bases) like THF, these reactivity ratios can be drastically changed, leading to randomness or even inversion of reactivity ratios (2500 eq THF: r_S = 12.58 r_I = 0.012).[10,13] The addition of polar modifiers such as THF changes the polymerization kinetics, as the chain end is solvated differently and Li-related aggregation is reduced.[10,14–16]

Besides styrene, different modified derivatives can be used as a hard block like 4-trimethylsilylstyrene (4TMSS), which not only alters the reactivity ratios but also the gas permeation properties of the polymer.[17][18] Yampolskii *et al.* showed that PTMSS has a 1.4-fold higher free volume compared to PS and has a significant influence on the higher permeability compared to poly(*tert*-butylstyrene).[19] Nagasaki *et al.* proved that the C-Si linkage exhibits strong affinity towards oxygen molecules which leads to an increase in the oxygen solubility coefficient.[20] Previous studies of the copolymerization of TMSS and isoprene using *in situ* ^{1}H-NMR kinetics revealed a less steep gradient structure (r_I = 3.28; r_{TMSS} = 0.152).[17] The introduction of the TMS group into the styrene monomer significantly increases its reactivity, and thus its reactivity ratio. The TMS group has an electron-donating (+I) and an electron-withdrawing (-M) effect when directly bound to an aromatic ring.[21,22] These effects are contractionary and several studies suggest that the -M effect dominates, when directly bound to the phenyl ring. Interaction of the empty 3d silicon orbitals with the π-orbitals of the phenyl ring leads to a downfield shift of the β-carbon and thus to a higher polarity and reactivity of TMSS.[21,23,24] This increased reactivity

compared to styrene could possibly be enhanced further by adding increasing amounts of THF to cyclohexane, which enables the synthesis of copolymers with various polymer compositions. For these studies we used *in-situ* near-infrared (NIR) spectroscopy, as described in our previous studies.[10,14,25] The copolymers of TMSS and isoprene are investigated with respect to their polymer composition, microstructure, and thermal properties for possible application in gas separation membranes.

2 Experimental Section

Materials, instrumentation, monomer synthesis and copolymerization procedures are given in the Supporting Information.

3. Results and Discussion

3.1 Copolymerisation kinetics

To investigate the effect of polar modifiers (THF) on the copolymerization of TMSS with isoprene, copolymerizations with different modifier content were performed in cyclohexane at 20 °C with *sec*-butyllithium (BuLi) as an initiator, similar to our previous studies.[10,14]] A molar ratio of 70 mol% of isoprene (ρ_{PI} = 0.91)[26] and 30 mol% of TMSS (ρ_{PTMSS} = 0.963)[27] was used for the copolymerization to obtain polymers with 47.3 wt% and 48.8 vol% of isoprene, respectively. The SEC elugrams of the copolymers (Figure S1) show that we obtained polymers with M_n between 85 and 138 kg/mol with dispersities between 1.09-1.22 (Table 1). Higher molecular weights can be explained by the approx. 10% overestimation of the PI samples when using a PS calibration.(ste) Some elugrams show a small peak or shoulder at lower elution volume stemming from oxygen coupling due to insufficient degassing of the termination reagent isopropanol.[8]

During the copolymerization, 13,000 to 20,000 NIR-spectra in the range of 5900 to 6250 cm^{-1} were recorded and analyzed by deconvoluting the measured spectra with the calibration spectra of all components present (TMSS, PTMSS and isoprene), as shown in Figure S2. Since the NIR spectrum of PI depends on its microstructure (given by the THF content) it was obtained by subtracting the spectra of the other components from the spectrum taken at full conversion. Time-conversion and plots of individual vs total conversion are given for 0.25 eq THF in Figure 1 and in the supporting information in Figures S3-S4. It is clearly seen that with increasing content of THF the rate of TMSS

consumption is strongly increasing, whereas the rate of isoprene conversion is much less affected.

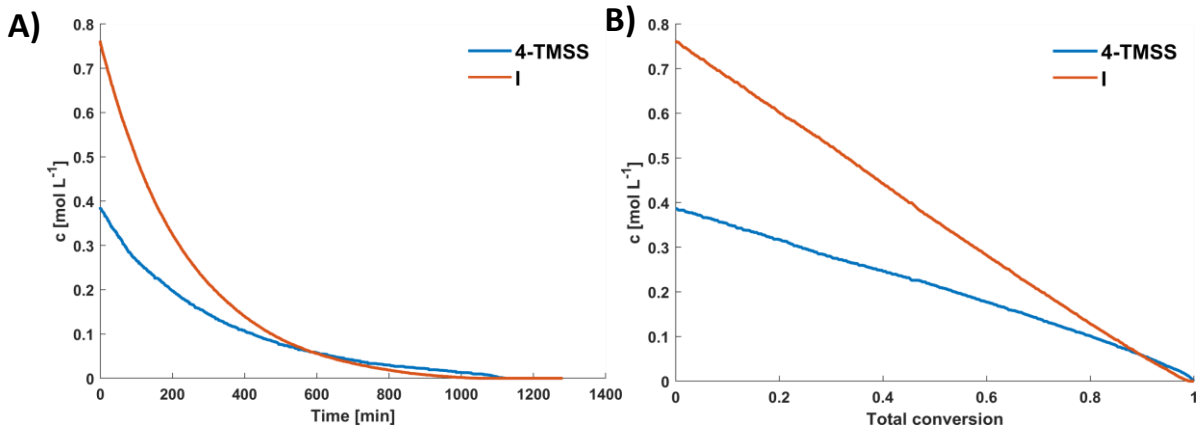

Figure 1: A) Time conversion and B) Monomer concentration as function of total conversion for [THF]/[Li] = 0.25.

The reactivity ratios r_{TMSS} and r_I were calculated using both the terminal and non-terminal models. The non-terminal model assumes an ideal copolymerization ($r_1 \cdot r_2 = 1$). If the plot according to Jaacks[28,29] is linear, this model is assumed to be valid, thus avoiding overfitting. A numerical fit to a plot according to Meyer and Lowry[30] is used to calculate r_1 and r_2 independently is only necessary to fit the copolymerization in pure cyclohexane.[31,32] The individual fits of the different methods can be seen in Figures S5-6.

Our results in pure cyclohexane are in reasonable agreement with values determined by Wadgaonkar *et al.* at room temperature with *in situ* ^{1}H-NMR (r_{TMSS} = 0.152 and r_I = 3.28)[17], The slight differences can be explained by different reaction temperature, concentrations, deuterated solvents, and slow diffusion in an NMR tube.

Table 1 and Figure 2 show a strong effect of THF on the reactivity ratios, particularly on r_{TMSS}. This is similar to earlier observations in the systems S/I and S/myrcene. Already at a ratio THF/Li ≈ 0.4 randomization is observed. In contrast, a ratio THF/Li ≈ 6 is needed to reach formation of ideally random copolymers in the S/I system. Thus, TMSS is much more sensitive to polar modifiers that styrene. This is explained by the higher reactivity of TMSS, caused by the electron withdrawing effect of the trimethylsilyl group, as described earlier.[17]

Table 1 Effect of THF on the reactivity ratios, molecular weight, dispersity and blockiness for P($TMSS_{0.3}$-co-$I_{0.7}$). Initiator and total monomer concentration are 1.75 mmol/L and 1.4 mol/L, resp.

[THF]/[Li]	Φ_{THF}, $\%_{Vol}$	ε[a]	r_{TMSS}	r_I	r_{TMSS} x r_I	blockiness	M_n[b] kg/mol	$Đ$[b]
0	0	2.023	0.066	2.37	0.16	27.4	84.6	1.15
0.25	0.0035	2.023	0.74	1.36	1	6.7	138.4	1.12
0.5	0.007	2.024	1.09	0.92	1	2.1	99.2	1.22
2	0.028	2.026	2.04	0.49	1	3.2	122.2	1.09
20	0.28	2.049	4.52	0.22	1	13.8	121.5	1.11
200	2.85	2.268	22.9	0.04	1	40.7	121.3	1.14

[a]dielectric constant of solvent, [b]SEC calibration with PS standard

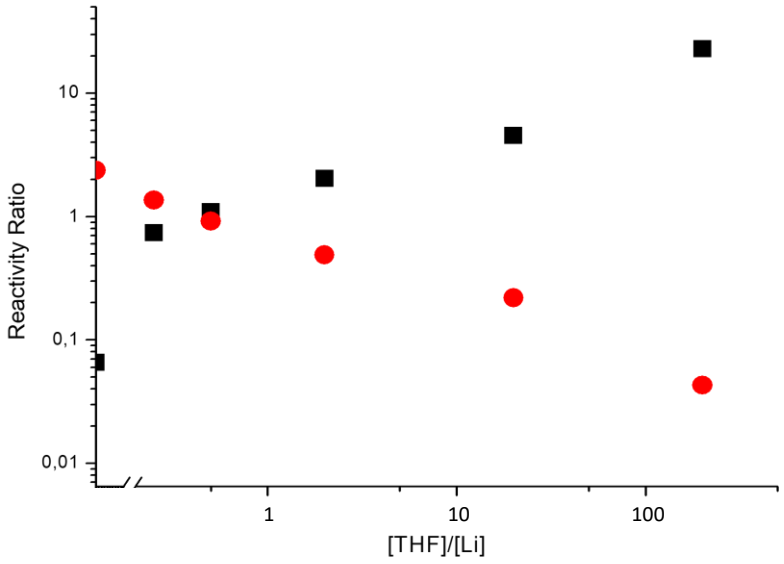

***Figure 2**:* Reactivity ratios of r_{TMSS} (black squares) and r_I (red circles) in dependence of the THF modifier content.

Shape of the gradient

The obtained reactivity ratios were used to calculate the gradients of comonomer compositions, Figure 3A shows the molar fraction of TMSS units, $F_{TMSS,}$ as a function of total conversion (i.e., along the polymer chain) and Figure 3B shows the volume incorporation, $F_{TMSS,V}$, along the chain.

The copolymerization without modifier yields a tapered copolymer that initially forms an isoprene block interspersed with short TMSS segments and, after all isoprene has been consumed, a pure PTMSS block is formed. Increasing the modifier content changes the composition: As the modifier content increases up to 0.5 eq, the gradient flattens out and almost random copolymers are obtained. Increasing the THF content further the gradient steepens again, and for ≥ 20 eq., a PTMSS block with short PI segments is formed and only after TMSS has been completely consumed is a pure PI block formed.

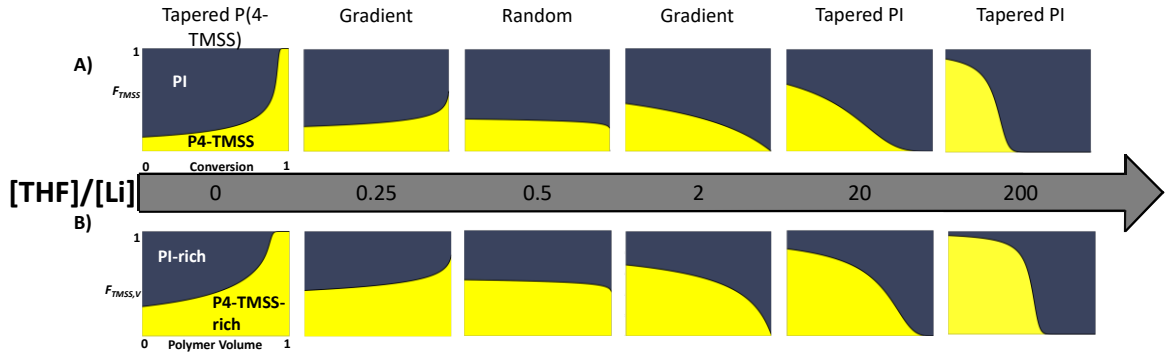

***Figure 3**:* A) Molar B) volume composition of the P($TMSS_{0.3}$-*co*-$I_{0.7}$) copolymer as a function of the [THF]/[Li] ratio.

In addition, the so-called "blockiness" was determined by analyzing the ^{1}H-NMR spectra of the copolymers in Figure 4.[33–36] The values are presented in Table 1 and confirm the kinetically obtained gradients. Details are given in the Supporting Information.

3.3 Microstructure of isoprene units:

^{1}H-NMR spectroscopy was used to determine the microstructure of the isoprene monomer units. This method differs from the one previously used by us consisting of a combination of inverse-gated ^{13}C NMR and ^{1}H NMR.[10] In contrast to the evaluation of the S/I system, for our monomer combination there is a significant overlap of the h and n signal (see Figure S10 + S15). A comparison of the two methods shows minor differences at lower 1,4-contents.[10] ^{1}H-, $^{13}C_{ig}$-, COSY, HSQC and HMBC spectra of the copolymers and the exact calculation can be found in Figures S7-16. An overview of the ^{1}H-NMR spectra is shown in Figure 4, and the PI microstructure is listed in Table 2.

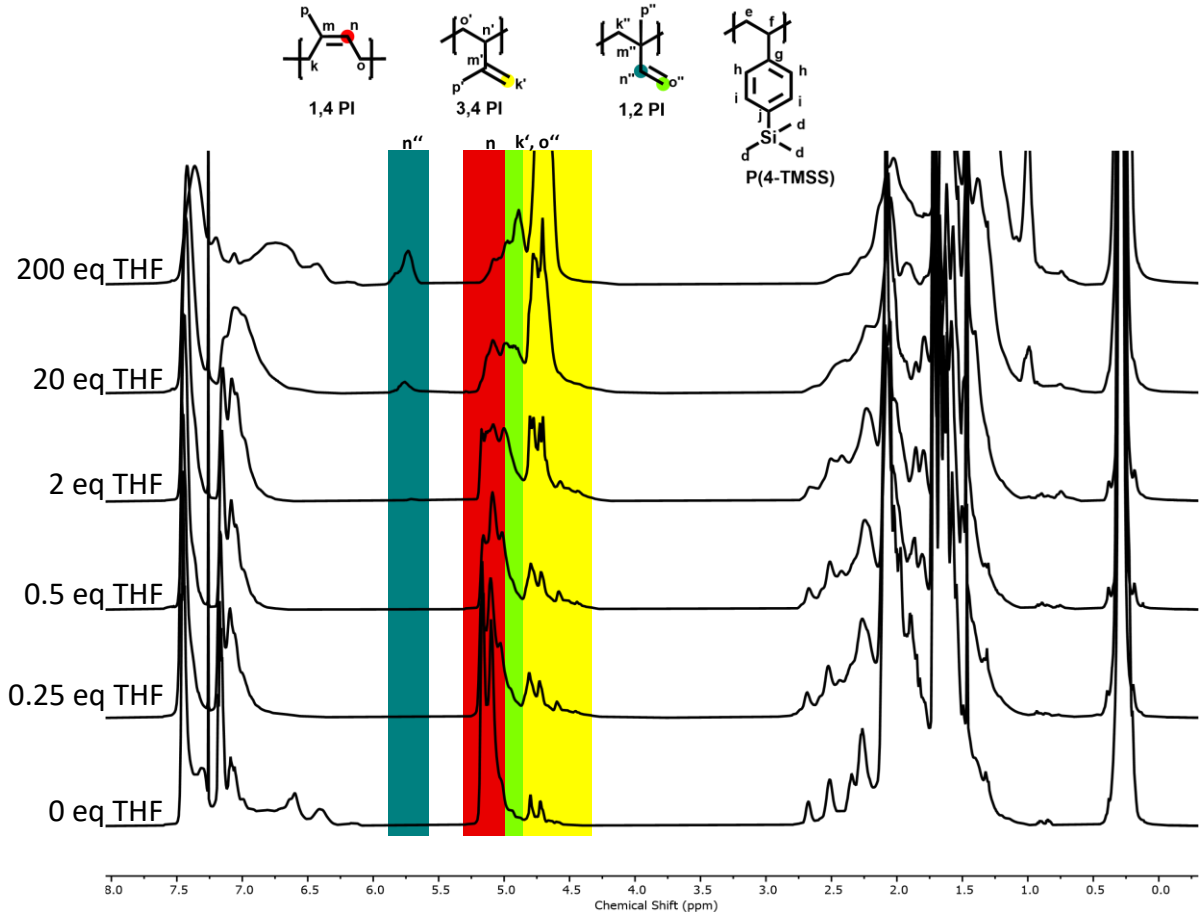

Figure 4: Overview of all ^{1}H-NMR spectra ($CDCl_3$, 600MHz) of P(TMSS-*co*-I) prepared in cyclohexane with 0 ≤ [THF]/[Li] ≤ 200.

When synthesized in pure cyclohexane, the isoprene units consist of 6% 3,4- and 94% 1,4-units, which is in good agreement with literature.[10,25,37,38] With increasing modifier concentration the 1,4- content decreases, and the 3,4- and 1,2- contents increase. For THF/Li ≥ 0.5 1,2-units appear, as shown in the green areas in Figure 4. Taking into account the different analytical methods, these results agree well with literature. In addition, different concentrations of monomers, chain ends, and an increased polarity by the TMSS comonomer may have an impact on the results. [10,39,40]

Table 2: Microstructure of isoprene monomer units in P(TMSS$_{0.3}$-*co*-I$_{0.7}$) determined by ^{1}H-NMR spectroscopy, the inherent glass transition temperatures (T_g) and the temperature at 5% wt. loss.

[THF]/[Li]	1,4-PI [%]	3,4-PI [%]	1,2-PI [%]	T_g [°C]	$T_{5\%}$ [°C]
0	93.7	6.3	0	-22	348
0.25	85	15	0	5	328
0.5	80.3	18.6	1.1	8	350
2	69.0	28.6	2.4	16	342
20	40.8	52.2	7.0	30	345
200	16.7	66.7	16.6	36	336

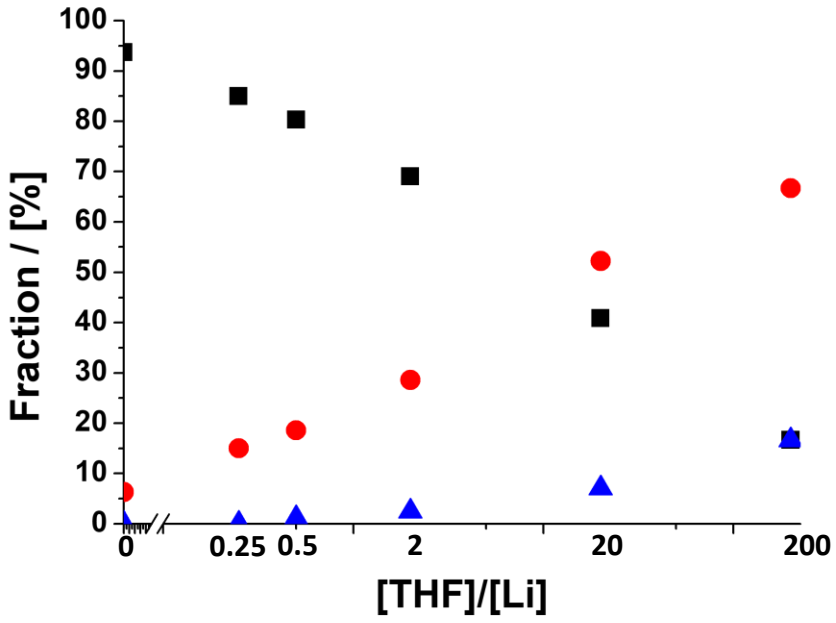

Figure 5*:* Microstructure of the isoprene units (1,4- black squares; 3,4- red dots; 1,2 blue triangle) as a function of the ratio [THF]/[Li] for the copolymer P(TMSS$_{0.3}$-*co*-I$_{0.7}$).

3.5 Thermal properties

The thermal properties of the copolymers were investigated by DSC, and the results are shown in Table 2 and Figures 6. The DSC curves are shown in Figure S17. For all samples, only a single glass transition temperature was measured, despite the high molecular weights of the materials in the range of 80 kg/mol to 138 kg/mol, indicating that no phase separation takes place. In our earlier paper this was also observed for the gradient copolymer synthesized in pure cyclohexane. In contrast, the block copolymer P($I_{0.5}$-*b*-$TMSS_{0.5}$), synthesized by sequential monomer additions, has two distinct glass transition temperatures (-49.9°C and 53.8°C).[17] They strongly differ from the respective homopolymers and suggest partial mixing of both phases, which indicates that the Flory Huggins parameter, $\chi_{TMSS/1,4\text{-}PI}$, is very small. Thus, it might be expected that a gradient-copolymer is not phase-separated, even for a rather strong gradient.

For 0 eq THF the glass transition was measured at -22°C which is in good agreement with literature and is explained by a mixture of both T_g, since both phases a miscible.[17] PI synthesized in cyclohexane has T_g = -64 °C[38] and PTMSS has T_g = 135°C.[17][41]

THF affects the microstructure of the PI units and thus the glass transition temperature of the copolymers.[42–45] As expected, with increasing modifier content, the glass transition temperature of this copolymer also increases.

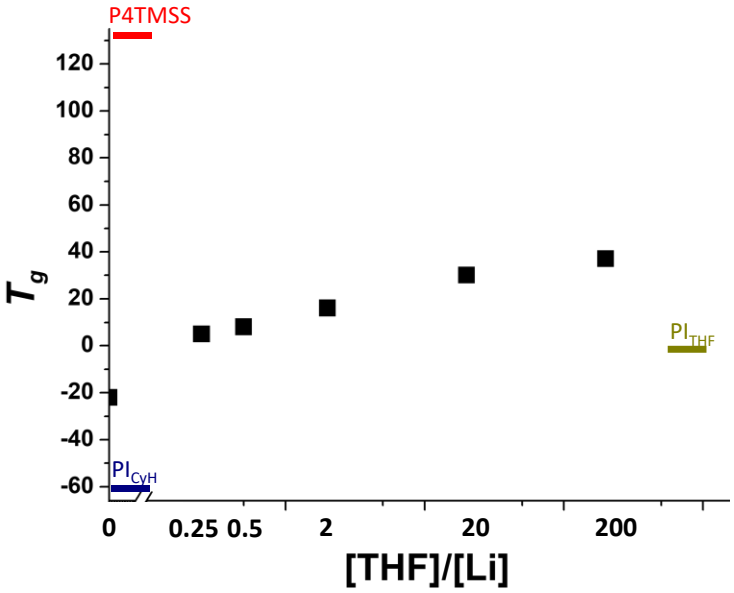

***Figure 6**:* Glass transition temperature of the copolymer P($TMSS_{0.3}$-*co*-$I_{0.7}$), as a function of the [THF]/[Li] ratio. The horizontal lines symbolize the glass transition temperature of the homopolymers PTMSS and PI synthesized in cyclohexane and THF.

From the similar system $\chi_{PS/PI}$, it is known that the Flory-Huggins parameter differs for the different PI microstructures.[46] Using the Hildebrand solubility parameters we estimated $\chi_{TMSS/1,4\text{-}PI} \approx 0.01$ and $\chi_{TMSS/3,4\text{-}PI} \approx 0$.[17] Since 3,4-PI is the predominant microstructure when synthesized in the presence of 200 eq THF no phase separation can be expected. All mixed-phase polymers form stable films by solvent casting (Figure S18). In addition, all samples were analyzed by thermogravimetric analysis (TGA) under nitrogen to investigate their thermostability. All samples showed a similar degradation temperature ($T_{5\%}$) of 330-350°C, at which a loss of 5 wt% occurred (see table 2 and figure S19); this is in the range of the homopolymers P(TMSS): 320°C [47] and PI: 393°C.[3] All polymers showed a one-step degradation and a complete decomposition at about 500°C.

4. Conclusions

The kinetics of the copolymerization of TMSS with isoprene in presence of different THF contents was successfully investigated by *in-situ* NIR spectroscopy. The monomer TMSS shows a higher reactivity than styrene; already less than 0.5 equivalents of the polar modifier THF relative to Li^+ are sufficient to alter the reactivity ratios from a strong gradient

into a random copolymerization. With increased modifier content the reactivity ratios are inverted leading to obtain almost blocklike structures. The absence of two glass transition temperatures indicates the absence of phase separation. These polymers are potential candidates for gas separation membranes. The 3,4- and 1,2-monomer units of isoprene can be used for potential crosslinking reactions to form a stable 3D network.

Conflict of interest:

There are no conflicts to declare.

Acknowledgements

D.F. thanks Jirui Zhang for helpful discussions, NMR analysis and critical evaluation of this article.

References

[1] M. Szwarc, *Nature* **1956**, *178*, 1168–1169.

[2] M. Meier-Merziger, M. Fickenscher, F. Hartmann, B. Kuttich, T. Kraus, M. Gallei, H. Frey, *Polym Chem* **2023**, *14*, 2820–2828.

[3] J. Zhang, W. Pointer, G. Patias, L. Al-Shok, R. A. Hand, T. Smith, D. M. Haddleton, *Eur Polym J* **2023**, *183*, 111755.

[4] H. Kim, R. Goseki, C. Homma, T. Ishizone, *Macromolecules* **2023**, *56*, 8796–8805.

[5] J. Glatzel, S. Noack, D. Schanzenbach, H. Schlaad, *Polym Int* **2021**, *70*, 181–184.

[6] A. Dev, A. Rösler, H. Schlaad, *Polym Chem* **2021**, *12*, 3084–3087.

[7] K. Ntetsikas, V. Ladelta, S. Bhaumik, N. Hadjichristidis, *ACS Polymers Au* **2023**, *3*, 158–181.

[8] M. Steube, T. Johann, R. D. Barent, A. H. E. Müller, H. Frey, *Prog Polym Sci* **2022**, *124*, 101488.

[9] R. Dong, A. Gao, Y. Zhu, B. Xu, J. Du, S. Ping, *Buildings* **2023**, *13*, 1451.

[10] M. Steube, T. Johann, H. Hübner, M. Koch, T. Dinh, M. Gallei, G. Floudas, H. Frey, A. H. E. Müller, *Macromolecules* **2020**, *53*, 5512–5527.

[11] Porter, R. Milkovich, Phillips Petroleum Co, *GB888624A Block Polymers and Process for Preparation Thereof*, **1959**.

[12] G. Holden, R. Milkovich, *U.S. Patent 3265765, Block Polymers of Monovinyl Aromatic Hydrocarbons and Conjugated Dienes.*, **1962**.

[13] L. Shaw, L. R. Hutchings, *Polym Chem* **2020**, *11*, 7020–7025.

[14] D. A. H. Fuchs, H. Hübner, T. Kraus, B.-J. Niebuur, M. Gallei, H. Frey, A. H. E. Müller, *Polym Chem* **2021**, *12*, 4632–4642.

[15] M. Morton, L. J. Fetters, *J Polym Sci A* **1964**, *2*, 3311–3326.

[16] S. Bywater, D. J. Worsfold, *Can J Chem* **1962**, *40*, 1564–1570.

[17] S. P. Wadgaonkar, S. Schüttner, E. Berger-Nicoletti, A. H. E. Müller, H. Frey, *Macromolecules* **2022**, *55*, 4721–4732.

[18] V. S. Khotimskii, V. G. Filippova, I. S. Bryantseva, V. I. Bondar, V. P. Shantarovich, Y. P. Yampolskii, *J Appl Polym Sci* **2000**, *78*, 1612–1620.

[19] A. C. Puleo, N. Muruganandam, D. R. Paul, *J Polym Sci B Polym Phys* **1989**, *27*, 2385–2406.

[20] Y. Nagasaki, Y. Hashimoto, M. Kato, T. Kimijima, *J Memb Sci* **1996**, *110*, 91–97.

[21] Y. Vignollet, J. C. Maire, M. Witanowski, *Chem. Commun. (London)* **1968**, *0*, 1187–1187.

[22] L. D. Freedman, H. Tauber, G. O. Doak, H. J. Magnuson, *J Am Chem Soc* **1953**, *75*, 1379–1381.

[23] T. Ishizone, A. Hirao, S. Nakahama, *Macromolecules* **1993**, *26*, 6964–6975.

[24] J. Nagy, J. Réffy, *J Organomet Chem* **1970**, *22*, 565–572.

[25] M. Steube, T. Johann, M. Plank, S. Tjaberings, A. H. Gröschel, M. Gallei, H. Frey, A. H. E. Müller, *Macromolecules* **2019**, *52*, 9299–9310.

[26] J. E. Mark, *Polymer Data Handbook*, **1999**.

[27] J. D. Cushen, L. Wan, G. Pandav, I. Mitra, G. E. Stein, V. Ganesan, R. Ruiz, C. G. Willson, C. J. Ellison, *J Polym Sci B Polym Phys* **2014**, *52*, 36–45.

[28] V. Jaacks, *Angewandte Chemie* **1967**, *79*, 419–419.

[29] V. Jaacks, *Makromol Chem* **1972**, *161*, 161–172.

[30] V. E. Meyer, G. G. Lowry, *J Polym Sci A* **1965**, *3*, 2843–2851.

[31] N. Kazemi, T. A. Duever, A. Penlidis, *Macromol React Eng* **2011**, *5*, 385–403.

[32] F. L. M. Hautus, A. L. German, H. N. Linssen, *J Polym Sci, Polym Lett Ed* **1985**, *23*, 311–315.

[33] K. Sardelis, H. J. Michels, G. Allen, F.R.S., *Polymer (Guildf)* **1984**, *25*, 1011–1019.

[34] V. D. Mochel, *Rubber Chem Technol* **1967**, *40*, 1200–1211.

[35] T. E. Hogan, W. Kiridena, L. Kocsis, *Rubber Chem Technol* **2017**, *90*, 325–336.

[36] D. L. Handlin, Block Copolymer US 6,699,941 B1, US 6,699,941 B1 to Kraton Polymers U.S. LLC, **2004**.

[37] C. Wahlen, J. Blankenburg, P. Von Tiedemann, J. Ewald, P. Sajkiewicz, A. H. E. Müller, G. Floudas, H. Frey, *Macromolecules* **2020**, *53*, 10397–10408.

[38] D. J. Worsfold, S. Bywater, *Can J Chem* **1964**, *42*, 2884–2892.

[39] T. A. Antkowiak, A. E. Oberster, A. F. Halasa, D. P. Tate, *J Polym Sci A1* **1972**, *10*, 1319–1334.

[40] C. A. Uraneck, *J Polym Sci A1* **1971**, *9*, 2273–2281.

[41] Y. Kawakami, H. Karasawa, T. Aoki, Y. Yamamura, H. Hisada, Y. Yamashita, *Polym J* **1985**, *17*, 1159–1172.

[42] J. M. Widmaier, G. C. Meyer, *Macromolecules* **1981**, *14*, 450–452.

[43] C. Rüttiger, M. Appold, H. Didzoleit, A. Eils, C. Dietz, R. W. Stark, B. Stühn, M. Gallei, *Macromolecules* **2016**, *49*, 3415–3426.

[44] L. Zhang, Y. Luo, Z. Hou, *J Am Chem Soc* **2005**, *127*, 14562–14563.

[45] X. Jia, X. Zhang, D. Gong, *J Polym Sci A Polym Chem* **2018**, *56*, 2286–2293.

[46] J. N. Owens, I. S. Gancarz, J. T. Koberstein, T. P. Russell, *Macromolecules* **1989**, *22*, 3380–3387.

[47] J. D. Cushen, C. M. Bates, E. L. Rausch, L. M. Dean, S. X. Zhou, C. G. Willson, C. J. Ellison, *Macromolecules* **2012**, *45*, 8722–8728.

Supporting Information

Effect of THF on the Anionic Copolymerization of 4-Trimethylsilylstyrene with Isoprene

Dominik A. H. Fuchs, [redacted]

1. Materials and experimental procedure

1.1 Materials

All chemicals were purchased from the following suppliers: Sigma-Aldrich, Thermo Fisher Scietific Inc, Acros, VWR International and Deutero GmbH. The monomers were chromatographed over basic alumina to remove stabilizers and dried in various ways (see ESI) before use. Argon 5.0 was used as an inert gas and purified through three gas wash bottles containing *sec.* BuLi, diphenylethylene and cyclohexane.

1.2 Instrumentation

NIR set up and data evaluation has been described in previous publications.[1] SEC was performed using an Agilent 1260 Infinity II set up with MZ-Gel SDPlus plus $10^5/10^3/100$ Å columns in THF and an RI detector (MZ-Analysetechnik, Mainz, Germany), the calibration was carried out by using PS standards. NMR spectra were obtained using a Bruker Avance III 600 spectrometer at 600 MHz for ^{1}H NMR and 151 MHz for ^{13}C NMR. Differential scanning calorimetry (DSC) thermal analysis was performed using a TA Instruments DSC 250 instrument connected to a TA Instruments RCS 90 refrigeration system, both from Waters Corporation, USA. Thermogravimetric analysis (TGA) was performed on a Mettler Toledo TGA 2 Star System in Alumina 70 µL crucible under 60.0 ml/min N_2 atmosphere. The sample was annealed at 30°C for 10 minutes, heated to 800°C at a heating rate of 10 K/min and annealed at 800°C for 20 minutes.

1.3 Monomer Synthesis

TMSS was synthesized by a one-step Grignard reaction of 4-chlorostyrene with chloro(trimethyl)silan as the electrophile, as previously described by S. P. Wadkaonkar *et al.*.[2]

1.4 Copolymerizations

TMSS was copolymerized with isoprene in the presence of various amounts of polar modifier THF. The general procedure is described here.

1.4.1 Purification of materials

All reactions and drying processes were carried out under Schlenk conditions. The used glassware was three times flame dried under high vacuum (10^{-3} mbar) prior to use and a pressure valve always maintained a constant overpressure of 50 mbar Argon. Isoprene was filtered through a column containing basic alumina to remove the stabilizer. Bothe monomers TMSS and I were dried over CaH_2 for a day, degassed by three freeze thaw cycles and cryo-transferred into another flask containing $Al(Oct)_3$ and again stirred for a day. The following day the monomer mixture was again cryo-transferred into a graduated ampoule, which always showed a loss of less 2 $\%_{Vol}$ in respect to the combined volume of the monomers. This loss is explained by partial auto polymerization due to heating during the cryo-transfer. Cyclohexane was dried under reflux with sodium and benzophenone. After a few days the former colorless solution changes to dark blue indicating absence of water. The solvent was transferred into the reaction flask (Morton flask glass reactor), equipped with a NIR probe, a temperature probe, and an additional glass joint. THF was dried with *sec.* BuLi in a small excess of 1,1-diphenylethylene (DPE), to avoid side reactions. After the red color remained, THF was prior to every use cryo-transferred and diluted with dry cyclohexane.

1.4.2 Copolymerization in the presence of polar modifiers

All polymerizations were carried out under the same conditions, solely the amount of modifier varies. As an example, the synthesis of P($TMSS_{0.3}$-*co*-$I_{0.7}$) with a modifier content of [THF]/[Li] = 20 is described. After the previous dried monomers (9.42 ml, 0.094 mol isoprene and 7.98 ml, 0.04 mol TMSS) were cryo-transferred into an ampoule and 80 ml dried cyclohexane and 0.27 ml dried THF were added into the reaction flask. After flame drying the joint the NIR baseline was recorded using Omnic and the monomers were added. The reaction was initiated via 0.13 ml (0.17 mmol, 1 eq) of a 1.3 molar solution of *sec.* BuLi in cyclohexane/hexane (92:8), which resulted in a color change from colorless to dark yellow, indicating the favored carbanionic polymerization of TMSS. After 700 minutes the intensity of the NIR signal at 6038 cm^{-1} does not change any further and the

copolymerization is completed. The reaction was terminated by the addition of 1 ml degassed isopropanol in argon counterflow and the polymer precipitated in 1L of a mixture 1:3 isopropanol:methanol. The colorless polymer was dried under reduced pressure for several days and stored at -20°C.

To maintain a reaction temperature of around 20 °C was a cryostat used to dissipate the reaction heat, which increased with increasing modifier content. For all copolymerizations the reaction temperature did not increase further than 10°C. However, previous works showed that the effect of temperature on the reactivity ratios is significantly less than that caused by the modifier. [1,3]

2 Molecular weight distributions

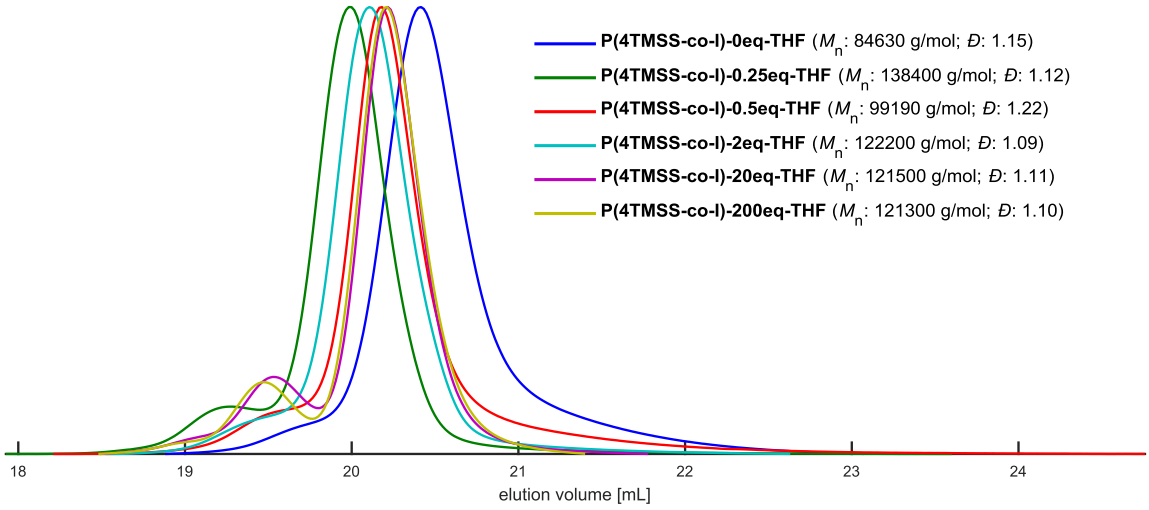

Figure S1: SEC (THF) traces of P($TMSS_{0.3}$-*co*-$I_{0.7}$) with different modifier to initiator ratios and PS calibration.

The targeted molecular weight for all copolymerizations was 80 kg/mol. The deviations are partly explained by the SEC-calibration with PS standards. PS calibration overestimates the molecular weight of a PI sample by about 10%. [3] No literature values are known for PTMSS, but due to the higher free volume, it is also expected to be overestimated. The SEC traces show a narrow molecular weight distribution, with a small shoulder at lower elution volumes (higher molecular weights), which is explained by oxygen coupling during the termination.

3 Copolymerization kinetics and determination of reactivity ratios:

The measured molar NIR attenuation coefficients spectra (4TMSS, P(4TMSS) and I) are used to calculate the missing PI spectra which depends on the microstructure of PI and therefore must be calculated for every reaction. Which works as follows: First the concentrations of monomers must be calculated by a deconvolution. Then the end spectra is taken and a PS spectra with the previous calculated concentration of styrene is subtracted and after multiplying it with the inverse concentration of isoprene the PI spectra is generated.

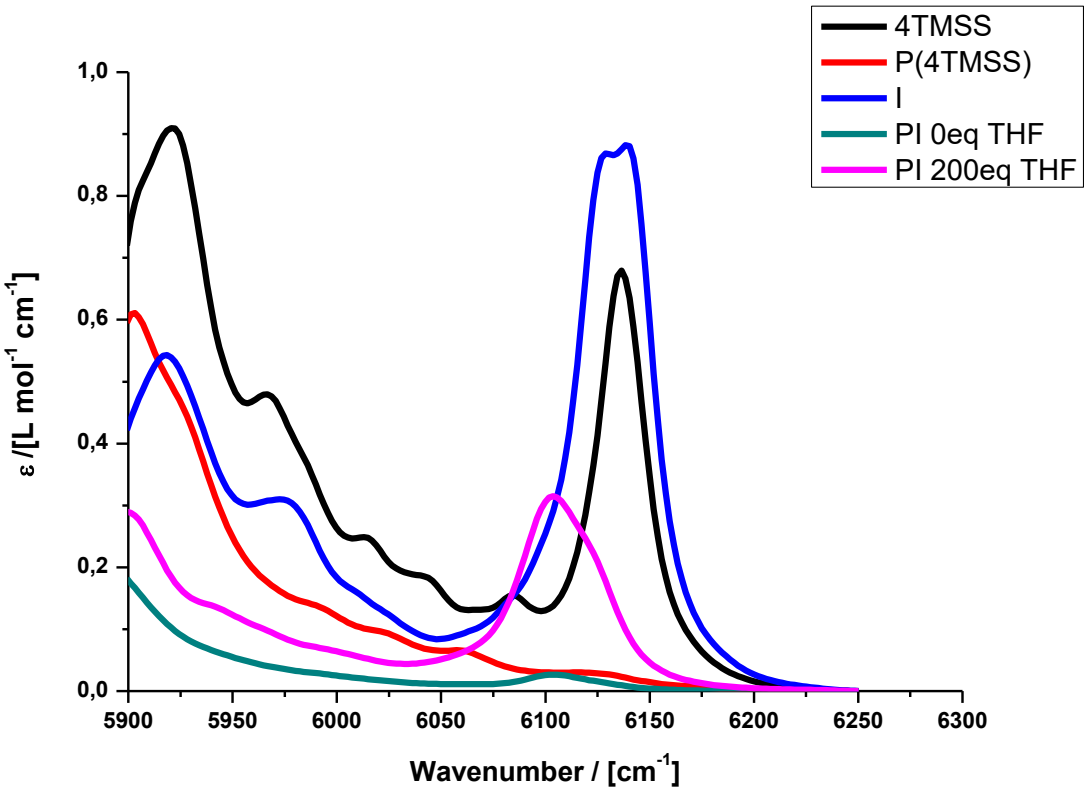

***Figure S2**:* Measured molar NIR attenuation coefficients of all species present in the reaction. The PI spectra are calculated.

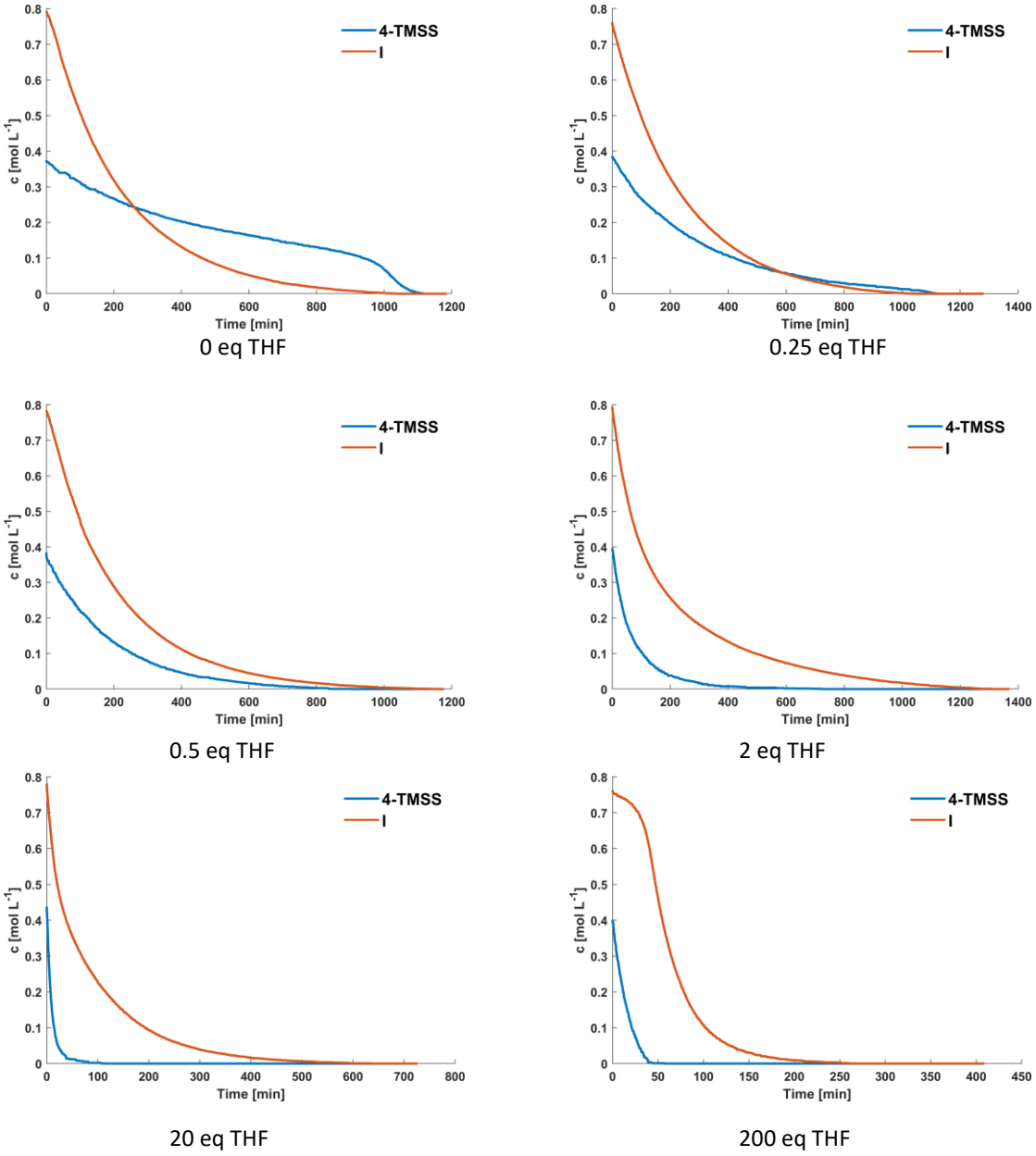

***Figure S3**:* Individual time-conversion plots at various THF contents.

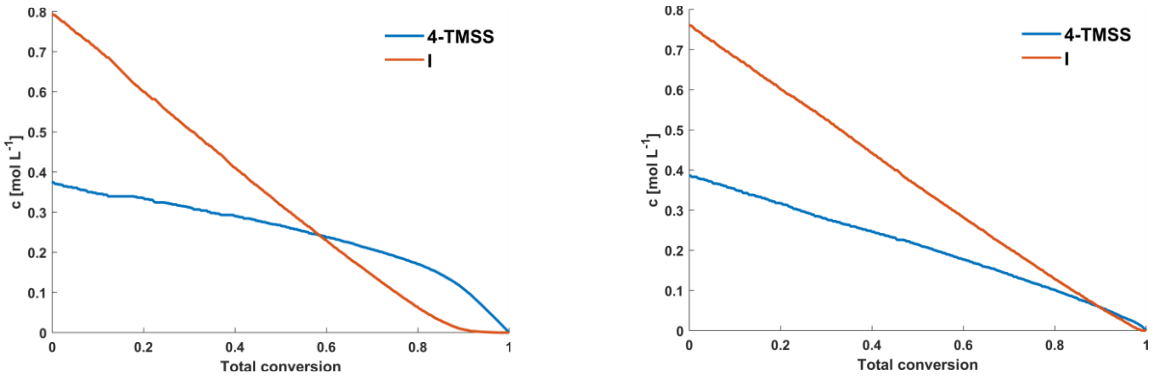

0 eq THF

0.25 eq THF

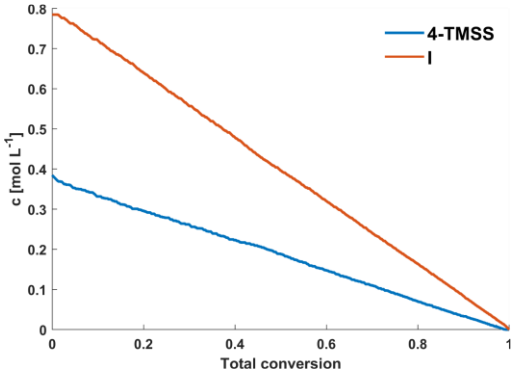

0.5 eq THF

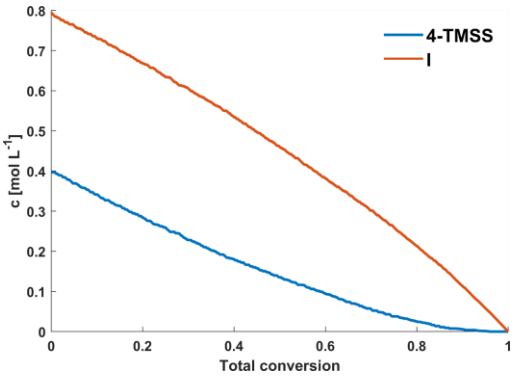

2 eq THF

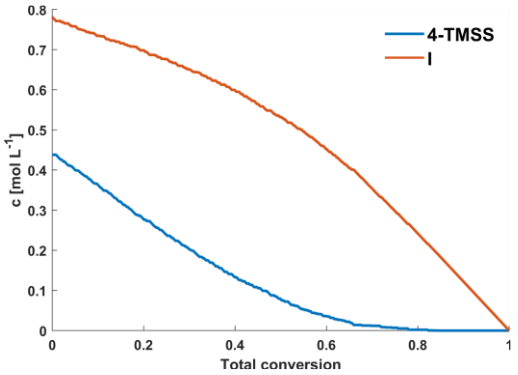

20 eq THF

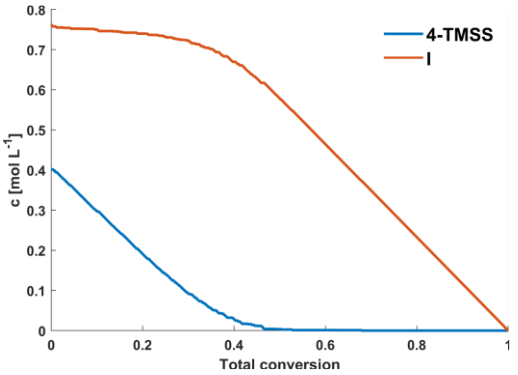

200 eq THF

***Figure S4**:* Individual monomer concentrations as a function of total conversion for different modifier contents.

3.1 Determination of reactivity ratios.

The reactivity ratios r_{TMSS} and r_I are calculated using both the terminal (Jaacks plot[4,5]) and non-terminal model (Meyer and Lowry[6]). The non-terminal model assumes an ideal copolymerization ($r_1 \cdot r_2 = 1$). If the linear plot according to this model is assumed to be valid, this model is preferred compared to the more complex non-terminal model, which tends to overfitting problems.[7] Else, a numerical fit to a plot according to Meyer and Lowry[6] is used to calculate r_1 and r_2 independently.

The determination of the reactivity ratios was calculated in the linear regime of the individual vs total conversion plots, until almost full conversion of the first monomer. The last 5 to 10% of the copolymerization was not considered, as these data are more strongly influenced by background noise and unstable baselines.

***Table S1**:* Reactivity ratios determined by different models of P($TMSS_{0.3}$-*co*-$I_{0.7}$) at various [THF]/[Li] ratios. The used values are printed in bold.

[THF]/[Li]	*Jaacks*				*Meyer-Lowry*				
	r_{TMSS}	Δr_{TMSS}	r_I	Δr_I	r_{TMSS}	Δr_{TMSS}	r_I	Δr_I	$r_{TMSS}r_I$
0	0.29	0.0005	3.40	0.006	**0.066**	**0.001**	**2.37**	**0.005**	**0.16**
0.25	**0.74**	**0.0004**	**1.36**	**0.0008**	0.19	0.01	0.87	0.008	0.17
0.5	**1.09**	**0.0004**	**0.92**	**0.0004**	-[a]	-	-	-	-
2	**2.04**	**0.001**	**0.49**	**0.0003**	1.44	0.02	0.40	0.0003	0.58
20	**4.52**	**0.01**	**0.22**	**0.0007**	4.0	0.1	0.22	0.0007	0.88
200	**22.9**	**0.2**	**0.04**	**0.003**	52	2	0.22	0.01	11.4

[a] no fit possible

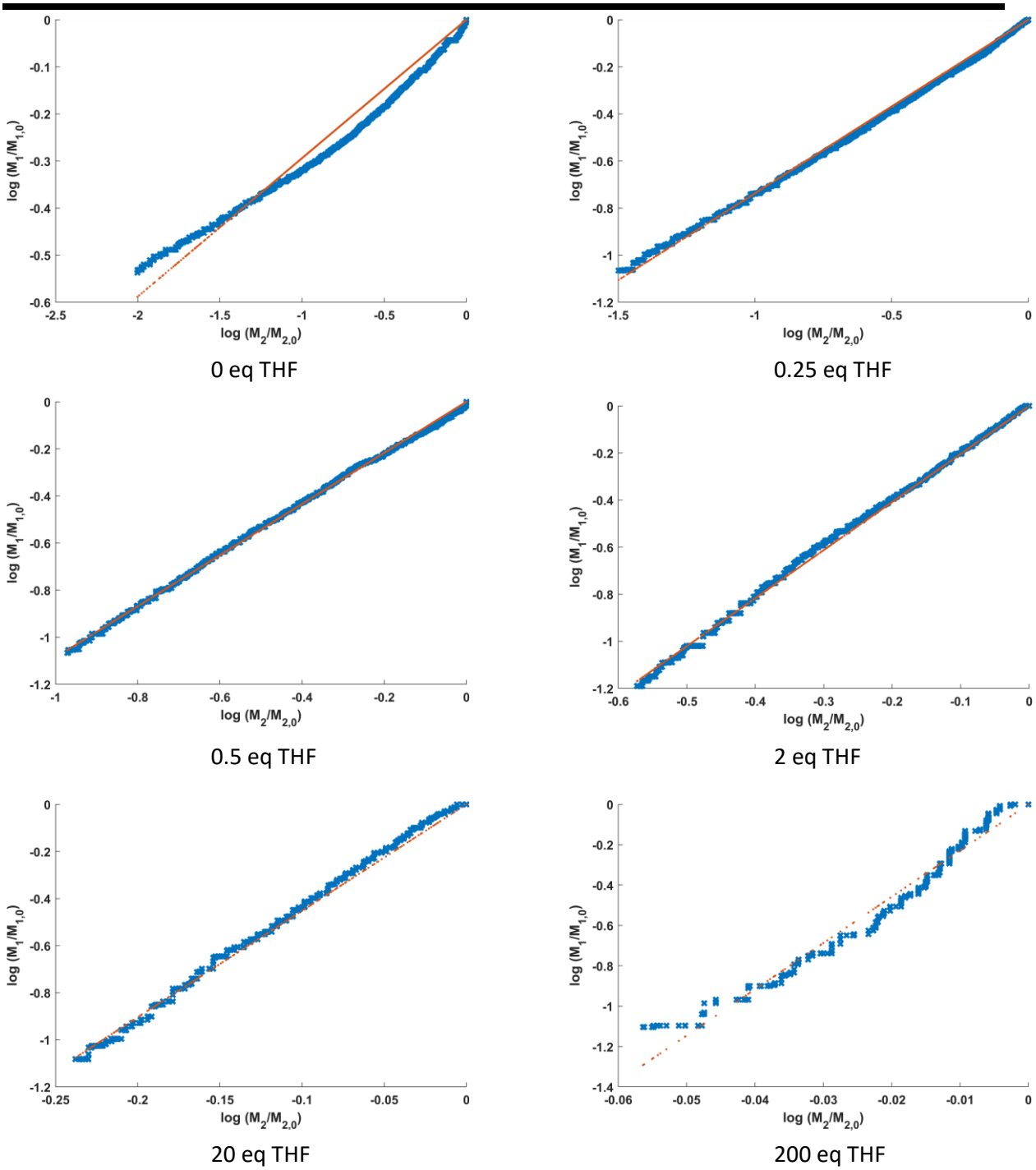

Figure* S5:* Jaacks fit (red line) of the copolymerization of P($TMSS_{0.3}$-*co*-$I_{0.7}$) with different amounts of modifier.

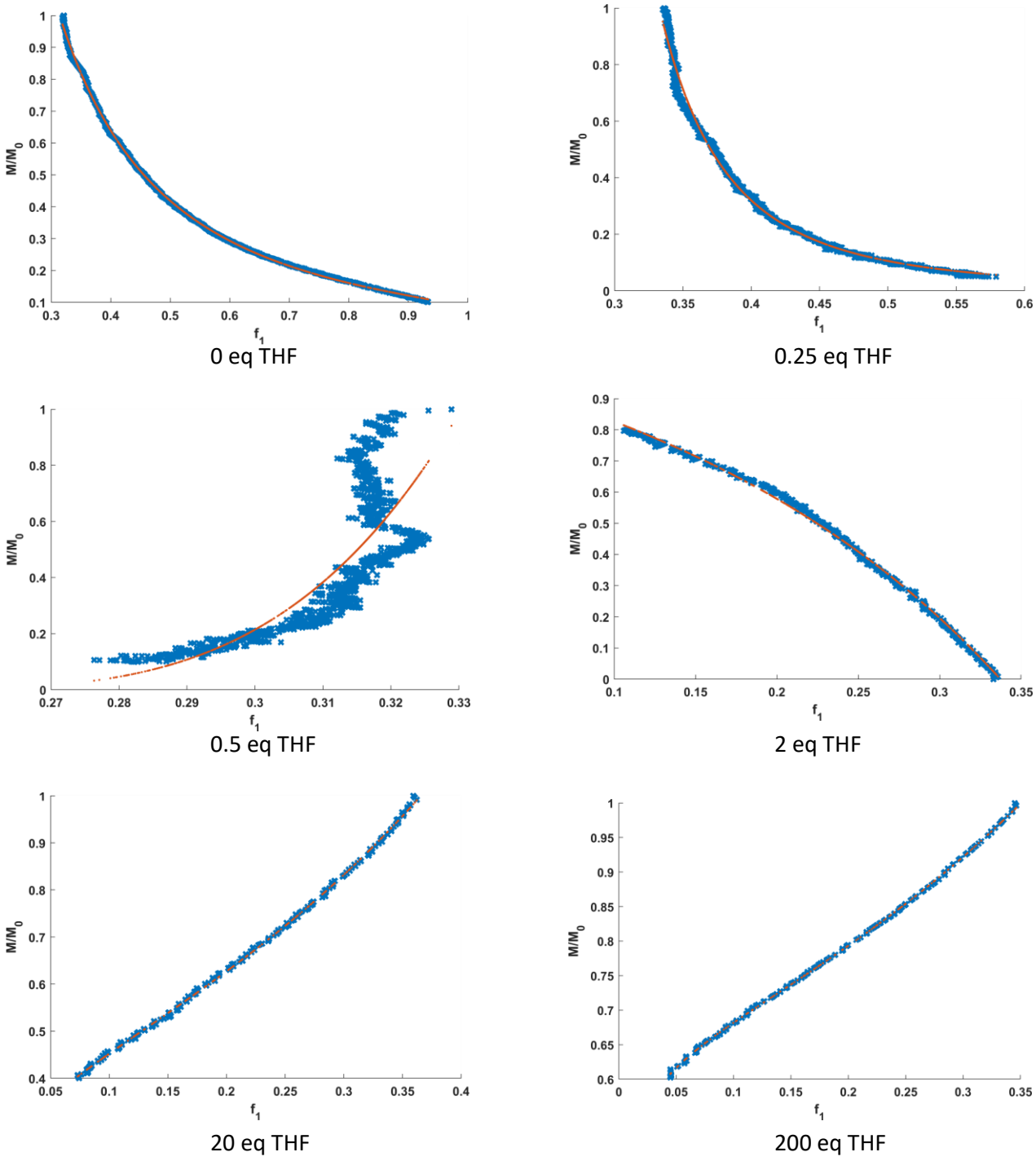

***Figure S6**:* Meyer-Lowry fit (red line) of the copolymerization of P($TMSS_{0.3}$-*co*-$I_{0.7}$) with different amounts of modifier.

4 Copolymer Composition

a. Volume composition profiles

Diagrams of the molar and volume compositions of the copolymer P($TMSS_{0.3}$-*co*-$I_{0.7}$) are shown in Figure 2. To calculate the volume compositions, both axes are weighted by the molecular weight and the density of the homopolymers, ρ_{PI} = 0.91 g/ml and $\rho_{P(TMSS)}$ = 0.963 g/ml.[8]

b. Blockiness

As an addition to the NIR based composition diagrams, the so-called blockiness of the TMSS units was investigated. [9–12] This relays on the following effect: the magnetic field of the NMR induces a ring current in the phenyl rings, which enhance the applied field at the edges of the ring. This effect affects all phenyl protons but especially the *ortho* protons, which are closer to the neighboring rings then the *meta* ones. In consequence the *ortho* protons are shifted high-field, as can be seen in Figure 3. In a block copolymer the *ortho* signal is between 6.85-6.00 ppm, but in a random copolymer the signal is shifted low-field to 7.20-6.85 ppm.[2] Both signals are always separated from the *meta* protons but have significant overlap among themselves.

To calculate the blockiness the ratio of all aromatic protons 7.60-6.00 ppm (I_1; 4 protons) and 6.85-6.00 ppm (I_2; 2 protons) is used:[9,13]

$$B = \frac{I_1/4}{I_2/2}$$

The results of the blockiness study (Table 1) are in good agreement with the kinetic data obtained by NIR (Table 1). The blockiness decreases from 27 to 2% from 0 to 0.5 eq THF and then increases again to 41% for 200 eq THF. For 0.5 eq THF we have a minimum on block structures and an almost ideal statistical copolymerization (r_{TMSS} = 1.09; r_I = 0.92) and with increasing modifier content the blockiness increases again.

5 Microstructure of PI monomer units

The determination of the polyisoprene microstructure is done via ^{1}H-NMR. The previous by Steube *et al*. introduced determination method ($^{13}C_{ig}$) is not suitable for this system since there is an overlap of the aromatic C (h) with the C (n) of the 1,4-microstructure triads. Additionally, the $^{13}C_{ig}$ Method has some flaws: the T_1 time was not determined and the signal to noise ratio is very low.

The ^{1}H-, ^{13}C-, COSY-, HSQC- and HMBC- spectra for 0 and 200 eq THF is shown in the following figures:

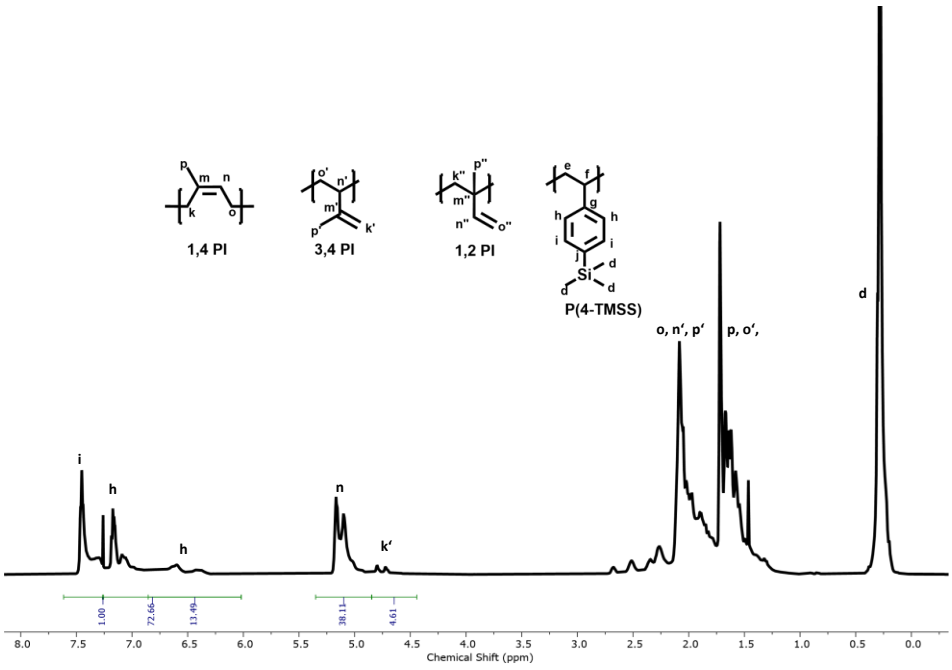

***Figure S7**:* Assigned ^{1}H-NMR spectra of the copolymer P($TMSS_{0.3}$-*co*-$I_{0.7}$) synthesized with 0 eq THF.

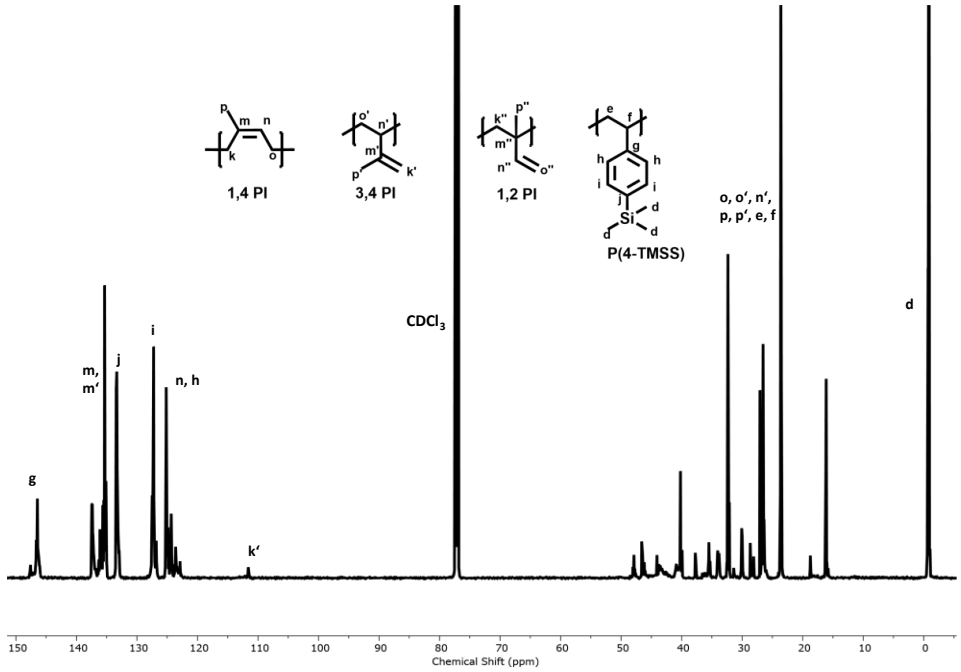

***Figure S8**:* Assigned ^{13}C-NMR spectra of the copolymer P(TMSS$_{0.3}$-*co*-I$_{0.7}$) synthesized with 0 eq THF.

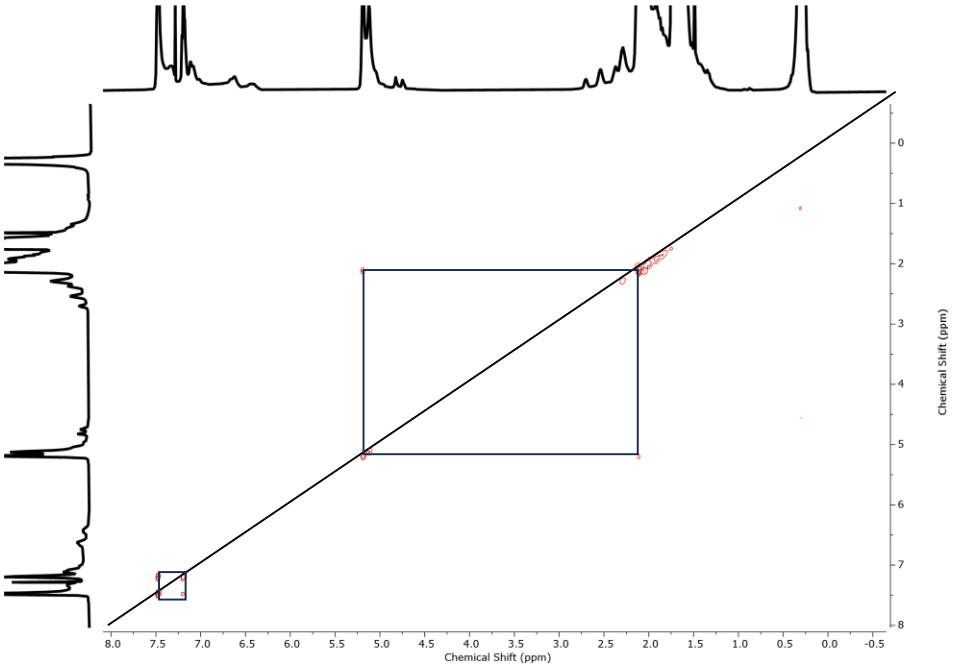

***Figure S9**:* Assigned COSY-NMR spectra of the copolymer P(TMSS$_{0.3}$-*co*-I$_{0.7}$) synthesized with 0 eq THF.

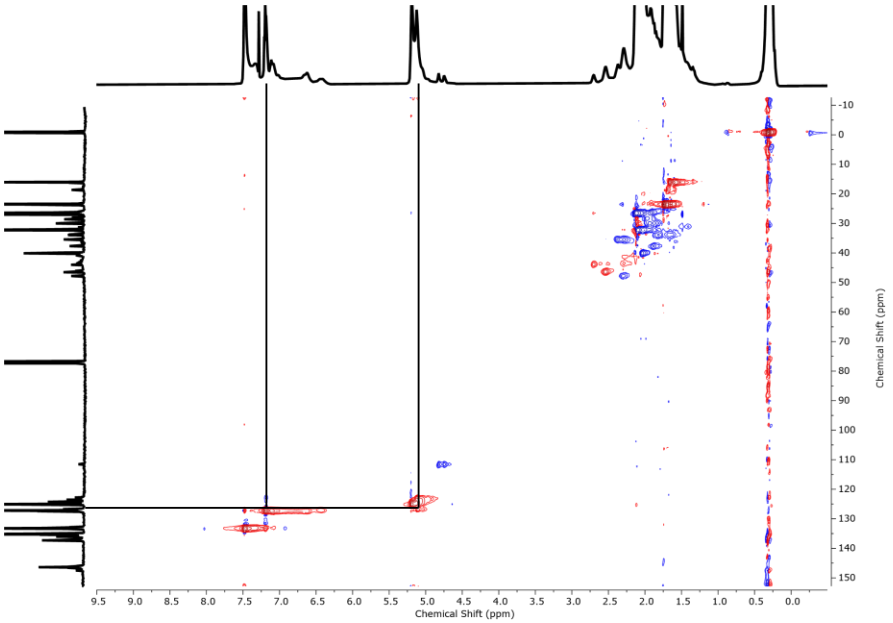

***Figure S10**:* Assigned HSQC-NMR spectra of the copolymer P($TMSS_{0.3}$-*co*-$I_{0.7}$) synthesized with 0 eq THF.

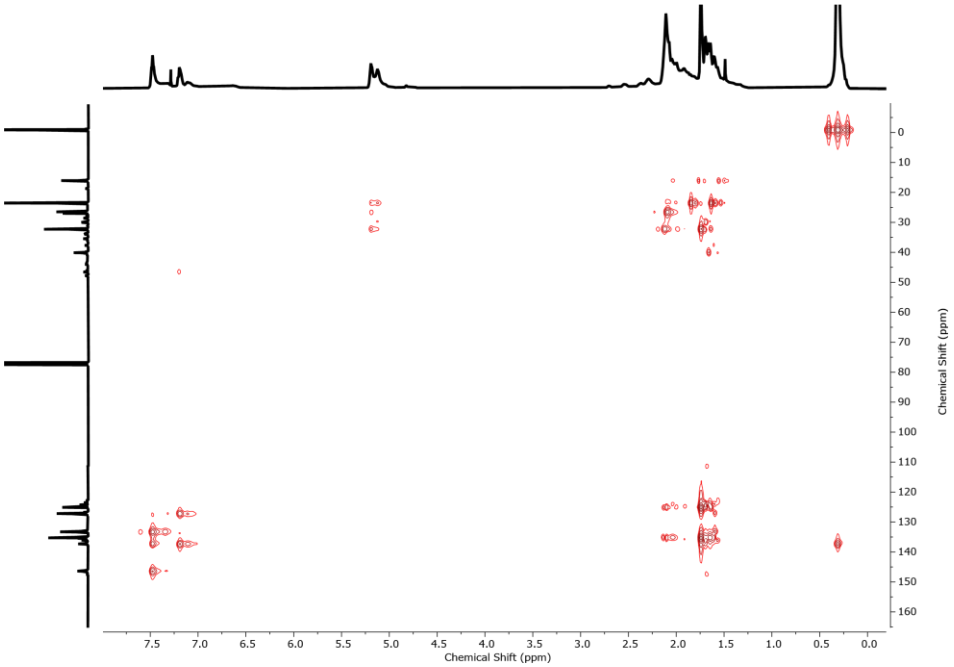

***Figure S11**:* Assigned HMBC-NMR spectra of the copolymer P($TMSS_{0.3}$-*co*-$I_{0.7}$) synthesized with 0 eq THF.

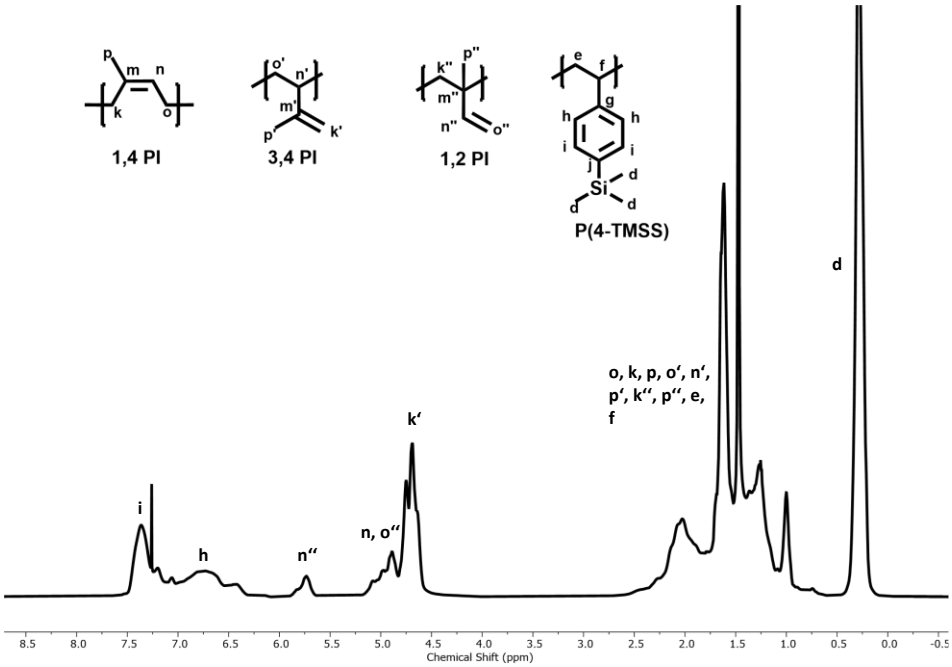

***Figure S12**:* Assigned ^{1}H-NMR spectra of the copolymer P($TMSS_{0.3}$-*co*-$I_{0.7}$) synthesized with 200 eq THF.

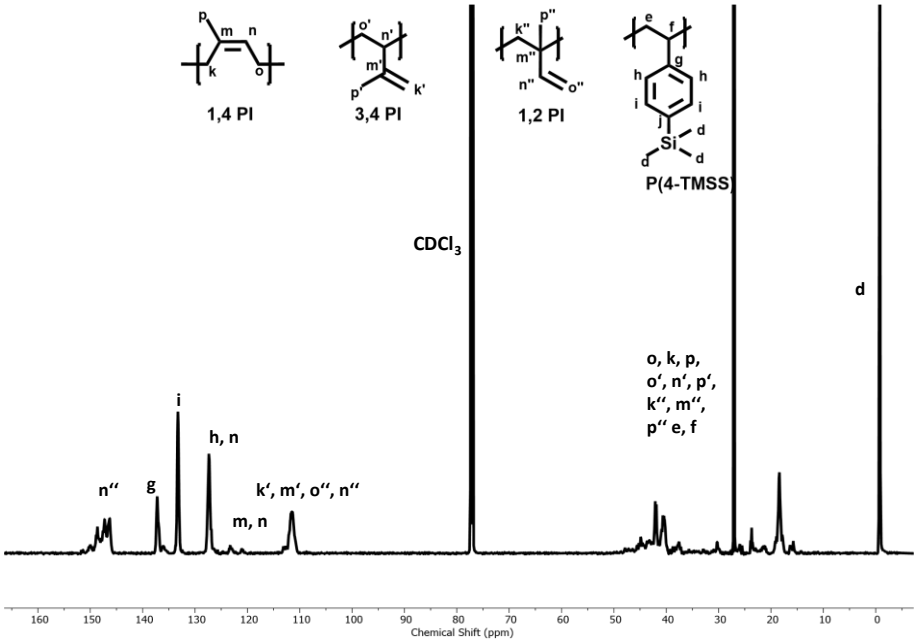

***Figure S13**:* Assigned ^{13}C-NMR spectra of the copolymer P($TMSS_{0.3}$-*co*-$I_{0.7}$) synthesized with 200 eq THF.

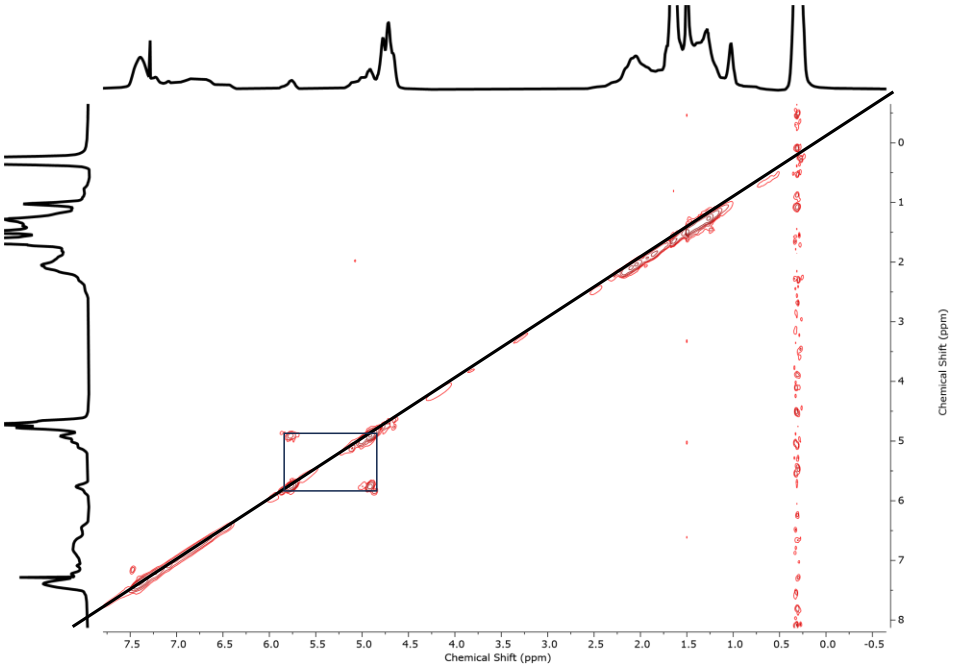

***Figure S14**:* Assigned COSY-NMR spectra of the copolymer P($TMSS_{0.3}$-*co*-$I_{0.7}$) synthesized with 200 eq THF.

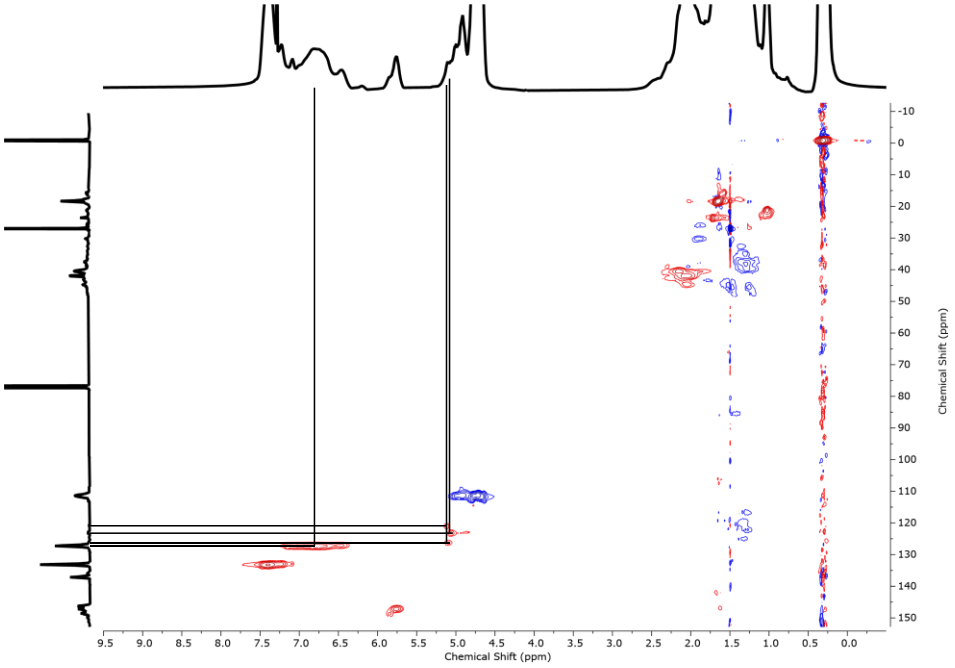

***Figure S15**:* Assigned HSQC-NMR spectra of the copolymer P($TMSS_{0.3}$-*co*-$I_{0.7}$) synthesized with 200 eq THF.

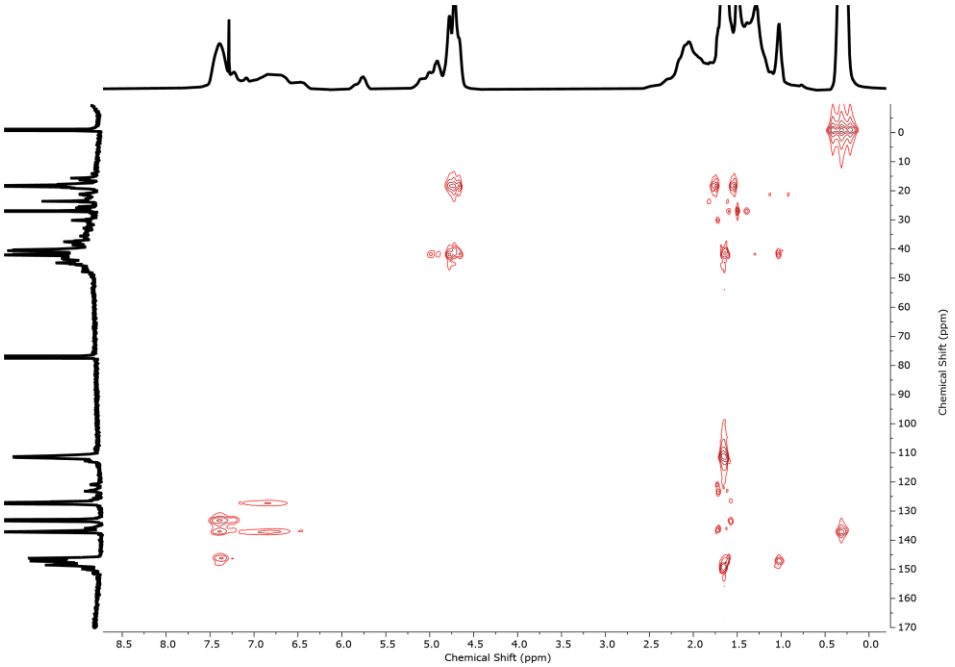

***Figure S16**:* Assigned HMBC-NMR spectra of the copolymer P($TMSS_{0.3}$-*co*-$I_{0.7}$) synthesized with 200 eq THF.

An overview over all ^{1}H-NMR spectra is shown in Figure 3. With increasing modifier content, the 1,2- and 3,4- units increase at the expense of 1,4-. For the determination of the microstructures the following signals are used: 5.91-5.59 (n''), 5.30-4.85 (n, o'') and 4.85-4.00 (k')

For the determination of the 1,2-units the integral of n'' is used and for the 3,4-units is the integral of k' used. But for the calculation of the 1,4 units the signals of n and o'' are overlapping, but since n'' is known and I(n'') = 2*I(o'') it can be calculated:

$$I_{1,2} = I(5.91 - 5.59)$$

$$I_{3,4} = I(4.85 - 4.00)$$

$$I_{1,4} = I(5.30 - 4.85) - 2 * I_{1,2}$$

$$C_{1,2} = \frac{I_{1,2}}{I_{1,2} + I_{3,4} + I_{1,4}}$$

$$C_{3,4} = \frac{I_{3,4}}{I_{1,2} + I_{3,4} + I_{1,4}}$$

$$C_{1,4} = \frac{I_{1,4}}{I_{1,2} + I_{3,4} + I_{1,4}}$$

C stands for the content of the represented microstructure in the polymer. Due to partially overlap of the signals the integral limits depend on the experimenter and the microstructure is subject to error. The values are in good agreement with literature, [3] slight differences are explained by experimental error, different reaction temperature[1,14],

different monomer- and chain end concentrations and an increased polarity by the TMSS comonomer.[15–17]

6 Thermal properties

The following Figure show an overlay of the second heating cycle of the copolymers P(TMSS$_{0.3}$-*co*-I$_{0.7}$), at a heating rate of 10K/min.

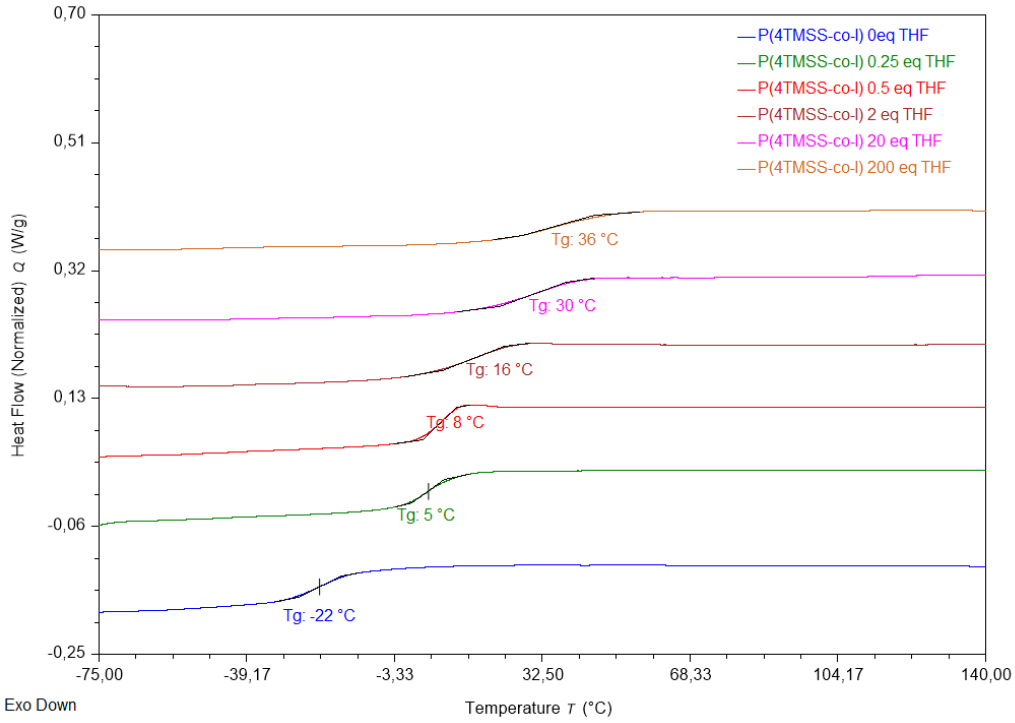

***Figure S17**:* Overlay of the second heating cycles of P(TMSS$_{0.3}$-*co*-I$_{0.7}$) synthesized with various amounts of THF, from -75 to 140°C with a heating rate of 10K/min and an indium and octane calibration.

7 Polymer film

To prove the polymers potential use in membranes a stable film was cast from $CHCl_3$.

***Figure S18**:* Polymer film of P($TMSS_{0.3}$-*co*-$I_{0.7}$) synthesized with 0 eq THF, casted from $CHCl_3$.

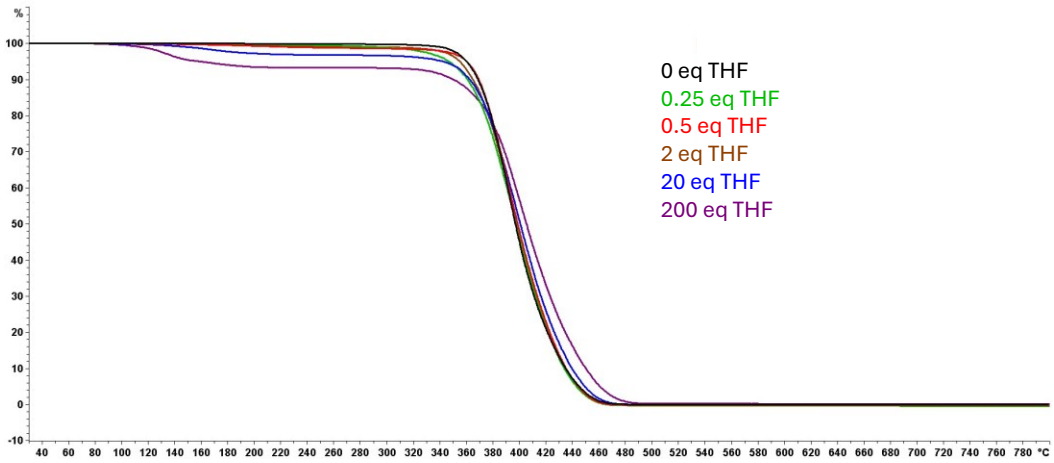

Figure S 19: Thermogravimetric analysis (TGA) of P($TMSS_{0.3}$-*co*-$I_{0.7}$) synthesized with different amounts of THF as randomizer under N_2 atmosphere with a heating rate of 10 K/min. The mass loss between 100 to 200°C for 20 and 200eq THF is attributed to residual solvent.

References

[1] M. Steube, T. Johann, M. Plank, S. Tjaberings, A. H. Gröschel, M. Gallei, H. Frey, A. H. E. Müller, Macromolecules 2019, 52, 9299–9310.

[2] S. P. Wadgaonkar, S. Schüttner, E. Berger-Nicoletti, A. H. E. Müller, H. Frey, Macromolecules 2022, 55, 4721–4732.

[3] M. Steube, T. Johann, H. Hübner, M. Koch, T. Dinh, M. Gallei, G. Floudas, H. Frey, A. H. E. Mül-ler, Macromolecules 2020, 53, 5512–5527.

[4] V. Jaacks, Angewandte Chemie 1967, 79, 419–419.

[5] V. Jaacks, Makromol Chem 1972, 161, 161–172.

[6] V. E. Meyer, G. G. Lowry, J Polym Sci A 1965, 3, 2843–2851.

[7] D. M. Hawkins, J Chem Inf Comput Sci 2004, 44, 1–12.

[8] M. Harada, T. Suzuki, M. Ohya, D. Kawaguchi, A. Takano, Y. Matsushita, Macromolecules 2005, 38, 1868–1873.

[9] D. L. Handlin, D. T. Williamson, C. L. Willis, US 6,699,941 B1 Block Copolymer, 2004.

[10] K. Sardelis, H. J. Michels, G. Allen, F.R.S., Polymer (Guildf) 1984, 25, 1011–1019.

[11] V. D. Mochel, Rubber Chem Technol 1967, 40, 1200–1211.

[12] T. E. Hogan, W. Kiridena, L. Kocsis, Rubber Chem Technol 2017, 90, 325–336.

[13] V. D. Mochel, Macromolecules 1969, 2, 537–540.

[14] C. A. Uraneck, J Polym Sci A1 1971, 9, 2273–2281.

[15] H. Hsieh, R. P. Quirk, Anionic Polymerization, CRC Press, 1996.

[16] M. Morton, E. E. Bostick, R. A. Livigni, L. J. Fetters, J Polym Sci A 1963, 1, 1735–1747.

[17] M. Morton, L. J. Fetters, J Polym Sci A 1964, 2, 3311–3326.

Chapter 3

Dramatic Effect of Alkali Metal Alkoxides on the Anionic Copolymerization of Styrene and Isoprene

Dominik A. H. Fuchs, [redacted]

Department of Chemistry, Johannes Gutenberg University Mainz, Duesbergweg 10-14, 55128 Mainz, Germany.

Submitted to *Macromolecules*

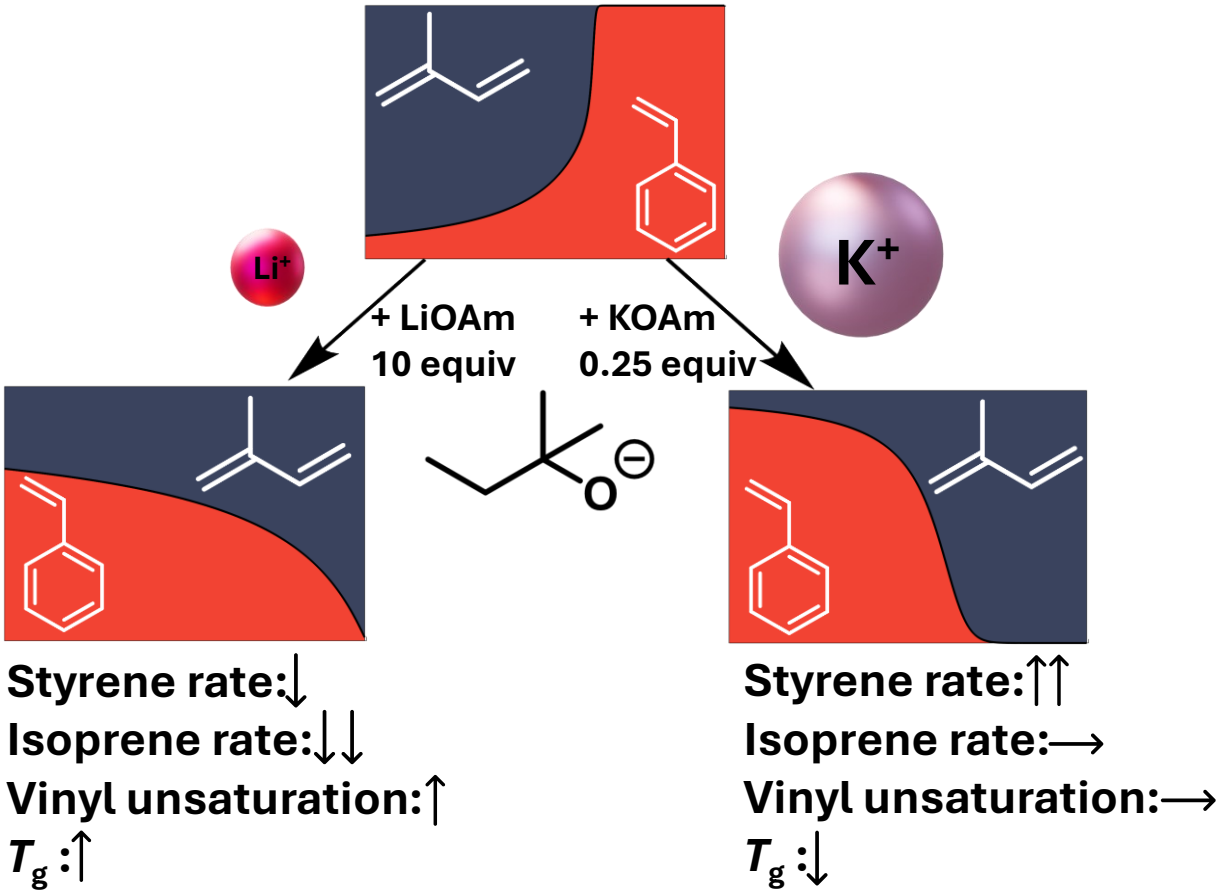

ABSTRACT: The effect of lithium-, sodium- and potassium *tert*-amylates on the kinetics of the statistical anionic copolymerization of styrene and isoprene in cyclohexane was investigated using *in-situ* near-infrared (NIR) spectroscopy. The reactivity ratios and the related comonomer gradients can be adjusted over the entire range resulting in both random and inverted gradient copolymers. Lithium *tert*-amylate retards the polymerization at over-stoichiometric concentrations. In contrast, even at low concentrations sodium and potassium *tert*-amylate increase the rate of styrene polymerization due to a counterion exchange. Only 1/30 equivalents potassium *tert*-amylate relative to butyllithium are necessary to obtain random copolymers, which unexpectedly consist of short blocks. Remarkably, a high content of isoprene 1,4-units is maintained leading a low glass transition temperature of -55 °C of random or inversely tapered poly(styrene-*co*-isoprene). Thus, in contrast to Lewis base modifiers, the diene microstructure can be decoupled from reaction kinetics, when potassium alkoxides are used.

Introduction

Living anionic polymerization, discovered by Szwarc in 1956, enables the synthesis of a wide range of well defined (multi) block copolymers.[1] Although this polymerization technique places high demands on the purity of both monomers and solvents, it has been used for the synthesis of thermoplastic elastomers (TPEs) for a long time. [2–4] These phase-separated materials consist of at least three different blocks in an ABA structure, where polymer A is a block with a high glass transition temperature, T_g, usually styrene (S), and the midblock B is a highly flexible polymer with a low T_g, usually a poly(1,3-diene), commonly based on butadiene (B) or isoprene (I).[5–7] A large variety of products are synthesized from the combination of styrene and diene by changing polymer architecture, composition, molecular weight and microstructure of the diene. Biobased and specialized monomers have also been used to synthesize (block)copolymers with tailored properties for high-performance materials.[6–14] Here, block copolymers are synthesized by a stepwise addition of the individual monomers.

Very early it was discovered that the statistical copolymerization of styrene and dienes initiated by butyllithium (BuLi) in non-polar solvents leads to "tapered" copolymers displaying similar properties as block copolymers. [2–4] In these solvents the diene polymerizes first and most of the styrene is incorporated after complete consumption of the diene. This translates to disparate reactivity ratios $r_S = 0.05$; $r_B = 15$ and $r_S = 0.013$; $r_I = 10.1$ for the S/B[15,16] and S/I[17] system, respectively, resulting in strong gradient copolymers.[2,3] The reason for these strong differences in the reactivity ratios are large discrepancies in the crossover rates, $k_{SI} >> k_{IS}$.[18,19]

Scheme 1: Aggregation of polystyryllithium in apolar solvents and the effect of Lewis bases (example: THF) on the aggregation equilibrium.[20]

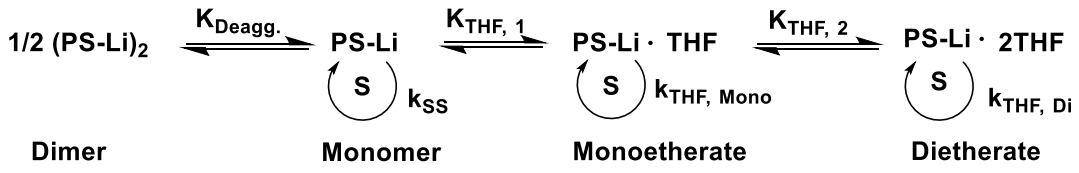

In apolar solvents, such as cyclohexane, the living, lithiated polymer chain ends form inactive dimers in equilibrium with the non-aggregated chains, acting as polymerization centers (Scheme 1).[15,16,21–24] The addition of polar additives, so called modifiers, breaks up

the aggregates and increases the reactivity of the comonomers to different extents. Typical modifiers are Lewis bases like methyl-*tert*-butylether (MTBE), THF, 2,2-di(2-tetrahydrofuryl)propane (DTHFP) or amines like tetramethylethylenediamine (TMEDA).[25–27] By using increasing equivalents (equiv) of these modifiers with respect to the butyllithium initiator, the reactivity ratios converge, leading to random copolymers or even inverted gradients.[20,25,28,29] However, the use of these polar modifiers leads to a strong decrease of 1,4- microstructures in the polydiene, thus increasing the glass transition temperature, which limits their usage as thermoplastic elastomers.[30–33]

In previous works, several authors have investigated the effects of Lewis acid ligands, and specifically alkali alkoxides (Li, Na, K, Rb, Cs), on the homo- and copolymerization of styrene and butadiene.[34–40] These highly aggregated modifiers form mixed aggregates with the polymer chain end, changing reactivity.[37,41] Addition of 6 equivalents (equiv) lithium *tert*-butoxide (LiOtBu) relative to butyllithium reduced the homopolymerization rate by a factor of 6.25 for butadiene and 2.3 for styrene.[36]

The introduction of higher alkali alkoxides does not only increase this aggregation but also results in an intermolecular exchange of counterions via mixed aggregates (Scheme 2). This equilibrium must be fast, as low dispersities ($Đ$ < 1.1) and the desired molecular weights were achieved.[34,40,42–46] However, different authors disagree on the question whether the mixed aggregate is active in polymerization.[47–49] As a general trend, increasing amounts of these modifiers and increasing counterion size increase the homopolymerization rate of both styrene and diene monomers, and styrene is more accelerated than the diene.[34,50]

Scheme 2*:* Two-State Model of Polymerization.[34]

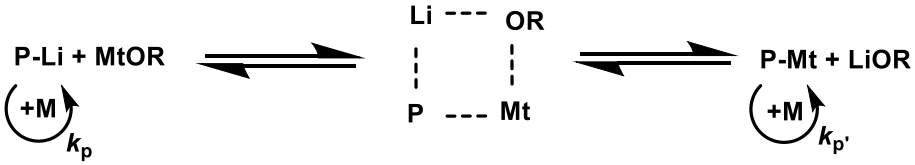

This influence is not limited to kinetics but also determines the microstructure of the polydiene and consequently the glass transition temperature. Literature results on the vinyl unsaturation of polybutadiene in the presence of an excess of lithium alkoxides scatter widely. Makowski recorded an increase up to 40% vinyl unsaturation while Hsieh

only found an increase to 10%.[36,51] In contrast, the addition of 1 equiv sodium *tert*-butoxide (NaO*t*Bu) already increases the vinyl unsaturation of polybutadiene from 5 % to 70 %,[34,52,53] which is the microstructure obtained with metallic or organosodium initiators.[39,52,54–56] Overall, sodium alkoxides exert the strongest modifier effect on the microstructure.[52]

Various groups investigated the effect of potassium alkoxides in sub- and over-stoichiometric concentrations for the polymerization of butadiene and isoprene on their respective microstructure.[34,44,50,57] Depending on the modifier concentration a wide range of vinyl unsaturations of 20 % to 50 % was observed. Both metallic and organopotassium initiators also increased vinyl unsaturation to 50 %.[52,55,56,58] Significant differences in the vinyl content were observed between butadiene and isoprene at comparable modifier concentrations,[35,50] which was explained by the PI/KOtBu adduct acting as a Schlosser-Lochmann base, deprotonating the 2-methyl group.[44,50,59–61] The higher alkali alkoxides of rubidium and cesium qualitatively had similar effects as potassium.[35]

The statistical copolymerization of styrene and butadiene in the presence of various alkali alkoxides was investigated in several studies. In all studies only the rate of total comonomer consumption and the fraction of styrene units in the copolymer as a function of conversion were determined, the latter being a rough estimate of the comonomer gradient along the chain.[35,36,62–64] The addition of up to 6 equiv LiO*t*Bu retarded the reaction but had no significant impact on the gradient, which is quite surprising in view of the previous results of the homopolymerizations.[35,36]

Higher alkali alkoxides had strong effects on the copolymerization rate and on the styrene incorporation, which increased from Na << K ~ Rb < Cs.[35] Already 0.2 equiv of NaO*t*Bu are sufficient to achieve random copolymerization.[35] Organosodium initiators were also investigated and reactivity ratios determined as r_S = 0.42 and r_B = 0.3.[65] These initiators undergo chain transfer to toluene, which can be suppressed by the addition of lithium alkoxides.[39] It could be assumed that the main reaction center is the polymer anion with lithium as the counterion, but the high vinyl content of 70 % is not consistent with this assumption.[34,52,53] Therefore, it was concluded that the main reaction center is a bimetallic mixed complex (intermediate in Scheme 2), which differs from either of the initial compounds.[54,66]

The use of potassium alkoxides in the copolymerization of styrene and butadiene drastically changes the comonomer incorporation; already 1/30 equiv is sufficient for a random copolymerization, and at higher ratios (up to 1 equiv) inversion of the gradient was observed.[35,63,64,67,68] Various publications[69,70] and patents describe the use of potassium alkoxides for the synthesis of random S/B copolymers.[71–74] Wofford and Hsieh as well as Arest-Yakubovich and coworkers studied the copolymerization of styrene and butadiene in cyclohexane at 25°C with an organopotassium initiator and also found an inversion of reactivities compared to butyllithium (r_S = 3.3 and r_B = 0.12).[35,62]

The mechanism of the homo- and copolymerization in the presence of sodium and potassium alkoxides is not fully understood. Two different mechanisms have been proposed,[40,75,76] a two-state mechanism[35,48] and a single-state mechanism consisting of a multicomponent complex, i.e. a mixed aggregate,[39,47,54] as the reaction center, as shown in Scheme 2. The two-state mechanism assumes a reversible exchange of counterions; a mixed aggregate is not considered or is inactive. Each of the two propagating centers, when active, leads to its own microstructure.[35,42–46,76]

This work presents the first in depth kinetic investigation on the copolymerization of styrene and isoprene in the presence of lithium-, sodium- and potassium-alkoxides in cyclohexane. Using *in-situ* near-infrared (NIR) spectroscopy enabled us to independently track the conversion of both monomers and thus determine reactivity ratios and comonomer gradients along the polymer chain. Investigations on their microstructure, blockiness and glass transition temperature enabled a better understanding of the polymerization mechanisms with Lewis acid modifiers.

Experimental Section

Materials, instrumentation and a general description of the copolymerization kinetic investigations are described in the Supporting Information.

Results and Discussion

The kinetic effect of alkali metal alkoxides in the copolymerization of styrene and isoprene in cyclohexane was investigated using *in-situ* near-infrared (NIR) spectroscopy at 20-23 °C. Lithium, sodium and potassium *tert*-amylates served as modifiers. Deprotonated *tert*-amyl alcohol (2-methyl-2-butanolate) was used due to its solubility in cyclohexane, commercial availability and industrial application.[63,67,72,73] The initiator *sec*-butyllithium (BuLi) was added to a premixed solution of alkoxide and monomers to avoid side reactions (see Scheme S1).[44] An equimolar monomer feed (f_S = f_I = 0.5) was used to generate a polymer with 60 wt% (57 vol%) of styrene. The targeted molecular weight of 80 kg/mol and low dispersities, Đ ≤ 1.1, were successfully achieved (Table 1, Figures S5-S7). Higher molecular weights, which in some cases exceed theory, can be partially explained by an overestimation of the PS calibration, which is noted to be approximately 10%[17], and to minor extent by termination reactions during initiation, as the alkoxides used cannot be dried further.

Time-conversion and individual vs total conversion plots for all counterions are given in the Supporting Information in Figures S8-S13. The reactivity ratios were calculated according to the terminal model (Meyer-Lowry[77] fit) or the non-terminal model (Jaacks [78,79] fit), see Figures S15-S20. As stated in our previous publications[9,17,18,25,26], we assume validity of the non-terminal model (r_1r_2 =1) whenever the Jaacks plot is linear, in order to avoid overfitting.[80] The Meyer-Lowry method was only used when the non-terminal model failed, i.e. for the copolymerization in pure cyclohexane[18,25,26] and for small amounts of modifier, [LiOAm]/[BuLi] ≤ 1; [NaOAm]/[BuLi] ≤ 0.1; [KOAm]/[BuLi] ≤ 0.025.

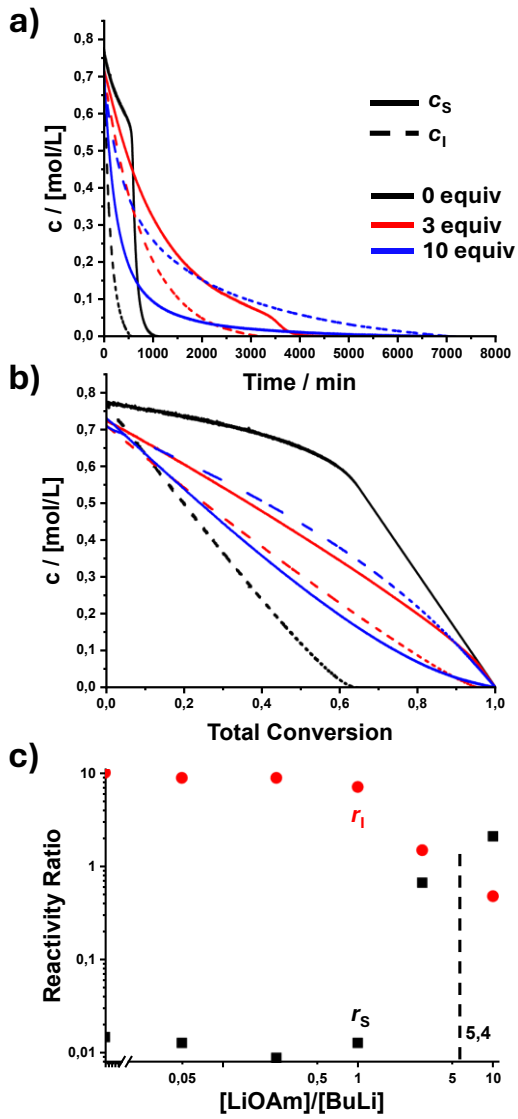

Figure 1: Effect of lithium *tert*-amylate (LiOAm) on the copolymerization kinetics. (a) time-conversion plots, (b) plots of comonomer concentrations versus total conversion, (c) reactivity ratios. Red circles: isoprene, black square: styrene. The dashed line indicates $r_S = r_I = 1$ and thus (ideal) random copolymerization. Please note the double-logarithmic scales.

Effect of lithium *tert*-amylate (LiOAm). Lithium *tert*-amylate was specifically chosen to separate the effect of the introduced alkoxide from that of the added counterion. Up to an equimolar ratio of LiOAm to BuLi no significant impact on the copolymerization kinetics is observed (Table 1, Figures 1, S8-S9); only when the LiOAm content is increased to ≥ 3 equiv, the reaction is retarded and reactivity ratios change. At 10 equiv of LiOAm the reaction slows down sevenfold for isoprene but less for styrene (for estimated half-lives, see Fig. S14 a). This is due to the formation of mixed aggregates $(P\text{-}Li)_x(LiOAm)_y$,

decreasing the concentration of non-aggregated chain ends (Scheme 3).[81] This effect is stronger for isoprene than for styrene.

Scheme 3: Possible aggregates of polystyryllithium in the presence of lithium alkoxides

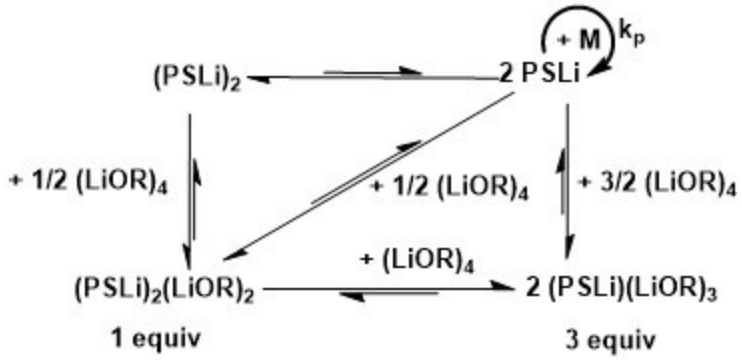

Figure 1c shows the reactivity ratios vs. modifier concentration, calculated from the plots in Figures S15-S16. With increasing amylate content, the reactivity ratios converge and intersect at an interpolated ratio of ~ 5.4 equiv, corresponding to a random copolymerization. At 10 equiv of LiOAm the gradient is inverted (Table 1 and Figure S21).

Our results for LiOAm quantitatively confirm literature data but significantly deviate from Hsieh's report on the styrene/butadiene system, who found no change in the comonomer gradient.[35,36] We tentatively explain these differences by the different diene used (butadiene) and by the poorer solubility of LiO*t*Bu in cyclohexane.

Table 1: Effect of alkali *tert*-amylates on the copolymerization of styrene and isoprene.

Amylate equivalents	M_n[a] [kg/mol]	Đ[a]	r_S[b]	r_I[b]	$r_S r_I$	Blockiness[c] [%]	1,4 [%][c]	3,4 [%][c]	1,2 [%][c]	T_g [°C][d]	Volume Gradient
0	83.9	1.05	0.009	9.05	0.081	75	94	6	0	-41/ 101	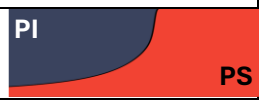
LiOAm											
0.05	79.5	1.05	0.013	8.83	0.12	75	94	6	0	-42 / 101	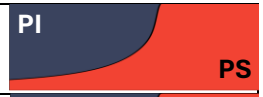
0.25	86.0	1.05	0.009	8.84	0.080	74	94	6	0	-42 / 101	
1	98.5	1.04	0.013	7.07	0.092	73	94	6	0	-40 /101	
3	91.4	1.10	0.67	1.49	1	56	84	16	0	8	
10	127	1.07	2.10	0.48	1	46	67	33	0.4	38	
NaOAm											
0.05	86.6	1.05	0.1	3.64	0.36	64	89	10	0.2	-28 / 87	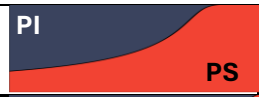
0.1	86.7	1.06	0.25	1.18	0.30	62	86	14	0.5	6	
0.25	88.3	1.05	1.71	0.59	1	52	66	33	1	15	

0.5	90.6	1.07	3.45	0.29	1	65	45	52	3	-13 /58	
0.75	91.4	1.10	5.11	0.20	1	78	21	68	11	3/75	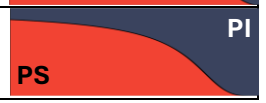

KOAm

0.025	85.6	1.06	0.23	1.76	0.41	80	91	9	0	-26 / 42	
0.033	91.6	1.06	0.88	1.14	1	85	92	8	0	-9	
0.05	79.5	1.06	1.35	0.74	1	89	91	9	0	-6	
0.1	80.0	1.08	5.72	0.17	1	92	88	11.5	0	-55 / 68	
0.25	77.9	1.09	13.8	0.07	1	92	81	18	0.3	-55 / 88	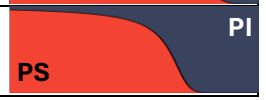

[a]Determined by SEC with PS calibration. [b] Calculated by either Jaacks or Meyer-Lowry. [c] Determined by ^{1}H-NMR spectroscopy (see supporting Information S23-25). Fraction of styrene units that have at least one other styrene neighbor. [d] Measured by DSC, value taken form the second heating cycle.

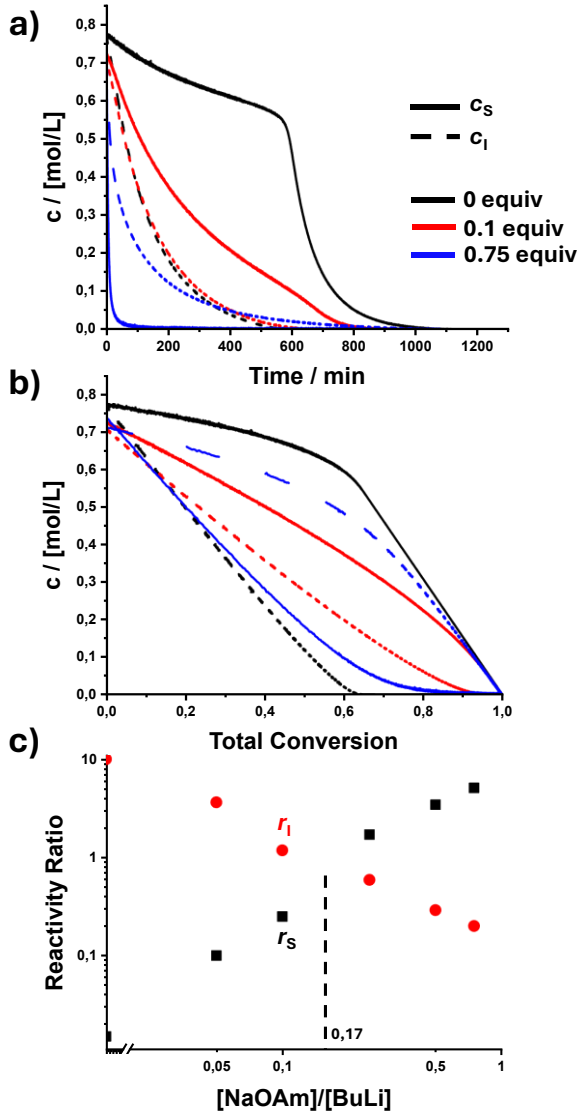

Figure 2: Effect of sodium *tert*-amylate (NaOAm) on the copolymerization kinetics. (a) time-conversion plots, (b) plots of comonomer concentrations versus total conversion, (c) reactivity ratios. Red circles: isoprene, black square: styrene. The dashed line indicates r_S = r_I = 1 and thus (ideal) random copolymerization. Please note the double-logarithmic scales.

Effect of sodium *tert*-amylate (NaOAm). As can be seen in the kinetic data (Table 1, Figures 2 and S10-S11) NaOAm has a completely different impact on the copolymerization compared to LiOAm. Already sub-stoichiometric amounts are sufficient to increase the rates of both comonomers (see Fig. S14 b for half-lives), whereby styrene is more accelerated than isoprene. The calculated reactivity ratios and the resulting gradients are listed in Table 1**:** and Figure S22. The underlying fits are shown in Figures S17-S18. Increasing the modifier content to 0.75 equiv, accelerates the styrene polymerization by two orders of magnitude, while the isoprene rate only increases by a factor of 5 (Figure S14). This leads to a complete inversion of the reactivity ratios and a

rather steep inverted gradient (r_S = 5.11 and r_I = 0.20). An almost random copolymerization is achieved with only 0.17 equiv of NaOAm, similar to the results published by Hsieh *et al.* and comparable to the effect of the bidentate ether modifier 2,2-di(2-tetrahydrofurfuryl)propane (DTHFP).[26,35] Thus, sodium alkoxides are much stronger modifiers than the previously investigated THF (random copolymerization at ca. 8 equiv).[18,26]

Our results are consistent with gradients reported by Hsieh and Wofford for the homo- and copolymerizations of styrene and butadiene initiated by NaO*t*Bu/*n*-BuLi, but they differ significantly from the reactivity ratios (r_S = 0.42, r_I = 0.3) reported by Arest-Yakubovich et al. for a pure sodium initiator.[34,35,65] This might indicate that the alkoxide ions play a role in the copolymerization by forming mixed complexes with the PI and PS chain ends (Scheme 3). The mechanism will be discussed further below in comparison to the other modifiers.

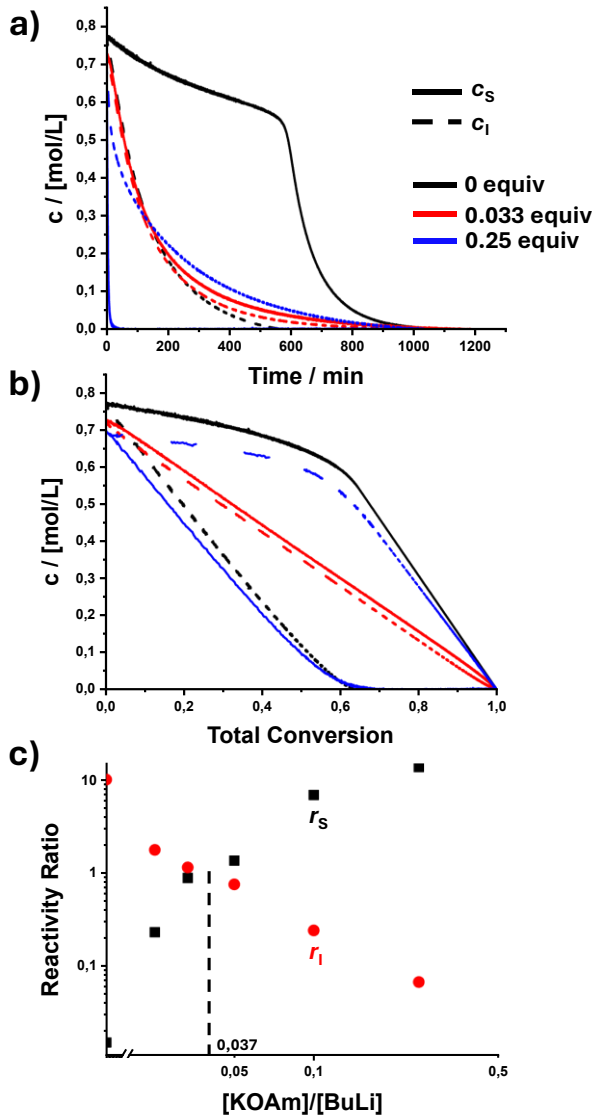

Figure 3: Effect of potassium *tert*-amylate (KOAm) on the copolymerization kinetics. (a) time-conversion plots, (b) plots of comonomer concentrations versus total conversion, (c) reactivity ratios vs. concentration. Red circles: isoprene, black square: styrene. The dashed line indicates $r_S = r_I = 1$ and thus (ideal) random copolymerization. Please note the double-logarithmic scales.

Effect of potassium *tert*-amylate (KOAm). Already minute amounts of KOAm have a dramatic impact on the copolymerization kinetics (Table 1, Figures 3 and S12-S13). As the potassium content increases, the rate of styrene consumption increases by two orders of magnitude at only 0.25 equiv, while the rate of isoprene consumption and reaction times for full conversion remain constant (Figure 3 a). Hsieh and Wofford found an increase in the rate of butadiene homopolymerization only at more than 0.2 equiv of KOtBu.[34] In contrast, ethers also affect the polymerization rate of isoprene.[18,28] The reactivity ratios and gradients are summarized in Table 1, Figures 3c and S23 (for fits, see Figures S19-S20). As little as 0.037 equiv of KOAm are necessary to obtain a random copolymerization.

A further increase of KOAm concentration leads to complete inversion of the gradient and to a tapered, block-like copolymer. Remarkably, the reactivity ratios (r_S = 13.8 and r_I = 0.07) obtained with 0.25 equiv of KOAm are similar to those obtained with 2500 equiv (29 vol-%) of THF. These results are in good agreement with qualitative and semi-quantitative results on the S/B copolymerization published by various authors. [35,63,64,67,68,74,82–85] However, they significantly differ from results published by Nakhmanovich et al. who investigated a pure organopotassium initiator (r_S = 3.3; r_B = 0.12), indicating that both counterions and the alkoxide affect the polymerization mechanism. A comprehensive discussion will be given in a later section of this paper.

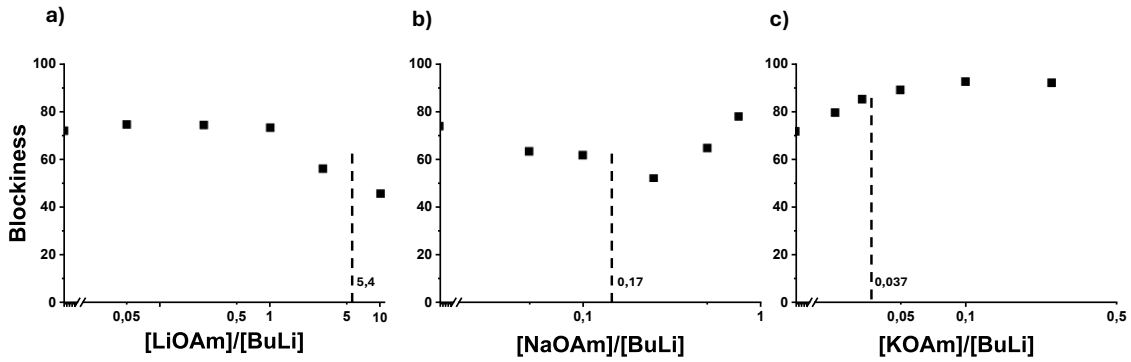

Figure 4: Blockiness of P(S-*co*-I) synthesized as a function of the MOAm/BuLi ratio. The vertical line represents random copolymerization.

Determination of Blockiness. The so-called "blockiness" is defined as the fraction of two or more consecutive styrene units in the copolymer, as analyzed by a characteristic shift of the *ortho* protons in ^{1}H-NMR.[86,87] The stacked NMR spectra are shown in Figures S24-26. The resulting blockiness values as a function of modifier equivalents are given in Table 1 and Figure 4. For details regarding determination of the blockiness, see Supporting Information, section 4.2.[9,18,26] The general trend for Lewis base modifiers is that with converging reactivity ratios the blockiness decreases, until a minimum for random copolymerization is reached.[9,18,26] Steube *et al*. observed this for THF as a modifier. The blockiness decreased from 75% in cyclohexane to 13% for random copolymerization with 4 to 8 equiv THF (Figure S27).[18] For LiOAm and NaOAm we observe a decrease to only 50%, indicating a deviation from an ideal randomness. KOAm shows an even more unexpected

behavior: the blockiness steadily increases up to 92% at complete gradient inversion. It is remarkable that at random copolymerization (0.037 equiv) we observe a higher blockiness than in a tapered, blocklike copolymer obtained in pure cyclohexane. This indicates the formation of short PS blocks. We explain this with an altered polymerization mechanism, which will be discussed in detail in a later section. To confirm this assumption a tapered copolymer synthesized in pure cyclohexane and a random one synthesized using 0.033 equiv of KOAm were submitted to oxidative degradation. [88,89] SEC distributions of the polymers before and after degradation are shown in Fig. S28. NMR (Fig. S29) confirmed that all double bonds were successfully degraded. As expected, degradation of the tapered copolymer yielded a pure PS block with a molecular weight of 36 kg/mol and low dispersity, whereas the random copolymer was broken down into smaller PS blocks with a molecular weight of ca. 1700 g/mol and a dispersity of 2.3.

Microstructure of isoprene units. The microstructure of diene polymers is a key feature for all application areas. ^{1}H-NMR spectroscopy was used to determine the microstructure of the isoprene units. Exemplary ^{1}H-, ^{13}C-, COSY, HSQC and HMBC spectra of copolymers synthesized in the presence of 0 eq, 0.75 equiv NaOAm and 0.25 equiv KOAm are shown in Figures S29-44, and the results are given in Table 1 and Figure 5. The microstructure of the copolymers synthesized in pure cyclohexane consists of 94% 1,4- and 6% 3,4-units, which is in good agreement with literature. [9,18,19,25,33,90] It is common that with increasing amount of modifier the 1,4-content decreases and the 3,4- and 1,2-content increases. Similar behavior has been reported for ether- or amine-based modifiers. As shown in Fig. 5, the extent to which this microstructure changes, varies greatly for the various counterions and is dramatically different for KOAm.

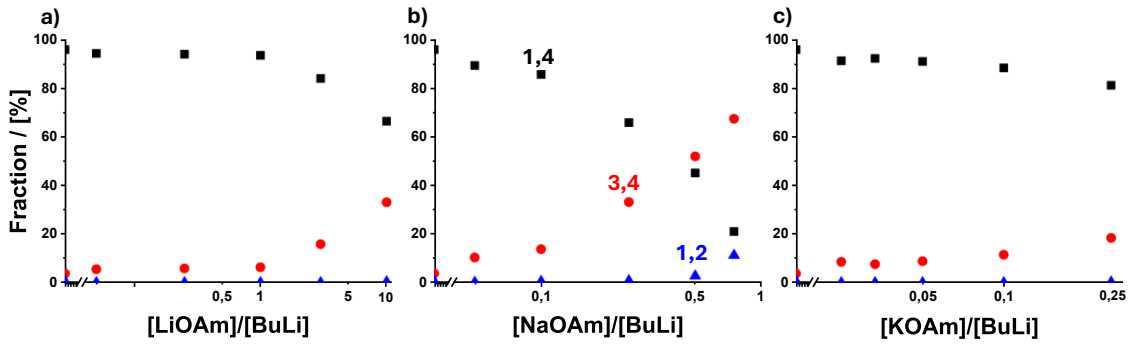

Figure 5: Microstructure of the isoprene units (1,4: black squares; 3,4: red dots; 1,2: blue triangle) obtained in presence of *tert*-amylates, a) lithium, b) sodium and c) potassium.

LiOAm only affects the microstructure in overstoichiometric concentrations, raising the vinyl content from 6 to 33%. This is similar to the results of Makowski[51] for polybutadiene at slightly lower alkoxide concentrations, but contradicts the results of Hsieh[36], where LiO*t*Bu had little effect on the polybutadiene microstructure. As discussed above, we suspect that LiO*t*Bu was probably not completely dissolved in Hsieh's experiments.

Even small amounts of NaOAm have a significant effect on the microstructure, which is in good agreement with literature.[34,57] Already 0.75 equiv NaOAm are sufficient to alter the vinyl content from 6 to 79%, similar to the effect of 2500 equiv of THF.[18] Metallic sodium or organosodium initiators lead to similar microstructures.[39,52,54,55] Thus, the microstructure of the isoprene units is dominated by the sodium counterion. Overall, sodium ions have the highest impact on the microstructure and are used to synthesize polymers with high vinyl unsaturation content.[35,52,53,91]

Surprisingly, KOAm, the most efficient modifier in this study, changed the microstructure only to a small extent (8% and 18 % vinyl units at random and at full inversion, respectively). This renders KOAm highly interesting for the synthesis of S/I or S/B random copolymers with high 1,4 microstructure, as documented by a number of patents.[2–4,72,73] These results are in contradiction to previous results for homo-polybutadiene, where a higher vinyl unsaturation of up to 50% was achieved by using potassium alkoxides in sub- and over-stoichiometric concentrations.[34,44,50,57] However it is in good agreement with the results published by Kirchevskaya *et al*. for polyisoprene.[50] We explain the differences between butadiene and isoprene units with the additional methyl group, increasing sterics, and a change in the microstructure determination method from infrared- to ^{1}H-NMR spectroscopy, which is more accurate.[25,33,92] In pronounced contrast, potassium metal and alkylpotassium initiators led to vinyl contents of about 50%.[32,52,55,56,93,94] This is a strong indication that both lithium, potassium and the alkoxide affect isoprene polymerization.

Comprehensive discussion. Our kinetic and microstructural investigation has shown strong differences in the behavior of the three modifiers. Retardation of the copolymerization by more than one equiv of LiOAm was explained by the existence of various mixed aggregates and a decrease of free, non-aggregated PS-Li and PI-Li. However, the only partial decrease of the blockiness and the increased vinyl content of

the isoprene units seem to indicate that a part of the active species are mixed complexes, e.g. (P-Li)(LiOAm)$_3$, see Scheme 3.

With sodium and potassium amylate we assume complete metal exchange (Scheme 2), but since they are used in deficit, only a fraction of polymer chains can be coordinated with sodium or potassium. This fraction depends on the nature of the chain end and the alkali metal (Scheme 4). The chain ends with Na^+ or K^+ counterions are more reactive than the lithiated ones ($k_{p,Mt} > k_{p,Li}$), explaining the observed increase in polymerization rate. The species formed in the metal exchange reaction can form mixed aggregates with the residual Li, Na, or K alkoxides, similar to Scheme 3 or a two-state equilibrium (Scheme 4). The open question is whether these mixed complexes participate in the polymerization.

Scheme 4: Effect of NaOAm and KOAm on the S/I copolymerization

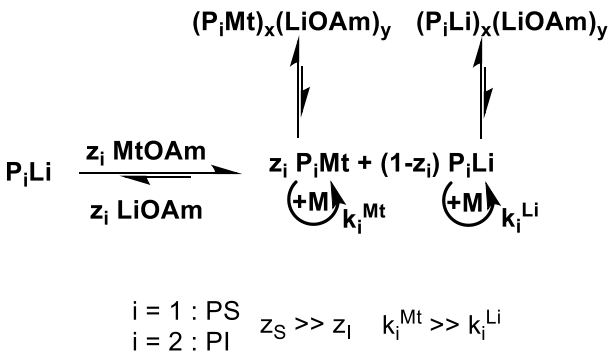

i = 1 : PS
i = 2 : PI
$z_S >> z_I$ $k_i^{Mt} >> k_i^{Li}$

This question is difficult to answer for the NaOAm modifier. On the one hand microstructures observed in our system are similar to those obtained with metallic sodium and organosodium initiators, indicating that the mechanism is dominated by a metal exchange in the two-state equilibrium. [39,52,54] On the other hand the reactivity ratios in our system significantly differ from those published for pure organosodium initiators, indicating participation of a mixed complex (PMt)$_x$(LiOAm)$_y$.[65] Furthermore, Arest-Yakubovich reported that addition of lithium alkoxide to 2-ethylhexylsodium suppresses chain transfer to toluene.[54] Thus, we conclude that both counterions and the alkoxide are relevant for the polymerization.[39,40,47,54,65,66]

KOAm has the strongest effect on the kinetics but still polymerizes isoprene in the predominant 1,4- microstructure. To the best of our knowledge, this is the only known modifier capable of altering reactivity ratios by accelerating styrene polymerization and

nevertheless having a negligible effect on isoprene polymerization and its microstructure. We explain this by the two-state polymerization mechanism in Schemes 2 and 4, where the equilibrium remains left for isoprene but shifts right for styrene. [34,35,40,48,76] According to the HSAB (hard and soft acids and bases) concept,[95] the delocalized (soft) polystyryl anions predominantly coordinate with soft (potassium) cations, whereas the (hard) polydienyl anions prefer the hard lithium cations, explaining the predominant 1,4-units. [48,72,73] Thus, styrene polymerization is strongly accelerated leading to the observed effect of the reactivity ratios. At the same time the microstructure of the isoprene units remains unaltered (Table 1, Figure 5) and blockiness increases (Figure 4).

The unexpected and unprecedented increase of blockiness and the formation of short PS blocks, even despite random copolymerization at ca. 1/30 equiv KOAm, needs special consideration. We explain this effect with the two-state polymerization mechanism. At 1/30 equiv of KOAm, there can be a potassium counterion at one of 30 polymer chain ends, most probably a PS chain end. Since they are considerably more reactive, the PS-K chain ends polymerize as much styrene as the other 29 PS-Li and PI-Li chain ends preferably polymerize isoprene, since $k_{SI} >> k_{SS}$.[18] Based on rapid exchange of the counterions monomodal polymers are accessible that consist of many short styrene and isoprene blocks, which increases the overall blockiness, since only two to three styrene units are required for the characteristic NMR shift of the ortho protons.[87] This is in contrast to previously studied Lewis bases, e.g. ethers, which lead to fully random copolymers. [9,18,25,26] Therefore, potassium alkoxide as a modifier enables decoupling of the diene microstructure from the reaction kinetics.

Thermal properties. The glass transition temperatures, T_g, of the P(S-*co*-I) copolymers were investigated by DSC. The results are presented in Table 1 and Figure 6. The second heating cycles are shown in Figures S45-47.

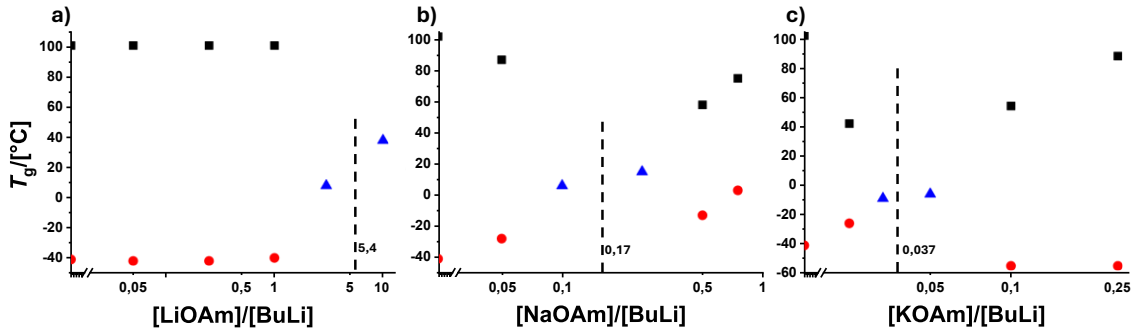

Figure 6: Glass transition temperatures of P(S-*co*-I) obtained in presence of *tert*-amylates, (a) LiOAm, (b) NaOAm, (c) KOAm. Black squares: PS-rich phase, red dots: PI-rich phase, blue triangles: mixed phase. The vertical lines indicate random copolymerization.

As expected, the addition of up to 1 equiv of LiOAm had no effect on the glass transition temperature of the resulting phase-separated polymers. The values for the PS-rich phase at 100 °C and for the PI-rich phase at about -40 °C are in good agreement with literature.[18] The T_g of the PI-rich phase is almost 20 °C higher than that of 1,4-PI homopolymer,[96,97] because of its contamination by short styrene units. Increasing the modifier content to ≥ 3 equiv LiOAm shifts the two distinct glass transition temperatures into one mixed phase. This is explained by the change in reactivity ratios (Table 1) and the increasing vinyl unsaturation of the diene.[58]

The glass transition temperature of copolymers polymerized with NaOAm behaves as expected from ether-based modifiers.[9,18,25,26] At 0.05 and ≥ 0.5 equiv of NaOAm, two distinct glass transition temperatures are observed, indicating phase separation due to the pronounced tapered structure. For 0.1 and 0.25 equiv NaOAm we again find phase mixing, as expected from the reactivity ratios (Table 1). When the phases are separated, the T_g of the PS-rich phase is below the T_g of PS homopolymer, since the polymer segments exhibit isoprene defects, and in a similar manner the T_g of the PI-rich phase increases due to the microstructure change (Figure 5).

The glass transition temperatures of copolymers polymerized with up to 0.05 equiv of KOAm show a similar behavior as with the other amylates. In particular, the copolymers formed at 0.033 and 0.05 equiv show a mixed T_g, indicating the absence of phase separation in spite of the formation of short blocks. These blocks are too short of undergo phase separation. At ≥ 0.1 equiv KOAm, the T_g of the PI-rich phase drops to -55 °C, a value

that is 14 degrees lower than that of a copolymer synthesized in pure cyclohexane. We explain this previously unreported phenomenon by the polymer composition. This tapered copolymer consists of a PS block contaminated with isoprene units (T_g lowered), predominantly grown with K^+ counterions. After the tapered region a pure PI block exists, with a high (88 and 81%) 1,4-content due to the preferred isoprene polymerization with lithium as a counterion. Since the 1,4-content in pure cyclohexane is still higher (95%), but the PI-rich phase has a lower T_g, we assume that the styrene contaminations have a stronger impact on the T_g than the increased content of vinyl units. A tapered copolymer with a pure PI block can also be obtained in the presence of 2500 equiv. of THF, which decreases the 1,4-content to 25% and thus increases the T_g to 5 °C.[18]

Conclusions

We have presented the first in-line NIR kinetic investigation of the copolymerization of styrene and isoprene initiated by *sec*-butyllithium (BuLi) in cyclohexane in the presence of alkali metal alkoxides as modifiers to calculate reactivity ratios and comonomer gradients. Additional information on the underlying mechanisms was obtained from NMR spectroscopy, namely the blockiness and the microstructure of the diene units. The glass transition temperatures of the gradient copolymers correlate with the copolymer microstructure. All investigated amylates affect the rate of polymerization, the reactivity ratios, the comonomer gradient and the diene microstructure, but at very different concentrations and with different reaction mechanisms. The general trend in modifier strength is Li < Na < K. The results show that these Lewis acid (μ-type) ligands act completely different to the well-known Lewis base (σ-type) ligands, e.g. ethers or amines.

LiOAm at over-stoichiometric concentrations decreases the rate of polymerization of both monomers to different degrees, affecting the respective reactivity ratios. This is due to a decrease in the concentration of active chains by formation of mixed aggregates. The only partial decrease of the blockiness and the moderately increased vinyl content of the isoprene units suggest that a part of the active species are mixed complexes.

Sub-stoichiometric addition of NaOAm accelerates styrene propagation but has only a minor effect on the rate of isoprene conversion. However, it significantly changes the

microstructure of the diene units, similar to metallic or organosodium initiators. Thus, exchange of the lithium counterion to sodium leads to the predominantly active species (Scheme 4). The reported fact that the addition of LiO*t*Bu to an organosodium initiator strongly decreases chain transfer to toluene indicates a contribution of mixed complexes. Thus, sodium alkoxides are promising modifiers for the synthesis of high vinyl polydienes suitable for post-polymerization modification.

KOAm selectively accelerates styrene polymerization even at minute concentrations, whereas isoprene rate and microstructure are unaffected. An unexpected phenomenon is the formation of short blocks in the random copolymer. This is explained the two-state polymerization mechanism involving a selective exchange from polystyryllithium to -potassium, resulting in a very low T_g of -55°C of the isoprene units. This unique feature of decoupling the reaction kinetics from the diene microstructure is the most impressive capability of potassium *tert*-amylate, rendering it a perfect choice for the synthesis of random copolymers and thermoplastic elastomers with high content of 1,4-isoprene units.

References

(1) Szwarc, M. 'Living' Polymers. *Nature* **1956**, *178* (4543), 1168–1169. https://doi.org/10.1038/1781168a0.

(2) Holden, G.; Milkovich, R. U.S. Patent 3265765, Block Polymers of Monovinyl Aromatic Hydrocarbons and Conjugated Dienes., 1962.

(3) Porter; Milkovich, R.; Phillips Petroleum Co. GB888624A Block Polymers and Process for Preparation Thereof, 1959.

(4) Holden, G.; Milkovich, R. Block Polymers of Monovinyl Aromatic Hydrocarbons and Conjugated Dienes US3265765A, US3265765A to Shell Oil Company, 1966.

(5) Qiao, L.; Leibig, C.; Hahn, S. F.; Winey, K. I. Isolating the Effects of Morphology and Chain Architecture on the Mechanical Properties of Triblock Copolymers. *Ind Eng Chem Res* **2006**, *45* (16), 5598–5602. https://doi.org/10.1021/ie0511940.

(6) Steube, M.; Johann, T.; Barent, R. D.; Müller, A. H. E.; Frey, H. Rational Design of Tapered Multiblock Copolymers for Thermoplastic Elastomers. *Prog Polym Sci* **2022**, *124*, 101488. https://doi.org/10.1016/j.progpolymsci.2021.101488.

(7) Ntetsikas, K.; Ladelta, V.; Bhaumik, S.; Hadjichristidis, N. Quo Vadis Carbanionic Polymerization? *ACS Polymers Au* **2023**, *3* (2), 158–181. https://doi.org/10.1021/acspolymersau.2c00058.

(8) Meier-Merziger, M.; Fickenscher, M.; Hartmann, F.; Kuttich, B.; Kraus, T.; Gallei, M.; Frey, H. Synthesis of Phase-Separated Super-H-Shaped Triblock Architectures: Poly(l-Lactide) Grafted from Telechelic Polyisoprene. *Polym Chem* **2023**, *14* (23), 2820–2828. https://doi.org/10.1039/d3py00230f.

(9) Fuchs, D. A. H.; Wadgaonkar, S. P.; Müller, A. H. E.; Frey, H. Effect of <scp>tetrahydrofuran</Scp> on the Anionic Copolymerization of 4-trimethylsilylstyrene with Isoprene. *Polym Adv Technol* **2024**, *35* (6). https://doi.org/10.1002/pat.6478.

(10) Zhang, J.; Pointer, W.; Patias, G.; Al-Shok, L.; Hand, R. A.; Smith, T.; Haddleton, D. M. End Functionalization of Polyisoprene and Polymyrcene Obtained by Anionic Polymerization via One-Pot Ring-Opening Mono-Addition of Epoxides. *Eur Polym J* **2023**, *183*, 111755. https://doi.org/10.1016/j.eurpolymj.2022.111755.

(11) Kim, H.; Goseki, R.; Homma, C.; Ishizone, T. Synthesis of Sequence-Controlled Homopolymer via Anionic Self-Alternating and Chemoselective Polymerization of 4-Vinyl-1,1-Diphenylethylene Derivatives. *Macromolecules* **2023**, *56* (21), 8796–8805. https://doi.org/10.1021/acs.macromol.3c01672.

(12) Glatzel, J.; Noack, S.; Schanzenbach, D.; Schlaad, H. Anionic Polymerization of Dienes in 'Green' Solvents. *Polym Int* **2021**, *70* (2), 181–184. https://doi.org/10.1002/pi.6152.

(13) Dev, A.; Rösler, A.; Schlaad, H. Limonene as a Renewable Unsaturated Hydrocarbon Solvent for Living Anionic Polymerization of β-Myrcene. *Polym Chem* **2021**, *12* (21), 3084–3087. https://doi.org/10.1039/D1PY00570G.

(14) Dong, R.; Gao, A.; Zhu, Y.; Xu, B.; Du, J.; Ping, S. The Development of a New Thermoplastic Elastomer (TPE)-Modified Asphalt. *Buildings* **2023**, *13* (6), 1451. https://doi.org/10.3390/buildings13061451.

(15) Korotkov, A. A.; Chesnokova, N. N. Catalytic Copolymerization of Styrene and Butadiene. *Polymer Science U.S.S.R.* **1961**, *2* (3), 284–298. https://doi.org/10.1016/0032-3950(61)90165-4.

(16) Kuntz, I. The Copolymerization of 1,3-butadiene with Styrene by Butyllithium Initiation. *Journal of Polymer Science* **1961**, *54* (160), 569–586. https://doi.org/10.1002/pol.1961.1205416020.

(17) Steube, M.; Johann, T.; Plank, M.; Tjaberings, S.; Gröschel, A. H.; Gallei, M.; Frey, H.; Müller, A. H. E. Kinetics of Anionic Living Copolymerization of Isoprene and Styrene Using in Situ NIR Spectroscopy: Temperature Effects on Monomer Sequence and Morphology. *Macromolecules* **2019**, *52* (23), 9299–9310. https://doi.org/10.1021/acs.macromol.9b01790.

(18) Steube, M.; Johann, T.; Hübner, H.; Koch, M.; Dinh, T.; Gallei, M.; Floudas, G.; Frey, H.; Müller, A. H. E. Tetrahydrofuran: More than a "Randomizer" in the Living Anionic Copolymerization of Styrene and Isoprene: Kinetics, Microstructures, Morphologies, and Mechanical Properties. *Macromolecules* **2020**, *53* (13), 5512–5527. https://doi.org/10.1021/acs.macromol.0c01022.

(19) Steube, M.; Johann, T.; Plank, M.; Tjaberings, S.; Gröschel, A. H.; Gallei, M.; Frey, H.; Müller, A. H. E. Kinetics of Anionic Living Copolymerization of Isoprene and Styrene Using in Situ NIR Spectroscopy: Temperature Effects on Monomer Sequence and Morphology. *Macromolecules* **2019**, *52* (23), 9299–9310. https://doi.org/10.1021/acs.macromol.9b01790.

(20) Bywater, S.; Worsfold, D. J. Anionic Polymerization of Styrene Effect of Tetrahydrofuran. *Can J Chem* **1962**, *40* (8), 1564–1570. https://doi.org/10.1139/v62-236.

(21) Margl, P. Mechanisms for Anionic Butadiene Polymerization with Alkyl Lithium Species. *Can J Chem* **2009**, *87* (7), 891–903. https://doi.org/10.1139/V09-032.

(22) Worsfold, D. J. Anionic Copolymerization of Styrene and Isoprene in Cyclohexane. *J Polym Sci A1* **1967**, *5* (11), 2783–2789. https://doi.org/10.1002/pol.1967.150051106.

(23) Quinebèche, S.; Navarro, C.; Gnanou, Y.; Fontanille, M. In Situ Mid-IR and UV-Visible Spectroscopies Applied to the Determination of Kinetic Parameters in the Anionic Copolymerization of Styrene and Isoprene. *Polymer (Guildf)* **2009**, *50* (6), 1351–1357. https://doi.org/10.1016/j.polymer.2009.01.041.

(24) Grune, E.; Johann, T.; Appold, M.; Wahlen, C.; Blankenburg, J.; Leibig, D.; Müller, A. H. E.; Gallei, M.; Frey, H. One-Step Block Copolymer Synthesis versus Sequential Monomer Addition: A Fundamental Study Reveals That One Methyl Group Makes a Difference. *Macromolecules* **2018**, *51* (9), 3527–3537. https://doi.org/10.1021/acs.macromol.8b00404.

(25) Meier-Merziger, M.; Fuchs, D. A. H.; Frey, H.; Müller, A. H. E. Spotlight on Methyl Tert-Butyl Ether–Underrated or Overlooked? Unveiling Its Role for Living Anionic Polymerization. *Macromolecules* **2024**. https://doi.org/10.1021/acs.macromol.4c01262.

(26) Fuchs, D. A. H.; Hübner, H.; Kraus, T.; Niebuur, B.-J.; Gallei, M.; Frey, H.; Müller, A. H. E. The Effect of THF and the Chelating Modifier DTHFP on the Copolymerisation of β-Myrcene and Styrene: Kinetics, Microstructures, Morphologies, and Mechanical Properties. *Polym Chem* **2021**, *12* (32), 4632–4642. https://doi.org/10.1039/D1PY00791B.

(27) Shaw, L.; Hutchings, L. R. Tales of the Unexpected. The Non-Random Statistical Copolymerisation of Myrcene and Styrene in the Presence of a Polar Modifier. *Polym Chem* **2020**, *11* (44), 7020–7025. https://doi.org/10.1039/d0py01099e.

(28) Morton, M.; Fetters, L. J. Homogeneous Anionic Polymerization. V. Association Phenomena in Organolithium Polymerization. *J Polym Sci A* **1964**, *2* (7), 3311–3326. https://doi.org/10.1002/pol.1964.100020726.

(29) Kim, J. M.; Chakrapani, S. B.; Beckingham, B. S. Tuning Compositional Drift in the Anionic Copolymerization of Styrene and Isoprene. *Macromolecules* **2020**, *53* (10), 3814–3821. https://doi.org/10.1021/acs.macromol.0c00526.

(30) Morton, M.; Fetters, L. J. Homogeneous Anionic Polymerization. V. Association Phenomena in Organolithium Polymerization. *J Polym Sci A* **1964**, *2* (7), 3311–3326. https://doi.org/10.1002/pol.1964.100020726.

(31) Morita, H.; Tobolsky, A. V. Isoprene Polymerization by Organometallic Compounds. I. *J Am Chem Soc* **1957**, *79* (22), 5853–5855. https://doi.org/10.1021/ja01579a004.

(32) Tobolsky, A. V.; Rogers, C. E. Isoprene Polymerization by Organometallic Compounds. II. *Journal of Polymer Science* **1959**, *40* (136), 73–89. https://doi.org/10.1002/pol.1959.1204013605.

(33) Worsfold, D. J.; Bywater, S. Anionic Polymerization of Isoprene. *Can J Chem* **1964**, *42* (12), 2884–2892. https://doi.org/10.1139/v64-426.

(34) Hsieh, H. L.; Wofford, C. F. Alkyllithium and Alkali Metal *Tert*-Butoxide as Polymerization Initiator. *J Polym Sci A1* **1969**, *7* (2), 449–460. https://doi.org/10.1002/pol.1969.150070204.

(35) Wofford, C. F.; Hsieh, H. L. Copolymerization of Butadiene and Styrene by Initiation with Alkyllithium and Alkali Metal *Tert*-Butoxides. *J Polym Sci A1* **1969**, *7* (2), 461–469. https://doi.org/10.1002/pol.1969.150070205.

(36) Hsieh, H. L. Effect of Lithium Alkoxide and Hydroxide on Polymerization Initiated with Alkyllithium. *J Polym Sci A1* **1970**, *8* (2), 533–543. https://doi.org/10.1002/pol.1970.150080223.

(37) Roovers, J. E. L.; Bywater, S. Butyl Lithium-Initiated Polymerization of Styrene. Effect of Lithium Butoxide. *Transactions of the Faraday Society* **1966**, *62*, 1876. https://doi.org/10.1039/tf9666201876.

(38) Roovers, J. E. L.; Bywater, S. The Polymerization of Isoprene with Sec-Butyllithium in Hexane. *Macromolecules* **1968**, *1* (4), 328–331.

(39) Cheng, T. C.; Halasa, A. F. Anionic Polymerization. III. Polymerization of Butadiene with Alkali Metal Alkoxide-modified Alkali Metal System. *Journal of Polymer Science: Polymer Chemistry Edition* **1976**, *14* (3), 573–581. https://doi.org/10.1002/pol.1976.170140306.

(40) Nakhmanovich, B. I.; Zolotareva, I. V.; Arest-Yakubovich, A. A. Study on the Mechanism of Anionic Polymerization with Mixed RLi-R'OK Initiators, 1. Polymerization of Butadiene. *Macromol Chem Phys* **1999**, *200* (9), 2015–2021. https://doi.org/10.1002/(SICI)1521-3935(19990901)200:9<2015::AID-MACP2015>3.0.CO;2-I.

(41) Halaška, V.; Lochmann, L.; Lím, D. Association Degree of T-Butoxides of Alkali Metals in Aprotic Solvents. *Collect Czechoslov Chem Commun* **1968**, *33* (10), 3245–3253. https://doi.org/10.1135/cccc19683245.

(42) Coleman, B. D.; Fox, T. G. A Multistate Mechanism for Homogeneous Ionic Polymerization. II. The Molecular Weight Distribution. *J Am Chem Soc* **1963**, *85* (9), 1241–1244. https://doi.org/10.1021/ja00892a007.

(43) Litvinenko, G.; Müller, A. H. E. General Kinetic Analysis and Comparison of Molecular Weight Distributions for Various Mechanisms of Activity Exchange in Living Polymerizations. *Macromolecules* **1997**, *30* (5), 1253–1266. https://doi.org/10.1021/ma960945u.

(44) Forens, A.; Roos, K.; Dire, C.; Gadenne, B.; Carlotti, S. Anionic Polymerization of Butadiene Using Lithium/Potassium Multi-Metallic Systems: Influence on Polymerization Control and Polybutadiene Microstructure. *Chinese Journal of Polymer Science (English Edition)* **2020**, *38* (4), 357–362. https://doi.org/10.1007/s10118-020-2355-4.

(45) Figini, V. R. V. Theoretische Analyse Der Bei Einem Zweiwegwachstumsmechanismus Auftretenden Molekulargewichtsverteilungen Und Ihre Anwendung Auf Die Anionische

Polymerisation von Styrol. *Die Makromolekulare Chemie* **1967**, *107* (1), 170–187. https://doi.org/10.1002/macp.1967.021070117.

(46) Coleman, B. D.; Fox, T. G. Multistate Mechanism for Homogeneous Ionic Polymerization. I. The Diastereosequence Distribution. *J Chem Phys* **1963**, *38* (5), 1065–1075. https://doi.org/10.1063/1.1733803.

(47) Arest-Yakubovich, A. A. Role of Bimetallic Active Centres in Anionic Polymerization of Hydrocarbon Monomers. *Macromol Symp* **1994**, *85* (1), 279–294. https://doi.org/10.1002/masy.19940850121.

(48) Grovenstein, E. Jr. Cation Effects in Organoalkali Metal Chemistry. In *Recent Advances in Anionic Polymerization*; Hogen-Esch, T. E., Smid, J., Eds.; Springer Netherlands: Dordrecht, 1987; pp 3–21. https://doi.org/10.1007/978-94-009-3175-6.

(49) Schlosser, M. Zur Aktivierung Lithiumorganischer Reagenzien. *J Organomet Chem* **1967**, *8* (1), 9–16. https://doi.org/10.1016/S0022-328X(00)84698-7.

(50) Kirchevskaya, I. Yu.; Samotsvetov, A. R.; Seredina, N. P.; Urazov, N. I.; Shatalov, V. P. Relations between Polymerization of Hydrocarbon Monomers in the Presence of Lithium Alkyls Modified with Potassium Tert.Butylate. *Polymer Science U.S.S.R.* **1976**, *18* (8), 2111–2118. https://doi.org/10.1016/0032-3950(76)90398-1.

(51) Makowski, H. S.; Lynn, M. Butyllithium Polymerization of Butadiene. III. Effect of Inactive Lithium Compounds. *Journal of Macromolecular Science: Part A - Chemistry* **1968**, *2* (4), 683–700. https://doi.org/10.1080/10601326808051434.

(52) Forens, A.; Roos, K.; Dire, C.; Gadenne, B.; Carlotti, S. Accessible Microstructures of Polybutadiene by Anionic Polymerization. *Polymer (Guildf)* **2018**, *153*, 103–122. https://doi.org/10.1016/j.polymer.2018.07.071.

(53) Kozak, R.; Matlengiewicz, M. Influence of Polar Modifiers on Microstructure of Polybutadiene Obtained by Anionic Polymerization. Part 5: Comparison of μ, σ, Σ+μ, and Σ−μ Complexes. *International Journal of Polymer Analysis and Characterization* **2017**, *22* (1), 51–61. https://doi.org/10.1080/1023666X.2016.1230264.

(54) Pakuro, N. I.; Zolotareva, I. V.; Kitayner, A. G.; Rogozhkina, E. D.; Izyumnikov, A. L.; Arest-Yakubovich, A. A. Diene Polymerization by Mixed Sodium- and Lithiumalkyl Initiators in Hydrocarbon Medium. *Macromol Chem Phys* **1995**, *196* (1), 375–383. https://doi.org/10.1002/macp.1995.021960127.

(55) Salle, R.; Essel, A.; Gole, J.; Pham, Q. Polymérisation Anionique Des Diènes. III. Etude Thermodynamique de La Propagation Du Butadiène et de i'isoprène Par Les Organo-alcalins. *Journal of Polymer Science: Polymer Chemistry Edition* **1975**, *13* (8), 1855–1867. https://doi.org/10.1002/pol.1975.170130810.

(56) Stearns, R. S.; Forman, L. E. The Stereoregular Polymerization of Isoprene with Lithium and Organolithium Compounds. *Journal of Polymer Science* **1959**, *41* (138), 381–397. https://doi.org/10.1002/pol.1959.1204113832.

(57) Patterson, D. B.; Halasa, A. F. Anionic Polymerization of 1,3-Butadiene to Highly Crystalline High Trans-1,4-Poly(Butadiene) with Potassium Catalysts Generated from an Alkyllithium and Potassium Tert-Amyloxide. *Macromolecules* **1991**, *24* (16), 4489–4494. https://doi.org/10.1021/ma00016a002.

(58) Hsieh, H. L. .; Quirk, R. P. . *Anionic Polymerization : Principles and Practical Applications*; CRC Press, an imprint of Taylor and Francis, 1996.

(59) Schlosser, M. Superbases for Organic Synthesis. *Pure and Applied Chemistry* **1988**, *60* (11), 1627–1634. https://doi.org/10.1351/pac198860111627.

(60) Lochmann, L.; Janata, M. 50 Years of Superbases Made from Organolithium Compounds and Heavier Alkali Metal Alkoxides. *Open Chem* **2014**, *12* (5), 537–548. https://doi.org/10.2478/s11532-014-0528-0.

(61) Halasa, A. F.; Mitchell, G. B.; Stayer, M.; Tate, D. P.; Oberster, A. E.; Koch, R. W. Metalation of Unsaturated Polymers by Using Activated Organolithium Compounds and the Formation of Graft Copolymers. II. *Journal of Polymer Science: Polymer Chemistry Edition* **1976**, *14* (2), 497–506. https://doi.org/10.1002/pol.1976.170140220.

(62) Nakhmanovich, B. I.; Arest-Yakubovich, A. A.; Prudskova, T. N.; Litvinenko, G. I. Styrene-butadiene Copolymerization Initiated by Organopotassium Compounds in Hydrocarbon Medium. *Macromol Rapid Commun* **1996**, *17* (1), 31–36. https://doi.org/10.1002/marc.1996.030170105.

(63) Smith, S. D.; Ashraf, A.; Clarson, S. J. Styrene-Diene Random Copolymers, Blends and "Random-Diblock" Copolymers. *Prepr., Am. Chem. Soc. Div. Polym. Chem.* **1994**, *35* (2), 466–467.

(64) Ashraf, A.; Smith, S. D.; Clarson, S. J. Synthesis and Characterization of PS-PI and PS-PBD Random Copolymers and "Random-Block" Copolymers via Anionic Polymerizations. *Prepr., Am. Chem. Soc. Div. Polym. Chem.* **1993**, *34* (2), 672–673.

(65) Arest-Yakubovich, A. A.; Litvinenko, G. I.; Basova, R. V. Synthesis of High Vinyl Styrene-Butadiene Random Copolymers with a New Soluble Organosodium Initiators. *Prepr., Am. Chem. Soc. Div. Polym. Chem.* **1994**, *2* (35), 544–545.

(66) Arest-Yakubovich, A. A.; Pakuro, N. I.; Zolotareva, I. V.; Kristal'nyi, E. V.; Basova, R. V. Polymerization of Conjugated Dienes Initiated by Soluble Organosodium Compounds in Hydrocarbon Solvents. *Polym Int* **1995**, *37* (3), 165–169. https://doi.org/10.1002/pi.1995.210370303.

(67) Knoll, K.; Nießner, N. Styrolux+ and Styroflex+ - From Transparent High Impact Polystyrene to New Thermoplastic Elastomers: Syntheses, Applications and Blends with Other Styrene Based Polymers. *Macromol Symp* **1998**, *132*, 231–243. https://doi.org/10.1002/masy.19981320122.

(68) Smith, S. D.; Ashraf, A.; Satkowski, M. M.; Spontak, R. J. Determination of the Phase Diagram for a New Class of Block Copolymers:"Random-Diblock" Copolymers. *Prepr., Am. Chem. Soc. Div. Polym. Chem.* **1994**, No. 35, 651–652.

(69) Laurer, J. H.; Ashraf, A.; Smith, S. D.; Samseth, J.; Spontak, R. J. Macromolecular Self-Assembly in Dilute Sequence-Controlled Block Copolymer/Homopolymer Blends. *Supramolecular Science* **1997**, *4* (1–2), 121–126. https://doi.org/10.1016/S0968-5677(96)00048-X.

(70) Laurer, J. H.; Ashraf, A.; Smith, S. D.; Spontak, R. J. Complex Phase Behavior of a Disordered "Random" Diblock Copolymer in the Presence of a Parent Homopolymer. *Langmuir* **1997**, *13* (8), 2250–2258. https://doi.org/10.1021/la960807y.

(71) Knoll, K.; Weber, M.; Gerhard, M. ; U.S. Patent 006162867A Thermoplastic Moulding Compounds, 1997.

(72) Niessner, N.; Jahnke, E.; Wagner, D.; Duerkheim, B.; Knoll, K. US 11,066,503 B2 Very Soft, Non-Sticky and Transparent Styrenic Thermoplastic Elastomer Composition, 2021.

(73) Knoll, K.; Gausepohl, H.; Niessner, N.; Naegele, P.; Fischer, W. EP0859803B1 Thermoplastische Formmasse, 1997.

(74) Schade, C.; Fischer, W.; Gausepohl, H.; Warzelhan, V.; Fontanille, M.; Deffieux, A.; Desbois, P. US6350834 Method for Retarded Anionic Polymerization, 2002.

(75) Litvinenko, G. I.; Arest-Yakubovich, A. A. Chain Transfer to Solvent in Two-state Anionic Polymerization, 2. Slow Exchange between Propagating Species. *Macromol Theory Simul* **1995**, *4* (2), 357–366. https://doi.org/10.1002/mats.1995.040040210.

(76) Litvinenko, G. I.; Arest-Yakubovich, A. A. Study on the Mechanism of Anionic Polymerization with Mixed RLi-R'OK Initiators, 2. Theoretical Study of Random Styrene-Butadiene Copolymerization. *Macromol Chem Phys* **2000**, *201* (17), 2417–2423. https://doi.org/10.1002/1521-3935(20001101)201:17<2417::AID-MACP2417>3.0.CO;2-T.

(77) Meyer, V. E.; Lowry, G. G. Integral and Differential Binary Copolymerization Equations. *J Polym Sci A* **1965**, *3* (8), 2843–2851. https://doi.org/10.1002/pol.1965.100030811.

(78) Jaacks, V. A Novel Method of Determination of Reactivity Ratios in Binary and Ternary Copolymerizations. *Makromol Chem* **1972**, *161* (1), 161–172. https://doi.org/10.1002/macp.1972.021610110.

(79) Jaacks, V. Eine Neuartige Methode Zur Bestimmung von Copolymerisationsparametern. *Angewandte Chemie* **1967**, *79* (9), 419–419. https://doi.org/10.1002/ange.19670790927.

(80) Hoffmann, R.; Minkin, V. I. Ockham's Razor and Chemistry. *International Journal for the Philosophy of Chemistry* **1996**, No. 3, 3–28.

(81) Quirk, R. P.; Ma, J. -J. Dilithium Initiators Based on 1,3-bis(1- Phenylethenyl)Benzene. Tetrahydrofuran and Lithium Sec-butoxide Effects. *Polym Int* **1991**, *24* (4), 197–206. https://doi.org/10.1002/pi.4990240402.

(82) Ashraf, A.; Smith, S. D.; Satkowski, M. M.; Spontak, R. J.; Clarson, S. J.; Lipscomb, G. G. Synthesis and Morphological Studies of Random Styrene-Diene Copolymers and "Random-Diblock" Copolymers. *Prepr., Am. Chem. Soc. Div. Polym. Chem.* **1994**, *35* (2), 581–582.

(83) Knoll, K.; Gausepohl, H.; Niessner, N.; Naegele, P. EP0927210B1 Thermoplastische Elastomere, 1997.

(84) Knoll, K.; Kindler, A.; Fischer, W. WO1999001490A1 Glycidylether Aliphatischer Polyalkohole Als Kopplungsmittel in Der Anionischen Polymerisation, 1997.

(85) Niessner, N.; Knoll, K.; Bender, D.; Gottschalk, A.; Weber, M. WO9620248 Impact-Resistent, Thermoplastic Mixture of Elastomers and Thermoplastic Materials, 1996.

(86) Handlin, D. L.; Williamson, D. T.; Willis, C. L. US 6,699,941 B1 Block Copolymer, 2004.

(87) Mochel, V. D. Nuclear Magnetic Resonance-Analog Computer Method for "Block Styrene." *Macromolecules* **1969**, *2* (5), 537–540. https://doi.org/10.1021/ma60011a017.

(88) Corbin, N.; Prud'Homme, J. Multiblock Copolymers of Styrene and Isoprene. I. Synthesis and Characterization. *Journal of Polymer Science: Polymer Chemistry Edition* **1976**, *14* (7), 1645–1659. https://doi.org/10.1002/pol.1976.170140708.

(89) Steube, M.; Johann, T.; Galanos, E.; Appold, M.; Rüttiger, C.; Mezger, M.; Gallei, M.; Müller, A. H. E.; Floudas, G.; Frey, H. Isoprene/Styrene Tapered Multiblock Copolymers with up to Ten Blocks: Synthesis, Phase Behavior, Order, and Mechanical Properties. *Macromolecules* **2018**, *51* (24), 10246–10258. https://doi.org/10.1021/acs.macromol.8b01961.

(90) Wahlen, C.; Blankenburg, J.; Von Tiedemann, P.; Ewald, J.; Sajkiewicz, P.; Müller, A. H. E.; Floudas, G.; Frey, H. Tapered Multiblock Copolymers Based on Farnesene and Styrene: Impact of Biobased

Polydiene Architectures on Material Properties. *Macromolecules* **2020**, *53* (23), 10397–10408. https://doi.org/10.1021/acs.macromol.0c02118.

(91) Meyer, A. W.; Hampton, R. R.; Davison, J. A. Structure of Alkali Metal-Catalyzed Butadiene Polymers [1,2]. *J Am Chem Soc* **1952**, *74* (9), 2294–2296. https://doi.org/10.1021/ja01129a037.

(92) Chen, H. Y. Nuclear Magnetic Resonance Study of Butadiene-Isoprene Copolymers. *Anal Chem* **1962**, *34* (9), 1134–1136. https://doi.org/10.1021/ac60189a032.

(93) Arest-Yakubovich, A. A.; Basova, R. V.; Nakhmanovich, B. I.; Kristalnyi, E. V. The Main Special Characteristics of Anionic Polymerization Initiated by Group II Metals. *Acta Polymerica* **1984**, *35* (1), 1–7. https://doi.org/10.1002/actp.1984.010350101.

(94) Foster, F. C.; Binder, J. L. Lithium and Other Alkali Metal Polymerization Catalysts. **1957**, 26–33. https://doi.org/10.1021/ba-1957-0019.ch004.

(95) Pearson, R. G. Hard and Soft Acids and Bases. *J Am Chem Soc* **1963**, *85* (22), 3533–3539. https://doi.org/10.1021/ja00905a001.

(96) Brandrup, J.; Immergut, E. H.; Grulke, E. A. *Polymer Handbook*; Wiley, 1999.

(97) Odian, G. *Principles of Polymerization*; Wiley & Sons Ltd, 2004. https://doi.org/10.1017/CBO9781139237031.013.

Supporting Information

Dramatic Effect of Alkali Metal Alkoxides on the Anionic Copolymerization of Styrene and Isoprene

Dominik A. H. Fuchs[1], [redacted]

*Corresponding authors

[1] Johannes Gutenberg-University, Duesbergweg 10-14, 55128 Mainz, Germany
[redacted]

1. Materials and experimental procedure:

1.1 Materials:

All chemicals were purchased from following suppliers: Sigma-Aldrich, Thermo Fisher Scientific Inc, Acros, VWR international and Deutero GmbH. The solution of potassium *tert*. Amylate was kindly provided by Ineos group limited. As inert gas was argon 5.0 used, which was further purified by passing it through three gas wash bottles containing *sec*. BuLi, diphenylethylene and cyclohexane.

1.2 Instrumentation

A description of the near infrared (NIR) set up and data evaluation can be found in previous publications.[1,2] NMR spectra were measured using a Bruker Avance III 600 spectrometer at 600 MHz for ^{1}H- and 151 MHz for ^{13}C-NMR. GPC samples were analyzed on an Agilent 1260 Infinity II set up with MZ-Gel SDPlus plus 10^5/10^3/100 Å columns from MZ-Analysetechnik, Mainz, Germany. All samples were measured at a concentration of 1 mg/ml with toluene as an internal standard with a PS calibration. Thermal DSC analysis of the copolymers were performed with a TA instruments DSC 250 connected to a TA instrument RCS 90 refrigeration system from Waters Corporation. Experiments were performed at a heating and cooling rate of 10K/min with a two-point calibration of indium and *n*-ocatane.

1.3 Copolymerisation

1.3.1 Purification of materials

The amylates used were not further dried, but their water content was quantified *via* Karl-Fischer titration to below 60 ppm of water and therefore no further drying was considered necessary.

Every glass flask used was flame dried three times under high vacuum (10^{-3} mbar) before use and all reactions and drying processes were carried out under schlenk conditions. A pressure valve maintained a constant overpressure of 50 mbar argon to ensure an inert gas atmosphere. The monomers were filtered through basic alumina to remove stabilizers and then dried over CaH_2 for a day. After degassing through three freeze thaw cycles, the monomers were cryotransferred to $Al(Oct)_3$ and further dried for a day. After the drying process, the monomers were cryotransferred

into a graduated ampoule, with less than 2 $\%_{Vol}$ loss in relation to the total volume of the monomers. The solvent cyclohexane was dried under reflux with sodium and benzophenone. After the blue color appeared, the solvent was transferred into the Morton flask glass reactor.

1.3.2 Copolymerization in the presence of different amylates

All polymerizations were carried out under the same conditions, only the amount of modifier was varied. The reaction flask was equipped with the NIR probe, a temperature probe and an additional glass joint. To maintain a constant reaction temperature, the flask was placed into a water bath that was cooled via a cryostat. In all reactions, the reaction heat was not exceeded by more than 10 °C (Figures S2-S4), and previous publications have shown that the effect of this temperature increase can be neglected as compared to the modifier effects.[1,3] Since mixtures of MtOR and BuLi are known as Lochmann-Schlosser superbases,[4,5] which have strong deprotonating abilities, due to their metal exchange (see Figure 2). These are no longer soluble in hydrocarbon solvents and form possible side reactions (Scheme S1).[6] Carlotti *et al.* could prove that it is essential for a controlled copolymerization that the initiator system of MtOR/BuLi had no preformation time to avoid side reactions and that MtOR had to be used in deficit to avoid crosslinking.[5,7–10] Therefore we have the goal of using the alkoxide in deficit and giving the initiator no preformation time.

The synthesis of P(S-*co*-I) in cyclohexane with 0.25 equiv. of [KOAm] is described here as example. First, 600 ml cyclohexane was added into the reaction flask followed by the modifier [KOAm] (0.25 equiv., 0.79 ml of a 0.33 mol/L solution in cyclohexane) to measure a background NIR spectra using Omnic software. An equimolar mixture of the monomers styrene (55.3 ml, 0.483 mol) and isoprene (48.35 ml, 0.483 mol) was added, and the polymerization was initiated by the injection of 0.8 ml (0.26 mmol, 1eq) of a 1.3 mol/L solution of *sec.* BuLi in cyclohexane/hexane (92:8). After initiation, the colorless solution turned dark red, indicating the preferential polymerization of styrene. After 1000 minutes the polymerization was complete and was terminated by adding 2 ml of degassed isopropanol in argon counterflow. The synthesized polymer was precipitated in a 1:3 mixture of isopropanol:methanol. The resulting colorless polymer was dried under reduced pressure and stored at -20°C.

For the kinetic investigation 13,000 to 20,000 NIR-spectra were recorded in the wavelength range from 5900 to 6250 cm^{-1} and analyzed by deconvolution, in analogy to our previous publications.[1–3,11,12] The calibration spectra of isoprene, styrene, polystyrene and polyisoprene are shown in Figure S1. The polyisoprene spectrum was calculated by subtracting the polystyrene spectrum from the spectrum at full conversion and normalizing it by the isoprene concentration, determined by the deconvolution of the starting spectrum. This is necessary because the NIR spectrum of PI is dependent on the microstructure, which depends on the modifier used.

1.4 Oxidative degradation

The oxidative degradation is performed analog to Corbin et al., with the exception that the polymer is not precipitated, but analyzed from the crude solution.[13]

To a solution of 1.5 g polymer in 200 mL benzene is 4.0 g *meta*-chloroperoxybenzoic acid (mCPBA) added and the solution stirred for 15 hours at room temperature. After removing the solvent under reduced pressure, the residue was dissolved in 150 mL dioxane and a solution of periodic acid (3.5 g in 20 mL water) is added. The solution was stirred for 24 hours at room temperature and then heated to 65°C for 30 minutes and the solvents removed under reduced pressure. The dried residue was washed with diluted NaOH and water. The obtained residual was analyzed via SEC

without prior work up. Please note that the PS oligomers carry aldehyde endgroups, which can affect the polystyrene calibration.

Scheme S1: Hypothetic mechanism of the elimination of potassium hydride.[6]

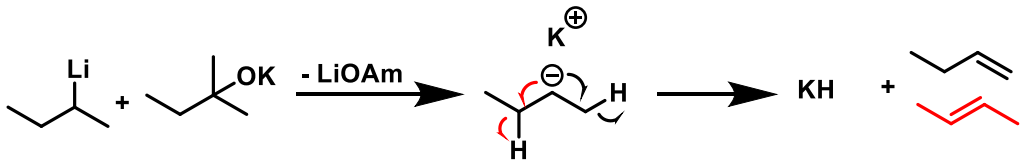

2. Copolymerization kinetics

2.1 NIR spectra

The measured (S, I and PS) and calculated (PI_{CyH} and $PI_{0.75eq\ Sodium}$) are displayed here. The microstructure depended PI spectrum is calculated by subtracting the PS spectrum from the final spectrum. These spectra are then used to perform a deconvolution to calculate the concentration of each component for each time point.

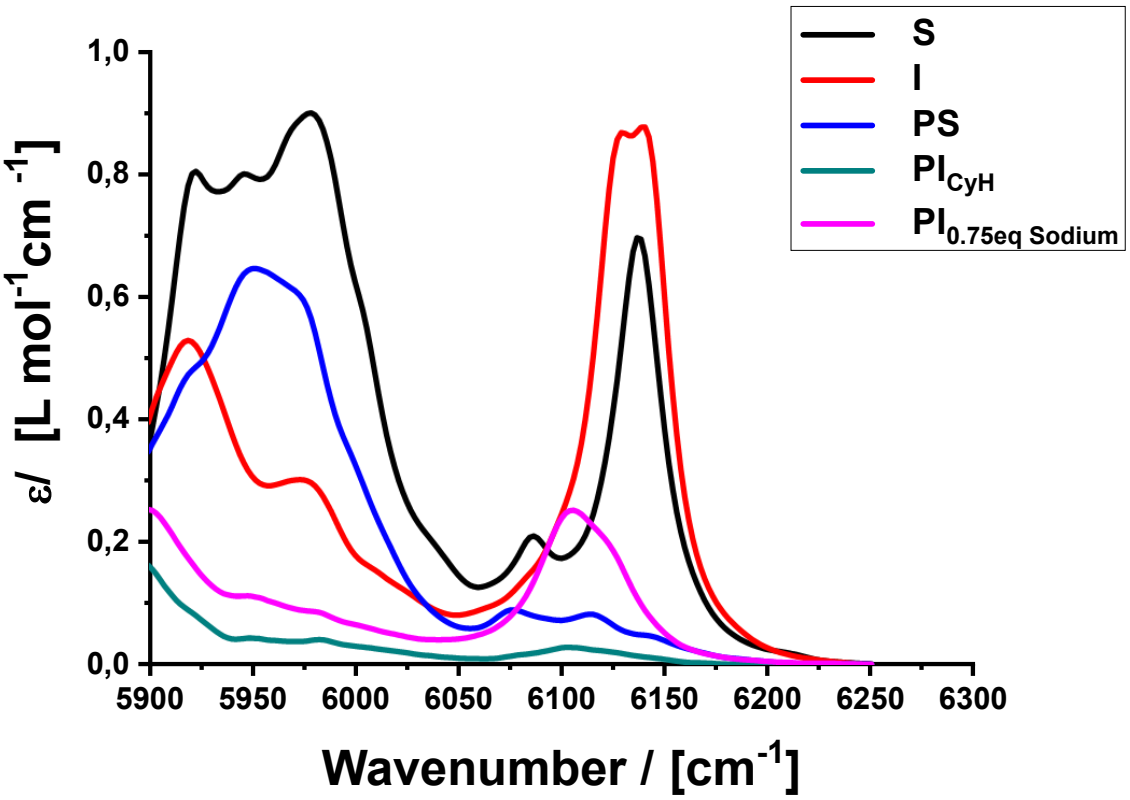

Figure S1: Measured molar attenuation coefficients of all in the reaction present reagents (S, I) and products (PS, PI). PI_{CyH} represents the spectra of polyisoprene synthesized in cyclohexane with the typical microstructure of (94% 1,4-; 6% 3,4-) and $PI_{0.75\ equiv\ NaOAm}$ the spectra of polyisoprene synthesized in cyclohexane with 0.75 equiv of NaOAm and a microstructure of (21% 1,4-; 68% 3,4-; and 11% 1,2-;) as determined by NMR spectroscopy.

2.2 Temperature profiles

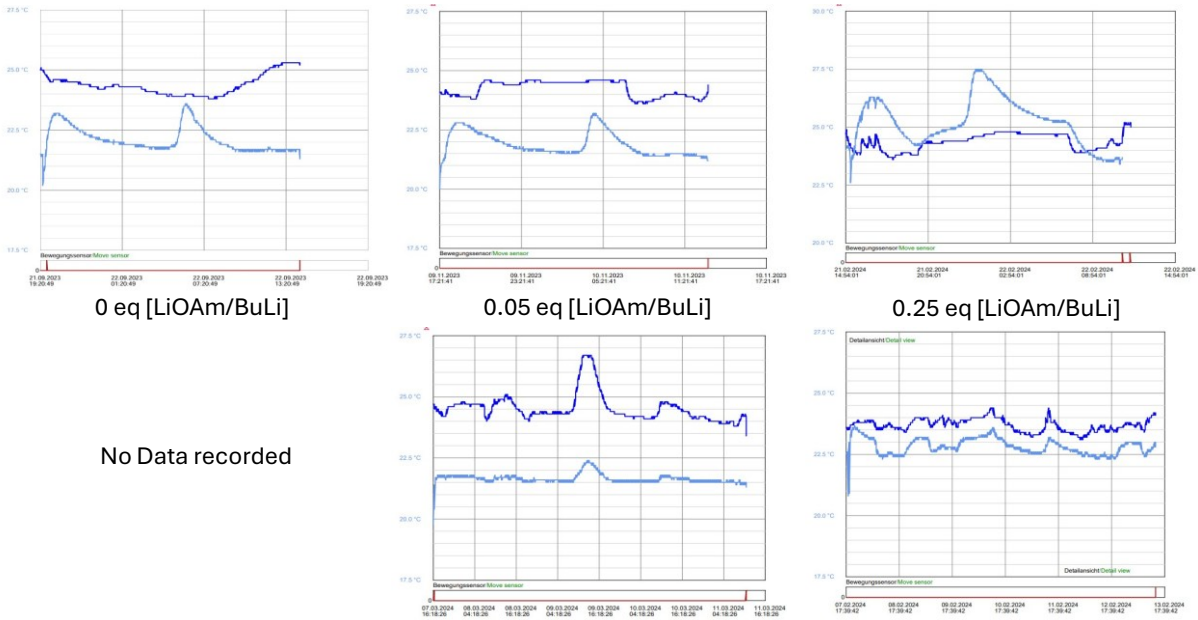

0 eq [LiOAm/BuLi] | 0.05 eq [LiOAm/BuLi] | 0.25 eq [LiOAm/BuLi]

No Data recorded | |

1 eq [LiOAm/BuLi] | 3 eq [LiOAm/BuLi] | 10 eq [LiOAm/BuLi]

Figure S2: Temperature recordings inside the reaction vessel for various [LiOAm/BuLi] ratios (light blue: temperature in the reaction vessel, drak blue room temperature).

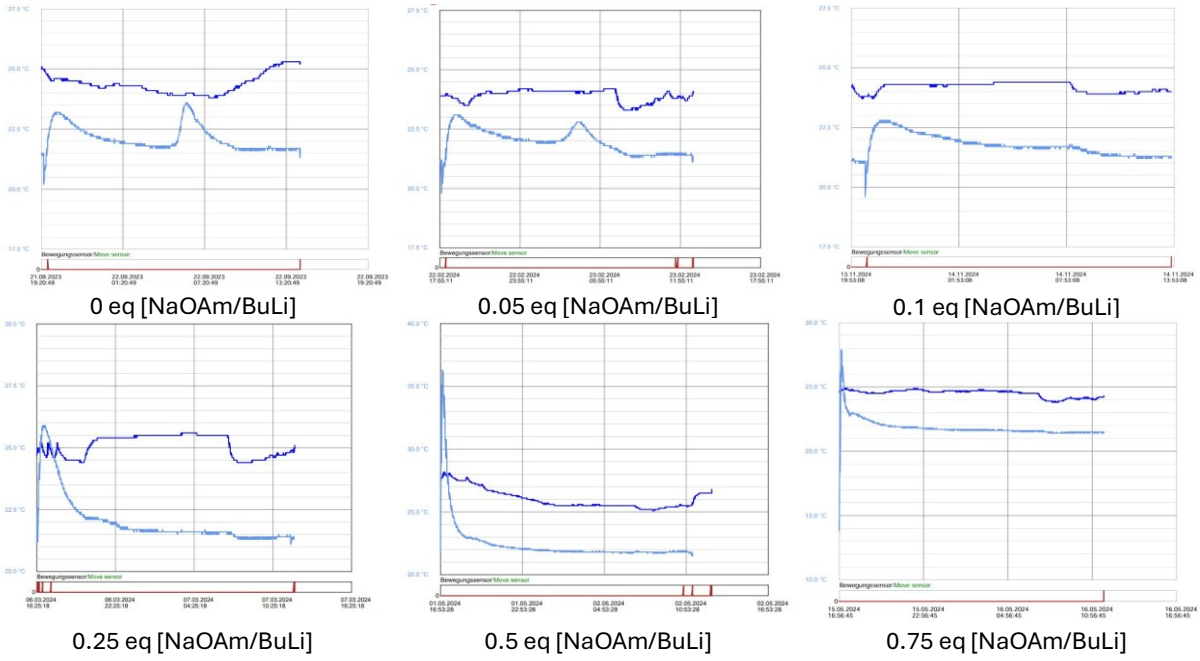

0 eq [NaOAm/BuLi] | 0.05 eq [NaOAm/BuLi] | 0.1 eq [NaOAm/BuLi]

0.25 eq [NaOAm/BuLi] | 0.5 eq [NaOAm/BuLi] | 0.75 eq [NaOAm/BuLi]

Figure S3: Temperature recordings inside the reaction vessel for various [NaOAm/BuLi] ratios (light blue: temperature in the reaction vessel, drak blue room temperature).

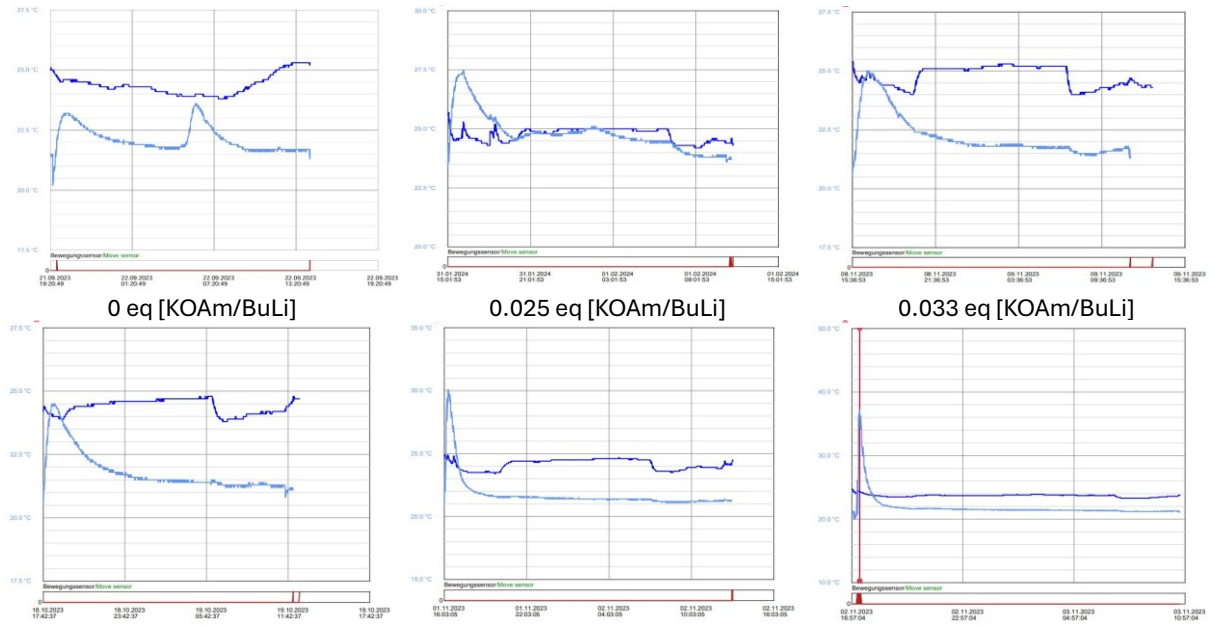

Figure S4: Temperature recordings inside the reaction vessel for various [KOAm/BuLi] ratios (light blue: temperature in the reaction vessel, drak blue room temperature).

2.3 SEC traces of Copolymers

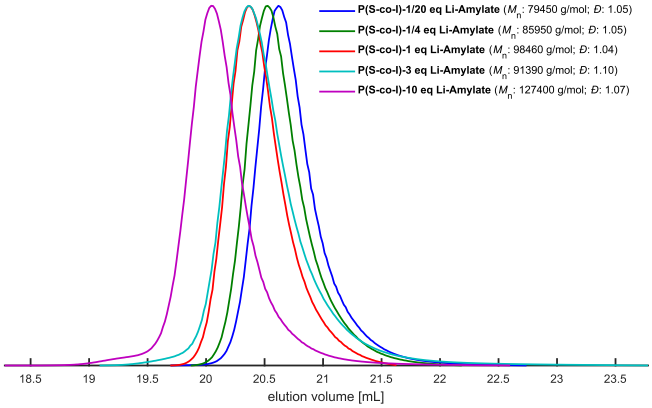

Figure S5: SEC (THF) traces of P(S-*co*-I) with different [LiOAm/BuLi] ratios and PS calibration.

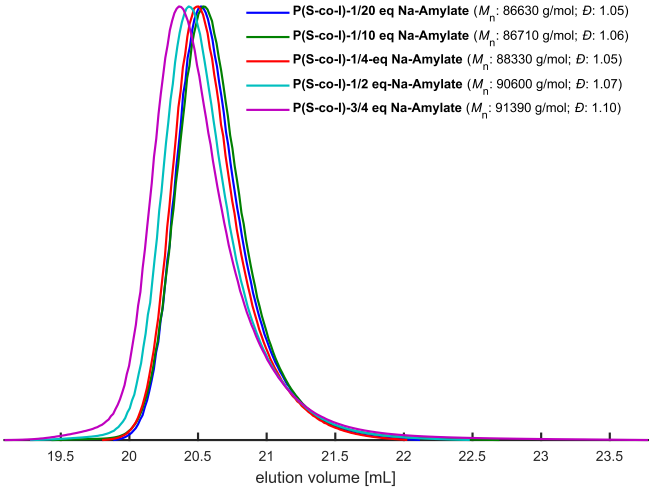

Figure S6: SEC (THF) traces of P(S-*co*-I) with different [NaOAm/BuLi] ratios and PS calibration.

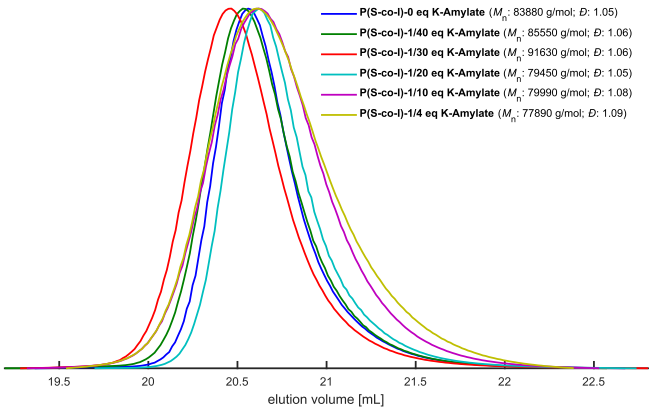

Figure S7: SEC (THF) traces of P(S-*co*-I) with different [KOAm/BuLi] ratios and PS calibration.

2.4 Kinetic Plots

2.4.1 LiOAm

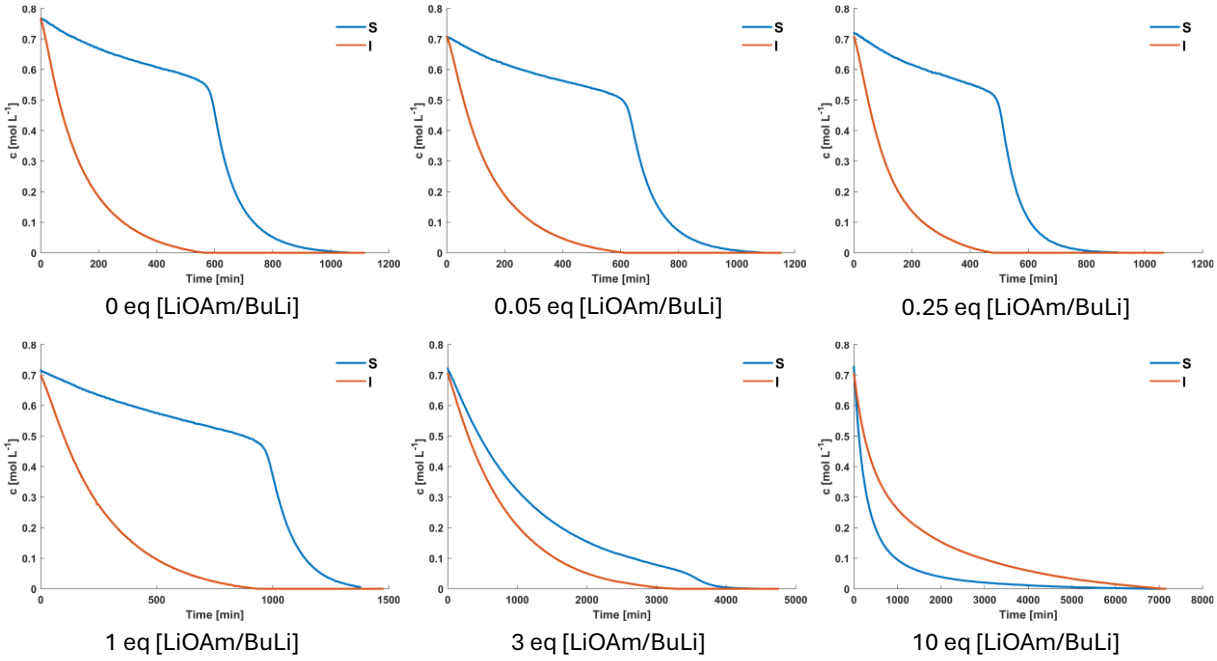

Figure S8: Individual time-conversion plots at various [LiOAm/BuLi] ratios.

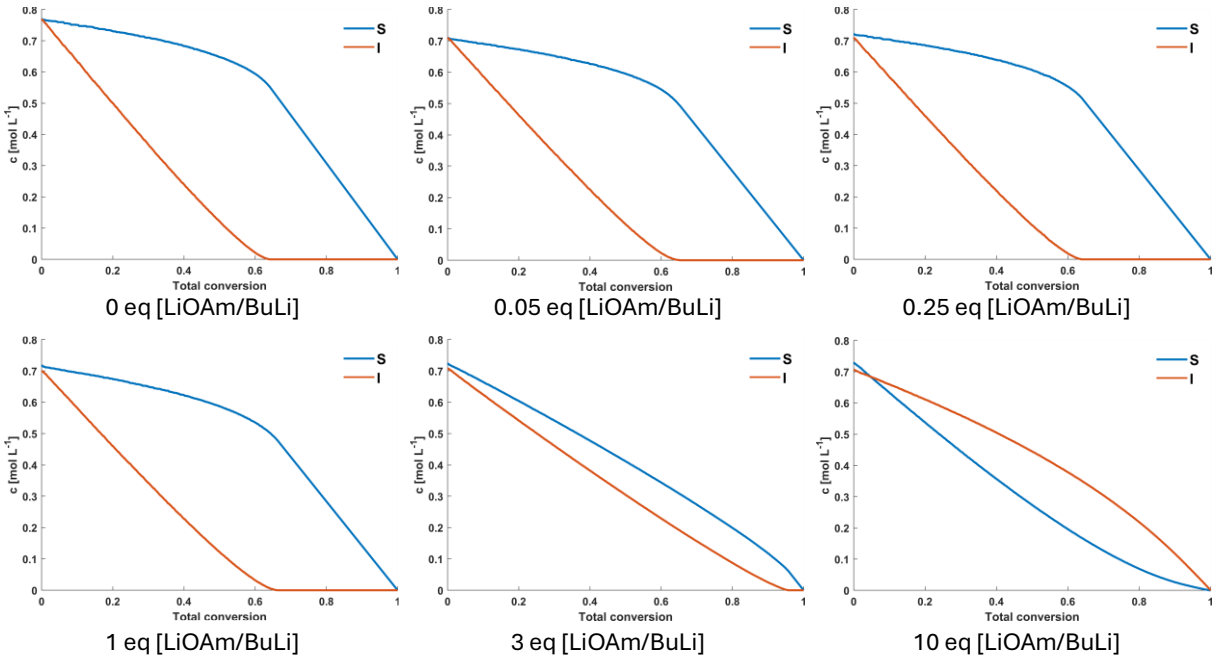

Figure S9: Individual monomer concentrations as a function of total conversion for various [LiOAm/BuLi] ratios.

2.4.2 NaOAm

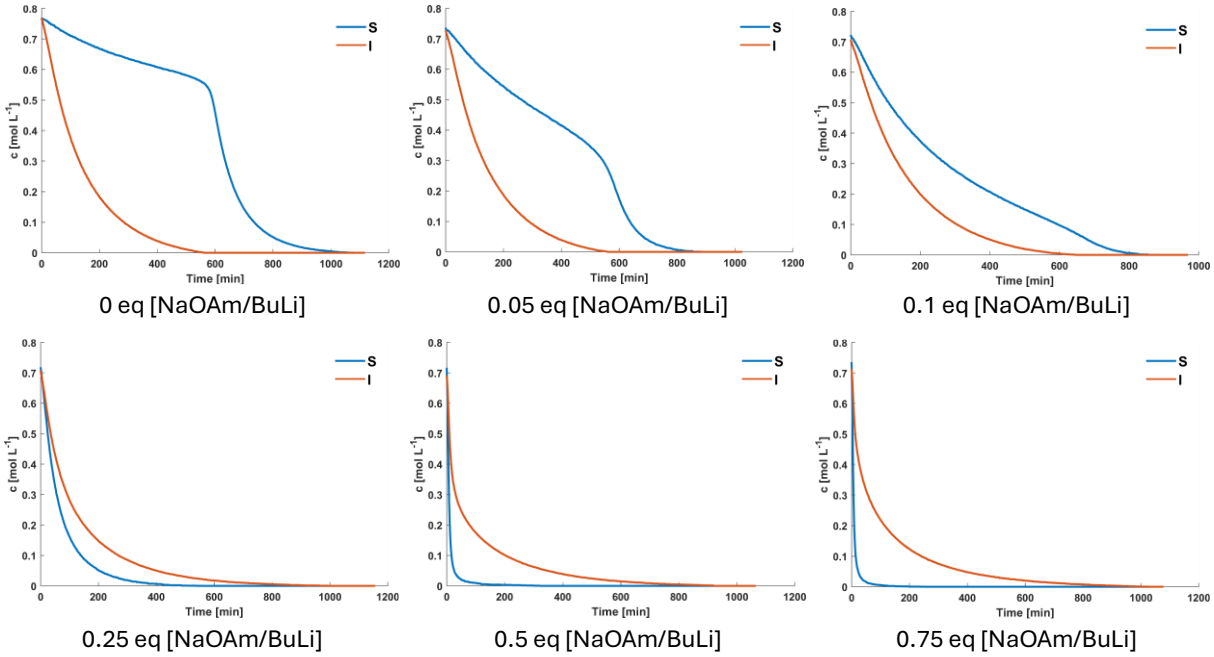

Figure S10: Individual time-conversion plots at various [NaOAm/BuLi] ratios.

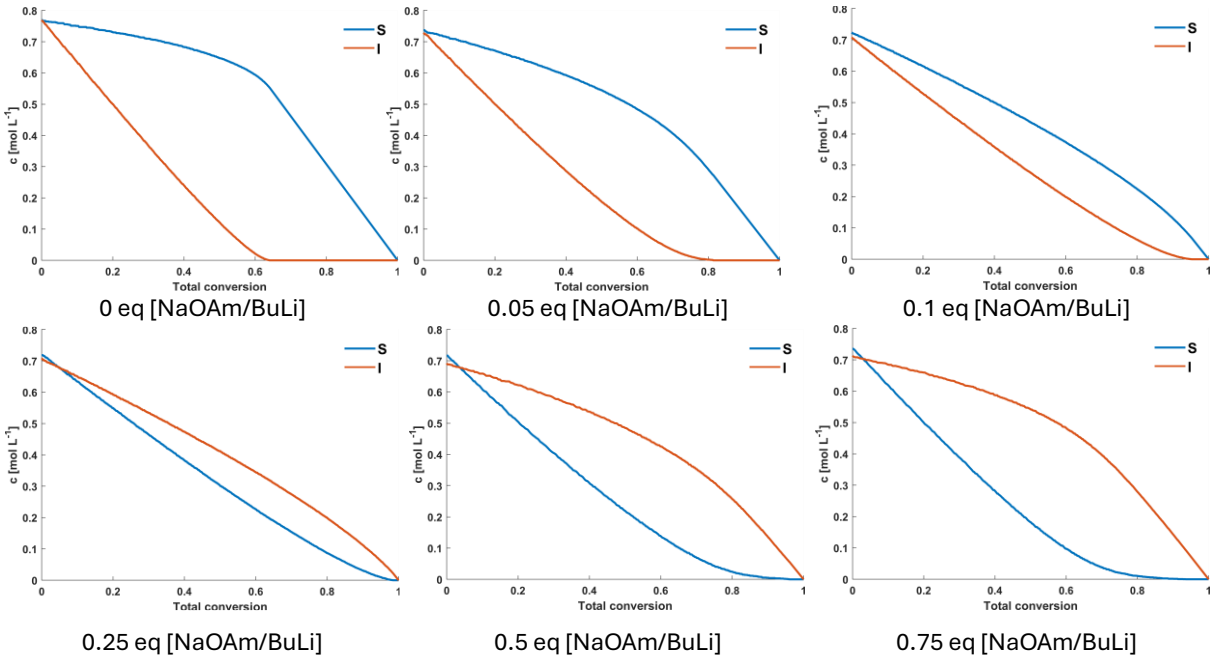

Figure S11: Individual monomer concentrations as a function of total conversion for various [NaOAm/BuLi] ratios.

2.4.3 KOAm

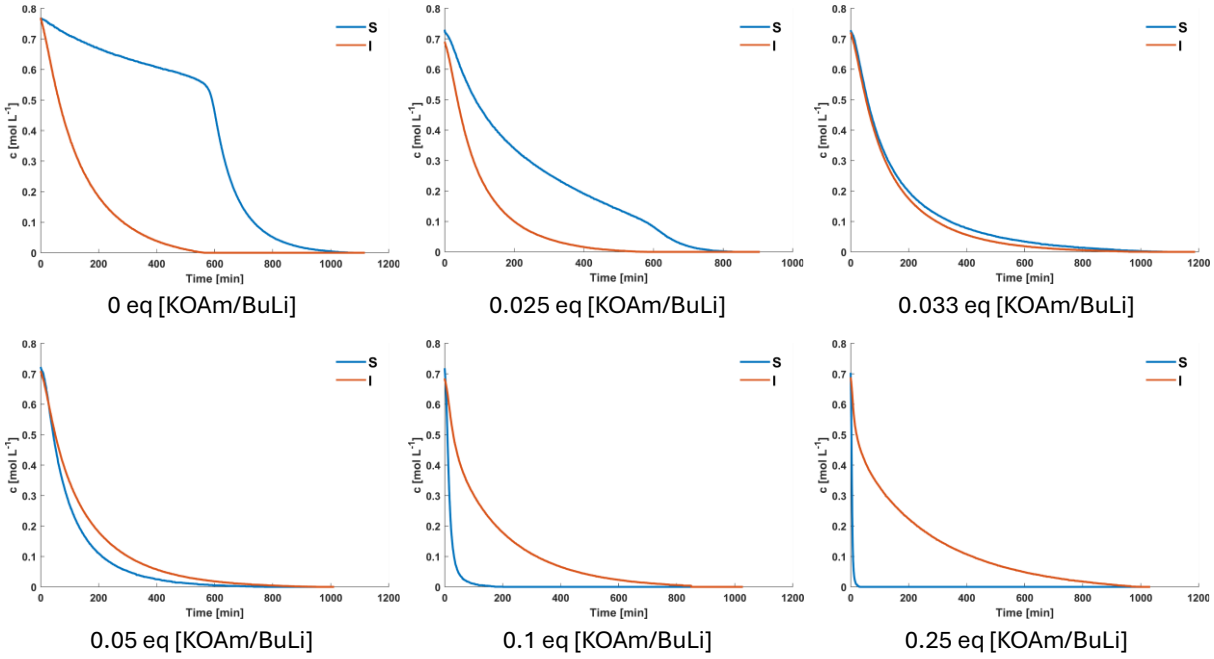

Figure S12: Individual time-conversion plots at various [KOAm]/BuLi] ratios.

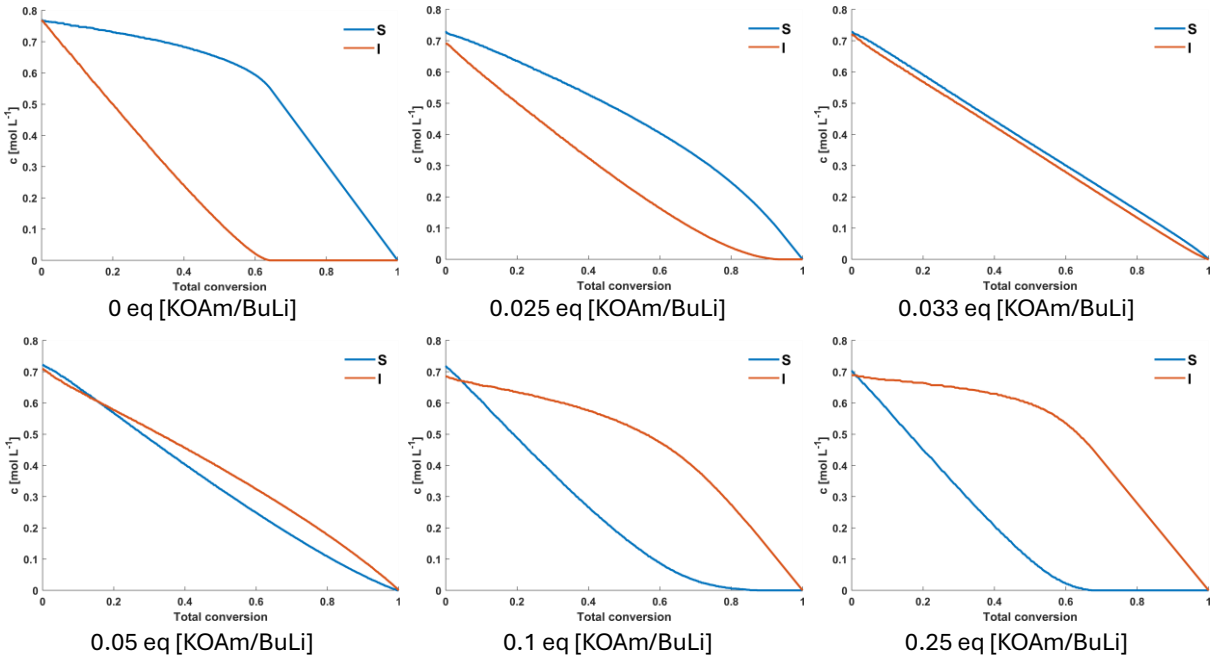

Figure S13: Individual monomer concentrations as a function of total conversion for various [KOAm/BuLi] ratios.

2.4.4 Half-lives of the copolymerizations

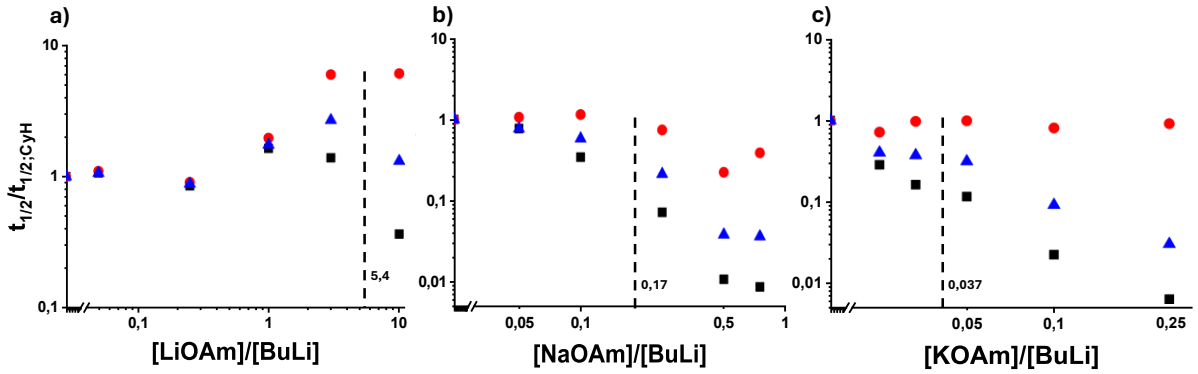

Figure S14: Estimated half-lives of isoprene (red circles), styrene (black squares) and both monomers (blue triangles) in the presence of different amylates. The half lives were normalized with the half-lives in pure cyclohexane, see Table 1.

3. Determination of reactivity ratios:

Reactivity ratios (r_I and r_S) were calculated using the terminal (Jaacks[14,15]) and the non-terminal (Meyer-Lowry[16]) model, which assumes an ideal copolymerization ($r_1 r_2 = 1$). Whenever the linear terminal plot was valid, this model is preferred to avoid overfitting in the non-terminal model.[17]

The reactivity ratios were calculated in the linear range of the individual vs total conversion plots up to 85-90% conversion of the monomer polymerizing faster. The last 5-10% were not taken into account, as these data points are more influenced by unstable baselines and background noises.

3.1 LiOAM

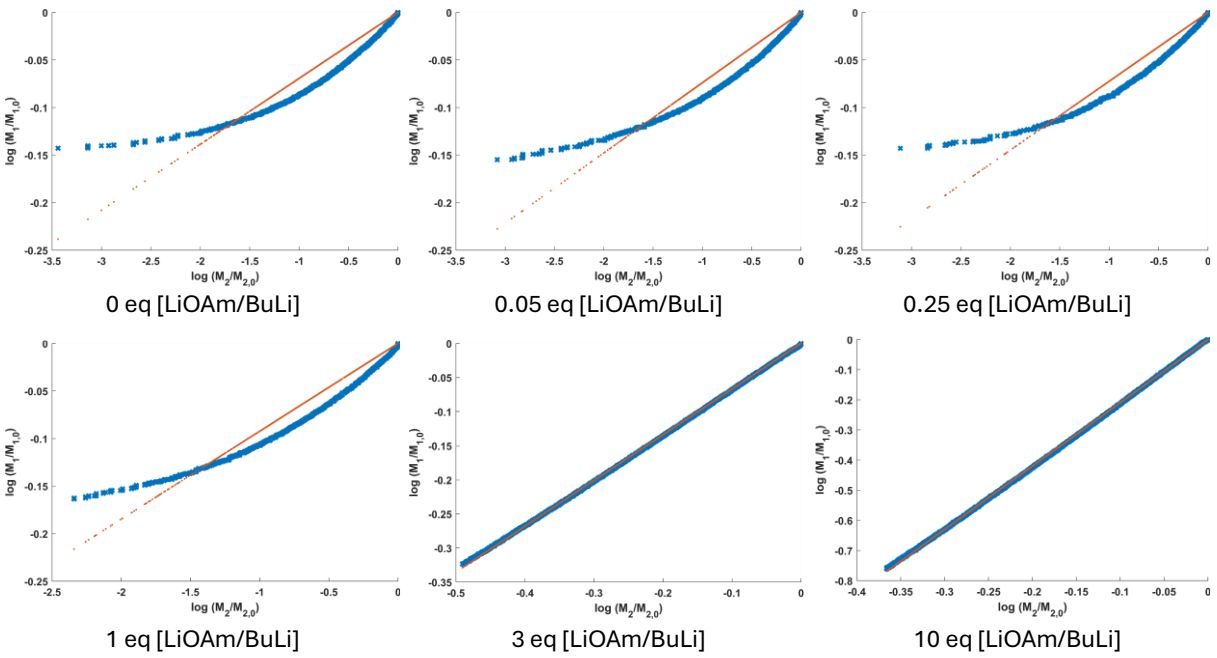

Figure S15: Jaacks fit (red line) of the copolymerization of P($S_{0.5}$-*co*-$I_{0.5}$) with different [LiOAm/BuLi] ratios.

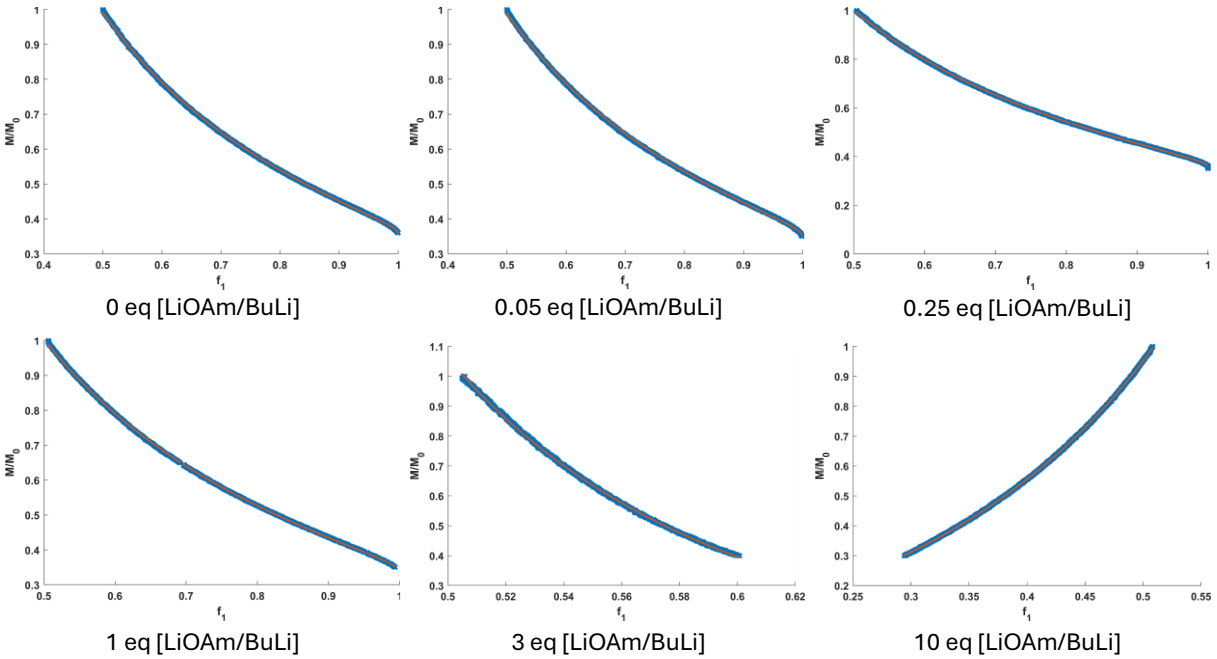

Figure S16: Meyer-Lowry fit (red line) of the copolymerization of P($S_{0.5}$-*co*-$I_{0.5}$) with different [LiOAm/BuLi] ratios.

3.2 NaOAm

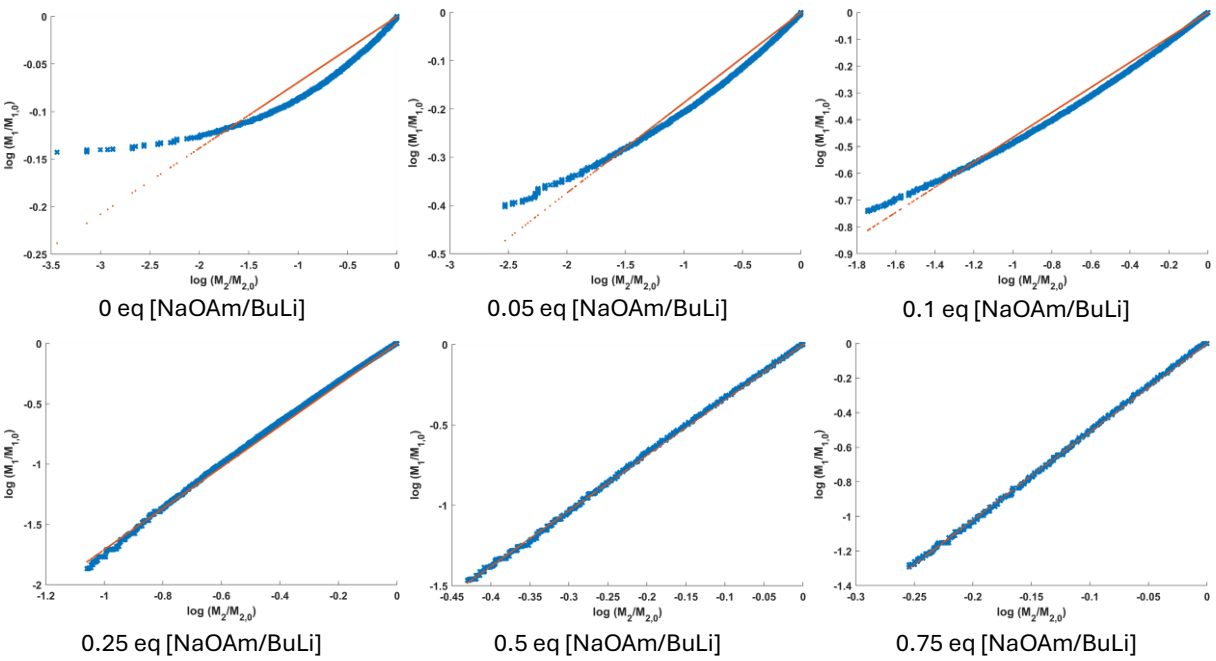

Figure S17: Jaacks fit (red line) of the copolymerization of P($S_{0.5}$-*co*-$I_{0.5}$) with different [NaOAm/BuLi] ratios.

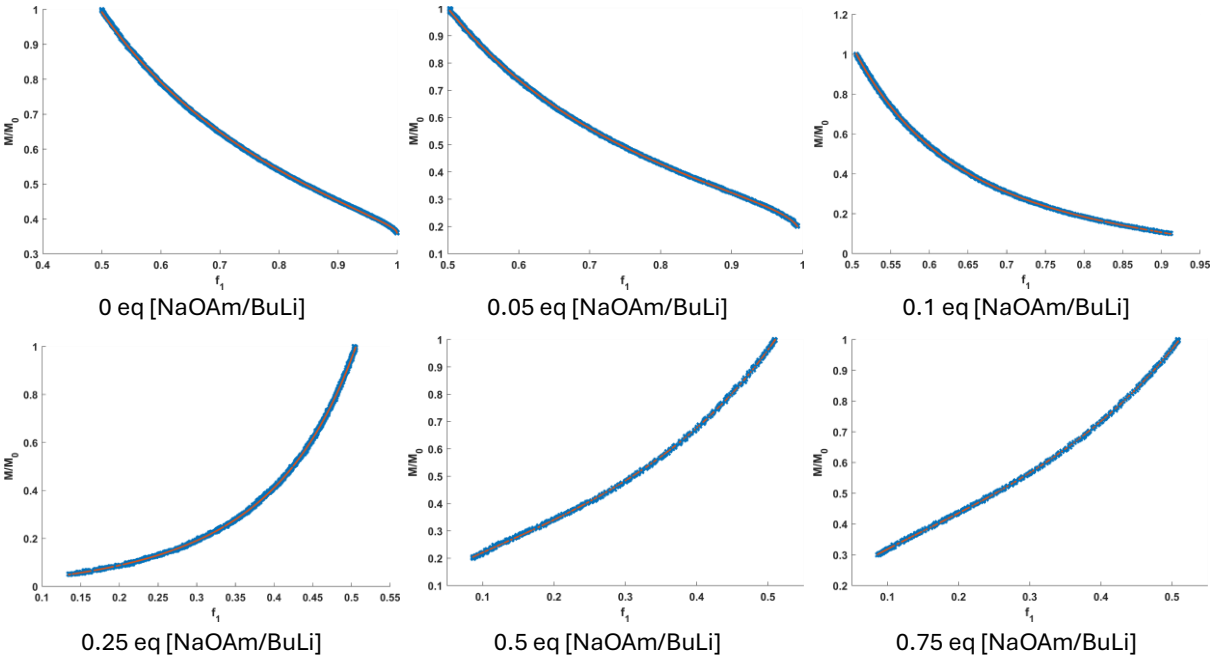

Figure S18 Meyer-Lowry fit (red line) of the copolymerization of P($S_{0.5}$-*co*-$I_{0.5}$) with different [NaOAm/BuLi] ratios.

3.3 KOAM

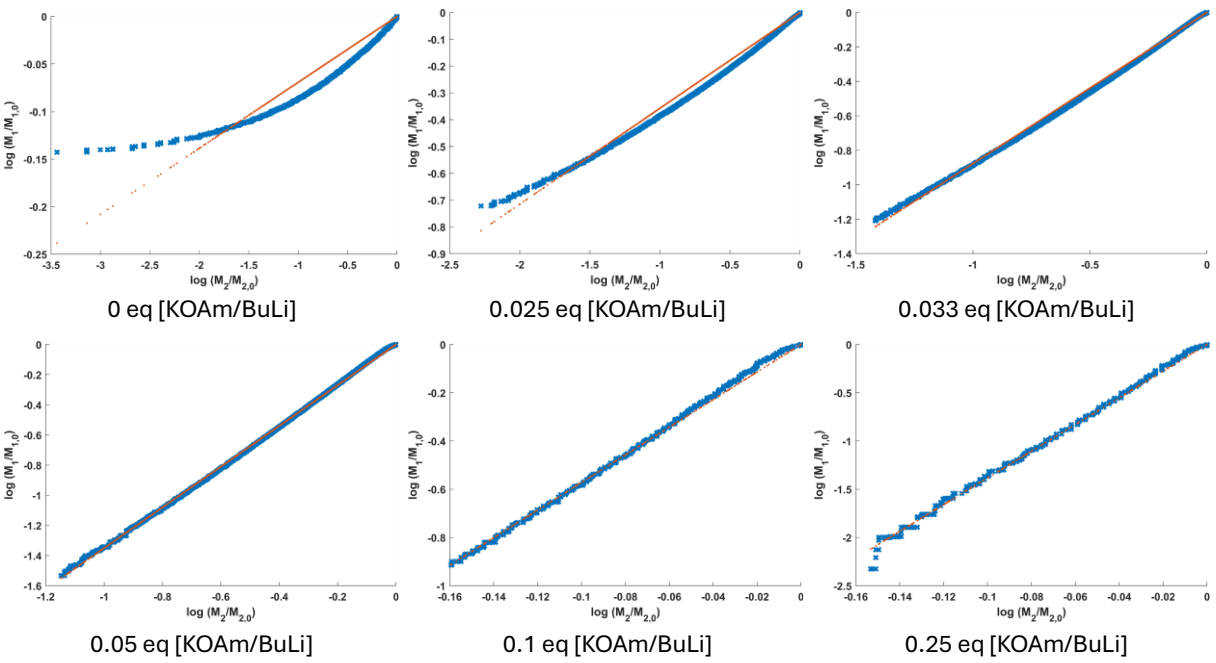

Figure S19: Jaacks fit (red line) of the copolymerization of P($S_{0.5}$-*co*-$I_{0.5}$) with different [KOAm/BuLi] ratios.

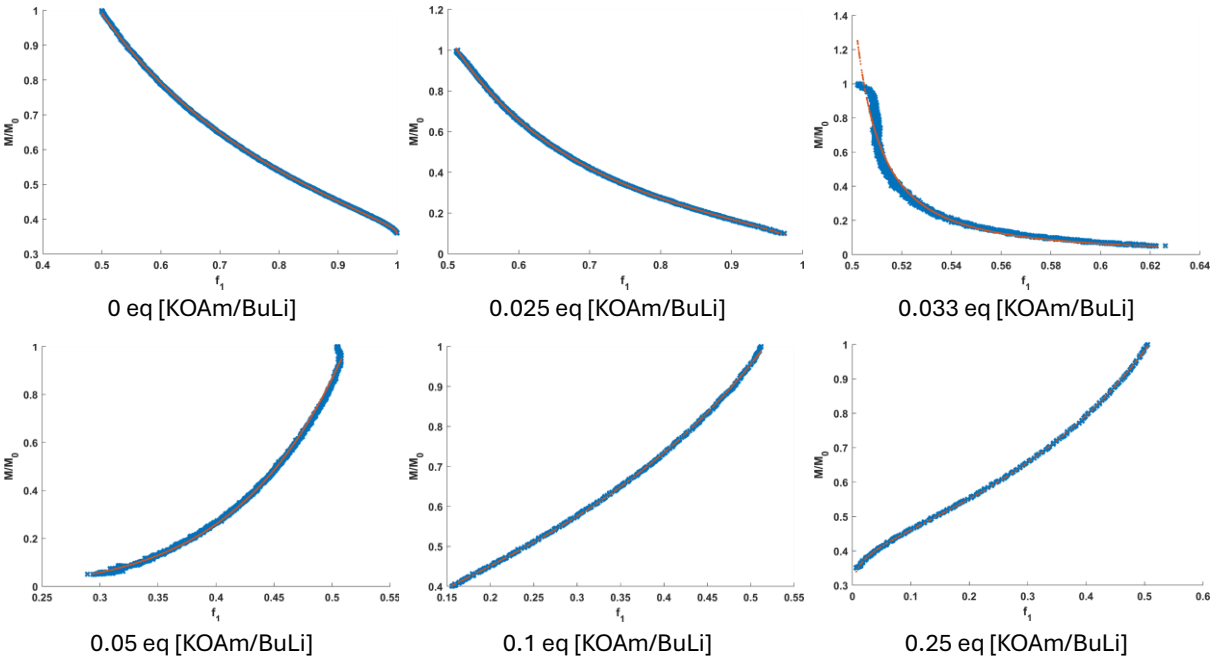

Figure S20: Meyer-Lowry fit (red line) of the copolymerization of P($S_{0.5}$-*co*-$I_{0.5}$) with different [KOAm/BuLi] ratios.

4. Copolymer composition

4.1 Molar and volume composition profiles

The molar copolymer composition were calculated using the reactivity ratios according to Wahlen et al.[18] For the volume based gradients, the monomer molecular weights and densities of the homopolymers, ρ_{PI} = 0.91 g/ml and ρ_{PS} = 1.05 g/ml, were used.

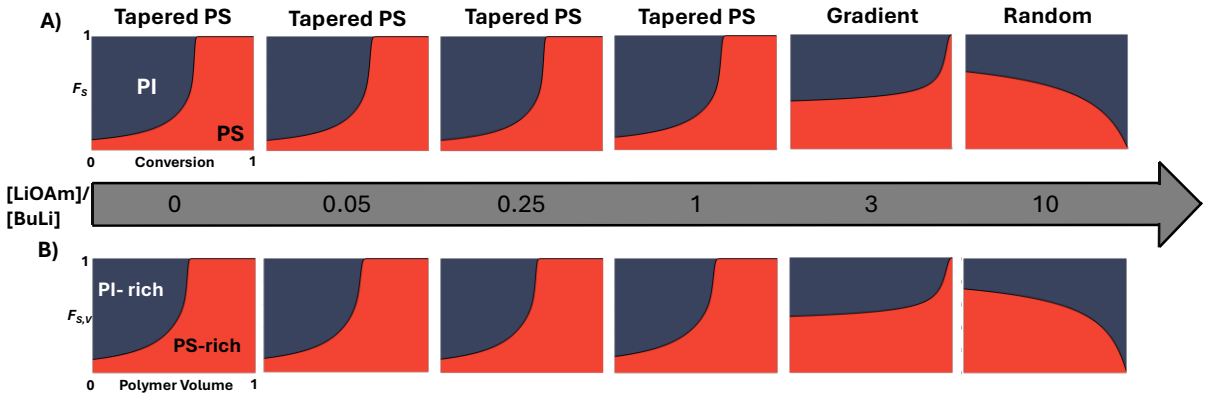

Figure S21: A) Molar B) volume composition profiles of the P($S_{0.5}$-*co*-$I_{0.5}$) copolymer as a function of the [LiOAm]/[BuLi] ratio.

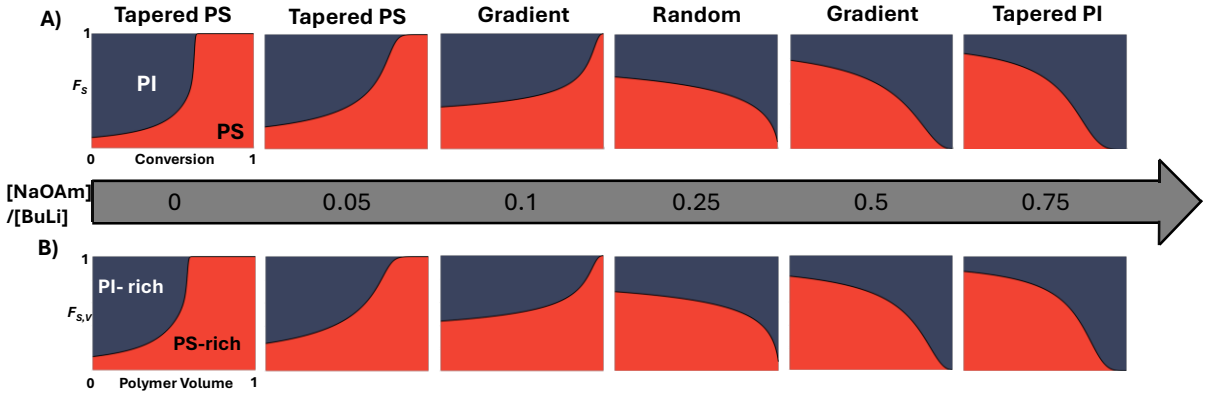

Figure S22: A) Molar B) volume composition profiles of the P($S_{0.5}$-*co*-$I_{0.5}$) copolymer as a function of the [NaOAm]/[BuLi] ratio.

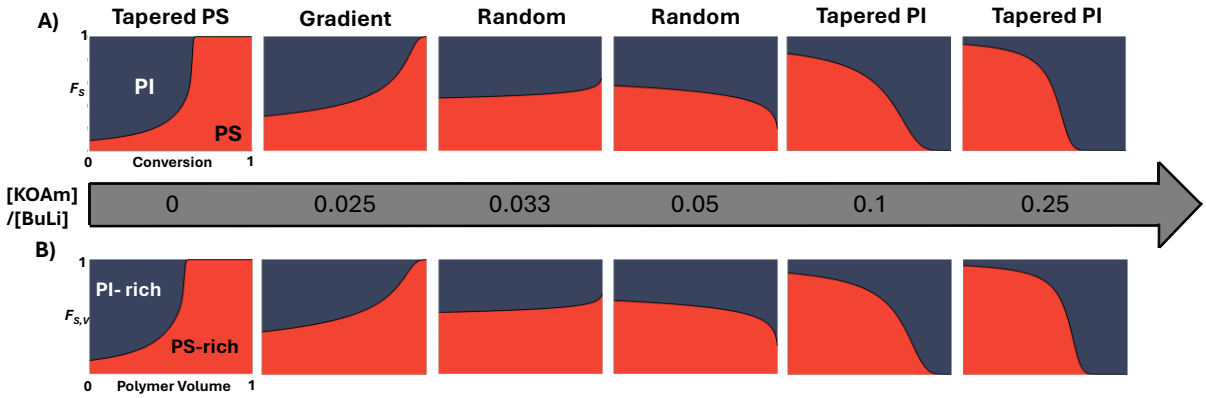

Figure S23: A) Molar B) volume composition profiles of the P($S_{0.5}$-*co*-$I_{0.5}$) copolymer as a function of the [KOAm]/[BuLi] ratio.

4.2 Blockiness

The so-called blockiness of the PS units is defined as the fraction of two to three contiguous styrene units in the copolymer. For block styrene are the ortho protons (h) shifted to 6.93-6.25 ppm in the NMR spectra and with increasing randomness they shift to 7.50-6.93 ppm.[19–22] Further information about this topic can be found in previous publications.[2,3,11,12]

The blockiness was calculated using the integrals of the total aromatic protons: I_1 = 7.50-6.25 ppm (5H) and those of the block styrene, I_2 = 6.93-6.25 ppm (2H):

$$B = \frac{I_2/2}{I_1/5}$$

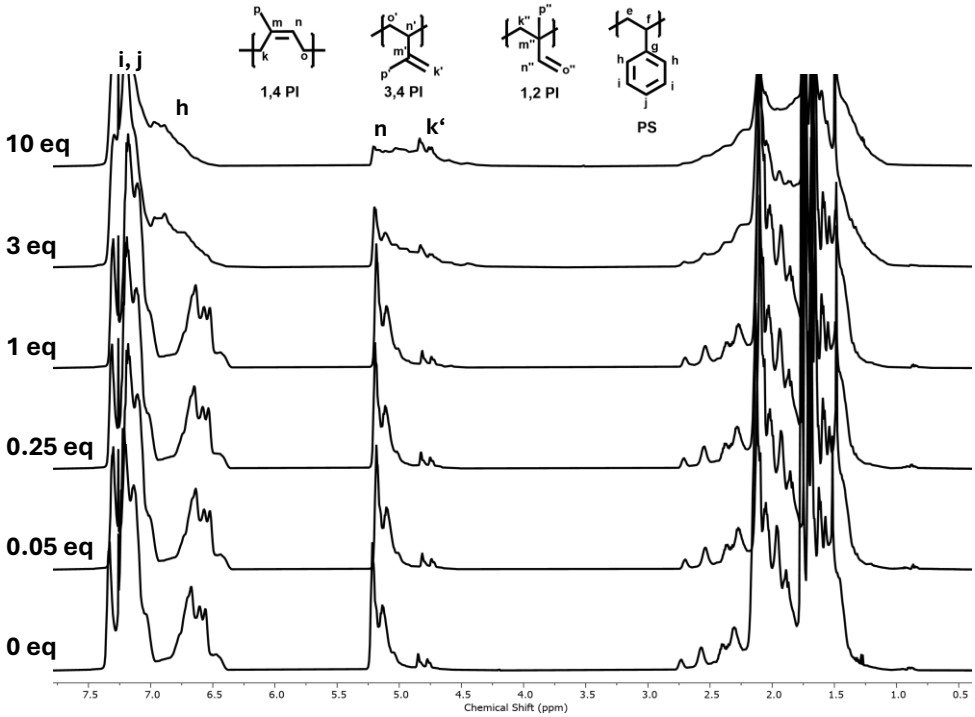

Figure S24: Stacked ^{1}H-NMR spectra of P(S-*co*-I) synthesized with different [LiOAm/BuLi] ratios.

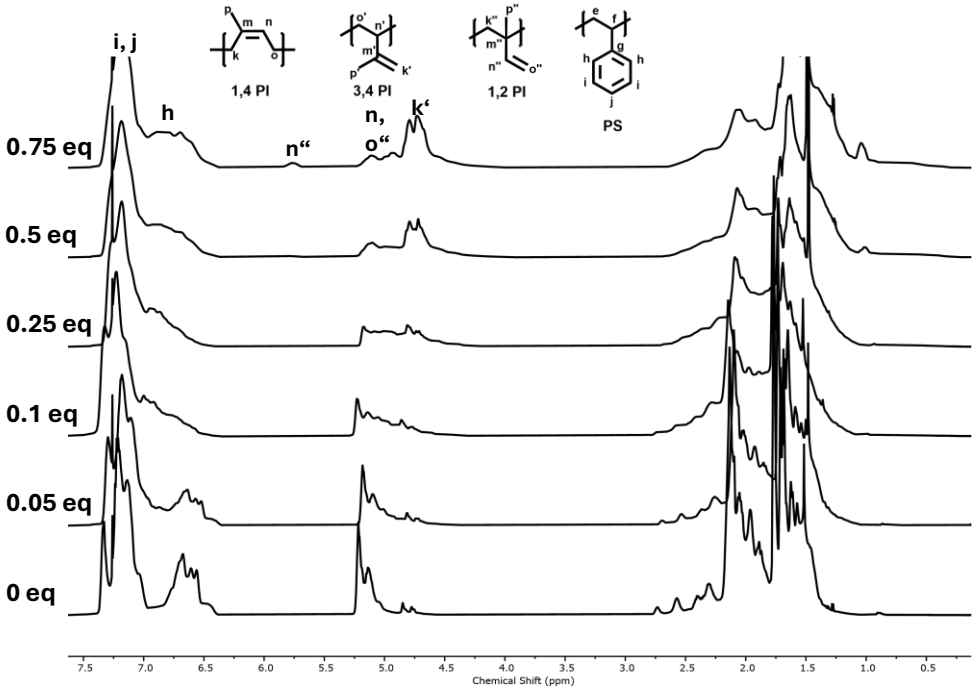

Figure S25 Stacked ^{1}H-NMR spectra of P(S-*co*-I) synthesized with different [NaOAm/BuLi] ratios.

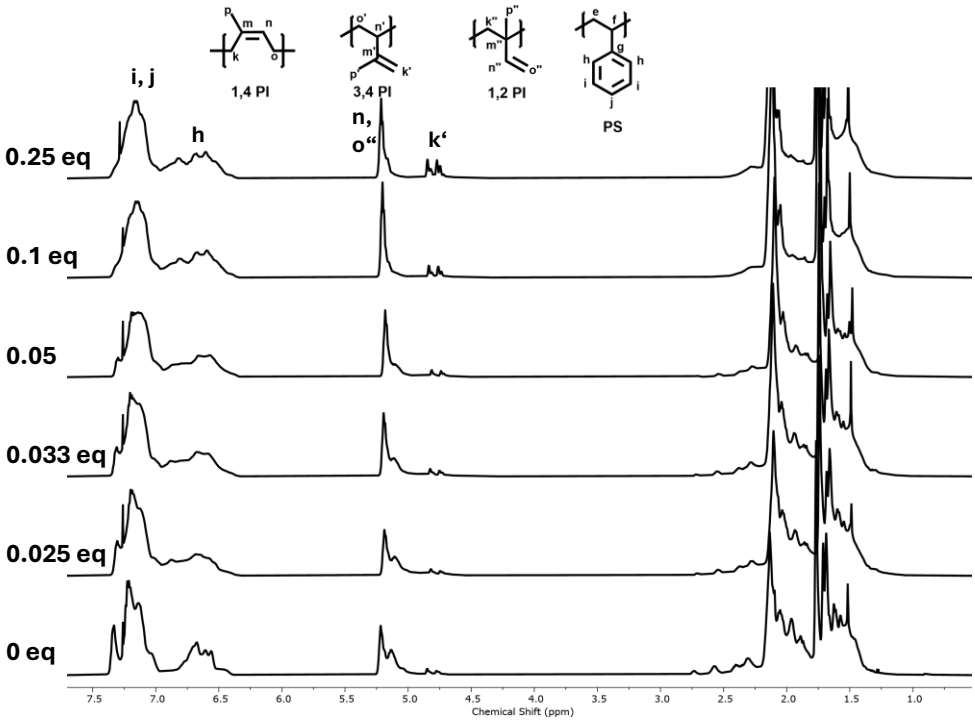

Figure S26 Stacked ^{1}H-NMR spectra of P(S-*co*-I) synthesized with different [KOAm/BuLi] ratios.

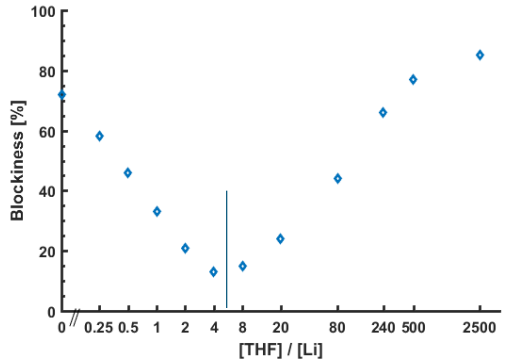

Figure S27. Blockiness of P(S-co-I) as a function of the [THF]/[Li] ratio. The vertical line represents random copolymerization.[3] Reproduced by permit of American Chemical Society.

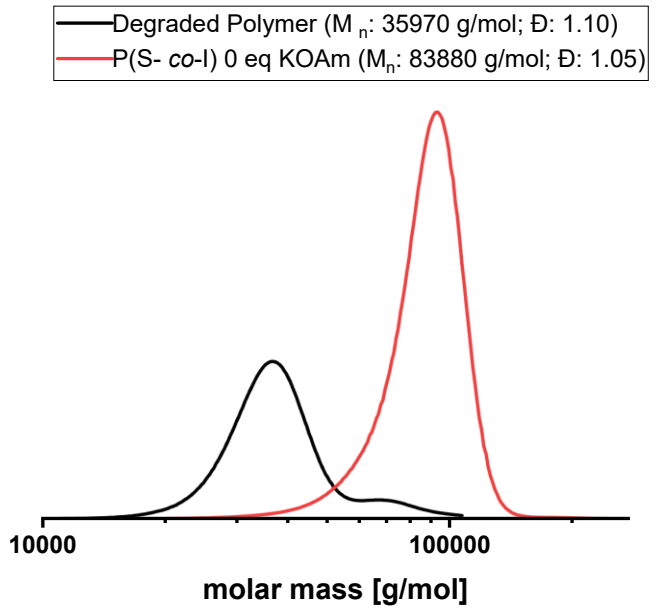

Figure S 28: SEC (THF, PS-calibration) traces of P(S-*co*-I) (red) synthesized in cyclohexane (top) and in the presence of 1/30 equiv potassium amylate (bottom) and the oxidative degradation product (black).

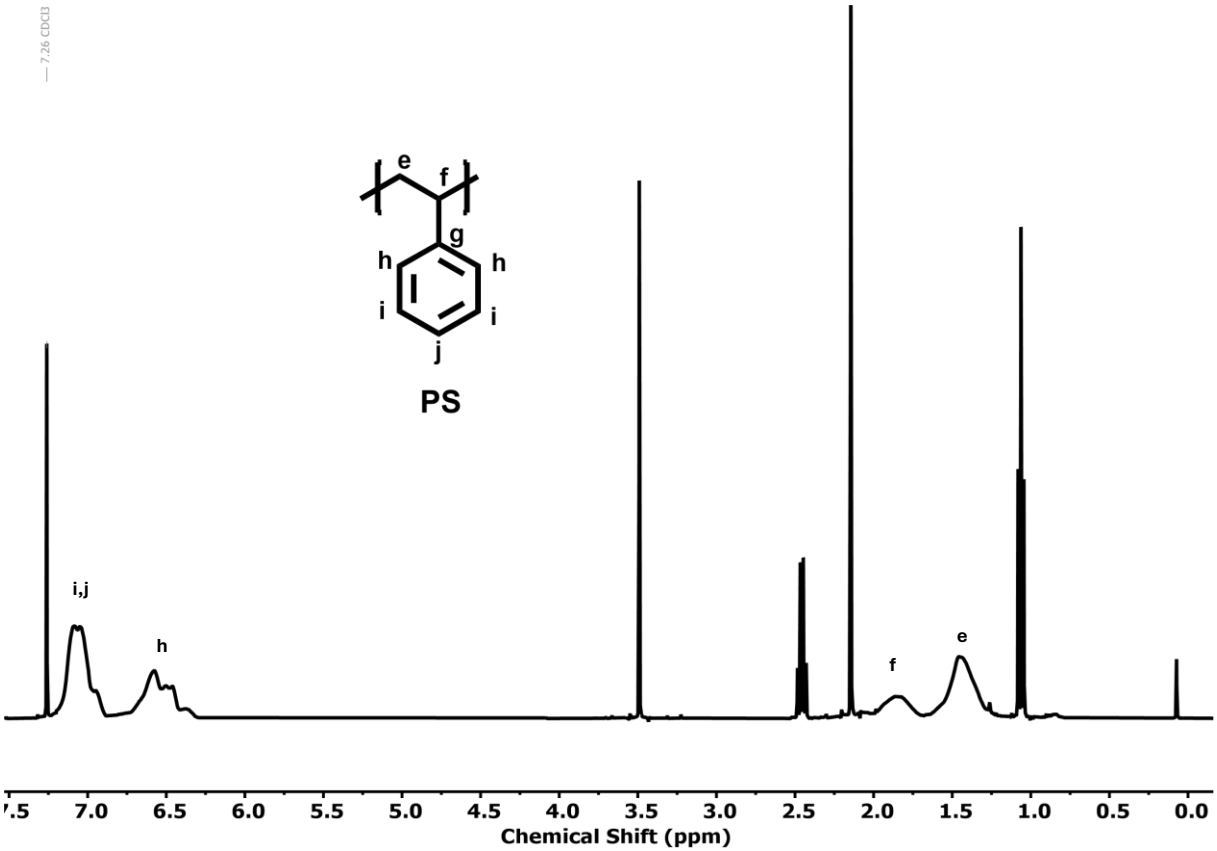

Figure S29: Assigned ^{1}H-NMR spectra of PS, obtained from degraded P(S-*co*-I) synthesized in cyclohexane with 0.033 equiv KOAm.

5. Microstructure of PI units

The microstructure of the PI units was determined via ^{1}H-NMR. With increasing modifier content increase the 3,4- and 1,2-units, which are represented by the following signals: 5.80-5.27 ppm (n''), 4.85-4.38 ppm (k') and 5.30-4.85 ppm (n, o'').

$$I_{1,2} = I(5.80 - 5.27)$$

$$I_{3,4} = I(4.85 - 4.38)$$

$$I_{1,4} = I(5.30 - 4.85) - 2 * I_{1,2}$$

$$C_{1,2} = \frac{I_{1,2}}{I_{1,2} + I_{3,4} + I_{1,4}}$$

$$C_{3,4} = \frac{I_{3,4}}{I_{1,2} + I_{3,4} + I_{1,4}}$$

$$C_{1,4} = \frac{I_{1,4}}{I_{1,2} + I_{3,4} + I_{1,4}}$$

C is the content of the microstructure in the polymer. Partially overlap, especially of the signals k' and n, o'', limits the accuracy of this method. But the results are in good agreement with literature,[1] slight differences can be explained by this overlap, different reaction temperature and different monomer and chain end concentrations.[23]

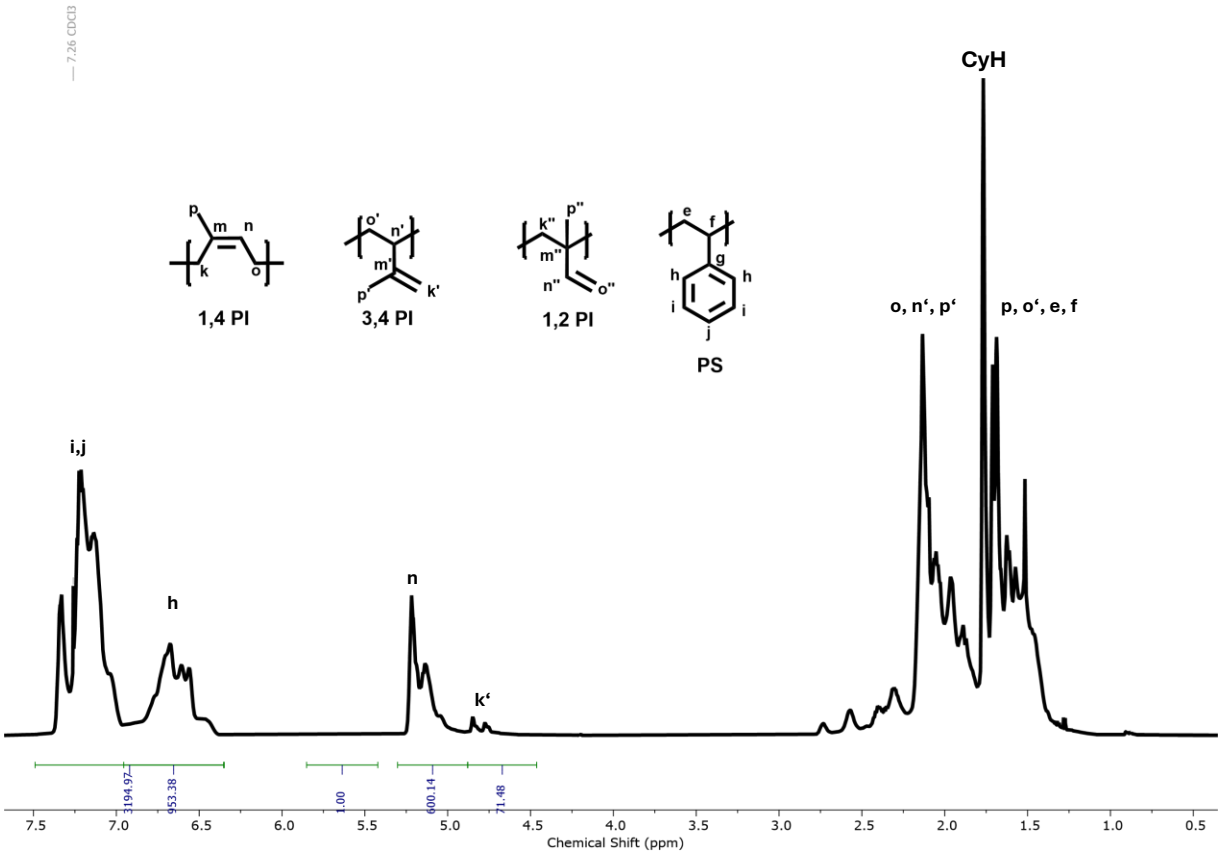

Figure S30: Assigned ^{1}H-NMR spectra of the copolymer P(S-*co*-I) synthesized in pure cyclohexane.

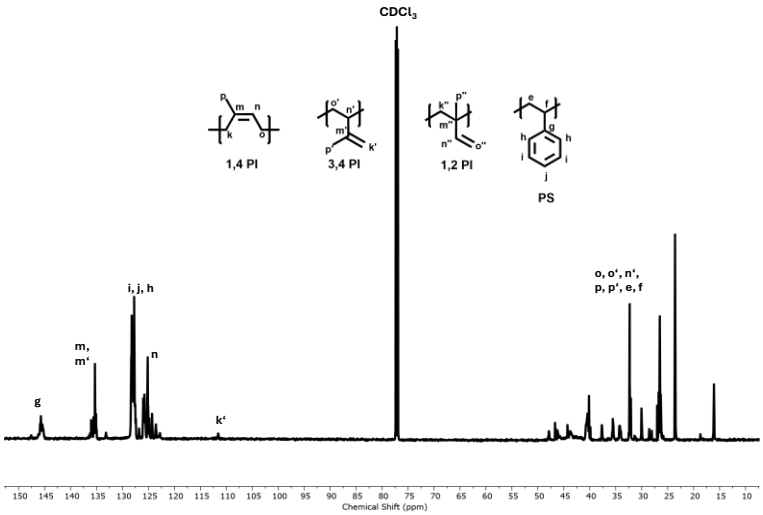

Figure S31: Assigned ^{13}C-NMR spectra of the copolymer P(S-*co*-I) synthesized in pure cyclohexane.

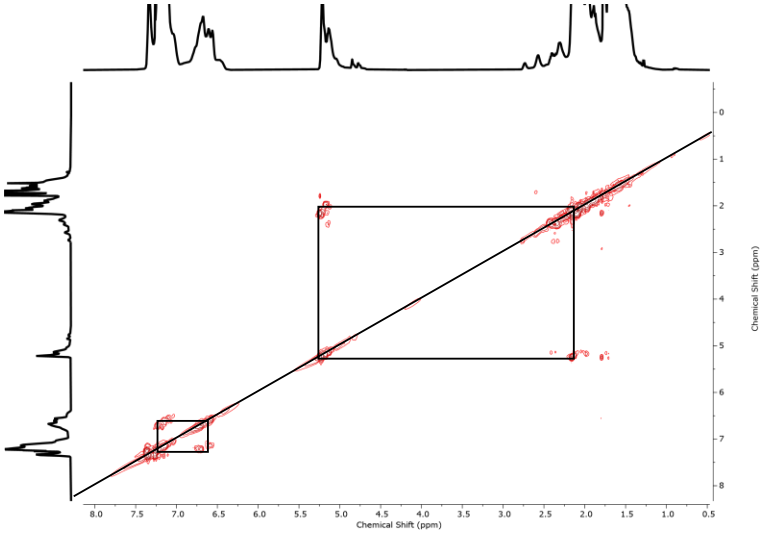

Figure S32: Assigned COSY-NMR spectra of the copolymer P(S-*co*-I) synthesized in pure cyclohexane.

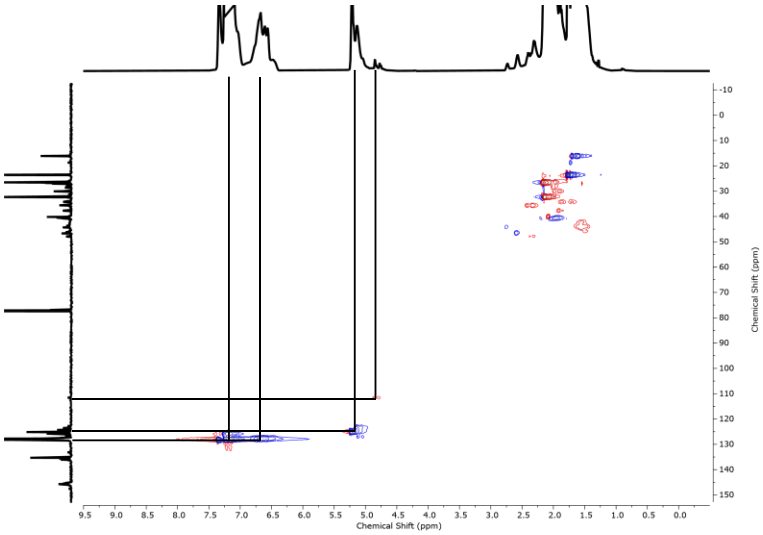

Figure S33: Assigned HSQC-NMR spectra of the copolymer P(S-*co*-I) synthesized in pure cyclohexane.

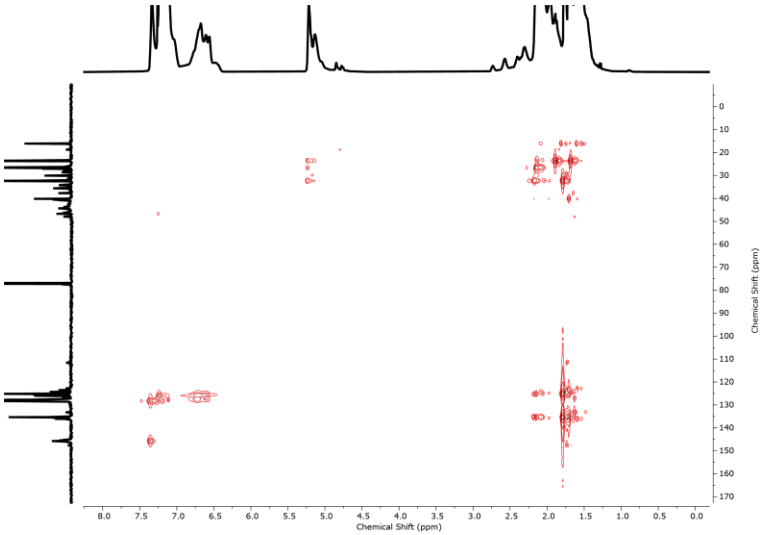

Figure S34: Assigned HMBC-NMR spectra of the copolymer P(S-*co*-I) synthesized in pure cyclohexane.

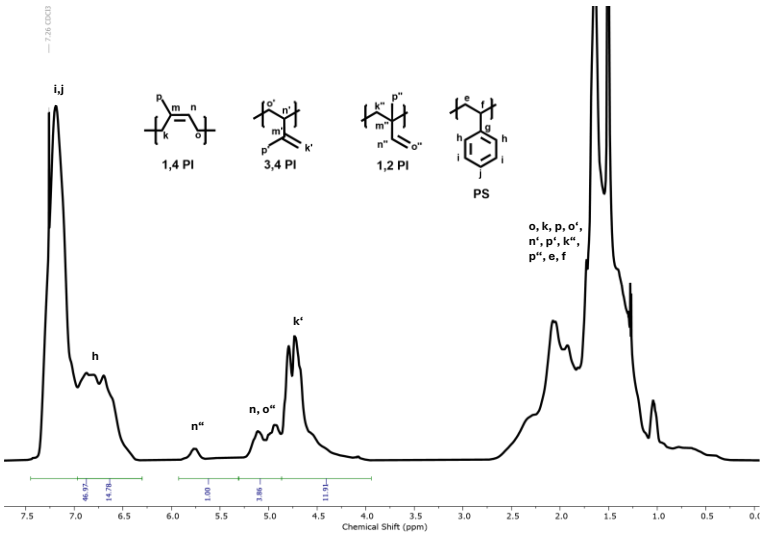

Figure S35: Assigned ^{1}H-NMR spectra of the copolymer P(S-*co*-I) synthesized in cyclohexane with 0.75 equiv. NaOAm.

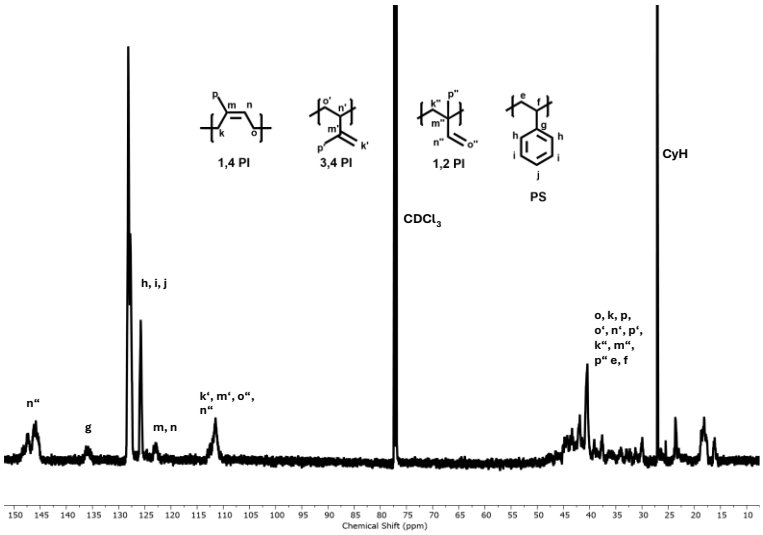

Figure S36: Assigned ^{13}C-NMR spectra of the copolymer P(S-*co*-I) synthesized in cyclohexane with 0.75 equiv. NaOAm.

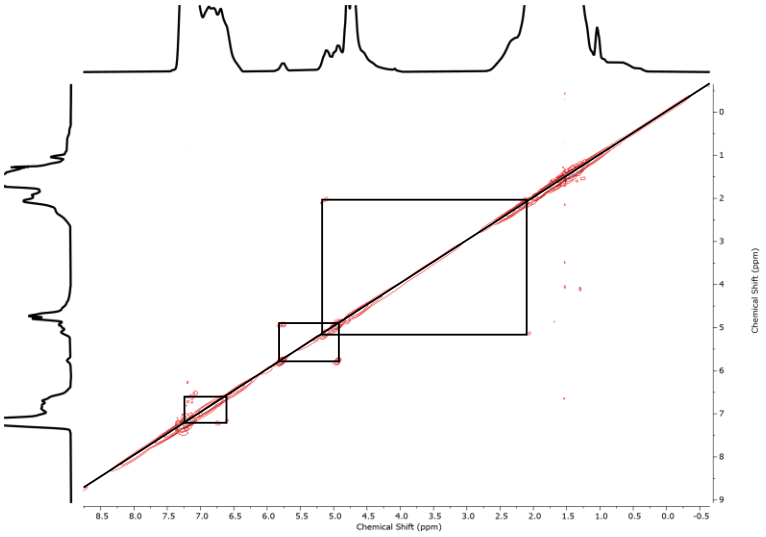

Figure S37: Assigned COSY-NMR spectra of the copolymer P(S-*co*-I) synthesized in cyclohexane with 0.75 equiv. NaOAm.

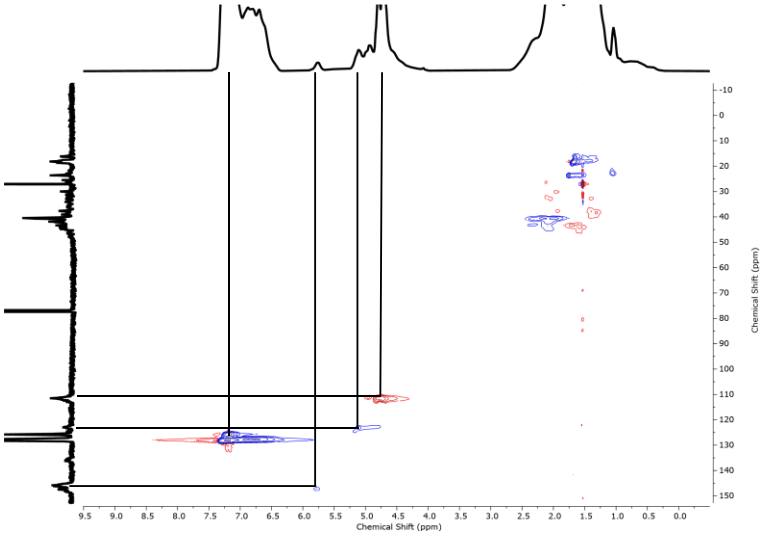

Figure S38: Assigned HSQC-NMR spectra of the copolymer P(S-*co*-I) synthesized in cyclohexane with 0.75 equiv. NaOAm.

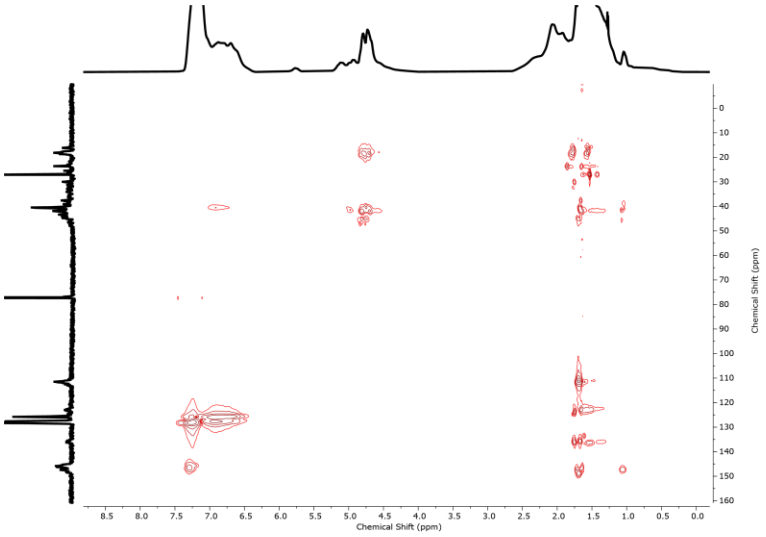

Figure S39: Assigned HMBC-NMR spectra of the copolymer P(S-*co*-I) synthesized in cyclohexane with 0.75 equiv. NaOAm.

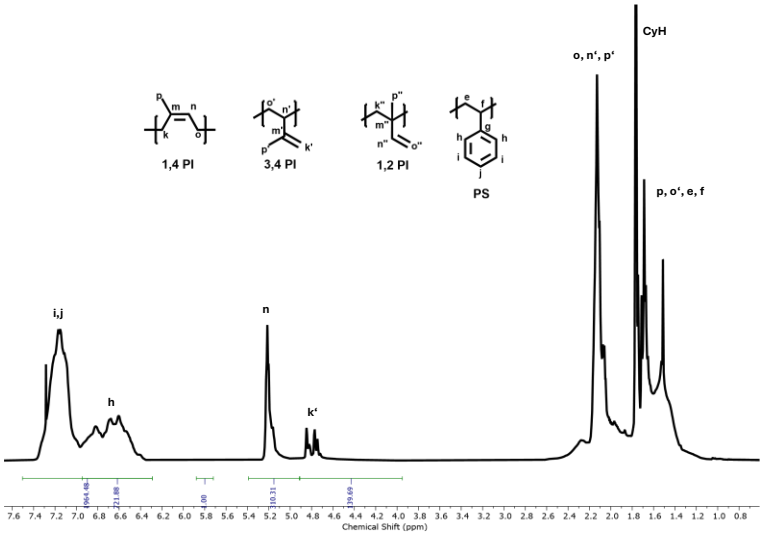

Figure S40: Assigned ^{1}H-NMR spectra of the copolymer P(S-*co*-I) synthesized in cyclohexane with 0.25 equiv. KOAm.

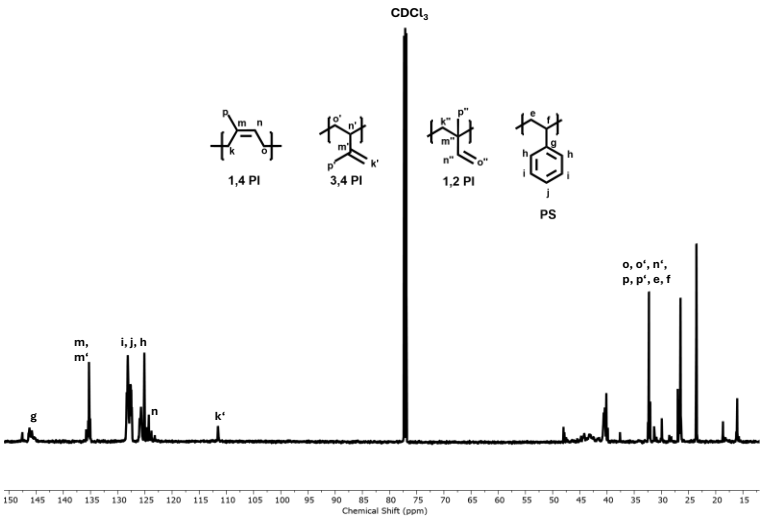

Figure S41: Assigned ^{13}C-NMR spectra of the copolymer P(S-*co*-I) synthesized in cyclohexane with 0.25 equiv. KOAm.

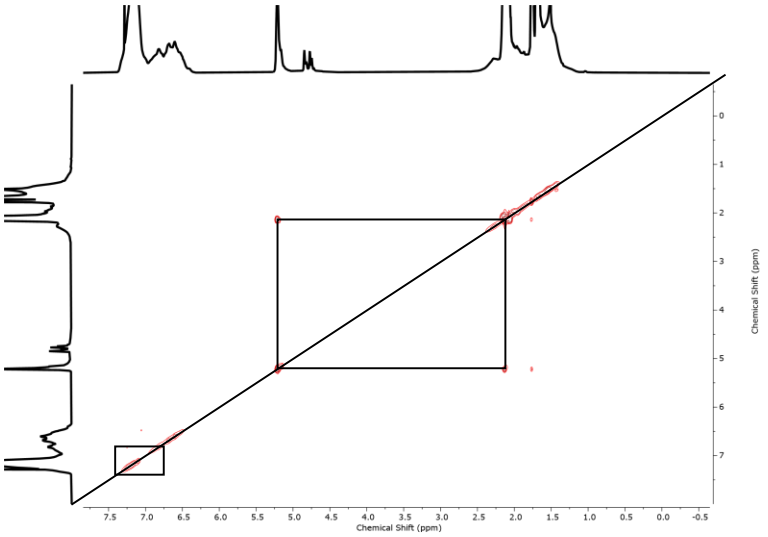

Figure S42: Assigned COSY-NMR spectra of the copolymer P(S-*co*-I) synthesized in cyclohexane with 0.25 equiv. KOAm.

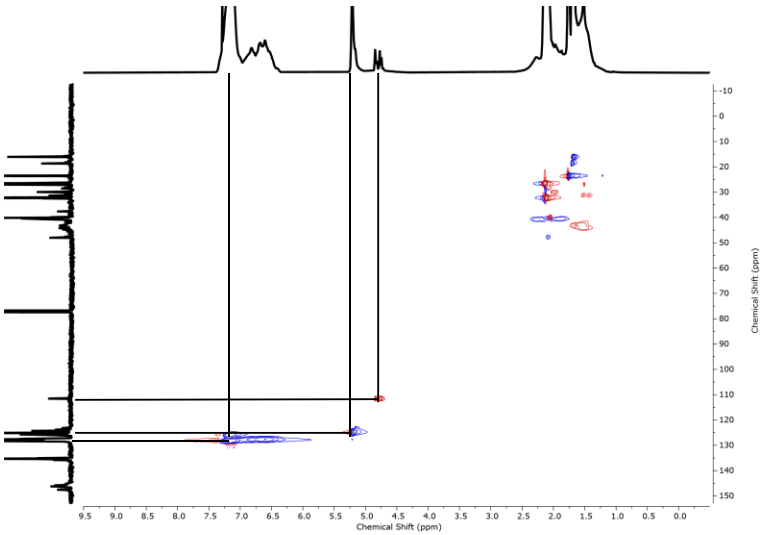

Figure S43: Assigned HSQC-NMR spectra of the copolymer P(S-*co*-I) synthesized in cyclohexane with 0.25 equiv. KOAm.

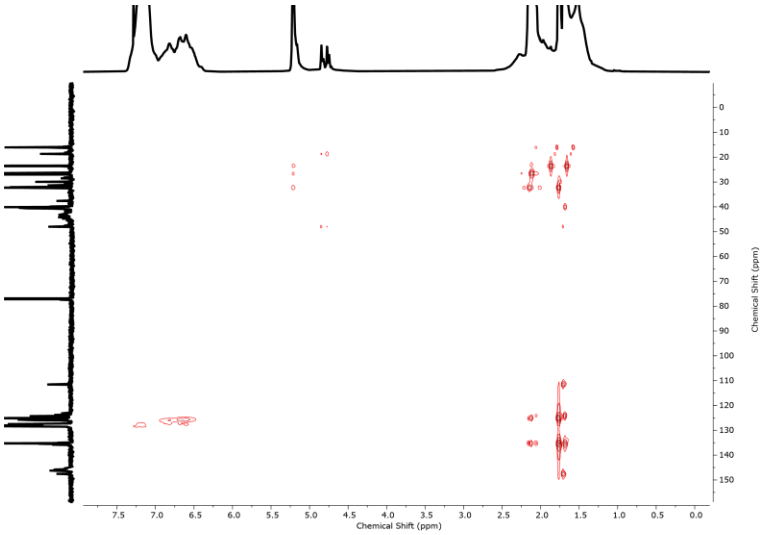

Figure S44: Assigned HMBC-NMR spectra of the copolymer P(S-*co*-I) synthesized in cyclohexane with 0.25 equiv. KOAm.

6. Glass transition temperatures

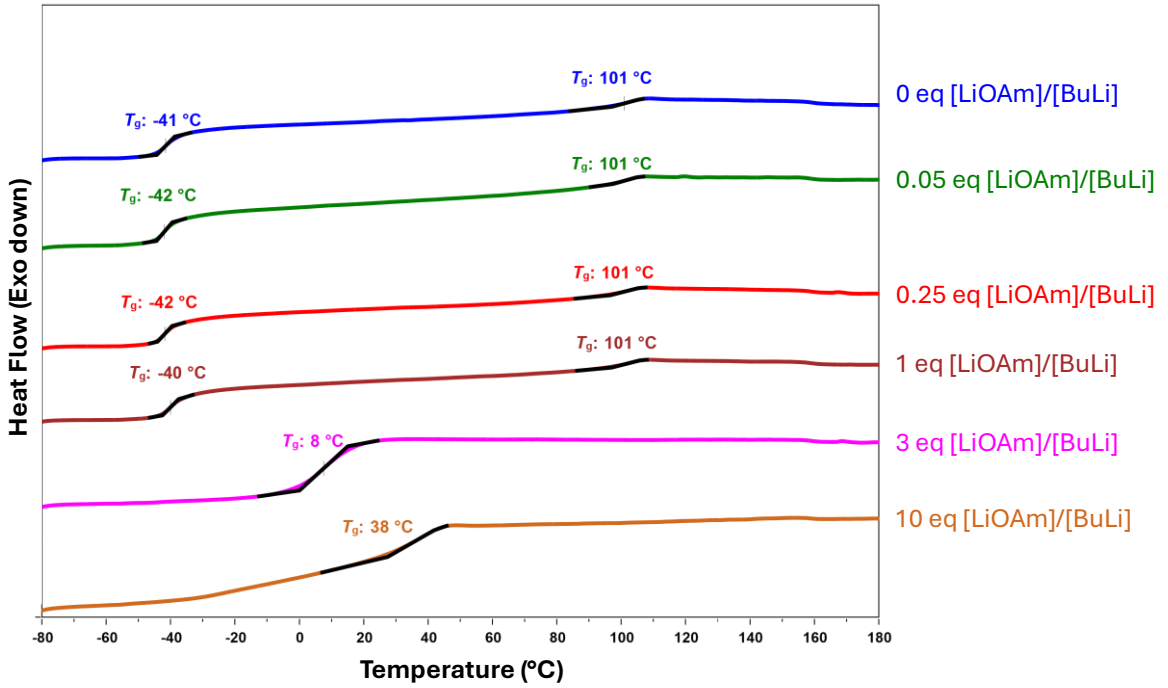

Figure S45: Second DSC heating curve of P(S-*co*-I) synthesized with different amounts of LiOAm, measured with a heating rate of 10 K min^{-1}.

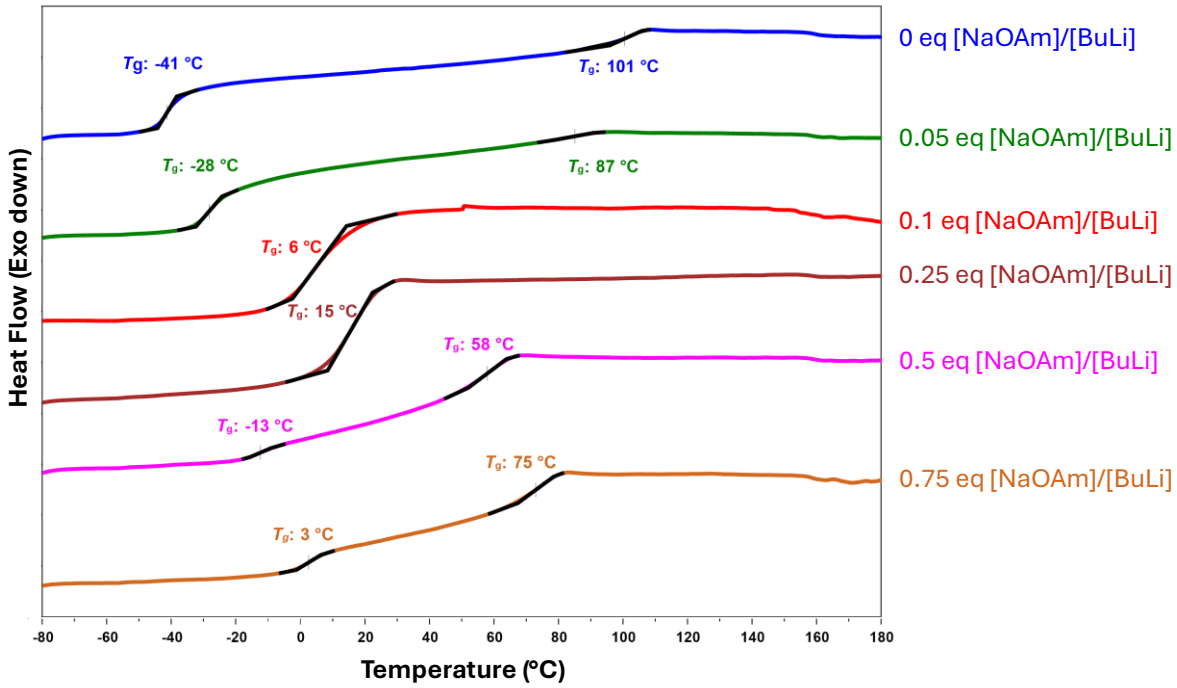

Figure S46: Second DSC heating curve of P(S-*co*-I) synthesized with different amounts of NaOAm, measured with a heating rate of 10 K min^{-1}.

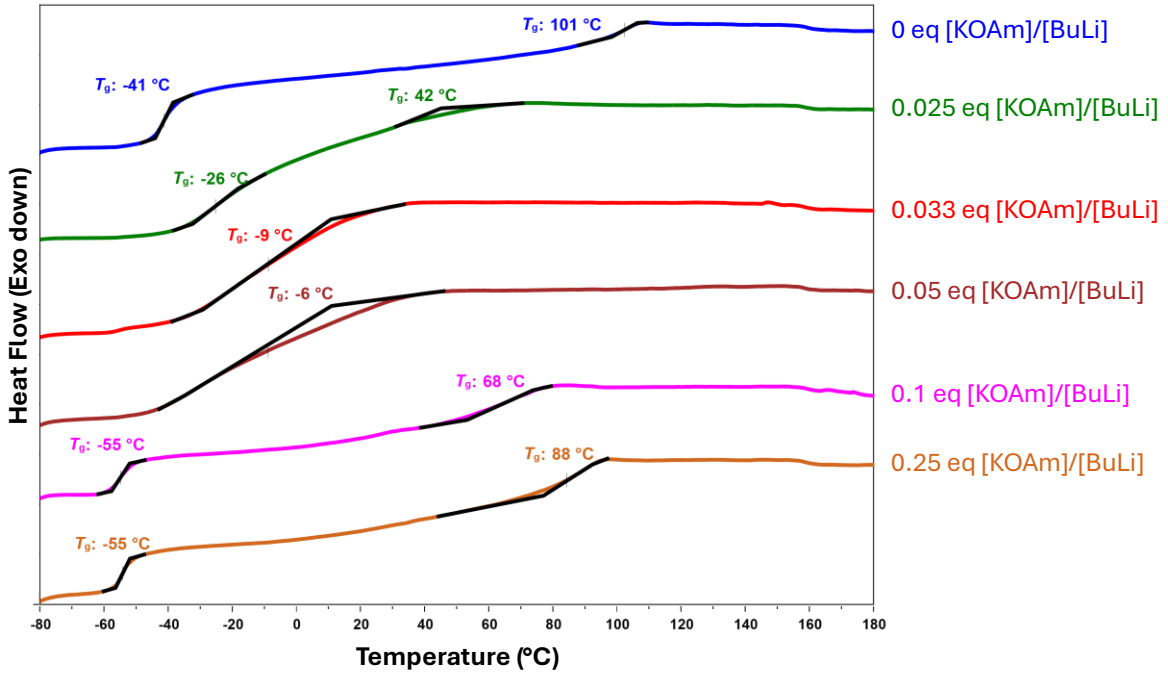

Figure S47: Second DSC heating curve of P(S-*co*-I) synthesized with different amounts of KOAm, measured with a heating rate of 10 K min^{-1}.

References

(1) Steube, M.; Johann, T.; Plank, M.; Tjaberings, S.; Gröschel, A. H.; Gallei, M.; Frey, H.; Müller, A. H. E. Kinetics of Anionic Living Copolymerization of Isoprene and Styrene Using in Situ NIR Spectroscopy: Temperature Effects on Monomer Sequence and Morphology. *Macromolecules* **2019**, *52* (23), 9299–9310. https://doi.org/10.1021/acs.macromol.9b01790.

(2) Fuchs, D. A. H.; Hübner, H.; Kraus, T.; Niebuur, B.-J.; Gallei, M.; Frey, H.; Müller, A. H. E. The Effect of THF and the Chelating Modifier DTHFP on the Copolymerisation of β-Myrcene and Styrene: Kinetics, Microstructures, Morphologies, and Mechanical Properties. *Polym Chem* **2021**, *12* (32), 4632–4642. https://doi.org/10.1039/D1PY00791B.

(3) Steube, M.; Johann, T.; Hübner, H.; Koch, M.; Dinh, T.; Gallei, M.; Floudas, G.; Frey, H.; Müller, A. H. E. Tetrahydrofuran: More than a "Randomizer" in the Living Anionic Copolymerization of Styrene and Isoprene: Kinetics, Microstructures, Morphologies, and Mechanical Properties. *Macromolecules* **2020**, *53* (13), 5512–5527. https://doi.org/10.1021/acs.macromol.0c01022.

(4) Schlosser, M. Superbases for Organic Synthesis. *Pure and Applied Chemistry* **1988**, *60* (11), 1627–1634. https://doi.org/10.1351/pac198860111627.

(5) Lochmann, L.; Janata, M. 50 Years of Superbases Made from Organolithium Compounds and Heavier Alkali Metal Alkoxides. *Open Chem* **2014**, *12* (5), 537–548. https://doi.org/10.2478/s11532-014-0528-0.

(6) Forens, A.; Roos, K.; Dire, C.; Gadenne, B.; Carlotti, S. Anionic Polymerization of Butadiene Using Lithium/Potassium Multi-Metallic Systems: Influence on Polymerization Control and Polybutadiene Microstructure. *Chinese Journal of Polymer Science (English Edition)* **2020**, *38* (4), 357–362. https://doi.org/10.1007/s10118-020-2355-4.

(7) Lochmann, L.; Pospíšil, J.; Lím, D. On the Interaction of Organolithium Compounds with Sodium and Potassium Alkoxides. A New Method for the Synthesis of Organosodium and Organopotassium Compounds. *Tetrahedron Lett* **1966**, *7* (2), 257–262. https://doi.org/10.1016/S0040-4039(00)70224-3.

(8) Kirchevskaya, I. Yu.; Samotsvetov, A. R.; Seredina, N. P.; Urazov, N. I.; Shatalov, V. P. Relations between Polymerization of Hydrocarbon Monomers in the Presence of Lithium Alkyls Modified with Potassium Tert.Butylate. *Polymer Science U.S.S.R.* **1976**, *18* (8), 2111–2118. https://doi.org/10.1016/0032-3950(76)90398-1.

(9) Forens, A.; Roos, K.; Dire, C.; Gadenne, B.; Carlotti, S. Anionic Polymerization of Butadiene Using Lithium/Potassium Multi-Metallic Systems: Influence on Polymerization Control and Polybutadiene Microstructure. *Chinese Journal of Polymer Science (English Edition)* **2020**, *38* (4), 357–362. https://doi.org/10.1007/s10118-020-2355-4.

(10) Halasa, A. F.; Mitchell, G. B.; Stayer, M.; Tate, D. P.; Oberster, A. E.; Koch, R. W. Metalation of Unsaturated Polymers by Using Activated Organolithium Compounds and the Formation of Graft Copolymers. II. *Journal of Polymer Science: Polymer Chemistry Edition* **1976**, *14* (2), 497–506. https://doi.org/10.1002/pol.1976.170140220.

(11) Fuchs, D. A. H.; Wadgaonkar, S. P.; Müller, A. H. E.; Frey, H. Effect of <scp>tetrahydrofuran</Scp> on the Anionic Copolymerization of 4-trimethylsilylstyrene with Isoprene. *Polym Adv Technol* **2024**, *35* (6). https://doi.org/10.1002/pat.6478.

(12) Meier-Merziger, M.; Fuchs, D. A. H.; Frey, H.; Müller, A. H. E. Spotlight on Methyl Tert-Butyl Ether–Underrated or Overlooked? Unveiling Its Role for Living Anionic Polymerization. *Macromolecules* **2024**. https://doi.org/10.1021/acs.macromol.4c01262.

(13) Corbin, N.; Prud'homme, J. MULTIBLOCK COPOLYMERS OF STYRENE AND ISOPRENE - 1. SYNTHESIS AND CHARACTERIZATION. *J Polym Sci Polym Chem Ed* **1976**, *14* (7), 1645–1659. https://doi.org/10.1002/pol.1976.170140708.

(14) Jaacks, V. Eine Neuartige Methode Zur Bestimmung von Copolymerisationsparametern. *Angewandte Chemie* **1967**, *79* (9), 419–419. https://doi.org/10.1002/ange.19670790927.

(15) Jaacks, V. A Novel Method of Determination of Reactivity Ratios in Binary and Ternary Copolymerizations. *Makromol Chem* **1972**, *161* (1), 161–172. https://doi.org/10.1002/macp.1972.021610110.

(16) Meyer, V. E.; Lowry, G. G. Integral and Differential Binary Copolymerization Equations. *J Polym Sci A* **1965**, *3* (8), 2843–2851. https://doi.org/10.1002/pol.1965.100030811.

(17) Hawkins, D. M. The Problem of Overfitting. *J Chem Inf Comput Sci* **2004**, *44* (1), 1–12. https://doi.org/10.1021/ci0342472.

(18) Wahlen, C.; Blankenburg, J.; Von Tiedemann, P.; Ewald, J.; Sajkiewicz, P.; Müller, A. H. E.; Floudas, G.; Frey, H. Tapered Multiblock Copolymers Based on Farnesene and Styrene: Impact of Biobased Polydiene Architectures on Material Properties. *Macromolecules* **2020**, *53* (23), 10397–10408. https://doi.org/10.1021/acs.macromol.0c02118.

(19) Handlin, D. L.; Williamson, D. T.; Willis, C. L. US 6,699,941 B1 Block Copolymer, 2004.

(20) Mochel, V. D. NMR Composition Analysis of Copolymers. *Rubber Chem Technol* **1967**, *40* (4), 1200–1211. https://doi.org/10.5254/1.3539131.

(21) Hogan, T. E.; Kiridena, W.; Kocsis, L. Effect of Stereochemistry in Anionic Polymerization Modifiers. *Rubber Chemistry and Technology* **2017**, *90* (2), 325–336. https://doi.org/10.5254/rct.17.82692.

(22) Sardelis, K.; Michels, H. J.; Allen, G.; F.R.S. Graded Block and Randomized Copolymers of Butadiene-Styrene. *Polymer (Guildf)* **1984**, *25* (7), 1011–1019. https://doi.org/10.1016/0032-3861(84)90089-2.

(23) Uraneck, C. A. Influence of Temperature on Microstructure of Anionic-initiated Polybutadiene. *J Polym Sci A1* **1971**, *9* (8), 2273–2281. https://doi.org/10.1002/pol.1971.150090814.

Chapter 4

Enteric drug coatings: Synthesis and copolymerization of novel α-hydroxy acid monomers to adjust the pH for dissolution

Shifting the pK_a value of enteric drug coatings for duodenum release: synthesis and copolymerization of novel α-hydroxy acid methacrylates

Dominik A. H. Fuchs, [redacted]

[a] Institute of Organic Chemistry, Johannes Gutenberg-University Mainz, Duesbergweg 10-14, 55128 Mainz, Germany
[b] Institute of Pharmacy, Department Pharmaceutical Technology and Biopharmacy, Johannes Gutenberg-University Mainz, Staudinger Weg 5, 55128 Mainz, Germany
[c] VeZerf Laborsynthesen GmbH, Langenfelder Straße 12, 55743 Idar-Oberstein

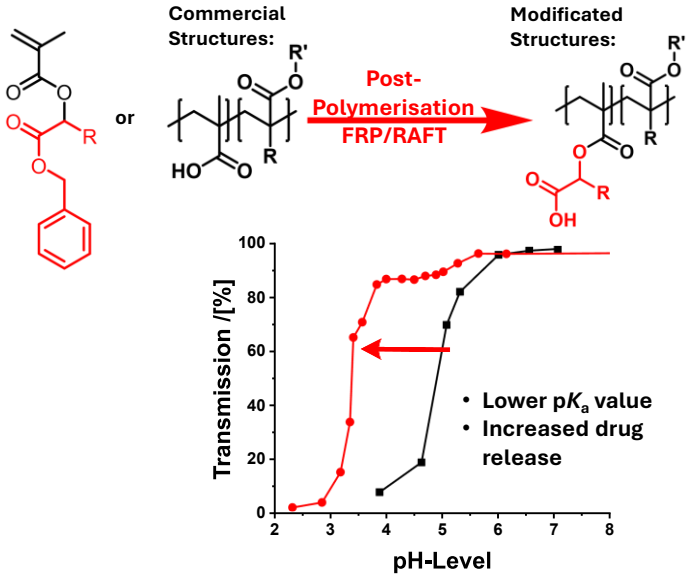

Abstract

Enteric drug coatings are often used to protect orally administered drugs from the acidic conditions of the stomach and vice versa. The most commonly used polymers for this purpose consist of methacrylic acid copolymerized with (meth)acrylates, better known under their trademark Eudragit® or Kollicoat®. We present two novel synthesis routes for modification of these copolymers with glycolic and lactid acid and their use for pH-responsive galenic formulations and coatings. By retaining the established poly(meth)acrylate backbone and modifying the acidic function with α-hydroxy-carboxylic acids, we were able to reduce the pK_a value of the copolymers while retaining the material properties. This was accomplished by two different synthesis routes: (i) copolymerization and (ii) post-polymerization modification. For the copolymerization, benzyl protected α-hydroxy-carboxylic acid modified methacrylic esters were employed as new monomers, which were copolymerized with various (meth)acrylates. For the post polymerization modification, commercially available Eudragit® was used in a nucleophilic substitution with benzyl protected α-bromo-carboxylic acid to obtain high molecular weight polymers with a degree of modification of > 99%. The monomers were copolymerized both via free radical (FRP) and reversible addition-fragmentation chain-transfer (RAFT) polymerization with methyl methacrylate and ethyl acrylate to synthesize polymers in the molecular weight range of 2,500-20,000 g mol^{-1}. While copolymers synthesized via FRP showed dispersities in the range of 1.5-2.2, RAFT yielded copolymers with narrow dispersities ($Đ \leq 1.3$) and adjustable molecular weights. Higher molecular weights (95-100 kg mol^{-1}) were synthesized by the quantitative post-polymerization modification of commercial available Eudragit®. The protective benzyl groups were successfully removed via hydrogenation with a palladium/carbon catalyst or hydrolyzed with trifluoracetic acid to obtain α-hydroxy-carboxylic acid modified poly(methacrylate). The pH responsivity of the modified copolymers was investigated by pH dependent cloud point titration, showing significantly improved solubility at pH 5, which should accelerate drug release in the duodenum. Further drug release experiments of coated capsules showed significantly faster disintegration for the modified copolymer coatings in comparison to the well established Eudragit® copolymers. This work provides the basis

for enteric formulations with faster drug release than the current state-of-the-art materials.

Introduction

Stimuli-responsive polymers can undergo extensive, but reversible structural alterations in response to changes in their environment. They play a key role for a large variety of established or envisaged applications like adaptive lenses,[1] nanofiltration,[2] targeted drug delivery systems [3,4] and tissue engineering scaffolds [5]. Stimuli responsive copolymers that dissolve at a predetermined pH are already indispensable for pharmaceutical purposes as well as controlled drug release and are widely applied in galenic coatings.[6] pH-responsive polymers for galenic coatings contain ionizable functional groups that donate or accept protons upon pH change. For instance, polycarboxylate structures in aqueous solution form collapsed structures at low pH due to hydrophobic interactions, resulting from the protonated acidic function. At higher pH, expanded coil structures are favoured due to electrostatic repulsion between the deprotonated, charged carboxylate groups. Rick et al. explored local and global structural changes of poly(methacrylic acid) *via* constant pH molecular dynamics computer simulations, which is responsible for the overall pH response.[7] Poly(methacrylic acid) exhibits pH-responsive properties with a pK_a value of around 5.5 and dissolves under basic conditions. [8,9] Poly(methacrylic acid-*co*-methyl methacrylate) offers strongly pH-dependent solubility, which depends on the extent of deprotonation.[10,11] The most important polymers for galenic coatings are methacrylate-based copolymers, consisting of methacrylic acid copolymerized with different (meth)acrylates (Eudragit® and Kollicoat®) [12–14] for pH dependent release in the intestines or alkylated amino-functional (meth)acrylates, for an immediate release in the stomach. The copolymers most commonly used for enteric coatings are copolymers based on methacrylic acid and ethyl acrylate: P(MA-*co*-EA) (Eudragit® L100-55) or methyl methacrylate P(MA-*co*-MMA) (Eudragit® L100), due to their high stability, resistance to water vapor permeation and protection of the cargo against acids due to their insolubility at acidic pH.[15,16] By altering the content of ionizable carboxylic acid groups, the

dissolution profile can be adjusted. Eudragit® L100 and Eudragit® L100-55 have a carboxylic acid/ester ratio of 1:1, respectively 1:2 for Eudragit® S100. Consequently Eudragit® L100 dissolves at a lower pH compared to Eudragit® S100. For Eudragit L-100 and L-100-55, solubility above a pH of 6 and 5.5, respectively has been reported.[17][18] However, *in vivo* as well as *in vitro* studies raise serious concerns about the effectiveness of the dissolution in the targeted small intestines, especially the duodenum, which has a very narrow time window for adsorption.[19–22] Discrepancies between *in vitro* and *in vivo* experiments can be explained by different drug release lag times, which are attributed to the difficulty of reproducing realistic *in vivo* test conditions in *in vitro* experiments. More specifically, the common test media have much higher buffer capacity than the intestinal fluid.[23] Therefore, they fail to reflect the fact that the micro-environmental pH of the dissolving coating is substantially lower than that of the bulk intestinal fluid. Consequently, the lag time of drug release in *in vivo* experiments are significantly longer than in *in vitro* experiments.[24] This is particularly problematic for drugs that are mainly absorbed in the duodenum. Further therapeutic problems are caused by site-unspecific drug release. For example, the enzyme pancreatin is administered to patients with exocrine pancreatic insufficiency. If the acid-labile pancreatin is not released immediately after the stomach passage, severe intestinal complaints frequently occur, because lipids contained in the diet are not completely digested.[25]

Considering these still insufficient properties of existing coatings, there is a need for enteric coatings that dissolve more rapidly after leaving the stomach at the considerably higher pH of the small intestines (5.1-7.8) than the materials currently available.[26] Ding *et al.* used hydrazide-modified polymethyl methacrylate as a promising candidate for pH responsive drug delivery systems.[27]

Despite an increasing number of publications and patents pertaining to Eudragit®, most are dealing with formulations and new applications of such polymers, but little has been reported regarding modification of this drug coating to address the problem of slow dissolution in the duodenum.[12,13,28] In the current approach we preserve the established (meth)acrylate copolymer backbone to retain the

material properties, but the carboxylic acid function is modified to obtain a polymer with a lower pK_a value. The concept relies on esterification with benzyl protected α-hydroxy acids (Fig. 1). This type of polymer was introduced by Theato et al. who used an active ester modified methacrylic acid to synthesize the homopolymer P(MA-Lac) in a transesterification reaction with L-lactide.[29][30] It is hypothesized that the carboxyl group has a negative inductive effect, lowering the pK_a value of the polymer. The resonance structure shown in Fig. 1 illustrates the inductive effect exerted by the partially positive charge at the oxygen atom of the carboxyl group.

Experimental Section

Materials, instrumentation, general experimental procedures as well as characterizations are described in the Supporting Information.

Results and discussion

This work aims at the synthesis of α-hydroxy-carboxylic acid modified MA structures as novel monomers for galenic coatings. We focus on the modification of MA with glycolic acid and L-lactic acid, respectively (Fig. 2A) and also demonstrate a novel post-polymerization modification route for commercially available Eudragit®, suitable for scale-up (Fig. 2B). Potential hydrolytic cleavage of the pendant ester bond would release the biocompatible Eudragit® copolymer and glycolic- or lactic acid into the gastrointestinal tract. L-lactic acid is an endogenous substance and is approved as a food additive (E 270)[31], and glycolic acid has a very low, physiologically irrelevant toxicity. To the best of our knowledge, we present the first successful example of the polymerization of α-hydroxy-carboxylic acid modified methacrylate under FRP and RAFT conditions. Furthermore, a post-polymerization method for the quantitative functionalization of high molecular weight Eudragit® L100 and Eudragit® L100-55 is presented. The resulting copolymers are investigated with respect to their pH-responsivity via cloud-point titration and controlled drug release by encapsulation tests.

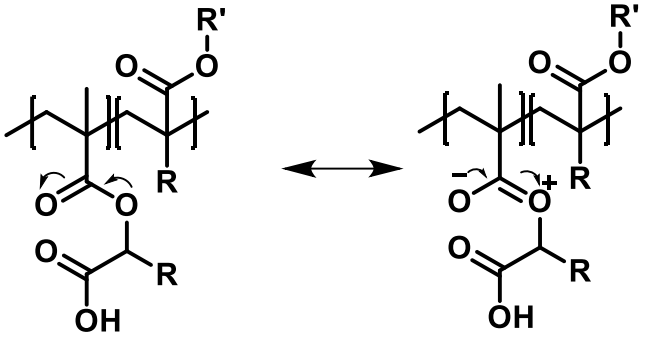

R = H, CH_3
R' = CH_3, CH_2CH_3

Figure 1: Resonance structures of poly(methacrylate)/poly(acrylate) copolymers modified with α-hydroxy carboxylic acids, resulting in -I-effect of adjacent carboxylic acid.

Monomer synthesis

The monomer synthesis is shown in Fig. 2. To modify methacrylic acid (MA) with α-hydroxy-carboxylic acids, it is crucial to protect the free carboxylic acid group of glycolic- or lactic acid. Several synthetic strategies were explored for direct modification of methacrylic acid with α-hydroxy-carboxylic acids, however this always resulted in the formation of oligomers and side products. Oligomerization occurs due to the bifunctionality of the α-hydroxy-carboxylic acids, leading to condensation reactions between hydroxyl-group and free carboxylic acid. Therefore, benzyl groups were chosen as protective groups for the carboxylic acid function, due to their high stability towards both acidic and basic conditions. After copolymerization, deprotection of the benzyl group can be carried out in a facile and selective manner via hydrogenation [32] or hydrolysis. [33][34] Using this protection strategy, the competitive esterification of the α-hydroxy-carboxylic acids can be completely avoided. The targeted monomers were synthesized in a two-step synthesis procedure: (i) protection of the α-hydroxy-carboxylic acids with benzyl bromide and (ii) Steglich esterification using *N,N'*-diisopropylcarbodiimde (DIPC) as a coupling agent and *N,N*-dimethylpyridin-4-amine (DMAP) as a catalyst. All starting compounds are inexpensive chemicals, widely used and commercially available. DIPC was used, because it is more reactive and less allergenic than dicyclohexylcarbodiimide (DCC), which is relevant in view of the envisaged pharmaceutical application. The undesired urea coupling product was removed via column chromatography.[35] The synthesis of benzyl (*S*)-hydroxypropanoate

(Lac-Bn) is well-known in literature. Based on this approach, the protection of glycolic acid was performed in a similar manner.[36] For this purpose, the sterically demanding base diazabicycloundecene (DBU) was used in a stoichiometric amount with respect to the α-hydroxy-carboxylic acids to synthesize the benzyl ester in a S_N-reaction with yields exceeding 80%. Extraction and distillation were performed to isolate the pure benzyl-protected product (Fig. 2A). Characterization by ^{1}H NMR spectroscopy confirmed the successful synthesis of Lac-Bn and Gly-Bn, respectively. ^{13}C- and additional 2D-spectra obtained by various NMR techniques are provided in the Supp. Info. (Fig. S1-10). The protected α-hydroxy-carboxylic acids were subsequently coupled with methacrylic acid (MA) in a Steglich esterification to obtain the glycolic- or lactic acid modified MA. The pure monomers were obtained in a yield of 70 % after extraction and subsequent purification via column chromatography. Characterization by ^{1}H NMR spectroscopy demonstrated the successful synthesis of MA-Lac-Bn and MA-Gly-Bn (Fig. 3), which were further characterized by other NMR techniques (Fig. S11-20).

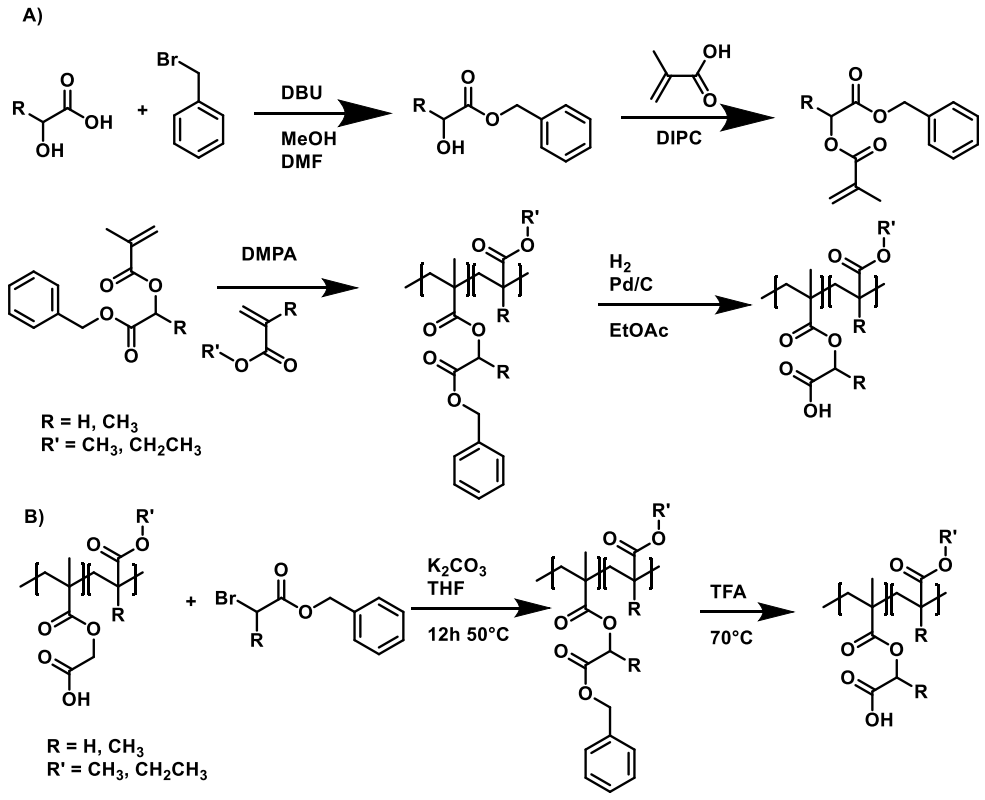

Figure 2: Synthesis overview of α-hydroxy-carboxylic acid modified methacrylic acid monomers and respective copolymerization with MMA or EA. A) Monomer route B) Postpolymerization route

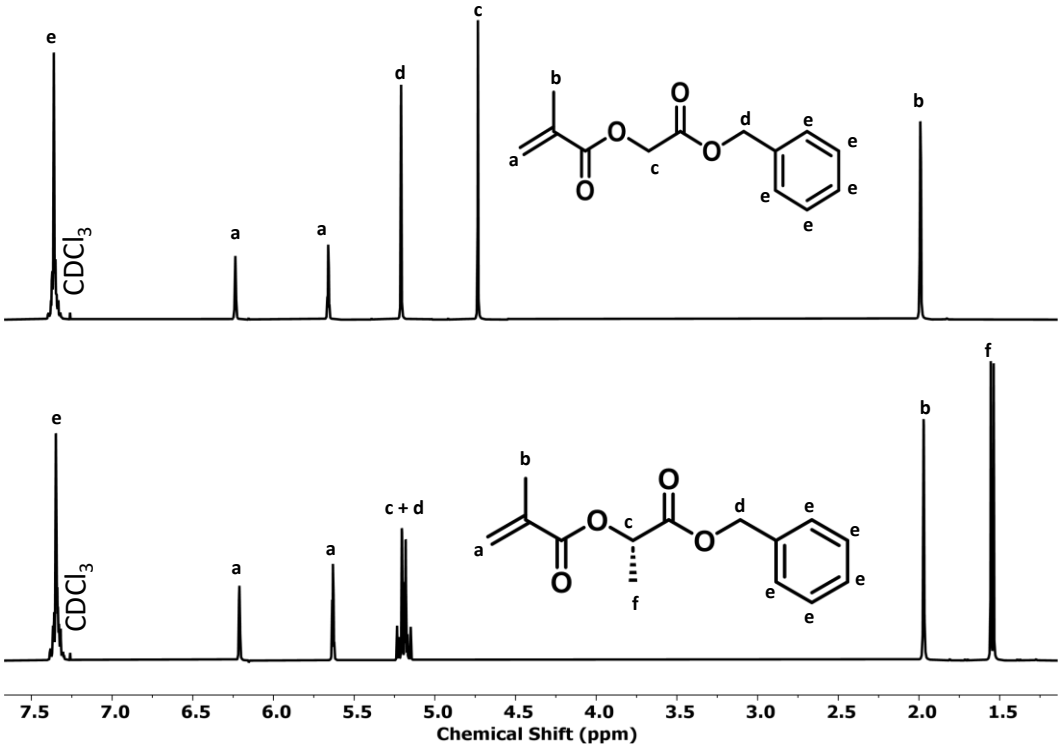

Figure 3: Stacked ^{1}H NMR spectra (400 MHz, $CDCl_3$) of glycolic acid modified methacrylate (top) and L-lactic acid modified methacrylate (bottom).

Copolymerization using free radical polymerization

The benzyl-protected monomers were copolymerized with methyl methacrylate (MMA) or ethyl acrylate (EA) using both free radical and RAFT polymerization to synthesize novel, pH-dependent materials suitable as drug coatings. For this purpose, two different initiator systems for the free radical polymerization were examined, 2,2-dimethoxy-2-phenylacetophenone (DMPA) a photoinitiator, which shows high efficiency for the polymerization of methacrylate monomers[37] and a thermal initiator, 2,2'-azobis(2-methylpropionitrile) (AIBN), a standard initiator in industry.[38] To investigate the polymerization potential of these new monomers, the initiator and monomer concentrations were changed to target different molecular weights from 11-36 kg/mol.[39–41] These could be achieved with the thermal initiator AIBN, but not with DMPA. The aim of this optimization was the synthesis of polymers with high yield, monomodal molecular weight distributions and low dispersity to investigate the intrinsic pH dependent properties of these polymers. Higher molecular weights, similar to the commercially available Eudragit® polymers (> 100kg/mol) are important for the formation of stable freestanding films and could be achieved by scalable postpolymerization modification with an α-bromo benzyl propionate (see the following sections). MMA and

EA were chosen as comonomers for the modified methacrylates, as they are already widely used in various commercially available copolymers for galenic drug coatings (Eudragit®). All copolymerizations were carried out in solution to avoid the Trommsdorff gelation effect and to obtain monomodal molecular weight distributions.[39] Benzene, a common solvent in FRP, was used due to its low radical transfer rate, good solubility of the monomers and polymers and its facile removal.[42]

According to the steady-state equation, the molecular weight is inversely proportional to the initiator concentration and increases with the monomer concentration.[39] These trends were observed, as expected. Copolymer yields, molecular weights and dispersities are listed in Tables S1-4.

Although the molecular weight decreased with increasing initiator concentration, the yield increased, and at least 5 wt.% had to be used for DMPA to achieve quantitative monomer conversion. Incomplete photolysis of the photoinitiator is unlikely and can be ruled out due to the long reaction times exceeding 14 hours. A possible explanation for the incomplete conversion with less than 5 wt% initiator is that the radicals formed by the initiator are terminated before polymerization is complete. As we investigated different monomer concentrations ranging from 1-2 mol/L, we could not observe a significant influence on the molecular weight and dispersity, so 1 mol/L was used to prevent a possible Trommsdorff effect and precipitation. The optimized conditions for high yields, monomodal distribution and low dispersity are therefore 5 wt% initiator at a monomer concentration of 1 mol/L (see Fig. S21-22 and Table S1-2).

This screening was also carried out for the thermal initiator AIBN. Changing the initiator system had the advantage of higher yields and molecular weights but also led to undesirable higher dispersities and non-monomodal molecular weight distributions. Therefore, 4 wt% initiator at a monomer concentration of 2.5 mol/L (see Fig. S23-24 and Table S3-4) was used to synthesize uniform copolymers, which were characterized by size exclusion chromatography (SEC) and NMR analysis. No low molecular weight products or unreacted monomers were detected by ^{1}H NMR spectroscopy after precipitation. SEC data were calibrated with a chemically different PEG standard, which leads to deviations and an underestimation of the observed molecular weights.

Comparing the two initiator systems, i.e. polymers synthesized with AIBN as an initiator have higher molecular weights and a broader molecular weight distribution (Fig. S37),

while polymers synthesized with DMPA showed overall lower molecular weights, but also lower dispersities and monomodal SEC curves (Fig. S40). Since this was more favorable for the studies on pH-responsive polymer behavior, independent of their molecular weight distribution, we focused on DMPA as an initiator. The deprotected low molecular weight polymers formed stable films. In addition to these molecular weights, methacrylic acid-copolymers were modified in a post-polymerization modification to synthesize polymers with at least twice the entanglement molecular weight (PMMA 18 kg/mol), which is described in the post-polymerization section. [43]

MMA copolymers: The monomers MA-Lac-Bn and MA-Gly-Bn were copolymerized with MMA using both optimized initiator systems. MMA was chosen as a comonomer for direct comparison with the established copolymer (Eudragit® L100), which consists of MA and MMA in the molar ratio 1:1. Additionally different molar ratios, in analogy to Eudragit® S100 were also synthesized (Table 1). The obtained copolymers were analyzed by ^{1}H-NMR (Fig. 4, S27) as well as 2D NMR spectroscopy (S28-36), and no unreacted monomer could be detected. The incorporation ratio of the monomers was calculated by ^{1}H-NMR spectroscopy by comparing the benzylic protons at 5.06-5.23 ppm and the methyl group of the ester at 3.40-3.68 ppm for P(MA-Lac-Bn-*co*-MMA), as shown in Fig. 4 and in S27 for P(MA-Gly-Bn-*co*-MMA). The determined molar incorporation ratio agrees with the monomer feed ratio for all copolymer samples (Table 1). Furthermore, the resulting copolymers were analyzed via SEC (see Fig. S25-26). All SEC traces showed monomodal weight distributions, but as expected for free-radical polymerizations all polymers showed higher dispersities in the range of 1.63 to 1.95 for DMPA as initiator. The molecular weight distribution, dispersities and the peak maxima of the SEC traces of the copolymers were in the same range for all samples. Tailing of the molecular weight distribution to lower or higher molecular weights was not detected.

The thermally initiated copolymers using AIBN as an initiator showed broader distributions with dispersities around 2.4 (see Fig. S37). In comparison to the copolymers initiated with DMPA, SEC traces of AIBN initiated copolymers showed tailing in the lower molecular weight region and no symmetrical distributions. The decomposition of DMPA is linear, resulting in a monomodal SEC curve, in contrast to AIBN, which has a half-life of

6.1 h at 70 °C in benzene.[44,45] For the copolymerization with AIBN more radicals are formed at the beginning of the reaction than at the end. This makes termination reactions at the beginning of the polymerization more likely, which may account for the shoulder in the low molecular weight range. The high molecular weight shoulder is tentatively explained by recombination of two polymer chains.

Table 1: Characterization of the MMA copolymers using DMPA as a photoinitiator.

Copolymer	Ratio[a]	M_n[b] / (g/mol)	$Đ$[b]
P(MA-LacBn$_{0.5}$-*co*-MMA$_{0.5}$)	1:1.03	3020	1.95
P(MA-LacBn$_{0.33}$-*co*-MMA$_{0.66}$)	1:1.98	3130	1.83
P(MA-LacBn$_{0.66}$-*co*-MMA$_{0.33}$)	1.96:1	2750	1.63
P(MA-GlyBn$_{0.5}$-*co*-MMA$_{0.5}$)	1:0.96	2790	1.87
P(MA-GlyBn$_{0.33}$-*co*-MMA$_{0.66}$)	1:1.87	2680	1.66
P(MA-GlyBn$_{0.66}$-*co*-MMA$_{0.33}$)	1.77:1	2760	1.77

[a] Determined by ^{1}H-NMR (400 MHz, DMSO-d_6) modified MA:MMA. [b] Determined by SEC (eluent: DMF, Calibration**: PEG).**

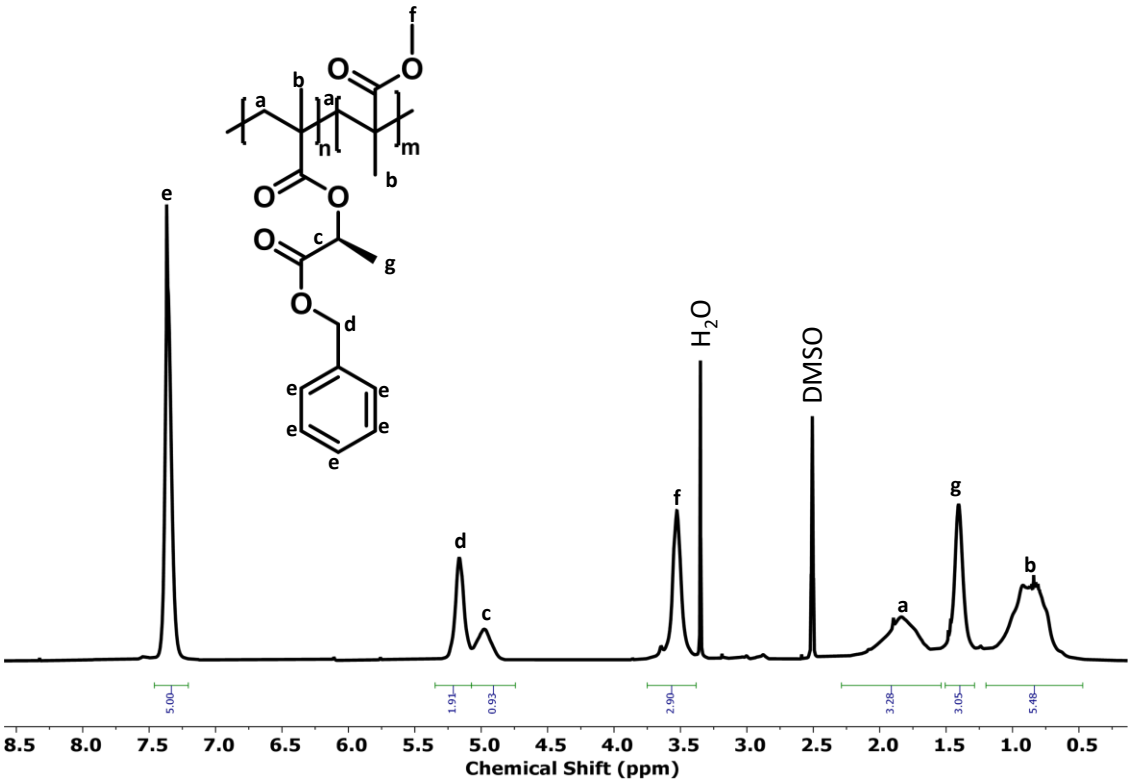

Figure 4: ^{1}H-NMR (400 MHz, DMSO-d_6) of P(MA-Lac-Bn-*co*-MMA) copolymer.

EA copolymers: Furthermore, the monomers MA-Lac-Bn and MA-Gly-Bn were also copolymerized with EA and DMPA as an initiator, according to the criteria defined in the previous section to obtain copolymer structures in analogy to Eudragit® L100-55 with the respective α-hydroxy acid in the side chain. ^{1}H-NMR spectra and SEC traces of the copolymers are depicted in the Supp. Inf. (Fig. S38-40). No residual monomer can be detected, and the MWD is monomodal. The composition of the copolymers can be verified by ^{1}H NMR spectroscopy by comparing the integral of the benzyl protons at 5.02-5.22 ppm with the integral of the methylene protons at 3.80-4.12 ppm. Compared to MMA as a comonomer, the copolymers with EA showed almost twice the molecular weight, a slightly higher dispersity, but comparable yields. One possible explanation for this is that for MMA the stabilizer was not completely removed by flash column chromatography with basic aluminum oxide.

These copolymers were synthesized to compare them with the established structure Eudragit® L100-55 in terms of pH-responsive dissolution behavior and targeted drug release, as can be seen in the following sections.

Copolymerization using RAFT technique

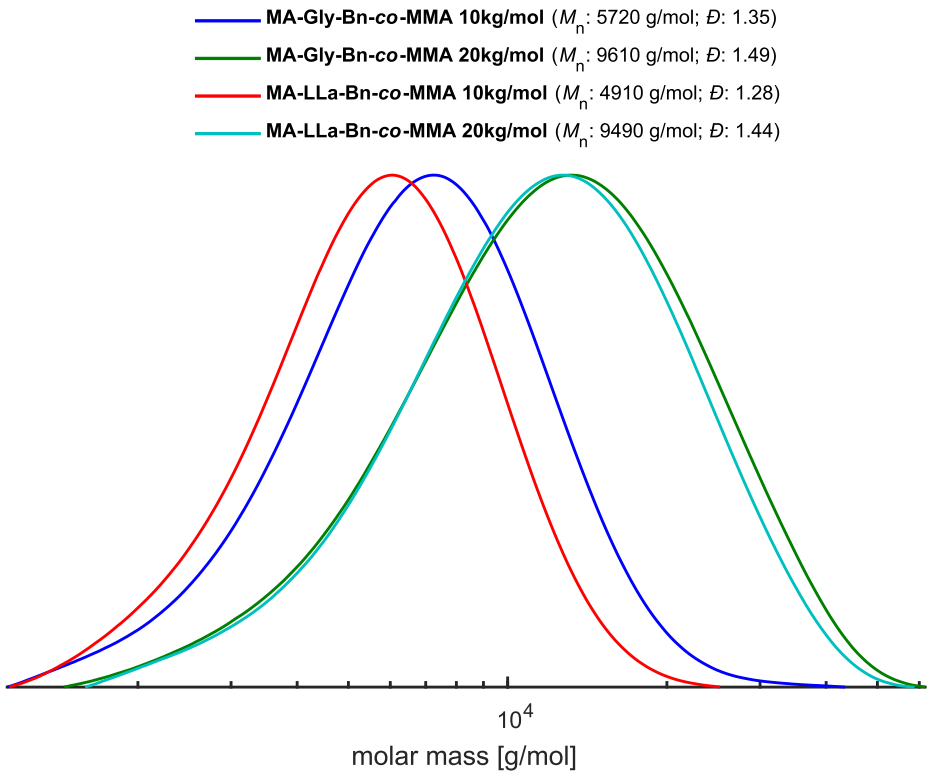

Figure 5: SEC curves (DMF, PEG calibration) for P(MA-Lac-Bn-*co*-MMA) and P(MA-Gly-Bn-*co*-MMA) copolymers using RAFT polymerization, see table S5.

Reversible addition-fragmentation chain-transfer (RAFT) polymerization has been employed to synthesize copolymers with lower dispersity and an adjustable molecular weight. RAFT polymerization is a controlled polymerization method. It is used as a versatile approach for manifold biomedical polymer applications.[46] One of the attractive benefits of RAFT polymerization is its simple setup involving radical polymerization, which is mediated by a chain transfer agent (CTA). For this purpose, the CTA 2-cyano-2-propyl dodecyl trithiocarbonate was added to the reaction mixture. This CTA was chosen because of its good compatibility with acrylates and methacrylates, as well as the evaluation of ^{1}H-NMR spectra. The methylene group in α-position to the thiocarbonate group at 3.22-3.29 ppm shows a slight overlap with the water signal at 3.33 ppm, but is separated from other polymer signals and is used to calculate the total number of monomer units and the molecular weight of the copolymer.

As a proof of concept, the different modified methacrylates were copolymerized with MMA. The RAFT reaction conditions are stated in the Supporting Information. Two different molecular weights of 10 and 20 kg/mol were targeted and characterized via SEC and ^{1}H-NMR calculations. ^{1}H-NMR and COSY spectra are shown in Fig. S41-43. They confirm successful copolymerization and are consistent with the samples synthesized by FRP, with the additional integrable initiator signal. The molecular weights determined by this method are listed in Table S5 and are very close to the targeted molecular weights of 10 and 20 kg/mol. The targeted molar ratio of 1:1 (functionalized MA:MMA) was almost reached for the 20 kg/mol samples, but the 10 kg/mol samples showed slight deviations from the targeted ratio. Not enough MMA was incorporated, which can be explained by statistical errors, as the amount of monomer was added to the reaction volumetrically by syringe and as only small amounts were synthesized, small deviations from the calculated volume have a strong effect on the copolymer composition. However, all copolymers were obtained in high yields (> 95 %) after precipitation.

The corresponding SEC traces are shown in Fig. 5. The obtained copolymers had moderate dispersities in a range of 1.28 to 1.44 and higher adjustable molecular weights compared to FRP. The comparison of the two methods for determining the

molecular weights shows that the NMR results are about twice as high as with SEC. It is difficult to judge which of these two methods is more reliable, as the NMR signal overlaps slightly, and SEC is based on PEG standard. In general, SEC-results are likely to be underestimated, while the NMR method overestimates the molecular weight.

Postpolymerization modification

Even though synthesis on gram scale by FRP and RAFT polymerization was successful, the time-consuming monomer synthesis involving purification via column chromatography significantly limits scalability and therefore the potential usage of the resulting polymers. Consequently, we also developed a scalable post polymerization modification based on the commercially available Eudragit® L-100 and L-100-55 structures. This simplified reaction is shown in Fig. 2B, and reaction conditions are listed in the Supp. Inf.. This approach allows the synthesis of the desired polymers on a hundred-gram scale, without the need for special chemicals or column chromatography, which shortens the reaction time considerably.

In the first step the carboxylate function of Eudragit® reacts in a nucleophilic substitution reaction with the α-bromo-phenyl ester to generate the protected polymer, which is deprotected in a second step with trifluoracetic acid (TFA) (see Fig. 2B). This sequence was carried out for the polymers P(MA-Gly-Bn-*co*-MMA) and P(MA-Lac-Bn-*co*-EA), since they were the most promising drug coatings in the following pharmaceutical tests. By this approach we were able to synthesize polymers with higher molar masses between 95 kg/mol for P(MA-Lac-Bn-*co*-EA) and 100 kg/mol for P(MA-Gly-Bn-*co*-MMA) (Fig S44), albeit with larger dispersities of 3.3-10.6. These higher molecular weight copolymers were produced on a hundred-gram scale, the molecular weight as well as dispersity are predefined by the Eudragit® L-100 and L-100-55 polymers used for modification. SEC was performed in THF with a PEG standard and is shown in Fig. S44. The higher molar masses achievable by this technique should improve material properties of the copolymers and help with film formation. The corresponding ^{1}H-NMR spectra (Fig. S45-46) can be found in the SI. As expected, the NMR spectra of polymers synthesized by the different routes are identical. The absence of proton signals

corresponding to the free carboxylic acid is evident for the quantitative functionalization (> 99%) for both copolymers.

Removal of the protective groups by hydrogenation:

In the final step of the synthesis, the benzyl protection group has to be removed to release the free α-hydroxy carboxylic acid groups (Scheme 2). However, other ester cleavage must be avoided, which complicates this step. Deprotection was carried out for P(MA-Gly-Bn-*co*-EA) and P(MA-Lac-Bn-*co*-EA) and the corresponding MMA copolymers synthesized by the monomer route using 20 wt% Pd/C as a catalyst for the hydrogenation according to a standard literature procedure.[33] The removal of the benzyl groups was performed at 40 bar hydrogen pressure and 40°C, for at least 4 days using ethyl acetate as a solvent. As depicted in Fig. 6, the exemplary ^{1}H-NMR spectrum of the deprotected sample of P(MA-Lac-*co*-EA) obtained in DMSO-d_6 shows full disappearance of the aromatic and benzyl proton signals (δ = 7.28 -7.42 ppm and 5.11 – 5.22 ppm) and the occurrence of the carboxylic acid signal at 13.02 ppm. The ^{1}H NMR spectra of the EA and MMA copolymers are shown in Fig. S 47-50, verifying the successful quantitative deprotection. Characterization by SEC was performed, but no signal was obtained with the refractive index detector and the UV detector, due to interaction of the multiple carboxylic acid functions with the column material of the SEC. However, quantitative yields and quantitative deprotection were achieved with this synthetic approach. Comparison of the copolymers via FTIR spectroscopy before and after deprotection confirmed the successful removal of the benzyl groups, by the disappearance of the aromatic bands at 700-750 cm^{-1}, the ester band of the protected polymer at 1750 cm^{-1} and the appearance of the carboxylic OH stretching vibration at 3300 cm^{-1} (Fig. 51). Additionally, thermal behavior was investigated via DSC, see Fig. S52-53. The copolymer P(MA-Gly-*co*-MMA) shows a glass transition temperature in the range of 121-126 °C, which is significantly lower than that of the unmodified copolymer (Eudragit® L-100) T_g = 169°C, which is explained by the flexible side chains. The T_g of the ethyl acrylate copolymer P(MA-Lac-*co*-EA) at 90°C is almost the same as that of the unmodified Eudragit® L-100-55 at 83 °C, see Fig. S54.

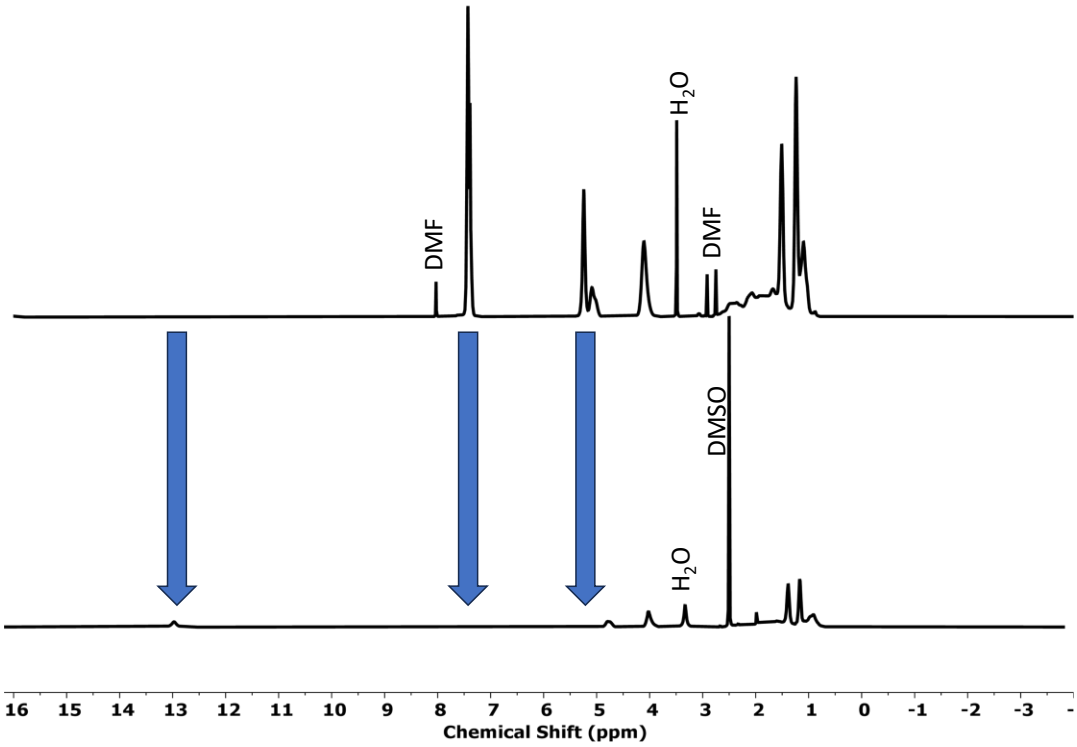

Figure 6: ^{1}H-NMR (400 MHz, DMF-d_7; DMSO-d_6) of top: P(MA-Lac-Bn-*co*-EA) and bottom: deprotected P(MA-Lac-*co*-EA).

Removal of the protective groups by hydrolysis:

Hydrogenation proved to be an unsuitable deprotection route for polymers synthesized by the post-polymerization modification, since the deprotection was incomplete due to the high molecular weights of around 100 kg/mol of the polymer. Additionally, the long reaction time of over 4 days, the hydrogen pressure of exceeding 40 bar and the amount of 20 wt% catalyst necessary for the reaction is too cost intensive for a possible upscaling. Therefore, a different synthesis approach had to be investigated and trifluoracetic acid (TFA) proved to be suitable for the quantitative hydrolysis of the benzyl protection unit. [34]

^{1}H- and ^{19}F-NMR spectra for the polymers for P(MA-Gly-co-MMA) and P(MA-Lac-co-EA) are shown in Fig. S 54-57. No benzylic protons can be detected, which indicates that the deprotection with ≥ 99% was complete, no methyl methacrylate or modified methacrylate was hydrolysed, and the absence of any signal in the ^{19}F-NMR spectra proves that all TFA was removed successfully. As already mentioned, SEC was not possible, but DSC measurements were performed (see Fig. S52-53).

All NMR spectra and glass transition temperatures are comparable with the polymers synthesized via the monomer route.

Using this approach we were able to reduce reaction time and the polymer was prepared on a hundred-gram scale with a yield exceeding 87%.

Cloud point titration

To study the pH dependent solubility of the synthesized copolymers in comparison to the commercially available galenic coatings Eudragit® L100-55 and L100, pH-dependent transmission measurements were carried out. All copolymers were dissolved under basic conditions at a polymer concentration of 5 mg mL^{-1}. The exact procedure is described in the Supp. Inf.. The transmission measurements were performed at 37°C to simulate the body temperature at which the galenic coating is dissolved in vivo. Titration was performed via subsequent stepwise addition of 0.1 molar hydrochloric acid, lowering the pH of the medium. At a certain pH level corresponding to the pK_a value of the α-hydroxy-carboxylic acid repeating units the polymer becomes insoluble, due to protonation of the carboxylate groups. This was investigated by turbidimetry: as the polymer precipitates, the mixture becomes increasingly turbid, and transmission decreases abruptly (Fig. 7 and S 58).

All of the α-hydroxy-carboxylic acid modified copolymers dissolve at lower pH compared to the unmodified copolymers, as their transmission increased earlier. The transmission at a pH level of 4.5 of the unmodified copolymers was about 10 %, whereas the modified copolymers still showed good solubility at this pH, indicated by the transmission of > 95%. The commercial Eudragit® L-100 and the synthesized copolymer P(MA-*co*-MMA) showed similar pH response, slight differences are explained by the higher molecular weight of the commercially available Eudragit® L-100 copolymer (around 125 kg/mol) and a slightly different comonomer ratio.[47] For all modified copolymers the results evidence dissolution at lower pH than their Eudragit® counterparts. There is no significant difference between the lactic and glycol modification and the different molecular weights.

The ethyl acrylate copolymers are shown in Fig. S58. All modified copolymers dissolve at lower pH than the commercial Eudragit® L-100-55 and the synthesized P(MA-*co*-EA) samples. At a pH of 5.0, the transmission for the unmodified polymer is lower than 10%, while the modified copolymers still exhibit more than 90% transmission. Both Eudragit® L-100-55 copolymers showed similar pH response behavior, small differences are explained by the different molecular weights and a slight variation of the comonomer ratio. The lactide modified copolymers obtained by the post polymerization modification dissolve even earlier than the low molecular weight polymer. This might be caused by slightly different comonomer ratios.

These results demonstrate the improved solubility of copolymers modified with α-hydroxy-carboxylic acids at lower pH compared to the unmodified copolymers. Therefore, we conclude that introducing these α-hydroxy-carboxylic acids lowers the pK_a value of the copolymers. This modification should therefore lead to faster drug release in the duodenum. In addition to the improved dissolution, it is crucial for a galenic drug coating to have acid resistance to the conditions in the stomach. This was also proven by the turbidity measurement, but additional experiments were carried out with coated capsules to investigate the acid absorption and drug release of a coated paracetamol capsule.

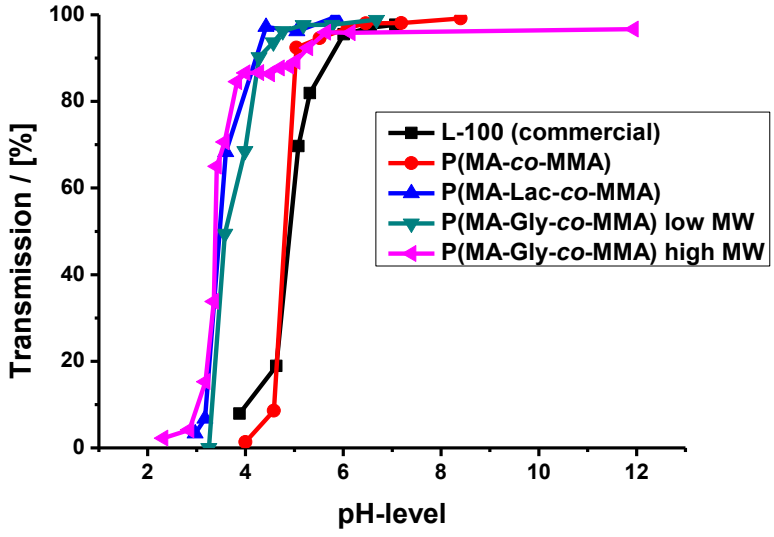

Figure 7: pH dependent transmission experiment for Eudragit® L100-type copolymers at 37 °C.

Acid uptake

For galenic drug coatings, it is essential that they are stable, insoluble and do not swell more than 10 wt % under the acidic conditions of the stomach.[48] To investigate this swelling behavior, the so-called “acid uptake”, we used a standardized procedure described in the European Pharmacopoeia, with the slight deviation of a pH of 2 to ensure acid stability even in a not fasted state.[49] Hydroxypropyl methylcellulose (HPMC) capsules filled with paracetamol were dip coated with the modified polymers until a coating density of approximately 10 mg/cm^2 was achieved, the determination is described in the Supp. Inf.. Since HPMC and paracetamol are water soluble, we attribute any swelling to the polymer coating. These capsules were immersed in a 0.01 M HCl solution for one hour to simulate gastric conditions. They were then carefully dried and weighed to calculate the acid uptake. This is shown in Fig. 8. The experimental conditions and calculations are listed in the Supporting Information.

All copolymers demonstrated an acid uptake of less than 10 %. As a reference low and high molecular weight Eudragit® copolymers were also measured. The low molecular weight Eudragit® like polymers showed a slightly higher acid uptake than the commercial Eudragit® polymers. This might be due to the lower molecular weight of the polymer. However, modification of the methacrylic acid seemed to compensate the lower molecular weight and showed improved resistance against acid uptake. The postpolymerization modified polymers P(MA-Gly-*co*-MMA) and P(MA-Lac-*co*-EA) exhibit a slightly higher acid uptake than their low molecular weight counterparts and their source Eudragit® material, but are still below the required 10%. For a complete analysis of the improved solubility of the new copolymers, the release of the drug paracetamol was investigated in dissolution tests of polymer-coated capsules.

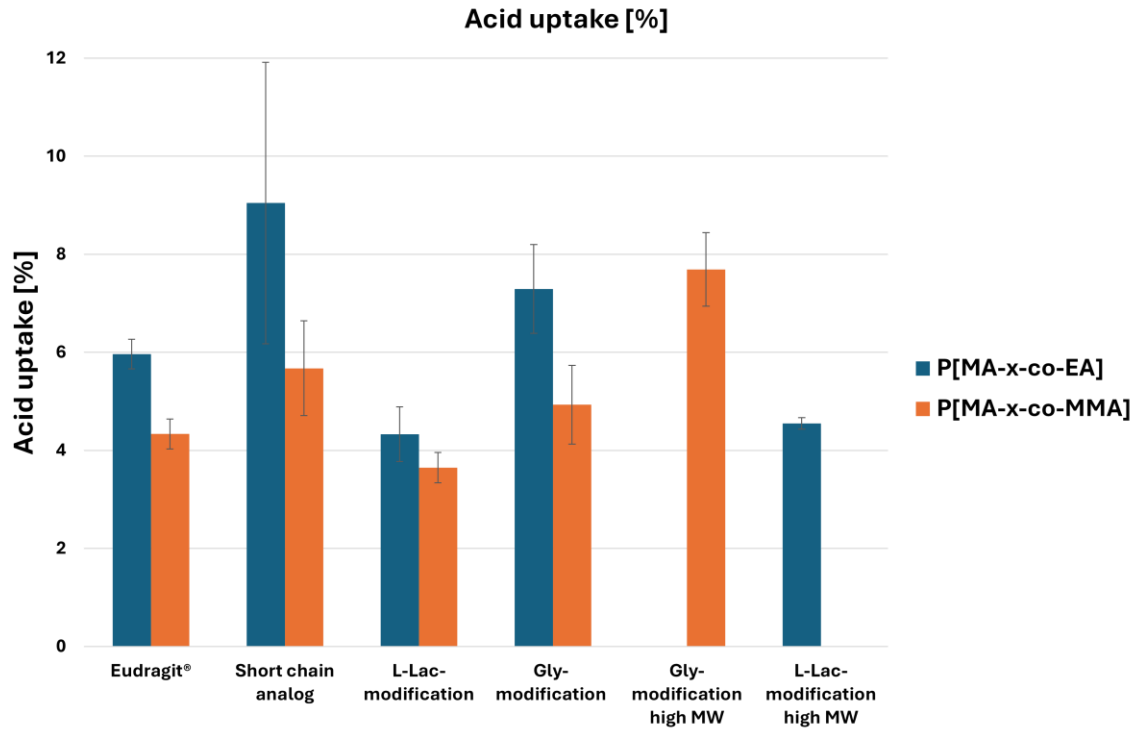

Figure 8: Acid uptake of the coated capsules after 1 hour in 0.01 M HCl. All copolymers showed an acid uptake < 10 % indicating a very good acid resistance. Eudragit® L-100 and analogs (red) and Eudragit® L-100-55 and analogs (blue).

Dissolution test of coated capsules

The drug release of hydroxypropyl methylcellulose (HPMC) capsules filled with paracetamol and coated with the new copolymers was investigated using the basket method (USP apparatus I) in a 15 mM phosphate buffer to simulate physiological conditions.[21] Paracetamol as well as HPMC are soluble in water, and therefore the drug release is primarily dependent on the dissolution of the copolymer. First, the capsules were tested in 900 ml of 0.01 M HCl for 1 hour followed by 2 hours in 900 ml of a 15 mM phosphate buffer at 37 °C. This buffer was described by Al-Gousous *et al.* for its bio-predictive representation of the proximal small intestinal conditions.[21] After set time points samples were withdrawn manually without replacement, and the paracetamol content was quantified with an UV-Vis spectrometer, as described in the experimental part. The results after 45 minutes are shown in Fig. 9. All copolymers showed no sign of drug release after 1 hour in 0.01 M HCl, indicating good acid resistance. Altogether, all modified copolymer showed significant faster drug release compared to the unmodified polymers, in accordance with the cloud point titrations, even though the modified copolymers exhibited the highest degree of coating.

Comparing the Eudragit® structures with its low molecular weight analogue in Figure 9 it becomes clear that the molecular weight of the copolymers has an influence on the polymer dissolution, as a higher molecular weight results in a slower dissolution of the polymer.[50] This result differs from the previous cloud point titration, in which the dissolution was independent from the molecular weight, this is especially pronounced in the EA copolymers, as can be seen in the comparison of the lactide modification in Fig. 9. The high molecular weight polymer showed almost no drug release after 45 minutes, which might be explained by the kinetically hindered dissolution of the higher molecular weights due to entanglements. This was not observed for the copolymer P(MA-Gly-*co*-MMA), as it still showed slightly lower drug release than the low molecular weight analog, but significantly higher than the established Eudragit® structures. Therefore, the enhanced drug release of the glycol modified polymers is largely independent of the molecular weight and is higher than that of Eudragit® L-100. Both Gly-copolymers showed increased drug release compared to L-100. Therefore, modification with an α-hydroxy-carboxylic acid, has a significant impact on the release rate, attributed to the lower pK_a-value of the resulting polymers. With a lower pK_a-value, a greater proportion of the polymer is ionized, even at the lower microenvironmental pH in the swollen film resulting in a faster dissolution.

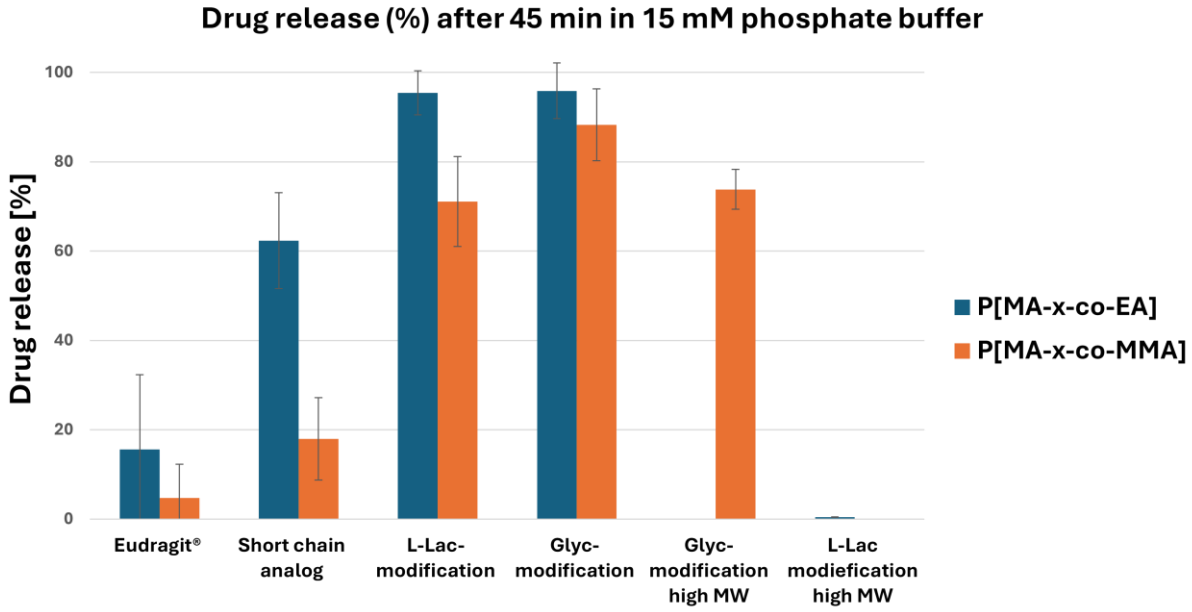

Figure 9: Drug release [%] at t=45 minutes in the dissolution test. The modified polymer shows a significantly faster drug release compared to the commercial Eudragit L100 and the P(MA-co-MMA) with a lower molecular weight. Eudragit® L-100 and analogs (red) and Eudragit® L-100-55 and analogs (blue).

Conclusions

We have described different synthetic procedures to obtain enteric Eudragit® like structures with lower pK_a values, improved pH-response and drug release. In a first step we describe the synthesis of novel benzyl protected α-hydroxy-carboxylic acid modified methacrylate monomers. Therefore, methacrylic acid monomers, esterified with benzyl-protected glycolic acid (MA-Gly-Bn) and L-lactic acid (MA-Lac-Bn) were synthesized and fully characterized. These functional monomers were copolymerized by free radical polymerization with ethyl acrylate (analogous to Eudragit® L100-55) as well as methyl methacrylate (analogous to Eudragit® L100). Furthermore, the monomers MA-Lac-Bn and MA-Gly-Bn were copolymerized with MMA using RAFT polymerization techniques to obtain copolymers with low dispersity and adjustable molecular weights. As proof of concept the low molecular weight polymers were deprotected and investigated regarding their intrinsic pH-dependent dissolution properties. The most promising copolymers P(MA-Gly-*co*-MMA) and P(MA-Lac-*co*-EA) were also synthesized in a scalable post polymerization modification, resulting in molecular weights > 100 kg/mol. The benzyl protective group could be completely removed by hydrogenation using heterogenous Pd/C catalysis or hydrolysis with TFA to release the free carboxylic acid functionality, introducing a pH responsive functionality to the copolymer. The dissolution profile of these copolymers was investigated using cloud point titration and all copolymers proved solubility at lower pH. In addition to dissolution, the acid resistance of all copolymers was tested by drug release experiments with polymer coated HPMC capsules containing paracetamol. All copolymers showed excellent acid resistance and an acceptable acid uptake of less than 10 wt.% after one hour in an acidic environment (0.01 M HCl). By changing the pH to 6.5 (15 mM phosphate buffer), the modified copolymers demonstrated much faster drug release compared to the unmodified copolymers as well as the commercial Eudragit® products, which we attribute to a lower pK_a-value of the copolymer. This effect is for the glycol modification almost independent of the molecular weight. The concept of modifying the polymethacrylate backbone with α-hydroxy-carboxylic acids to lower the pK_a-value of the resulting copolymers, has proven to increase drug release. Consequently, the new copolymers with lower pK_a-values could help address some

product performance issues of enteric coated dosage forms, such as the failure of antiplatelet low dose aspirin therapy commonly observed with the enteric-coated products. This failure has been attributed to the poor bioavailability of aspirin due to the slow dissolution of the enteric coating.[51–53] Therefore, the herein presented post polymerization modified commercial Eudragit® copolymers are a promising alternative to commercial Eudragit® L-100 and L-100-55, with an improved drug release at lower pH. Further studies on cytotoxicity, long term stability and formulation will be discussed in a follow-up article. Other α-hydroxy acids such as mandelic and malic acid will also be the subject of further investigations.

Conflicts of interest

The authors J.A., J.B., E.K., P.L. and H. F. are owners of Patent DE102018129419A1, which relates to the synthesis and characterization of modified Eudragit® structures for enteric drug coatings. All authors may benefit from potential licensing agreements or further revenue associated with this patent. Therefore, this patent may be considered a competing interest, as the authors have an economic interest in the commercialization of the research findings presented in this manuscript.

Acknowledgements

The authors thank WIPANO-Wissens- und Technologietransfer durch Patente und Normen" (9644602) for financial support, especially for the opportunity to synthesize the copolymers external on a larger scale (Grant number: 03THWRP003). D.F. thanks Maximilian ´King´ Kaiser for helpful discussions and critical evaluation of this article.

References:

[1] L. Dong, A.K. Agarwal, D.J. Beebe, H. Jiang, Adaptive liquid microlenses activated by stimuli-responsive hydrogels, Nature 442 (2006) 551–554. https://doi.org/10.1038/nature05024.

[2] R. Du, J. Zhao, Positively charged composite nanofiltration membrane prepared by poly(N,N-dimethylaminoethyl methacrylate)/polysulfone, J Appl Polym Sci 91 (2004) 2721–2728. https://doi.org/10.1002/app.13477.

[3] S. Brahim, D. Narinesingh, A. Guiseppi-Elie, Release Characteristics of Novel pH-Sensitive p(HEMA-DMAEMA) Hydrogels Containing 3-(Trimethoxy-silyl) Propyl Methacrylate, Biomacromolecules 4 (2003) 1224–1231. https://doi.org/10.1021/bm034048r.

[4] Q. Wu, L. Wang, H. Yu, J. Wang, Z. Chen, Organization of glucose-responsive systems and their properties, Chem Rev 111 (2011) 7855–7875. https://doi.org/10.1021/cr200027j.

[5] J. Kroupová, D. Horák, J. Pacherník, P. Dvořák, M. Šlouf, Functional polymer hydrogels for embryonic stem cell support, J Biomed Mater Res B Appl Biomater 76B (2006) 315–325. https://doi.org/10.1002/jbm.b.30366.

[6] J.M. Ting, W.W. Porter, J.M. Mecca, F.S. Bates, T.M. Reineke, Advances in Polymer Design for Enhancing Oral Drug Solubility and Delivery, Bioconjug Chem 29 (2018) 939–952. https://doi.org/10.1021/acs.bioconjchem.7b00646.

[7] A. Sharma, J.D. Smith, K.B. Walters, S.W. Rick, Constant pH simulations of pH responsive polymers, J Chem Phys 145 (2016). https://doi.org/10.1063/1.4972062.

[8] E. He, C.Y. Yue, K.C. Tam, Association behavior of star-shaped pH-responsive block copolymer: Four-arm poly(ethylene oxide)-b-poly(methacrylic acid) in aqueous medium, Langmuir 25 (2009) 4892–4899. https://doi.org/10.1021/la804056p.

[9] P. Ravi, S. Dai, C.H. Tan, K.C. Tam, Self-assembly of alkali-soluble [60]fullerene containing poly(methacrylic acid) in aqueous solution, Macromolecules 38 (2005) 933–939. https://doi.org/10.1021/ma0480547.

[10] A. Bettencourt, A.J. Almeida, Poly(methyl methacrylate) particulate carriers in drug delivery, J Microencapsul 29 (2012) 353–367. https://doi.org/10.3109/02652048.2011.651500.

[11] D.A. LaVan, T. McGuire, R. Langer, Small-scale systems for in vivo drug delivery, Nat Biotechnol 21 (2003) 1184–1191. https://doi.org/10.1038/nbt876.

[12] A. Nikam, P.R. Sahoo, S. Musale, R.R. Pagar, A.C. Paiva-Santos, P.S. Giram, A Systematic Overview of Eudragit® Based Copolymer for Smart Healthcare, Pharmaceutics 15 (2023) 587. https://doi.org/10.3390/pharmaceutics15020587.

[13] S.K. Jain, A.K. Jain, K. Rajpoot, Expedition of Eudragit® Polymers in the Development of Novel Drug Delivery Systems, Curr Drug Deliv 17 (2020) 448–469. https://doi.org/10.2174/1567201817666200512093639.

[14] Ch.N. Patra, R. Priya, S. Swain, G. Kumar Jena, K.C. Panigrahi, D. Ghose, Pharmaceutical significance of Eudragit: A review, Futur J Pharm Sci 3 (2017) 33–45. https://doi.org/10.1016/j.fjps.2017.02.001.

[15] H. Schreier, Drug Targeting Technology, CRC Press, 2001. https://doi.org/10.1201/9780203908563.

[16] J. Breitkreutz, Leakage of enteric (Eudragit® L)-coated dosage forms in simulated gastric juice in the presence of poly(ethylene glycol), Journal of Controlled Release 67 (2000) 79–88. https://doi.org/10.1016/S0168-3659(00)00197-8.

[17] T. Parikh, S. Singh Gupta, A. Meena, A.T.M. Serajuddin, Investigation of thermal and viscoelastic properties of polymers relevant to hot melt extrusion-III: Polymethacrylates and polymethacrylic acid based polymers, Journal of Excipients and Food Chemicals 5 (2014) 56–64.

[18] Evonik Industries AG, Functional polymers to take control of your release profile Versatility and reliability for oral solid dosage forms, Https://Healthcare.Evonik.Com/En/Drugdelivery/Oral-Drug-Delivery/Oral-Excipients/Eudragit-Portfolio/Attachment/149083?Rev=fd91102acf8d769a56d0716b20544216 (2022).

[19] E.T. Cole, R.A. Scott, A.L. Connor, I.R. Wilding, H.U. Petereit, C. Schminke, T. Beckert, D. Cadé, Enteric coated HPMC capsules designed to achieve intestinal targeting, Int J Pharm 231 (2002) 83–95. https://doi.org/10.1016/S0378-5173(01)00871-7.

[20] P. Decuzzi, B. Godin, T. Tanaka, S.Y. Lee, C. Chiappini, X. Liu, M. Ferrari, Size and shape effects in the biodistribution of intravascularly injected particles, Journal of Controlled Release 141 (2010) 320–327. https://doi.org/10.1016/j.jconrel.2009.10.014.

[21] J. Al-Gousous, G.L. Amidon, P. Langguth, Toward Biopredictive Dissolution for Enteric Coated Dosage Forms, Mol Pharm 13 (2016) 1927–1936. https://doi.org/10.1021/acs.molpharmaceut.6b00077.

[22] M.Z.I. Khan, Ž. Prebeg, N. Kurjaković, A pH-dependent colon targeted oral drug delivery system using methacrylic acid copolymers, Journal of Controlled Release 58 (1999) 215–222. https://doi.org/10.1016/S0168-3659(98)00151-5.

[23] J. Al-Gousous, H. Ruan, J.A. Blechar, K.X. Sun, N. Salehi, P. Langguth, N.M. Job, E. Lipka, R. Loebenberg, M. Bermejo, G.E. Amidon, G.L. Amidon, Mechanistic analysis and experimental verification of bicarbonate-controlled enteric coat dissolution: Potential in vivo implications, European Journal of Pharmaceutics and Biopharmaceutics 139 (2019) 47–58. https://doi.org/10.1016/j.ejpb.2019.03.012.

[24] J. Al-Gousous, Y. Tsume, M. Fu, I.I. Salem, P. Langguth, Unpredictable Performance of pH-Dependent Coatings Accentuates the Need for Improved Predictive in Vitro Test Systems, Mol Pharm 14 (2017) 4209–4219. https://doi.org/10.1021/acs.molpharmaceut.6b00877.

[25] J. Mössner, V. Keim, Pancreatic Enzyme Therapy, Dtsch Arztebl Int 108 (2011) 578–582. https://doi.org/10.3238/arztebl.2011.0578.

[26] A.E. Felber, M.-H. Dufresne, J.-C. Leroux, pH-sensitive vesicles, polymeric micelles, and nanospheres prepared with polycarboxylates, Adv Drug Deliv Rev 64 (2012) 979–992. https://doi.org/10.1016/j.addr.2011.09.006.

[27] X. Ding, Y. Liu, J. Li, Z. Luo, Y. Hu, B. Zhang, J. Liu, J. Zhou, K. Cai, Hydrazone-bearing PMMA-functionalized magnetic nanocubes as pH-responsive drug carriers for remotely targeted cancer therapy in vitro and in vivo, ACS Appl Mater Interfaces 6 (2014) 7395–7407. https://doi.org/10.1021/am500818m.

[28] M. Fu, J.A. Blechar, A. Sauer, J. Al-Gousous, P. Langguth, In vitro evaluation of enteric-coated hpmc capsules—Effect of formulation factors on product performance, Pharmaceutics 12 (2020) 1–17. https://doi.org/10.3390/pharmaceutics12080696.

[29] M. Eberhardt, R. Mruk, R. Zentel, P. Théato, Synthesis of pentafluorophenyl(meth)acrylate polymers: New precursor polymers for the synthesis of multifunctional materials, Eur Polym J 41 (2005) 1569–1575. https://doi.org/10.1016/j.eurpolymj.2005.01.025.

[30] A. Das, P. Theato, Multifaceted Synthetic Route to Functional Polyacrylates by Transesterification of Poly(pentafluorophenyl acrylates), Macromolecules 48 (2015) 8695–8707. https://doi.org/10.1021/acs.macromol.5b02293.

[31] R. D. Schmid, Taschenatlas der Biotechnologie und Gentechnik, 3rd ed., Wiley-VCH, Weinheim, 2016.

[32] D.J. Abraham, Rational Drug Design Edited by D. G. Truhlar, W. J. Howe, A. J. Hopfinger, J. Blaney, and R. Dammkoehler. Springer-Verlag, New York. 1999. xxii + 206 pp. 16 × 24 cm. ISBN 0-387-98753-3. $69.95., J Med Chem 42 (1999) 5284–5284. https://doi.org/10.1021/jm990497r.

[33] J. Geschwind, H. Frey, Poly(1,2-glycerol carbonate): A fundamental polymer structure synthesized from CO2 and glycidyl ethers, Macromolecules 46 (2013) 3280–3287. https://doi.org/10.1021/ma400090m.

[34] Y. Hsu, M. Chuang, T. Hirano, K. Ute, Multivariate analysis of 13C NMR spectra to extract information about monomer sequences in poly(methyl methacrylate-co-benzyl methacrylate)s prepared by various polymer reactions, Polym J 50 (2018) 355–363. https://doi.org/10.1038/s41428-018-0027-9.

[35] J.M. Collins, K.S. Sandeep, Coupling method for peptide synthesis at elevated temperatures US2017/0342104A1, 2017.

[36] Y. Tabata, H. Abe, Synthesis and properties of alternating copolymers of 3-hydroxybutyrate and lactate units with different stereocompositions, Macromolecules 47 (2014) 7354–7361. https://doi.org/10.1021/ma501783f.

[37] V. Mucci, C. Vallo, Efficiency of 2,2-dimethoxy-2-phenylacetophenone for the photopolymerization of methacrylate monomers in thick sections, J Appl Polym Sci 123 (2012) 418–425. https://doi.org/10.1002/app.34473.

[38] P. Nesvadba, Radical Polymerization in Industry, in: Encyclopedia of Radicals in Chemistry, Biology and Materials, Wiley, 2012. https://doi.org/10.1002/9781119953678.rad080.

[39] S. Koltzenburg, M. Maskos, O. Nuyken, Polymere: Synthese, Eigenschaften und Anwendungen, Springer Berlin Heidelberg, Berlin, Heidelberg, 2014. https://doi.org/10.1007/978-3-642-34773-3.

[40] T.G. Carswell, D.J.T. Hill, D.I. Londero, J.H. O'Donnell, P.J. Pomery, C.L. Winzor, Kinetic parameters for polymerization of methyl methacrylate at 60°C, Polymer (Guildf) 33 (1992) 137–140. https://doi.org/10.1016/0032-3861(92)90573-F.

[41] J. Krstina, G. Moad, R. Ian Willing, S.K. Danek, D.P. Kelly, S.L. Jones, D.H. Solomon, Further studies on the thermal decomposition of AIBN—implications concerning the mechanism of termination in methacrylonitrile polymerization, Eur Polym J 29 (1993) 379–388. https://doi.org/10.1016/0014-3057(93)90108-R.

[42] K.H. Büchel, J. Falbe, H. Hagemann, M. Hanack, D. Klamann, R. Kreher, H. Kropf, M. Regitz, Register der Stoffklassen, Georg Thieme Verlag KG, Stuttgart, 1987. https://doi.org/10.1055/b-003-111695.

[43] R.P. Wool, Polymer entanglements, Macromolecules 26 (1993) 1564–1569. https://doi.org/10.1021/ma00059a012.

[44] G. Weickert, Modellierung von Polymerisationsreaktoren, Springer Berlin Heidelberg, 1997. https://doi.org/10.1007/978-3-642-60516-1.

[45] M. Wen, A. V. McCormick, Kinetic model for radical trapping in photopolymerization of multifunctional monomers, Macromolecules 33 (2000) 9247–9254. https://doi.org/10.1021/ma0003351.

[46] C. Boyer, V. Bulmus, T.P. Davis, V. Ladmiral, J. Liu, S. Perrier, Bioapplications of RAFT polymerization, Chem Rev 109 (2009) 5402–5436. https://doi.org/10.1021/cr9001403.

[47] M. Widjaja, J. Gan, J. Talpaneni, R. Tjandrawinata, Determination of Eudragit® L100 in an Enteric-Coated Tablet Formulation Using Size-Exclusion Chromatography with Charged-Aerosol Detection, Sci Pharm 86 (2018) 38. https://doi.org/10.3390/scipharm86030038.

[48] S. Missaghi, C. Young, K. Fegely, A.R. Rajabi-Siahboomi, Delayed release film coating applications on oral solid dosage forms of proton pump inhibitors: Case studies Delayed release solid dosage forms of proton pump inhibitors, Drug Dev Ind Pharm 36 (2010) 180–189. https://doi.org/10.3109/03639040903468811.

[49] Tablets, in: European Pharmacopoeia, 2018: pp. 1004–1006.

[50] A.T. Florence, D. Attwood, Physicochemical Principles of Pharmacy: In Manufacture, Formulation and Clinical Use, 6. Edition, Pharmaceutical Press, 2015.

[51] T. Grosser, S. Fries, J.A. Lawson, S.C. Kapoor, G.R. Grant, G.A. FitzGerald, Drug resistance and pseudoresistance: An unintended consequence of enteric coating aspirin, Circulation 127 (2013) 377–385. https://doi.org/10.1161/CIRCULATIONAHA.112.117283.

[52] J.J. McNeil, R. Wolfe, R.L. Woods, A.M. Tonkin, G.A. Donnan, M.R. Nelson, C.M. Reid, J.E. Lockery, B. Kirpach, E. Storey, R.C. Shah, J.D. Williamson, K.L. Margolis, M.E. Ernst, W.P. Abhayaratna, N. Stocks, S.M. Fitzgerald, S.G. Orchard, R.E. Trevaks, L.J. Beilin, C.I. Johnston, J. Ryan, B. Radziszewska, M. Jelinek, M. Malik, C.B. Eaton, D. Brauer, G. Cloud, E.M. Wood, S.E. Mahady, S. Satterfield, R. Grimm, A.M. Murray, Effect of Aspirin on Cardiovascular Events and Bleeding in the Healthy Elderly, New England Journal of Medicine 379 (2018) 1509–1518. https://doi.org/10.1056/NEJMoa1805819.

[53] D.L. Bhatt, T. Grosser, J. Dong, D. Logan, W. Jeske, D.J. Angiolillo, A.L. Frelinger, L. Lei, J. Liang, J.E. Moore, B. Cryer, U. Marathi, Enteric Coating and Aspirin Nonresponsiveness in Patients With Type 2 Diabetes Mellitus, J Am Coll Cardiol 69 (2017) 603–612. https://doi.org/10.1016/j.jacc.2016.11.050.

Supporting Information

Enteric drug coatings: Synthesis and copolymerization of novel α-hydroxy acid monomers to adjust the pH for dissolution

Shifting the pK_a value of enteric drug coatings for duodenum release: synthesis and copolymerization of novel α-hydroxy acid methacrylates

Dominik A. H. Fuchs,[a] [redacted]

[d.] Institute of Organic Chemistry, Johannes Gutenberg-University Mainz, Duesbergweg 10-14, 55128 Mainz, Germany
[e.] Institute of Pharmacy, Department Pharmaceutical Technology and Biopharmacy, Johannes Gutenberg-University Mainz, Staudinger Weg 5, 55128 Mainz, Germany
[f.] VeZerf Laborsynthesen GmbH, Langenfelder Straße 12, 55743 Idar-Oberstein

Experimental Part

Reagents

Solvents and chemicals were typically purchased from Acros Organics, Thermo Fischer Scientific Inc., TCI, Sigma-Aldrich, Merck, Fluka, VWR International or Carl Roth GmbH and used as received, unless otherwise stated. Deuterated solvents were received from Deutero GmbH. The synthesized monomers were subjected to flash chromatography with neutral aluminium oxide to remove the stabilizer. Technical petrol ether was distilled before use. Eudragit® L100-55 and L100 were provided by Evonik Industries AG. Paracetamol was obtained from Caesar & Loretz GmbH (Hilden, Germany). The transparent hydroxypropyl methylcellulose (HPMC) capsules (ACG Nature Caps Plus) were received as gift from ACG Associated Capsule PvT Ltd (Ashagadh, Maharashtra, India).

Instrumentation

^{1}H NMR (400 MHz) spectra were recorded on a Bruker Avance III HD (400 MHz, 5 mm BBFO-head with z-gradient and ATM, BACS 60 sample changer) and referenced internally to the proton signal of the deuterated solvent ($CDCl_3$, DMSO-d_6).
Size exclusion chromatography (SEC) analysis was performed in dimethylformamide (DMF) (containing 1 g L^{-1} lithium bromide) as an eluent and Polymer Standards Service (PSS) HEMA columns (300/100/40 Å porosity) at 50 °C, using a RI detector at a flow rate of 1 mL min^{-1}. Molecular weights were determined by a calibration with poly(ethylene oxide) standards in the molecular range of 194-44700 g mol^{-1} provided by PSS.
Differential scanning calorimetry (DSC) measurements were carried out under a nitrogen atmosphere using a TA instruments DSC 250 connected to a TA instrument RCS 90 refrigeration system from Waters Corporation. Experiments were performed in the temperature range of −90 °C to 200 °C, with a heating and cooling rate of 10 °K min^{-1} using a two-point calibration of indium and *n*-octane. The values of the second heating cycle were used for analysis.
Cloud point measurements were performed on a JASCO V-640 photometer, equipped with a JASCO ETC-717 Peltier element at 600 nm. It was heated from 30 to 40 °C with a heating rate of 3 K min^{-1} while stirring. The transmission value at 37 °C was used for determination of the transmission at specific pH values.
FT-IR spectra were recorded using a Thermo Scientific iS10 FT-IR spectrometer, equipped with a diamond ATR unit.
Capsule dissolution experiments were performed in a USP type I apparatus (PTW S III, Pharma Test, Germany). The analysis of the dissolution samples was done spectrophotometrically (UV-1700 PharmaSpec, Shimadzu, Japan).
The *photoinitiated radical copolymerization* experiments were performed using a UV lamp (XX-15B) from Ultra-Violet Products Ltd. The UV lamp was equipped with two UV tubes of the manufacturer Vilber Lourmat Deutschland GmbH of different wavelengths: 312 nm (T-15.M) and 365 nm (T-15.L).

Synthesis of benzyl 2-hydroxyacetate (GlyBn)

GlyBn was prepared similarly to the described procedure in the literature.[23] Glycolic acid (29.98 g, 0.394 mol, 1.0 eq) was dissolved in 150 mL of methanol in a 500 mL flask. The base 1,8-diazabicyclo(5.4.0)undec-7-ene (59.98 g, 0.394 mol, 1.0 eq) was added dropwise under stirring. After stirring for 1 hour the solvent was removed under reduced pressure. The oily liquid was dissolved in 240 mL of dimethylformamide (DMF) and

cooled to 10 °C. At this temperature benzyl bromide (67.54 g, 0.394 mol, 1.0 eq) was added dropwise. The reaction mixture was stirred overnight at room temperature. The yellow solution was diluted with 250 mL of ethyl acetate and 400 mL of deionized water. The aqueous phase was extracted with 150 mL of ethyl acetate for 4 times. The combined organic phase was extracted with 150 mL of water, three times with 150 mL of 5 wt.% citric acid and two times with 150 mL of brine and dried over sodium sulfate. Ethyl acetate was removed under reduced pressure to obtain the crude product. The purity was improved by distillation at 98 °C and at $1*10^{-3}$ mbar to obtain the pure product in 82 % yield. ^{1}H NMR (400 MHz, chloroform-*d*) δ (ppm) = 2.36 (s, 1H, CH_2 O*H*), 4.20 (s, 2H, C*H*$_2$ OH), 5.24 (s, 2H, C*H*$_2$ C_6H_5), 7.34-7.40 (m, 5H, CH_2 C_6*H*$_5$).

Benzyl (*S*)-hydroxypropanoate (Lac-Bn) and **Benzyl-hydroxypropanoate (DLLacBn)** were prepared analogous to Gly-Bn. The purification was performed by distillation at 100 °C and at $1*10^{-3}$ mbar to obtain the pure product in a yield of 72 %. ^{1}H NMR (400 MHz, chloroform-*d*) δ (ppm) = 1.46 (d, *J* = 6.9 Hz, 3H, C*H*$_3$ CH (OH)), 2.85 (s, 1H, CH_3 CH (O*H*)), 4.35 (q, *J* = 6.9 Hz 1H, CH_3 C*H* (OH)), 5.24 (s, 2H, C*H*$_2$ C_6H_5), 7.33-7.40 (m, 5H, CH_2 C_6*H*$_5$).

Monomer synthesis 2-(benzyloxy)-2-oxoethyl methacrylate (MA-GlyBn)

GlyBn (10,00 g, 0.061 mol, 1.0 eq), methacrylic acid (5,70 g, 0.062 mol, 1.1 eq) and *N,N*-Dimethylpyridin-4-amine DMAP (0,74 g, 0.006 mol, 0.1 eq) were dissolved in a brown glass flask in 50 mL of DMF. The solution was cooled with an ice bath to 0 °C. *N,N'*-Diisopropylcarbodiimde DIPC (11.39 g, 0.09 mol, 1.5 eq) was dissolved in 15 mL of DMF and added dropwise to the cooled solution. Additional 10 mL of DMF were added to rinse all DIPC. After complete addition of DIPC, the ice bath was removed and the reaction mixture was stirred for 5 days at room temperature. The white solid was filtered. The yellow solution was diluted with 100 mL of ethyl acetate and 100 mL of deionized water. The aqueous phase was extracted 3 times with 150 mL of ethyl acetate. The combined organic phase was extracted with 150 mL of deionized water and 2 times with 100 mL of brine and dried over magnesium sulfate. A stabilizer 2,6-Di-*tert*-butyl-4-methylphenol (BHT) was added and the solvent was removed under reduced pressure to obtain the crude product. The crude product was stored at -20 °C to crystallize the remaining urea. The white solid was removed by filtration and washed with ice cold ethyl acetate. The solvent was removed under reduced pressure. The purification was performed by column chromatography with ethyl acetate and petrol ether (1:5) to obtain the pure product in a yield of 70 %. ^{1}H NMR (400 MHz, chloroform-*d*) δ (ppm) = 1.99 (m, 3H, CH_2 C (C*H*$_3$)), 4.73 (s, 2H, O C*H*$_2$ C (O) O), 5.21 (s, 2H, C*H*$_2$ C_6H_5), 5.66-5.75 (m, 1H, C*H*$_2$ C (CH_3)), 6.18-6.27 (m, 1H, C*H*$_2$ C (CH_3)), 7.30-7.44 (m, 5H, CH_2 C_6*H*$_5$).

(S)-1-(benzyloxy)-1-oxopropan-2-yl methacrylate (MA-Lac-Bn) and **1-(benzyloxy)-1-oxopropan-2-yl methacrylate (MA-DLLac-Bn)** were prepared analogous to MA-Gly-Bn in 59 % yield. ^{1}H NMR (400 MHz, chloroform-*d*) δ (ppm) = 1.55 (d, *J* = 7.1 Hz 3H, O CH (C*H*$_3$)), 1.97 (m, 3H, CH_2 C (C*H*$_3$)), 5.08-5.29 (m, 1H, O C*H* (CH_3)) and 2H, C*H*$_2$ C_6H_5), 5.63 (m, 1H, , C*H*$_2$ C (CH_3)), 6.20 (m, 1H, C*H*$_2$ C (CH_3)), 7.28-7.44 (m, 5H, CH_2 C_6*H*$_5$).

Copolymerization of modified MA copolymers

The synthesis procedure of an exemplary **P(MA-GlyBn$_{0.50}$-*co*-MMA$_{0.50}$)** with a molar ratio of 1:1 was performed as follows. The monomers MA-GlyBn (0.800 g, 0.0034 mol, 1.0 eq) and methyl methacrylate (MMA) (0.342 g, 0.0034 mol, 1.0 eq) were columned over neutral aluminium oxide to remove the stabilizer and transferred to a schlenk flask. The monomer mixture was diluted with 6 mL benzene to obtain a monomer concentration of 1 mol/L. The photoinitiator 2,2-dimethoxy-2-phenylacetophenone (DMPA) (57.5 mg, 0.22 mmol, 5 wt.%) was dissolved in 0.4 mL of benzene and added to the monomer mixture. The schlenk flask was sealed and the reaction mixture was degassed three times with the freeze-pump-thaw technique. Subsequently, the solution was stirred under irradiation of UV light for 14 hours. The polymer product was precipitated twice in ice cold petrol ether and separated by centrifugation. Typical yields were in the range of 90-99 %. ^{1}H NMR (400 MHz, DMSO-d_6) δ (ppm) = 0.53-1.32 (m, 6H, CH_2 C (C*H*$_3$)), 1.38-2.27 (m, 4H, polymer backbone C*H*$_2$ C (CH_3)), 3.51 (broad s, 3H, O C*H*$_3$), 4.68 (s, 2H, O C (O)C*H*$_2$ O), 5.15 (broad s, 2H, C*H*$_2$ C_6H_5), 7.05-7.63 (m, 5H, CH_2 C_6*H*$_5$).

P(MA-Lac-Bn-*co*-MMA) and **P(MA-DLLac-Bn-*co*-MMA)** copolymers were prepared analogous to P(MA-GlyBn$_{0.50}$-*co*-MMA$_{0.50}$) in yields of approximately 90 %. ^{1}H NMR (400 MHz, DMSO-d_6) δ (ppm) = 0.51-1.20 (m, 6H, CH_2 C (C*H*$_3$)), 1.38 (broad s, 3H, CH (C*H*$_3$)), 1.57-2.23 (m, 4H, polymer backbone C*H*$_2$ C (CH_3)), 3.51 (broad s, 3H, O C*H*$_3$), 4.95 (broad s, 1H, C*H* (CH_3)), 5.14 (broad s, 2H, C*H*$_2$ C_6H_5) 7.03-7.62 (m, 5H, CH_2 C_6*H*$_5$).

P(MA-Lac-Bn-*co*-EA), P(MA-DLLac-Bn-*co*-EA) and P(MA-GlyBn-*co*-EA) were prepared analogous to P(MA-GlyBn$_{0.50}$-*co*-MMA$_{0.50}$) as described above. **P(MA-Lac-Bn-*co*-EA)** ^{1}H NMR (400 MHz, DMSO-d_6) δ (ppm) = 0.60-1.02 (m, 3H, CH_2 C (C*H*$_3$)), 1.11 (broad s, 3H, C*H*$_3$ CH_2 O), 1.36 (broad s, 3H, CH (C*H*$_3$)), 1.46-2.31 (m, 5H, polymer backbone C*H*$_2$ C (CH_3) and C*H*$_2$ C*H*), 3.97 (broad s, 2H, O C*H*$_2$ CH_3), 4.93 (broad s, 1H, C*H* (C*H*$_3$)), 5.12 (broad s, 2H, C*H*$_2$ C_6H_5) 7.03-7.62 (m, 5H, CH_2 C_6*H*$_5$). **P(MA-GlyBn-*co*-EA)** ^{1}H NMR (400 MHz, DMSO-d_6) δ (ppm) = 0.67-1.03 (m, 3H, CH_2 C (C*H*$_3$)), 1.11 (broad s, 3H, C*H*$_3$ CH_2 O), 1.24-2.38 (m, 5H, polymer backbone C*H*$_2$ C

(CH_3) and CH_2 CH), 3.97 (broad s, 2H, O CH_2CH$_3$), 4.64 (broad s, 2H, O C (O)CH_2 O), 5.13 (broad s, 2H, CH_2 C_6H_5) 7.03-7.65 (m, 5H, CH_2 C_6H_5).

The thermal initiated copolymerization was performed analogous to the photoinitiated copolymerization. The photoinitiator DMPA was substituted with 2,2'-Azobis(2-methylpropionitrile) (AIBN) using 4 wt% and a monomer concentration of 2.5 mol/L. The copolymerization was performed at 70 °C for 14 hours. The product was obatined in 99 % yield after precipitation.

Copolymerization of unmodified MA copolymers

The synthesis procedure of an exemplary **P(MA$_{0.50}$-*co*-MMA$_{0.50}$)** was carried out as follows. The monomers MA (1.50 g, 17.4 mmol, 1.0 eq) and MMA (1.74 g, 17.4 mmol, 1.0 eq) were columned over neutral aluminium oxide to remove the stabilizer and transferred to a Schlenk flask. The monomer mixture was diluted with 35 mL of benzene to obtain a monomer concentration of 1 mol/L. The photoinitiator 2,2-dimethoxy-2-phenylacetophenone (DMPA) (162.0 mg, 0.63 mmol, 5 wt.%) was added to the monomer mixture. The Schlenk flask was sealed and the reaction mixture was degassed three times with the freeze-pump-thaw technique. Subsequently, the solution was stirred under irradiation of UV light for 14 hours. The polymer product was precipitated in ice cold petrol ether, separated by centrifugation and dissolved 3 times in benzene. The copolymer was obtained in a yield of 98 %. ^{1}H NMR (400 MHz, DMSO-d_6) δ (ppm) = 0.49-1.27 (m, 6H, polymer backbone CH_2 C (CH_3)), 1.30-2.18 (m, 4H, polymer backboneCH_2 C (CH_3)), 3.55 (broad s, 3H, O CH_3), 12.38 (broad s, 1H, COOH). The synthesis procedure **P(MA$_{0.50}$-*co*-EA$_{0.50}$)** was performed as described for P(MA-*co*-MMA). The colorless copolymer was obtained in 96 % yield. ^{1}H NMR (400 MHz, DMSO-d_6) δ (ppm) = 0.77-1.08 (m, 3H, polymer backbone CH_2 C (CH_3)), 1.09-1.28 (m, 3H, O CH_2 CH_3), 1.30-2.40 (m, 5H, polymer backbone CH_2 C (CH_3) and CH_2 C CH), 3.76-4.31 (m, 2H, O CH_2 CH_3), 12.32 (broad s, 1H, COOH).

RAFT Copolymerization

In the following the synthesis of P(MA-GlyBn$_{0.50}$-*co*-MMA$_{0.50}$) is described, all other copolymers were synthesized accordingly. The stabilizer was removed from the monomers MA-GlyBn (0.2000 g, 0.001 mol, 1.0 eq) and MMA (0.0851 g, 0.001 mol, 1.0 eq) using column chromatography with aluminium oxide as packing material. Subsequently the monomers were transferred to a Schlenk flask. The initiator 2,2'-Azobis(2-methylpropionitrile (AIBN) (0.2 mg, 0.0014 mmol, cat.) and the RAFT agent 2-Cyano-2-propyl dodecyl trithiocarbonate (9.7 mg, 0.03 mmol, cat) were dissolved in 1.74 mL of benzene and added to the monomer mixture to obtain a monomer concentration of 1 mol/L. The Schlenk flask was sealed and the reaction mixture was degassed three times with the freeze-pump-thaw technique. Subsequently, the solution was stirred for 48 h at 70 °C. The polymer product was precipitated twice in ice cold petrol ether and purified by centrifugation. Typical yields were in the range of 95-99 %. ^{1}H NMR (400 MHz, DMSO-d_6) δ (ppm) = 0.58-1.34 (m, 9H, CH_2 C (CH_3) and CH_3 $(CH_2)_{10}$ CH_2 S; 26H, CH_3 $(CH_2)_{10}$ CH_2 S and NC C(CH_3)$_2$), 1.35-2.23 (m, 4H, polymer backbone CH_2 C (CH_3)), 3.23-3.29 (m, 2H, CH_3 $(CH_2)_{10}$ CH_2 S), 3.49 (broad s, 3H, O CH_3), 4.67 (broad s, 2H, O C (O)CH_2 O), 5.15 (broad s, 2H, CH_2 C_6H_5) 7.03-7.64 (m, 5H, CH_2 C_6H_5). **P(MA-Lac-Bn$_{0.50}$-*co*-MMA$_{0.50}$)** copolymer was prepared analogous to the other RAFT copolymers P(MA-GlyBn$_{0.50}$-*co*-MMA$_{0.50}$) in yields of around 94 %. ^{1}H NMR (400 MHz, DMSO-d_6) δ (ppm) = 0.51-1.27 (m, 9H, CH_2 C (CH_3) and CH_3 $(CH_2)_{10}$ CH_2 S; 26H, CH_3 $(CH_2)_{10}$ CH_2 S and NC C(CH_3)$_2$), 1.38 (broad s, 3H, CH (CH_3)), 1.52-2.26 (m, 4H, polymer backbone CH_2 C (CH_3)), 3.21-3.30 (m, 2H, CH_3 $(CH_2)_{10}$ CH_2 S), 3.50 (broad s, 3H, O CH_3), 4.96 (broad s, 1H, CH (CH_3)), 5.14 (s, 2H, CH_2 C_6H_5), 7.01-7.61 (m, 5H, CH_2 C_6H_5)

Benzyl 2-bromopropianate:

2-Brompropionic acid (15.29 g, 0.1 mol, 1eq), benzyl alcohol (10.81 g, 0.1 mol, 1eq) and para toluene sulfonic acid (0.19 g, 0.1 mmol, 0.01 eq) was dissolved in 50 ml dry toluene and heated at 125 °C for 1 h in a water separator set up and then heated at 145°C for 3h. After cooling down to room temperature diethyl ether was added and the solution washed with a cold 5 wt% sodium hydroxide solution, water and brine. The organic phase was dried over sodium sulfate, filtrated and concentrated under vacuum. The purity was improved by distillation at 75 °C and at 1*10^{-3} mbar to obtain the pure product in 86 % yield.[1]

^{1}H NMR (400 MHz, $CDCl_3$-d_1) δ (ppm) = 1.83-1.85 (d, 3H, CH_3), 4.39-4.44 (q, 1H, CH3CHBr), 5.21 (s, 2H, CH_2Ph), 7.31-7.42 (s, 5H, C_6H_5).

Postpolymerization modifications:

The polymer (Eudragit L-100 or L-100-55) (120 g, 1eq) was dissolved slowly in 4.5 L THF, after complete dissolution potassium carbonate (613 g, 7 eq) was added and the solution was stirred for 30 minutes and the alpha-Bromo ester was added slowly. The solution was stirred and heated at 50°C for 12h. The solid was removed via centrifugation and

the solvent under reduced pressure, until only 1.6 L THF were remaining, and the polymer was precipitated in pentane. Almost all carboxylic functions were modified (99%) with a yield of 78%.

P(MA-Gly-Bn-co-MMA) ^{1}H NMR (400 MHz, DMSO-d_6) δ (ppm) = 0.53-1.32 (m, 6H, $CH_2C(CH_3)$), 1.38-2.27 (m, 4H, polymer backbone CH_2 C (CH_3)), 3.51 (broad s, 3H, O CH_3), 4.68 (s, 2H, O C (O)CH_2 O), 5.15 (broad s, 2H, CH_2 C_6H_5), 7.05-7.63 (m, 5H, CH_2 C_6H_5).
P(MA-La-Bn-co-EA) ^{1}H NMR (400 MHz, DMSO-d_6) δ (ppm) = 0.60-1.02 (m, 3H, CH_2 C (CH_3)), 1.11 (broad s, 3H, CH_3 CH_2 O), 1.36 (broad s, 3H, CH (CH_3)), 1.46-2.31 (m, 5H, polymer backbone CH_2 C (CH_3) and CH_2 CH), 3.97 (broad s, 2H, O CH_2 CH_3), 4.93 (broad s, 1H, CH (CH_3)), 5.12 (broad s, 2H, CH_2 C_6H_5) 7.03-7.62 (m, 5H, CH_2 C_6H_5).

Hydrogenation: removal of the protective groups

The copolymer (1.00 g) was dissolved in 100 mL ethyl acetate. In the glovebox 20 wt.% Pd/C-catalyst (0.200 g) was added to a vial and transferred into the reactor vessel. The copolymer solution was added carefully to the inlay by dropwise addition. The inlay with the suspension was transferred into a reaction vessel and a hydrogen pressure of 40 bar was applied. The reaction mixture was stirred and heated at 40 °C for 4 days. The suspension was filtered and the solvent was removed under reduced pressure. The copolymer was dried in a high vacuum at 40 °C overnight to obtain the colourless copolymer in a quantitative yield.

P(MA-Lac-*co*-EA) ^{1}H NMR (400 MHz, DMSO-d_6) δ (ppm) = 0.78-1.02 (m, 3H, polymer backbone CH_2 C (CH_3)), 1.08-1.28 (m, 3H, CH_3 CH_2 O), 1.39 (s, 3H, CH (CH_3)), 1.46-2.31 (m, 5H, polymer backbone CH_2 C (CH_3) and CH_2 CH), 3.76-4.32 (m, 2H, O CH_2 CH_3), 4.78 (broad s, 1H, CH (CH_3)), 12.97 (s, 1H, COOH).
P(MA-Gly-*co*-EA) ^{1}H NMR (400 MHz, DMSO-d_6) δ (ppm) = 0.71-1.06 (m, 3H, polymer backbone CH_2 C (CH_3)), 1.07-1.24 (m, 3H, CH_3 CH_2 O), 1.27-2.36 (m, 5H, polymer backbone CH_2 C (CH_3) and CH_2 CH), 3.77-4.24 (m, 2H, O CH_2CH_3), 4.50 (broad s, 2H, CH_2 COOH), 13.04 (s, 1H, COOH).
P(MA-Lac-*co*-MMA) ^{1}H NMR (400 MHz, DMSO-d_6) δ (ppm) = 0.52-1.12 (m, 6H, CH_2 C (CH_3)), 1.30-1.58 (m, 3H, CH (CH_3)), 1.62-2.24 (m, 4H, CH_2 C (CH_3)), 3.55 (broad s, 3H, O CH_3), 4.81 (broad s, 1H, CH (CH_3)), 13.00 (s, 1H, COOH).
P(MA-Gly-*co*-MMA) ^{1}H NMR (400 MHz, DMSO-d_6) δ (ppm) = 0.61-1.28 (m, 6H, CH_2 C (CH_3)), 1.44-2.23 (m, 4H, CH_2 C (CH_3)), 3.54 (broad s, 3H, O CH_3), 4.50 (broad s, 2H, CH_2 COOH), 13.03 (broad s, 1H, COOH).

Hydrolysis: removal of the protective groups

The postpolymerization modified polymers were dissolved in Trifluoracetic acid in a concentration of 0.1g/ml at room temperature and heated up to 70°C for 16h. The colourless liquid changes to a beige colour. TFA is removed under reduced pressure and can be used again. The remaining polymer is dissolved in ethyl acetate and washed at least 5 times against water to remove remaining TFA, until the ^{19}F-NMR has no remaining signals. Almost all benzylic protecting units were removed (99%) with a yield of 85%.

P(MA-Gly-co-MMA) ^{1}H NMR (400 MHz, DMSO-d_6) δ (ppm) = 0.47-1.10 (m, 6H, $CH_2C(CH_3)$), 1.33-2.21 (m, 4H, polymer backbone CH_2 C (CH_3)), 3.54 (s, 3H, OCH_3), 4.51 (s, 2H, OCH_2COOH), 12.23-13.67 (s, 1H, COOH).

P(MA-Lac-co-EA) ^{1}H NMR (400 MHz, DMSO-d_6) δ (ppm) = 0.64-1.07 (m, 3H, $CH_2C(CH_3)$), 1.16 (s, 3H, CH_3CH_2O), 1.38 (s, 3H, $CH(CH_3)$), 1.46-2.42 (m, 5H, polymer backbone $CH_2C(CH_3)$ and CH_2CH), 4.01 (s, 2H, OCH_2CH3), 4.78 (s, 1H, $CH(CH_3)$), 12.33-13.25 (s, 1H, COOH).

Cloud point titration

The copolymer was dissolved in 0.01 molar NaOH solution to obtain a 5 mg/mL polymer solution. The polymer solution was stirred for 1 hour to ensure complete dissolution of the copolymer. The pH value of the copolymer solution was determined and the transmission was measured in a temperature range from 30 to 40 °C with a heating rate of 3 K min $^{-1}$ while stirring. The transmission value at 37 °C was used for determination of the transmission at specific pH values. The pH value was lowered stepwise by addition of 0.1 molar hydrochloric acid (HCl), and the measurement was repeated.

Capsule Coating

Paracetamol was filled manually into size zero hydroxypropyl methylcellulose (HPMC) capsules. The empty shell weighs an average of 98.4 mg (n=100). Each capsule was weighed before and after the coating to determine the individual dose and the coating level of each capsule. The copolymer solution was prepared as follows. 60 mg of triethyl citrate (TEC) and 300 mg of the polymer were dissolved in 5 g of acetone/ethanol (1:1 v/v). The capsules were dipped in the copolymer solution for 1-3 seconds and dried at room temperature for 10-15 minutes. The dipping process was repeated 10 to 13 times until a sufficient amount of coating was obtained. After the last immersion, the capsules were dried at room temperature for one hour. Afterwards any

irregularities due to the holding position of the forceps were corrected with a brush and the coating solution. The coating level was calculated by the following equation:

$$Coating\ level = \frac{(m_c - m_u)}{5\ cm^2} \times 0.83$$

where m_c is the capsule weight after coating and m_u is the capsule weight before coating. The mean coating level and the standard deviation (SD) of the copolymer coated capsules are 10.16 ± 0.79 mg*cm^{-2} for Eudragit® L100, 9.63 ± 0.19 mg*cm^{-2} for P(MA$_{0.50}$-*co*-MMA$_{0.50}$) and 11.70 ± 1.80 mg*cm^{-2} for P(MA-Gly$_{0.50}$-*co*-MMA$_{0.50}$), respectively.

Dissolution testing of coated capsules

Dissolution testing was performed using the basket method (USP apparatus I) at 100 rpm. First, the capsules were tested in 900 ml of 0.01 M HCl for 1 hour followed by 2 hours in 900 ml of a 15 mM phosphate buffer at 37 °C. The buffer was described by Al-Gousous *et al.* and showed to give a fairly bio predictive representation of the proximal small intestinal conditions.[2] After set time points 5 mL samples were withdrawn manually without replacement. The amount of released paracetamol was quantified at λ=243 nm spectrophotometrically.

Acid uptake

For the investigation of the acid uptake the capsules were gently dried after one hour in 0.01 M HCl and weighed again and the acid uptake calculated as follows:

$$Acid\ uptake\ (\%) = \frac{(m_a - m_c)}{m_c} * 100\ \%$$

where m_a is the capsule weight after the acid stage, m_c is the initial capsule weight before the dissolution testing.

Monomer characterisation:

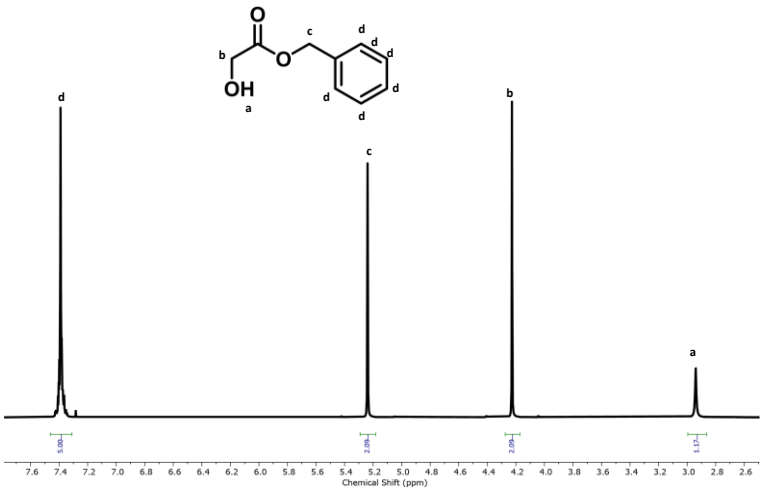

Figure S1: ^{1}H-NMR spectrum (400 MHz, $CDCl_3$) of benzyl protected glycolic acid (Gly-Bn).

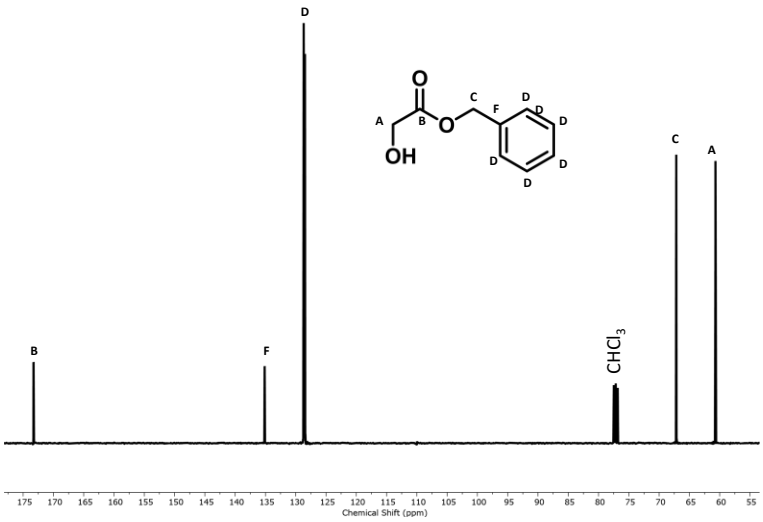

Figure S2: ^{13}C-NMR spectrum (101 MHz, $CDCl_3$) of benzyl protected glycolic acid (Gly-Bn).

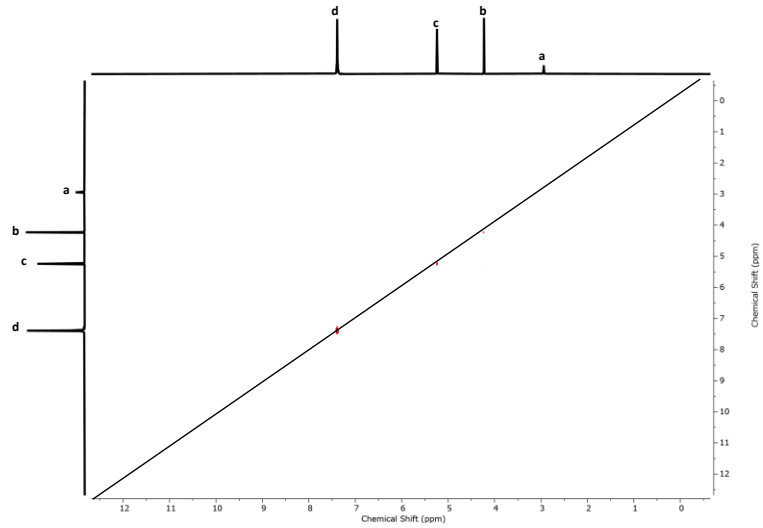

Figure S3: COSY spectrum (400 MHz, $CDCl_3$) of bezyl protected glycolic acid (Gly-Bn).

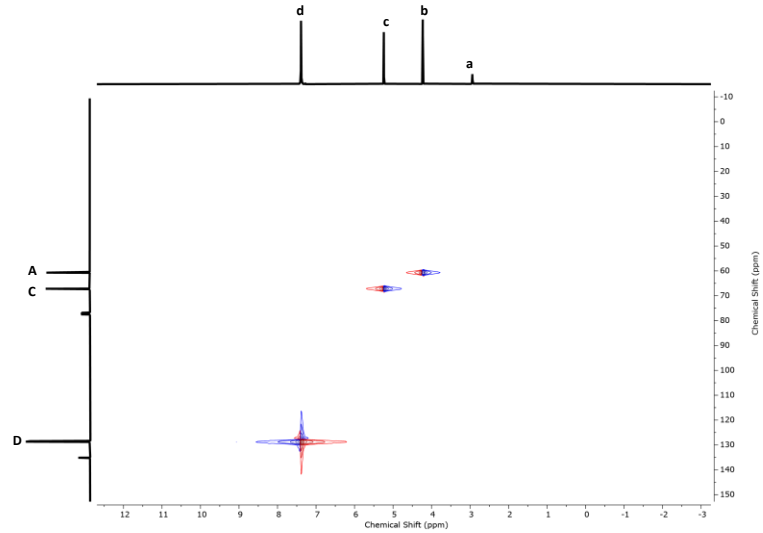

Figure S4: HSQC spectrum (400 MHz, $CDCl_3$) of benzyl protected glycolic acid (Gly-Bn).

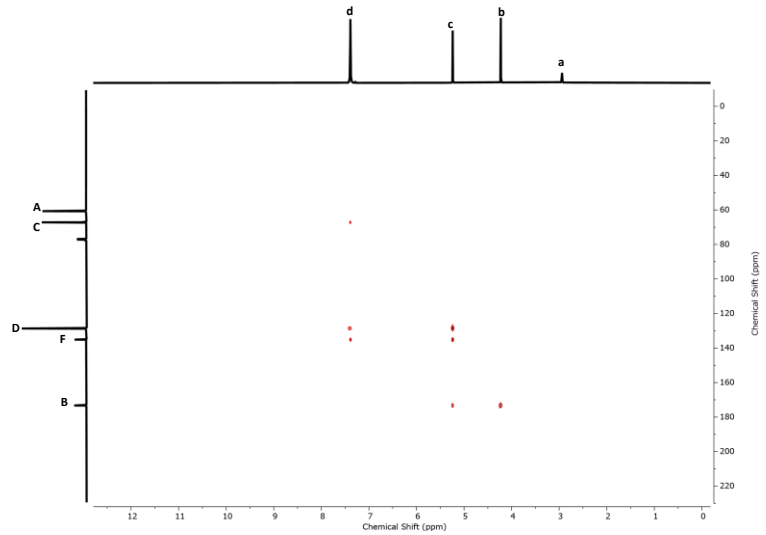

Figure S5: HMBC spectrum (400 MHz, $CDCl_3$) of benzyl protected glycolic acid (Gly-Bn).

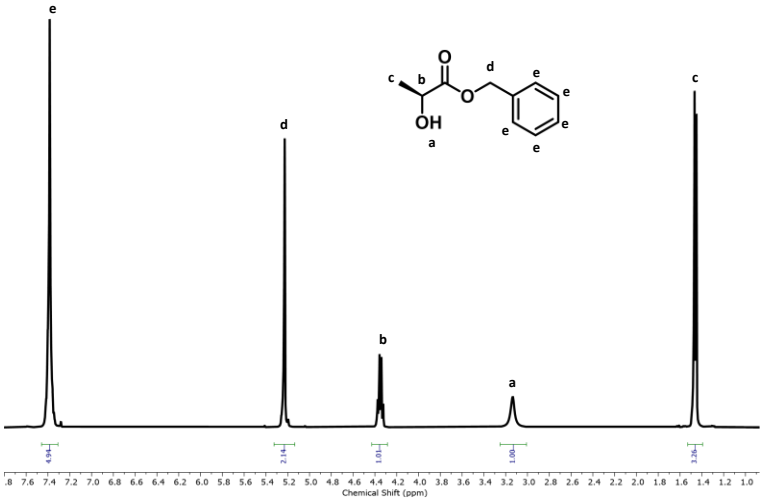

Figure S6: ^{1}H-NMR spectrum (400 MHz, $CDCl_3$) of benzyl protected L-lactic acid (Lac-Bn).

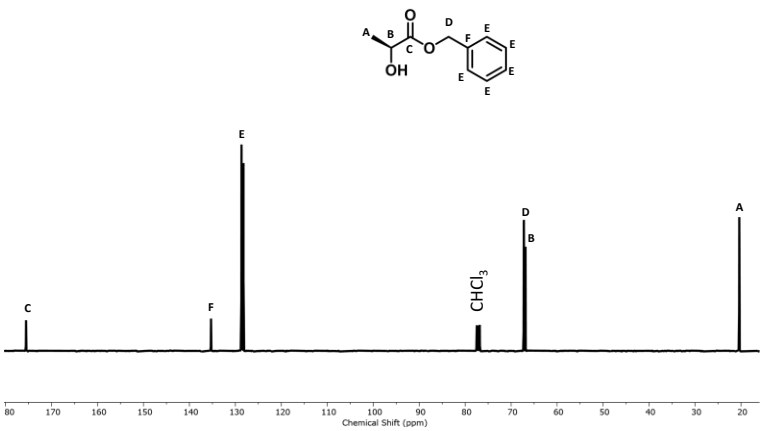

Figure S7: ^{13}C-NMR spectrum (101 MHz, $CDCl_3$) of benzyl protected L-lactic acid (Lac-Bn).

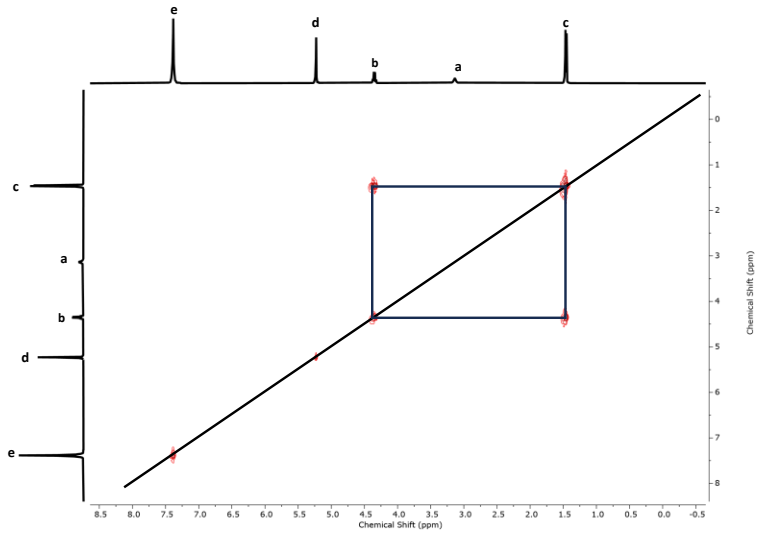

Figure S8: COSY spectrum (400 MHz, $CDCl_3$) of bezyl protected L-lactic acid (Lac-Bn).

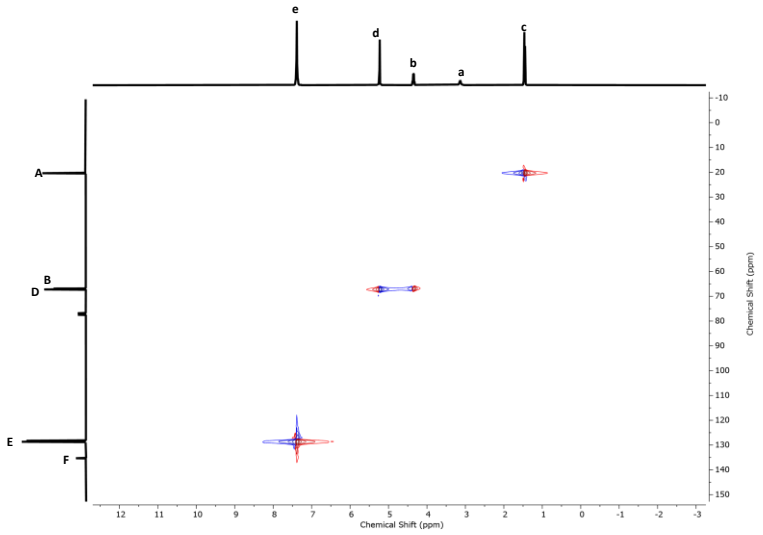

Figure S9: HSQC spectrum (400 MHz, $CDCl_3$) of benzyl protected L-lactic acid (Lac-Bn).

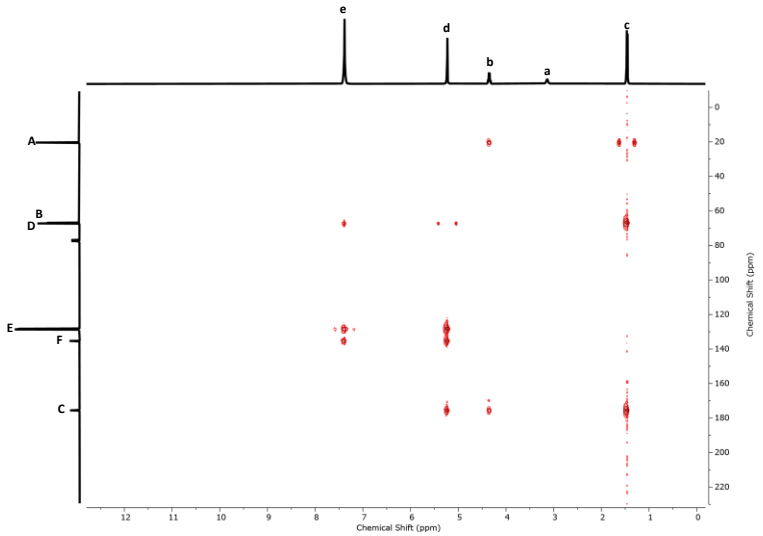

Figure S10: HMBC spectrum (400 MHz, $CDCl_3$) of benzyl protected L-lactic acid (Lac-Bn).

Figure S11: ^{1}H-NMR spectrum (400 MHz, $CDCl_3$) of benzyl protected glycolic acid modified methacrylic acid (MA-Gly-Bn).

Figure S12: ^{13}C-NMR spectrum (101 MHz, $CDCl_3$) of benzyl protected glycolic acid modified methacrylic acid (MA-Gly-Bn).

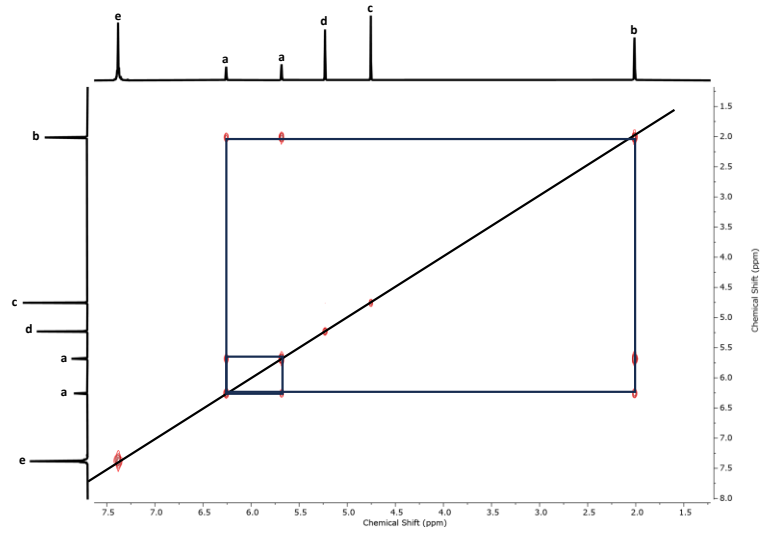

Figure S13: COSY spectrum (400 MHz, $CDCl_3$) of bezyl protected glycolic acid modified methacrylic acid (MA-Gly-Bn).

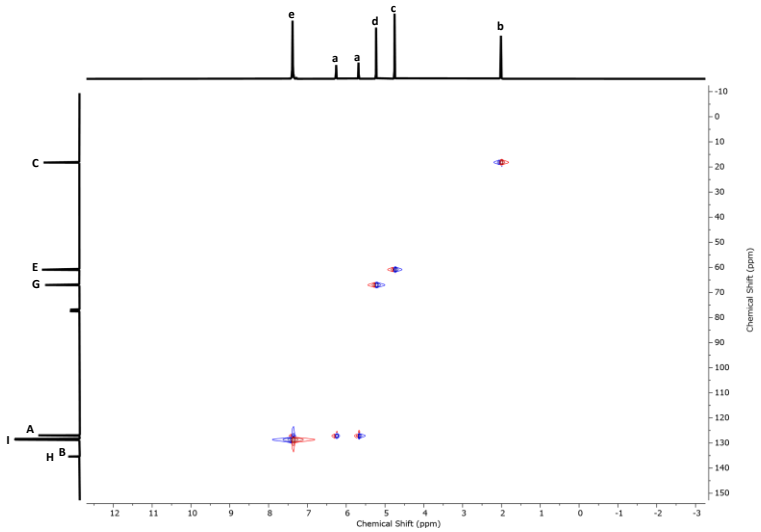

Figure S14: HSQC spectrum (400 MHz, $CDCl_3$) of benzyl protected glycolic acid modified methacrylic acid (MA-Gly-Bn).

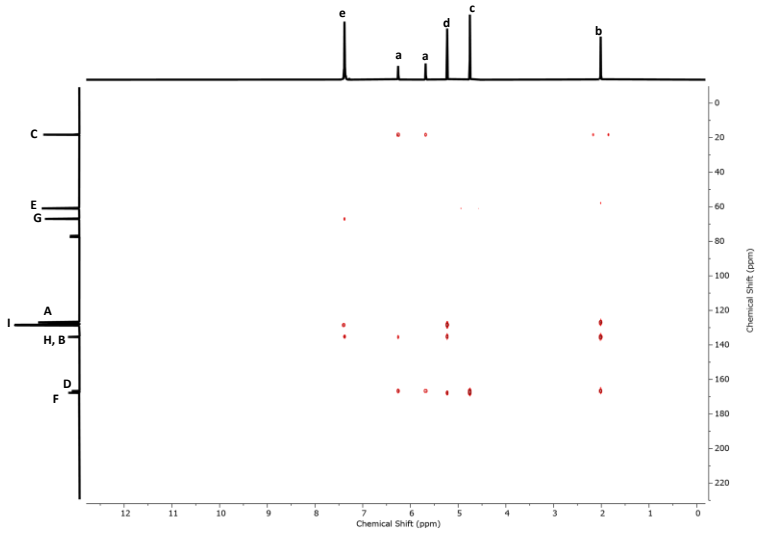

Figure S15: HMBC spectrum (400 MHz, $CDCl_3$) of benzyl protected glycolic acid modified methacrylic acid (MA-Gly-Bn).

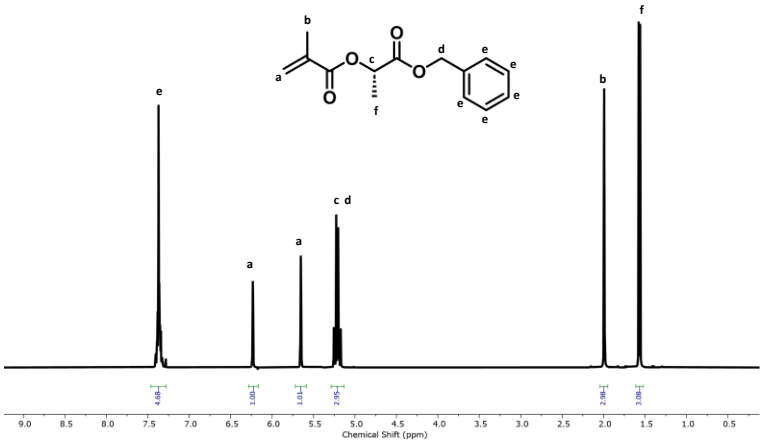

Figure S16: ^{1}H-NMR spectrum (400 MHz, $CDCl_3$) of benzyl protected L-lactic acid modified methacrylic acid (MA-Lac-Bn).

Figure S17: ^{13}C-NMR spectrum (101 MHz, $CDCl_3$) of benzyl protected L-lactic acid modified methacrylic acid (MA-Lac-Bn).

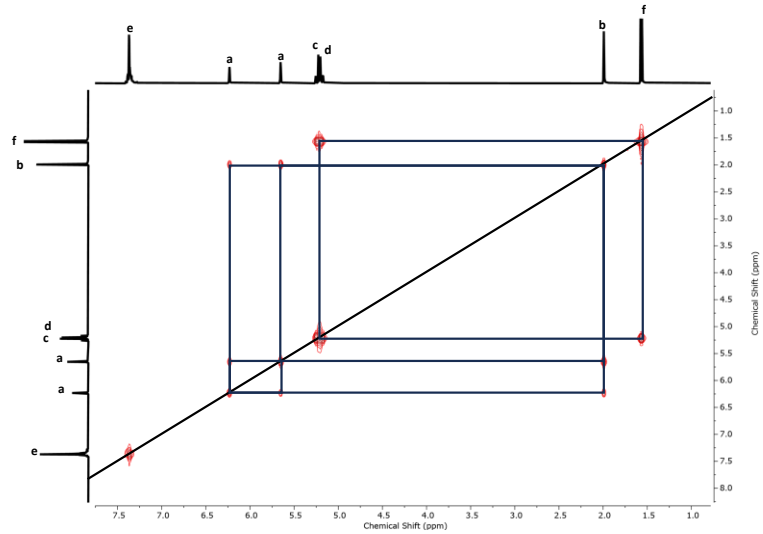

Figure S18: COSY spectrum (400 MHz, $CDCl_3$) of bezyl protected L-lactic acid modified methacrylic acid (MA-Lac-Bn).

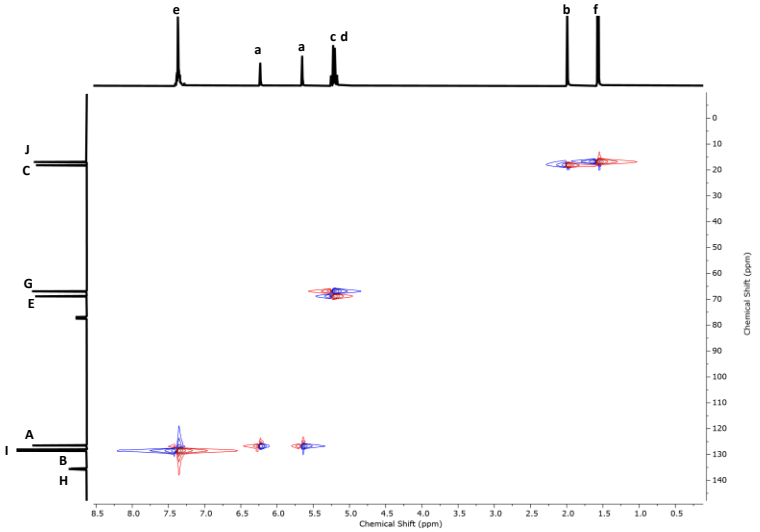

Figure S19: HSQC spectrum (400 MHz, $CDCl_3$) of benzyl protected L-lactic acid modified methacrylic acid (MA-Lac-Bn).

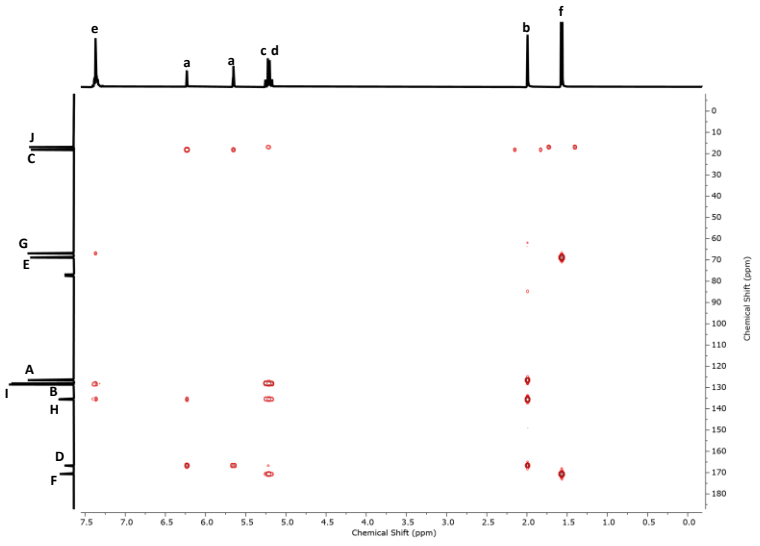

Figure S20: HMBC spectrum (400 MHz, $CDCl_3$) of benzyl protected L-lactic acid modified methacrylic acid (MA-Lac-Bn).

Copolymer characterisation:

Table S1: Results of the copolymerization of P(MA-Gly-Bn-co-EA) using different amounts of DMPA initiator at a monomer concentration of 1.0 mol/L, using a PEG calibration.

		DMF SEC	
DMPA / (wt.%)	**Yield / (%)**	**M_n / (10^3 g/mol)**	**Đ**
0.5	39	11.8	1.93
1.0	65	8.69	2.14
2.0	78	7.71	1.95
5.0	92	6.14	2.54

Table S2: Results of the copolymerization of P(MA-Gly-Bn-co-EA) using 5 wt% DMPA initiator at different monomer concentration, using a PEG calibration

		DMF SEC	
Monomer concentration / (mol/l)	**Yield / (%)**	**M_n / (10^3 g/mol)**	**Đ**
1.0	82	2.57	1.96
1.5	89	2.95	1.75
2.0	99	3.25	1.89

Table S3: Results of the copolymerization of P(MA-co-EA) using different amounts of AIBN initiator at a monomer concentration of 2.5 mol/L, using a PEG calibration.

		DMF SEC	
AIBN / (wt.%)	**Yield / (%)**	**M_n / (10^3 g/mol)**	**Đ**
3	99	14.5	2.20
4	99	34.5	1.35
5	99	13.5	1.95
6	99	22.1	1.76

Table S4: Results of the copolymerization of P(MA-co-EA) using 4 wt% AIBN initiator at different monomer concentration, using a PEG calibration.

		DMF SEC	
Monomer concentration / (mol/L)	**Yield / (%)**	**M_n / (10^3 g/mol)**	**Đ**
1.5	75	21.3	1.61
2.0	64	30.8	1.39
2.5	99	34.5	1.35

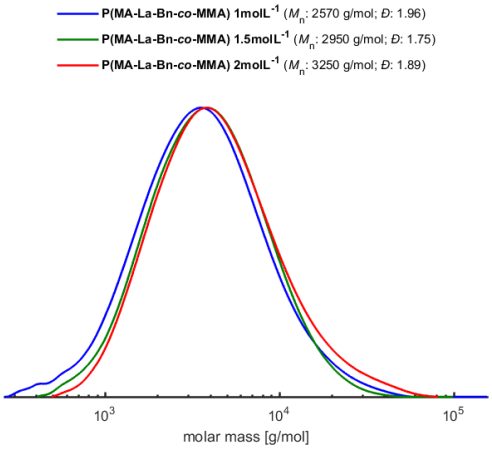

Figure S21: SEC curves (DMF, PEG calibration) for P(MA-Lac-Bn-co-MMA) in a ratio 1:1 using 5 wt% DMPA as initiator.

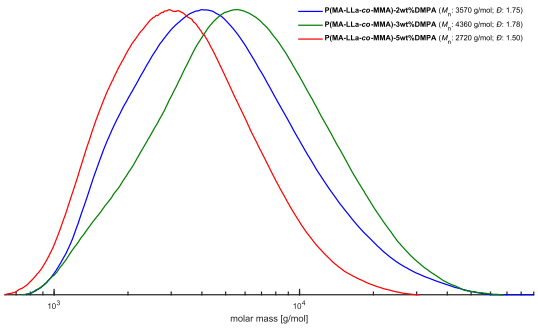

Figure S22: SEC curves (DMF, PEG calibration) for P(MA-Lac-Bn-co-MMA) in a ratio 1:1 in a concentration of 1mol/L using different wt% DMPA as initiator.

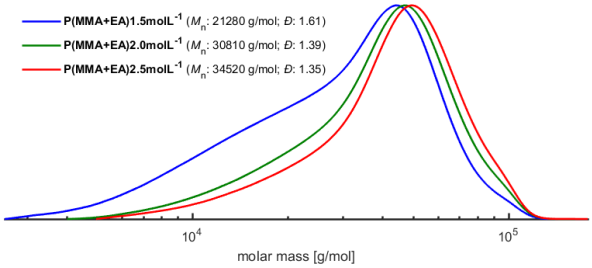

Figure S23: SEC curves (DMF, PEG calibration) for P(MMA-co-EA) in a ratio 1:1 using 4 wt% AIBN as initiator.

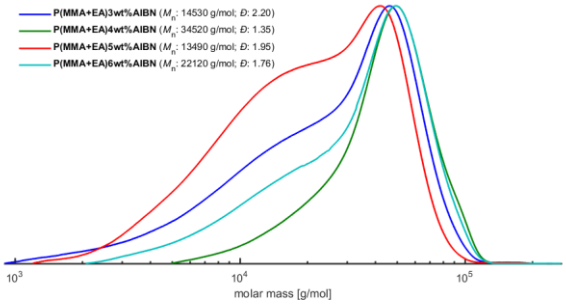

Figure S24: SEC curves (DMF, PEG calibration) for P(MMA-co-EA) in a ratio 1:1 in a concentration of 2.5 mol/L and different wt% AIBN as initiator.

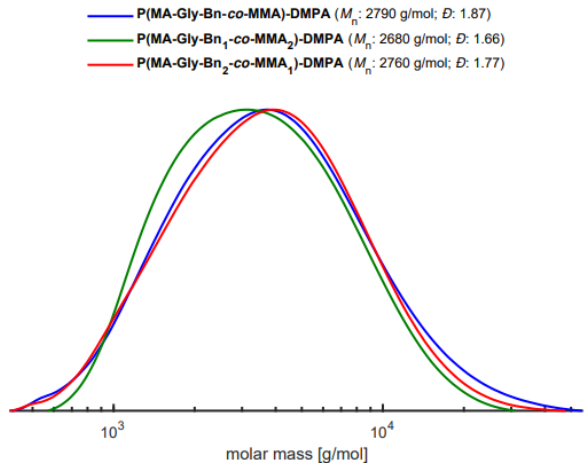

Figure S25: SEC curves (DMF, PEG calibration) for P(MA-GlyBn-co-MMA) in a ratio 1:1, 1:2 and 2:1 in a concentration of 1.0 mol/L and 5 wt% DMPA as initiator.

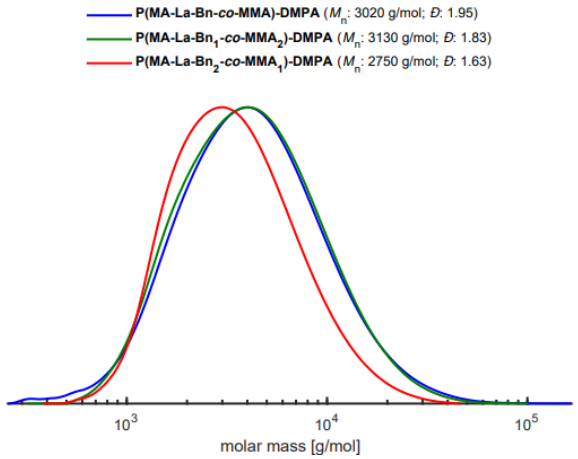

Figure S26: SEC curves (DMF, PEG calibration) for P(MA-Lac-Bn-co-MMA) in a ratio 1:1, 1:2 and 2:1 in a concentration of 1.0 mol/L and 5 wt% DMPA as initiator.

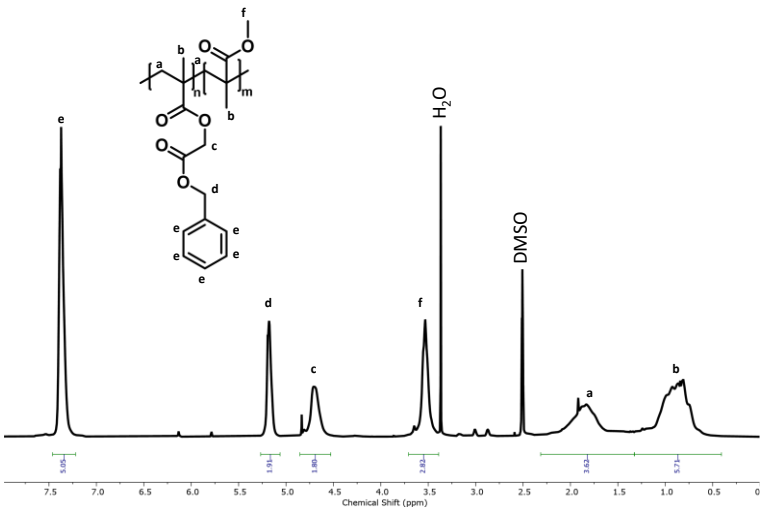

Figure S27: ^{1}H-NMR spectrum (400 MHz, DMSO-d_6) of P(MA-Gly-Bn-co-MMA) copolymer.

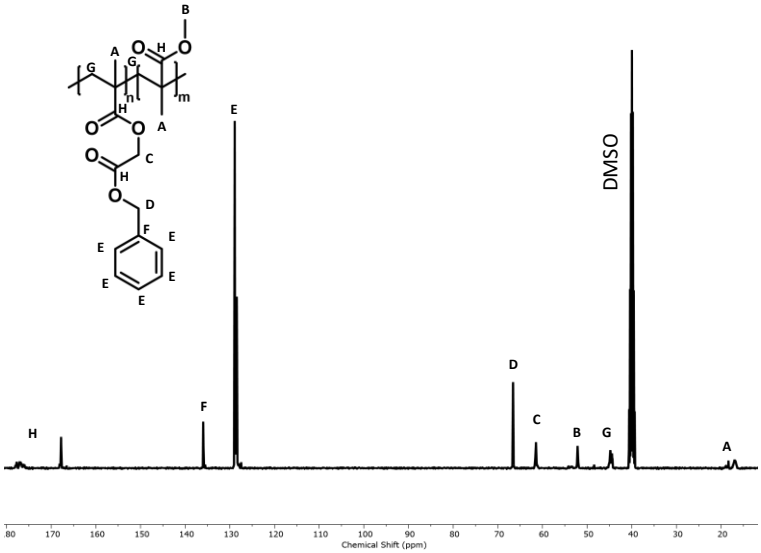

Figure S28: ^{13}C-NMR spectrum (101 MHz, DMSO-d_6) of P(MA-Gly-Bn-co-MMA) copolymer.

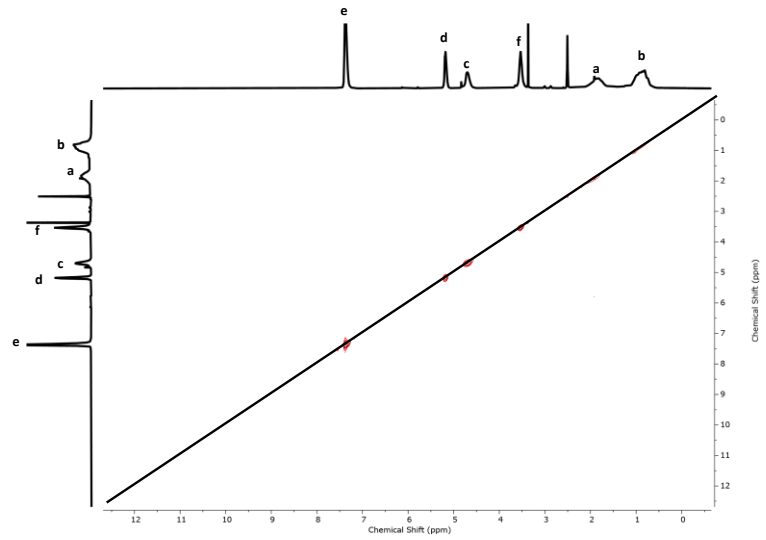

Figure S29: COSY spectrum (400 MHz, DMSO-d_6) of P(MA-Gly-Bn-co-MMA) copolymer.

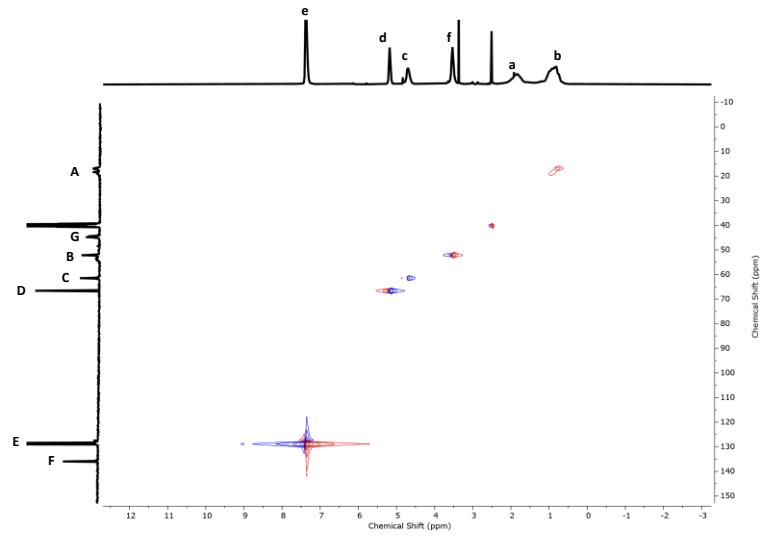

Figure S30: HSQC spectrum (400 MHz, DMSO-d_6) of P(MA-Gly-Bn-co-MMA) copolymer.

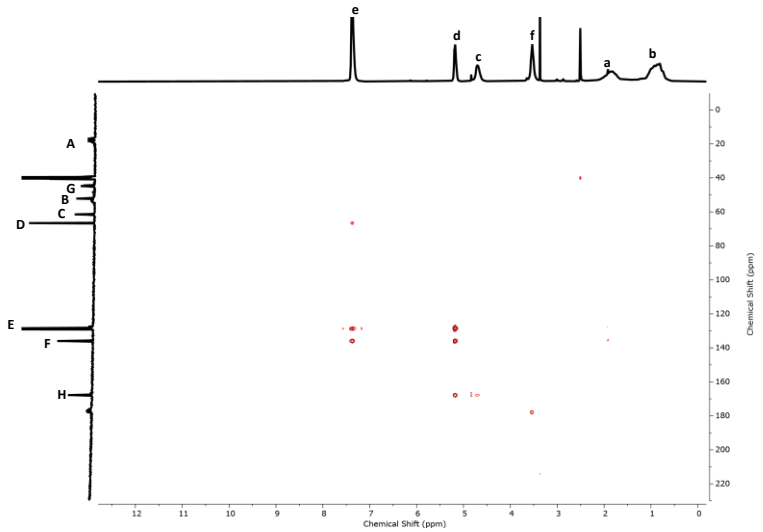

Figure S31: HMBC spectrum (400 MHz, DMSO-d_6) of P(MA-Gly-Bn-co-MMA) copolymer.

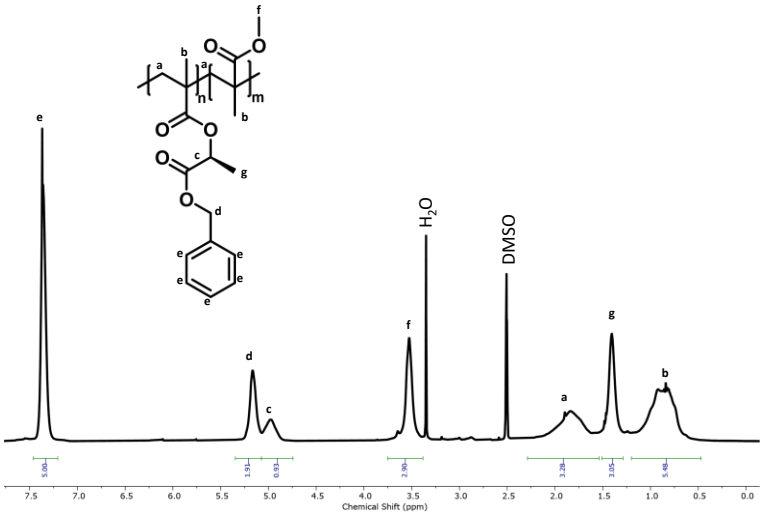

Figure S32: ^{1}H-NMR spectrum (400 MHz, DMSO-d_6) of P(MA-Lac-Bn-co-MMA) copolymer.

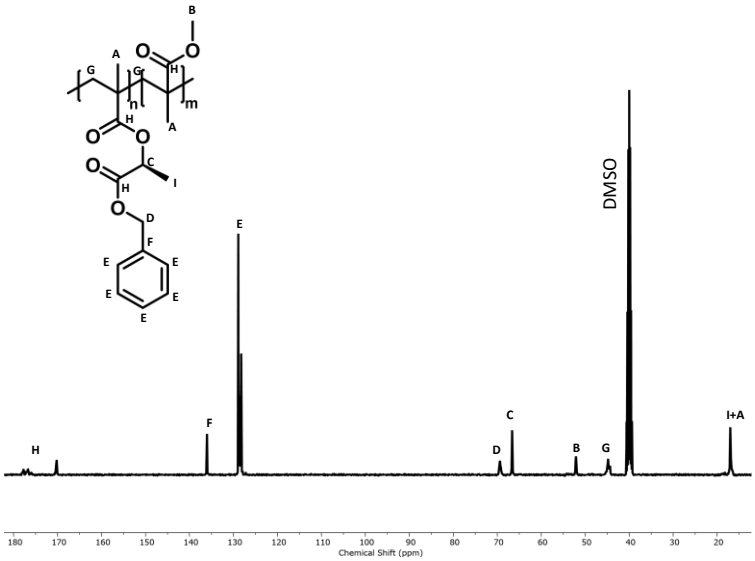

Figure S33: ^{13}C-NMR spectrum (101 MHz, DMSO-d_6) of P(MA-Lac-Bn-co-MMA) copolymer.

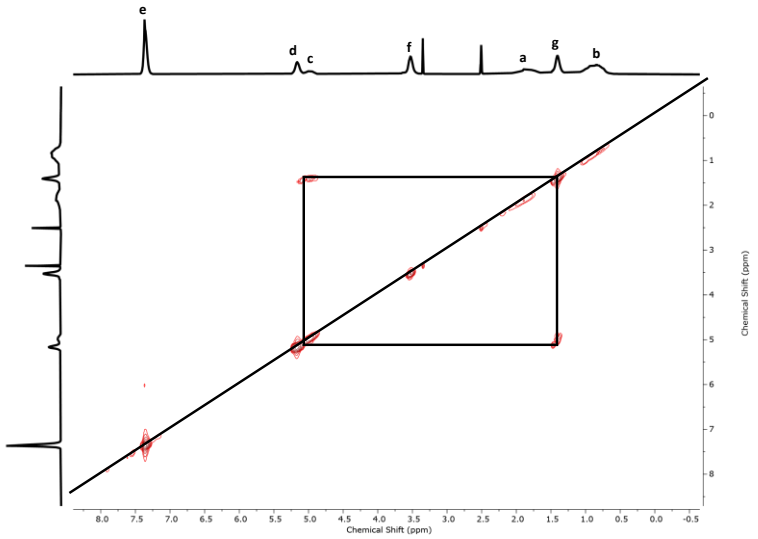

Figure S34: COSY spectrum (400 MHz, DMSO-d_6) of P(MA-Lac-Bn-co-MMA) copolymer.

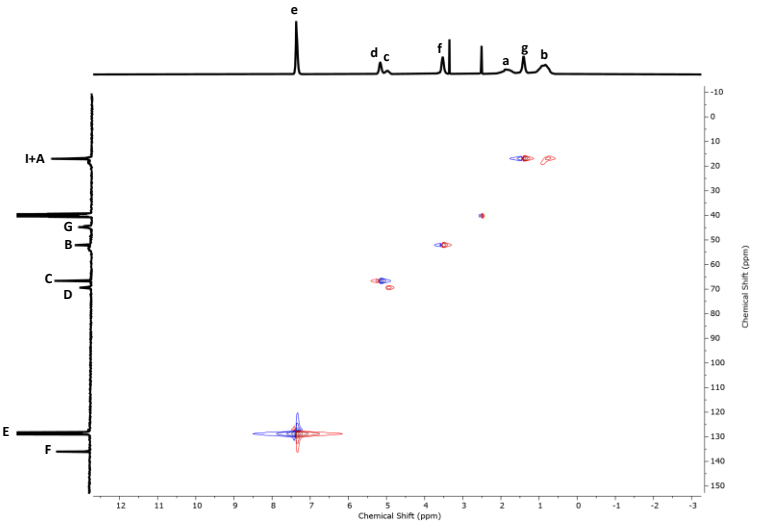

Figure S35: HSQC spectrum (400 MHz, DMSO-d_6) of P(MA-Gly-Bn-co-MMA) copolymer.

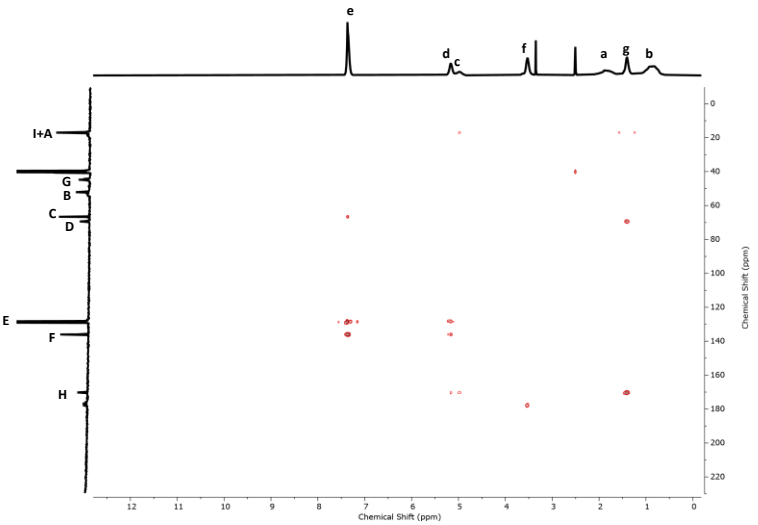

Figure S36: HMBC spectrum (400 MHz, DMSO-d_6) of P(MA-Gly-Bn-co-MMA) copolymer.

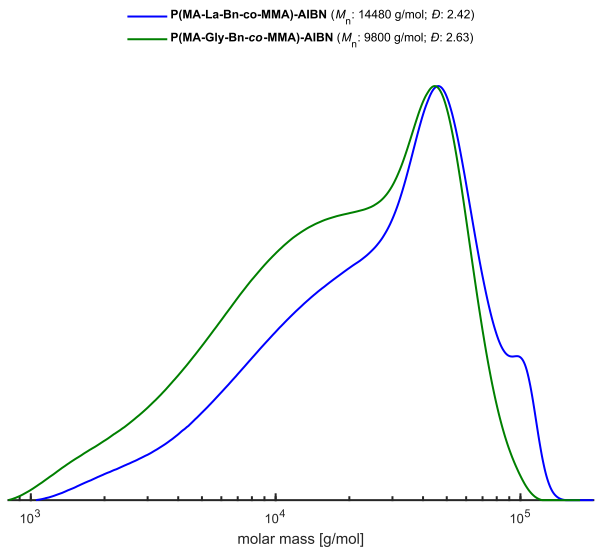

Figure S37: SEC curves (DMF, PEG calibration) for P(MA-XBn-*co*-MMA) in a ratio 1:1 in a concentration of 2.5 mol/L and 4 wt% AIBN as initiator.

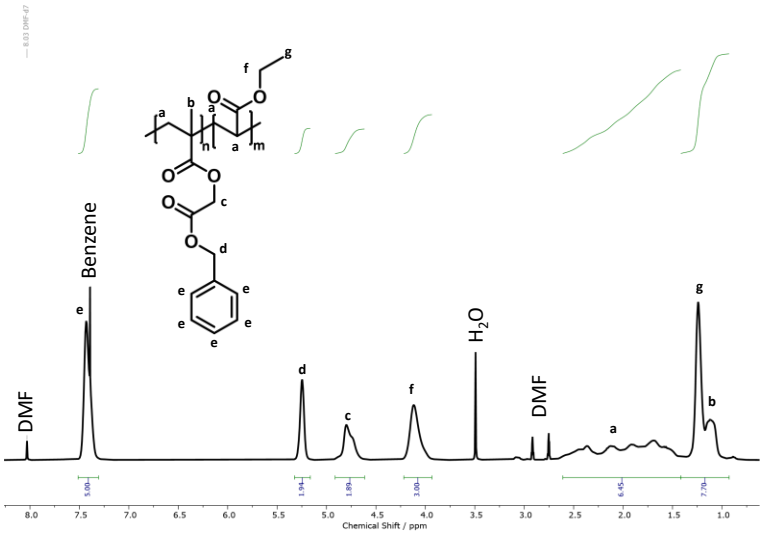

Figure S38: ^{1}H-NMR spectrum (400 MHz, DMF-d_7) of P(MA-Gly-Bn-*co*-EA) copolymer.

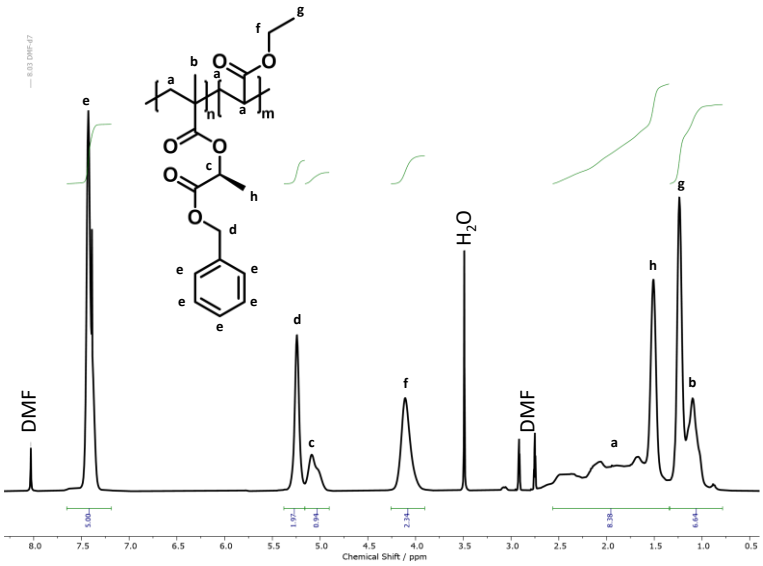

Figure S39: ^{1}H-NMR spectrum (400 MHz, DMF-d_7) of P(MA-Lac-Bn-*co*-EA) copolymer.

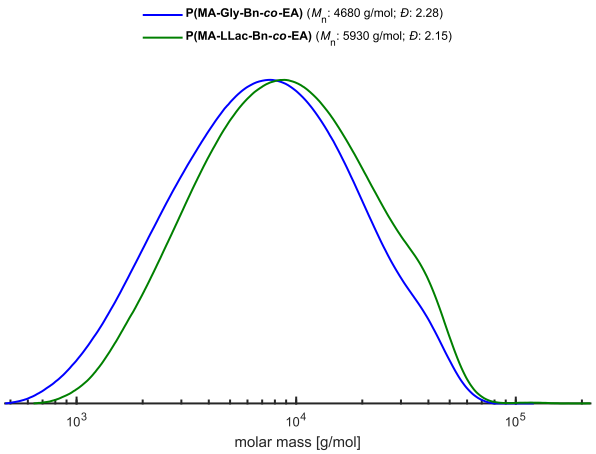

Figure S40: SEC curves (DMF, PEG calibration) for P(MA-X-Bn-*co*-EA) synthesized with 5 wt% DMPA at a concentration of 1 mol/L.

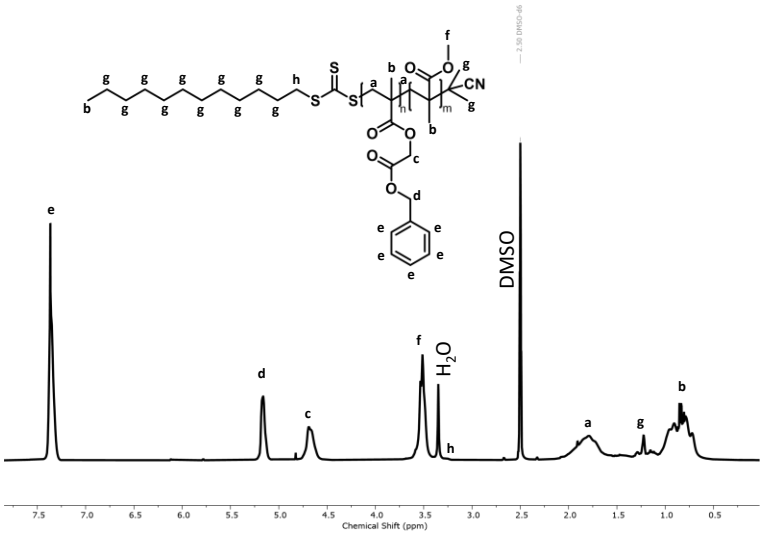

Figure S41: ^{1}H-NMR spectrum (400 MHz, DMSO-d_6) of P(MA-Gly-Bn-*co*-MMA) copolymers using RAFT polymerisation.

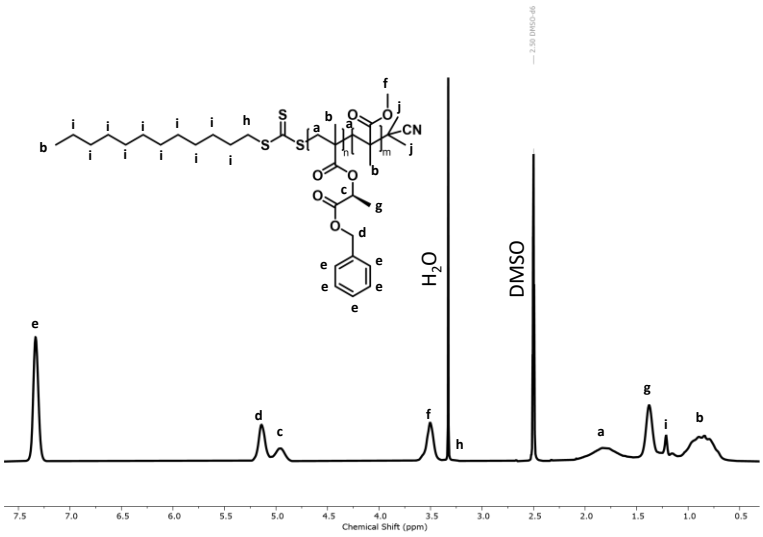

Figure S42: ^{1}H-NMR spectrum (400 MHz, DMSO-d_6) of P(MA-Lac-Bn-*co*-MMA) copolymers using RAFT polymerisation.

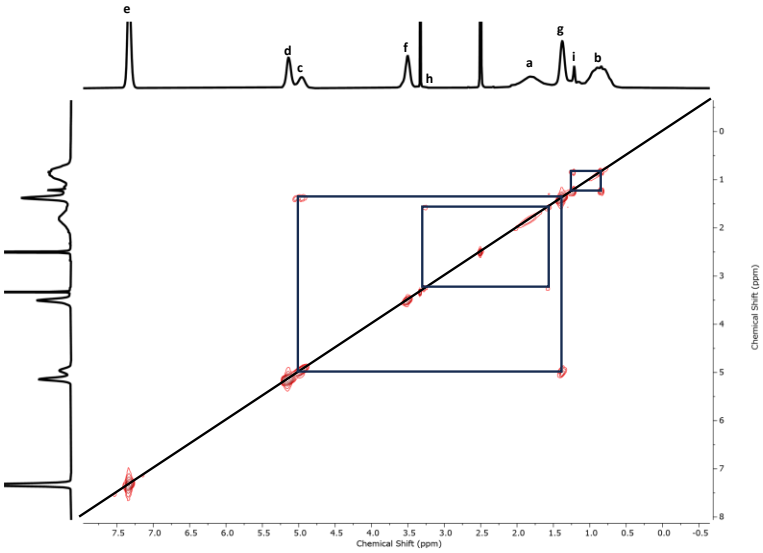

Figure S43: COSY spectrum (400 MHz, DMSO-d_6) of P(MA-Lac-Bn-*co*-MMA) copolymers using RAFT polymerisation.

Table S5: Characterization of the MMA copolymers using RAFT polymerisation.

Copolymer	M_n^{target} / (g/mol)	Ratio[a]	M_n[a] / (g/mol)	M_n[b] / (g/mol)	Đ[b]
P(MA-Gly-Bn$_{0.5}$-*co*-MMA$_{0.5}$)	10000	1:0.75	11100	5720	1.35
P(MA-Gly-Bn$_{0.5}$-*co*-MMA$_{0.5}$)	20000	1:0.92	26700	9610	1.49
P(MA-Lac-Bn$_{0.5}$-*co*-MMA$_{0.5}$)	10000	1:0.75	8700	4910	1.28
P(MA-Lac-Bn$_{0.5}$-*co*-MMA$_{0.5}$)	20000	1:0.95	19300	9490	1.44

[a] Determined by ^{1}H-NMR (400 MHz, DMSO-d_6). [b] Determined by SEC (eluent: DMF, calibration: PEG).

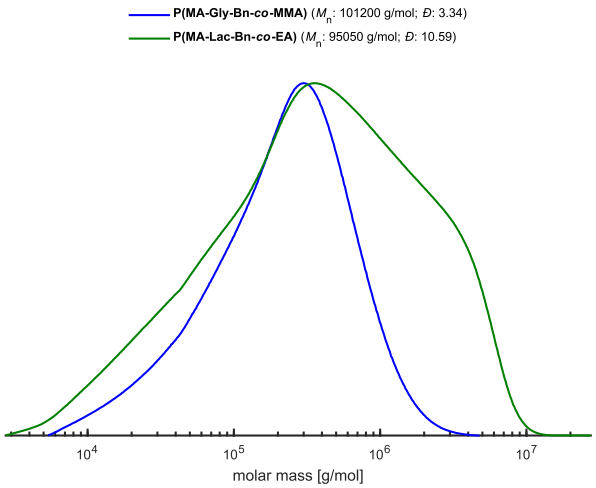

Figure S44: SEC curves (THF, PEG calibration) for P(MA-Gly-Bn-*co*-MMA) and P(MA-Lac-Bn-*co*-EA) synthesized by postpolymerization modification of Eudragit l-100 and l-100-55.

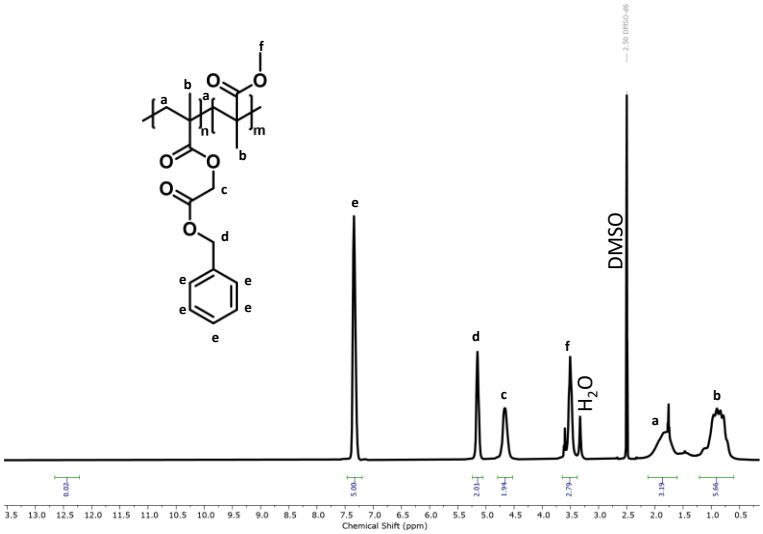

Figure S45: ^{1}H-NMR spectrum (400 MHz, DMSO-d_6) of P(MA-Gly-Bn-co-MMA) copolymer, synthesized by a postpolymerization modification.

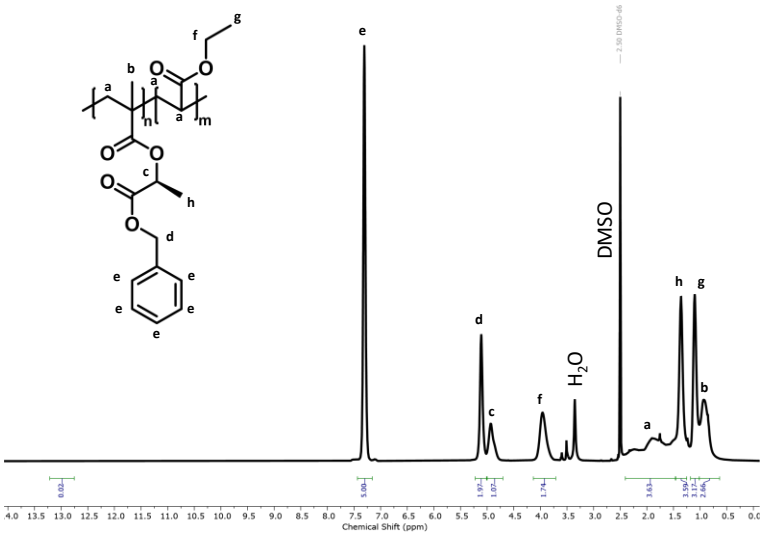

Figure S46: ^{1}H-NMR spectrum (400 MHz, DMSO-d_6) of P(MA-Lac-Bn-co-MMA) copolymer, synthesized by a postpolymerization modification.

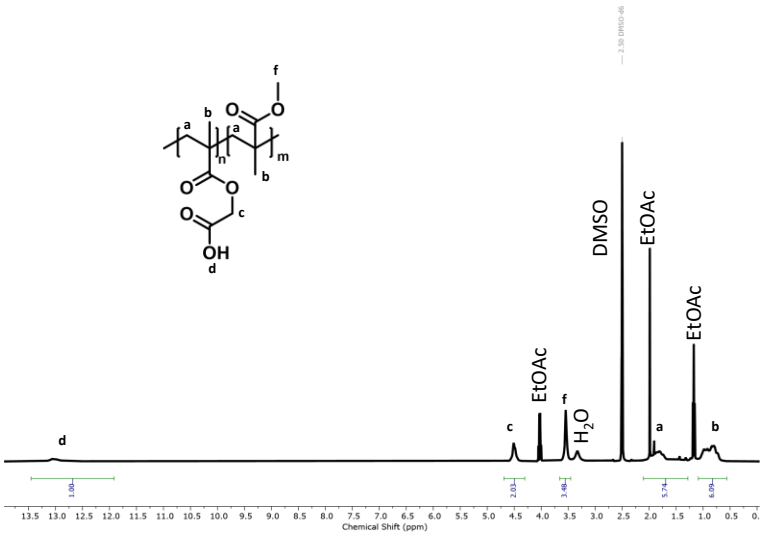

Figure S47: ^{1}H-NMR spectrum (400 MHz, DMSO-d_6) of deprotected P(MA-Gly-*co*-MMA) copolymer.

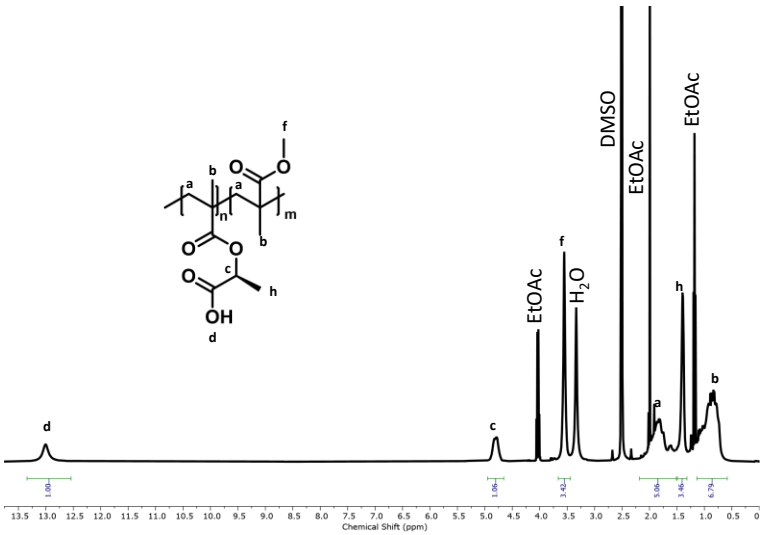

Figure S48: ^{1}H-NMR spectrum (400 MHz, DMSO-d_6) of deprotected P(MA-Lac-*co*-MMA) copolymer.

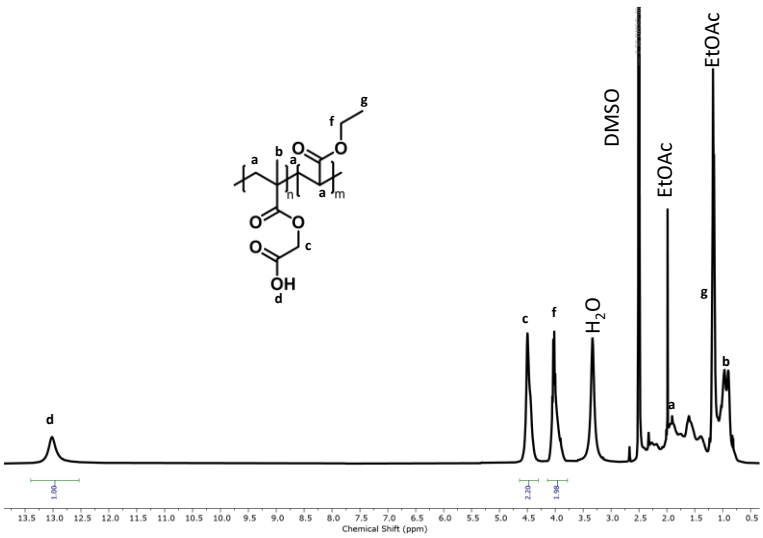

Figure S49: ^{1}H-NMR spectrum (400 MHz, DMSO-d_6) of deprotected P(MA-Gly-*co*-EA) copolymer.

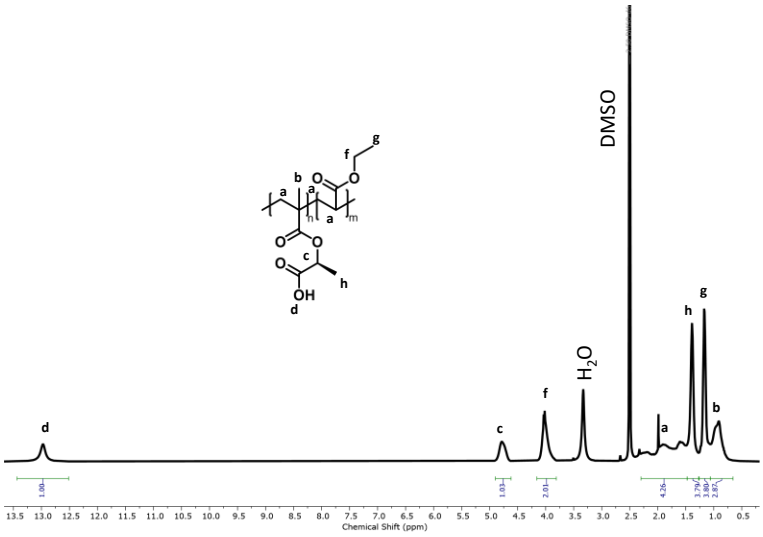

Figure S50: ^{1}H-NMR spectrum (400 MHz, DMSO-d_6) of deprotected P(MA-Lac-*co*-EA) copolymer.

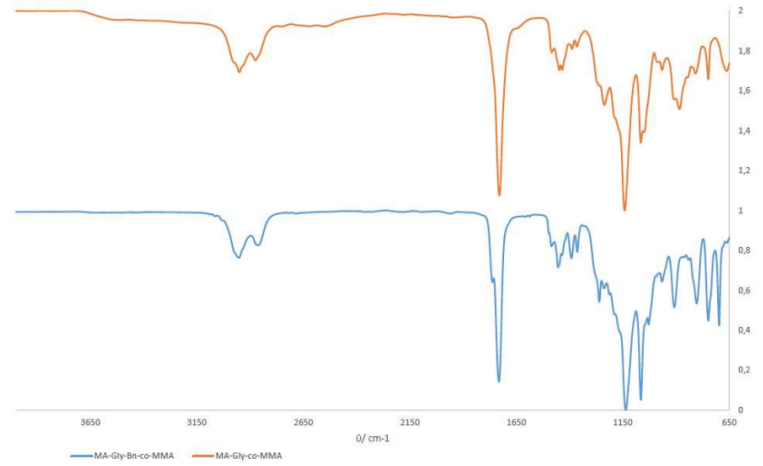

Figure S51: IR spectrum of P(MA-Gly-Bn-*co*-MMA) copolymer (bottom) and P(MA-Gly-*co*-MMA) copolymer (top).

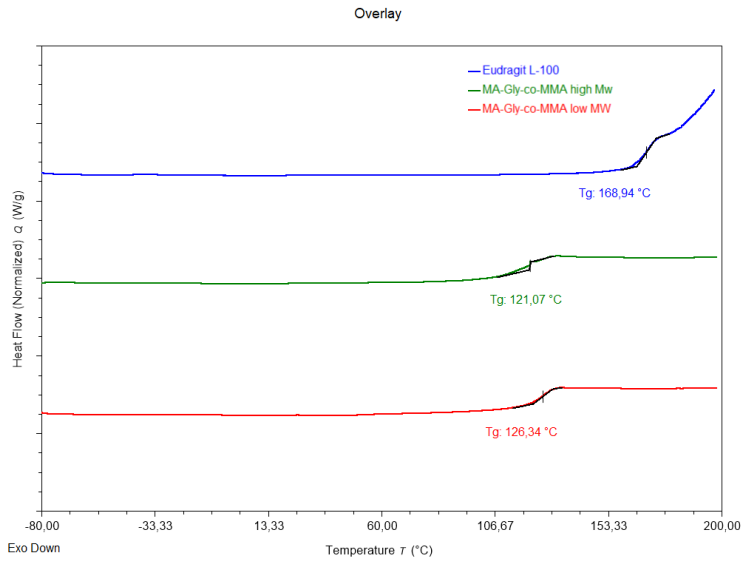

Figure S52: DSC data of P(MA-Gly-*co*-MMA) synthesized by post polymerization and monomer route.

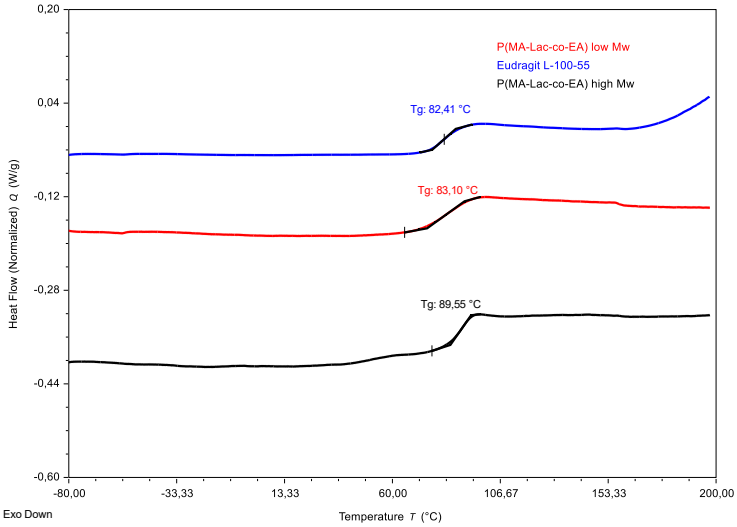

Figure S53: DSC data of P(MA-Lac-*co*-EA) synthesized by post polymerization and monomer route.

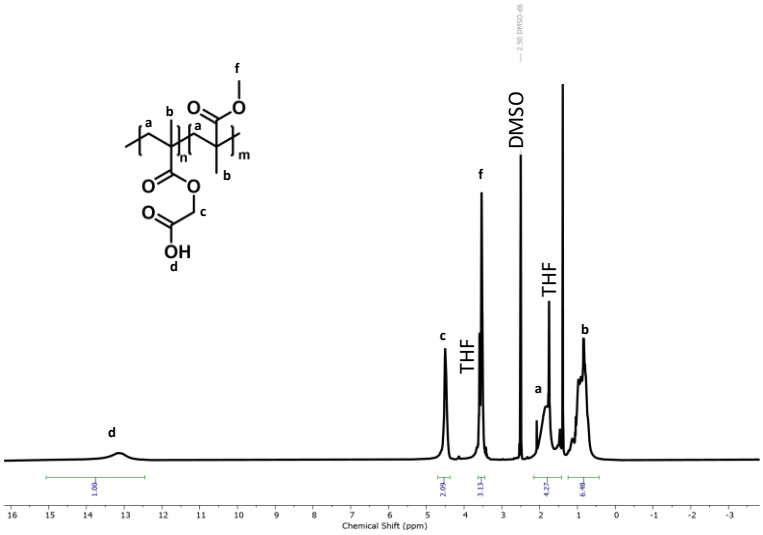

Figure S54: ^{1}H-NMR spectrum (400 MHz, DMSO-d_6) of with TFA deprotected P(MA-Gly-*co*-MMA) copolymer.

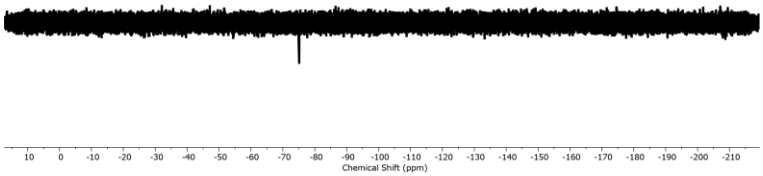

Figure S55: ^{19}F-NMR spectrum (400 MHz, DMSO-d_6) of with TFA deprotected P(MA-Gly-*co*-MMA) copolymer.

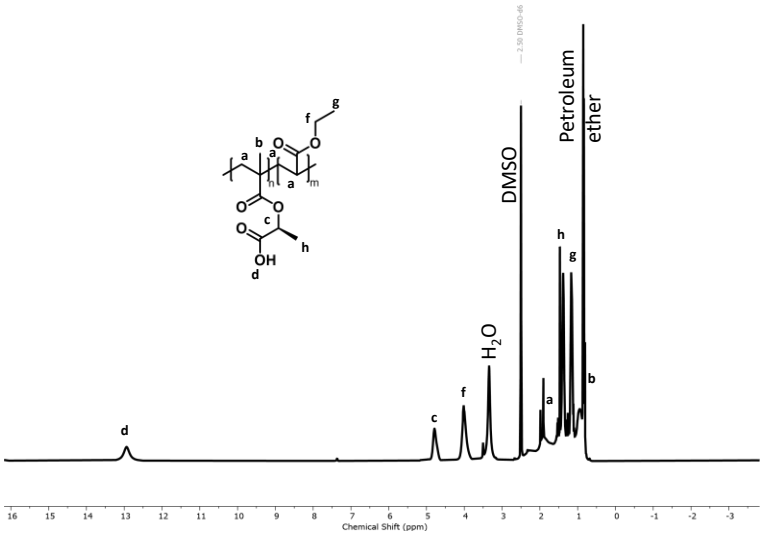

Figure S56: ^{1}H-NMR spectrum (400 MHz, DMSO-d_6) of with TFA deprotected P(MA-Lac-*co*-EA) copolymer.

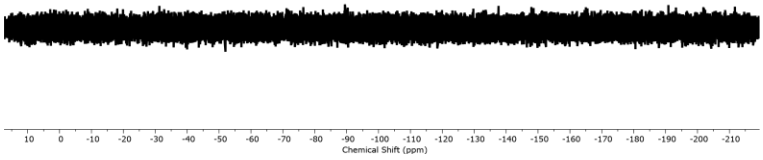

Figure S57: ^{19}F-NMR spectrum (400 MHz, DMSO-d_6) of with TFA deprotected P(MA-Lac-*co*-EA) copolymer.

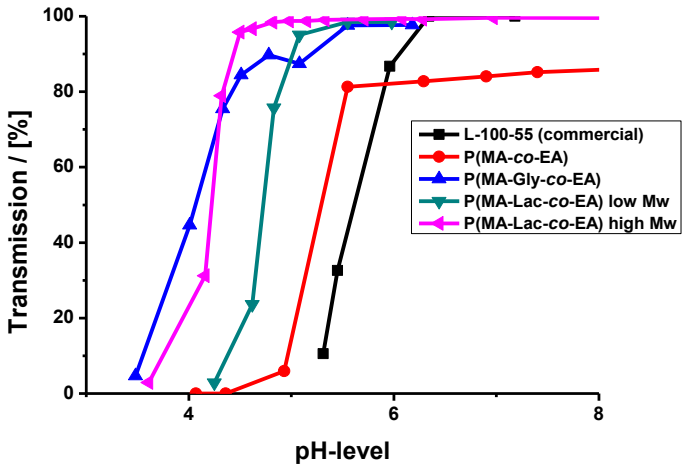

Figure S58: pH dependent transmission experiment for Eudragit® L-100-55 type copolymers at 37°C.

References:

[1] M. A. Tehfe, S. Schweizer, A. C. Chany, C. Ysacco, J. L. Clément, D. Gigmes, F. Morlet-Savary, J. P. Fouassier, M. Neuburger, T. Tschamber, N. Blanchard, J. Lalevée, *Chemistry - A European Journal* **2014**, *20*, 5054–5063.

[2] J. Al-Gousous, G. L. Amidon, P. Langguth, *Mol Pharm* **2016**, *13*, 1927–1936.

Chapter 5

Enteric drug coatings: Improving drug release and acid resistance by the synthesis and polymerization of novel mandelic and malic acid monomers.

Dominik A. H. Fuchs,[a] [redacted]

[g] Institute of Organic Chemistry, Johannes Gutenberg-University Mainz, Duesbergweg 10-14, 55128 Mainz, Germany
[h] Institute of Pharmacy, Department Pharmaceutical Technology and Biopharmacy, Johannes Gutenberg-University Mainz, Staudinger Weg 5, 55128 Mainz, Germany

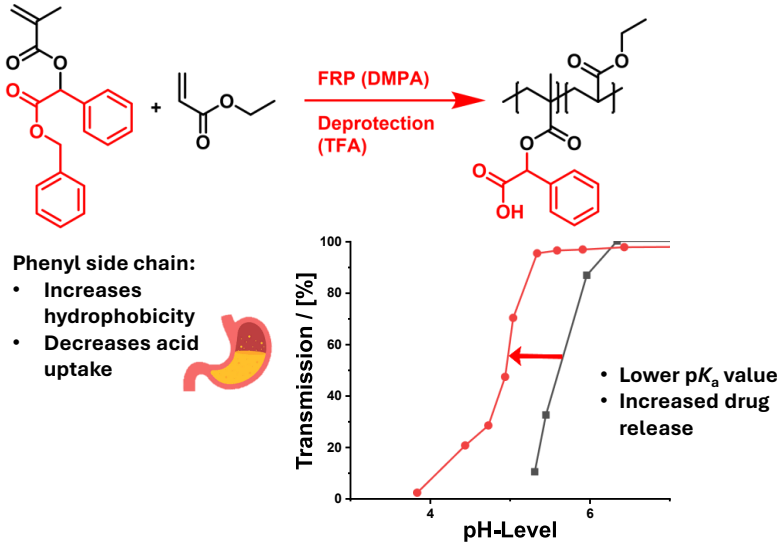

Abstract:

Drug coatings serve multiple purposes, with the primary goals being the protection of the drug from the acidic conditions of the stomach and the protection of the stomach from potentially irritating drug compounds. However, conventional enteric coatings often exhibit a too slow dissolution after passing the stomach, to target drug release in the duodenum.[1,2] To address this issue we presented in our previous paper a synthetic strategy to adjust the pH-responsiveness of these copolymers and increase the drug release. This was achieved by modifying the pK_a value of the copolymer (P(MA-*co*-X), X = MMA or EA) by esterification with an α-hydroxy carboxylic acid, see Fig. 1. Using this strategy, in which the polymer backbone is retained, we also hope to preserve the material properties and non-toxicity of the copolymers. Since both earlier modifications with glycolic and lactic acid were successful and improved the drug release we were keen to investigate two additional α-hydroxy carboxylic acids, mandelic and malic acid. Mandelic acid was specifically chosen because of its phenyl side chain, which is expected to increase the hydrophobicity of the resulting copolymer and reduce acid uptake in the stomach. Malic acid was chosen to further enhance dissolution by introducing a second acid functionality with a slightly higher pK_{a2} value. These monomers (MA-Mand-Bn and MA-Mal-Bn) were copolymerized with methyl methacrylate (MMA) or ethyl acrylate (EA) via free radical polymerization to obtain copolymers with a molar mass of < 10 kg/mol. Trifluoracetic acid (TFA) was used to remove the benzylic protection units to obtain pH-responsive copolymers. This pH-responsiveness was evaluated using cloud point titration and all synthesized copolymers showed solubility at lower pH levels than commercial Eudragit® polymers. Further acid resistance and drug release profiles were investigated using coated paracetamol capsules. Among the tested polymers, only P(MA-Mand-*co*-EA) was stable under the acidic conditions. As predicted, this copolymer also showed a reduced acid uptake, attributed to the increased hydrophobicity, as well as an improved drug release performance, making it a promising candidate for further investigations. This work presents an advancement over our previously studied glycol and lactic modified coatings by addressing the challenge of increased acid uptake while further enhancing the drug release.

Introduction

Drugs can be administered through various routes, with oral delivery being by far the most common, accounting for over 60% of all marketed pharmaceuticals. This popularity is largely due to its convenience: oral administration typically requires no medical personnel, minimal equipment (often just a small cup of water) and are packed in the right doses.[3] Additionally, tablets are economically favorable due to their scalable, cost-effective production, as well as their efficient storage and transportation.[3–5] In contrast, intravenously administered drugs are often stored in plastic containers that may leach potentially harmful chemicals into the drug solution, a particular concerning issue for chronic diseases.[6,7] Tablets, therefore present a safer an less invasive alternative, eliminating the need for needles.

However, oral drug delivery presents its own challenges. Unlike intravenous administration, orally delivered drugs must pass through the digestive system to be absorbed into the bloodstream. This means they must survive the harsh, acidic environment of the stomach. Some drugs, such as pancreatin,[8] are acid labile and can be degraded before reaching the intestines, while others may irritate the stomach, leading to unwanted side effects. To address these issues, protective drug coatings have been developed. These coatings shield the active drug from gastric fluids and dissolves only once the drug reaches the more neutral pH environment of the intestines. For this purpose pH-responsive polymers are utilized and one of the most common is poly(methacrylic-acid-*co*-methyl-methacrylate) (P(MA-*co*-MMA)) also known as Eudragit® L-100 (Evonik AG). This polymer is insoluble under acidic conditions but dissolves at pH above 6, making it suitable for targeting drug release in the small intestine.[9] The functionality of this polymer is closely related to the pK_a value of methacrylic acid of 4.65,[10] which ensures its insolubility in the stomach. The pH of the stomach is between 1-3 in a fasted state but can increase up to 6 if the patient is fed.[11,12]

Eudragit® coatings are widely used and have become a standard in enteric drug coatings. In addition to Eudragit® L-100, Eudragit® L-100-55, a copolymer based on MA and ethyl acrylate (EA) dissolves at pH 5.5, is commonly used to target drug release in the small intestines, specifically the duodenum. Other Eudragit® variants serve different purposes:

Eudragit® E100 enables immediate release, Eudragit® RS100 provides sustained release and Eudragit® S100 is designed for colon-specific release at a pH of 7.[9]

Despite their widespread use, studies have questioned the effectiveness of Eudragit® L-100-55 coatings to achieve a fast enough drug release to actually target the duodenum.[1,2] Especially if you consider that most *in vitro* experiments overestimate the drug release compared to *in vivo* conditions, due to exaggerated assumptions, such as the buffer capacity as well as the volume of liquid in the intestines.[13–15] Therefore, under *in vivo* conditions is the pH level in direct contact with the tablet significantly lower than that of the intestinal fluid. In both studies, more than one hour was required for the complete dissolution at a pH of 6.5, which is problematic given the fact that the normal transit time in the small intestines is only 1-3 hours. This is particularly concerning for iron-based drugs, which are primarily absorbed in the duodenum, the first and shortest segment of the small intestines.[16,17] Additionally, enteric drug coatings seem to decrease the bioavailability of acetylsalicylic acid, commonly used for antiplatelet therapy, due to the prolonged solvation and absorption of the enteric-coated formulation.[18,19] One way to compensate for the slow dissolution is to increase the drug loading in the tablets, raising the local concentration of the drug over the whole intestine. However, this approach increases the risk of side effects and is economically unfavored.[20]

To address this issue, we introduced in the previous chapter structural modifications to Eudragit® L-100 and L-100-55 using α-hydroxy acids to lower the copolymers pK_a value. This was successfully achieved with glycolic and lactic acid and is attributed to the electron withdrawing effect (-I effect) of the ester group, as illustrated in Fig. 1.

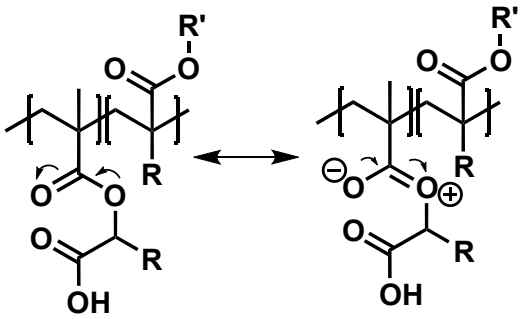

-I Effect of the proposed structures

Figure 1: Resonance structures of modified poly(methacrylate)/poly(acrylate) copolymers and the resulting -I effect.

These modifications resulted in a faster drug release profile and increased acid uptake. Although the glycol-modified copolymer still exhibited less than 10 wt% acidic uptake, which is correlated to no drug release or degradation in the acid phase, it still increased about 2 % compared to the commercial Eudragit®.[21] To reduce this acid uptake, but still maintain a faster dissolution it was hypothesized that increasing the hydrophobicity of the copolymer would also reduce the acid uptake. Therefore, the α-hydroxy acid mandelic acid was chosen due to its phenyl side chain. Additionally, to further enhance the drug release, malic acid was introduced to explore the effects of a second acid functionality with a different pK_a value on the dissolution behavior.

Experimental Section

Materials, instrumentation, general experimental procedures as well as characterizations are shown in the Supporting Information.

Results and discussion:

In the previous chapter, we introduced lactic- and glycolic acid modified methacrylic acid (MA) as novel monomers for the synthesis of enteric drug coatings, which are summarized as α-hydroxy carboxylic acid modified MA structures. Copolymerizations with methyl methacrylate (MMA) or ethyl acrylate (EA) lead to new copolymers suitable for enteric drug coatings. Compared to Eudragit® polymers, these new copolymers exhibited accelerated drug release profiles, attributed to their reduced pK_a values. However, this benefit was accompanied by an increased acid uptake, particularly pronounced in the glycol acid modification, which is undesirable for enteric coatings. To address this problem and further enhance the drug release, we explored more structurally complex α-hydroxy carboxylic acids, mandelic and malic acid. Both acids were specifically chosen to investigate different effects. Mandelic acid was chosen for its phenyl side chain, which we assume increases hydrophobicity and therefore reduces the acid uptake of the copolymer. And malic acid to investigate the influence of a second acid functionality with a higher pK_a value on the dissolution of the copolymer. Both acids are non-toxic and biocompatible: malic acid is naturally occurring in the citric acid cycle and plays a role in the malate-aspartate shuttle.[22,23] It is also found in fruits like apples and is

widely used as a food additive (E296) for its acidulant and taste enhancer properties.[24] Beyond food applications it is also used in personal care products,[25] pharmaceuticals,[26] semiconductor fabrication[27] as well as in animal feed additives[28] and was already used in a different drug coating.[29] Mandelic acid, on the other hand, is known for its antibacterial properties and is used in treating urinary tract infections.[30,31] Therefore, potential acid cleavages of the ester bonds will not be an issue, since this would result in the formation of already FDA approved Eudragit® structures and α-hydroxy carboxylic acids, which are approved for medical and nutritional applications. We also expect that incorporation of mandelic and malic acid will further lower the pK_a value of the copolymer and thus further enhance the dissolution rate. Notably, mandelic acid (pK_a = 3.37) and malic acid (pK_{a1} = 3.24; pK_{a2} = 4.68) exhibit stronger acidity than glycolic (pK_a = 3.83) and lactic acid (pK_a = 3.90).[30,32]

The synthesis of the new monomers follows the strategy previously developed for glycolic and lactic acid-modified methacrylic acid, as illustrated in Fig. 2.[33] In the first step it is crucial to protect the acid functionality of the α-hydroxy carboxylic acids to prevent unwanted oligomerization and side reactions. As in the previous chapter 4, benzyl groups are used as protective groups since they have proven themselves due to their acid and basic stability, compatibility with the reaction conditions and easy cleavage via hydrogenation or hydrolysis.[34–36] For the protection were stoichiometric amounts of the sterically hindered base diazabicycloundecene (DBU) used to deprotonate the α-hydroxy carboxylic acid, which then undergoes a S_N-reaction with benzyl bromide. After extraction and distillation, the protected esters Mandelic-Bn (Mand-Bn) and Malic-Bn (Mal-Bn) were obtained in yields exceeding 80%. Mand-Bn was isolated as colorless crystals with a melting point of 92°C and Mal-Bn as a pale yellow liquid with a boiling point of 220°C at a pressure of 10^{-3} mbar. Both monomers were characterized using ^{1}H-NMR spectroscopy, which can be found in the Supporting Information (Fig. S1-2). Notably, for Mal-Bn complete protection was achieved without any mono benzylated product.

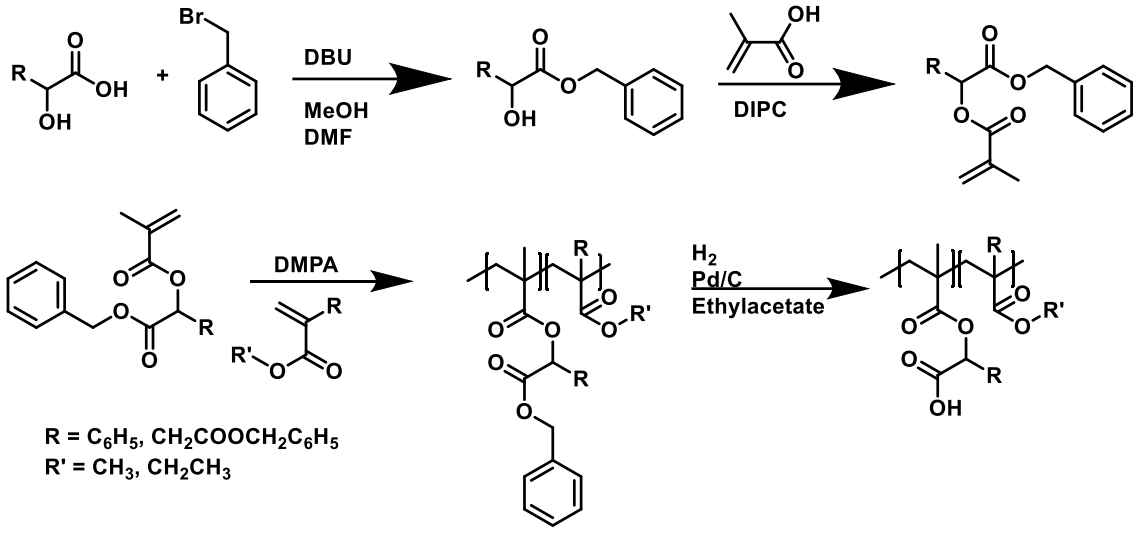

Figure 2: Synthesis overview of new monomers and copolymerizations for enteric drug coatings based on mandelic and malic acid.

After the successful protection of all acid functionalities the next step was to introduce a polymerizable double bond into the monomer. Therefore, the α-hydroxy carboxylic esters were coupled with methacrylic acid (MA) in a Steglich esterification. This was carried out using *N,N'*-diisopropylcarbodiimide (DIPC) as the coupling agent and *N.N*-dimethylpyridin-4-amine (DMAP) as the catalyst, similar to our previous synthesis of MA-Gly-Bn and MA-Lac-Bn. After purification via column chromatography the targeted monomers MA-Mand-Bn and MA-Mal-Bn were obtained with yields of 46% and 33% respectively.[37] While the esterification of Mand-Bn proceeded quantitatively, some unreacted Mal-Bn was recovered during the purification and can be reused, to increase the yield. Both monomers were analyzed via ^{1}H-NMR in Fig. 3 and with various other NMR techniques in Fig. S3-12.

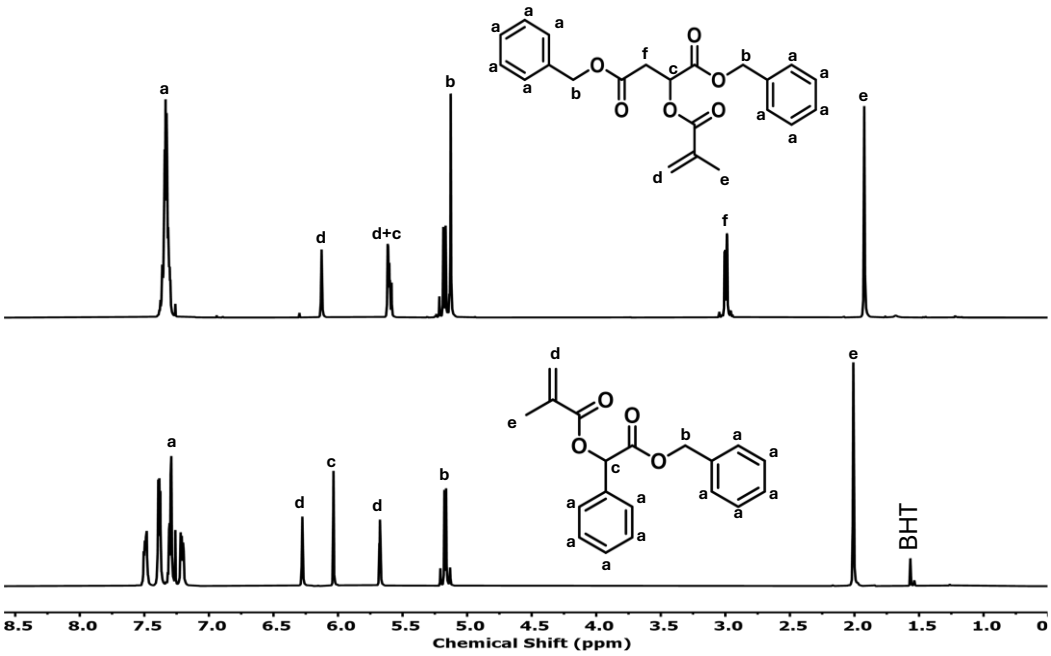

Figure 3: Stacked ^{1}H-NMR spectra (400 MHz, $CDCl_3$) of benzyl protected malic acid modified MA (MA-Mal-Bn) on the top and benzyl protected mandelic acid modified MA (MA-Mand-Bn) on the bottom.

Homopolymerization

As an initial proof of concept, the newly synthesized monomers MA-Mal-Bn and MA-Mand-Bn were homopolymerized via radical polymerization. The homopolymers were characterized using SEC and ^{1}H-NMR spectroscopy, as shown in Fig. S13-15. Since the goal was to test if polymerizations are possible, reaction conditions were selected to favor polymerization rather than optimizing.

Since in previous studies the thermal initiator AIBN has proven to obtain higher yields compared to the photo initiator DMPA, AIBN was chosen as initiator. Benzene was used as solvent due to its low radical transfer rate, good solubility for both monomers and polymers and its easy removal.[38] Additionally, this solvent has proven its compatibility with the previous investigated MA-Lac-Bn and MA-Gly-Bn monomers in the previous chapter.

This study represents the first successful synthesis and characterization of the homopolymers P(MA-Mand-Bn) and P(MA-Mal-Bn). SEC measurements were performed with DMF as eluent and a PMMA calibration. However, the SEC columns had an insufficient resolution limit at around 300 kg/mol, which the homopolymers exceeded. Therefore the reported molecular weights, 183 kg/mol for P(MA-Mal-Bn) and 52 kg/mol for

P(MA-Mand-Bn) are likely underestimated and dispersities are narrower than expected. The high molecular weights are attributed to the Trommsdorff effect, where increased viscosity reduces termination rates and promotes chain propagation.[39]

Copolymerization

For the synthesis of new improved drug coatings, methyl methacrylate (MMA) and ethyl acrylate (EA) were chosen as comonomers due to their established use in enteric drug coatings like Eudragit® and were copolymerized with MA-Mand-Bn and MA-Mal-Bn in a free radical polymerization. This technique was chosen for its simplicity, scalability and minimal handling requirements. Additionally, narrow dispersities and precise molar mass control are not required for enteric drug coatings and the focus of this study lies on evaluating the pH-responsive behavior of the new materials. However, for stable film formation, it is generally desirable to achieve molar masses at least twice the entanglement molecular weight.[40]

For the copolymerizations was DMPA used, since photoinitiators generate radicals in a more linear and controlled fashion, in contrast to thermal initiators like AIBN, which generate radicals exponentially and lead to non-monomodal molar mass distributions.[41,42] Polymerization conditions were optimized in regard to yields, monomodal weight distributions and low dispersities. Achieving a high molar mass, often associated with better film building properties, was considered less critical, as the intrinsic properties of the copolymers, such as solubility and pH-responsiveness, were the focus of this study. Therefore, both monomers were copolymerized with MMA with different initiator and monomer concentrations. SEC results for the copolymers are presented in Fig. S16-19 and Tables S1-4. Both monomers showed similar copolymerization behavior with MMA, yielding polymers with molar masses between 3.5-5.4 kg/mol and a dispersity between 1.63-1.94. All SEC curves were monomodal and calibrated using a PMMA standard. Copolymerizations were carried out in benzene as solvent, as in the homopolymerizations, to suppress a possible Trommsdorff effect.

As expected from free radical polymerizations in which the steady state-equation applies, increasing the initiator concentration leads to a decrease in molar mass, while an

increase in monomer concentration leads to higher molar mass. These trends were consistently observed across all copolymerizations.

Optimal reaction conditions were identified for both MA-Mand-Bn and MA-Mal-Bn: 1 mol/L total monomer concentration and 5 wt% DMPA. Under these conditions polymers with ≥ 70% yields, molar masses over 4 kg/mol and monomodal SEC curves were obtained. For further tests, which require larger polymer quantities and higher molar masses, alternative polymerization methods such as emulsion polymerization or post-polymerization modifications, analog to those discussed in the previous chapter, can be utilized.

MMA copolymers:

Both monomers MA-Mand-Bn and MA-Mal-Bn were copolymerized in a 1:1 (molar) ratio with MMA to obtain copolymers similar to Eudragit® L-100. In addition, MA-Mal-Bn was copolymerized with MMA in a 1:2 (molar) ratio similar to Eudragit® S-100. Unlike the previously investigated modified methacrylic acids, MA-Mal-Bn introduces two acid functionalities per repeating unit, therefore this ratio was also tested to maintain a 1:1 ratio of acid functionality to comonomer. This was done, because it was assumed that in the 2:1 (functionality) ratio the copolymer could not be stable under the acidic conditions of the stomach.

All synthesized copolymers were analyzed via ^{1}H-, ^{13}C- and various 2D-NMR spectroscopy, see Fig. S20-30. No residual monomer signals were detected. $CDCl_3$ was used as the NMR solvent instead of DMSO to prevent the overlap between the methyl signal of MMA and the water peak at 3.33 ppm. Therefore, the monomer incorporation was calculated using the protected copolymers, since the unprotected were no longer soluble in $CDCl_3$.

Monomer incorporation is calculated for mandelic acid by comparing the benzylic proton signal (5.34-4.86 ppm, divided by 2) to that of the MMA ester methyl group (3.64-3.34 ppm, divided by 3). And for malic acid based copolymers were the benzylic proton signals (5.20-4.75 ppm, divided by 4) compared to the MMA ester methyl group signal (3.78-3.28 ppm, divided by 3). Table 1 summarizes the incorporation ratios, molar masses and

dispersities for all synthesized copolymers. The corresponding SEC curves can be seen in Fig. S42 + 43.

Table 1: Characterization of mandelic and malic acid based copolymers, synthesized using 5 wt% DMPA and 1 mol/L monomer concentration.

Copolymer	Ratio[a]	M_n[b] / (g/mol)	$Đ$[b]
P(MA-Mand-$Bn_{0.5}$-*co*-$MMA_{0.5}$)	1:0.97	4880	2.17
P(MA-Mal-$Bn_{0.5}$-*co*-$MMA_{0.5}$)	1:0.96	4410	2.93
P(MA-Mal-$Bn_{0.33}$-*co*-$MMA_{0.66}$)	1:1.75	3980	1.89
P(MA-Mand-$Bn_{0.5}$-*co*-$EA_{0.5}$)	1:0.85	8010	2.79
P(MA-Mal-$Bn_{0.5}$-*co*-$EA_{0.5}$)	1:0.92	8750	4.42
P(MA-Mal-$Bn_{0.33}$-*co*-$EA_{0.66}$)	1:1.72	8900	2.21

[a] Determined by ^{1}H-NMR (400 MHz, $CDCl_3$) spectroscopy, MA:X. [b] Determined by SEC (DMF, Calibration PMMA)

All MMA based copolymers were obtained with yields ≥ 80%, molar masses between 4.0-4.9 kg/mol and dispersities between 1.89-2.93. For all copolymers was the MMA content slightly lower than the targeted feed ratio. This can be explained by several reasons: only small amounts (< 1 mL) were used, the comonomer could be partially removed during the freeze-pump thaw cycles or different reactivity ratios promote the modified MA incorporation.

Interestingly, the observed molar masses of MMA-based copolymers were significantly lower than those of the EA-based copolymers, nearly by a factor of two. This discrepancy is likely due to incomplete removal of the stabilizer 4-methoxyphenol (MEHQ), which is present at higher concentrations in MMA compare to EA. Residual MEHQ acts as a radical scavenger, limiting chain growth and lowers molar mass.

EA copolymers:

In addition to MMA, both MA-Mand-Bn and MA-Mal-Bn were copolymerized with EA under the same conditions. These copolymers were synthesized as structural analogs to Eudragit® L-100-55. ^{1}H-, ^{13}C- as well as various 2D-NMR techniques have been used to analyze the copolymer and to calculate the monomer incorporation, see Fig. 4 and Fig. S31-41. No residual monomer signals were detected. The molar incorporation was

calculated using the same equations, as for the MMA-based copolymers, with slight alterations due to the different side chain of ethyl acrylate.

For mandelic acid modified copolymers is the benzylic proton signal (5.20-4.75 ppm, divided by 2) compared to the methylene signal of the ethyl ester (4.30-3.75 ppm, divided by 2). For malic acid modified copolymers is the calculation similar, only the benzylic signal is divided by four to attribute the two protection units per molecule. The molar incorporation ratio is shown in Table 1, as well as the SEC results. Similar to the MMA-based copolymers, the EA content is in all cases consistently lower than the targeted feed ratio.

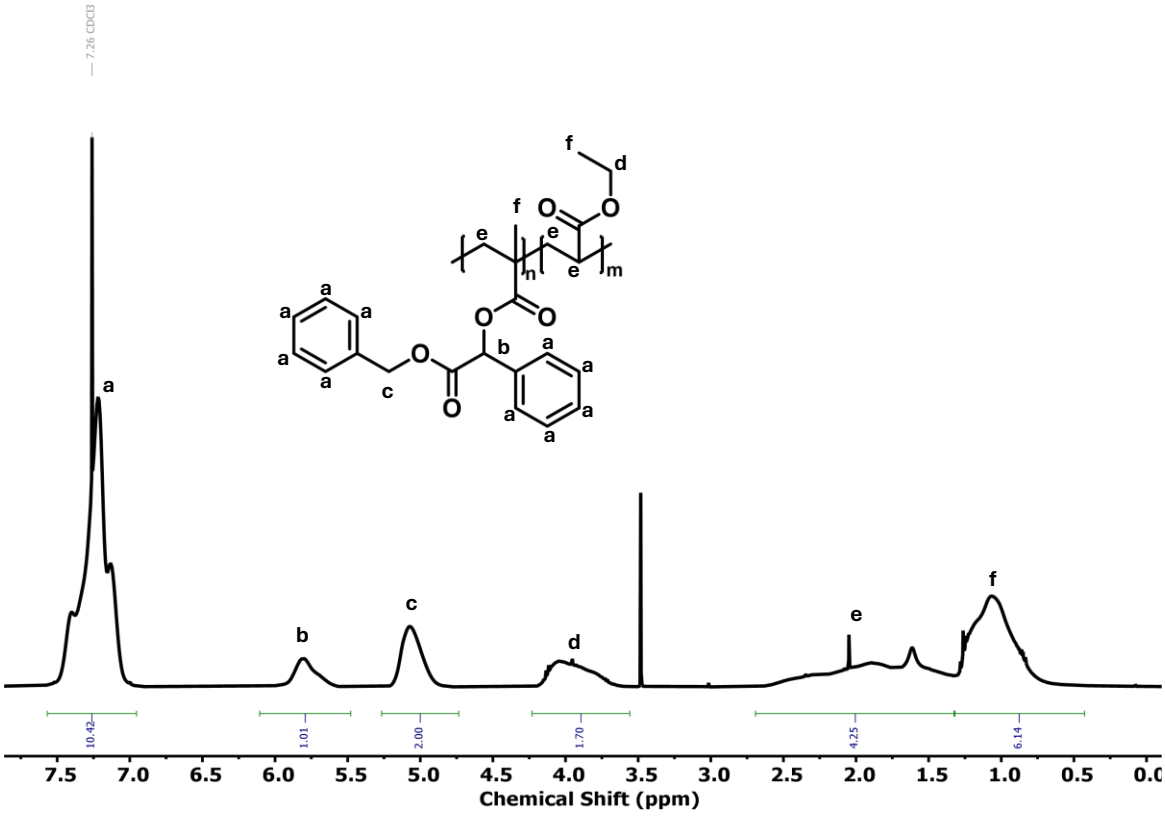

Figure 4: ^{1}H-NMR (400 MHz, $CDCl_3$) spectrum of P(MA-Mand-Bn-*co*-EA).

Molar masses and dispersities of the new copolymers were investigated using SEC (DMF, PMMA calibration), the mass distributions can be found in Fig. S42 + 43. Molar masses range from 8.1-8.9 kg/mol with dispersities between 2.21-4.42. Despite being synthesized under identical conditions to their MMA counterparts, the EA-based copolymers exhibit significantly higher molar masses, by a factor of two. This is as earlier stated attributed to the incomplete removal of MEHQ and the different inhibitor content in MMA and EA.

Deprotection

Following the successful synthesis and characterization of all copolymers, the next step was the removal of the benzylic protection groups to obtain the pH-responsive copolymer, while maintaining the other ester bonds. For this purpose different synthetic routes like hydrogenation[35] or hydrolysis by trifluoracetic acid (TFA) have been tested.[36]

A first attempt was made using hydrogenation under conditions previously successful for glycol and lactic acid-based copolymers (40 bar hydrogen pressure, 40 °C, 4 days). However, these conditions were insufficient for a complete deprotection. Increasing the hydrogen pressure to almost 80 bar led to a partial cleavage of the ester bonds in MMA. Therefore hydrogenation was considered unsuitable for these copolymers and it was relayed on hydrolysis with TFA.

Hydrolysis with TFA was performed analog to the previous chapter and the successfully deprotected copolymers were characterized via ^{1}H-, ^{13}C- and different 2D-NMR spectroscopy, see Fig. S44-71. The degree of deprotection was calculated by comparing the phenyl signal (7.60-6.99 ppm, divided by 5) to the methine signal (5.28-4.73, c) of the corresponding α-hydroxyl acid. In contrast to the previously investigated glycolic and lactic acid modified copolymers, complete deprotection was not achieved. Approximately 10-15 mol % of the acid functionalities remained protected, which is attributed to the decreasing solubility of the deprotected copolymers in TFA. Importantly, no side reactions or undesired hydrolysis of other ester bonds was observed, indicating that both the modified MA and the comonomers are stable under these conditions. Attempts to improve the deprotection yield through extended reaction time or modified conditions were unsuccessful. Nevertheless, partial deprotection was seen as acceptable for the scope of this study, which focusses on investigating the intrinsic pH-responsiveness of these copolymers. If the copolymers show improved properties compared to commercial Eudragit® structures, future work will require the development of alternative, scalable synthetic routes for higher molar masses and quantitively deprotection. Deprotection yields as well as the degree of deprotection are listed in Table S5. Most yields were around 80%, with the exception of malic acid-modified copolymers at a 1:1 ratio, which showed significantly lower yields.

To ensure complete removal of residual TFA, all deprotected copolymers were washed at least three times with slightly acidified water. ^{19}F-NMR analysis of the copolymers revealed no detectable fluorine-containing species, confirming the quantitative removal of TFA and that the polymer did not undergo any side reactions with TFA.

Attempts to characterize the deprotected copolymers via SEC using DMF as solvent were unsuccessful. No signals were observed in either the refractive index or UV detector, likely due to strong interactions between the acidic functionalities of the polymers and the column or pre-column material. Besides this, thermal properties were successfully investigated using DSC, see Fig. S72+73. All copolymers displayed a single glass transition temperature (T_g).

For the MMA based copolymers, analog to Eudragit® L-100, the T_g decreases due to the incorporation of flexible side chains. While the commercial Eudragit® L-100 has a T_g of 168 °C, mandelic acid modification reduced it to 149 °C and malic acid modifications lowered it further to 109 °C (1:1 ratio) and 81 °C (1:2 ratio). Despite this decrease of almost 90 °C, the resulting T_g is comparable to Eudragit® L-100-55 (T_g = 82°C), indicating this is acceptable for an enteric drug coating. For the EA based copolymers, analog to Eudragit® L-100-55, the mandelic acid modification increased the T_g to 113 °C. In contrast the malic acid modification led to a T_g of 65 °C (1:1 ratio) and 60 °C (1:2 ratio). These T_g's could be an issue since drug coatings are usually mixed with plasticizers, which further decrease the T_g. These lower T_g's could pose challenges in processing and handling of the drug coating, as glass transitions are not first order phase transitions, material properties are weakened gradually, potentially resulting in sticky or viscous materials unsuitable for enteric drug coatings.

Cloud point titration

To investigate the altered pH-responsive behavior of the newly synthesized copolymers, pH-dependent transmission measurements were performed, with commercially available Eudragit® L-100 and L-100-55 as benchmarks. All experiments were carried out under identical conditions to those described in the previous chapter to enable direct comparison. Each polymer was dissolved in 10 mL of 0.01 M NaOH at a concentration of 5 mg/mL and measurements were performed at 37 °C to simulate body temperature.

Detailed information on the procedure can be found in the Supporting Information. To avoid too much dilution, the pH was gradually lowered by the addition of 0.1 M hydrochloric acid. As the pH level decreases, carboxylate groups are protonated, leading to coil collapse and polymer precipitation, increasing turbidity of the solution and reducing laser transmission. The cloud point titration curves are shown in Fig. 5 for MMA based copolymers and in Fig. S75 for EA based copolymers.

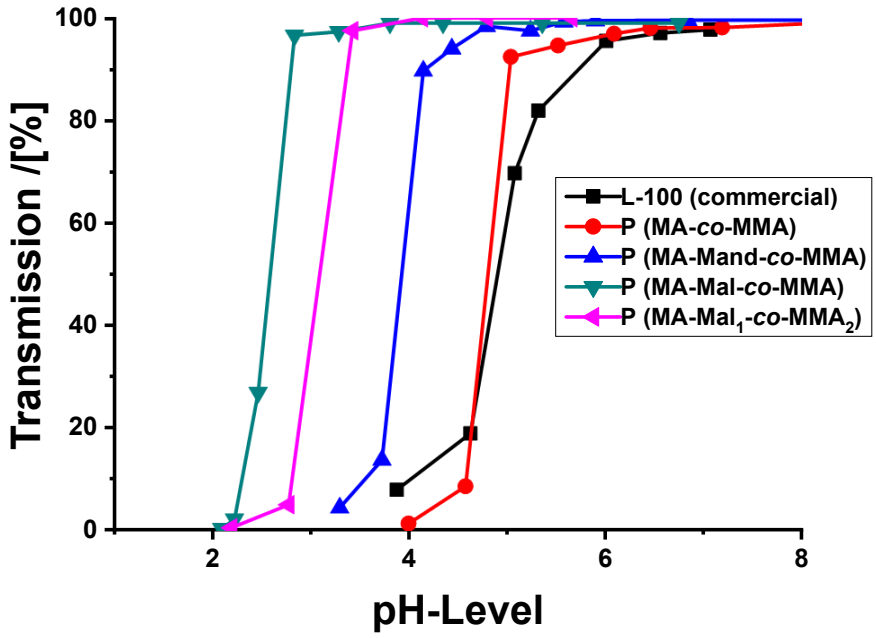

Figure 5: pH dependent cloud point titrations for Eudragit® L-100 analog copolymers. The black curve represents commercial available high molar mass Eudragit® L-100, while the red curve corresponds to self-synthesized P(MA-*co*-MMA).

All modified copolymers demonstrated significantly enhanced solubility at lower pH compared to their Eudragit® based polymers, confirming that α-hydroxy acid modifications effectively lower the pK_a. Interestingly, the dissolution behavior of Eudragit® polymers was consistent even with very different molar mass, indicating that the dissolution behavior is independent of molar mass. The slight differences can be explained by the slightly different monomer ratios.

The modified Eudragit® L-100 copolymers remain soluble at lower pH than both commercial and self-synthesized low molar mass P(MA-*co*-MMA). For instance, while unmodified Eudragit® L-100 reaches only ~10 % transmission at a pH of 4.5, the modified

copolymers showed more than 90 % transmission, indicating high solubility at this pH. The mandelic acid modified copolymers began precipitating at a pH of 4, suggesting improved drug release performance due to earlier solubilization, while retaining stability under the typical acidic conditions of the stomach (pH = 1-3).[11,12] In contrast malic acid modified copolymers were fully soluble even at pH 3, raising concerns about their gastric insolubility. Reducing the malic acid content increases the pK_a value of the copolymer, enabling tunable pH-responsiveness and controlled drug release profiles by altering the malic acid content.

The EA based copolymers, analog to Eudragit® L-100-55 are shown in Fig. S75. As for the MMA based copolymers all EA based copolymers show an improved solubility at lower pH, indicating their reduced pK_a value. The mandelic acid modified copolymers began precipitating at a pH of 4.5, slightly higher than the MMA copolymer, suggesting again enhanced release characteristics, while maintaining acid stability. In contrast the malic acid modified copolymers dissolve completely at a pH of 2-2.5, questioning again their insolubility under gastric conditions. As for the MMA copolymers, the malic acid content can be used to fine tune the release profile.

In summary both modifications with mandelic and malic acid have proven to be successful in lowering the pK_a value of the copolymers. Hereby has malic acid a greater influence than mandelic acid, which is explained by the different pK_a values of the different acids. Mandelic acid has a pK_a value of 3.37, which is between the pK_a's of malic acid: pK_{a1} = 3.24 and pK_{a2} = 4.68.[32,43] Interestingly it seems like the dissolution behavior of the malic acid based copolymers are only dependent on the first pK_a value. However, for enteric drug coatings, both rapid dissolution and acid resistance are essential. Since gastric acid can vary from pH = 1 in a fasted state to 6 in a fed state, drug coatings have to be stable not only at a pH of 1.[11] Normally a pH of 1-3 is assumed and regulatory standards require the stability of drug coatings at a pH of 1.2 for at least one, preferably for 2-3 hours.[44] While mandelic acid modified copolymers appear to meet this criteria, malic acid modified copolymers may not. To further investigate the acid resistance and drug release of these systems, additional studies were conducted using coated paracetamol capsules.

Acid uptake

As previously discussed, a critical requirement for enteric drug coatings is their stability and insolubility under gastric conditions. In addition they must not absorb significant amounts of the surrounding media, as this can negatively impact both material properties and dissolution behavior. Generally, an acid uptake below 10 wt% is considered acceptable and is correlated to acid resistance.[21] To evaluate this, dip coated capsules were immersed into a 0.01 M HCl solution for two hours to simulate stomach conditions. The experimental setup and calculation are described in the Supporting Information and the results are summarized in Fig. 6.

With the exception of one copolymer P(MA-Mand-*co*-EA), all coatings failed the acid stability test. The other polymers either partially dissolved or swelled excessively and ruptured during the transfer from the steel basket (due to being stuck on the metal surface) onto the scale, making the determination of the acid uptake impossible. Shortening the time frame to one hour for the malic acid based copolymers did not improve their performance. This is attributed to their reduced pK_a value, which allows deprotonation even at such low pH. Due to the lack of acid stability, malic acid modified copolymers were no longer considered viable candidates for enteric drug coatings and were not further investigated. Therefore P(MA-Mand-*co*-EA), the only stable copolymer, is compared to previously studied glycolic and lactic acid modified copolymers, as well as the benchmark Eudragit® L-100-55, see Fig. 6. The mandelic acid modified EA showed significant less acid uptake than the others, supporting the hypothesis that increased hydrophobicity decreases the acid uptake. In contrast P(MA-Mand-*co*-MMA) failed the test, likely due to its slightly lower pK_a value, disqualifying it as a suitable coating material. Although only one copolymer passed the acid uptake test, P(MA-Mand-*co*-EA) demonstrated excellent acid resistance and will be further tested in dissolution studies.

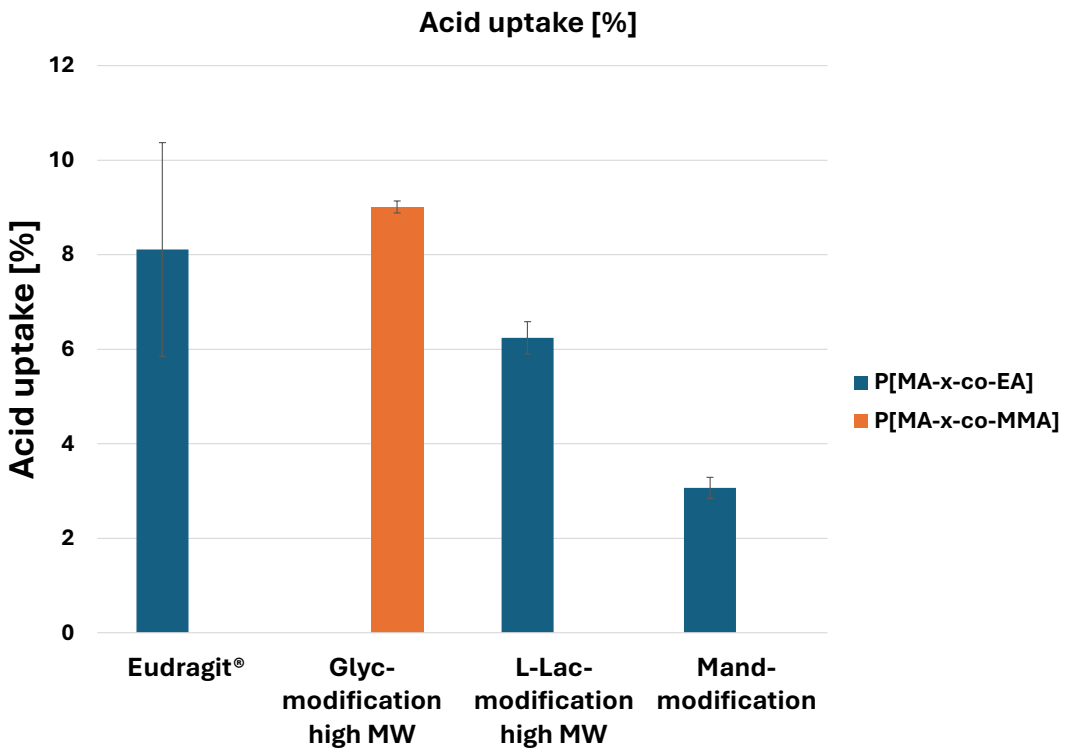

Figure 6: Acid uptake of coated capsules after 2 hours in a 0.01 M HCl solution. Only P(MA-Mand-*co*-EA) was stable under these conditions.

Dissolution tests of coated capsules

To further investigate the drug release performance of P(MA-Mand-*co*-EA), hydroxypropyl methylcellulose (HPMC) capsules filled with paracetamol were coated with the polymer and tested using the basket method (USP apparatus I). The coated capsules were initially immersed into 900 mL of 0.01 M HCl for two hours (commercial Eudragit® only one hour) to simulate gastric conditions and analyze the dissolution properties of the copolymer under more realistic conditions. The absorption of gastric fluids changes the microenvironmental pH level around the coating and therefore the dissolution. After the acid stability of the copolymers had been confirmed, the medium was replaced with 900 mL of 15 mM phosphate butter (pH = 6.5). This buffer was chosen because of its fairly bio-predictive representation of the proximal small intestinal conditions.[45] Since both HPMC capsules and paracetamol are water-soluble, drug release is primarily dependent on the polymer dissolution. A detailed experimental procedure is shown in the Supporting Information. Since all polymers besides P(MA-Mand-*co*-EA) failed the acid stability test,

P(MA-Mand-*co*-EA) was again compared to the in the previous chapter investigated copolymers, but with an extended acid absorption period of two hours.

Notably, extending the acid exposure from one to two hours altered dissolution outcomes. For example P(MA-Lac-*co*-EA), which failed to release the drug in previous experiments now outperforms commercial Eudragit® copolymers, which were only submerged for one hour. In fact, all modified copolymers demonstrated faster drug release than the commercial coatings, validating the concept of a lowered pK_a via α-hydroxy acid modification to enhance polymer dissolution. Among these, P(MA-Mand-*co*-EA) showed drug release comparable to P(MA-Gly-*co*-MMA) and significantly faster than both lactic modified and unmodified copolymers. A more detailed time dependent release profile is shown in Fig. S75.

These findings support P(MA-Mand-*co*-EA) as a promising candidate for enteric coatings, offering both reduced acid uptake and faster drug release. This reduced acid uptake is particularly notable as the release kinetics appear to depend on the duration of prior acid exposure. It can be assumed that copolymers with higher acid uptake are more sensitive to exposure time, potentially leading to variability in the drug release profiles, depending on the gastric emptying. Since gastric emptying times can range from one to six hours,[46,47] a more hydrophobic, acid resistant polymer like P(MA-Mand-*co*-EA) could help achieve more consistent drug release profiles. Additionally, due to the faster release this drug coating may also address some limitations of current Eudragit® coatings, such as improving bioavailability of iron based drugs or aspirin for antiplatelet therapy.[16,17,48–50]

However, before this copolymer can be considered an alternative enteric drug coating, several synthetic problems have to be solved and further pharmaceutical tests must be performed. The primary synthetic issues are increasing the copolymers molar mass, improving scalability and achieving quantitative deprotection. These challenges may be overcome through the post-polymerization strategy described in the previous chapter.

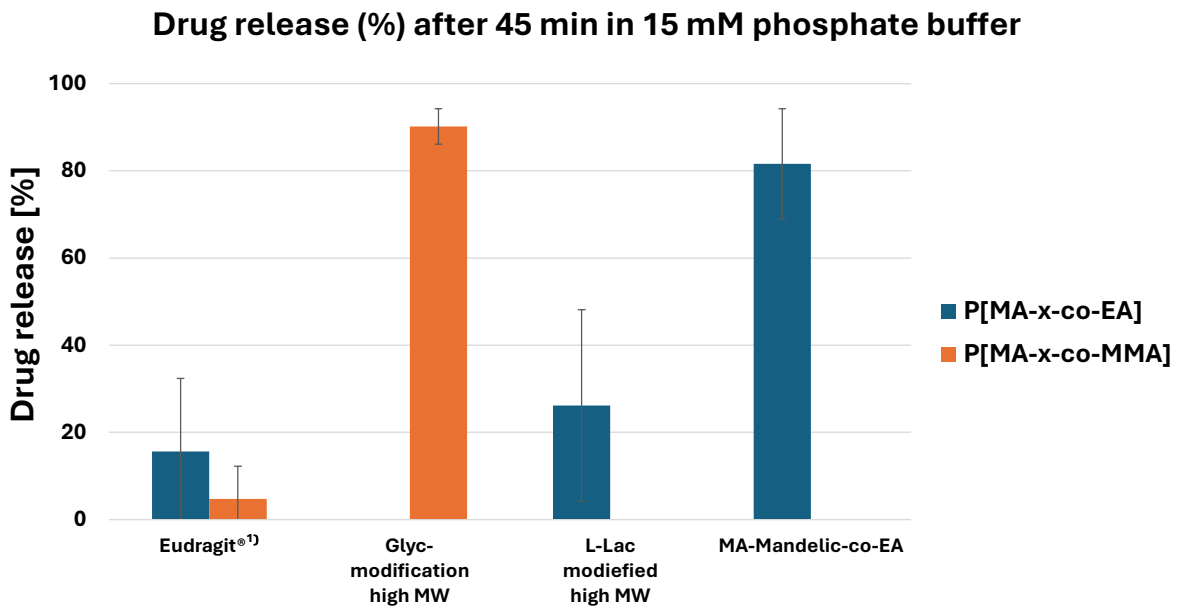

Figure 7: Drug release [%] after 45 minutes of different modified copolymers and the commercial Eudragit® polymers at a pH level of 6.5. [1)] was only exposed for one hour to the 0.01 M HCl solution, all other copolymers were for two hours.

Conclusions

We successfully synthesized and fully characterized two novel monomers (MA-Mand-Bn and MA-Mal-Bn) and polymerized them via free radical polymerization. MA-Mand-Bn was specifically designed to lower the pK_a value of the copolymer, similar to other α-hydroxy-carboxylic acids, while also increasing hydrophobicity due to its phenyl side chain, which is expected to reduce acid uptake of gastric fluid. Malic acid was selected to examine the effect of introducing a second carboxylic acid functionality with a slightly higher pK_a value. Since this increases the density of acid functions, malic modified copolymers were synthesized not only in a 1:1 ratio like the mandelic acid modified copolymers, but also in a 1:2 ratio to maintain the 1:1 ratio of acid functionalities to comonomer.

Both monomers were homo- and copolymerized with MMA and EA to obtain Eudragit® L-100 and L-100-55 analog structures. The resulting polymers were characterized using NMR and SEC to determine the monomer incorporation and molar weight distribution. These polymers were deprotected to almost 90% using TFA. These copolymers were then investigated towards their intrinsic pH-dependent dissolution properties via cloud point titration. All modified polymers exhibited dissolution at lower pH levels than the commercially available Eudragit® polymers, confirming a successful decrease of the pK_a.

Acid stability, uptake and drug release tests were performed using dip-coated paracetamol capsules. Unexpectedly only one copolymer P(MA-Mand-*co*-EA), demonstrated sufficient stability at a pH of 2, making it the only candidate for further dissolution testing. This copolymer showed significantly lower acid uptake than both previously investigated copolymers and commercial Eudragit®, supporting the hypothesis that the phenyl side chain enhances hydrophobicity. Moreover, it exhibits a faster drug release, further validating the reduced pK_a value, see Fig. 1.

Due to poor acid resistance, the malic based copolymers were excluded from subsequent dissolution studies. Overall, P(MA-Mand-*co*-EA) presents a promising candidate for enteric drug coatings, offering improved acid stability and enhanced release properties. However, key challenges remain, including the need for higher molar mass, improved synthetic scalability and comprehensive pharmaceutical evaluation, such as cytotoxicity, long-term stability and formulation development. A potential solution to the synthetic limitations may lie in the post-polymerization strategy described in the previous chapter.

References:

(1) Khan, M. Z. I.; Prebeg, Ž.; Kurjaković, N. A PH-Dependent Colon Targeted Oral Drug Delivery System Using Methacrylic Acid Copolymers. *Journal of Controlled Release* **1999**, *58* (2), 215–222. https://doi.org/10.1016/S0168-3659(98)00151-5.

(2) Cole, E. T.; Scott, R. A.; Connor, A. L.; Wilding, I. R.; Petereit, H. U.; Schminke, C.; Beckert, T.; Cadé, D. Enteric Coated HPMC Capsules Designed to Achieve Intestinal Targeting. *Int J Pharm* **2002**, *231* (1), 83–95. https://doi.org/10.1016/S0378-5173(01)00871-7.

(3) Xu, W.; Ling, P.; Zhang, T. Polymeric Micelles, a Promising Drug Delivery System to Enhance Bioavailability of Poorly Water-Soluble Drugs. *J Drug Deliv* **2013**, *2013*, 1–15. https://doi.org/10.1155/2013/340315.

(4) Findlay, M.; von Minckwitz, G.; Wardley, A. Effective Oral Chemotherapy for Breast Cancer: Pillars of Strength. *Annals of Oncology* **2008**, *19* (2), 212–222. https://doi.org/10.1093/annonc/mdm285.

(5) De Portu, S.; Mantovani, L. G.; Ravaioli, A.; Tamburini, E.; Bollina, R.; Cozzi, C.; Grimaldi, A. M.; Testa, T. E.; Bianchessi, C.; Cartenì, G. Cost Analysis of Capecitabine vs 5-Fluorouracil-Based Treatment for Metastatic Colorectal Cancer Patients. *Journal of Chemotherapy* **2010**, *22* (2), 125–128. https://doi.org/10.1179/joc.2010.22.2.125.

(6) Schröter, A.; Mahler, H.-C.; Sayed, N. Ben; Koulov, A. V.; Huwyler, J.; Jahn, M. 4-Hydroxynonenal – A Toxic Leachable from Clinically Used Administration Materials. *J Pharm Sci* **2021**, *110* (9), 3268–3275. https://doi.org/10.1016/j.xphs.2021.05.014.

(7) Jenke, D.; Carlson, T. A Compilation of Safety Impact Information for Extractables Associated with Materials Used in Pharmaceutical Packaging, Delivery, Administration, and Manufacturing Systems. *PDA J Pharm Sci Technol* **2014**, *68* (5), 407–455. https://doi.org/10.5731/pdajpst.2014.00995.

(8) Mössner, J.; Keim, V. Pancreatic Enzyme Therapy. *Dtsch Arztebl Int* **2011**, *108* (34–35), 578–582. https://doi.org/10.3238/arztebl.2011.0578.

(9) Evonik Industries AG. *Functional polymers to take control of your release profile Versatility and reliability for oral solid dosage forms*. https://healthcare.evonik.com/en/drugdelivery/oral-drug-delivery/oral-excipients/eudragit-portfolio/attachment/149083?rev=fd91102acf8d769a56d0716b20544216.

(10) Ibarra-Montaño, E. L.; Rodríguez-Laguna, N.; Sánchez-Hernández, A.; Rojas-Hernández, A. Determination of PKa Values for Acrylic, Methacrylic and Itaconic Acids by 1H and 13C NMR in Deuterated Water. *Journal of Applied Solution Chemistry and Modeling* **2015**, *4* (1), 7–18. https://doi.org/10.6000/1929-5030.2015.04.01.2.

(11) Stamatopoulos, K.; O'Farrell, C.; Simmons, M.; Batchelor, H. In Vivo Models to Evaluate Ingestible Devices: Present Status and Current Trends. *Adv Drug Deliv Rev* **2021**, *177*, 113915. https://doi.org/10.1016/j.addr.2021.113915.

(12) Beasley, D. E.; Koltz, A. M.; Lambert, J. E.; Fierer, N.; Dunn, R. R. The Evolution of Stomach Acidity and Its Relevance to the Human Microbiome. *PLoS One* **2015**, *10* (7), e0134116. https://doi.org/10.1371/journal.pone.0134116.

(13) Al-Gousous, J.; Amidon, G. L.; Langguth, P. Toward Biopredictive Dissolution for Enteric Coated Dosage Forms. *Mol Pharm* **2016**, *13* (6), 1927–1936. https://doi.org/10.1021/acs.molpharmaceut.6b00077.

(14) Al-Gousous, J.; Ruan, H.; Blechar, J. A.; Sun, K. X.; Salehi, N.; Langguth, P.; Job, N. M.; Lipka, E.; Loebenberg, R.; Bermejo, M.; Amidon, G. E.; Amidon, G. L. Mechanistic Analysis and Experimental Verification of Bicarbonate-Controlled Enteric Coat Dissolution: Potential in Vivo Implications. *European Journal of Pharmaceutics and Biopharmaceutics* **2019**, *139*, 47–58. https://doi.org/10.1016/j.ejpb.2019.03.012.

(15) Blechar, J. A.; Al-Gousous, J.; Wilhelmy, C.; Postina, A. M.; Getto, M.; Langguth, P. Toward Mechanistic Design of Surrogate Buffers for Dissolution Testing of PH-Dependent Drug Delivery Systems. *Pharmaceutics* **2020**, *12* (12), 1197. https://doi.org/10.3390/pharmaceutics12121197.

(16) Rudinskas, L.; Paton, T. W.; Walker, S. E.; Dotten, D. A.; Cowan, D. H. Poor Clinical Response to Enteric-Coated Iron Preparations. *CMAJ* **1989**, *141* (6), 565–566.

(17) Walker, S. E.; Paton, T. W.; Cowan, D. H.; Manuel, M. A.; Dranitsaris, G. Bioavailability of Iron in Oral Ferrous Sulfate Preparations in Healthy Volunteers. *CMAJ* **1989**, *141* (6), 543–547.

(18) Haastrup, P. F.; Grønlykke, T.; Jarbøl, D. E. Enteric Coating Can Lead to Reduced Antiplatelet Effect of Low-Dose Acetylsalicylic Acid. *Basic Clin Pharmacol Toxicol* **2015**, *116* (3), 212–215. https://doi.org/10.1111/bcpt.12362.

(19) Grosser, T.; Fries, S.; Lawson, J. A.; Kapoor, S. C.; Grant, G. R.; FitzGerald, G. A. Drug Resistance and Pseudoresistance. *Circulation* **2013**, *127* (3), 377–385. https://doi.org/10.1161/CIRCULATIONAHA.112.117283.

(20) LaVan, D. A.; McGuire, T.; Langer, R. Small-Scale Systems for in Vivo Drug Delivery. *Nat Biotechnol* **2003**, *21* (10), 1184–1191. https://doi.org/10.1038/nbt876.

(21) Missaghi, S.; Young, C.; Fegely, K.; Rajabi-Siahboomi, A. R. Delayed Release Film Coating Applications on Oral Solid Dosage Forms of Proton Pump Inhibitors: Case Studies. *Drug Dev Ind Pharm* **2010**, *36* (2), 180–189. https://doi.org/10.3109/03639040903468811.

(22) Williamson, J. R.; Cooper, R. H. Regulation of the Citric Acid Cycle in Mammalian Systems. *FEBS Lett* **1980**, *117* (S1). https://doi.org/10.1016/0014-5793(80)80572-2.

(23) Borst, P. The Malate–Aspartate Shuttle (Borst Cycle): How It Started and Developed into a Major Metabolic Pathway. *IUBMB Life* **2020**, *72* (11), 2241–2259. https://doi.org/10.1002/iub.2367.

(24) Kövilein, A.; Kubisch, C.; Cai, L.; Ochsenreither, K. Malic Acid Production from Renewables: A Review. *Journal of Chemical Technology & Biotechnology* **2020**, *95* (3), 513–526. https://doi.org/10.1002/jctb.6269.

(25) Bellon, P. EP001291012A1 Cosmetic Complex Based on Malic Acid, 2003.

(26) Gore, V.; Gadkar, M.; Pokharkar, K. US 20100392290A1 Novel Process to Prepare Almotriptan, 2010.

(27) Zhang, Z.; Wang, B.; Zhou, P.; Guo, D.; Kang, R.; Zhang, B. A Novel Approach of Chemical Mechanical Polishing Using Environment-Friendly Slurry for Mercury Cadmium Telluride Semiconductors. *Sci Rep* **2016**, *6* (1), 22466. https://doi.org/10.1038/srep22466.

(28) Stallcup, O. T. US4161539 Use of Malic Acid as a Ruminant Feed Additive, 1979.

(29) ruzzaman, Md. S.; Islam, Md. S.; Haque, Md. M.; Hossain, Md. S.; Bakr, Dr. Md. A. Malic Acid Butane-1, 4-Diol-Glycerol Co-Polyester as an Enteric Coating Material. *Int J Sci Eng Res* **2015**, *6* (3), 1460–1463. https://doi.org/10.14299/ijser.2015.03.007.

(30) Brittain, H. G. Mandelic Acid. In *Analytical Profiles of Drug Substances and Excipients*; 2002; Vol. 29, pp 179–211. https://doi.org/10.1016/S1075-6280(02)29007-2.

(31) van Putten, P. L. Mandelic Acid and Urinary Tract Infections. *Antonie Van Leeuwenhoek* **1979**, *45* (4), 622–623. https://doi.org/10.1007/BF00403669.

(32) Hamada, Y. Z.; Harris, M.; Burt, K.; Greene, J.; Rosli, K. Detailed Potentiometric Study of Al3+ and Cr3+ with Malic Acid in Aqueous Solutions. *Journal of Membrane and Separation Technology* **2013**, *2* (4), 213–218. https://doi.org/10.6000/1929-6037.2013.02.04.2.

(33) Tabata, Y.; Abe, H. Synthesis and Properties of Alternating Copolymers of 3-Hydroxybutyrate and Lactate Units with Different Stereocompositions. *Macromolecules* **2014**, *47* (21), 7354–7361. https://doi.org/10.1021/ma501783f.

(34) Abraham, D. J. Rational Drug Design Edited by D. G. Truhlar, W. J. Howe, A. J. Hopfinger, J. Blaney, and R. Dammkoehler. Springer-Verlag, New York. 1999. Xxii + 206 Pp. 16 × 24 Cm. ISBN 0-387-98753-3. $69.95. *J Med Chem* **1999**, *42* (25), 5284–5284. https://doi.org/10.1021/jm990497r.

(35) Geschwind, J.; Frey, H. Poly(1,2-Glycerol Carbonate): A Fundamental Polymer Structure Synthesized from CO2 and Glycidyl Ethers. *Macromolecules* **2013**, *46* (9), 3280–3287. https://doi.org/10.1021/ma400090m.

(36) Hsu, Y.; Chuang, M.; Hirano, T.; Ute, K. Multivariate Analysis of 13C NMR Spectra to Extract Information about Monomer Sequences in Poly(Methyl Methacrylate-Co-Benzyl Methacrylate)s Prepared by Various Polymer Reactions. *Polym J* **2018**, *50* (5), 355–363. https://doi.org/10.1038/s41428-018-0027-9.

(37) Collins, J. M.; Sandeep, K. S. Coupling Method for Peptide Synthesis at Elevated Temperatures US2017/0342104A1, 2017.

(38) Büchel, K. H.; Falbe, J.; Hagemann, H.; Hanack, M.; Klamann, D.; Kreher, R.; Kropf, H.; Regitz, M. *Register Der Stoffklassen*; Georg Thieme Verlag KG: Stuttgart, 1987. https://doi.org/10.1055/b-003-111695.

(39) Koltzenburg, S.; Maskos, M.; Nuyken, O. *Polymere: Synthese, Eigenschaften Und Anwendungen*; Springer Berlin Heidelberg: Berlin, Heidelberg, 2014. https://doi.org/10.1007/978-3-642-34773-3.

(40) Wool, R. P. Polymer Entanglements. *Macromolecules* **1993**, *26* (7), 1564–1569. https://doi.org/10.1021/ma00059a012.

(41) Weickert, G. *Modellierung von Polymerisationsreaktoren*; Springer Berlin Heidelberg, 1997. https://doi.org/10.1007/978-3-642-60516-1.

(42) Wen, M.; McCormick, A. V. Kinetic Model for Radical Trapping in Photopolymerization of Multifunctional Monomers. *Macromolecules* **2000**, *33* (25), 9247–9254. https://doi.org/10.1021/ma0003351.

(43) Lide, D. R.; Baysinger, G.; Berger, L. I.; Goldberg, R. N.; Kehiaian, H. V; Kuchitsu, K.; Roth, D. L.; Zwillinger, D. *CRC Handbook of Chemistry and Physics*; Haynes, W. M., Ed.; CRC Press, 2014. https://doi.org/10.1201/b17118.

(44) Tablets. In *European Pharmacopoeia*; 2018; Vol. 11, pp 1004–1006.

(45) Al-Gousous, J.; Amidon, G. L.; Langguth, P. Toward Biopredictive Dissolution for Enteric Coated Dosage Forms. *Mol Pharm* **2016**, *13* (6), 1927–1936. https://doi.org/10.1021/acs.molpharmaceut.6b00077.

(46) Szarka, L. A.; Camilleri, M. Gastric Emptying. *Clinical Gastroenterology and Hepatology* **2009**, *7* (8), 823–827. https://doi.org/10.1016/j.cgh.2009.04.011.

(47) Goyal, R. K.; Guo, Y.; Mashimo, H. Advances in the Physiology of Gastric Emptying. *Neurogastroenterology & Motility* **2019**, *31* (4). https://doi.org/10.1111/nmo.13546.

(48) Grosser, T.; Fries, S.; Lawson, J. A.; Kapoor, S. C.; Grant, G. R.; FitzGerald, G. A. Drug Resistance and Pseudoresistance: An Unintended Consequence of Enteric Coating Aspirin. *Circulation* **2013**, *127* (3), 377–385. https://doi.org/10.1161/CIRCULATIONAHA.112.117283.

(49) McNeil, J. J.; Wolfe, R.; Woods, R. L.; Tonkin, A. M.; Donnan, G. A.; Nelson, M. R.; Reid, C. M.; Lockery, J. E.; Kirpach, B.; Storey, E.; Shah, R. C.; Williamson, J. D.; Margolis, K. L.; Ernst, M. E.; Abhayaratna, W. P.; Stocks, N.; Fitzgerald, S. M.; Orchard, S. G.; Trevaks, R. E.; Beilin, L. J.; Johnston, C. I.; Ryan, J.; Radziszewska, B.; Jelinek, M.; Malik, M.; Eaton, C. B.; Brauer, D.; Cloud, G.; Wood, E. M.; Mahady, S. E.; Satterfield, S.; Grimm, R.; Murray, A. M. Effect of Aspirin on Cardiovascular Events and Bleeding in the Healthy Elderly. *New England Journal of Medicine* **2018**, *379* (16), 1509–1518. https://doi.org/10.1056/NEJMoa1805819.

(50) Bhatt, D. L.; Grosser, T.; Dong, J.; Logan, D.; Jeske, W.; Angiolillo, D. J.; Frelinger, A. L.; Lei, L.; Liang, J.; Moore, J. E.; Cryer, B.; Marathi, U. Enteric Coating and Aspirin Nonresponsiveness in Patients With Type 2 Diabetes Mellitus. *J Am Coll Cardiol* **2017**, *69* (6), 603–612. https://doi.org/10.1016/j.jacc.2016.11.050.

Supporting Information

Enteric drug coatings: Improving drug release and acid resistance by the synthesis and polymerization of novel mandelic and malic acid monomers.

Dominik A. H. Fuchs,[a] [redacted]X

[i] *Institute of Organic Chemistry, Johannes Gutenberg-University Mainz, Duesbergweg 10-14, 55128 Mainz, Germany*
[j] *Institute of Pharmacy, Department Pharmaceutical Technology and Biopharmacy, Johannes Gutenberg-University Mainz, Staudinger Weg 5, 55128 Mainz, Germany*

1. Materials and experimental procedure

1.1 Materials

All chemicals, including solvents and reagents were purchased from Acros Organics, Thermo Fisher Scientific Inc, Sigma Aldrich, VWR International, TCI, Fluka or Carl Roth and were used as received, unless otherwise stated. Deuterated solvents were purchased from Deutero GmbH. Petrol ether was distilled before use to remove high boiling impurities. Stabilizers in the monomers MEHQ (for purchased EA and MMA) and BHT (for self-synthesized monomers) were removed using a flash column filled with neutral aluminium oxide. Eudragit® L-100 and L-100-55 were gifted by Evonik Industries AG and Paracetamol was provided by Caesar and Lorentz GmbH. The hydroxypropyl methylcellulose (HPMC) capsules were gifted by ACG Associated Capsule PvT Ltd.

1.2 Instrumentation

For the copolymerizations using DMPA as photo initiator was an UV lamp (*XX-15B*) from Ultra-Violet Products Ltd, equipped with two UV tubes with different wavelengths 312 nm (*T-15.M*) and 365 nm (*T-15.L*) used. NMR spectra were measured on a *Bruker Acance II 400* spectrometer with 400 MHz for ^{1}H and 101 MHz for ^{13}C-measurements with a 5 mm BBFO probe head with z-gradient and ATM. The spectra are referenced internally to the residual proton signal of the deuterated solvents ($CDCl_3$ and DMSO-d_6). SEC measurements were performed using an *Agilent 1100 series* with 300/100/40 Å HEMA columns and DMF (containing 1 g/L LiBr) as a solvent. The measurement was performed at a flow rate of 1 ml/min at 50°C with toluene as an internal standard. Data recording and processing were performed using *PSS WinGPC UniChrom*. DSC measurements were carried out on a *TA Instruments DSC 250* equipped with a *Recovery Cooling System 90* in a temperature range of -90-200°C. All measurements were done under a dry nitrogen atmosphere at a heating and cooling rate of 10K/min using a two-point calibration of indium and *n*-octane. The second heating cycle was used for the analysis of the glass transition temperature. The cloud point measurements were carried out on a *JASCO V-640* photometer, equipped with a *JASCO ETC-717* Peltier element at 600 nm. The measuring cell was stirred and heated to 37°C. Capsule dissolution experiments were performed on an USP type I apparatus (*PTW SIII, Pharma Test*) and the released paracetamol was spectrophotometrically quantified using a *UV-1700 PharmaSpec* spectrometer.

2. Synthesis

2.1 Protection groups (Mand-Bn & Mal-Bn)

Mand-Bn and Mal-Bn were synthesized analog to literature and the previous chapter.[1] Mandelic acid (40.0 g; 0.26 mol; 1 eq) was dissolved in 150 ml methanol and the base 1,8-diazabicyclo(5.4.0)undec-7-ene (DBU) (40.0 g; 0.26 mol; 1 eq) was added dropwise under stirring. After one hour, methanol was removed under reduced pressure and the resulting oily liquid was dissolved in 240 ml DMF and cooled to 10 °C. Benzyl bromide (45.0 g; 0.26 mol; 1 eq) was added dropwise, and the reaction mixture stirred overnight. After turning yellow the solution was diluted with 250 ml ethyl acetate and 400 ml water. The aqueous phase was extracted four times with 150 ml ethyl acetate and the combined organic phases were extracted with 150 ml water, three times with 5 wt % citric acid solution and two times with brine. The organic phase was dried with sodium sulfate and the solvent was removed under reduced pressure. The crude

products were purified by distillation under reduced pressure (10^{-3} mbar) at 120°C for Mand-Bn and 220°C for Mal-Bn, yielding 93% Mand-Bn and 84% Mal-Bn.

Mand-Bn: ^{1}H-NMR (400 Mhz, $CDCl_3$) δ (ppm) = 7.48-7.10 (m, 5H, a), 5.28-5.07 (m, 3H, b), 3.43 (d, 1H, c)

Mal-Bn: ^{1}H-NMR (400 Mhz, $CDCl_3$) δ (ppm) = 7.43-7.28 (m, 10H, a), 5.19-5.13 (s, 4H, b), 4.59 (t, 1H, d) 2.91 (m, 2H, e)

2.2 Steglich esterification (MA-Mand-Bn & MA-Mal-Bn)

For the Steglich esterification, Mand-Bn (25.0 g; 0.1 mol; 1eq), methacrylic acid (9.8 g; 0.11 mol; 1.1eq) and *N,N*-Dimethylpyridin-4-amine (DMAP) (1.26 g; 0.01 mol; 0.1 eq) were dissolved in 70 ml DMF and cooled to 0°C. *N,N'*-Diisopropylcarbodiimid (DIPC) (19.5 g; 0.15 mol; 1.5 eq) dissolved in 30 ml DMF was added dropwise to keep the reaction temperature below 10 °C. After the addition of DIPC was complete, the cooling bath was removed and the reaction mixture was stirred at room temperature for three days. Afterwards were the colorless crystals removed using filtration and the yellow solution was diluted with 100 mL of ethyl acetate as well as water. The aqueous phase was extracted three times with 150 mL of ethyl acetate and the combined organic phases one time with 150 mL water and twice with 100 mL of brine. The organic phase was dried over magnesium sulfate, and 2,6-Di-*tert*-butyl-4-methylphenol (BHT) was added as a stabilizer. The solvent was removed under reduced pressure. The crude product was stored at – 20 °C and purified using column chromatography using a 1:5 mixture of ethyl acetate to petrol ether as eluent. The two monomers were obtained in pure form with yields of 45 % for MA-Mand-Bn and 31 % for MA-Mal-Bn,

MA-Mand-Bn: ^{1}H-NMR (400 Mhz, $CDCl_3$) δ (ppm) = 7.56-7.13 (m, 10H, a); 6.27 (s, 1H, d); 6.03 (s, 1H, c); 5.67 (s, 1H, d); 5.17 (m, 2H, b); 2.00 (s, 3H, e)

MA-Mal-Bn: ^{1}H-NMR (400 Mhz, $CDCl_3$) δ (ppm) =7.42-7.21 (m, 10H, a); 6.12 (s, 1H, d); 5.64-5.52 (s, 1H, d); 5.63-5.53 (m, 2H, d+c); 5.24-5.04 (m, 4H, b); 2.98 (m, 2H, f); 1.92 (s, 3H, e)

2.3 Copolymerization

The copolymerization procedure is illustrated using P(MA-Mand-Bn-*co*-MMA) as an example. MA-Mand-Bn (3.0 g; 0.01 mol; 1eq) and methyl methacrylate (0.97 g; 0.01 mol; 1eq) were filtered over neutral aluminum oxide to remove any stabilizers. The purified monomers were than transferred into a Schlenk flask. Benzene was used as a solvent, and the reaction mixture was diluted with 19.3 mL to achieve a monomer concentration of 1 mol/L. The photoinitiator DMPA (0.198 g; 0.7 mmol; 5wt.%) was added and the reaction mixture was degassed by three freeze-pump-thaw cycles. The reaction mixture was then irradiated with UV light for 18 hours. After polymerization, unreacted monomers were removed by precipitation of the polymer at least three times into ice-cold petroleum ether, followed by centrifugation. The typical yield was in the range of 80% and all copolymerizations were carried out following this procedure under identical conditions.

P(MA-Mand-Bn-*co*-MMA): ^{1}H-NMR (400 Mhz, $CDCl_3$) δ (ppm) = 7.56-6.99 (10H, a); 6.06-5.57 (1H, b); 5.28-4.85 (2H, c); 3.77-3.14 (3H, d); 2.30-1.33 (4H, e); 1.19-0.46 (6H, f)

P(MA-Mand-Bn-*co*-EA): ^{1}H-NMR (400 Mhz, $CDCl_3$) δ (ppm) = 7.57-6.95 (10H, a); 6.10-5.47 (1H, b); 5.26-4.73 (2H, c); 4.23-3.55 (2H, d); 2.69-1.32 (4H, e); 1.31-0.42 (6H, f)

P(MA-Mal-Bn-*co*-MMA): ^{1}H-NMR (400 Mhz, $CDCl_3$) δ (ppm) = 7.40-7.15 (10H, a); 5.45-5.23 (1H, b); 5.21-4.85 (4H, c); 3.76-3.36 (3H, d); 3.06-2.73 (2H, e); 2.31-1.36 (4H, f); 1.34-0.60 (6H, g)

P(MA-Mal-Bn-*co*-EA): ^{1}H-NMR (400 Mhz, $CDCl_3$) δ (ppm) = 7.37-7.12 (10H, a); 5.48-5.21 (1H, b); 5.20-4.79 (4H, c); 4.28-3.76 (2H, d); 3.10-2.68 (2H, e); 2.62-1.34 (5H, f); 1.34-0.73 (6H, g)

2.4 Deprotection

For the deprotection of the acid functionalities the benzylic esters had to be cleaved. Therefore, the protected copolymers were dissolved in trifluoracetic acid (TFA) in a concentration of 0.1 g/mL at room temperature and heated up to 70°C for 16h. After successful deprotection, the initial colorless solution turned beige and the polymer precipitated. TFA was removed under reduced pressure and collected for reuse. The resulting beige polymer was dissolved in EtOAc and washed at least five times with water to remove any residual TFA. This was confirmed by ^{19}F-NMR spectroscopy. Yields and degrees of deprotection can be found in Table S5.

P(MA-Mand-*co*-MMA): ^{1}H-NMR (400 Mhz, DMSO-d_6) δ (ppm) = 14.10-11.86 (1H, b); 8.07-6.38 (5H, a); 6.00-5.28 (1H, c); 3.93-3.01 (4H,); 2.24-1.22 (3H, d); 1.16-0.27 (6H, f)

P(MA-Mand-*co*-EA): ^{1}H-NMR (400 Mhz, DMSO-d_6) δ (ppm) = 14.26-12.1 (1H, b); 7.76-6.52 (5H, a); 5.95-5.29 (1H, c); 4.21-3.57 (2H, d); 2.43-1.22 (5H, e); 1.21-0.49 (6H, f)

P(MA-Mal-*co*-MMA): ^{1}H-NMR (400 Mhz, DMSO-d_6) δ (ppm) = 14.07-11.61(2H, a); 5.40-4.79 (1H, b); 3.90-3.08 (3H, d); 2.93-2.58 (2H, e); 2.22-1.30 (4H, f); 1.12-0.56 (6H, g)

P(MA-Mal-*co*-EA): ^{1}H-NMR (400 Mhz, DMSO-d_6) δ (ppm) = 13.69-11.99 (2H, a); 5.37-4.83 (1H, b); 4.19-3.75 (3H, d); 2.89-2.59 (2H, e); 2.46-1.26 (4H, f); 1.24-1.07 (3H, g); 1.06-0.66 (3H, h)

2.5 Cloud point titration

For cloud point titration, the deprotected copolymer was dissolved in a 0.01 M NaOH solution at a concentration of 5 mg/mL. If the polymer did not fully dissolve, a few drops of 0.1 M NaOH were added until a clear solution was formed. Once dissolution was complete, the pH was measured, as well as the transmission at 37 °C. This measurement was then repeated after the addition of 0.1 M HCl solution to gradually lower the pH.

2.6 Capsule Coating

Hydroxypropyl methylcellulose (HPMC) capsules (size 0) were filled with paracetamol and coated with different copolymers. For each copolymer, four capsules were prepared, and their individual coating levels were calculated. To prepare the coating solution 60 mg of triethyl citrate (TEC) and 300 mg of the copolymer were dissolved in 5 g of a (1:1 v/v) acetone/ethanol mixture. Capsules were immersed into the solution for 1-3 seconds and then dried for 10-15 minutes, until a target coating density of 10 mg/cm^2 was achieved. After the final dipping cycle, capsules were dried for an additional hour. Any irregularities in the coating were manually corrected using a brush and the coating solution. The coating level was calculated using the following equation, where m_c is the capsule weight after coating and m_u the weight prior to coating. The factor of 0.83 is due to the incorporation of TEC as a plasticizer.

$$Coating\ level = \frac{(m_c - m_u)}{5\ cm^2} \cdot 0.83$$

The mean coating level and the standard deviation for P(MA-Mand-*co*-EA) was 9.22 ± 0.81 mg/cm^2.

2.7 Acid uptake

The acid uptake of the different copolymers was calculated using the following equation:

$$Acid\ uptake\ (\%) = \frac{(m_a - m_c)}{m_c} \cdot 100\%$$

Hereby stands m_a for the weight of the capsule after the capsule was submerged for two hours in a 0.01 M HCl solution.

2.8 Dissolution testing

Dissolution testing was performed using an USP apparatus I with the basket method at 100 rpm and 37 ± 0.5 °C. To evaluate the acid resistance and uptake, the coated capsules were first submerged into 900 mL of 0.01 M HCl solution for two hours (malic acid modified, as well as the Eudragit® polymers were only submerged for one hour). Afterwards the capsules were carefully dried and weighed. The acidic solution was then replaced with 900 mL of 15 mM phosphate buffer at a pH of 6.5. At set time points were 5 mL samples withdrawn without replacement to determine the drug release. The concentration of paracetamol was spectrophotometrically determined at λ = 243 nm.

3. Monomer characterization:

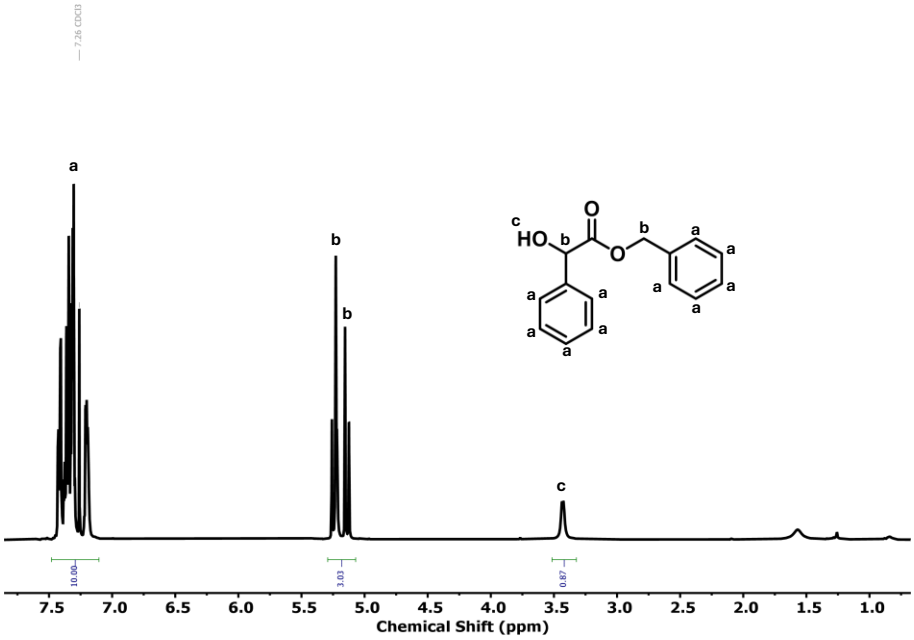

Figure S1: ^{1}H-NMR spectrum (400 MHz, $CDCl_3$) of benzyl protected mandelic acid (Mand-Bn).

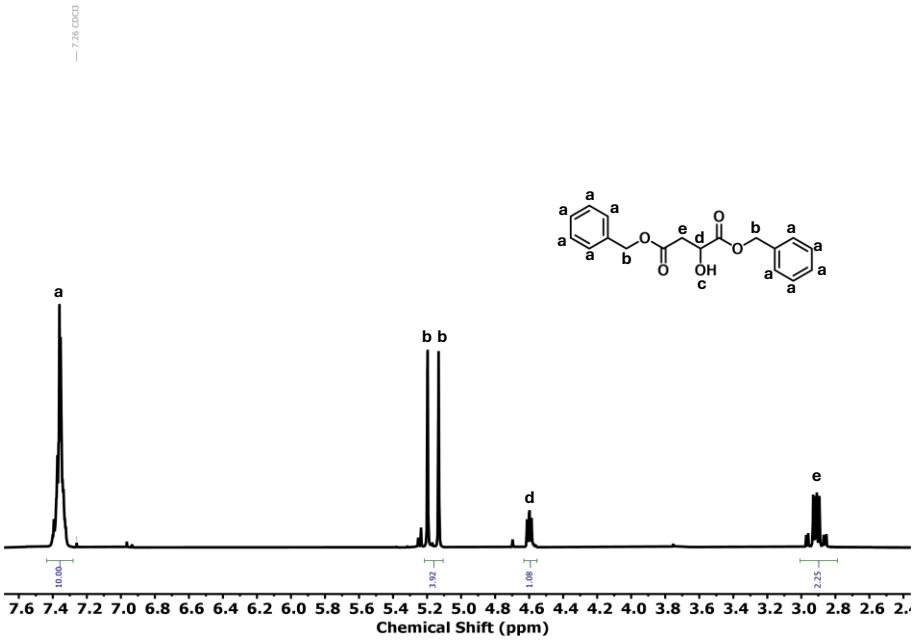

Figure S2: ^{1}H-NMR spectrum (400 MHz, $CDCl_3$) of benzyl protected malic acid (Mal-Bn).

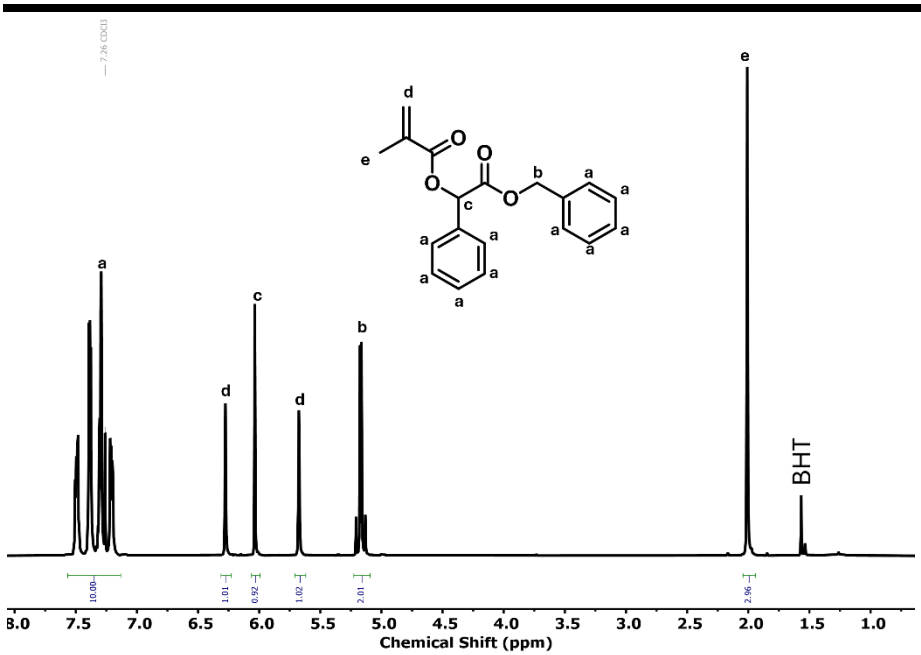

Figure S3: ^{1}H-NMR spectrum (400 MHz, $CDCl_3$) of benzyl protected mandelic acid modified MA (MA-Mand-Bn).

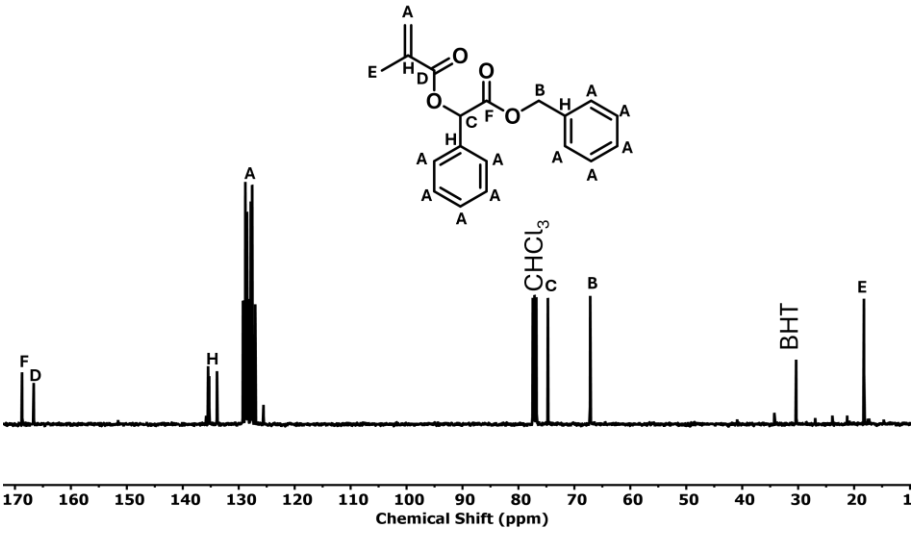

Figure S4: ^{13}C-NMR spectrum (101 MHz, $CDCl_3$) of benzyl protected mandelic acid modified MA (MA-Mand-Bn).

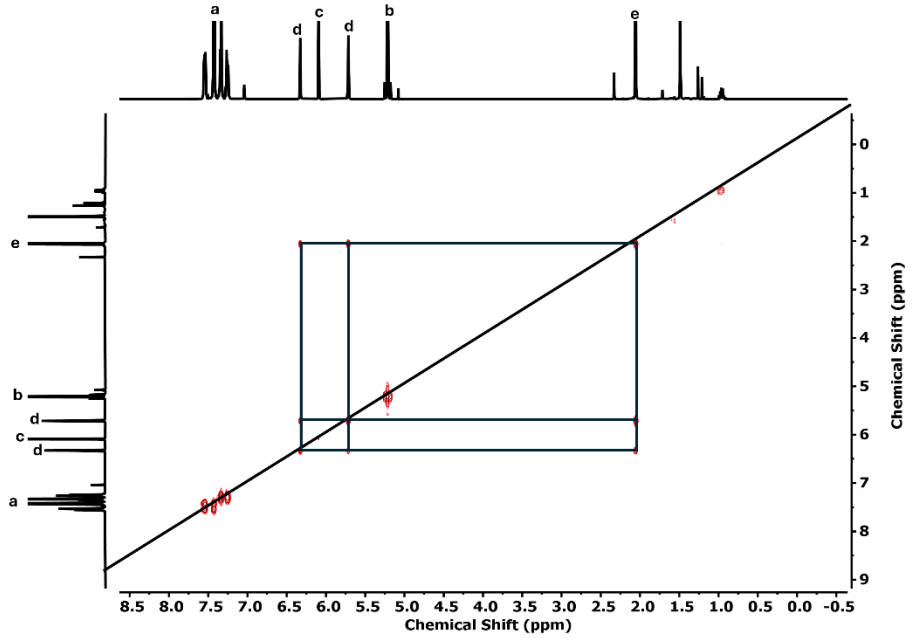

Figure S5: COSY spectrum (400 MHz, $CDCl_3$) of benzyl protected mandelic acid modified MA (MA-Mand-Bn).

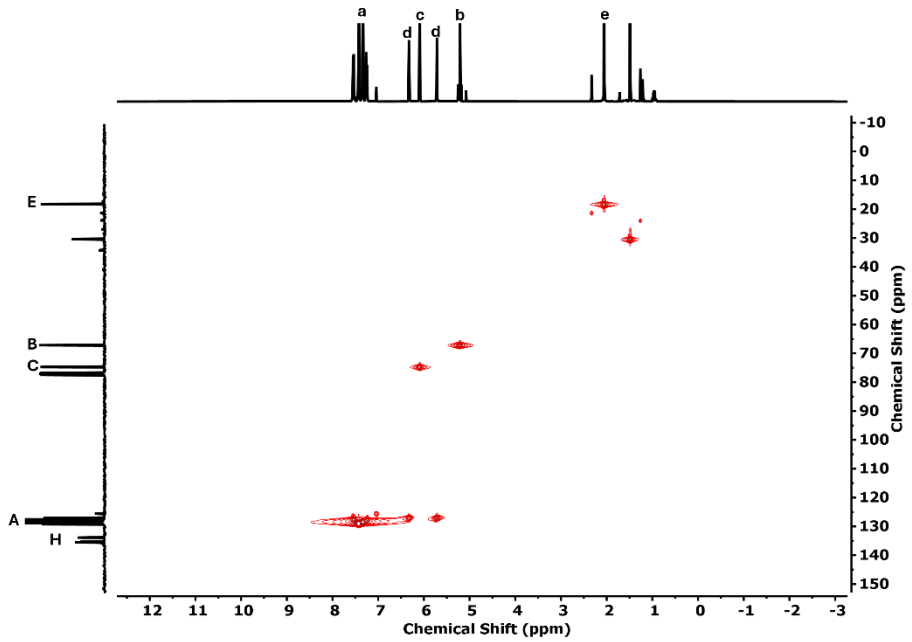

Figure S6: HSQC spectrum (400 MHz, $CDCl_3$) of benzyl protected mandelic acid modified MA (MA-Mand-Bn).

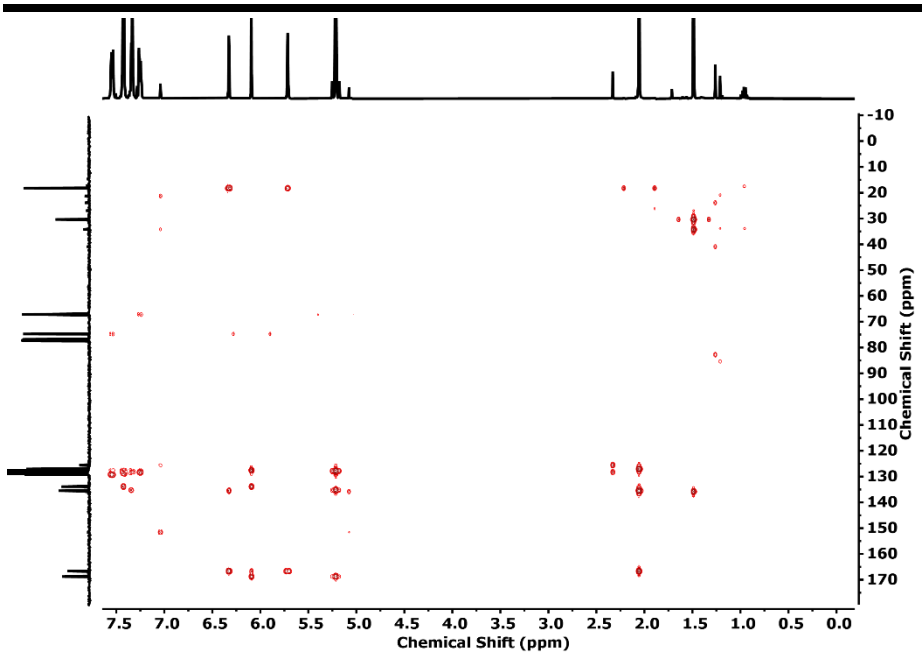

Figure S7: HMBC spectrum (400 MHz, $CDCl_3$) of benzyl protected mandelic acid modified MA (MA-Mand-Bn).

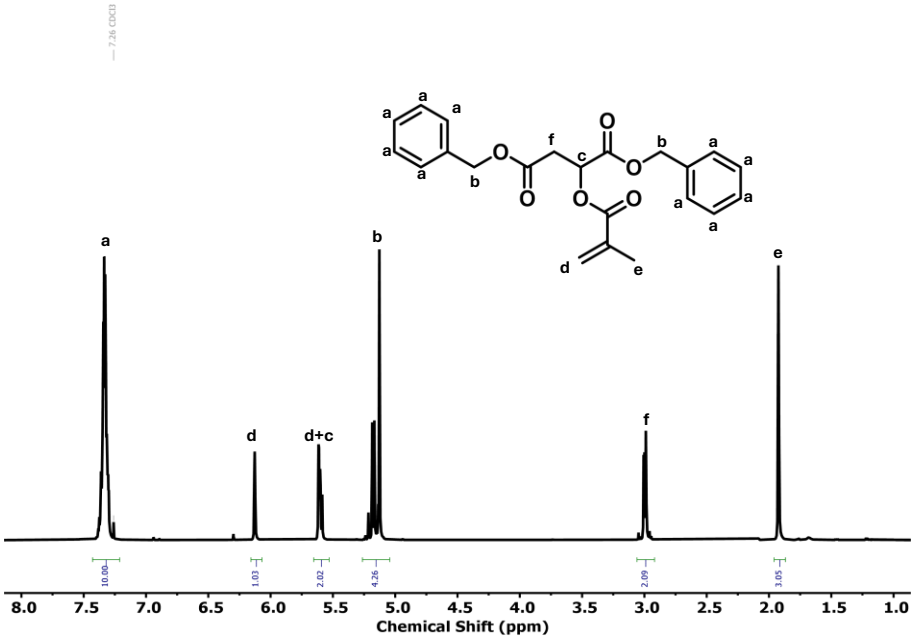

Figure S8: ^{1}H-NMR spectrum (400 MHz, $CDCl_3$) of benzyl protected malic acid modified MA (MA-Mal-Bn).

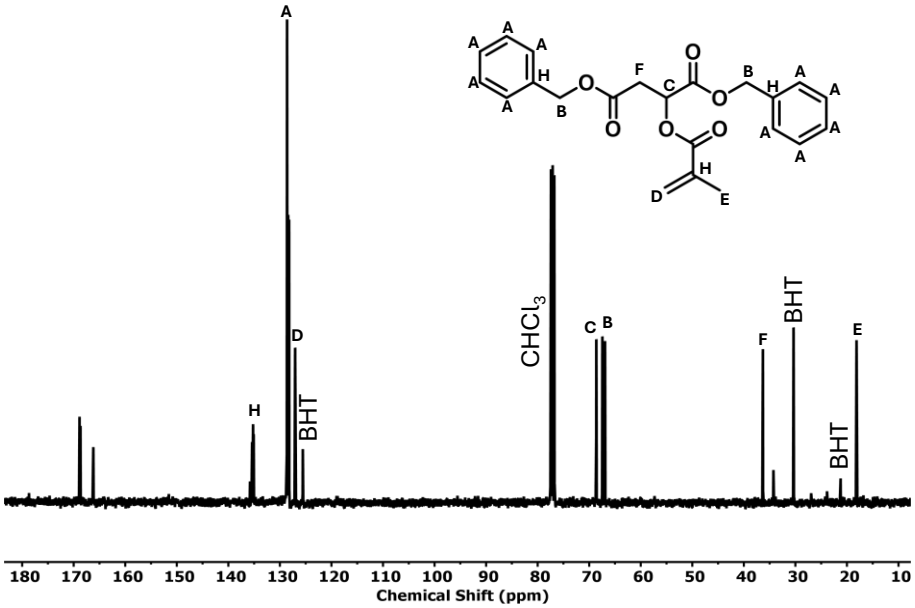

Figure S9: ^{13}C-NMR spectrum (101 MHz, $CDCl_3$) of benzyl protected malic acid modified MA (MA-Mal-Bn).

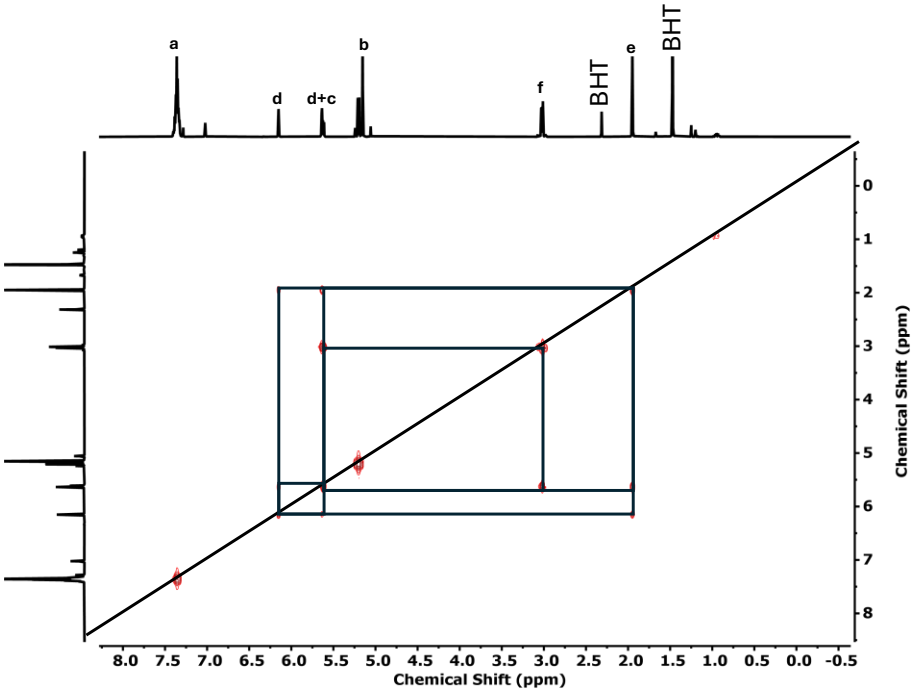

Figure S10: COSY spectrum (400 MHz, $CDCl_3$) of benzyl protected malic acid modified MA (MA-Mal-Bn).

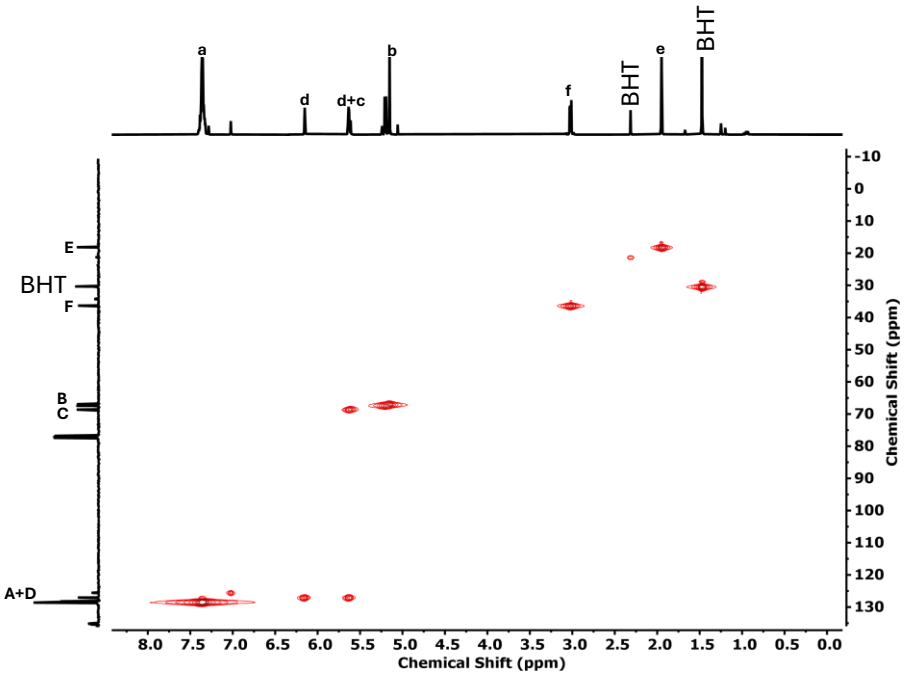

Figure S11: HSQC spectrum (400 MHz, $CDCl_3$) of benzyl protected malic acid modified MA (MA-Mal-Bn).

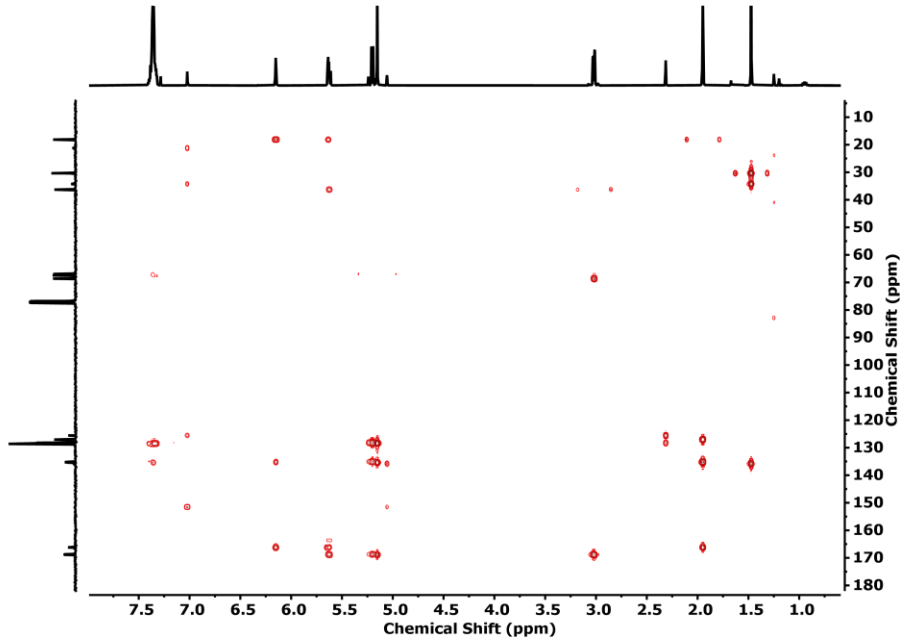

Figure S12: HMBC spectrum (400 MHz, $CDCl_3$) of benzyl protected malic acid modified MA (MA-Mal-Bn).

4. Homopolymer characterization

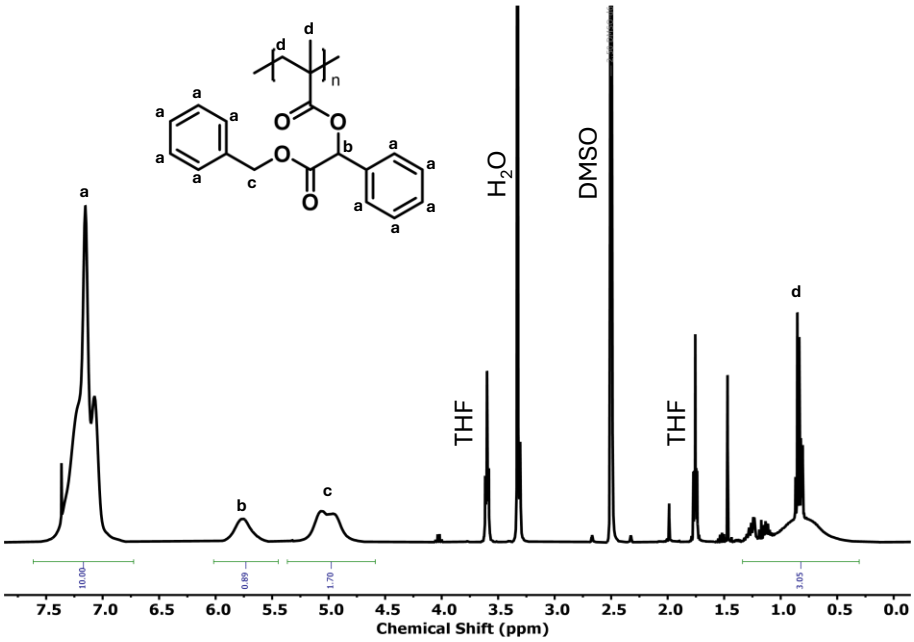

Figure S13: ^{1}H-NMR spectrum (400 MHz, $CDCl_3$) of P(MA-Mand-Bn).

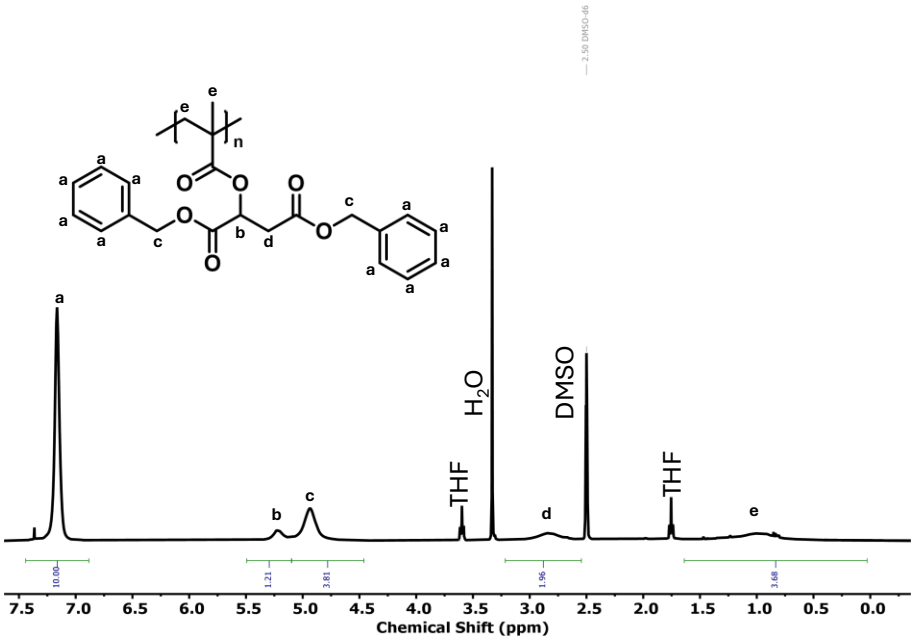

Figure S14: ^{1}H-NMR spectrum (400 MHz, $CDCl_3$) of P(MA-Mal-Bn).

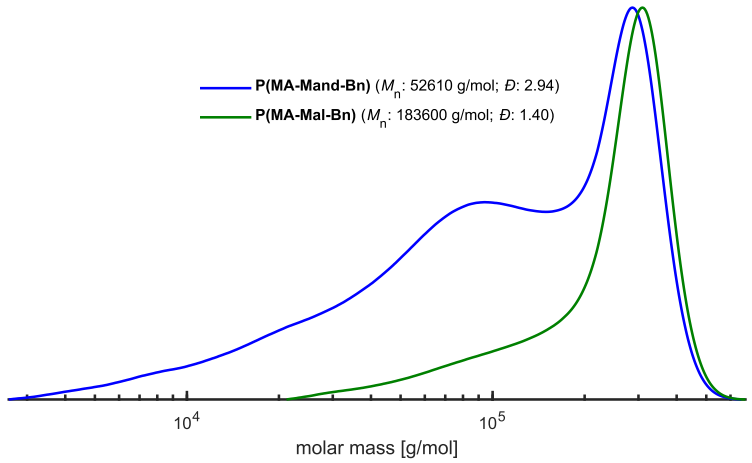

Figure S15: SEC curves (DMF, PMMA calibration) for the homopolymers P(MA-Mand-Bn) and P(MA-Mal-Bn).

5. Copolymer characterization

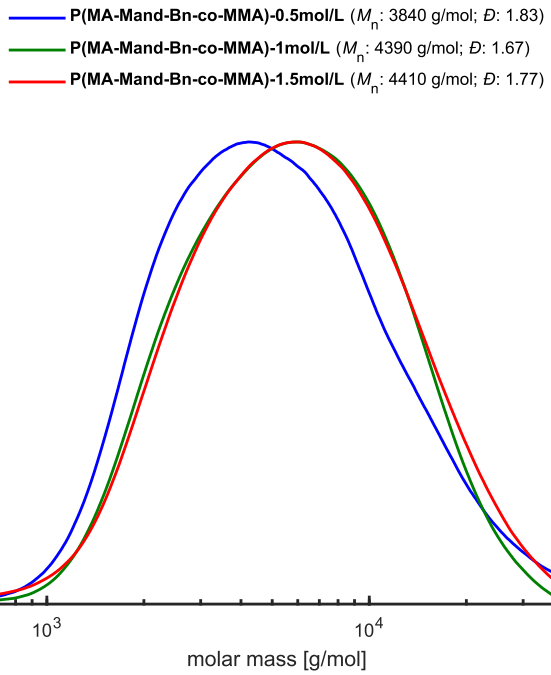

Figure S16: SEC curves (DMF, PMMA calibration) for the copolymer P(MA-Mand-Bn-co-MMA) in a 1:1 ratio, synthesized with 5 wt% DMPA at different monomer concentrations.

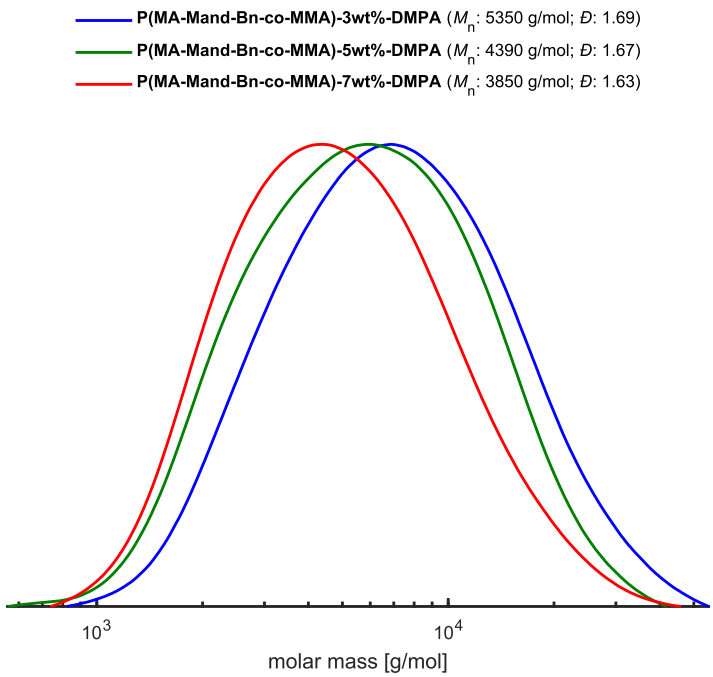

Figure S17: SEC curves (DMF, PMMA calibration) for the copolymer P(MA-Mand-Bn-co-MMA) in a 1:1 ratio, synthesized at 1 mol/L monomer concentration and varying DMPA concentrations.

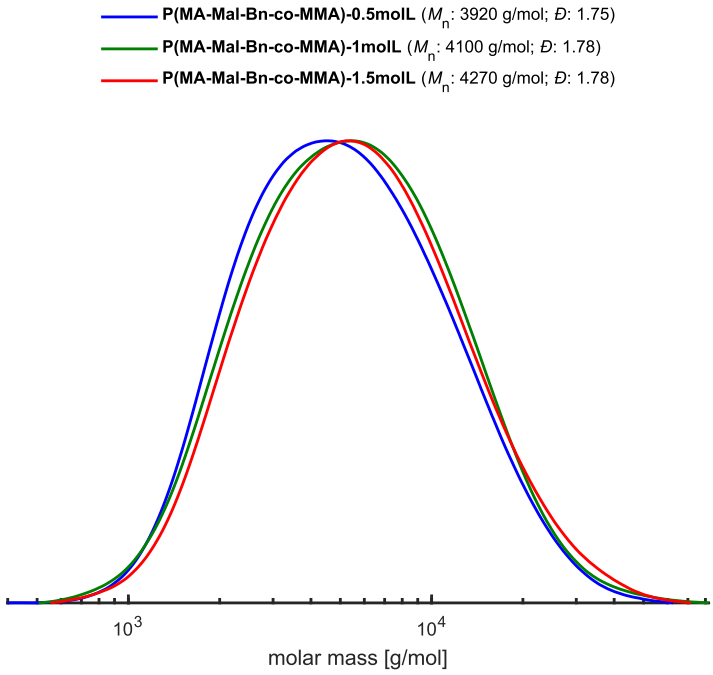

Figure S18: SEC curves (DMF, PMMA calibration) for the copolymer P(MA-Mal-Bn-co-MMA) in a 1:1 ratio, synthesized with 5 wt% DMPA at different monomer concentrations.

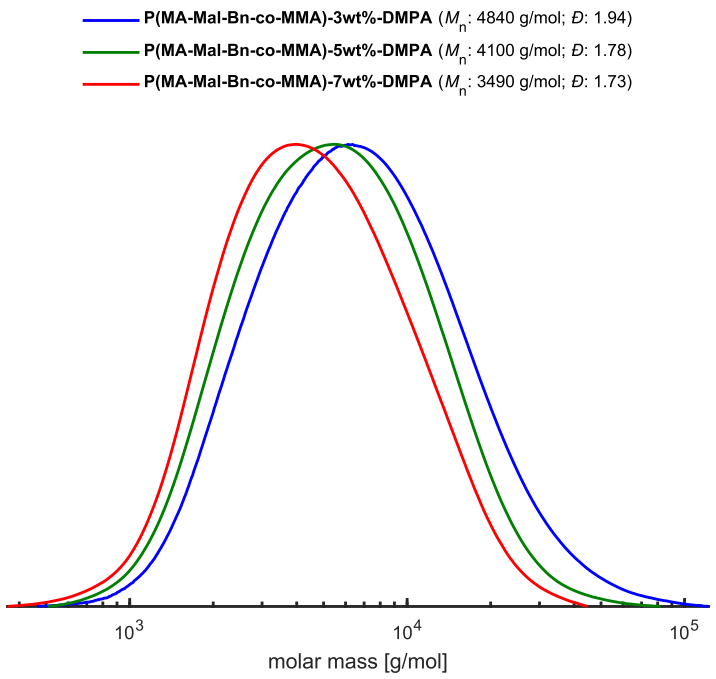

Figure S19: SEC curves (DMF, PMMA calibration) for the copolymer P(MA-Mal-Bn-co-MMA) in a 1:1 ratio, synthesized at 1 mol/L monomer concentration and varying DMPA concentrations.

Table S1: Results of the copolymerization of P(MA-Mand-Bn-co-MMA) using 5 wt% DMPA initiator at different monomer concentration, using a PMMA calibration.

		DMF SEC	
Monomer concentration / (mol/l)	**Yield / (%)**	**M_n / (10^3 g/mol)**	**Đ**
0.5	60	3.8	1.83
1	78	4.4	1.67
1.5	82	4.4	1.77

Table S2: Results of the copolymerization of P(MA-Mand-Bn-co-MMA) using different amounts of DMPA initiator at a monomer concentration of 1.0 mol/L, using a PMMA calibration.

		DMF SEC	
DMPA / (wt.%)	**Yield / (%)**	**M_n / (10^3 g/mol)**	**Đ**
3	68	5.4	1.69
5	78	4.4	1.67
7	82	3.9	1.63

Table S3: Results of the copolymerization of P(MA-Mal-Bn-co-MMA) using 5 wt% DMPA initiator at different monomer concentration, using a PMMA calibration.

		DMF SEC	
Monomer concentration / (mol/l)	**Yield / (%)**	**M_n / (10^3 g/mol)**	**Đ**
0.5	58	3.9	1.75
1	70	4.1	1.78
1.5	75	4.3	1.78

Table S4: Results of the copolymerization of P(MA-Mal-Bn-co-MMA) using different amounts of DMPA initiator at a monomer concentration of 1.0 mol/L, using a PMMA calibration.

		DMF SEC	
DMPA / (wt.%)	**Yield / (%)**	**M_n / (10^3 g/mol)**	**Đ**
3	48	4.8	1.94
5	70	4.1	1.78
7	74	3.5	1.73

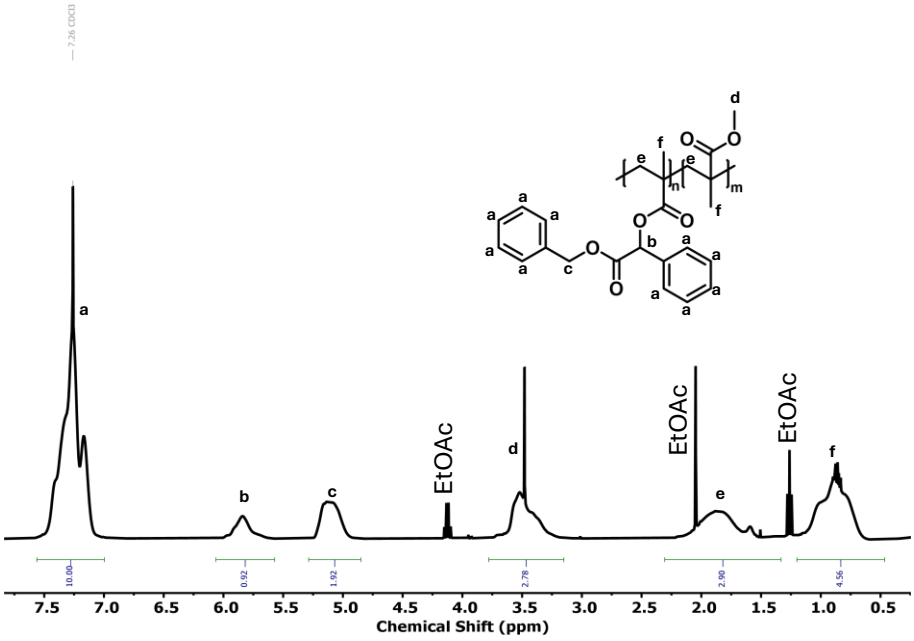

Figure S20: ^{1}H-NMR spectrum (400 MHz, $CDCl_3$) of P(MA-Mand-Bn-*co*-MMA).

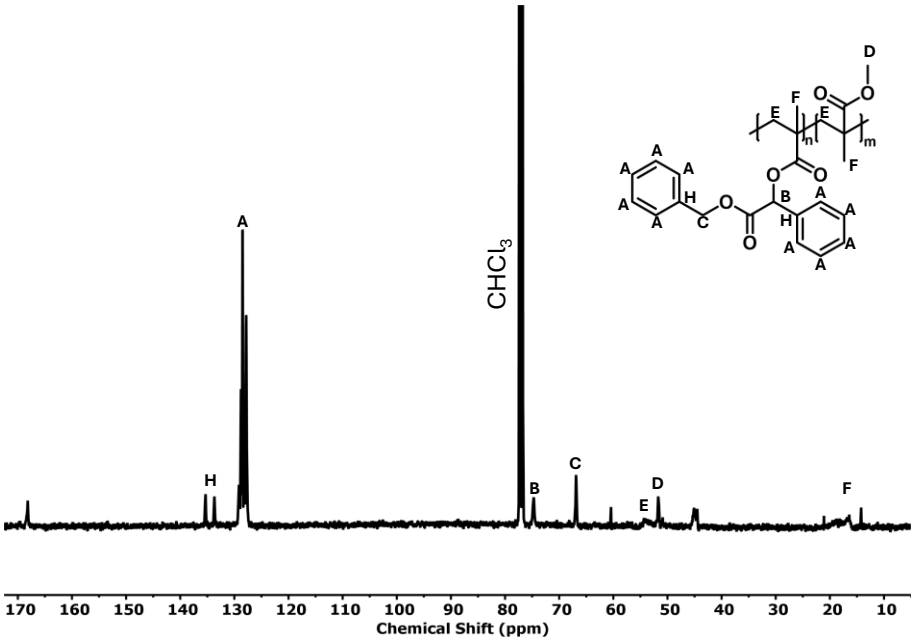

Figure S21: ^{13}C-NMR spectrum (101 MHz, $CDCl_3$) of P(MA-Mand-Bn-*co*-MMA).

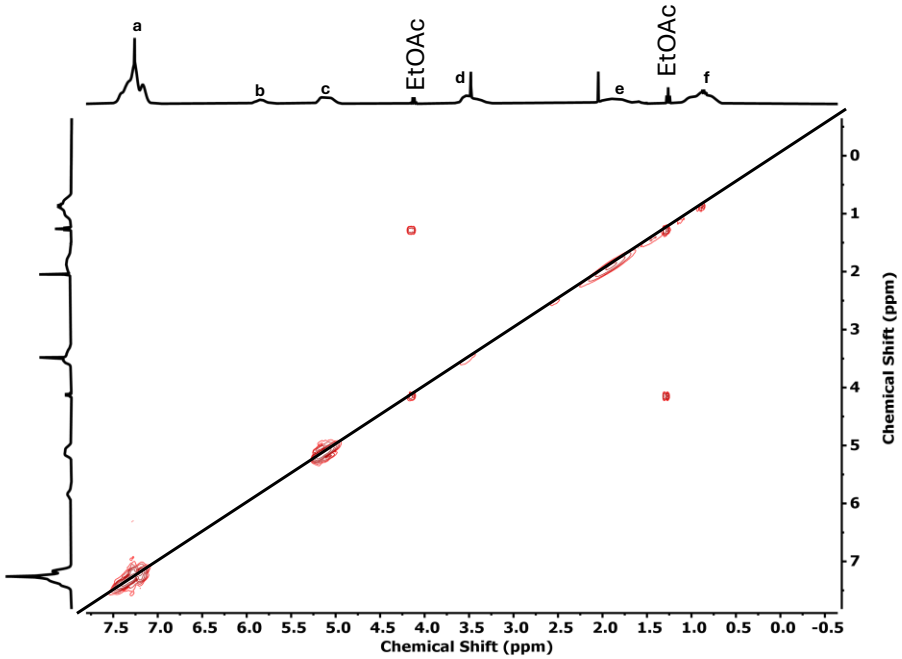

Figure S22: : COSY-NMR spectrum (400 MHz, $CDCl_3$) of P(MA-Mand-Bn-*co*-MMA).

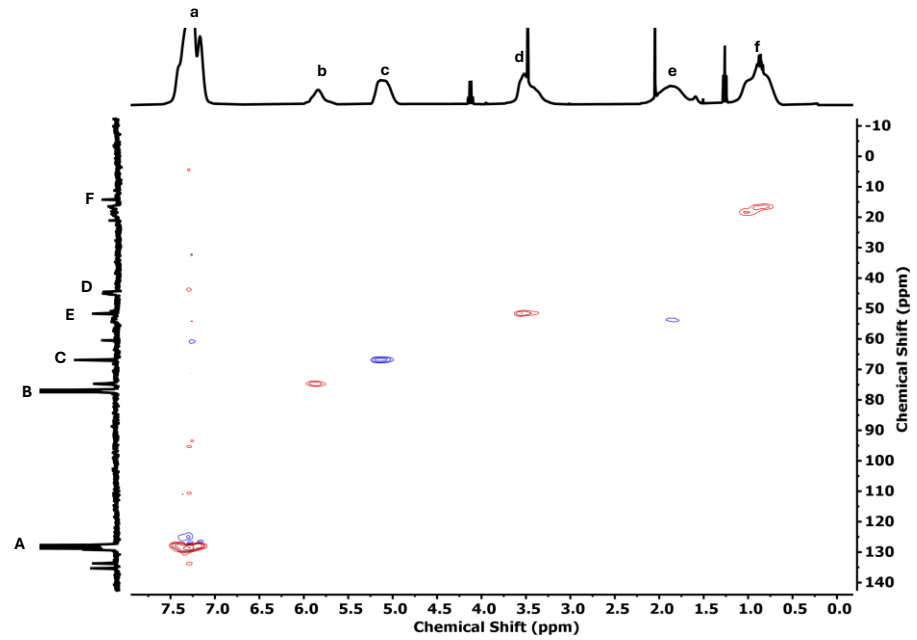

Figure S23: HSQC- NMR spectrum (400 MHz, $CDCl_3$) of P(MA-Mand-Bn-*co*-MMA).

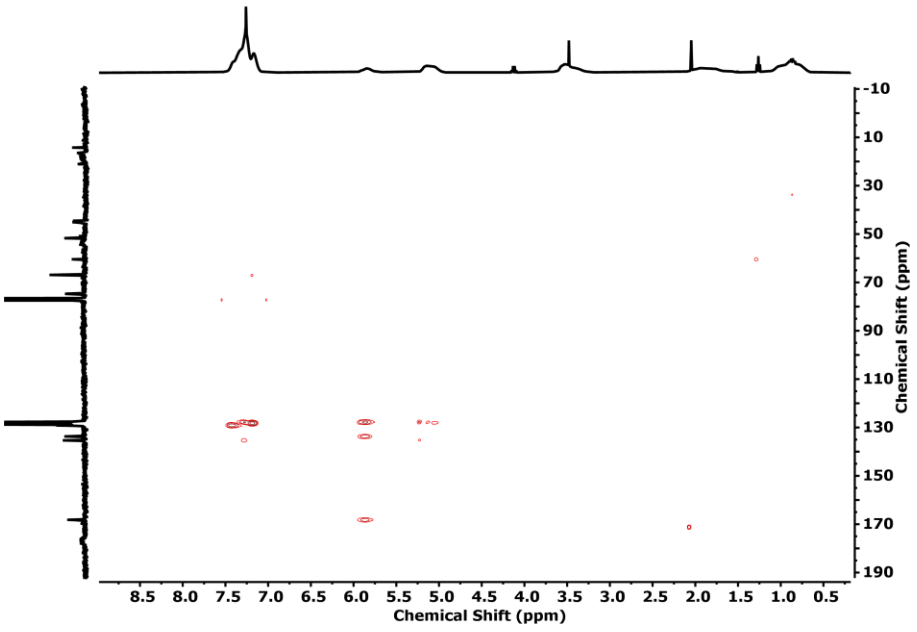

Figure S24: HMBC- NMR spectrum (400 MHz, $CDCl_3$) of P(MA-Mand-Bn-*co*-MMA).

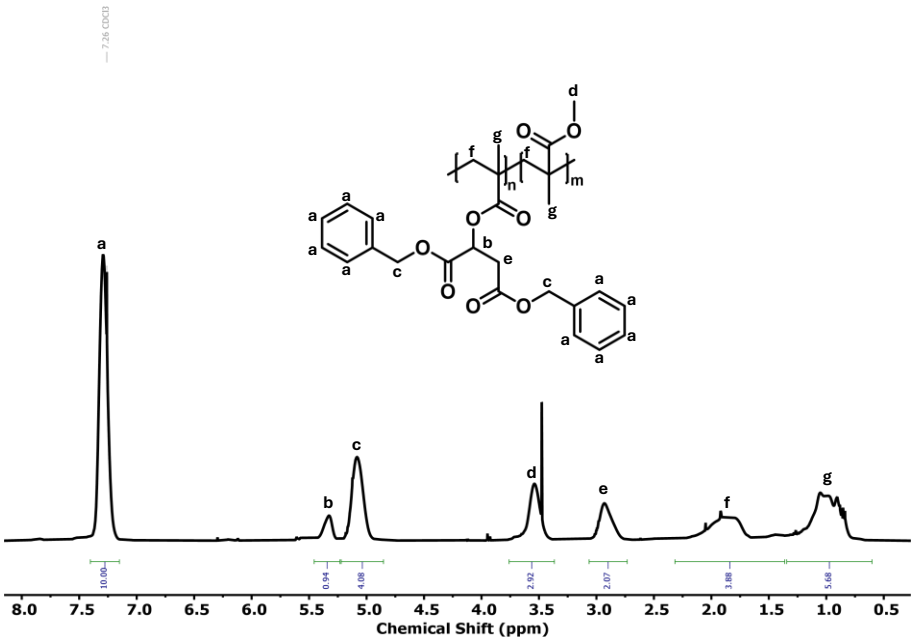

Figure S25: ^{1}H-NMR spectrum (400 MHz, $CDCl_3$) of P(MA-Mal-Bn-*co*-MMA).

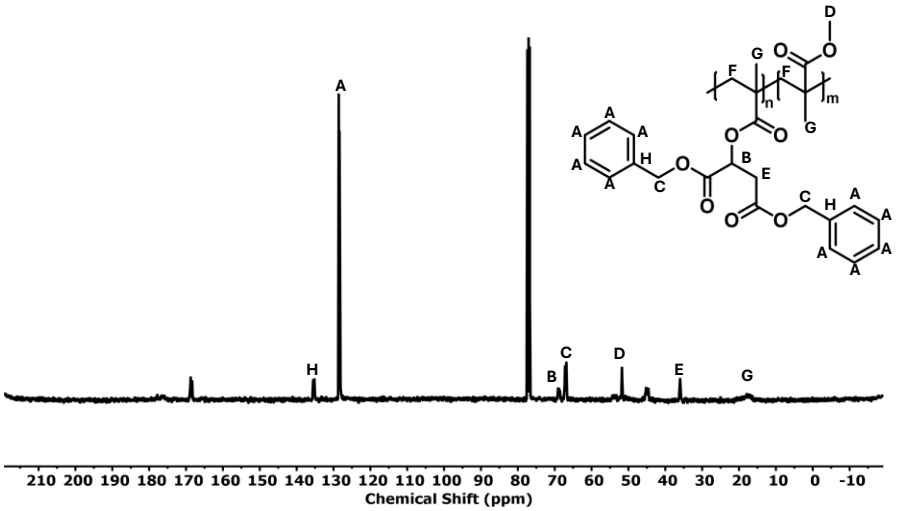

Figure S26: ^{13}C-NMR spectrum (101 MHz, $CDCl_3$) of P(MA-Mal-Bn-*co*-MMA).

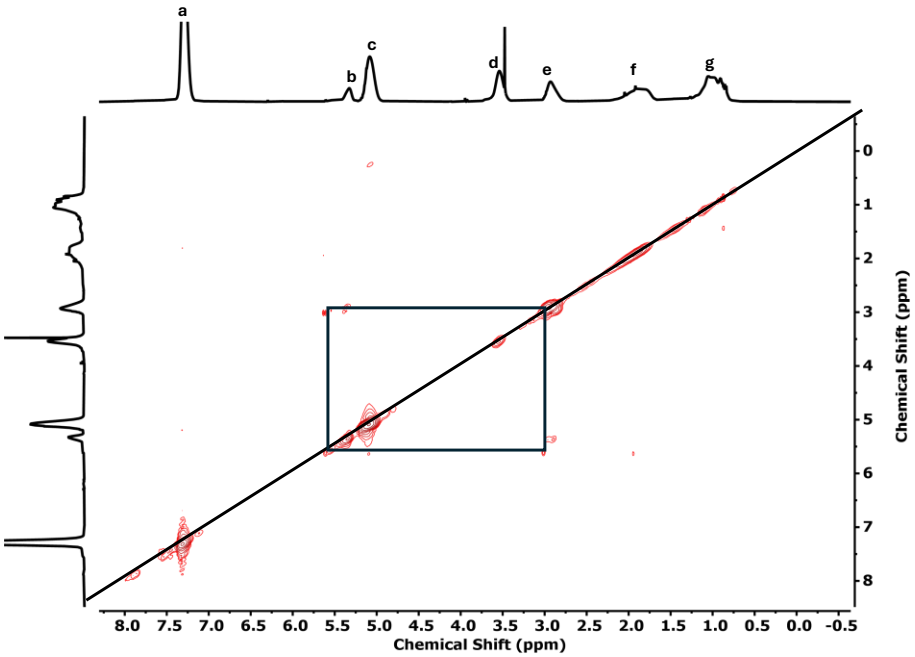

Figure S27: COSY-NMR spectrum (400 MHz, $CDCl_3$) of P(MA-Mal-Bn-*co*-MMA).

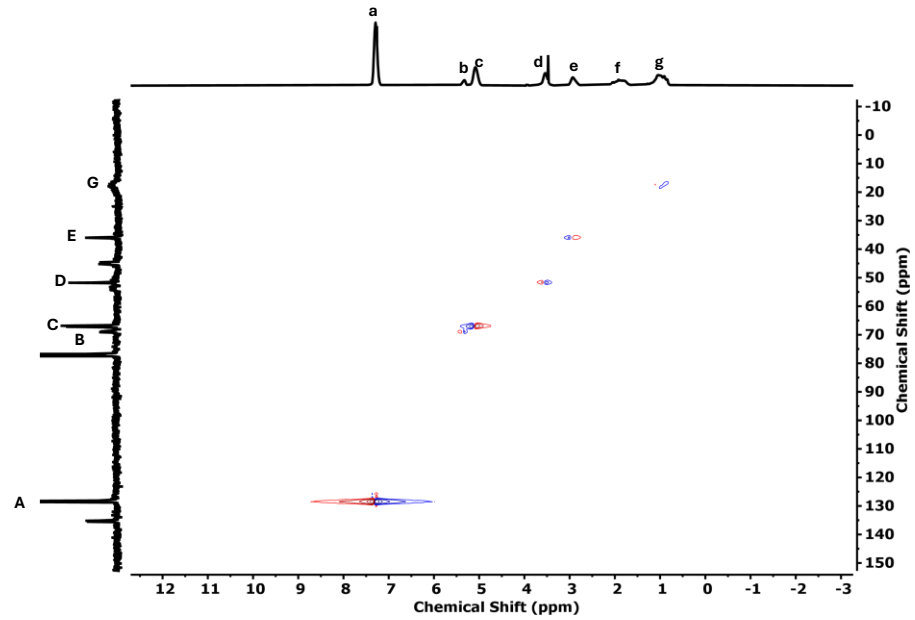

Figure S28: HSQC-NMR spectrum (400 MHz, $CDCl_3$) of P(MA-Mal-Bn-*co*-MMA).

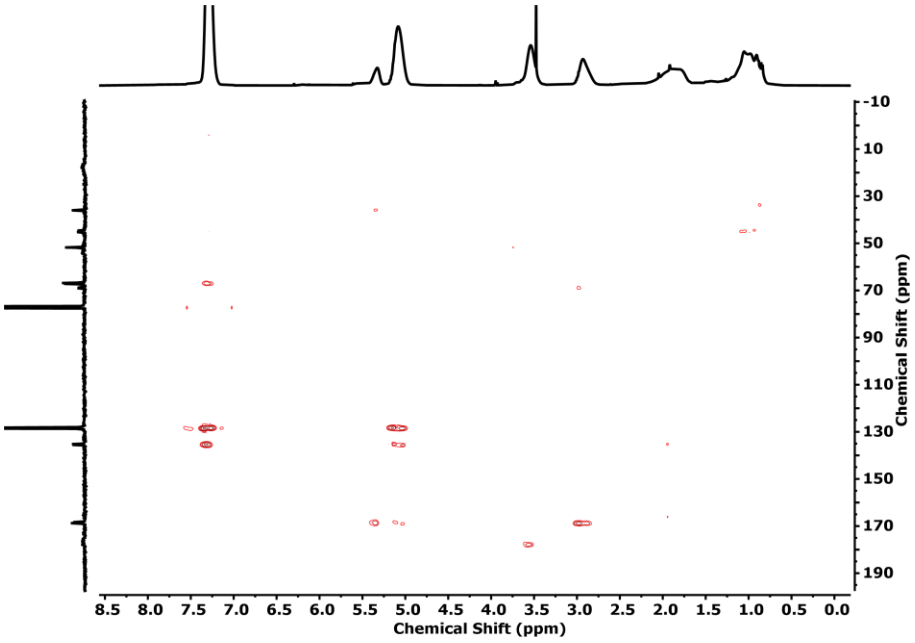

Figure S29: HMBC-NMR spectrum (400 MHz, $CDCl_3$) of P(MA-Mal-Bn-*co*-MMA).

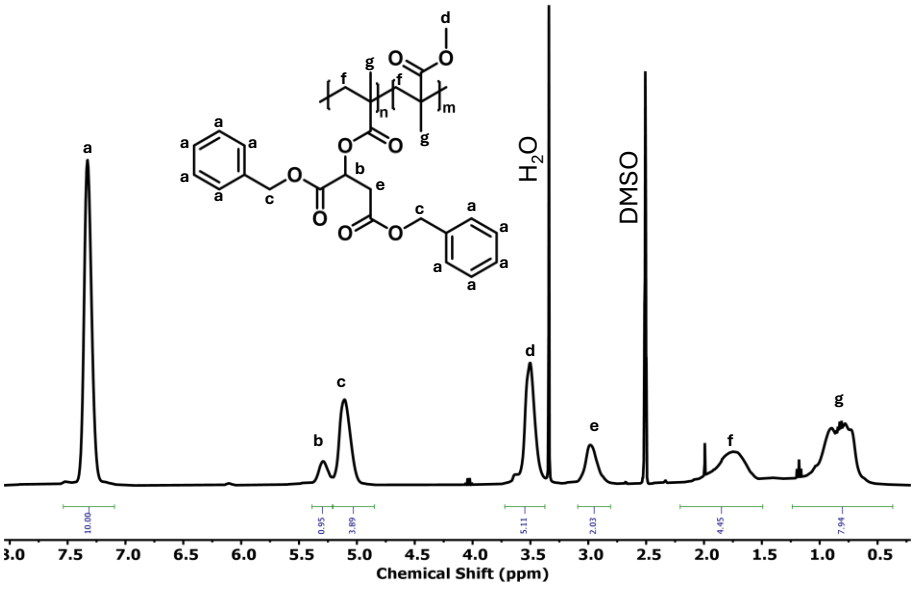

Figure S30: ^{1}H-NMR spectrum (400 MHz, DMSO-d_6) of P(MA-Mal-Bn_1-*co*-MMA_2).

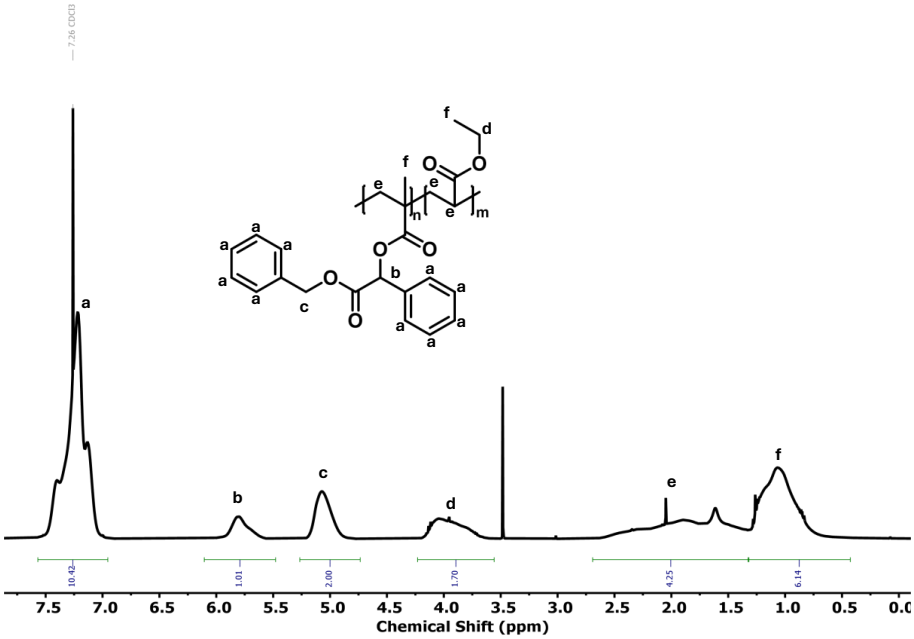

Figure S31: ^{1}H-NMR spectrum (400 MHz, $CDCl_3$) of P(MA-Mand-Bn-*co*-EA).

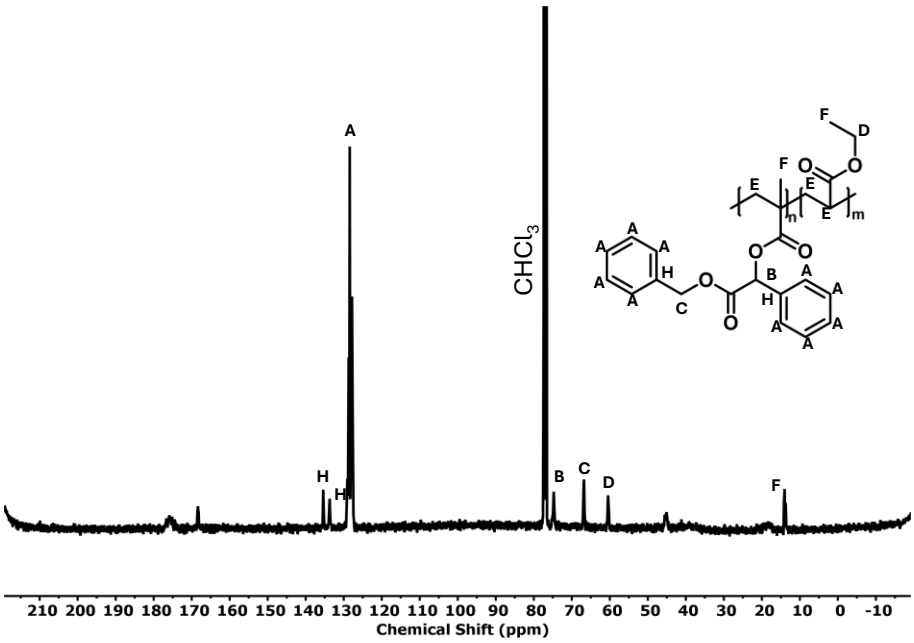

Figure S32: ^{13}C-NMR spectrum (101 MHz, $CDCl_3$) of P(MA-Mand-Bn-*co*-EA).

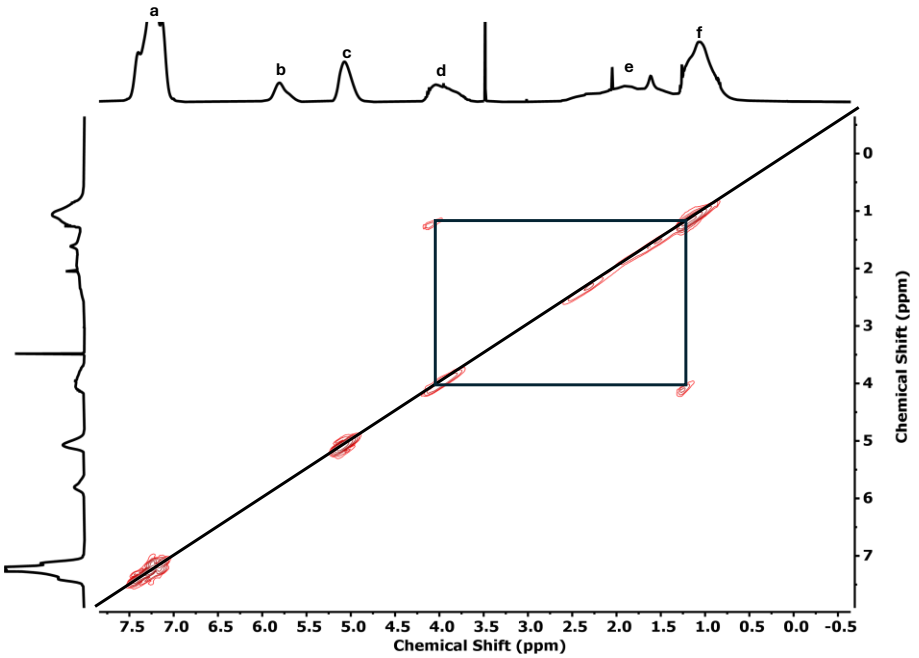

Figure S33: COSY-NMR spectrum (400 MHz, $CDCl_3$) of P(MA-Mand-Bn-*co*-EA).

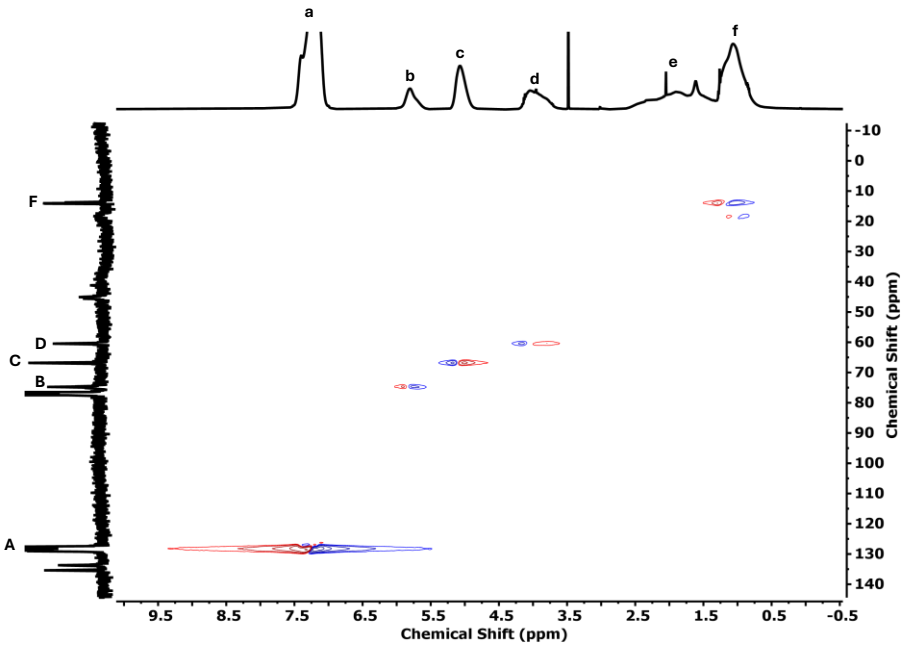

Figure S34: HSQC-NMR spectrum (400 MHz, $CDCl_3$) of P(MA-Mand-Bn-*co*-EA).

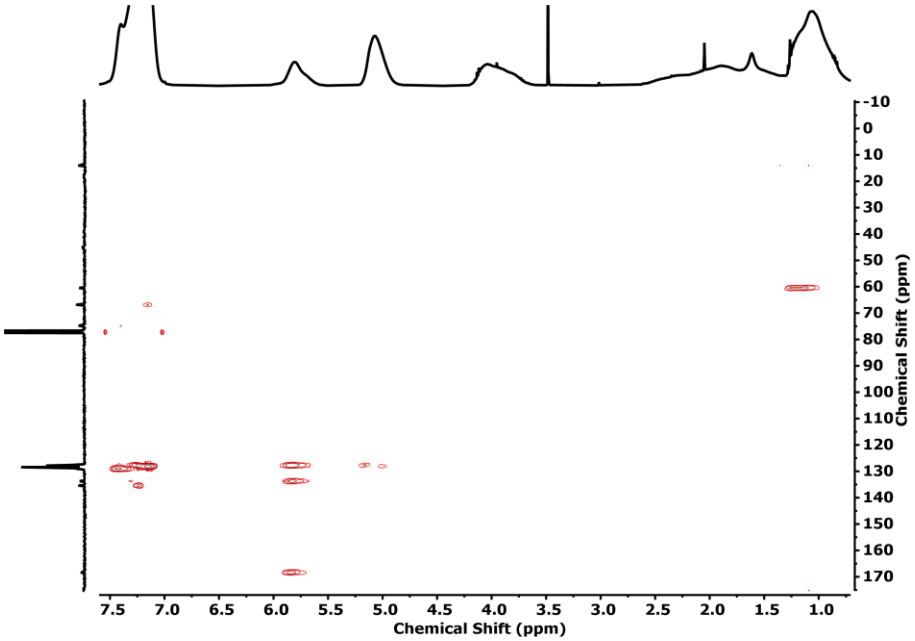

Figure S35: HMBC-NMR spectrum (400 MHz, $CDCl_3$) of P(MA-Mand-Bn-*co*-EA).

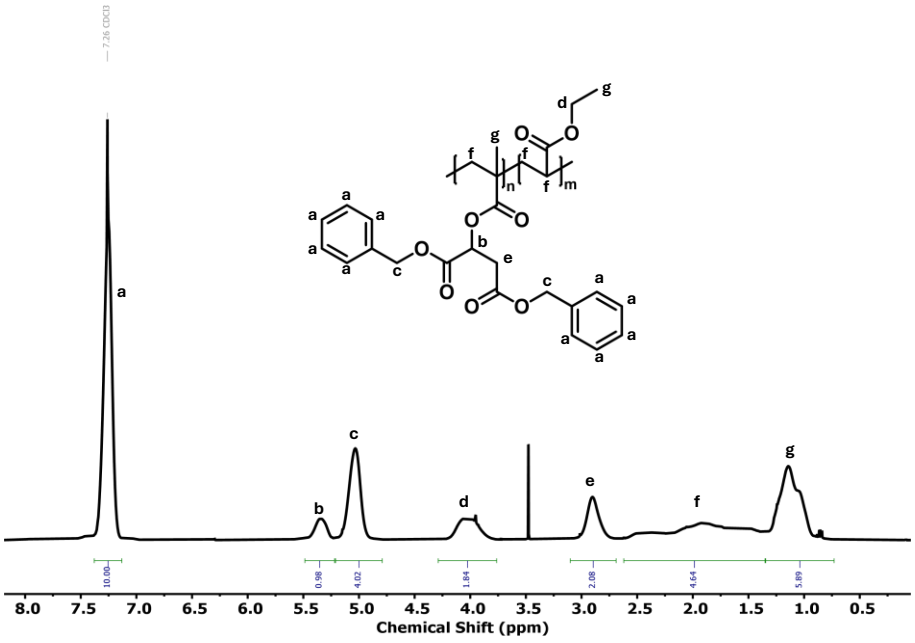

Figure S36: ^{1}H-NMR spectrum (400 MHz, $CDCl_3$) of P(MA-Mal-Bn-*co*-EA).

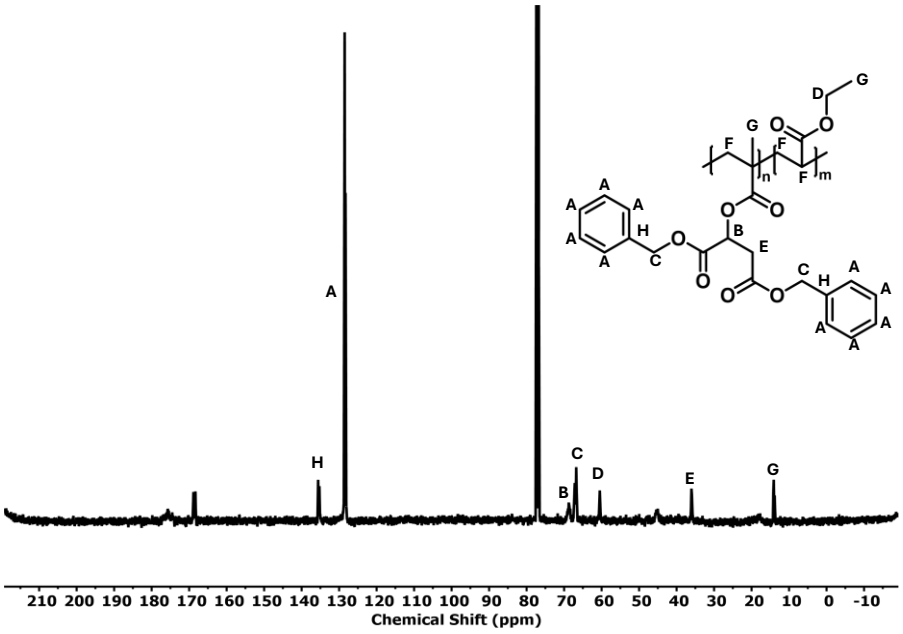

Figure S37: ^{13}C-NMR spectrum (101 MHz, $CDCl_3$) of P(MA-Mal-Bn-*co*-EA).

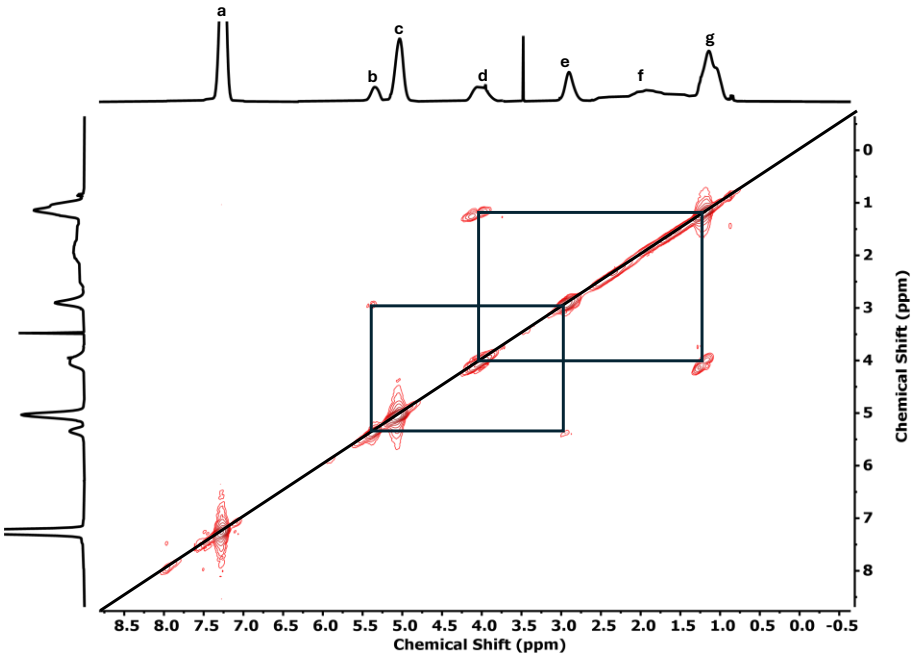

Figure S38: COSY-NMR spectrum (400 MHz, $CDCl_3$) of P(MA-Mal-Bn-*co*-EA).

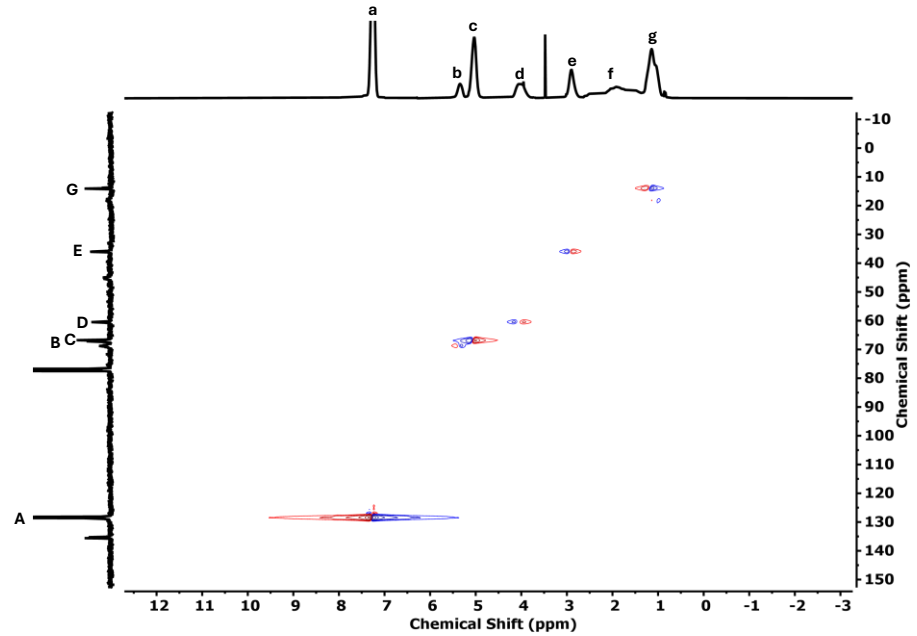

Figure S39: HSQC-NMR spectrum (400 MHz, $CDCl_3$) of P(MA-Mal-Bn-*co*-EA).

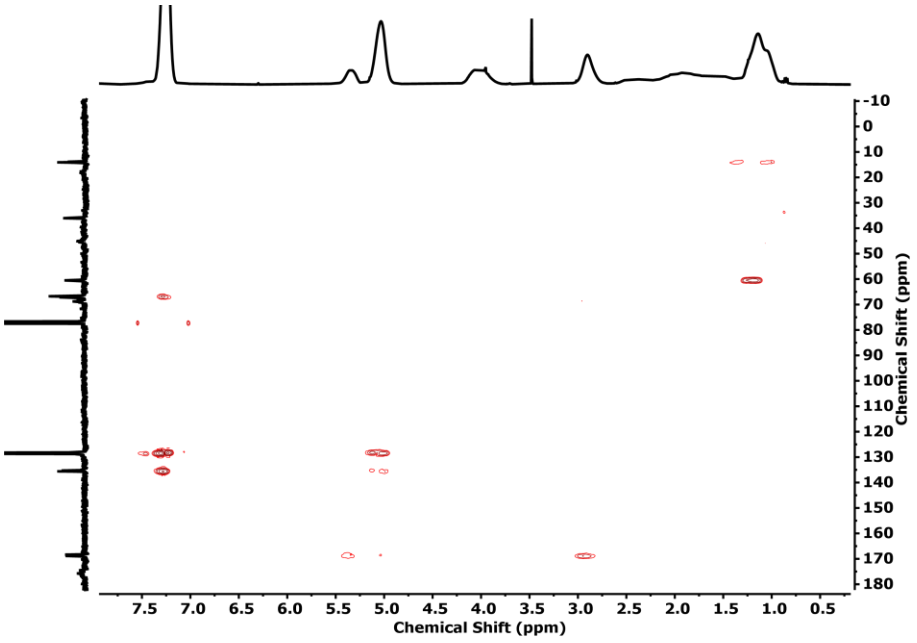

Figure S40: HMBC-NMR spectrum (400 MHz, $CDCl_3$) of P(MA-Mal-Bn-*co*-EA).

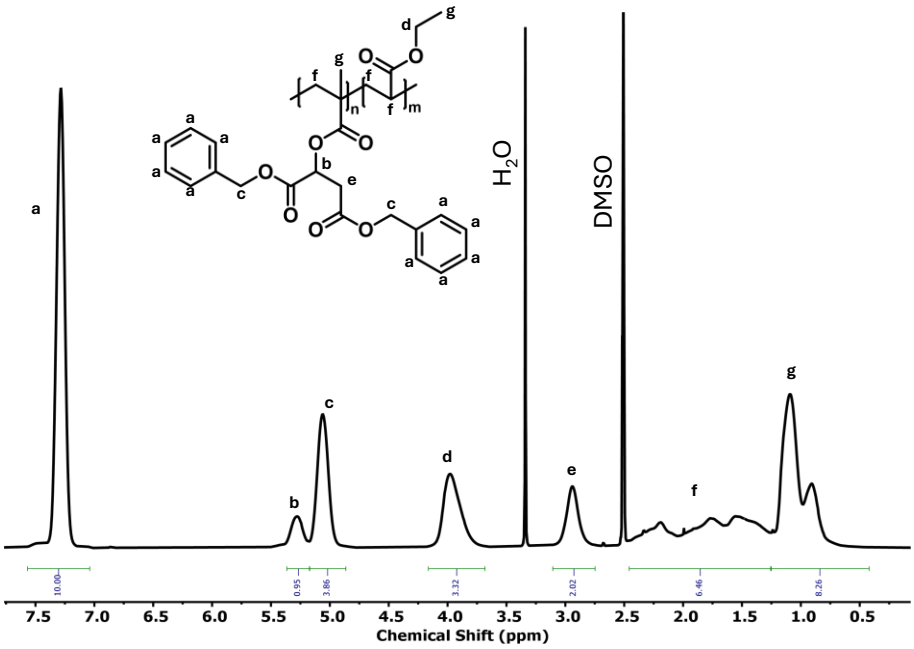

Figure S41: ^{1}H-NMR spectrum (400 MHz, DMSO-d_6) of P(MA-Mal-Bn$_1$-*co*-EA$_2$).

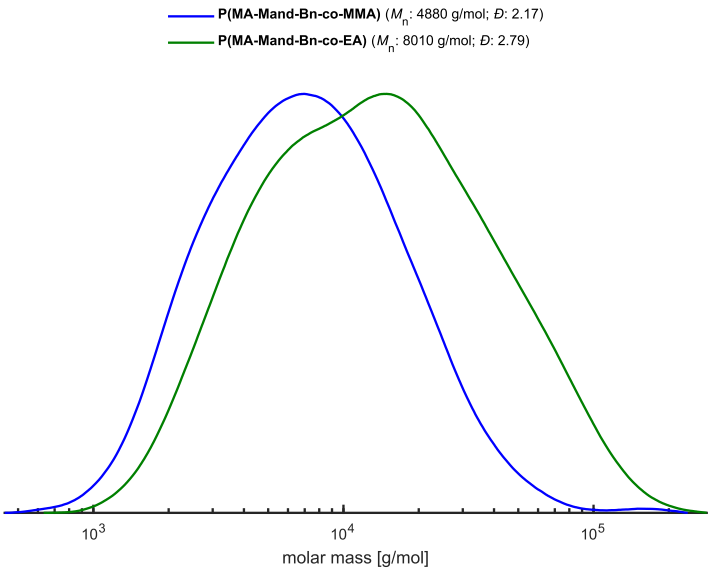

Figure S42: SEC curves (DMF, PMMA calibration) for the copolymer P(MA-Mand-Bn-*co*-X) synthesized in a 1:1 ratio with 5 wt% DMPA at 1 mol/L monomer concentration.

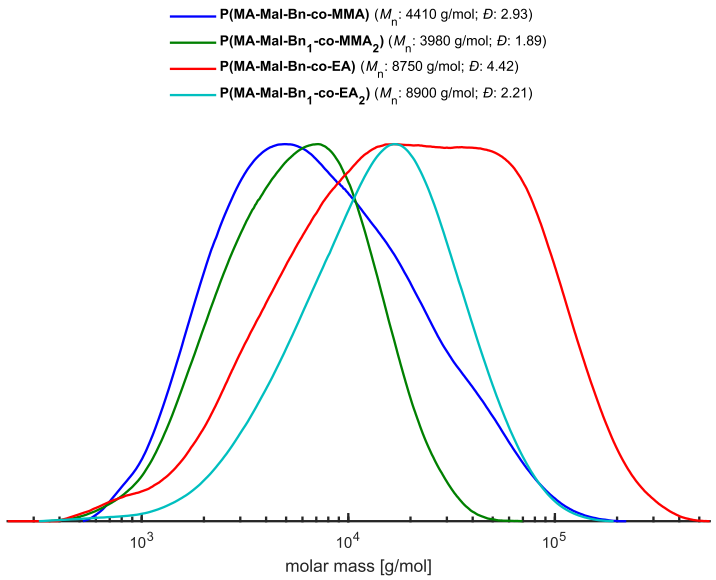

Figure S43: SEC curves (DMF, PMMA calibration) for the copolymer P(MA-Mal-Bn-*co*-X) synthesized in a 1:1 and 1:2 ratio with 5 wt% DMPA at 1 mol/L monomer concentration.

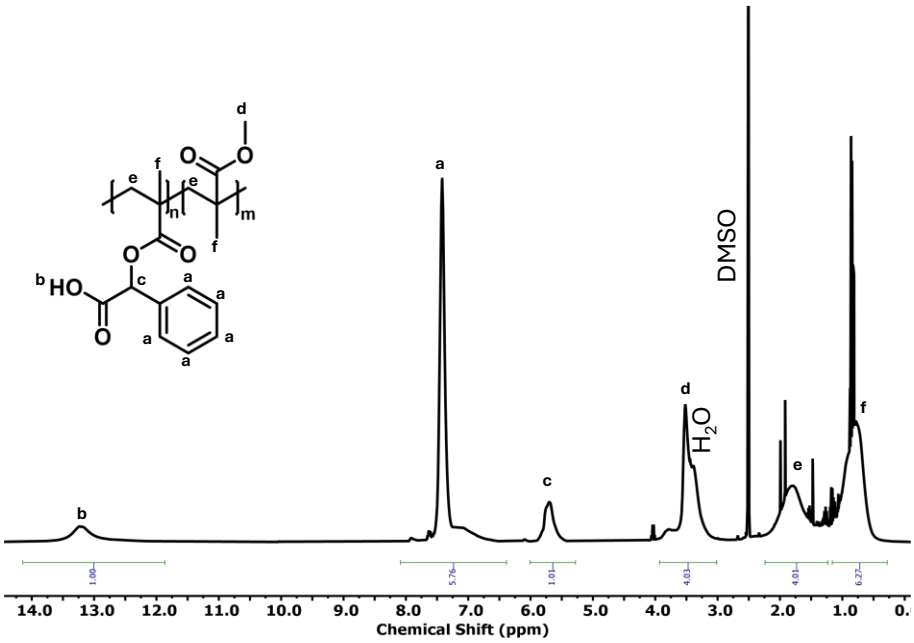

Figure S44: ^{1}H-NMR spectrum (400 MHz, DMSO-d_6) of P(MA-Mand-*co*-MMA).

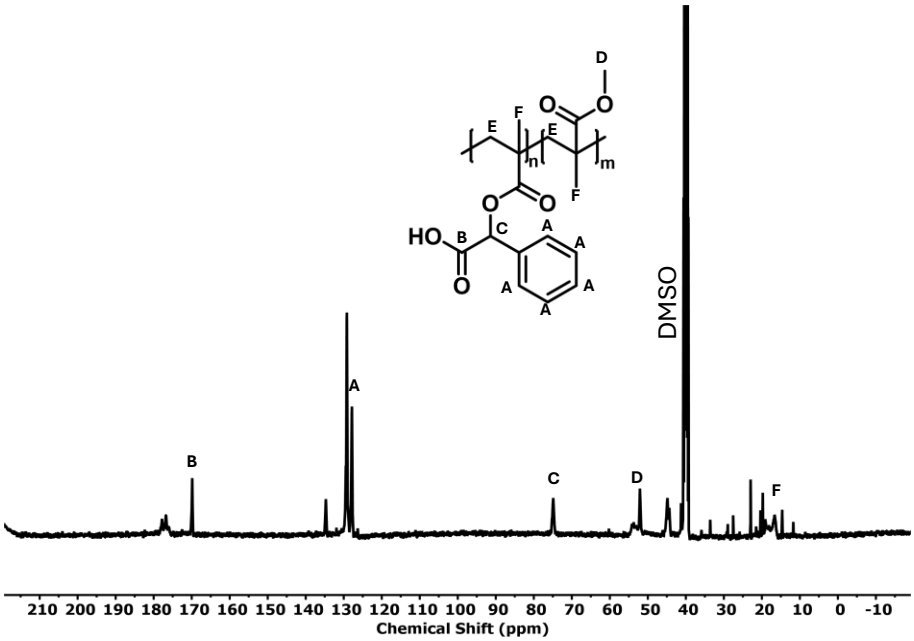

Figure S45: ^{13}C-NMR spectrum (101 MHz, DMSO-d_6) of P(MA-Mand-*co*-MMA).

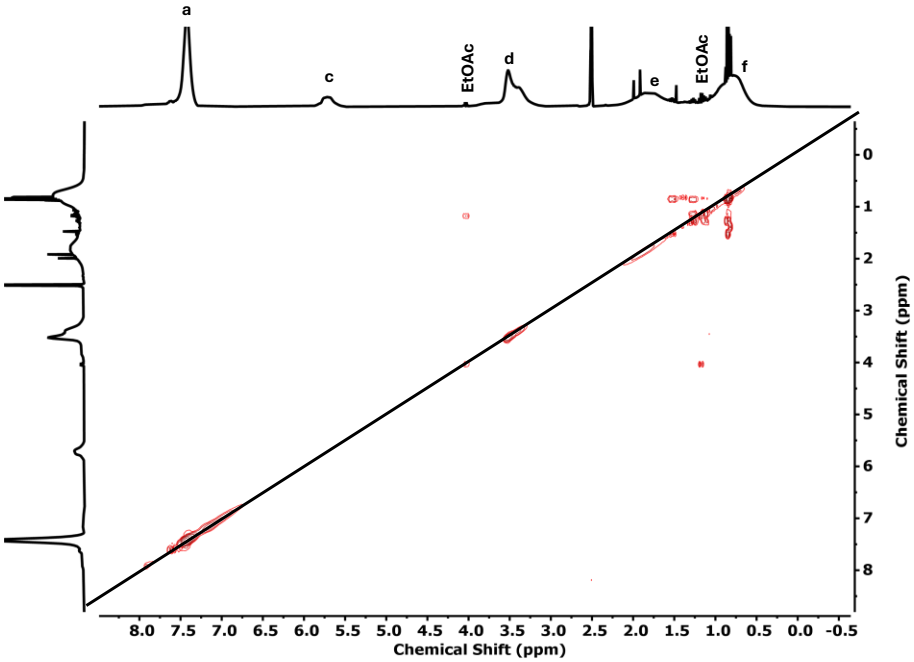

Figure S46: COSY-NMR spectrum (400 MHz, DMSO-d_6) of P(MA-Mand-*co*-MMA).

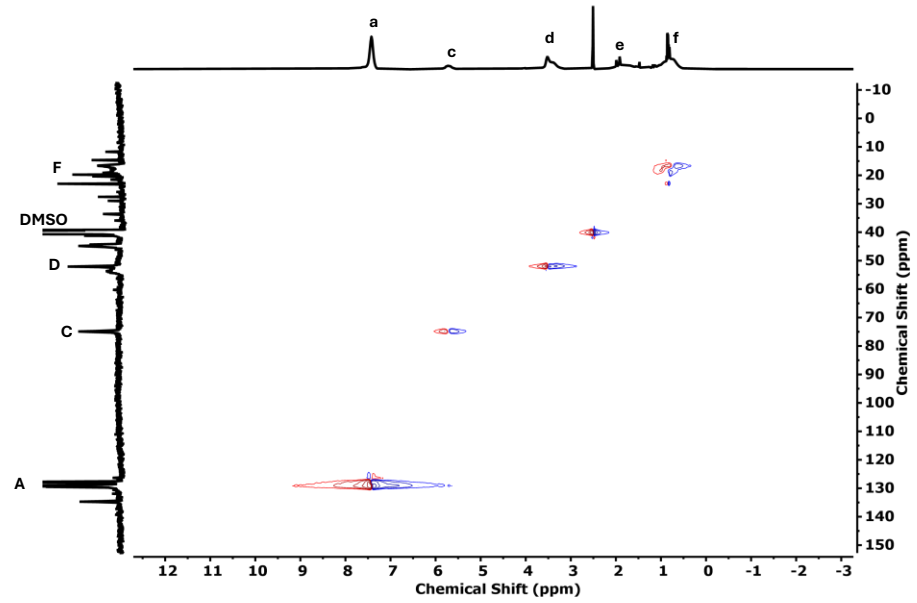

Figure S47: HSQC-NMR spectrum (400 MHz, DMSO-d_6) of P(MA-Mand-*co*-MMA).

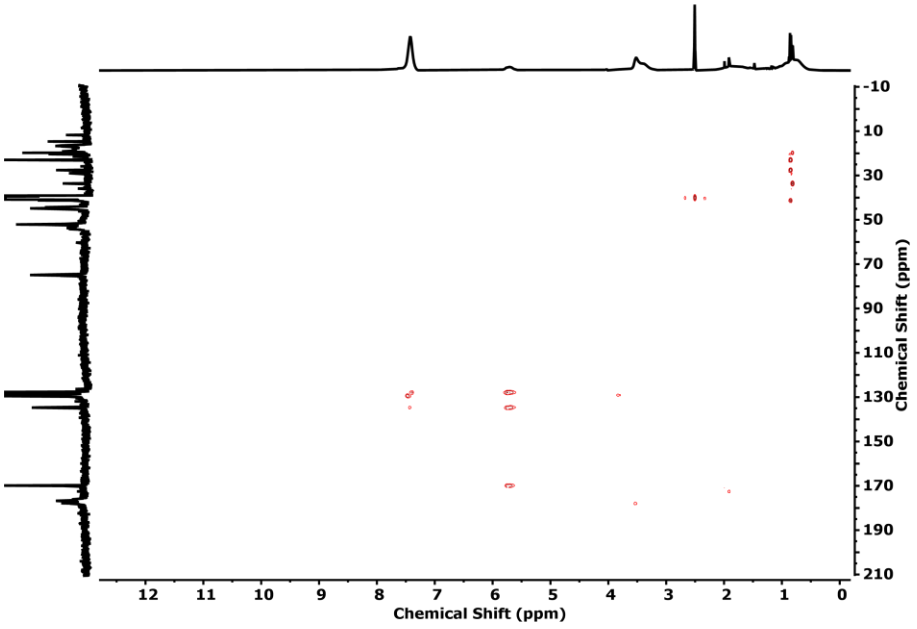

Figure S48: HMBC-NMR spectrum (400 MHz, DMSO-d_6) of P(MA-Mand-*co*-MMA).

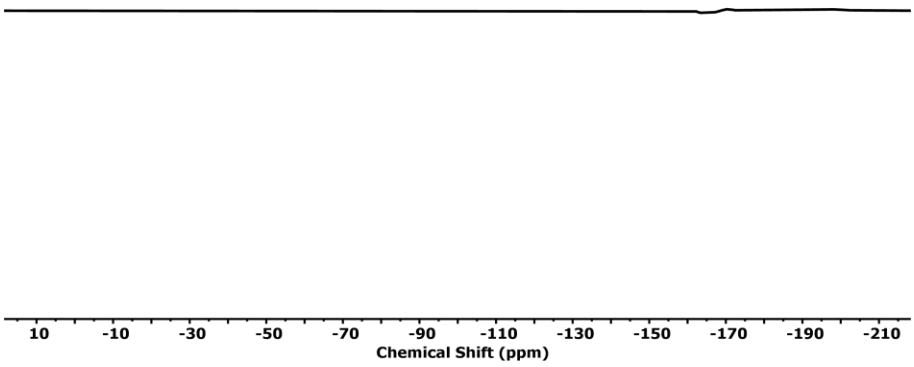

Figure S49: ^{19}F-NMR spectrum (400 MHz, DMSO-d_6) of P(MA-Mand-*co*-MMA).

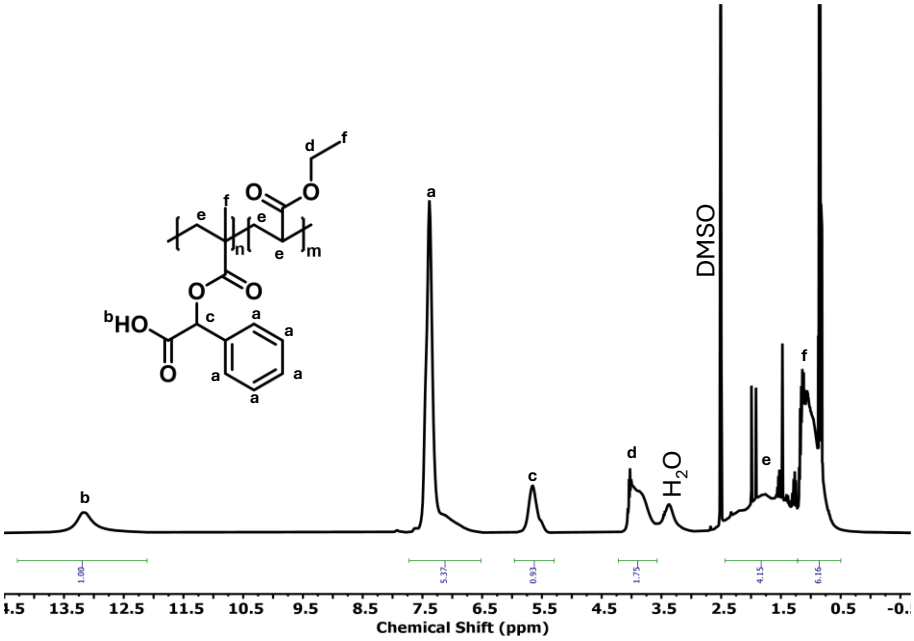

Figure S50: ^{1}H-NMR spectrum (400 MHz, DMSO-d_6) of P(MA-Mand-*co*-EA).

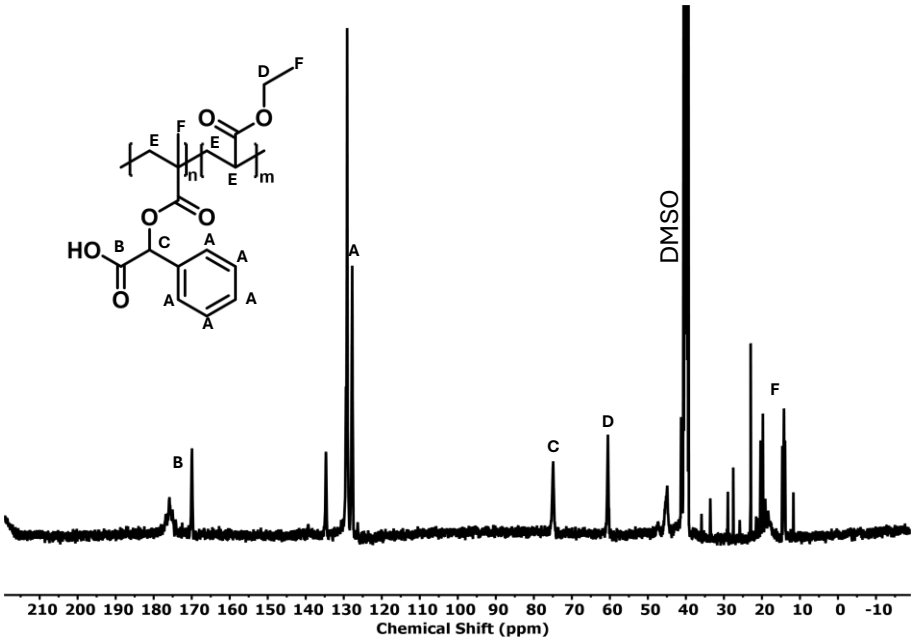

Figure S51: ^{13}C-NMR spectrum (101 MHz, DMSO-d_6) of P(MA-Mand-*co*-EA).

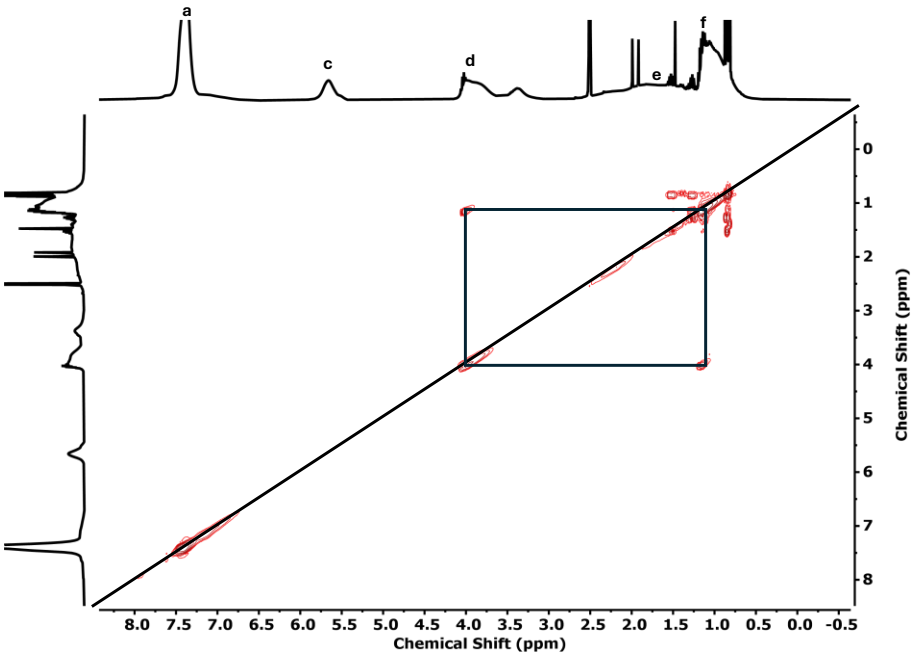

Figure S52: COSY-NMR spectrum (400 MHz, DMSO-d_6) of P(MA-Mand-*co*-EA).

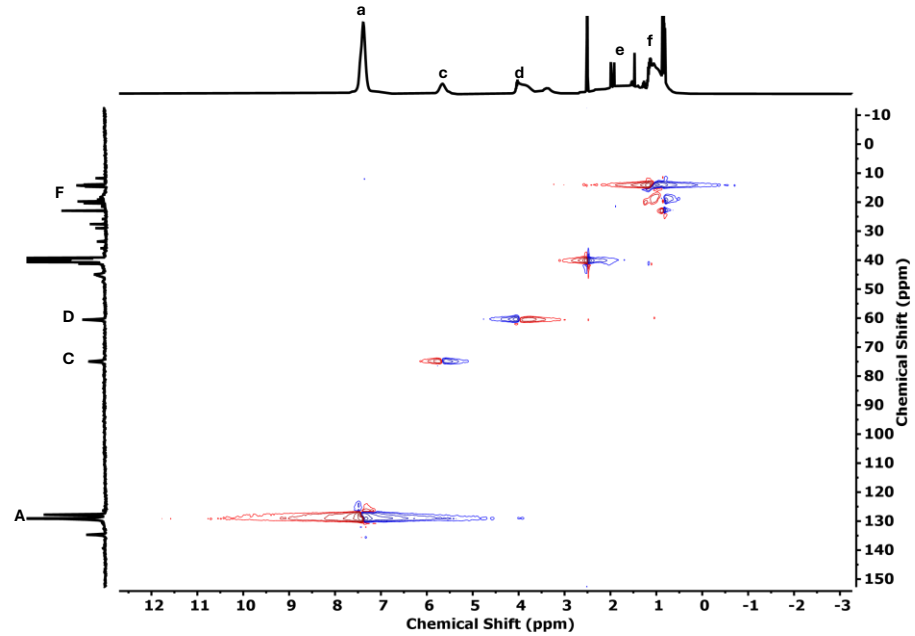

Figure S53: HSQC-NMR spectrum (400 MHz, DMSO-d_6) of P(MA-Mand-*co*-EA).

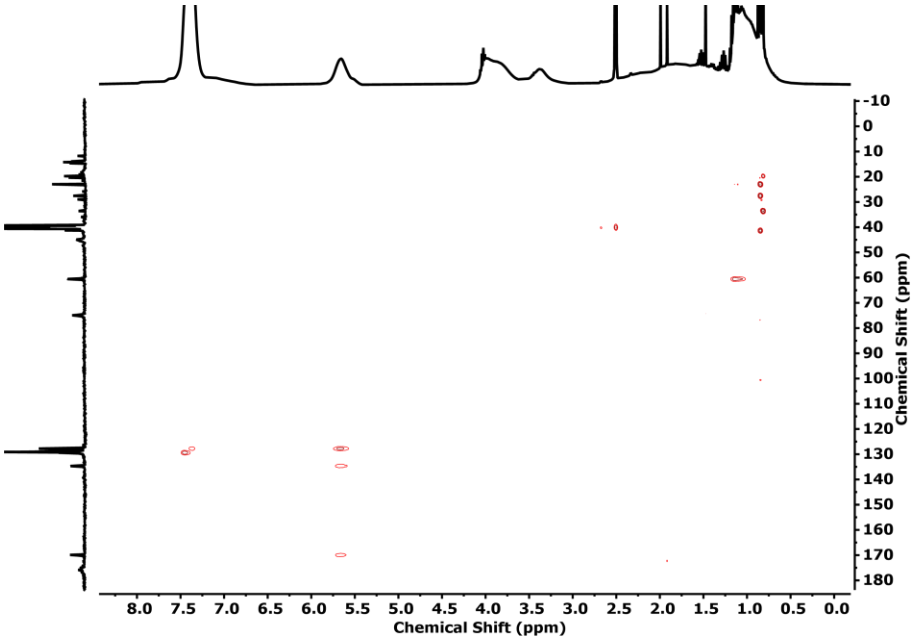

Figure S54: HMBC-NMR spectrum (400 MHz, DMSO-d_6) of P(MA-Mand-*co*-EA).

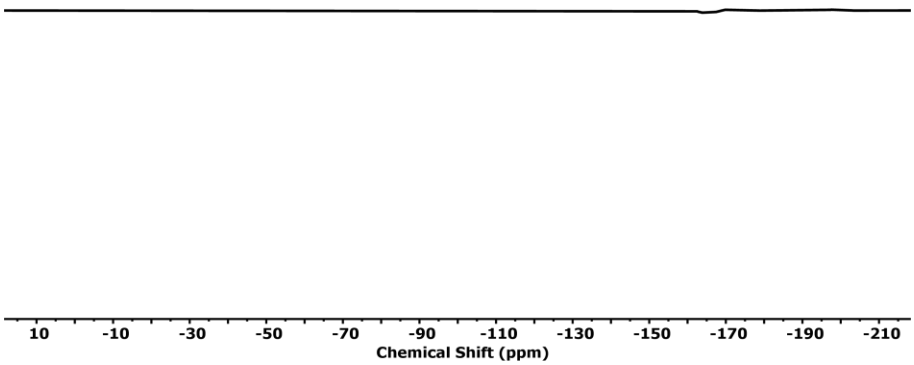

Figure S55: ^{19}F-NMR spectrum (400 MHz, DMSO-d_6) of P(MA-Mand-*co*-EA).

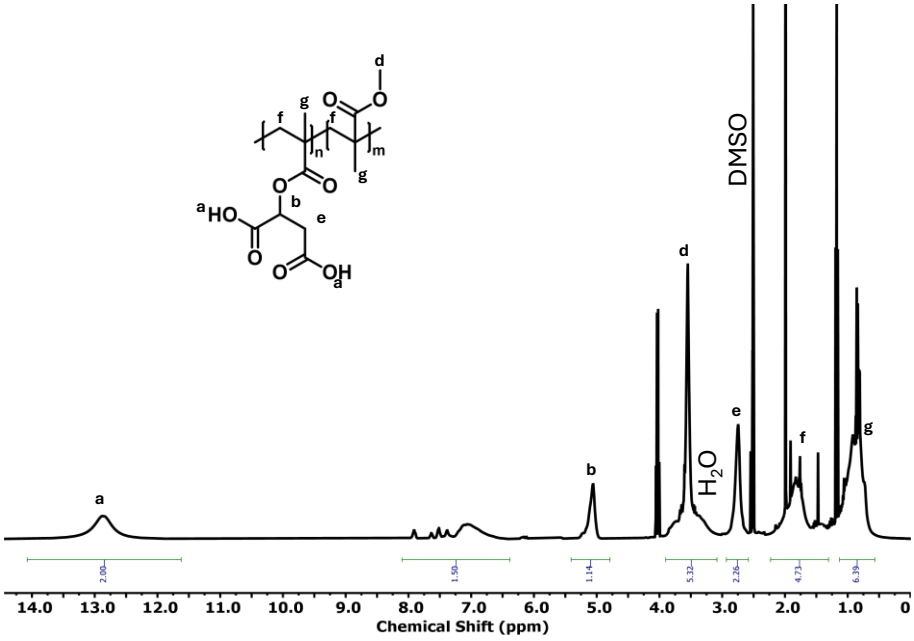

Figure S56: ^{1}H-NMR spectrum (400 MHz, DMSO-d_6) of P(MA-Mal-*co*-MMA).

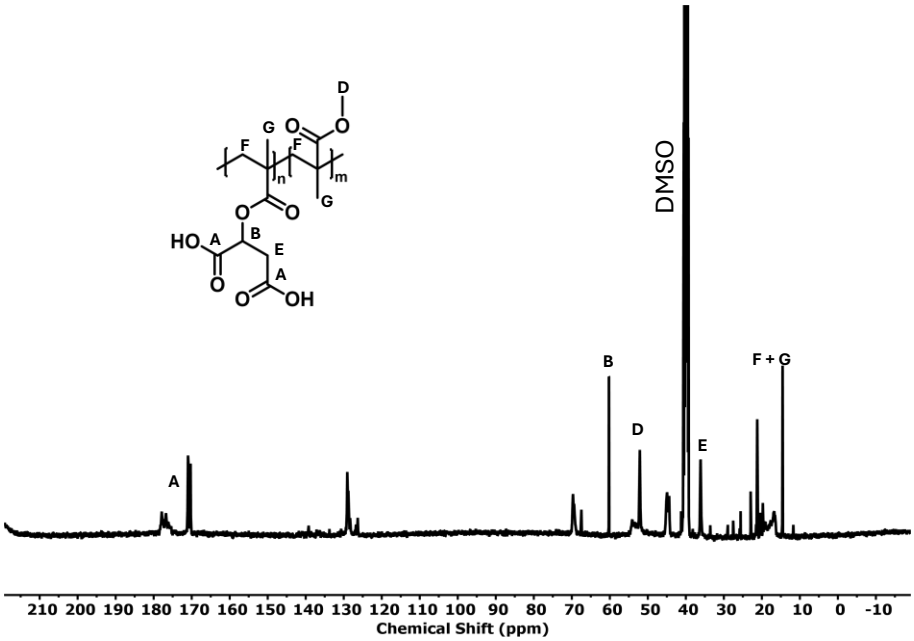

Figure S57: ^{13}C-NMR spectrum (101 MHz, DMSO-d_6) of P(MA-Mal-*co*-MMA).

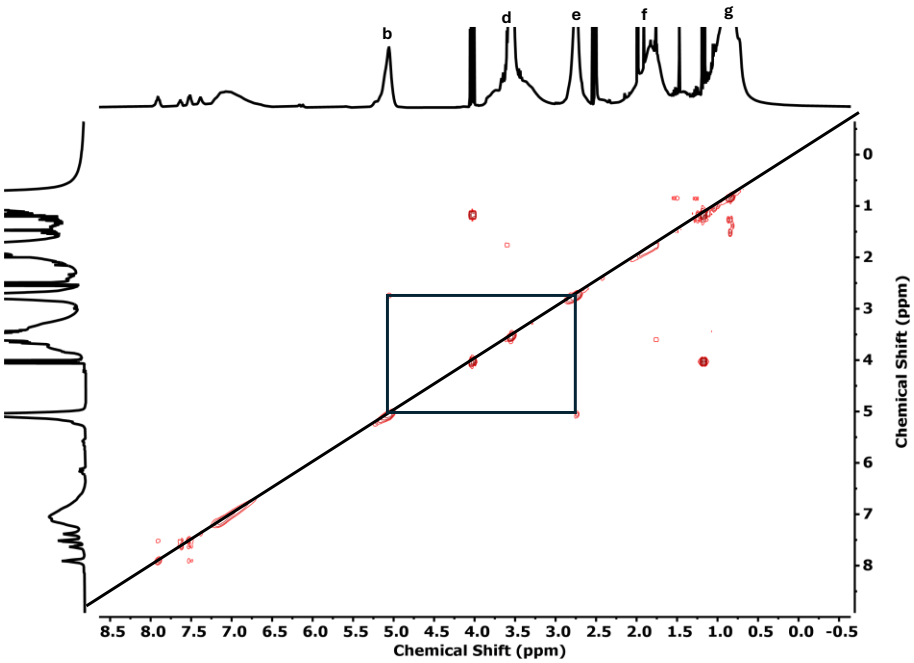

Figure S58: COSY-NMR spectrum (400 MHz, DMSO-d_6) of P(MA-Mal-*co*-MMA).

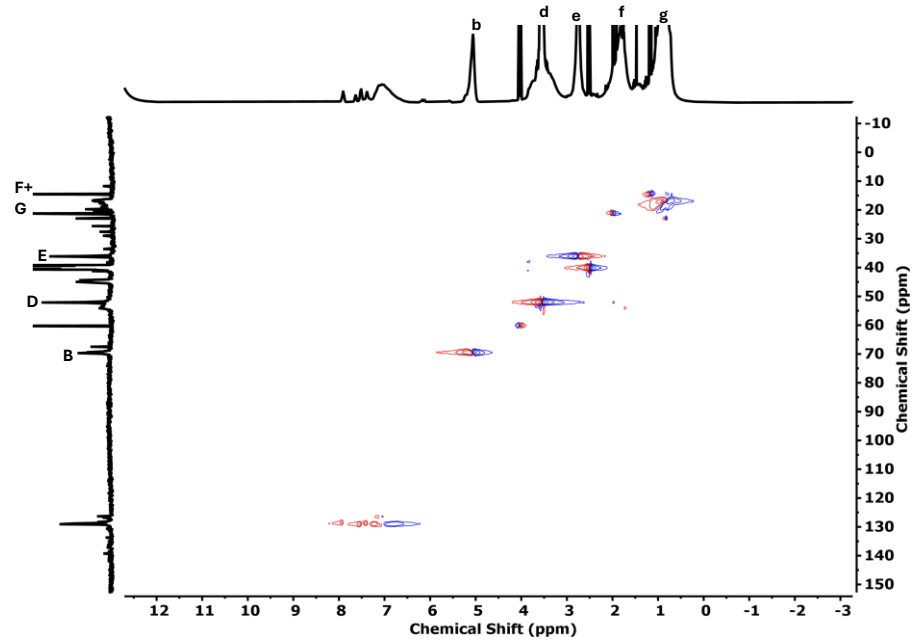

Figure S59: HSQC-NMR spectrum (400 MHz, DMSO-d_6) of P(MA-Mal-*co*-MMA).

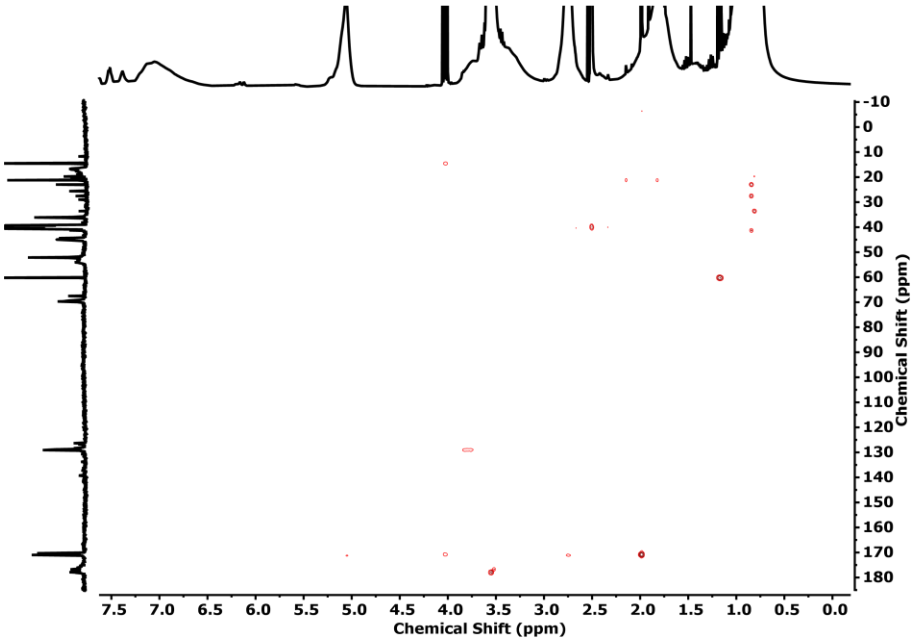

Figure S60: HMBC-NMR spectrum (400 MHz, DMSO-d_6) of P(MA-Mal-*co*-MMA).

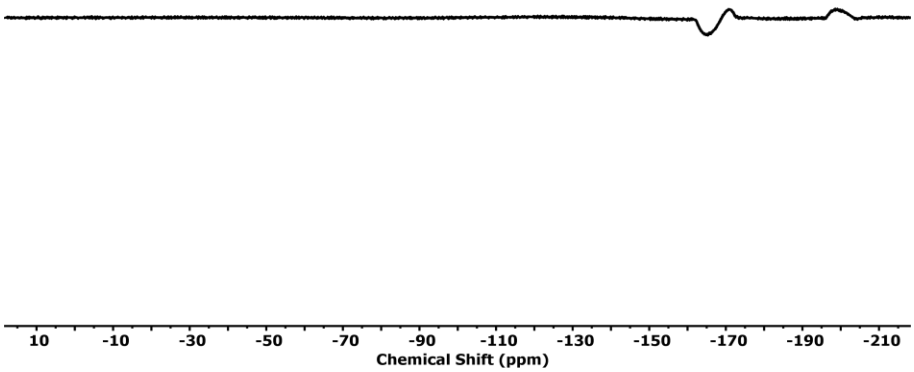

Figure S61: ^{19}F-NMR spectrum (400 MHz, DMSO-d_6) of P(MA-Mal-*co*-MMA).

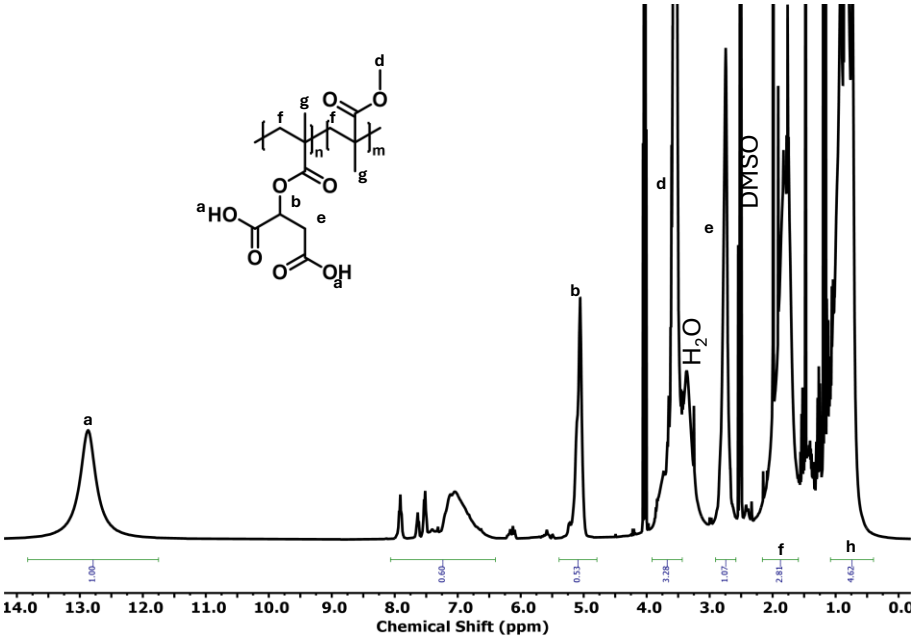

Figure S62: ^{1}H-NMR spectrum (400 MHz, DMSO-d_6) of P(MA-Mal$_1$-*co*-MMA$_2$).

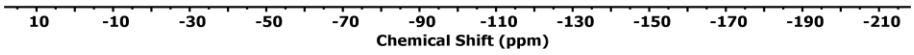

Figure S63: ^{19}F-NMR spectrum (400 MHz, DMSO-d_6) of P(MA-Mal$_1$-*co*-MMA$_2$).

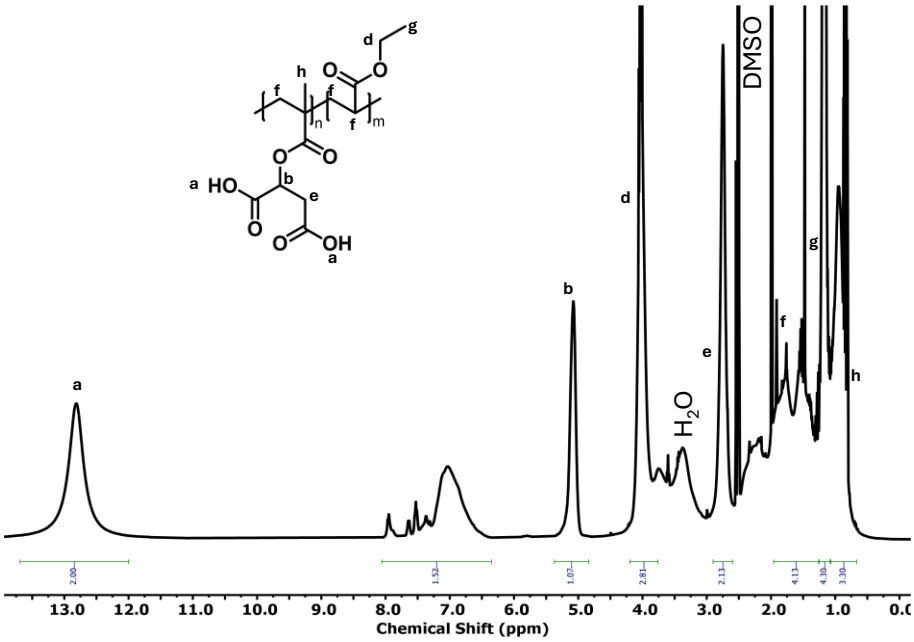

Figure S64: ^{1}H-NMR spectrum (400 MHz, DMSO-d_6) of P(MA-Mal-*co*-EA).

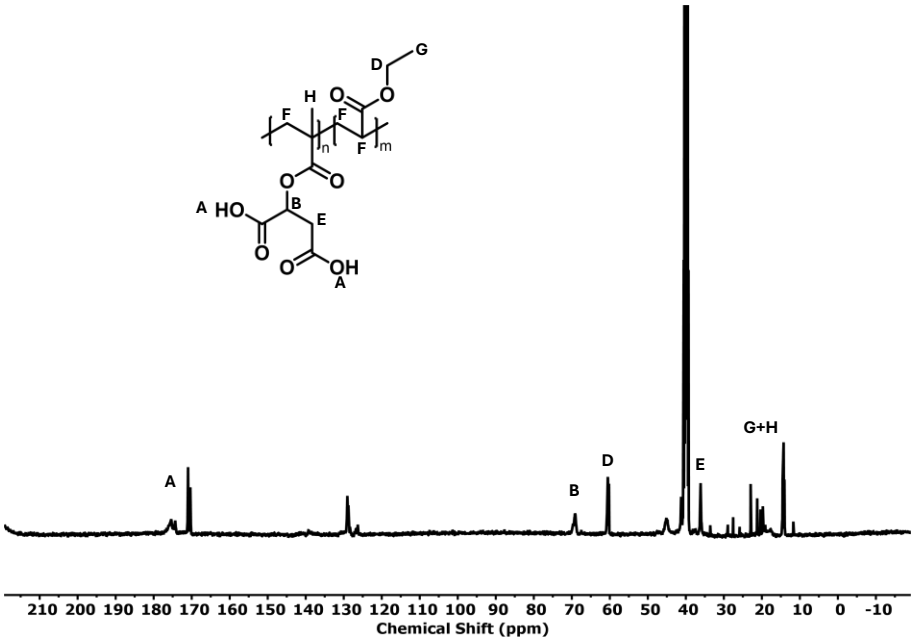

Figure S65: ^{13}C-NMR spectrum (101 MHz, DMSO-d_6) of P(MA-Mal-*co*-EA).

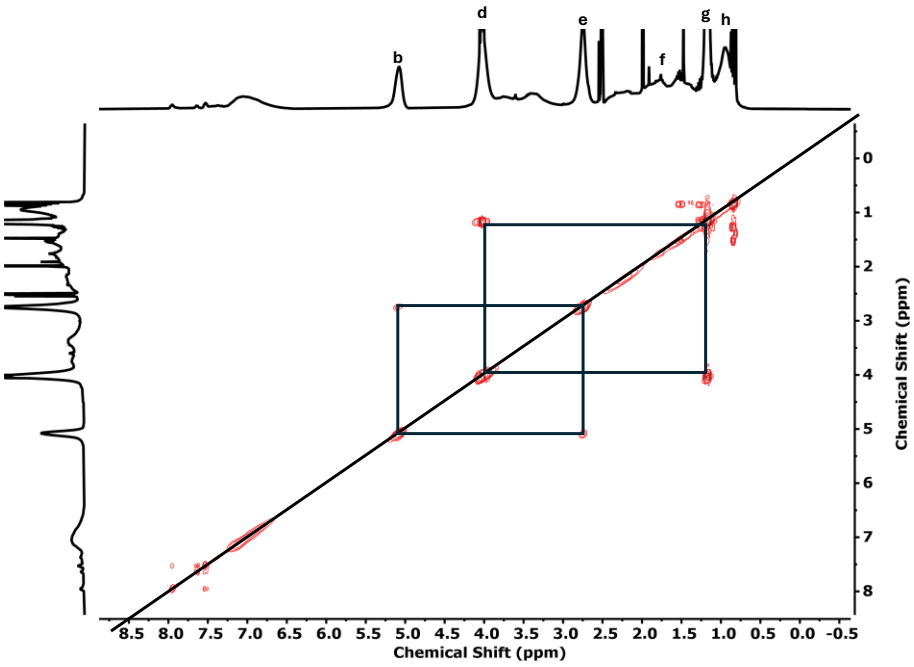

Figure S66: COSY-NMR spectrum (400 MHz, DMSO-d_6) of P(MA-Mal-*co*-EA).

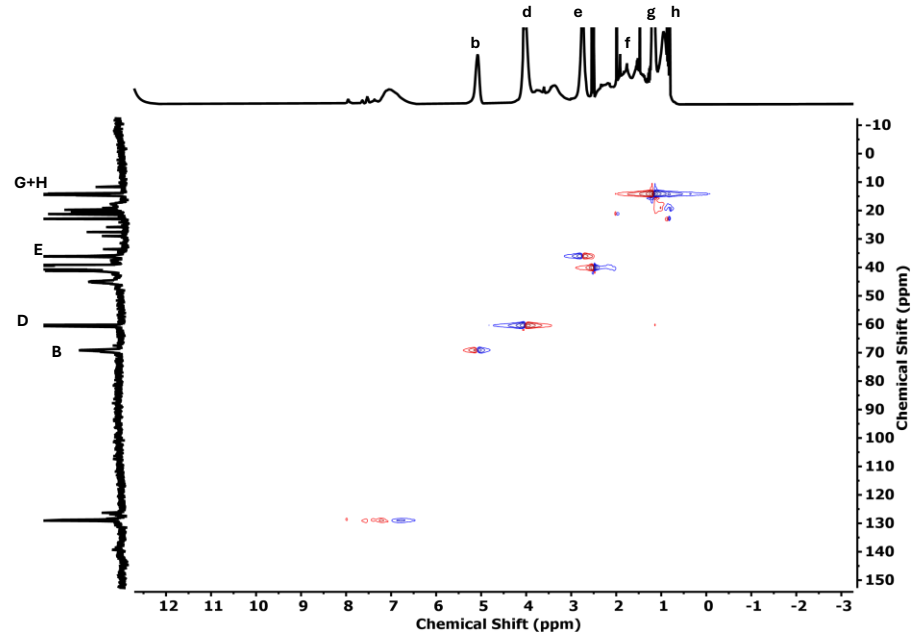

Figure S67: HSQC-NMR spectrum (400 MHz, DMSO-d_6) of P(MA-Mal-*co*-EA).

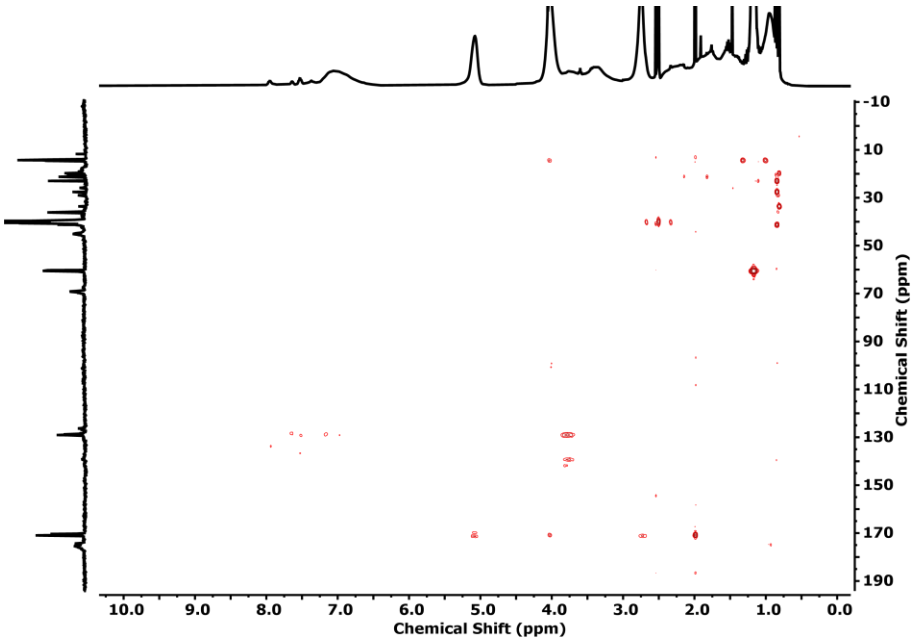

Figure S68: HMBC-NMR spectrum (400 MHz, DMSO-d_6) of P(MA-Mal-*co*-EA).

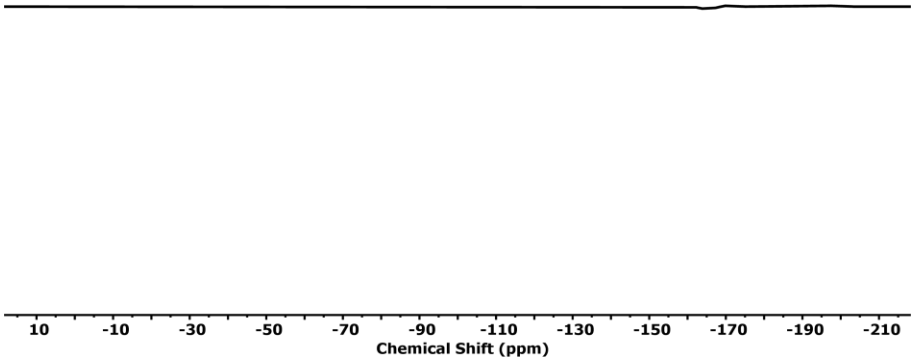

Figure S69: ^{19}F-NMR spectrum (400 MHz, DMSO-d_6) of P(MA-Mal-*co*-EA).

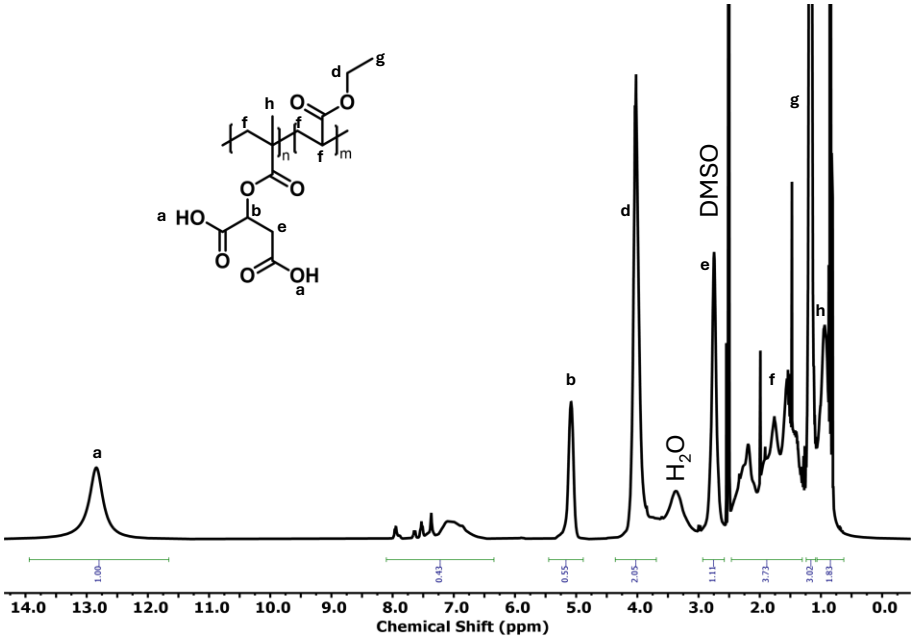

Figure S70: ^{1}H-NMR spectrum (400 MHz, DMSO-d_6) of P(MA-Mal$_1$-*co*-EA$_2$).

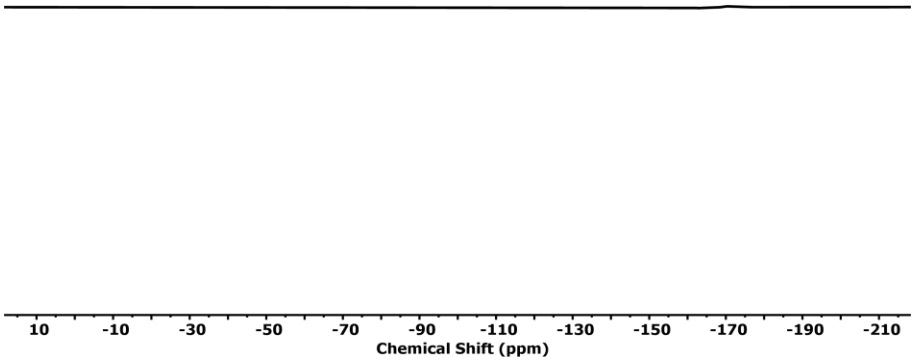

Figure S71: ^{19}F-NMR spectrum (400 MHz, DMSO-d_6) of P(MA-Mal-*co*-EA).

Table S6: Summary of yield, degree of deprotection as well as the glass transition temperature for deprotected copolymers.

Copolymer	Yield / (%)	Degree of deprotection / (%)	T_g /(°C)
Eudragit L-100	-	-	168
P(MA-Mand-*co*-MMA)	87	86.2	140
P(MA-Mal-*co*-MMA)	56	84.8	109
P(MA-Mal$_1$-*co*-MMA$_2$)	95	86.8	81
Eudragit L-100-55	-	-	82
P(MA-Mand-*co*-EA)	84	88.7	113
P(MA-Mal-*co*-EA)	47	85.8	65
P(MA-Mal$_1$-*co*-EA$_2$)	81	92.1	60

6. Glass transition temperatures

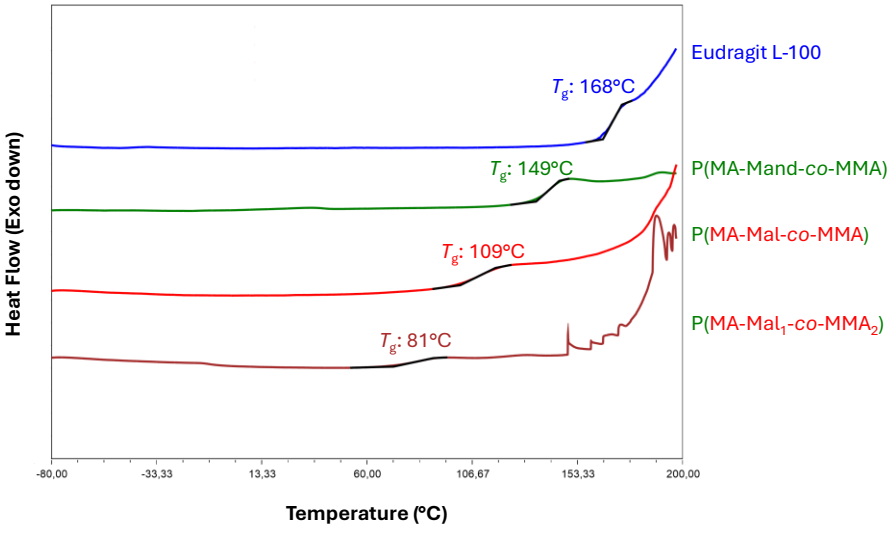

Figure S72: DSC curves of the second heating cycle of Eudragit® L-100, P(MA-Mand-*co*-MMA) and P(MA-Mal-*co*-MMA).

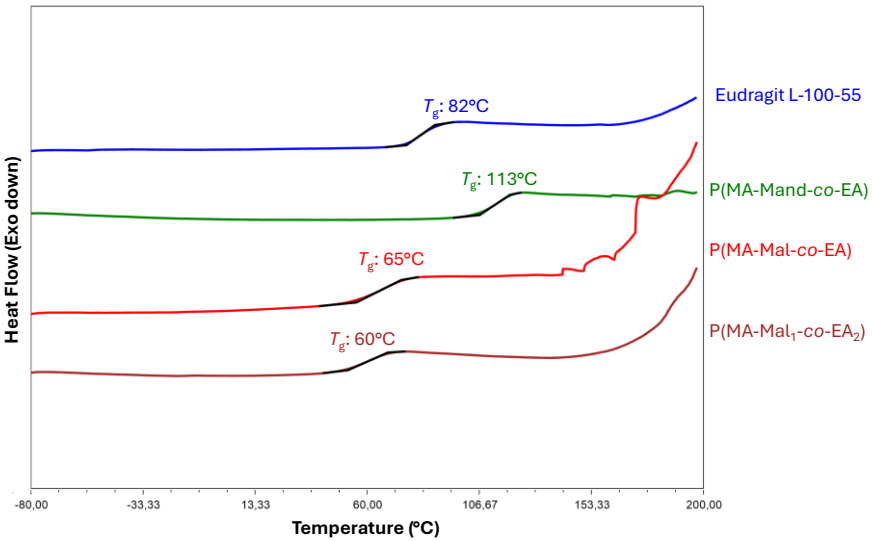

Figure S73: DSC curves of the second heating cycle of Eudragit® L-100-55, P(MA-Mand-*co*-EA) and P(MA-Mal-*co*-EA).

7. Cloud point titration

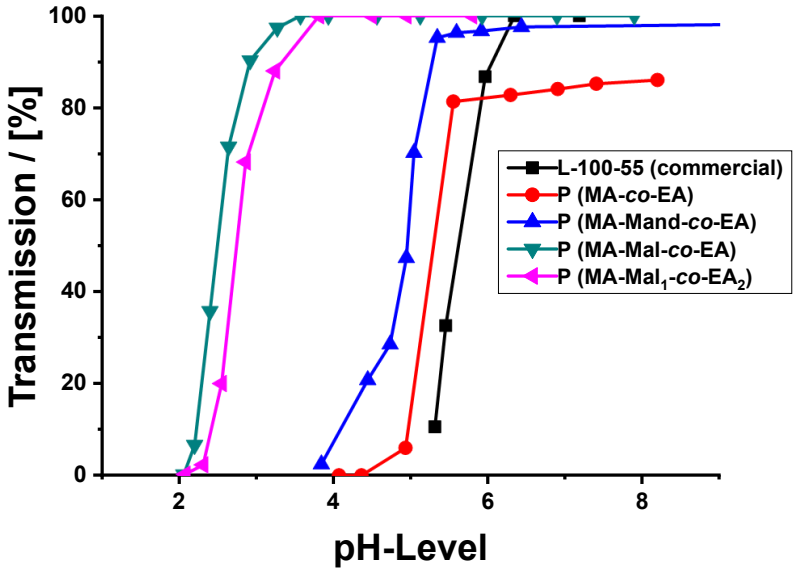

Figure S74: pH dependent transmission experiments for Eudragit® L-100-55 type copolymers at 37°C.

8. Time dependent drug release profile

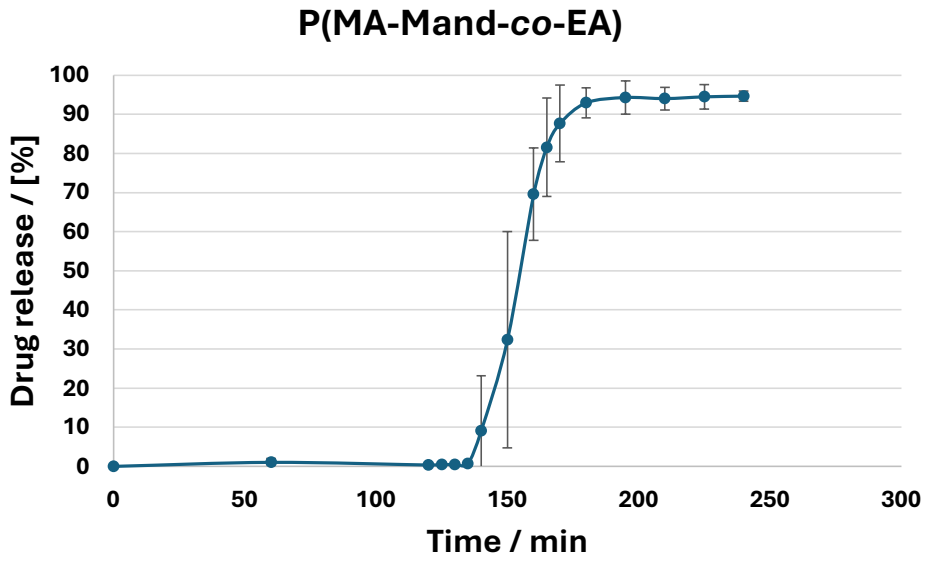

Figure S75: Drug release of paracetamol of a HPMC capsule coated with P(MA-Mand-*co*-EA). For the first two hours at a pH of 2, which was changed to a 15 mM phosphate buffer with a pH of 6.5.

Appendix

Chapter A1

Spotlight on Methyl *tert*-Butyl Ether - Underrated or Overlooked? Unveiling Its Role for Living Anionic Polymerization

[redacted], *Dominik A. H. Fuchs*, [redacted]

* *Corresponding authors*

[1] Johannes Gutenberg-University, Duesbergweg 10-14, 55128 Mainz, Germany

[redacted]

Published in: *Macromolecules*, **2024**, *57*(16), 8154–8161.

https://doi.org/10.1021/acs.macromol.4c01262

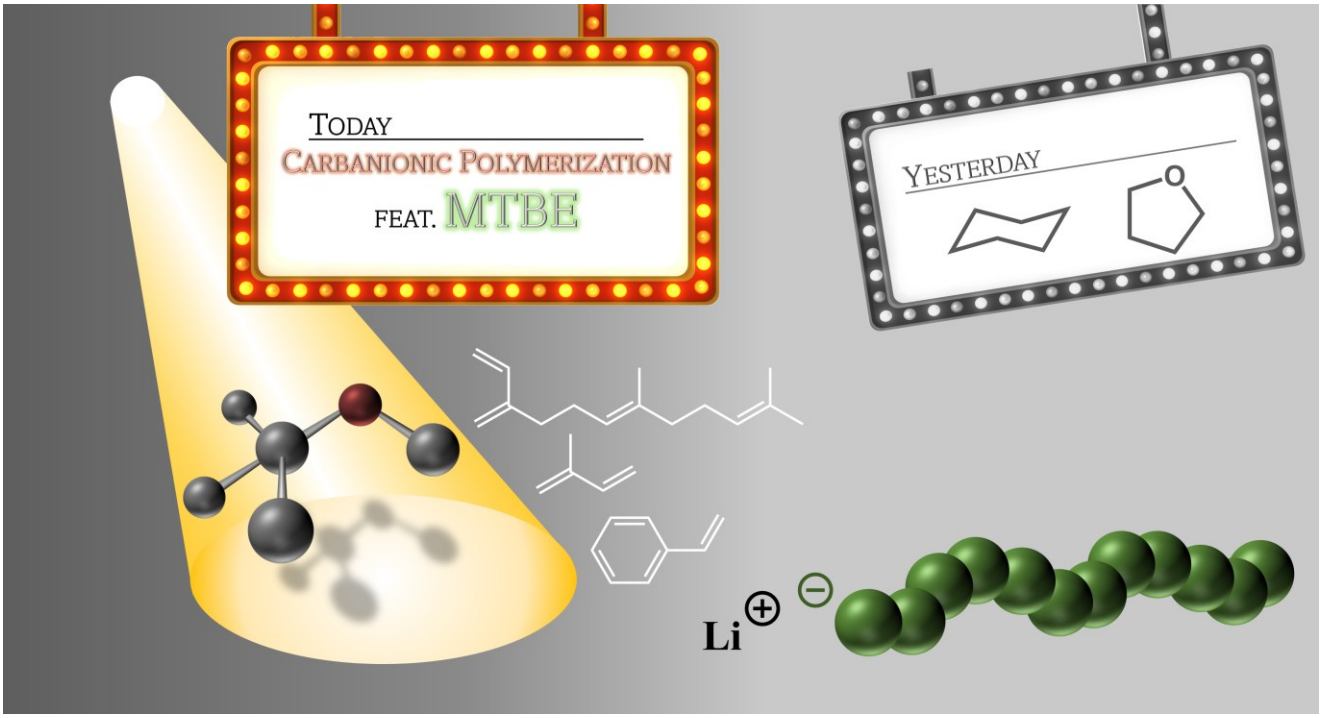

The following publication is adapted with permission from [redacted]., Fuchs, D. A. H. [redacted] Spotlight on Methyl tert-Butyl Ether – Underrated or Overlooked? Unveiling Its Role for Living Anionic Polymerization, *Macromolecules*, **2024**, 57 (16), 8154-8161.

ABSTRACT: The moderately polar solvent methyl *tert*-butyl ether (MTBE) was investigated as reaction medium for the carbanionic polymerization of the 1,3-dienes isoprene and *β*-farnesene. Key characteristics of MTBE, e.g., 50 times longer half-life of *n*-butyllithium compared to tetrahydrofuran and polymerization rate constants were determined. *In situ* ^{1}H NMR kinetics showed a polymerization rate in MTBE in between the commonly utilized solvents cyclohexane and tetrahydrofuran for diene polymerization. Remarkably, the living polydienyllithium chains in MTBE are predominantly present as non-aggregated unimers. The copolymerization of styrene and isoprene in cyclohexane with increasing MTBE fraction was investigated via *in situ* near-infrared kinetics. The gradient structure successively changes to random monomer incorporation and ultimately yields an inverted, yet still almost random incorporation in pure MTBE, reflected by the reactivity ratios r_S^{MTBE} = 1.82 and r_I^{MTBE} = 0.55. A spotlight is placed on the great potential of this highly available, albeit rarely used solvent for anionic polymerization.

INTRODUCTION

The choice of a solvent is often crucial in determining the success of a given reaction. This particularly applies to ionic polymerizations. In the case of carbanionic polymerization, the main requirement is a non-protic solvent and the strict absence of all protic impurities. Therefore, for the case of non-polar monomers hydrocarbon solvents, e.g., alkanes, toluene or benzene, typically have been used,[1,2] some of which bear disadvantages. For example, proton transfer reactions were reported for toluene.[3] Carbanionic ion pairs form aggregates with Li counterions, posing a well-known problem for the solubility of bifunctional initiators.[4–6] Thus, non-protic ether solvents, predominantly tetrahydrofuran (THF), have been used in this case. The better solvation of the counterion prevents formation of aggregates. However, the increased polarity affects the resulting microstructure, namely regio- and stereostructure, of a poly(1,3-diene) leading to a low extent of 1,4-incorporation and consequently an undesired high glass temperature (T_g) for, e.g. polybutadiene and polyisoprene. In addition, THF is notorious for its decomposition reactions with alkyllithium compounds, limiting its use to low temperatures.[7] The half-life of *n*-butyllithium in THF at 20 °C was reported to be just 107 min.[8] Finally, ether solvents are also known to form peroxides, restricting or even prohibiting their use in large-scale industrial processes.

Surprisingly, very little research has been published on the use of solvents of intermediate polarity for the anionic polymerization. One representative of this class is methyl *tert*-butyl ether (MTBE). One the one hand MTBE shows improved safety due to the absence of peroxide formation.[9] Secondly, one expects higher stability towards alkyllithium compounds due to fewer protons in α-position as well as significant steric hindrance and moderate polarity, reflected by a dielectric constant, $\varepsilon^{MTBE} = 2.6$, in between the non-polar cyclohexane (CHx; $\varepsilon^{CHx} = 2.02$) and THF, $\varepsilon^{THF} = 7.6$.[10–12] Despite these advantages, MTBE has received surprisingly little attention, although it is readily available on large scale. In a few works MTBE was used as a polar modifier to modify the vinyl content of polybutadiene and to randomize the copolymerization of butadiene with styrene or divinylbenzene.[13–16] The addition of 40 equivalents of MTBE relative to *n*-BuLi in cyclohexane at 50 °C led to an increase of the vinyl content from ~7% to 28%.[13,17] This effect is much weaker than the ~41% vinyl content reported for 45 equivalents of THF in hexane at 50 °C.[18] Another interesting feature of MTBE is its greater solvating strength for bifunctional initiators preventing aggregation.[19,20] This is primarily relevant for diene monomers, for which the change in the resulting microstructure is not of great concern for their properties. This refers for instance to the microstructure-independent low T_g of polyfarnesene (PFar).[20,21] Consequently, we recently introduced the bifunctional synthesis of fully bio-based thermoplastic elastomers in MTBE.[22,23]

The use of MTBE as a neat solvent for carbanionic polymerization was reported in 1987 in a Czech patent, targeting the bifunctional synthesis of SBS rubber.[24–27] Surprisingly, this has been almost overlooked ever since.

Increasing awareness for sustainability has resulted in the examination of new bio-based solvents in recent years. For instance, Schlaad et al. introduced DL-limonene and 2-methyltetrahydrofuran (2-MeTHF) as more sustainable solvents for carbanionic polymerization.[28,29] Other examples comprise the hydrogenated triterpene squalane, bearing a C_{30} framework, and cyclopentyl methyl ether.[30,31] The drawback of these solvents is their limited accessibility, which makes large-scale application unlikely. MTBE, which is already available on large scale due to multiple industrial applications, e.g., as fuel component, is therefore much more attractive. Even though today's MTBE large-scale production relies on a fossil feedstock, the high demand has resulted in a variety of alternative bio-based production pathways. MTBE can be obtained from methanol, that is easily available in a sustainable manner, and isobutylene.[32] The latter can be synthesized from carbon dioxide and green hydrogen in the zirconium oxide catalyzed isosynthesis.[33–35] The process can also be operated with syngas from biomass or biomass can be used directly to afford isobutylene via fermentation.[36–39] Despite the many benefits, it is important to also be aware of the reported disadvantages of MTBE, such as health concerns linked to endocrine disruption and incompatibility with some established metalation reactions, e.g., Grignard reagent formation.[40,41]

This work presents the first fundamental examination of MTBE as a solvent for carbanionic polymer synthesis. It covers an investigation on the stability towards alkyllithium compounds in comparison to the established polar solvent THF. Further, the performance in the anionic polymerization is quantified and demonstrated by investigating the kinetics of the homopolymerization of isoprene and β-farnesene as well as the copolymerization of isoprene and styrene using increasing fractions of MTBE.

Results and Discussion

Stability of THF and MTBE Towards Butyllithium

To compare the stability of alkyllithium compounds in THF and MTBE, the nucleophile *n*-butyllithium (*n*-BuLi) was chosen. Its more widely used isomer, *sec*-BuLi, is not feasible for this investigation due to its rapid decomposition in THF even at lower temperatures (78 min at – 20 °C).[8] The reaction was investigated by *in situ* ^{1}H NMR kinetics at 20 °C by tracking the decrease of the methylene signal of *n*-BuLi at ~ -0.75 ppm, see **Figure S1** (Supporting Information). **Figure 1a** shows that the concentration of *n*-BuLi decreases rapidly. The pseudo-first order plot of

ln([BuLi]$_0$/[BuLi]) vs time is linear with a half-life of 44 min. Detailed information on the NMR method is given in the **Supporting Information**.

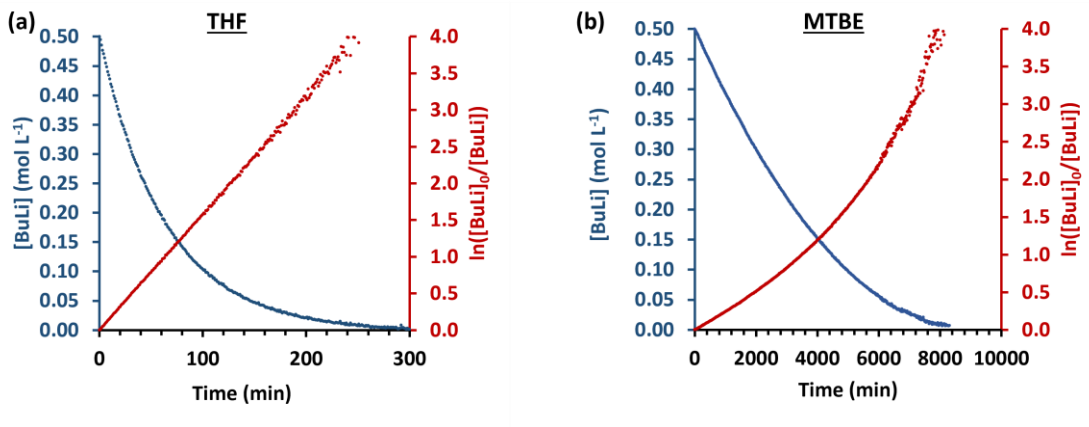

Figure 1. *Decrease of n-BuLi concentration at 20 °C (blue), along with the pseudo-first order plot (red); (a) in THF, (b) in MTBE.*

In contrast, the decomposition of MTBE is more than 50 times slower than THF, with a half-life of ~ 2600 min, see **Figure 1b** and **Figure S2**. Since neither the pseudo-first order, nor the pseudo-second order plot (1/[BuLi] vs time, **Figure S3**) follow a linear trend, the consumption of *n*-BuLi cannot easily be assigned to a specific kinetic order. We assume that a secondary process emerges during the decomposition of MTBE. As known in literature, the methoxy group of MTBE can be deprotonated under harsh conditions using *sec*-BuLi and potassium *tert*-butoxide.[42] This implies the following proposed reaction shown in **Scheme 1**.

Scheme 1. *Proposed decomposition reaction of MTBE in the presence of n-BuLi.*

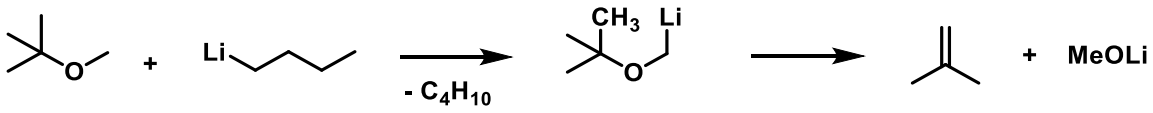

As a result, isobutylene and lithium methoxide are produced. Evidence for this can be found in the *in situ* ^{1}H NMR kinetics in **Figure S2**. While the characteristic *n*-BuLi signal at ca. -0.75 ppm decreases, new signals emerge at 4.7 ppm and 1.8 ppm. They can be attributed to the olefin and methyl signal of isobutylene, respectively. Their formation follows the expected integral ratio of two and six protons. Simultaneously, lithium methoxide is formed, in which we assume the origin

of the deviating pseudo-first order kinetics. Polar structures are known to affect the kinetics of carbanionic polymerization.[1,43]

The far higher stability of MTBE compared to THF indicates that it is ideally suited as an alternative solvent for the carbanionic polymerization, as investigated in the following.

KINETICS OF POLYMERIZATION OF ISOPRENE IN MTBE

The diene monomers isoprene and *β*-farnesene (Far) were investigated for their polymerization kinetics in MTBE. Isoprene is a commonly utilized monomer of which many data regarding polymerization rates, aggregation number, and polymer microstructure in classical solvents are known, rendering it highly suitable for comparison. *β*-Farnesene on the other hand, is much better suited for synthesis in polar media for its microstructure-independent low T_g.[20]

The polymerization of isoprene was performed at three different temperatures, 23 °C, 30 °C and 40 °C. Polymerizations were investigated using *in situ* ^{1}H NMR kinetic experiments following the decrease of the methine signal of isoprene at ~ 6.6 ppm, see **Figure S4**. **Figure 2a** shows the linear pseudo-first order plots indicating living polymerization of isoprene in MTBE.

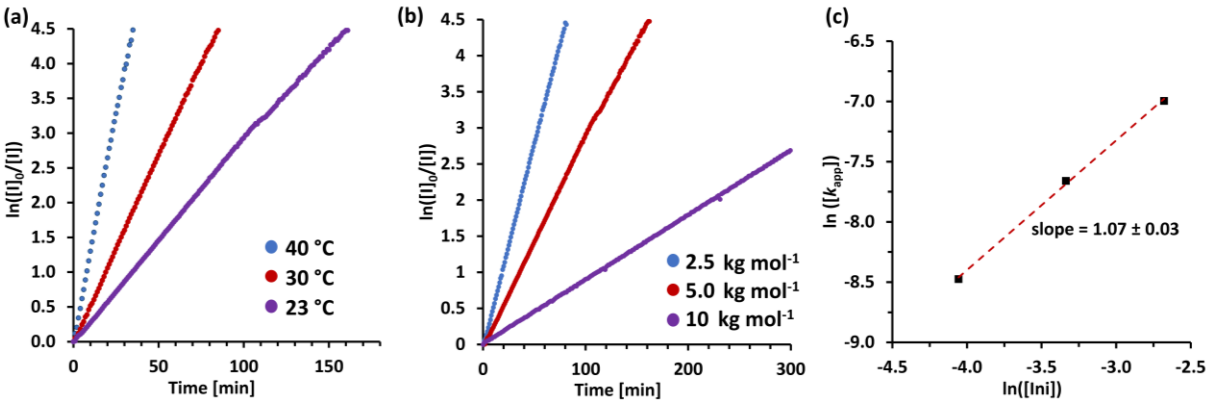

Figure 2. *In situ ^{1}H NMR kinetics results of isoprene polymerization in MTBE using sec-BuLi as initiator; (a) pseudo-first-order plots at different temperatures at $[Ini]_0 \approx 35$ mmol L^{-1}; (b) pseudo-first-order plots using different $[Ini]_0$ at 23 °C; (c) double logarithmic plot of the apparent rate constants of isoprene at different initiator concentrations at 23 °C.*

The apparent rate constant, k_{app}, is the slope of the pseudo first-order plot, and **Equation 1** renders the rate constant, k_p^{MTBE}, using the initiator concentration $[Ini]_0$ and the aggregation number *n*,

$$k_p = \frac{k_{app}}{[Ini]_0^{1/n}} \quad \textbf{(1)}$$

These values were compared to previously reported values of isoprene polymerized in cyclohexane, see **Table 1**.[44,45] The propagation rate of isoprene in MTBE is about one magnitude higher than in cyclohexane. In contrast, the propagation rate in THF is four times higher than in MTBE, $k_p^{THF,29\,°C} = 105 \cdot 10^{-3}\ M^{-1}\ s^{-1}$.[46]

An important factor that needs to be considered is the degree of aggregation of the active chain ends, *n*, in the respective solvents. Polyisoprenyllithium chains are known to form tetramers in cyclohexane at concentrations relevant to polymerization.[47] The higher polarity of MTBE suggests a change in the aggregation state. **Equation 2** was used to determine the aggregation number.

$$\ln k_{app} = (1/n) \ln[Ini]_0 \qquad \textbf{(2)}$$

The polymerization was performed at three different initiator concentrations, $[Ini]_0$, targeting different molar masses of 2.5 kg mol^{-1}, 5 kg mol^{-1} and 10 kg mol^{-1}, see **Figure 2**b. The initiator concentrations were determined from the number-average molecular weights of the polymers determined by ^{1}H NMR (see **Table 1**). Based on the linear fit (**Figure 2**c) an aggregation number of $n \approx 1$ was determined, suggesting the unimeric nature of polyisoprenyllithium chains in MTBE. Additional information on the polymerization kinetics, e.g. time-conversion plots, SEC traces and NMR spectra, can be found in **Figures S5, S6, S10, S12 and S13**.

Table 1. *Summary of polymerization rates of isoprene and β-farnesene in MTBE and published values obtained in cyclohexane (CHx), assuming n=1 in MTBE and n=4 in cyclohexane.*

Temperature (°C)	$[Ini]_0$ [a] (mmol L^{-1})	k_{app}^{MTBE} (10^{-3} s^{-1})	k_p^{MTBE} (10^{-3} M^{-1} s^{-1})	k_p^{CHx} (10^{-3} M$^{-1/4}$ s^{-1})
Isoprene				
23	35.5	0.47	13.3	0.61[44 b)]
30	36.9	0.89	24.1	1.47[45 c)]
40	37.1	2.11	56.9	3.81[45 c)]
Farnesene				
23	34.9	0.80	22.9	3.23[48 b)]
30	35.7	1.57	44.0	6.31[48 b)]
40	34.3	3.69	107.6	23.1[48 b)]

[a)] calculated using $M_n = M_{Mon} \cdot [M]_0 \cdot [Ini]_0^{-1}$; $[I]_0 = 1.94$ mol L^{-1}, $[Far]_0 = 0.65$ mol L^{-1}

[b)] determined by *in situ* ^{1}H NMR kinetics;[44,48] [c)] determined by *in situ* NIR kinetics.[45]

KINETICS OF POLYMERIZATION OF *β*-FARNESENE IN MTBE

The conversion of *β*-farnesene (Far) can be tracked by *in situ* ^{1}H NMR kinetics following the decrease of the proton at ~6.4 ppm. The respective spectra are presented in **Figure S7**. Following the investigation for isoprene we investigated the dependence on temperature and initiator concentration. The linearity of the pseudo-first order plots, see **Figure 3a** and **b**, proves the living behavior, and using **Equation 1** the apparent rate constants were converted to the respective rate constants of Far in MTBE, k_p^{MTBE}, summarized in **Table 1**. As evident from **Figure 3c**, polyfarnesenyllithium chains in MTBE form primarily unimers (aggregation number of $n \approx 1$), similar to polyisoprenyllithium. Additional data are presented in **Figures S8, S9, S11, S14 and S15**.

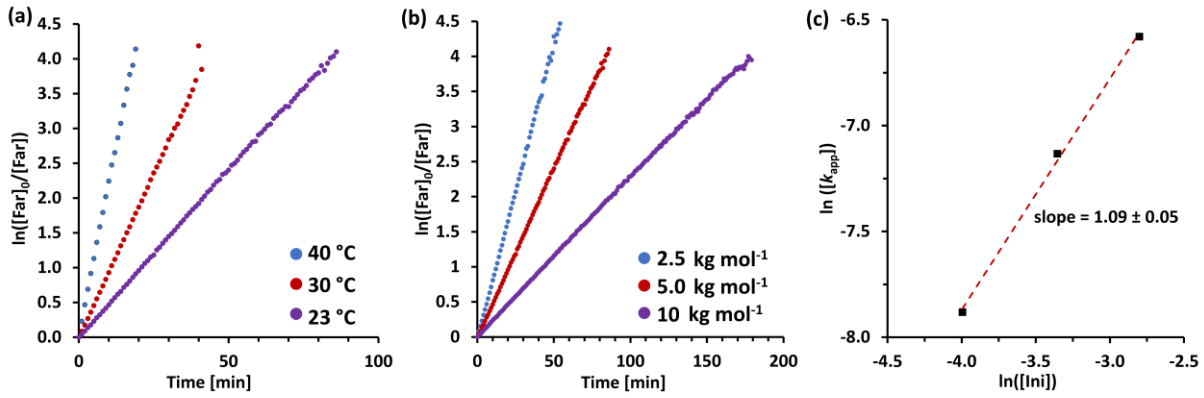

Figure 3. *In situ ^{1}H NMR kinetics results of β-farnesene polymerization in MTBE using sec-BuLi as initiator; (a) pseudo-first-order plots at different temperatures at $[Ini]_0 \approx 35$ mmol L^{-1}; (b) pseudo-first-order plots using different $[Ini]_0$ at 23 °C; (c) double logarithmic plot of the apparent rate constants of isoprene at different initiator concentrations at 23 °C.*

As observed earlier, *β*-farnesene reacts faster than myrcene and isoprene in cyclohexane. This was associated to the bulky chain-ends of the longer homologues of isoprene, decreasing their aggregation.[48,49] Further it is evident that in MTBE *β*-farnesene polymerizes about 70% faster than isoprene, independent of the temperature. Taking the absence of aggregation into account, this is unexpected, considering the bulkiness of the monomer and the chain end. The full set of rate constants is analyzed by an Arrhenius plot (**Equation 3**; **Figure 4)**.

$$\ln k_p = \ln A + E_A/RT \qquad \textbf{(3)}$$

The activation energies, E_A, of both *β*-farnesene and isoprene are much lower in MTBE than in cyclohexane. This can be attributed to the fact that the activation energy in cyclohexane also

contains the enthalpy of the aggregation/dissociation equilibrium. Further polymer characteristics, e.g. microstructure and molar mass determinations via SEC and NMR, are summarized in **Table S1**.

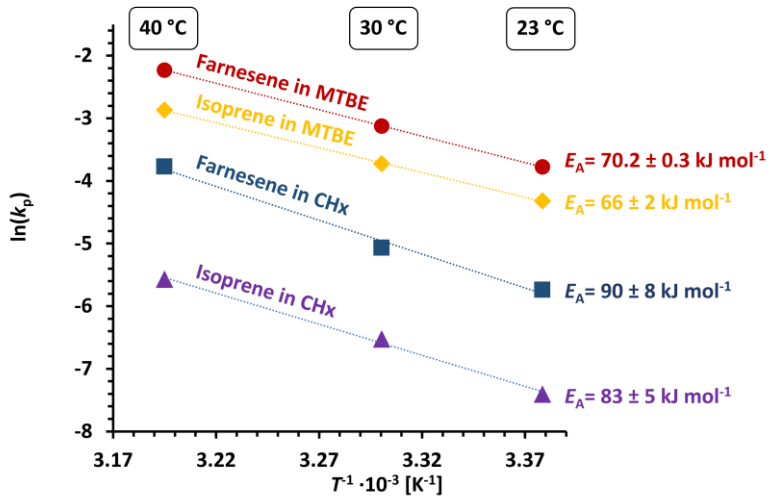

Figure 4. *Arrhenius plots of isoprene and β-farnesene polymerization in MTBE and cyclohexane.*

Noteworthy, the change in polarity of the solvent influences the resulting microstructure of the respective polydienes. For example, *β*-farnesene polymerized in hydrocarbons leads to ~ 93% of 1,4-units and ~ 7% 3,4-units, which decreases to approximately 62% 1,4-units and 38% 3,4-units when polymerized in MTBE.[22] In contrast, the effect on the polyisoprene microstructure is slightly stronger, as the amount of vinyl units increases to approx. 49% 3,4-units and 4% 1,2-units, whereas the amount of 1,4-units decreases to 47%. In comparison, the higher polarity of THF is known to further increase the vinyl content to 62% 3,4-units, 24% 1,2-units and only 14% of 1,4-units.[29]

Copolymerization of Isoprene and Styrene in MTBE/Cyclohexane Mixtures

Recently, our group utilized MTBE as a solvent for the bifunctional copolymerization of *β*-farnesene and nopadiene (Nopa), a biobased 1,2-substituded bicyclic 1,3-diene. Herein, the change from cyclohexane to MTBE showed only minor variation of the respective reactivity ratios of the copolymerization ($r_{Far}^{CHx} = 6.5$, $r_{Nopa}^{CHx} = 0.156$ and $r_{Far}^{MTBE} = 7.23$, $r_{Nopa}^{MTBE} = 0.138$).[23] In the following section, the copolymerization of styrene (S) and isoprene (I), as an established

copolymerization pair in carbanionic polymerization, is investigated in MTBE/cyclohexane mixtures.

The copolymerization in pure cyclohexane leads to a steep comonomer gradient along the chain, reflected by the reactivity ratios r_I^{CHx} = 10 and r_S^{CHx} = 0.015, respectively.[50] The change in the polarity of the reaction medium is known to have a strong impact on the copolymerization and the associated reactivity ratios. Polar additives, like THF or 2,2-di(2-tetrahydrofurfuryl)propane (DTHFP), are known to entirely invert the comonomer gradient, and consequently styrene is preferably incorporated during the copolymerization.[49,50] The copolymerization of styrene and isoprene with increasing MTBE content was therefore investigated using in situ near-infrared (NIR) kinetics. The procedure followed the protocol explained in a previous publication.[45]

The ratio [MTBE]/[Li] in cyclohexane was steadily increased until MTBE was present as a pure solvent. The reactivity ratios are determined from the individual monomer consumptions using the non-terminal (Jaacks)[51,52] and terminal model (Meyer and Lowry)[53]. Preferentially, the non-terminal model — assuming an ideal copolymerization ($r_1 \cdot r_2$=1) — is used, since it is less prone to overfitting compared to the more complex terminal model.[54] The non-linear Meyer-Lowry fit was only used for the ratios [MTBE]/[Li] = 0, 5 and 20, as the data deviated from linearity in the respective Jaacks fit.[53] Exemplary, the NIR kinetic results in neat MTBE is presented in **Figure 5**.

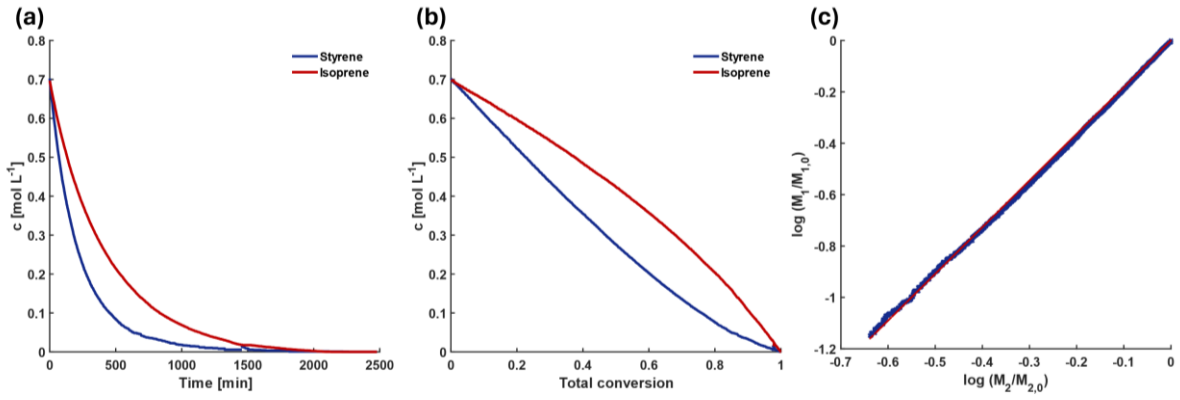

Figure 5. *In situ NIR kinetics of the copolymerization of styrene and isoprene in neat MTBE at 20 °C, (a) time-conversion plot, (b) monomer consumption vs. total consumption, (c) Jaacks-fit of the copolymerization, r_I=0.55 and r_S=1.82.*

All kinetic results are summarized in **Table 2** and additional data is given in the SI (**Figures S18-25**). The effect of the MTBE content on the reactivity ratios is shown in **Figure 6**.

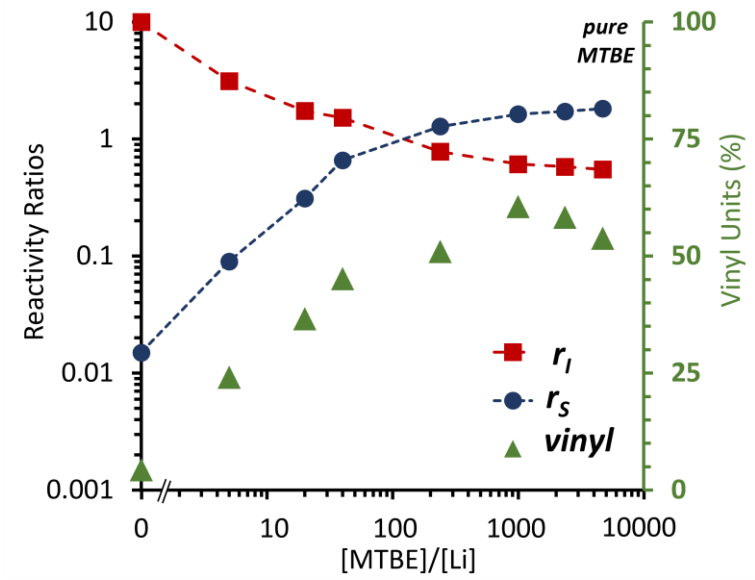

Figure 6. *Effect of the addition of MTBE on the reactivity ratios of the copolymerization of S, red, and I, blue, and the amount if vinyl units, green; lines connecting the symbols are a guide to the eye only; measured with in situ NIR kinetics at 20 °C.*

It is evident that the reactivity ratios converge and eventually invert, so that finally styrene is incorporated first. By interpolation we see that a random copolymer ($r_S = r_I \approx 1$) is expected at [MTBE]/[Li] ≈ 166 (3.5 vol%) and no significant change is observed by exceeding a [MTBE]/[Li] ratio of 1000 equivalents. Additionally, the reaction half-life, $t_{1/2}$ (inverse rate), is decreased by the addition of MTBE up to 1000 eq, whereas further addition of MTBE leads to an increase in reaction time again. Eventually, the half-life of isoprene even exceeds the $t_{1/2}$ in pure cyclohexane, see **Figure S29**. A similar minimum of $t_{1/2}$ was observed with THF as ligand at a THF/Li ratio ≈ 80 already.[50] Analogously, randomization with THF is already achieved at [THF]/[Li] ≈ 6.[50] Significantly, an additional in situ NMR kinetic experiment in neat MTBE showed nearly identical results to the one obtained via the in situ NIR measurement, proving the comparability of both techniques. The reactivity ratios in neat MTBE, determined by either NMR or NIR are in good agreement, r_S^{MTBE} = 1.82 (NIR); 1.87 (NMR) and r_I^{MTBE} = 0.55 (NIR); 0.53 (NMR), and reveal a weak compositional gradient not very far from an ideal, random incorporation of styrene and isoprene. This is also reflected by a the low so-called blockiness of the styrene content, see **Figure S30**. This is in line with results obtained in previous works where the addition of polar modifiers, e.g., THF or DTHFP, was used to manipulate the tapered structure of diene/styrene copolymers.[49,50] Notably, the gradient is much weaker than in

pure THF, where $r_S^{THF} \approx 9$ and $r_I^{THF} \approx 0.1$ was reported.[55] Thus, pure MTBE is a suitable solvent to synthesize near-random S/I copolymers.

Table 2. *Polymer characteristics of all synthesized S/I copolymers.*

[MTBE]/[Li] [a]	MTBE [vol%]	M_n^{SEC} [b] [kg mol^{-1}]	$Đ$ [b]	r_I [c]	r_S [c]	1,4- [d] [%]	3,4- [d] [%]	1,2- [d] [%]	T_g [e] [°C]	Volume Gradient [f]
In situ NIR kinetics										
0 [Ref: 50]	0	88.2	1.06	10.03	0.015	96	3.8	0.6	-39/83	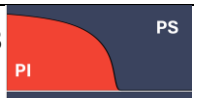
5	0.1	88.3	1.04	3.13	0.09	75.9	22.6	1.5	-14	
20	0.4	89.6	1.04	1.74	0.31	63.4	34.9	1.7	11	
40	0.9	86.4	1.04	1.52	0.66	54.8	42.3	2.9	24	
240	5.1	90.4	1.04	0.78	1.28	49.0	48.3	2.7	32	
1000	21.3	83.7	1.04	0.61	1.63	39.4	56.5	4.1	33	
2350	50.0	94.6	1.05	0.58	1.72	41.7	53.9	4.4	33	
pure MTBE	100	84.1	1.06	0.55	1.82	46.2	51.3	2.5	29	
In situ ^{1}H NMR kinetics										
pure MTBE	100	4.1	1.11	0.53	1.87	45.7[g]	50.4[g]	3.9[g]	NA	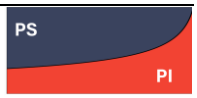

[a] Equivalents based on the [MTBE]/[Li], [b] Determined by SEC (eluent: THF, PS-calibration), [c] Determined from the Jaacks-Fit or Mayer-Lowry-Fit, [d] Determined by ^{1}H NMR,[56] [e] Glass transition determined *via* DSC using a heat rate of 10 K min^{-1}, [f] Volume gradients were determined assuming the following densities of the homopolymers: ρ_{PS}=0.97 g·cm^{-3}, ρ_{PI}=0.83 g·cm^{-3}, respectively,[57] [g] Values taken from PI homopolymerization in pure MTBE, see Table S1.

The increasing polarity of the medium affects the fraction of resulting vinyl units, i.e. 3,4- and 1,2-units, as can be seen in **Figure 6** and **S26** and **Table 2**. Exceeding 1000 eq of MTBE has no further significant impact on the reactivity ratios. This is also evident from thermal properties determined by DSC experiments, **Figures S27** and **S28**. The near random S/I-

copolymers show only one mixed T_g in the range of -14 °C to 33 °C, depending on the content of vinyl units.

CONCLUSIONS

MTBE, produced on megaton scale, offers numerous advantages beyond the absence of peroxide formation, making it particularly preferable to other ethers for large-scale processes. The key objective of this work was to give a fundamental introduction and overview of the characteristics of MTBE as a moderately polar solvent for the carbanionic polymerization. As one key result, the study reveals that MTBE shows a more than 50 times higher stability towards alkyllithium compounds than THF, the most often used polar solvent. *In situ* ^{1}H NMR kinetics of isoprene and *β*-farnesene polymerizations show a propagation rate in MTBE in between those in THF and cyclohexane. In pronounced contrast to cyclohexane and similar to THF the chain ends are present as non-aggregated unimers, leading to higher reaction rates for propagation. *In situ* NIR kinetics revealed that the effect of MTBE on the copolymerization of styrene and isoprene as a relevant copolymerization system in cyclohexane is weaker than that of THF, eventually yielding an inverted near-random incorporation of both comonomers in neat MTBE. Due to its higher stability, moderate polarity, excellent solubility of bifunctional initiators, and absence of peroxide formation, MTBE as a cheap and very abundant chemical has great potential for further applications in polymer chemistry. The use of this solvent for polar and heterocyclic monomers is subject of future investigations.

REFERENCES

(1) Hsieh, H. L.; Quirk, R. P. *Anionic Polymerization*:*Principles and Practical Applications*; Plastics Engineering Ser, v.34; Chapman and Hall/CRC**,** 1996.

(2) Hadjichristidis, N.; Iatrou, H.; Pispas, S.; Pitsikalis, M. Anionic polymerization: High vacuum techniques. *J. Polym. Sci. A Polym. Chem.***, 2000**, *38* (18), 3211–3234. DOI: 10.1002/1099-0518(20000915)38:18<3211:AID-POLA10>3.0.CO;2-L.

(3) Gatzke, A. L. Chain transfer in anionic polymerization. Determination of chain-transfer constants by using carbon-14-labeled chain transfer agents. *J. Polym. Sci. A-1 Polym. Chem.***, 1969**, *7* (8), 2281–2292. DOI: 10.1002/pol.1969.150070823.

(4) Sanderson, R. D.; Roediger, A. H. A.; Summers, G. J. Hydrocarbon-soluble difunctional organolithium anionic initiators. A gas–liquid chromatographic study of the reaction of sec -butyllithium with m -divinylbenzene. *Polym. Int.***, 1994**, *35* (3), 263–272. DOI: 10.1002/pi.1994.210350308.

(5) Margerison, D.; Newport, J. P. Degree of association of n-butyl lithium in hydrocarbon media. *Trans. Faraday Soc.***, 1963**, *59*, 2058. DOI: 10.1039/tf9635902058.

(6) Hadjichristidis, N.; Pitsikalis, M.; Pispas, S.; Iatrou, H. Polymers with complex architecture by living anionic polymerization. *Chem. Rev.***, 2001**, *101* (12), 3747–3792. DOI: 10.1021/cr9901337.

(7) Clayden, J.; Yasin, S. A. Pathways for decomposition of THF by organolithiums: the role of HMPA. *New J. Chem.***, 2002**, *26* (2), 191–192. DOI: 10.1039/b109604d.

(8) Stanetty, P.; Mihovilovic, M. D. Half-Lives of Organolithium Reagents in Common Ethereal Solvents. *J. Org. Chem.***, 1997**, *62* (5), 1514–1515. DOI: 10.1021/jo961701a.

(9) Hamid, S. H.; Ali, M. A. Effect of MTBE Blending on the Properties of Gasoline. *Fuel Sci. Technol. Int.***, 1995**, *13* (5), 509–544. DOI: 10.1080/08843759508947692.

(10) Zhang, H.; Zeng, Z.; Ma, F.; Wu, Q.; Wang, X.; Cheng, S.; Xie, J. Cyclopentylmethyl Ether, a Non-Fluorinated, Weakly Solvating and Wide Temperature Solvent for High-Performance Lithium Metal Battery. *Angew. Chem. Int. Ed.***, 2023**, *62* (21), e202300771. DOI: 10.1002/anie.202300771.

(11) Critchfield, F. E.; Gibson, J. A.; Hall, J. L. Dielectric Constant and Refractive Index from 20 to 35° and Density at 25° for the System Tetrahydrofuran—Water. *J. Am. Chem. Soc.*, **1953**, *75* (23), 6044–6045. DOI: 10.1021/ja01119a509.

(12) Songsiri, N.; Rempel, G. L.; Prasassarakich, P. Liquid-Phase Synthesis of Isoprene from Methyl tert -Butyl Ether and Formalin Using Keggin-Type Heteropolyacids. *Ind. Eng. Chem. Res.*, **2016**, *55* (33), 8933–8940. DOI: 10.1021/acs.iecr.6b02452.

(13) Iovu, M. C.; Buzdugan, E.; Teodorescu, M.; Britchi, A. G.; Hubca, G.; Iovu, H. Copolymerization of styrene with butadiene using methyl tert -butyl ether as active center modifier. *Angew. Makromol. Chemie*, **1999**, *271* (1), 18–23. DOI: 10.1002/(SICI)1522-9505(19991101)271:1<18:AID-APMC18>3.0.CO;2-%23.

(14) Iovu, M.-C.; Mapolie, S.; Britchi, A. G. Styrene-butadiene rubber synthesized by anionic polymerization. *Macromol. Symp.*, **2001**, *165* (1), 55–62.

(15) Iovu, M.-C.; Buzdugan, E.; Ghioca, P.; Britchi, A. G. Random Anionic Polymerization of Styrene with Butadiene using Methyl Tert-Butyl Ether/n-Butyl Lithium as Initiator System. Reation Mechanism and Kinetic Model. *Rev. Roum. Chim.*, **2003**, *48* (2), 163–171.

(16) Novoa-Carballal, R.; Nosov, S.; Pfaff, S.; Schmalz, H.; Müller, A. H. E. Hyperbranched and Hyperstar Polybutadienes via Anionic Self-Condensing Vinyl Copolymerization. *Macromolecules*, **2021**, *54* (12), 5774–5783. DOI: 10.1021/acs.macromol.1c00537.

(17) Uraneck, C. A. Influence of temperature on microstructure of anionic-initiated polybutadiene. *J. Polym. Sci. A-1 Polym. Chem.*, **1971**, *9* (8), 2273–2281. DOI: 10.1002/pol.1971.150090814.

(18) Antkowiak, T. A.; Oberster, A. E.; Halasa, A. F.; Tate, D. P. Temperature and concentration effects on polar-modified alkyllithium polymerizations and copolymerizations. *J. Polym. Sci. A-1 Polym. Chem.*, **1972**, *10* (5), 1319–1334. DOI: 10.1002/pol.1972.150100504.

(19) Yu, Y.; Dubois, P.; Teyssié, P.; Jérôme, R. Difunctional Initiator Based on 1,3-Diisopropenylbenzene. 6. Synthesis of Methyl Methacrylate−Butadiene−Methyl Methacrylate Triblock Copolymers. *Macromolecules*, **1997**, *30* (15), 4254–4261. DOI: 10.1021/ma961819t.

(20) Yoo, T.; Henning, S. K. Synthesis and Characterization of Farnesene-Based Polymers. *Rubber Chem. Technol.*, **2017**, *90* (2), 308–324. DOI: 10.5254/rct.17.82683.

(21) Wahlen, C.; Frey, H. Anionic Polymerization of Terpene Monomers: New Options for Bio-Based Thermoplastic Elastomers. *Macromolecules*, **2021**, *54* (16), 7323–7336. DOI: 10.1021/acs.macromol.1c00770.

(22) Meier-Merziger, M.; Imschweiler, J.; Hartmann, F.; Niebuur, B.-J.; Kraus, T.; Gallei, M.; Frey, H. Bifunctional Carbanionic Synthesis of Fully Bio-Based Triblock Structures Derived from β-Farnesene and ll-Dilactide: Thermoplastic Elastomers. *Angew. Chem. Int. Ed.*, **2023**, *62* (42), e202310519. DOI: 10.1002/anie.202310519.

(23) Meier-Merziger, M.; Fotaras, N.; Tzourtzouklis, I.; Allouch, C.; Wagner, M.; Müller, A. H. E.; Frey, H. One-Step Synthesis of Fully Bio-based Two-Sided Tapered ABA-Type Thermoplastic Elastomers. *In Print ACS Sustainable Chem. Eng.*, **2024**.

(24) Čermák, J., Hašová, V.; Mačka, M.; Petrů, V.; Pleska, A.; Reiss, J.; Sufčák, M.; Večerka, F.; Vyoral, L. Způsob roztokové kopolymerace konjugovaných dienů s vinylaromatickými uhlovodíky, **1986**, CZ 254630.

(25) Horák, Z.; Hlavatá, D.; Hromádková, J.; Kotek, J.; Hašová, V.; Mikešová, J.; Pleska, A. Effect of selected structural parameters of styrene–butadiene block copolymers on their compatibilization efficiency in polystyrene/polybutadiene blends. *J. Polym. Sci. B Polym. Phys.*, **2002**, *40* (23), 2612–2623. DOI: 10.1002/polb.10323.

(26) Hlavatá, D.; Hromádková, J.; Fortelný, I.; Hašová, V.; Pulda, J. Compatibilization efficiency of styrene–butadiene triblock copolymers in polystyrene–polypropylene blends with varying compositions. *J. Appl. Polym. Sci.*, **2004**, *92* (4), 2431–2441. DOI: 10.1002/app.20216.

(27) Fortelný, I.; Minkova, L. I.; Kotek, J.; Lapčíková, M.; Michálková, D. Morphology and mechanical properties of polypropylene/polystyrene blends compatibilized with styrene–butadiene block copolymers. *Polym. Eng. Sci.*, **2012**, *52* (1), 191–204. DOI: 10.1002/pen.22066.

(28) Dev, A.; Rösler, A.; Schlaad, H. Limonene as a renewable unsaturated hydrocarbon solvent for living anionic polymerization of β-myrcene. *Polym. Chem.*, **2021**, *12* (21), 3084–3087. DOI: 10.1039/D1PY00570G.

(29) Glatzel, J.; Noack, S.; Schanzenbach, D.; Schlaad, H. Anionic polymerization of dienes in 'green' solvents. *Polym. Int.*, **2021**, *70* (2), 181–184. DOI: 10.1002/pi.6152.

(30) Zhang, J.; Aydogan, C.; Patias, G.; Smith, T.; Al-Shok, L.; Liu, H.; Eissa, A. M.; Haddleton, D. M. Polymerization of Myrcene in Both Conventional and Renewable

Solvents: Postpolymerization Modification via Regioselective Photoinduced Thiol-Ene Chemistry for Use as Carbon Renewable Dispersants. *ACS Sustainable Chem. Eng.*, **2022**, *10* (29), 9654–9664. DOI: 10.1021/acssuschemeng.2c03755.

(31) Fu, Y.; Yang, S.; Xiong, Q.; Gu, Z.; Dai, Q.; Tan, H.; Le Zhou; Geng, M.; Xie, F.; Yi, W.; Li, L.; Liu, K. Synthesis, kinetic study and characterization of C5 -dienes/styrene copolymers via living anionic polymerization in cyclopentyl methyl ether solvent. *Polym. Int.*, **2023**, *73* (4), 326–336. DOI: 10.1002/pi.6598.

(32) Nawaz, Z. Methyl-Tert-Butyl-Ether Synthesis Reactor Modelling and Optimization Using an Aspen Custom Modeler. *Hung. J. Ind. Chem.*, **2017**, *45* (2), 1–7. DOI: 10.1515/hjic-2017-0012.

(33) Bown, R. M.; Joyce, M.; Zhang, Q.; Reina, T. R.; Duyar, M. S. Identifying Commercial Opportunities for the Reverse Water Gas Shift Reaction. *Energy Tech*, **2021**, *9* (11). DOI: 10.1002/ente.202100554.

(34) Zhu, M.; Ge, Q.; Zhu, X. Catalytic Reduction of CO2 to CO via Reverse Water Gas Shift Reaction: Recent Advances in the Design of Active and Selective Supported Metal Catalysts. *Trans. Tianjin Univ.*, **2020**, *26* (3), 172–187. DOI: 10.1007/s12209-020-00246-8.

(35) Wu, X.; Tan, M.; Tian, S.; Song, F.; Ma, Q.; He, Y.; Yang, G.; Tsubaki, N.; Tan, Y. Designing ZrO2-based catalysts for the direct synthesis of isobutene from syngas: The studies on Zn promoter role. *Fuel*, **2019**, *243*, 34–40. DOI: 10.1016/j.fuel.2019.01.098.

(36) Fukada, H.; FUJII, T.; OGAWA, T. Microbial production of C3- and C4-hydrocarbons under aerobic conditions. *Agricultural and Biological Chemistry*, **1984**, *48* (6), 1679–1682. DOI: 10.1271/bbb1961.48.1679.

(37) Wilson, J.; Gering, S.; Pinard, J.; Lucas, R.; Briggs, B. R. Bio-production of gaseous alkenes: ethylene, isoprene, isobutene. *Biotechnology for biofuels*, **2018**, *11*, 234. DOI: 10.1186/s13068-018-1230-9.

(38) van Leeuwen, B. N. M.; van der Wulp, A. M.; Duijnstee, I.; van Maris, A. J. A.; Straathof, A. J. J. Fermentative production of isobutene. *Applied microbiology and biotechnology*, **2012**, *93* (4), 1377–1387. DOI: 10.1007/s00253-011-3853-7.

(39) Rauch, R.; Hrbek, J.; Hofbauer, H. Biomass Gasification for Synthesis Gas Production and Applications of the Syngas. *WIRS Energy Environ*, **2014**, *3* (4), 343–362.

(40) Moser, G. J.; Wolf, D. C.; Sar, M.; Gaido, K. W.; Janszen, D.; Goldsworthy, T. L. Methyl tertiary butyl ether-induced endocrine alterations in mice are not mediated through the estrogen receptor. *Toxicological Sciences*, **1998**, *41* (1), 77–87. DOI: 10.1006/toxs.1997.2366.

(41) Jordan, A.; Hall, C. G. J.; Thorp, L. R.; Sneddon, H. F. Replacement of Less-Preferred Dipolar Aprotic and Ethereal Solvents in Synthetic Organic Chemistry with More Sustainable Alternatives. *Chem. Rev.*, **2022**, *122* (6), 6749–6794. DOI: 10.1021/acs.chemrev.1c00672.

(42) Corey, E. J.; Eckrich, T. M. t-Butoxymethyllithium: Direct preparation from t-butyl methyl ether and applications as a hydroxymethyl anion equivalent. *Tetrahedron Lett.*, **1983**, *24* (31), 3165–3168. DOI: 10.1016/S0040-4039(00)88125-3.

(43) Bywater, S. Anionic Polymerization of Olefins. In *Non-Radical Polymerisation*; Comprehensive Chemical Kinetics; Elsevier, **1976**; pp 1–65. DOI: 10.1016/S0069-8040(08)70047-5.

(44) Tiedemann, P. von; Blankenburg, J.; Maciol, K.; Johann, T.; Müller, A. H. E.; Frey, H. Copolymerization of Isoprene with p-Alkylstyrene Monomers: Disparate Reactivity Ratios and the Shape of the Gradient. *Macromolecules*, **2019**, *52* (3), 796–806. DOI: 10.1021/acs.macromol.8b02280.

(45) Steube, M.; Johann, T.; Plank, M.; Tjaberings, S.; Gröschel, A. H.; Gallei, M.; Frey, H.; Müller, A. H. E. Kinetics of Anionic Living Copolymerization of Isoprene and Styrene Using in Situ NIR Spectroscopy: Temperature Effects on Monomer Sequence and Morphology. *Macromolecules*, **2019**, *52* (23), 9299–9310. DOI: 10.1021/acs.macromol.9b01790.

(46) Morton, M.; Bostick, E. E.; Livigni, R. A.; Fetters, L. J. Homogeneous anionic polymerization. IV. Kinetics of butadiene and isoprene polymerization with butyllithium. *J. Polym. Sci. A Gen. Pap.*, **1963**, *1* (5), 1735–1747. DOI: 10.1002/pol.1963.100010525.

(47) Worsfold, D. J.; Bywater, S. Degree of Association of Polystyryl-, Polyisoprenyl-, and Polybutadienyllithium in Hydrocarbon Solvents. *Macromolecules*, **1972**, *5* (4), 393–397. DOI: 10.1021/ma60028a012.

(48) Wahlen, C.; Blankenburg, J.; Tiedemann, P. von; Ewald, J.; Sajkiewicz, P.; Müller, A. H. E.; Floudas, G.; Frey, H. Tapered Multiblock Copolymers Based on Farnesene and Styrene: Impact of Biobased Polydiene Architectures on Material Properties. *Macromolecules*, **2020**, *53* (23), 10397–10408. DOI: 10.1021/acs.macromol.0c02118.

(49) Fuchs, D. A. H.; Hübner, H.; Kraus, T.; Niebuur, B.-J.; Gallei, M.; Frey, H.; Müller, A. H. E. The effect of THF and the chelating modifier DTHFP on the copolymerisation of β-myrcene and styrene: kinetics, microstructures, morphologies, and mechanical properties. *Polym. Chem.*, **2021**, *12* (32), 4632–4642. DOI: 10.1039/D1PY00791B.

(50) Steube, M.; Johann, T.; Hübner, H.; Koch, M.; Dinh, T.; Gallei, M.; Floudas, G.; Frey, H.; Müller, A. H. E. Tetrahydrofuran: More than a "Randomizer" in the Living Anionic Copolymerization of Styrene and Isoprene: Kinetics, Microstructures, Morphologies, and Mechanical Properties. *Macromolecules*, **2020**, *53* (13), 5512–5527. DOI: 10.1021/acs.macromol.0c01022.

(51) Jaacks, V. Eine neuartige Methode zur Bestimmung von Copolymerisationsparametern. *Angew. Chem.*, **1967**, *79* (9), 419. DOI: 10.1002/ange.19670790927.

(52) Jaacks, V. A Novel Method of Determination of Reactivity Ratios in Binary and Ternary Copolymerizations. *Makromol. Chem.*, **1972**, *161* (1), 161–172. DOI: 10.1002/macp.1972.021610110.

(53) Meyer, V. E.; Lowry, G. G. Integral and differential binary copolymerization equations. *J. Polym. Sci. A Gen. Pap.*, **1965**, *3* (8), 2843–2851. DOI: 10.1002/pol.1965.100030811.

(54) Hawkins, D. M. The problem of overfitting. *J. Chem. Inf. Comput. Sci.*, **2004**, *44* (1), 1–12. DOI: 10.1021/ci0342472.

(55) Spirin, Y. L.; Arest-Yakubovich, A. A.; Polyakov, D. K.; Gantmakher, A. R.; Medvedev, S. S. Polymerization catalyzed by lithium and lithium alkyl. *J. Polym. Sci.*, **1962**, *58* (166), 1181–1189. DOI: 10.1002/pol.1962.1205816674.

(56) Meier-Merziger, M.; Fickenscher, M.; Hartmann, F.; Kuttich, B.; Kraus, T.; Gallei, M.; Frey, H. Synthesis of phase-separated super-H-shaped triblock architectures: poly(l-lactide) grafted from telechelic polyisoprene. *Polym. Chem.*, **2023**, *14* (23), 2820–2828. DOI: 10.1039/D3PY00230F.

(57) Fetters, L. J.; Lohse, D. J.; Richter, D.; Witten, T. A.; Zirkel, A. Connection between Polymer Molecular Weight, Density, Chain Dimensions, and Melt Viscoelastic Properties. *Macromolecules*, **1994**, *27* (17), 4639–4647. DOI: 10.1021/ma00095a001.

Supporting Information

1. Experimental Section

All experiments had to be performed under inert atmosphere in absence of any protic impurities. Therefore, the glassware was flame-dried at least three times before usage, and high-vacuum (10^{-3} mbar) techniques were used to transfer monomers and solvents. The argon used was treated by passing through cyclohexane/BuLi/diphenylethylene solutions to remove any remaining reactive substances.

1.1. Materials

All chemicals were used as received from the respective suppliers and all treatments are indicated at the point of the procedure. Substances were obtained from the following suppliers: *Amyris*: *β*-farnesene (95%); *Fisher Scientific:* THF (99.8%), cyclohexane (99.8%), isopropyl alcohol (99.8%); *Thermo Fisher:* MTBE (99.9%); *Thermo Scientific: n*-BuLi (2.5 mol L^{-1}), *sec*-BuLi (2.5 mol L^{-1}), isoprene (98%), calcium hydride (93%), basic aluminum oxide (40-300 µm 60A), *Sigma Aldrich:* styrene (99%), toluene (99.8%); *Lanxess:* trioctyl aluminum; *TCI:* diphenyl ethylene (98%); *Deutero*: cyclohexane-d_{12} (99.5%), chloroform-d_1 (99.5%).

1.2. Instruments

Nuclear Magnetic Resonance Spectroscopy (NMR). Measurements were performed on different NMR instruments. All 400 MHz spectra were recorded on either *Bruker Avance II HD* 400 MHz *(*5 mm *BBFO-head* with z-gradient, ATM and *SampleXPress 60* autosampler) or *Bruker Avance III HD* 400 MHz (5 mm N_2-cooled *BBO-cryo-head (BB/H+F)* with z-gradient, ATM and *SampleXPress 60* autosampler). Whereas 500 MHz spectra were measured on a *Bruker Avance III* 500 MHz instrument (5 mm *BBFO-Probe* with z-gradient and ATM, temperature control was done with a *VTU* (variable temperature unit) with an accuracy of ± 0.1 K). Data processing was done using the software *MestReNova* by *Mestrelab Research S.L.*, Spain.

Size Exclusion Chromatography (SEC). Samples were prepared at a concentration of 1 mg mL^{-1} in THF. They were measured using an Agilent *1260 Infinity II* setup using a *MZ-*

Gel SDPlus e5/e3/100 column set provided by *MZ-Analysetechnik,* Mainz, Germany. All measured samples were normalized to an internal toluene standard. Samples were referenced to either polyisoprene or polystyrene calibration standards obtained from *Polymer Standard Service*, Mainz, Germany.

Differential Scanning Calorimetry (DSC). Thermal analysis of the copolymers was performed using a *TA Instruments DSC 250* in combination with a *TA Instruments RCS 90* cooling system from *Waters Corporation*, United States. Experiments were performed using a heating rate of 10 K min^{-1}, and the instrument was calibrated using a two-point calibration of indium and *n*-octane.

1.3. *IN SITU* ^{1}H NMR DETERMINATION OF THE HALF-LIFE OF *N*-BULI

The solvents MTBE and THF were dried over *n*-BuLi and diphenylethylene and freshly distilled when used. The solvent was inserted into an argon filled glovebox. For the measurement of THF, 0.8 mL of THF was added to an NMR tube and sealed with an septa cap. It was taken out of the glovebox and cooled in an isopropyl alcohol bath (cooled to < -20 °C). Then, 0.2 mL of 2.5 mol L^{-1} *n*-BuLi stock solution in hexane/cyclohexane was added. The NMR tube was kept at < -20 °C, until it was directly inserted into the NMR instrument, which was already set to 20 °C. *In situ* ^{1}H NMR kinetics were recorded without the addition of deuterated solvent. To obtain quantitative proton signals, the delay was set to 60 seconds and 1-scan spectra were recorded to yield a data point each minute.

For MTBE a similar procedure was applied. Again, 0.8 mL of solvent (MTBE) was added to an NMR tube with the addition of 0.05 mL of deuterated cyclohexane (C_5D_{12}). After removal from the glovebox the NMR tube was cooled to < -20 °C in an isopropyl alcohol cooling bath and 0.2 mL of 2.5 mol L^{-1} *n*-BuLi stock solution in hexane/cyclohexane was added. Keeping the NMR tube at < -20 °C it was moved to the NMR instrument. It was inserted to the NMR instrument, already set to 20 °C. As the measurement was carried out over a period of over 5 days, the measurement was performed with the addition of a deuterated solvent to minimize the drift of the spectra. It was recorded with a relaxation delay of 60 seconds and 16 scans per spectra to yield a higher signal-to-noise ratio. Thereby, every 16 min a data point is collected.

1.4 *IN SITU* ^{1}H NMR KINETICS OF HOMOPOLYMERIZATION OF ISOPRENE

MTBE was dried over *n*-BuLi and diphenylethylene and freshly distilled when used. Isoprene was first freed from its stabilizer by passing through alkaline aluminum oxide and dried for 24 hours over calcium hydride. Hydrogen and other gases were removed via three *freeze-pump-thaw* cycles. A second empty reaction flask was loaded with 10 vol% of 25 wt% trioctyl aluminum solution in cyclohexane, and cyclohexane was removed under vacuum. Then isoprene was transferred from calcium hydride onto trioctyl aluminum and stirred for 24 hours. Isoprene was transferred into an empty flask and along with dry MTBE inserted into an argon filled glove box. NMR tubes were loaded with 0.1 g (0.489 mmol) of isoprene and 0.7 mL MTBE each. The tubes were sealed with a septa cap and removed from the glove box. The *in situ* ^{1}H NMR kinetic was measured without the addition of deuterated solvents and initiated with 15.6 µL of 1.3 mol L^{-1} *sec*-BuLi solution in hexane/cyclohexane. The NMR experiment was performed with a relaxation delay of 60 seconds, and 1-scan spectra were recorded until no monomer signal remained. The kinetics data were measured at 23 °C, 30 °C and 40 °C. The polymerization was terminated by the addition of one drop degassed isopropyl alcohol and the product was precipitated in pure isopropyl alcohol.

1.5. *IN SITU* ^{1}H NMR KINETICS OF HOMOPOLYMERIZATION OF *β*-FARNESENE

MTBE was dried over *n*-BuLi and diphenylethylene and freshly distilled when used. *β*-Farnesene was first freed from its stabilizer by passing through alkaline aluminum oxide and dried 24 hours over calcium hydride. Hydrogen and other gases were removed by vacuum. Then 10 vol% of 25 wt% trioctyl aluminum solution in cyclohexane was added and stirred for another 24 hours. Cyclohexane was removed under vacuum. Then *β*-farnesene was distilled, and along with MTBE inserted into an argon filled glove box. NMR tubes were loaded with 0.1 g (0.489 mmol) of *β*-farnesene and 0.7 mL MTBE each. The tubes were sealed with a septa cap and removed from the glove box. The *in situ* ^{1}H

NMR kinetics were measured without the addition of deuterated solvents and initiated with 15.6 µL of 1.3 mol L^{-1} *sec*-BuLi solution in hexane/cyclohexane. NMR experiments were performed with a relaxation delay of 60 seconds, and 1-scan spectra were recorded until no monomer signal remained. The kinetics were measured at 23 °C, 30 °C and 40 °C. The polymerization was terminated by the addition of one drop degassed isopropyl alcohol and precipitated in pure isopropyl alcohol.

1.6. *IN SITU* ^{1}H NMR KINETICS OF THE COPOLYMERIZATION STYRENE AND ISOPRENE

MTBE was dried over *n*-BuLi and diphenylethylene and freshly distilled when used. Isoprene and styrene were first freed from their stabilizer by passing through alkaline aluminum oxide and dried 24 hours over calcium hydride. Hydrogen and other gases were removed via three *freeze-pump-thaw* cycles. A second empty reaction flask was loaded with 10 vol% of 25 wt% trioctyl aluminum solution in cyclohexane and cyclohexane was removed under vacuum. Then the monomers were transferred from calcium hydride onto trioctyl aluminum and stirred for another 24 hours. Isoprene and styrene were transferred into an empty flask and along with dry MTBE transferred into an argon filled glove box. An NMR tube was loaded with 0.55 mL MTBE, 0.052 g (0.76 mmol) isoprene and 0.078 g (0.75 mmol) styrene. The tube was sealed with a septa cap and removed from the glove box. The *in situ* ^{1}H NMR kinetics were measured without the addition of deuterated solvents and initiated with 14.5 µL of 1.3 mol L^{-1} *sec*-BuLi solution in hexane/cyclohexane. The NMR experiment was performed with a relaxation delay of 60 seconds and 1-scan spectra were recorded until no monomer signals remained. The kinetics were measured at 23 °C. The polymerization was terminated by the addition of one drop degassed isopropyl alcohol and the product precipitated in pure isopropyl alcohol.

1.7. *IN SITU* NIR KINETICS OF THE COPOLYMERIZATION STYRENE AND ISOPRENE

The NIR set-up and data analysis have been described in previous publications.[1] Solvents and monomers were dried as in the other experiments, and they were cryo-transferred

into an ampule rather than the glovebox. Cyclohexane was dried under reflux with sodium and benzophenone. After drying, indicated by a blue coloration, the solvent was transferred into the NIR-reaction flask (Morton flask glass reactor), which was equipped with the NIR probe head, the monomer glass ampule, a temperature probe and an additional glass joint. All reactions were carried out under the same conditions, only the amount of MTBE added varies. The synthesis of P($S_{0.5}$-*co*-$I_{0.5}$) with [MTBE]/[Li] = 5 is described as an example. Both dried monomers (48.35 ml, 0.483 mol) isoprene and (55.3 ml, 0.483 ml) styrene were cryo-transferred into an ampule and added to the reaction flask, containing 585 ml cyclohexane and 0.62 ml MTBE. The polymerization was initiated with 0.8 ml (1.04 mmol; 1 eq) of a 1.3 M *sec*-BuLi solution. The addition of the initiator resulted in a color change from colorless to pale yellow at the beginning of the reaction, indicating the preferred isoprene polymerization, to red at the end of the polymerization, indicating the preferred styrene incorporation at this point. After a reaction time of 600 minutes and no further decrease of the NIR signal at 6138 cm^{-1}, the reaction was completed and terminated by adding 2 ml of degassed isopropanol under argon counterflow. The resulting colorless polymer was precipitated in a 3:1 mixture of methanol:isopropanol, dried under reduced pressure and stored at -20 °C.

The reaction temperature was monitored with a temperature probe, and a cryostat was used to maintain a reaction temperature of 20 °C. In all copolymerizations the measured reaction temperature increase did not exceed 10 °C. Previous works demonstrated that the effect of temperature is negligible compared to the effect the modifiers have on the reactivity ratios.[1,2]

2.Kinetics of *n*-BuLi decomposition in THF and MTBE

The kinetics of *n*-BuLi decomposition in THF was tracked via *in situ* ^{1}H NMR kinetics, using the methylene signal at ~ -0.75 ppm. A delay of 60 s between each data point was selected to ensure a full relaxation of the proton signal and 1-scan spectra were recorded. The decrease in the proton integral can be seen in **Figure S1**:

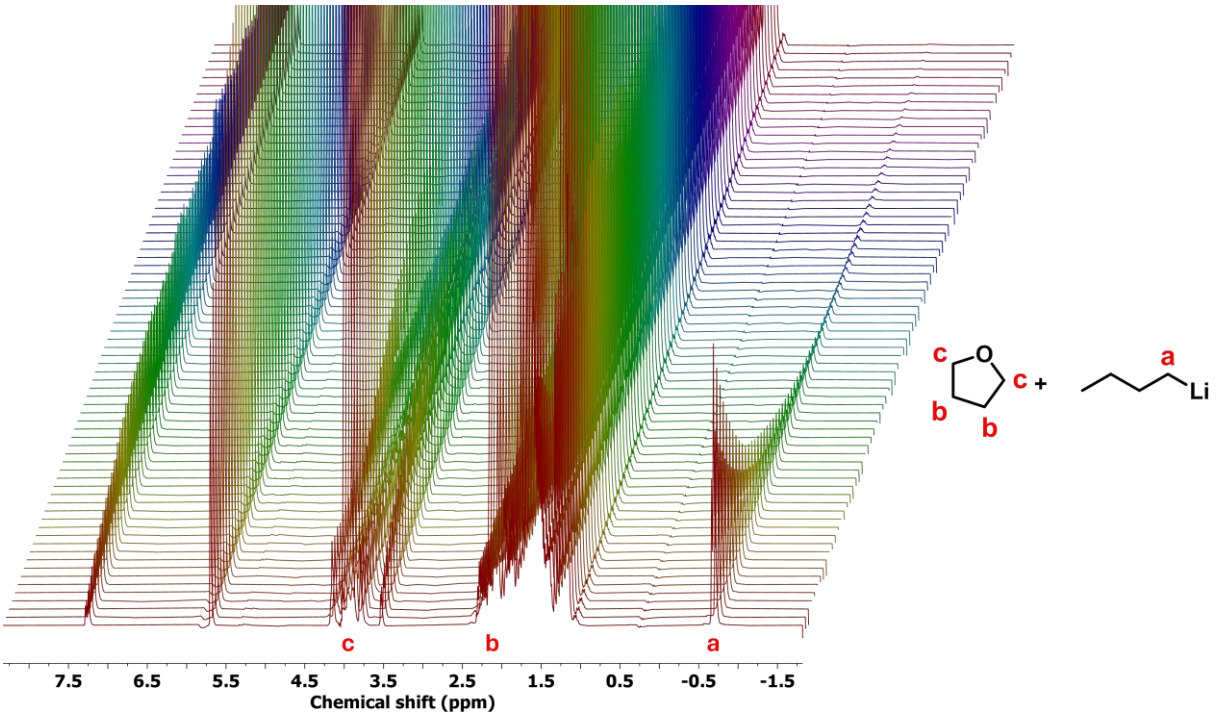

Figure S1. ^{1}H NMR kinetic of n-BuLi in THF, 1-scan spectra recorded with a delay of 60 s without deuterated solvent at 400 MHz, proton signals assigned to THF and n-BuLi, every 5th spectrum is shown.

A similar procedure was performed for *n*-BuLi in MTBE. However, as the process is much slower, 16-scan spectra with a delay of 60 s in between each pulse were recorded, yielding an even better signal-to-noise ratio, see **Figure S2**.

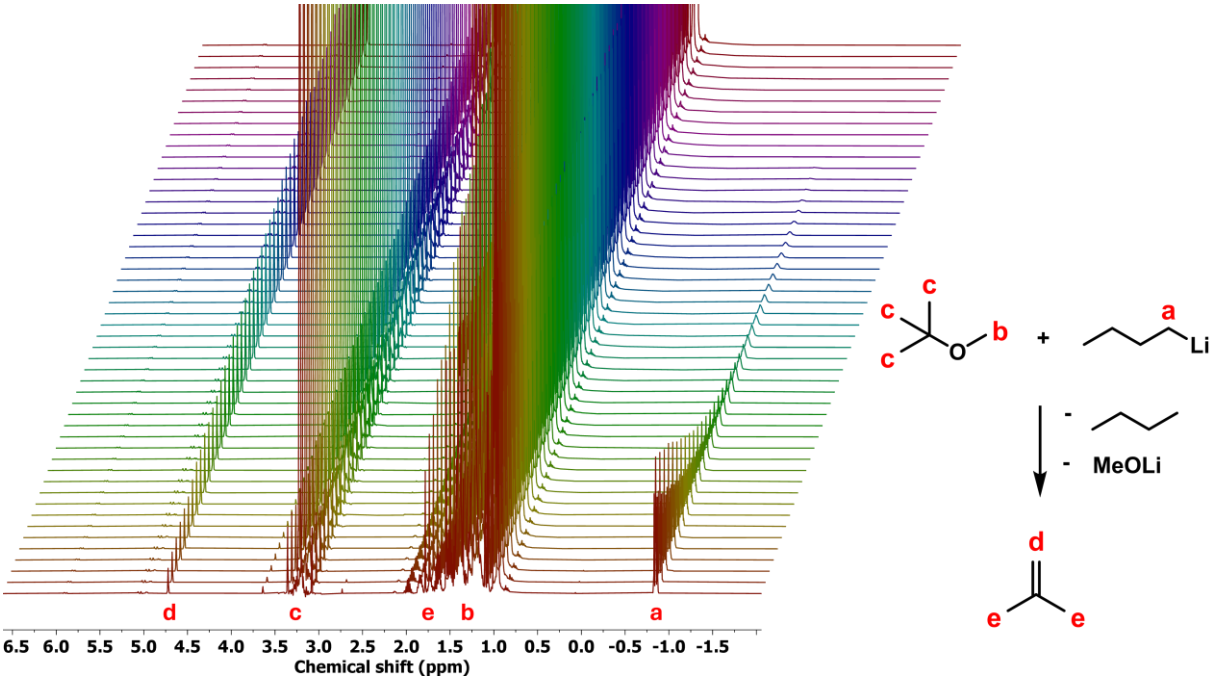

Figure S2. ^{1}H NMR kinetics of n-BuLi in MTBE, 16-scan spectra recorded with a delay of 60 s without deuterated solvent at 500 MHz, proton signals assigned to MTBE, n-BuLi and isobutylene, every 10th spectrum is shown.

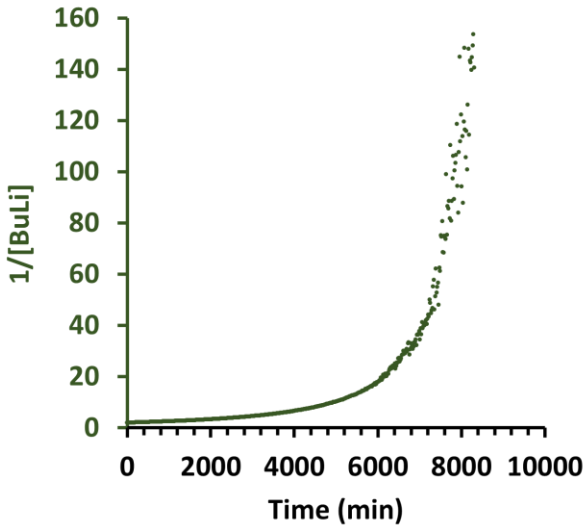

Figure S3. Plot of n-BuLi in MTBE shown as 1/[BuLi] vs time, corresponding to a second order plot.

3. Homopolymerization of Isoprene and β-Farnesene in MTBE

Homopolymerizations of isoprene were performed in MTBE at 23 °C, 30 °C and 40 °C. *In situ* ^{1}H NMR kinetics were measured, and the consumption of isoprene was tracked by following the decrease of the proton integral of the conjugated diene at ~ 6.6 ppm. The respective spectra are presented in **Figure S4** for the polymerization at 23 °C.

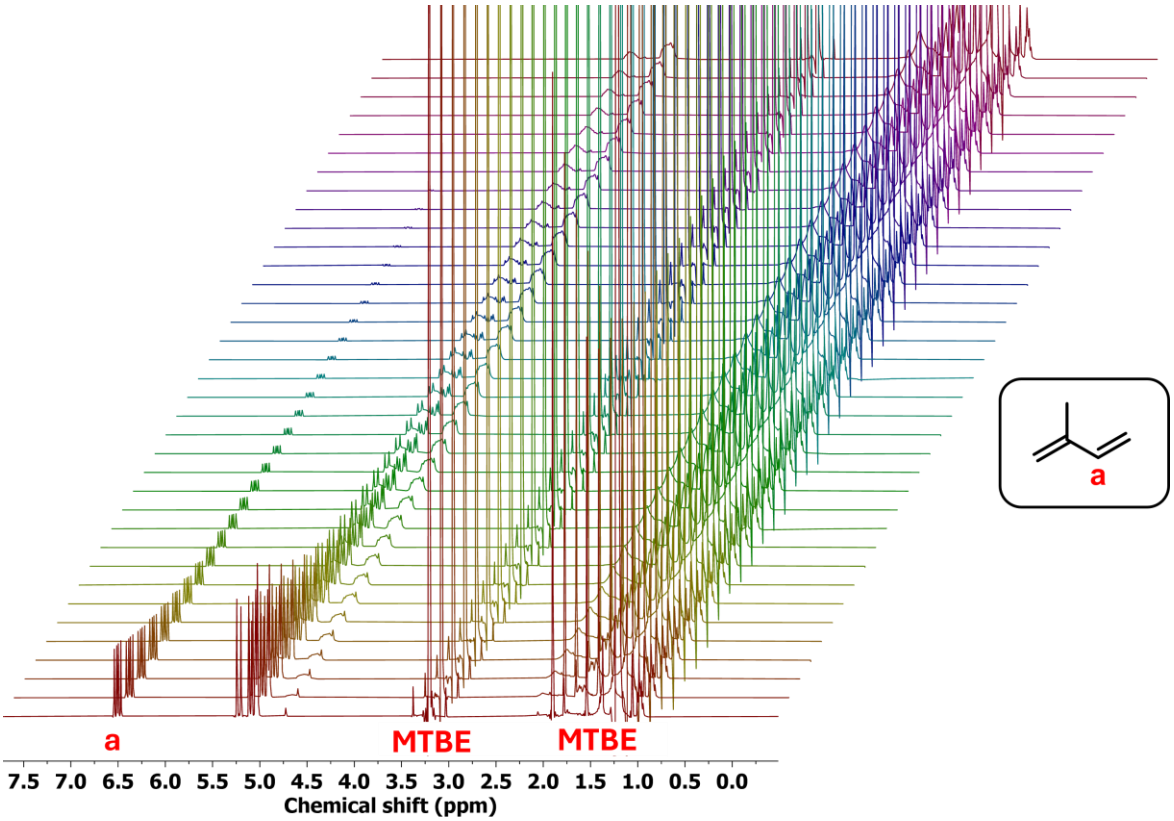

Figure S4. *In situ* ^{1}H NMR kinetics of isoprene in MTBE, 1-scan spectra recorded with a delay of 60 s without deuterated solvent at 400 MHz. The characteristic diene proton signal at 6.6 ppm was used to determine the consumption of isoprene, every 5th spectrum is shown.

Olefin signals in the range of 4.5 ppm to 5.3 ppm represent the methylene protons of the diene structure. The signals change from sharp signals originating from the monomer to broad signals assigned to the olefinic protons of the polymer backbone. The time-conversion plot for each polymerization is presented in **Figure S5**, indicating faster consumption of isoprene at higher temperatures.

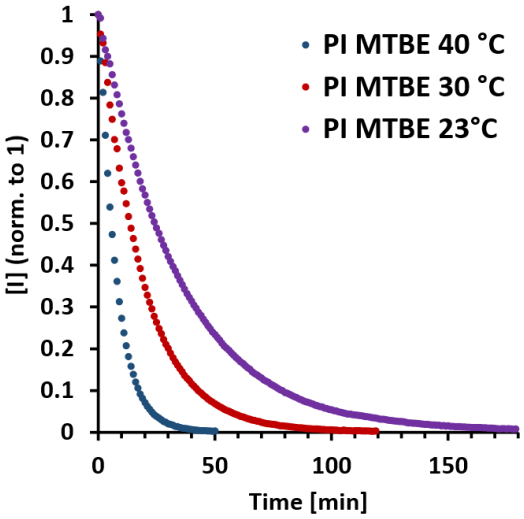

Figure S5. Time-conversion plots of the homopolymerization of isoprene in MTBE carried out at 23 °C, 30 °C and 40 °C.

Additionally, the homopolymerization of isoprene in MTBE was investigated at three different initiator concentrations to determine the degree of aggregation. The time-conversion plots of the respective *in situ* ^{1}H NMR kinetics are shown in the following **Figure S6**:

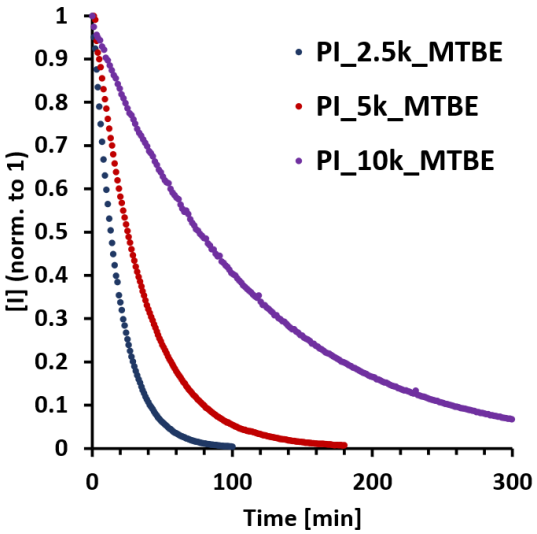

Figure S6. Time-conversion plots of the homopolymerizations of isoprene in MTBE targeting a molar mass of 2.5 kg mol^{-1}, 5 kg mol^{-1} and 10 kg mol^{-1}, respectively.

The homopolymerization was likewise performed for *β*-farnesene in MTBE. **Figure S7** exemplarily shows the *in situ* ^{1}H NMR kinetics of *β*-farnesene polymerized in MTBE at 23 °C. The time-conversion plots of the polymerizations performed at three different

temperatures, 23 °C, 30 °C, and 40 °C, are presented in **Figure S8**. The results of the homopolymerizations targeting different molar masses can be followed in **Figure S9**.

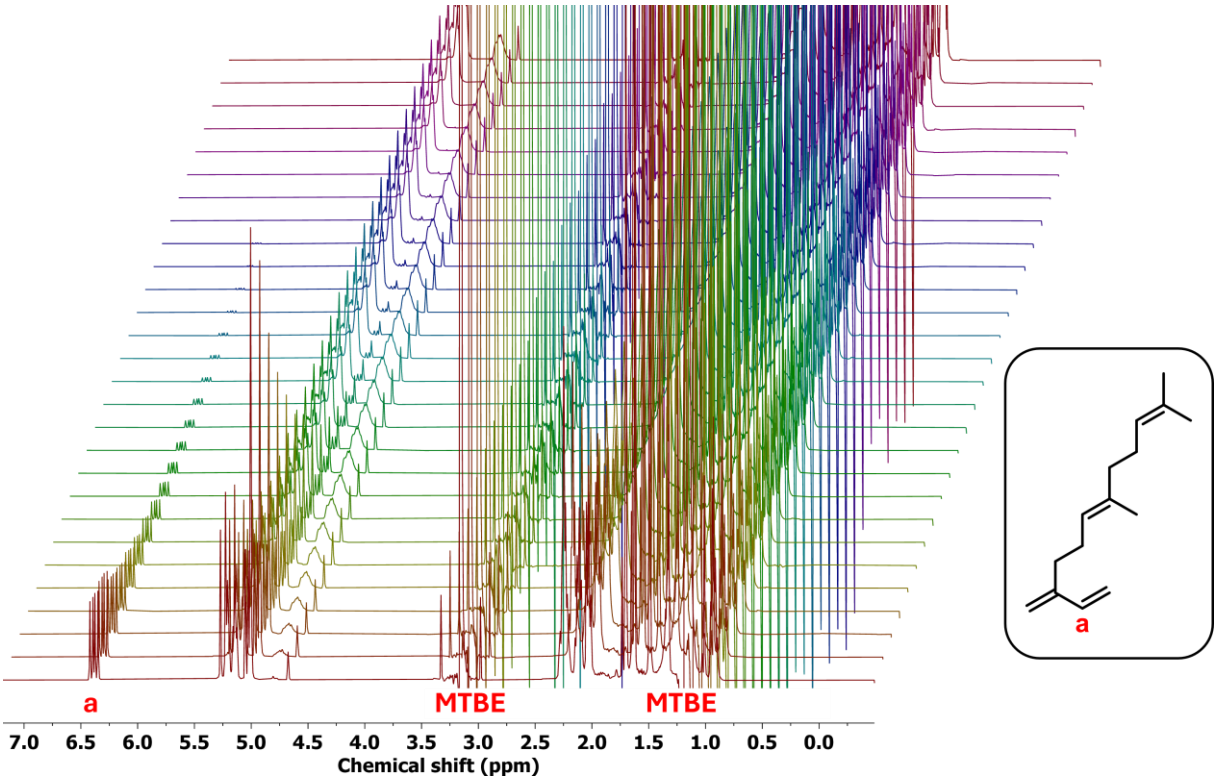

Figure S7. In situ ^{1}H NMR kinetics of β-farnesene in MTBE, 1-scan spectra recorded with a delay of 60 s without deuterated solvent at 400 MHz. The characteristic diene proton signal at ~ 6.4 ppm was used to determine the consumption of β-farnesene, every 5th spectrum is shown.

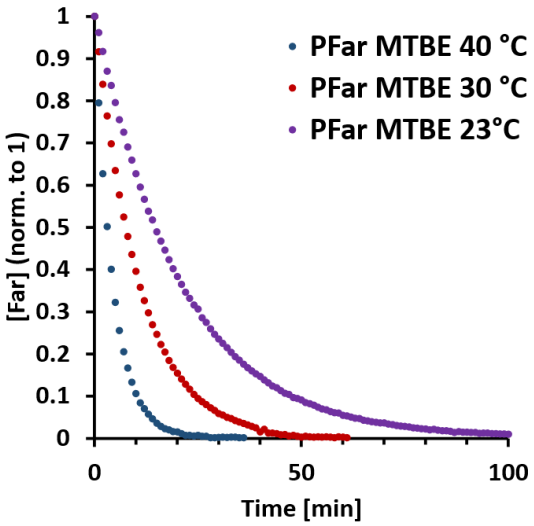

Figure S8. Time-conversion plots of the homopolymerization of β-farnesene in MTBE carried out at 23 °C, 30 °C and 40 °C.

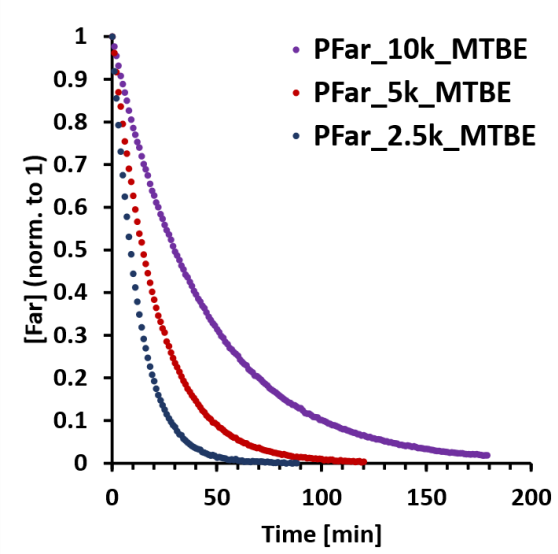

Figure S9. Time-conversion plots of the homopolymerizations of β-farnesene in MTBE at 23 °C targeting a molar mass of 2.5 kg mol^{-1}, 5 kg mol^{-1} and 10 kg mol^{-1}, respectively.

For all kinetics samples polymer characteristics, e.g., the initiator concentration $[Ini]_0$, molar mass by SEC (M_n^{SEC}) and by NMR (M_n^{NMR}) as well as their respective microstructure are summarized in the following **Table S1**:

Table S1. Summary of all collected data of polymer samples obtained in the in situ ^{1}H NMR kinetics of isoprene, $[I]_0$ = 1.94 mol L^{-1}, and β-farnesene, $[Far]_0$ = 0.65 mol L^{-1}, polymerized in MTBE.

$M_n^{theo.}$ [kg mol^{-1}]	Temp. [°C]	$[Ini]_0$ [a)] [mmol L^{-1}]	M_n^{SEC} [b)] [kg mol^{-1}]	$Đ$ [b)]	M_n^{NMR} [c)] [kg mol^{-1}]	1,4- [c)] [%]	3,4- [c)] [%]	1,2- [c)] [%]
Isoprene								
5.0	23	35.5	5.6	1.11	3.7	45.7	50.4	3.9
5.0	30	36.9	5.8	1.11	3.6	47.3	49.0	3.7
5.0	40	37.1	5.5	1.11	3.6	48.5	48.3	3.1
2.5	23	68.6	2.7	1.06	1.9	46.2	49.1	4.7
10.0	23	17.3	15.7	1.05	7.7	47.3	49.1	3.6
Farnesene								
5.0	23	34.9	4.2	1.15	3.8	60.9	39.1	0.0
5.0	30	35.7	4.1	1.16	3.7	59.7	40.3	0.0
5.0	40	34.3	4.1	1.16	3.9	63.0	37.0	0.0
2.5	23	60.7	2.2	1.10	2.2	64.4	35.6	0.0
10.0	23	18.4	9.7	1.04	7.2	60.0	40.0	0.0

[a)] Calculated using the absolute molecular weight M_n^{NMR} and total volume of the reaction mixture. [b)] Determined by SEC (eluent: THF, PI-calibration). [c)] Determined by ^{1}H NMR.[3,4]

4. NMR Spectra of Homopolymers

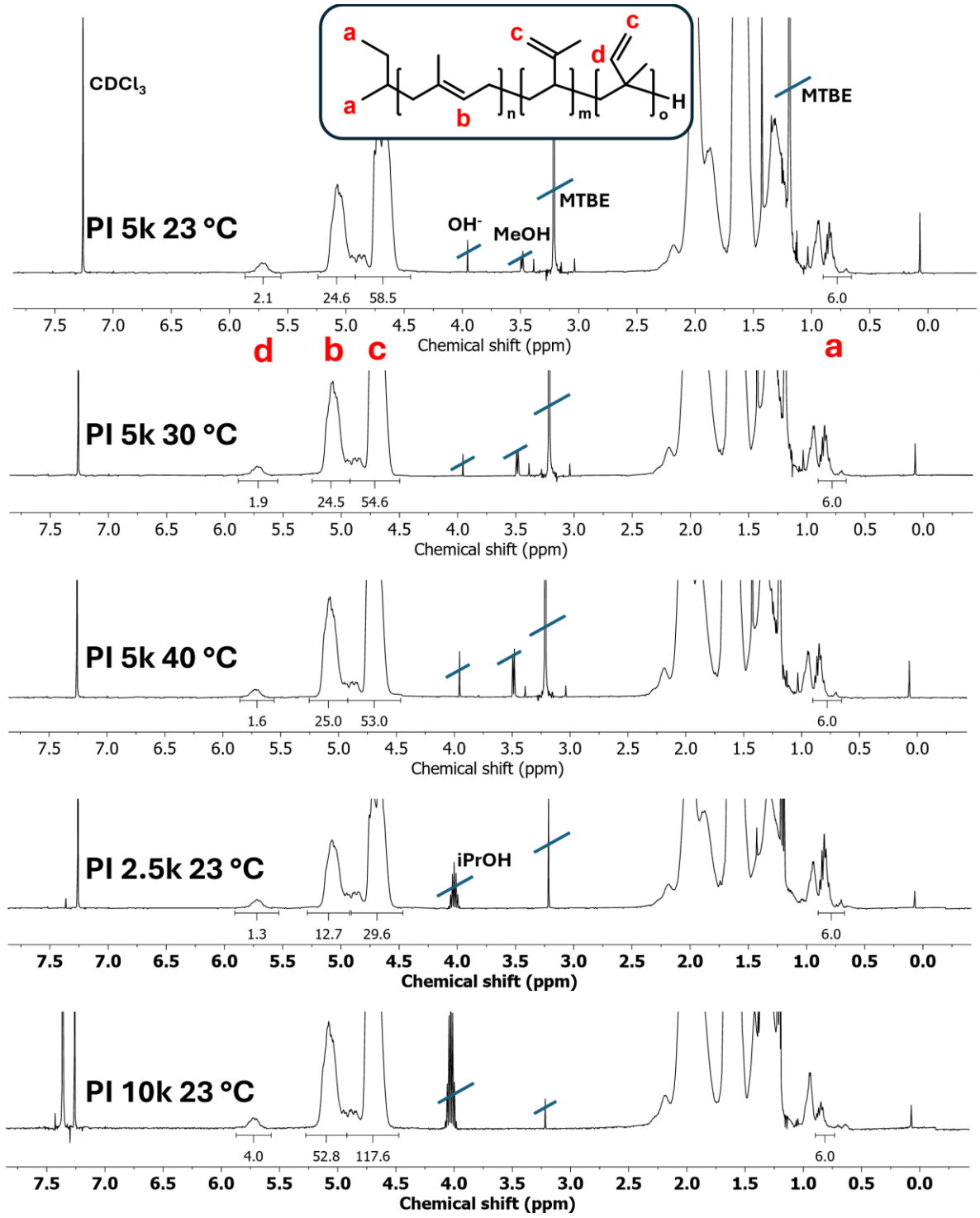

Figure S10. ^{1}H NMR spectra of all PI samples and their proton integrals assigned to the respective characteristic microstructure, measured in $CDCl_3$ at 400 MHz.

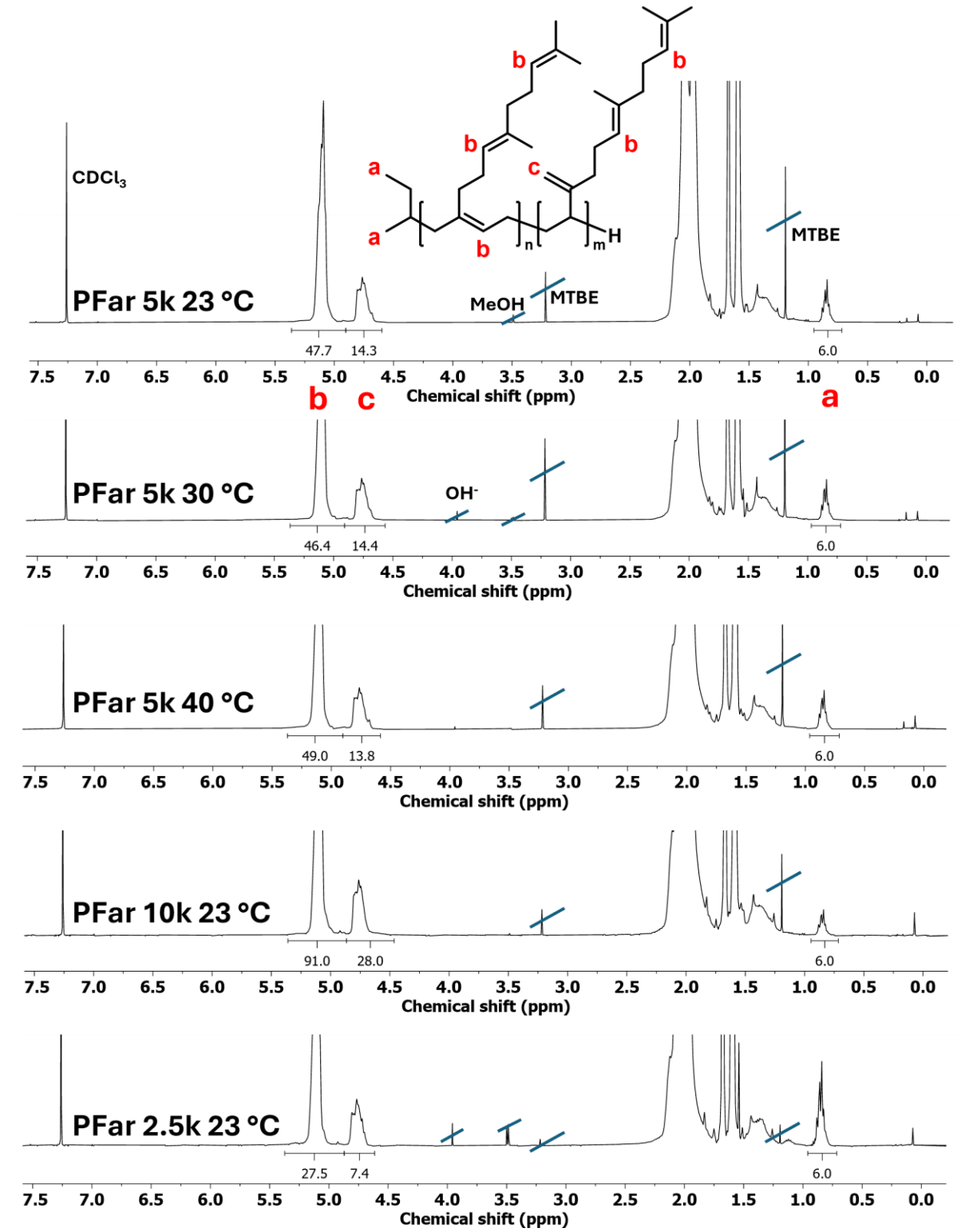

Figure S11. ^{1}H NMR spectra of all PFar samples and their proton integrals assigned to the respective characteristic microstructure, measured in $CDCl_3$ at 400 MHz.

5. SEC Results

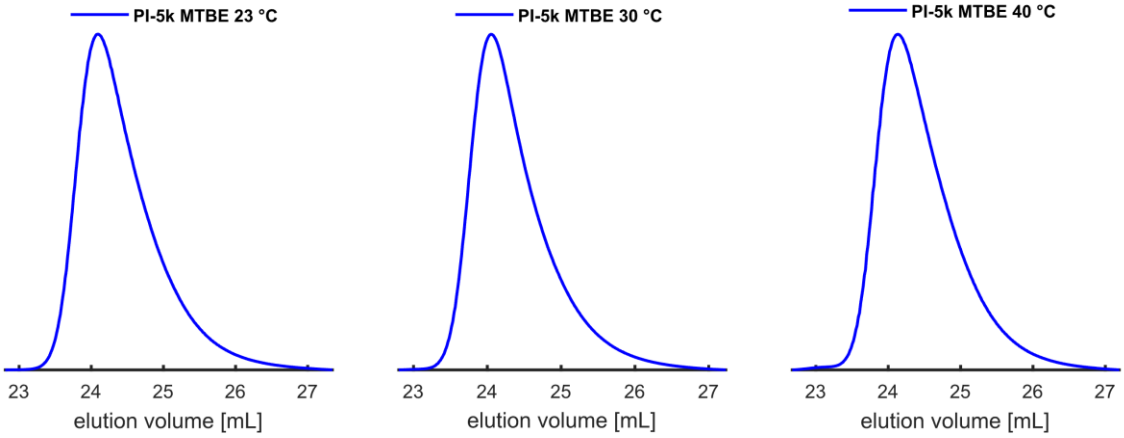

Figure S12. SEC traces of in situ ^{1}H NMR kinetics PI-samples of polymerizations performed at different temperatures, measured in THF using a PI-calibration. For M_n and dispersity, see Table S1.

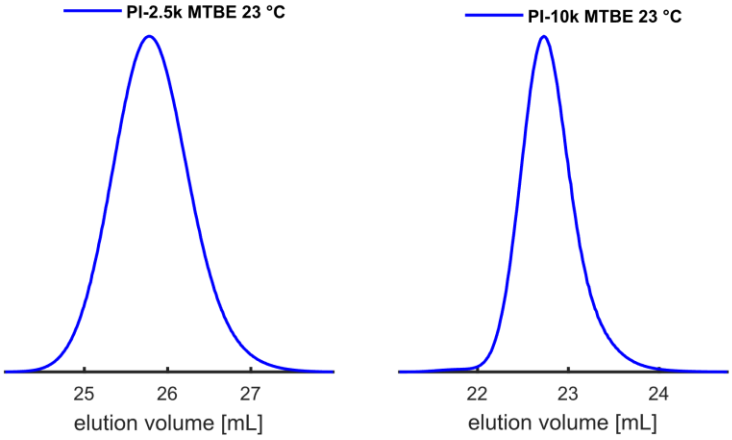

Figure S13. SEC traces of in situ ^{1}H NMR kinetics PI-samples targeting 2.5 kg mol^{-1} and 10 kg mol^{-1}, measured in THF using a PI-calibration. For M_n and dispersity, see Table S1.

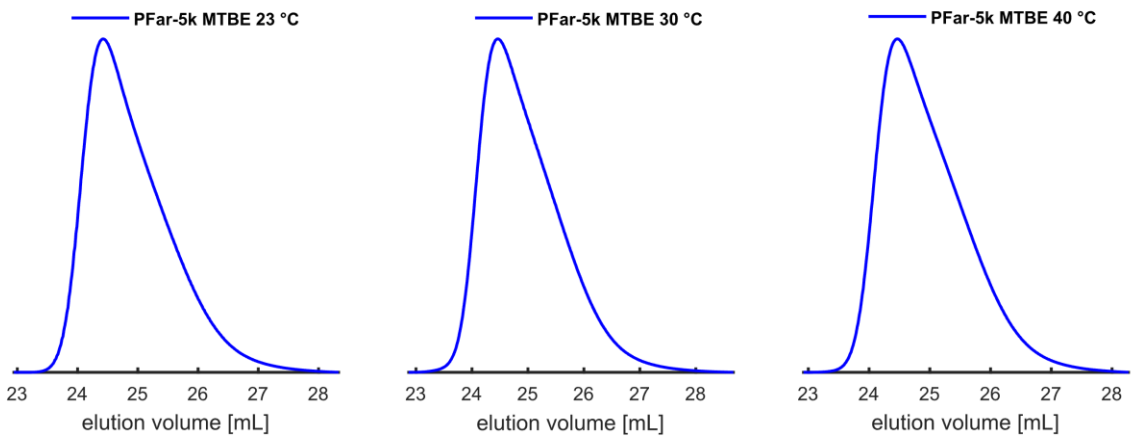

Figure S14. SEC traces of in situ ^{1}H NMR kinetics PFar-samples of polymerizations performed at different temperatures, measured in THF using a PI-calibration. For M_n and dispersity, see Table S1.

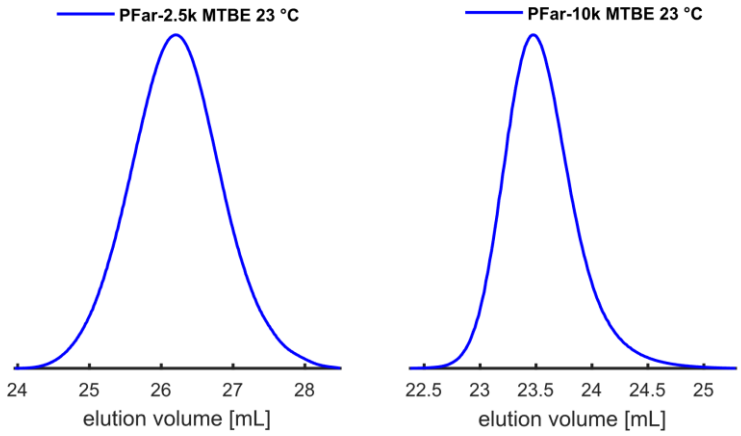

Figure S15. SEC traces of in situ ^{1}H NMR kinetics PFar-samples targeting 2.5 kg mol^{-1} and 10 kg mol^{-1}, measured in THF using a PI-calibration. For M_n and dispersity, see Table S1.

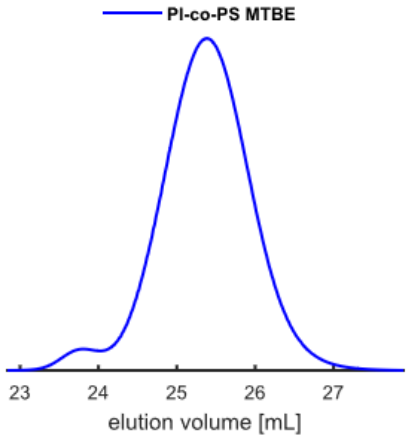

Figure S16. SEC trace of in situ ^{1}H NMR kinetics sample of the copolymerization of isoprene and styrene in MTBE at 23 °C, measured in THF with a PS-calibration.

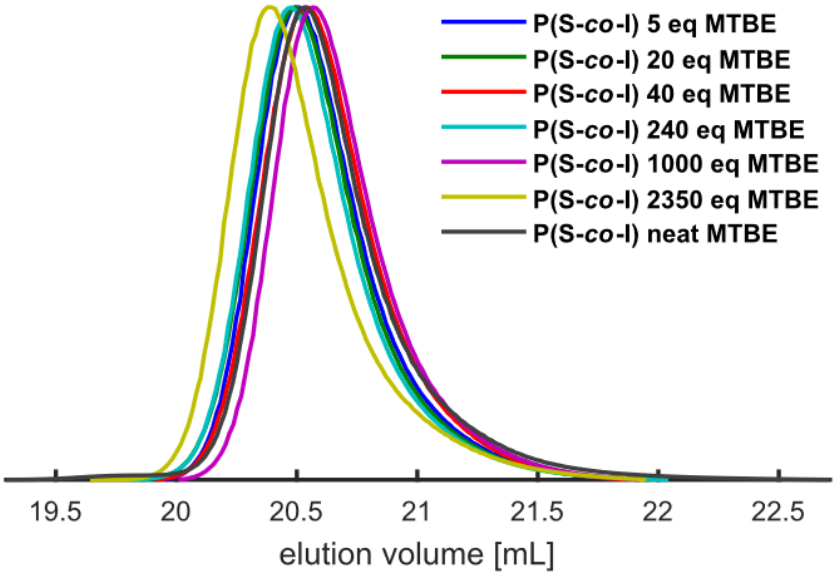

Figure S17. SEC trace of in situ NIR kinetic samples of the copolymerization of isoprene and styrene in cyclohexane with different equivalents of MTBE at 20 °C, measured in THF with a PS-calibration.

6. Copolymerization of Isoprene and Styrene

6.1 *In situ* ^{1}H NMR Kinetics

The copolymerization of isoprene and styrene was investigated both *via in situ* ^{1}H NMR kinetics and *in situ* NIR kinetics. First, neat MTBE was used as a solvent in the NMR experiment, see **Figure S18**. The individual monomer consumption is plotted versus time and total conversion and the Jaacks equation,[5] **Equation S1**, is used to determine the reactivity ratios, r_I and r_S. All three plots are illustrated in **Figure S19**, and the results is summarized in **Table 2.**

$$\ln\frac{[M_1]_0}{[M_1]_t} = r_1 \ln\frac{[M_2]_0}{[M_2]_t}; \qquad r_2 = 1/r_1 \qquad \textbf{(Equation S1)}$$

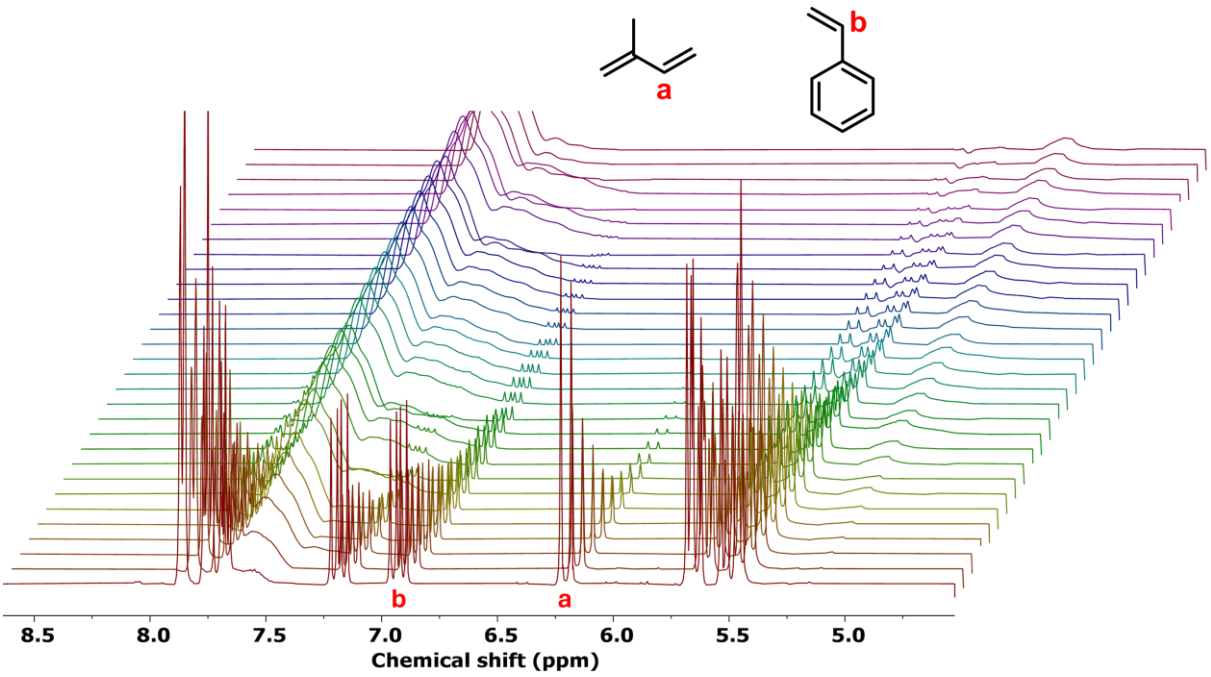

Figure S18. In situ ^{1}H NMR spectra of the copolymerization of styrene and isoprene in neat MTBE, measured in non-deuterated MTBE at 23 °C and 400 MHz.

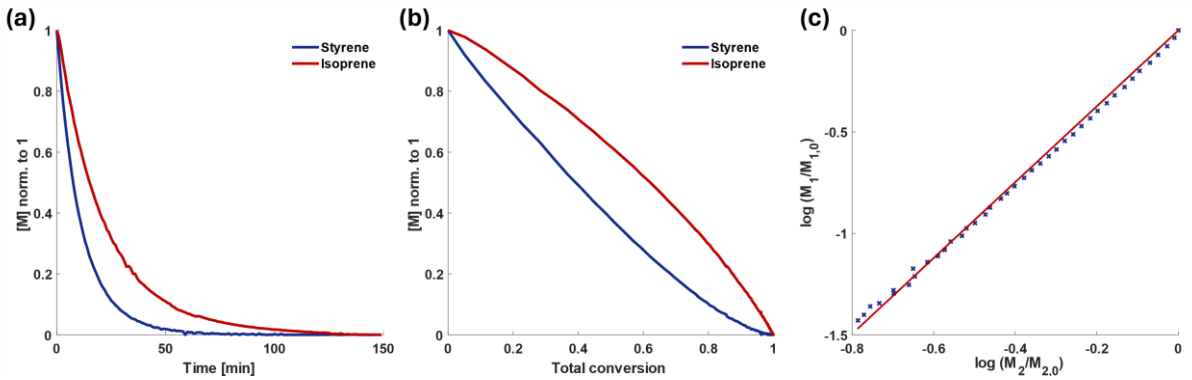

Figure S19. In situ ^{1}H NMR kinetics of the copolymerization of styrene and isoprene in MTBE at 23 °C, (a) time-conversion plot, (b) monomer consumption vs. total consumption, (c) Jaacks-fit of the copolymerization; r_I=0.53 and r_S=1.87.

6.2 In Situ NIR Kinetics

For the determination of the influence of an increasing amount of MTBE added to the copolymerization in cyclohexane, *in situ* NIR kinetics experiments were performed. The equivalents of [MTBE]/[Li] were steadily increased from 5 to 20, 40, 240, 1000, 2350 to 4700 equivalents, respectively. Pure MTBE was achieved by 4700 equivalents. In the following, the time-conversion and monomer-total conversion-plots and the respective fits for the determination of the reactivity ratios are given, see **Figure S20-S25**.

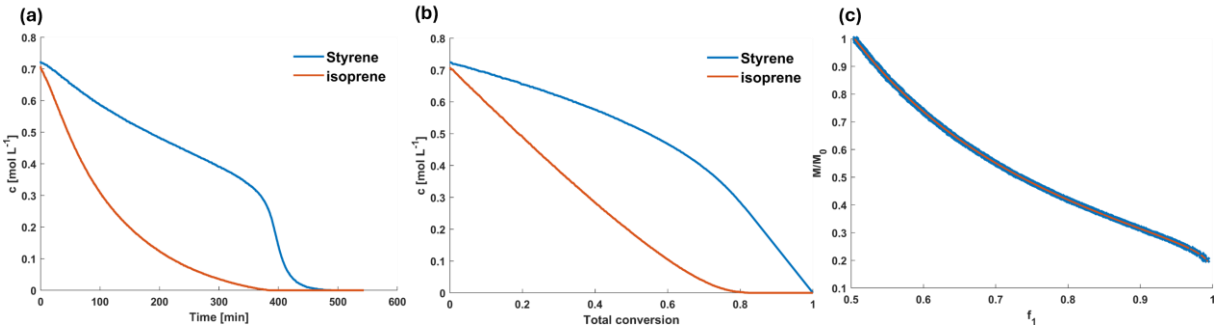

Figure S20. In situ NIR kinetics of the copolymerization of styrene and isoprene in CHx and 5 eq MTBE at 20 °C, (a) time-conversion plot, (b) monomer consumption vs. total consumption, (c) Meyer Lowry-fit of the copolymerization, r_I=3.13 and r_S=0.09.

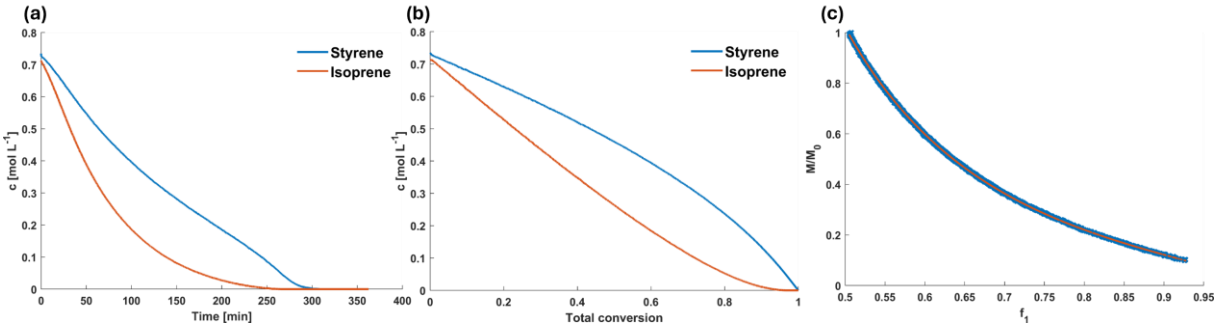

Figure S21. In situ NIR kinetics of the copolymerization of styrene and isoprene in CHx and 20 eq MTBE at 20 °C, (a) time-conversion plot, (b) monomer consumption vs. total consumption, (c) Meyer Lowry-fit of the copolymerization, r_I=1.74 and r_S=0.31.

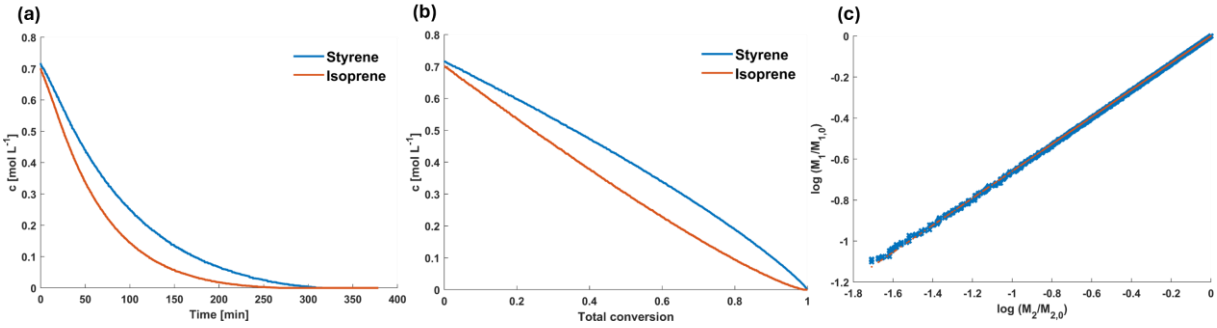

Figure S22. In situ NIR kinetics of the copolymerization of styrene and isoprene in CHx and 40 eq MTBE at 20 °C, (a) time-conversion plot, (b) monomer consumption vs. total consumption, (c) Jaacks-fit of the copolymerization, r_I=1.52 and r_S=0.66.

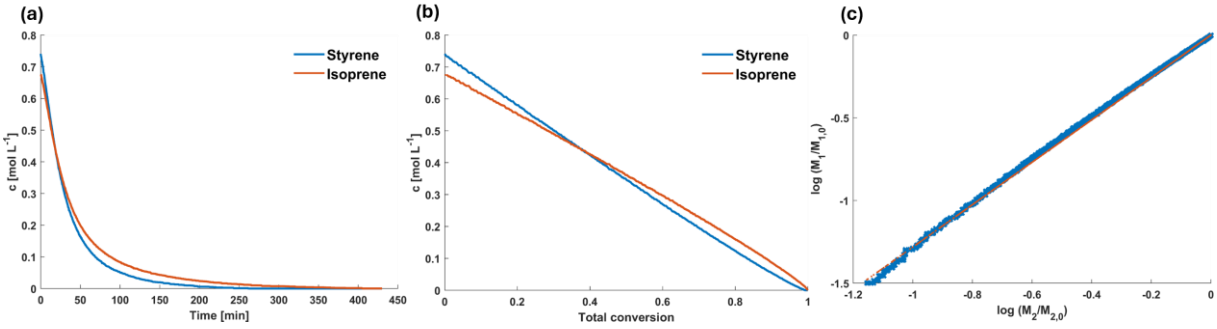

Figure S23. In situ NIR kinetics of the copolymerization of styrene and isoprene in CHx and 240 eq MTBE at 20 °C, (a) time-conversion plot, (b) monomer consumption vs. total consumption, (c) Jaacks-fit of the copolymerization, r_I=0.78 and r_S=1.28.

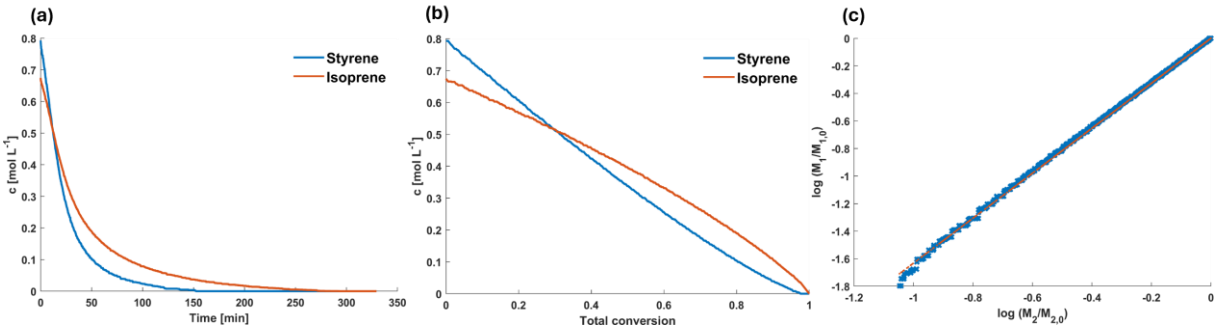

Figure S24. In situ NIR kinetics of the copolymerization of styrene and isoprene in CHx and 1000 eq MTBE at 20 °C, (a) time-conversion plot, (b) monomer consumption vs. total consumption, (c) Jaacks-fit of the copolymerization, r_I=0.61 and r_S=1.63.

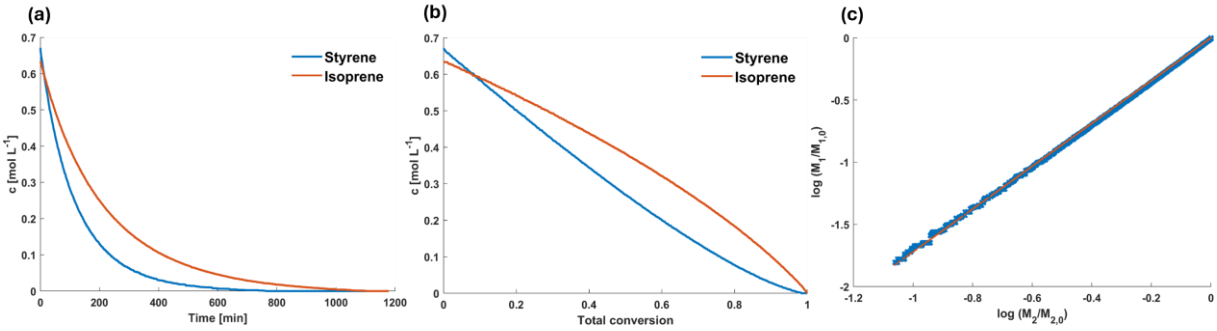

Figure S25. In situ NIR kinetics of the copolymerization of styrene and isoprene in CHx and 2350 eq MTBE at 20 °C, (a) time-conversion plot, (b) monomer consumption vs. total consumption, (c) Jaacks-fit of the copolymerization, r_I=0.58 and r_S=1.72.

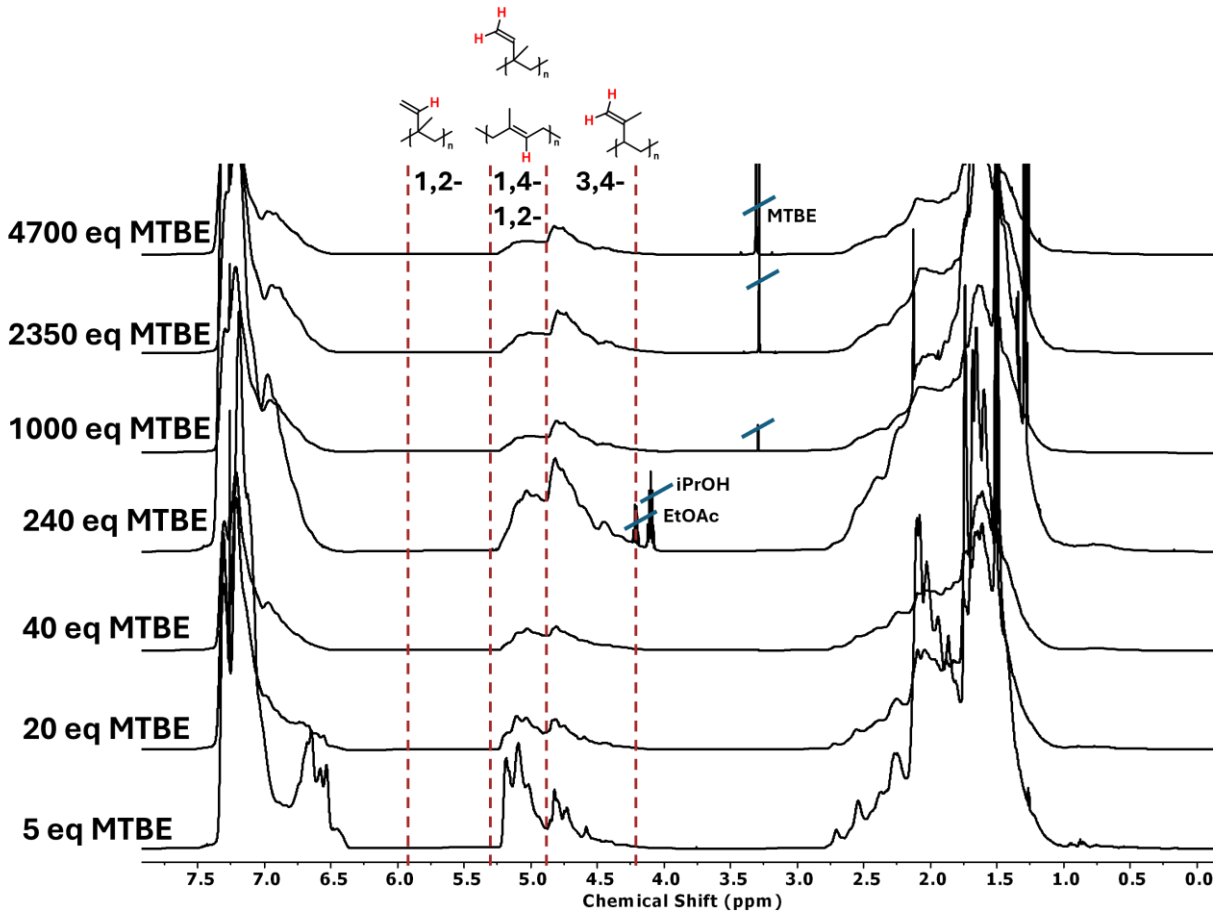

Figure S26. ^{1}H NMR results of all synthesized in situ NIR PS-co-PI copolymers indicating signals of the respective PI microstructure, measured in $CDCl_3$ and 600 MHz.

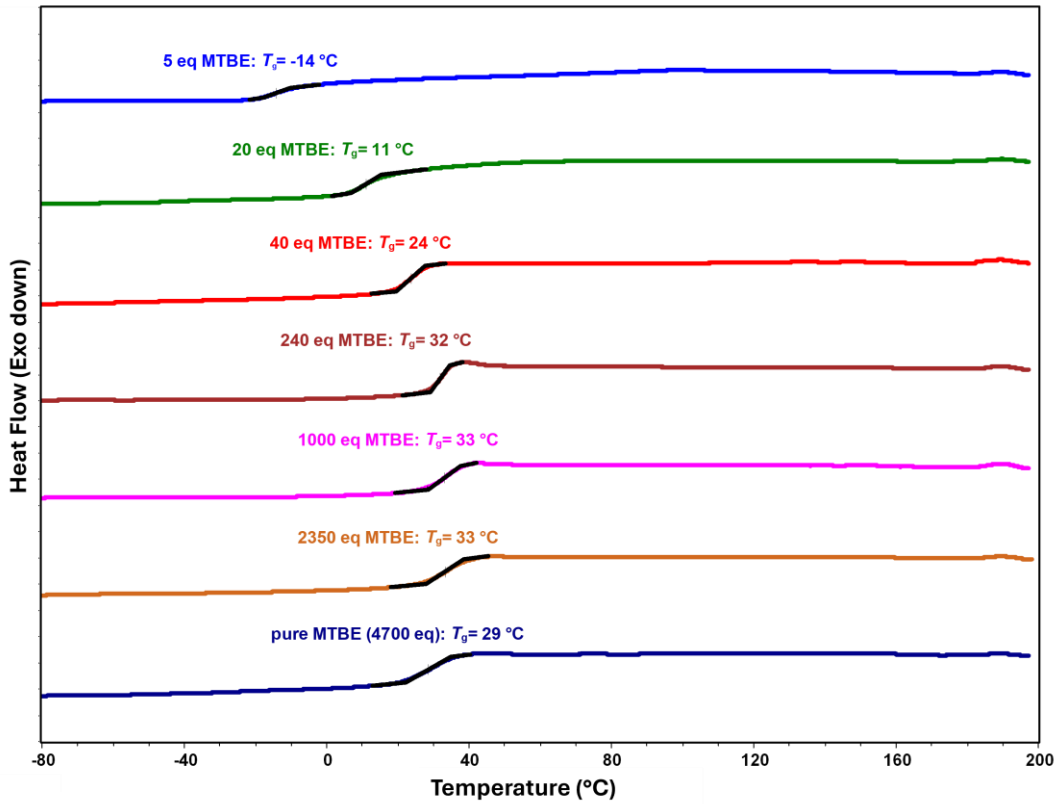

Figure S27. Second DSC heating curve of all synthesized PS-co-PI copolymers, measured with a heating rate of 10 K min^{-1}.

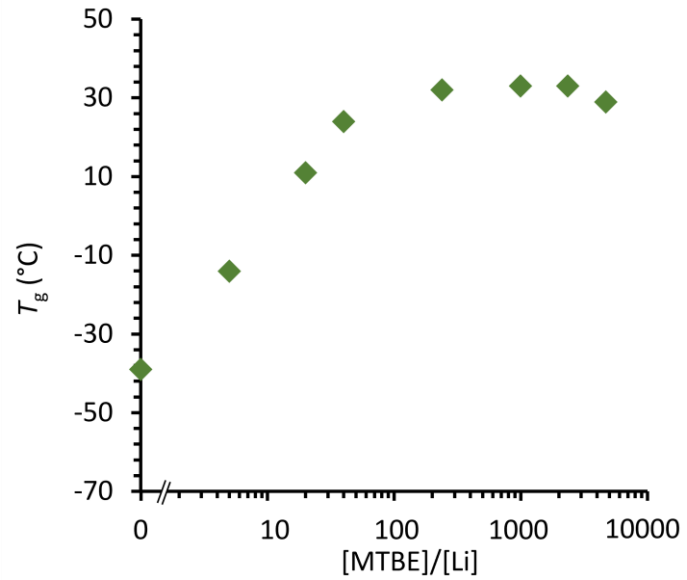

Figure S28. Glass transition temperature versus [MTBE]/[Li] ratio of all PS-co-PI copolymers.

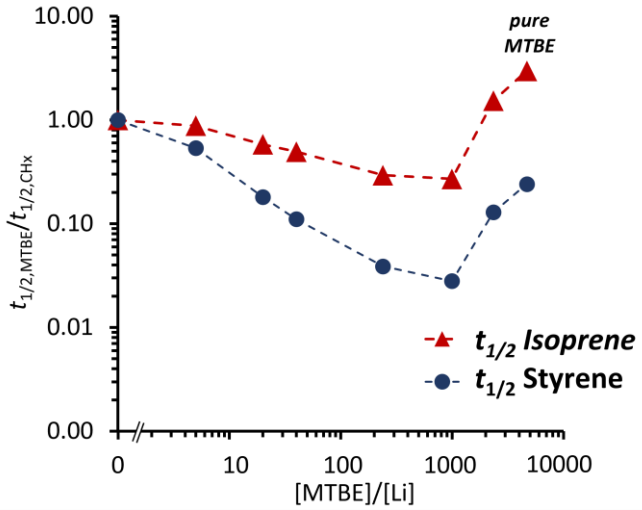

Figure S29. Half-lives of styrene and isoprene with increasing ratio [MTBE]/[Li] normalized to values in cyclohexane ($t_{1/2}^{S,CHx}$= 614 min, $t_{1/2}^{I,CHx}$= 96 min), lines connecting the symbols are a guide to the eye only.

6.3 Blockiness Study

The so-called blockiness of a PS-*co*-PI copolymer can be described by the ratio of SSS-triads in relation to all triads (ISS, ISI, SSS). The triads have slightly different shifts in the respective ^{1}H NMR spectra and can be used to quantify the SSS-triads. This can be used to get a rough estimate on the parameter "blockiness" that corresponds to the block-like PS-domains of at least 3 repeating units.[2,6–8] The results for all PS-*co*-PI copolymer samples of this work is summarized in **Figure S30**.

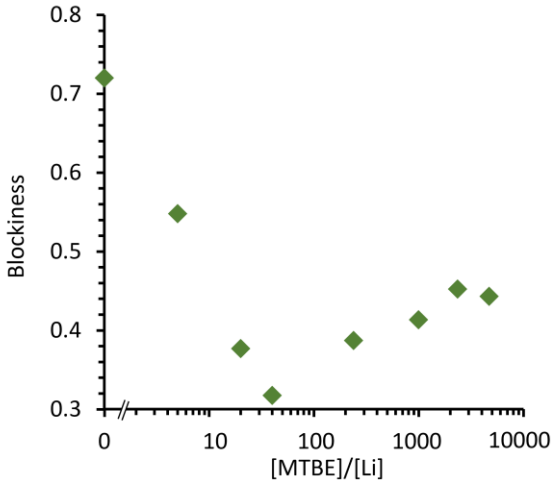

Figure S30. Blockiness of PS content of all PS-*co*-PI copolymers with increasing ratio [MTBE]/[Li], value in pure cyclohexane taken from ref[2].

References

(1) Steube, M.; Johann, T.; Plank, M.; Tjaberings, S.; Gröschel, A. H.; Gallei, M.; Frey, H.; Müller, A. H. E. Kinetics of Anionic Living Copolymerization of Isoprene and Styrene Using in Situ NIR Spectroscopy: Temperature Effects on Monomer Sequence and Morphology. *Macromolecules* **2019**, *52* (23), 9299–9310. DOI: 10.1021/acs.macromol.9b01790.

(2) Steube, M.; Johann, T.; Hübner, H.; Koch, M.; Dinh, T.; Gallei, M.; Floudas, G.; Frey, H.; Müller, A. H. E. Tetrahydrofuran: More than a "Randomizer" in the Living Anionic Copolymerization of Styrene and Isoprene: Kinetics, Microstructures, Morphologies, and Mechanical Properties. *Macromolecules* **2020**, *53* (13), 5512–5527. DOI: 10.1021/acs.macromol.0c01022.

(3) Meier-Merziger, M.; Fickenscher, M.; Hartmann, F.; Kuttich, B.; Kraus, T.; Gallei, M.; Frey, H. Synthesis of phase-separated super-H-shaped triblock architectures: poly(l-lactide) grafted from telechelic polyisoprene. *Polym. Chem.* **2023**, *14* (23), 2820–2828. DOI: 10.1039/D3PY00230F.

(4) Meier-Merziger, M.; Imschweiler, J.; Hartmann, F.; Niebuur, B.-J.; Kraus, T.; Gallei, M.; Frey, H. Bifunctional Carbanionic Synthesis of Fully Bio-Based Triblock Structures Derived from β-Farnesene and ll-Dilactide: Thermoplastic Elastomers. *Angew. Chem. Int. Ed.* **2023**, *62* (42), e202310519. DOI: 10.1002/anie.202310519. Published Online: Jul. 28, 2023.

(5) Jaacks, V. A Novel Method of Determination of Reactivity Ratios in Binary and Ternary Copolymerizations. *Makromol. Chem.* **1972**, *161* (1), 161–172. DOI: 10.1002/macp.1972.021610110.

(6) Bovey, F. A.; v. d. Tiers, G.; Filipovich, G. Polymer NSR spectroscopy. I. The motion and configuration of polymer chains in solution. *J. Polym. Sci.* **1959**, *38* (133), 73–90. DOI: 10.1002/pol.1959.1203813308.

(7) v. d. Mochel. Nuclear Magnetic Resonance-Analog Computer Method for "Block Styrene". *Macromolecules* **1969**, *2* (5), 537–540. DOI: 10.1021/ma60011a017.

(8) Handlin, D. L.; Williamson, D. T.; Willis, C. L. Block copolymer. US20020289833 20021107.

Chapter A2

Evaluation of a novel series of enteric -copolymers for pharmaceutical applications: α-hydroxycarboxylic acid modified polymethacrylates

[redacted], Dominik Albrecht Hugo Fuchs[3], [redacted]

[1] Department Pharmaceutical Technology and Biopharmaceutics, Johannes Gutenberg-University Mainz, Staudinger Weg 5, 55128 Mainz, Germany

[2] Department of Pharmaceutical Sciences, University of Michigan, Ann Arbor, MI 48104, USA

[3] Institute of Organic Chemistry, Johannes Gutenberg-University Mainz, Duesbergweg 10-14, 55128 Mainz, Germany

[4] Institute of Pharmaceutical and Biomedical Sciences, Johannes Gutenberg-University Mainz, Staudingerweg 5, 55128, Mainz, Germany.

* Correspondence: [redacted]

† Equal first authors.

Abstract

Enteric-coated dosage forms often suffer from sluggish post-gastric emptying drug release. Addressing this issue, this work focuses on developing novel enteric polymers as an approach to overcome this problem. The well-known polymer structures of Eudragit® L and L55 were esterified with the α-hydroxycarboxylic acids L- and D,L-lactic and glycolic acid. A resulting partial positive charge arises within the ester linkage, reducing the pK_a value of the polymer. This translates to more facile deprotonation of the carboxylic acid moieties, which enables more rapid polymer dissolution and consequently faster drug release. The dissolution pH threshold was reduced from pH 5.5 for the established Eudragit® L 55 to around 5, while the valuable acid-resistant properties of the polymethacrylates were preserved. Capsules filled with paracetamol were coated with the modified polymers as well as with the commercially available materials Eudragit® L and L55. In 0.01 M hydrochloric acid all coated capsules remained intact without any significant drug release. However, the drug release in 15 mM phosphate buffer (pH 6.5) from the formulations based on the novel polymers was significantly enhanced compared to formulations with Eudragit® L and L55. The increased release rate was connected to the faster dissolution of the modified polymers. This novel series of enteric polymers could help to overcome clinical problems associated with the currently used enteric Eudragit® polymers.

Introduction

Enteric coatings are frequently used in the formulation of oral dosage forms to delay drug release until the dosage form is emptied from the stomach and reaches the small intestine. [1] The rationale behind the use of pH-dependent coatings is e.g., to protect the drug from degradation in the stomach or to protect the stomach from irritation by drugs [1]. Usually, enteric coatings consist of acidic polymers that are protonated in the gastric fluid and therefore insoluble. When the coated dosage form reaches the small intestine with an increased pH-environment the polymer gets deprotonated and thus soluble. As a result, the enteric coating begins to dissolve and the active pharmaceutical ingredient (API) is released from the dosage form and can be absorbed from the proximal small intestine. The most frequently used enteric polymer is the methacrylic acid-ethyl acrylate 1:1 copolymer (P[MA-*co*-EA]) with the trade name Eudragit® L30-D55/Eudragit® L100-55 or Kollicoat® MAE [2]. The manufacturer states that the polymer has a dissolution pH threshold of 5.5 and therefore targets the drug release in the duodenum [3].

However, recent studies indicate too slow post-gastric disintegration of enteric-coated dosage forms and consequently drug release in a lower part of the small intestine, missing their targeted release destination [4]. A slow *in vivo* release of the API can sometimes lead to serious bioavailability problems of drugs with a major absorption site in the duodenum. Rudinskas *et al*. reported cases where poor bioavailability of iron sulfate from enteric-coated formulations is due to drug release taking place after the dosage form has passed the duodenum and jejunum, the preferential absorption site of iron salts [5]. Mössner and Keim proposed that the insufficient treatment of gastrointestinal distress symptoms associated with an exocrine pancreatic insufficiency is related to the delayed onset of pancreatin release from enteric-coated dosage forms [6]. A more recent study showed that low-doses of enteric-coated aspirin have no benefit in lowering the risk of cardiovascular diseases towards placebo [7]. On the other hand, it is well known that low-dose aspirin decreases the risk of cardiovascular events [8]. The studies indicates that the failure of enteric-coated low-dose aspirin is related to a dissolution failure of the enteric coating. Cox *et al*. performed a bioequivalence study on five different aspirin preparations (three 75 mg enteric-coated (EC) dosage forms, one 75 mg dispersible form and one combination of 25 mg immediate release (IR) aspirin/200 mg modified release dipyridamole). They found that the EC aspirin showed a lower bioavailability compared to

the IR formulation and concluded that the lower absorption from the EC dosage form is due to the enteric coating [9]. The authors proposed that an increase in the dose of the EC formulation could overcome the clinical failure of the EC products [9]. However, Cox *et al.* also stated that this could increase the risk for bleeding events [9,10]. Consequently, there is a need for novel formulation strategies to enhance the drug release from EC formulations, thus overcoming the low bioavailability and treatment failure of these products.

There has been progress in the development of EC dosage forms with enhanced post gastric dissolution rates. Liu *et al.* introduced a double-coating approach of pellets. Their coat consists of two different coating layers, namely an inner coat with partially neutralized Eudragit® L30 D-55 with addition of a buffering agent (e.g., citric acid or adipic acid) and an outer coat with a standard Eudragit® L30D-55 formulation. Through the high local buffer concentrations, they could show a strongly improved release of the API even at a decreased bulk pH of 5.6 [11,12]. However, this approach includes two coating steps and is therefore more time consuming and maybe costlier in comparison to a single coat approach. In addition, even this approach could benefit from improved polymers. For an even greater improvement can be achieved by using inherently faster dissolving polymers in the described double coat.

In this study, we propose a novel strategy to enhance the post gastric disintegration and dissolution using modified methacrylic polymers In our patent application (DE 10 2018 129 419) the successful synthesis of a novel type of methacrylic acid-based polymers is described in chapter 4. [13] In brief, the well-known and established structure of P[MA-*co*-EA] and methacrylic acid-methyl methacrylate 1:1 copolymer P[MA-*co*-MMA] (corresponding the Eudragit® L55 and Eudragit® L polymer, respectively) were modified by esterification of the functional carboxylic group with the α-hydroxycarboxylic acids lactic acid (D,L-Lac or L-Lac) and glycolic acid (Gly) (Figure 1).

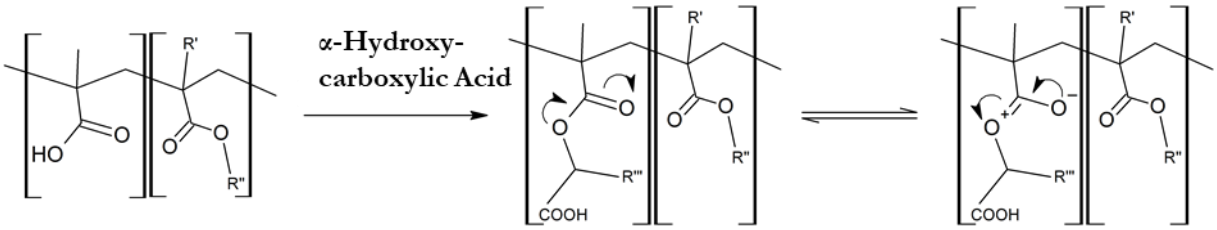

Figure 1. Modification of methacrylic acid-ethyl acrylate (R' =H; R''= COOEt) by esterifying the free acid group with the hydroxy group of lactic acid (R''' = Me) or glycolic acid (R''' = H) and the resonance structures of the modified polymers. The partial positive charge at the oxygen atom reduces the pK_a of the carboxylic group.

The novel structure exhibits resonance creating a partial positive charge at the oxygen atom in the ester bond. The resulting strong electron withdrawing effect lowers the pK_a of the carboxylic acid group. As described in literature, the pK_a of carboxylic acid groups has a strong effect on the dissolution rate, and with a lower pK_a value of the dissolving acid the dissolution rate is usually enhanced [14–16]. Consequently, the drug release after gastric emptying from enteric coated dosage forms with the proposed polymer should be more rapid compared to the commercially available polymers (P[MA-*co*-EA] and P[MA-*co*-MMA]), while maintaining acid stability. An *in silico* prediction of the effect of the modification on the pK_a and intrinsic solubility of the repeating monomer unit was performed using the ADMET Predictor 8.0 (Simulations Plus, Inc., Lancaster, CA, USA) (Table 1). It is self-evident that the polymers have different value, but the general trend will be reflected in the polymers as well, supporting this hypothesis.

Table 1. Predictions made by ADMET Predictor concerning the physico-chemical properties of the repeating monomer blocks of the original and proposed polymers.

Property	**Input structure**	**pK_a**	**Intrinsic solubility (mg/ml)**	**Ionized form solubility (mg/ml)**
Methacrylic acid-ethyl acrylate repeating monomer	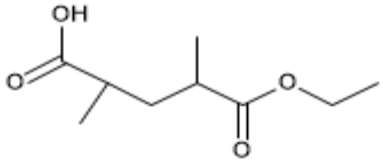	4.81	7.358	112.772

Glycolic acid ester	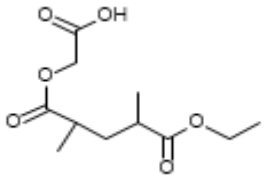	3.49	5.105	113.235
Lactic acid ester	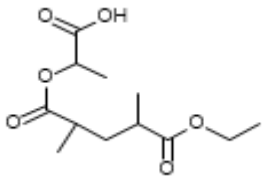	3.66	3.113	95.143

The aim of this work was to evaluate the newly synthesized polymers regarding their dissolution behavior and suitability for enteric coatings.

Materials and methods

Materials

Size 0 hydroxypropyl methylcellulose (HPMC) capsules (ACG Nature Caps Plus) were received from ACG Associated Capsules Pvt Ltd (Ashagadh, Maharashtra, India). Paracetamol was brought from Caesar & Loretz GmbH (Hilden, Germany) and triethyl citrate (TEC) from Merck Schuchardt OHG (Hohenbrunn, Germany) Manniltol, fumed silica and talcum were pharmacopeial quality and bought from Fagron GmbH (Glinde, Germany). 3-(4,5-di methyl thiazol-2-yl)-2,5-diphenyltetrazolium bromide (MTT), dimethyl sulfoxide (DMSO) and sodium dodecyl sulfate (SDS) were bought form Thermo Fischer Scientific(Waltham, USA), Eudragit® L100 and L100-55 were received as free samples from Evonik Röhm GmbH (Darmstadt, Germany). The modified polymers were synthesized in-house. For the detailed synthesis the reader is referred to the patent application (DE 10 2018 129 419) or chapter 4 [13]. All other reagents used were of analytical grade and bought from CarlRoth or VWR.

Dissolution pH-threshold

The solubility of the tested polymers was assessed at different pH values (pH 2 to pH 7 in increments of 1). In vials the polymers were dispersed in buffer at a concentration of 5 mg/ml at room-temperature. The turbidity of the dispersion was visually assessed.

Preparation of enteric-coated capsules

The size zero HPMC capsules were filled manually (aponorm Kapselfüllgerät, WEPA Apothekenbedarf GmbH & Co. KG, Germany) with paracetamol. Paracetamol and hydroxypropyl methylcellulose (HPMC) were chosen because of their high solubility in aqueous medium. To determine the dose of each capsule, 100 empty capsule shells were weighed, and the average weight was determined and subtracted from the mass of the filled capsules. While for the dip-coating pure paracetamol was enough, for the capsules coated with Mini-Coater a mass-based filling with a mixture of paracetamol, fumed silica and mannitol was chosen. This was necessary since tracking of the individual capsule mass through the coating is impossible and the coating level could only be determined on average. The capsules made this way had a dose of 100 mg paracetamol and passed the test for uniformity of mass (2.9.5), uniformity of dose (2.9.6) and uniformity of single dose dosage forms (2.9.40) of the European Pharmacopoeia [17].

Dip-Coating

The capsules were coated with a dip-coating procedure. The coating solution was prepared by dissolving 300 mg of the polymer with 20 % (based on polymer weight) of TEC in 5 g of an acetone-ethanol-mixture (1:1 v/v). Forceps were used to hold the capsules and completely submerge them into the coating solution. Next, the capsules were raised out of the solution and dried at room temperature. A sufficient coating level was achieved after ten to 14 dip cycles. Any irregularities in the coating owing to the holding position of the forceps were corrected by applying the coating solution with a brush.

The coating level is calculated with the following equation:

$$Coating\ level = \frac{(m_c - m_u)}{5\ cm^2} \times 0.83 \quad (1)$$

where m_c is the weight of the coated capsule and m_u the weight of the capsule before coating. The coating level is based on the dry polymer weight. To eliminate the TEC fraction in the calculation, the factor 0.83 is used. Table 2 summarizes the coating levels of the capsules.

Mini-Coater

The coating was performed with a Labotec Mini-Coater at an air presser of 1.5 bar and a tube length of 7.1 cm. The coating solution was prepared by dissolving 3.6 g of the

polymer with 20 % (based on polymer weight) of TEC in 150 g of an acetone. Afterwards 50 % (based on polymer weight) of talcum was added and fully dispersed. The dispersion was kept under constant stirring to prevent sedimentation. The coating was performed with 30 capsules, which were weighed before and after the coating to determine the coating level. The pump rate was set to 4 apm which led to a flow rate of 1 g/min for the dispersion. The capsules were coated for 125 minutes while the flow rate was constantly checked. After that they were kept for five minutes in the coater and overnight under a funnel at room temperature.

The coating level is calculated with the following equation:

$$Coating\ level = \frac{(m_{ct} - m_{ut})}{5\ cm^2} \times 0.588 \quad (2)$$

where m_{ct} is the weight of the coated capsules and m_{ut} the weight of the capsules before coating. The coating level is based on the dry polymer weight. To eliminate the TEC and talcum fraction in the calculation, the factor 0.588 is used. Table 2 summarizes the coating levels of the capsules.

Table 2. Coating level of enteric-coated HPMC capsules based on dry polymer mass.

Polymer	Number of capsules in dissolution test	Experimental setup (Table 3)	Mean ± Standard deviation (mg×cm^{-2})	Approx. molecular weight (Da)
P[MA-*co*-MMA] Eudragit® L100	n = 4	1	8.13 ± 0.63	125 000*
P[MA-*co*-MMA] short chain analog	n = 3	1	7.70 ± 0.15	§
P[MA- D,L-Lac-*co*-MMA]	n = 4	1	11.39 ± 0.22	36 875 $#
P[MA- L -Lac-*co*-MMA]	n = 4	1	8.48 ± 0.50	35 042 $#
P[MA-Gly-*co*-MMA]	n = 4	1	9.36 ± 1.44	25 778 $#
P[MA-Gly-*co*-MMA] high molecular weight	n = 3 n = 3 n = 3 each	1 2 3,4,5,6	10.75 ± 0.74 12.20 ± 0.29 5.02	>125 000#
P[MA-*co*-EA] Eudragit® L100-55	n = 4 n = 6 n = 3 each	1 2 3,4,5	9.26 ± 0.27 10.14 ± 1.65 5.15	320 000*
P[MA-*co*-EA] short chain analog	n = 3	1	9.32 ± 0.09	§
P[MA- D,L -Lac-*co*-EA]	n = 4	1	10.63 ± 0.72	12 750 $#

P[MA-L-Lac-*co*-EA]	n = 3	1	8.94 ± 0.51	18 400 $^{\$\#}$
P[MA-Gly-*co*-EA]	n = 3	1	8.25 ± 0.94	10 670 $^{\$\#}$
P[MA-Lac-*co*-EA]	n = 3	1	9.50 ± 0.34	>320 000$^{\#}$
high molecular weight	n = 3	2	10.26 ± 0.07	

*[3]

§ Polymerization was done under similar conditions as with the modified polymers. Therefore, the molecular weight should be comparable to the modified polymers.

$^{\$}$ [13]

$^{\#}$ Due to the poly-anionic nature of the polymer, only the molecular weight of the polymer with protective group (benzyl-group) could be determined.

Dissolution test

For dissolution testing a USP type I apparatus (PTWS III, Pharma Test, Germany) was used at 100 rpm and 900 mL of dissolution medium at 37 ± 0.5 °C. 5 mL samples were withdrawn at predefined time points without volume replacement. The deionized water used for the media was degassed for two hours at 30 °C with an automatic degasser (PT-DDS, Pharma Test, Germany) and let cool down over night to room temperature before use. All capsules were first tested in 0.01 M HCl for one or two hours (see Table 3). Afterwards the medium for the dip coated capsules was changed to 15 mM phosphate buffer pH 6.5 ± 0.05, that promotes enteric coat dissolution similar to physiological conditions [18]. The ionic strength of the phosphate buffer was adjusted to 139 mM with NaCl and the pH adjustet with 1 M NaOH and HCl For the capsules from the Mini-Coater different media were used for the post gastric stage, as can be seen in Table 3. For the bicarbonate media the media were sparged constantly with an CO_2/air mixture to keep the pH stable. The pH was measured constantly, and the dissolution was only started, if it was stable for half an hour. The dissolved amount of paracetamol was determined spectrophotometrically (UV-1700 PharmaSpec, Shimadzu, Japan) at ƛ=243 nm.

After one hour in the acidic medium the capsules were gently dried using a paper towel. The capsules were weighed, and the % acid uptake was calculated using the following formula:

$$\%\ acid\ uptake = \frac{(m_a - m_c)}{m_c} \times 100\ \% \quad (3)$$

where m_a is the weight of the capsule after acid treatment and m_c the weight of the coated capsule.

Table 3: Dissolution setup

Setup	Experiment	1st Stage Media	2nd Stage Media	Filling	Coating
1	Polymer screening	0.01M HCl for 1 h	15 mM phosphate buffer pH 6.5	Pure paracetamol	Dip-coating
2	Polymer testing	0.01M HCl for 2 h	15 mM phosphate buffer pH 6.5	Pure paracetamol	Dip-coating
3	Polymer testing	0.01M HCl for 2 h	15 mM phosphate buffer pH 6.5	100 mg paracetamol Fumed silica Mannitol	Mini-Coater
4	Polymer testing	0.01M HCl for 2 h	8 mM bicarbonate buffer pH 6.5	100 mg paracetamol Fumed silica Mannitol	Mini-Coater
5	Polymer testing	0.01M HCl for 2 h	2 mM bicarbonate buffer pH 5.5	100 mg paracetamol Fumed silica Mannitol	Mini-Coater
6	Stability testing	0.01M HCl for 2 h	15mM phosphate buffer pH 6.5	100 mg paracetamol Fumed silica Mannitol	Mini-Coater

Stability testing

The stability of the coating of the capsules coated with P[MA-Gly-*co*-MMA] was tested by performing a dissolution experiment (see Table 3) right after the coating and then after six and twelve months. During the time the capsules were kept at standard conditions 25 °C temperature and 65 % relative humidity [19] in a KBF-S 240 controlled climate chamber manufactured by BINDER GmbH (Tuttlingen, Germany).

MTT-Test

The essay was performed in 96-well tissue culture plates. The human embryo kidney (HEKut) cells used in this experiment were seeded with a cell density of 5000 cells per well and let incubate for 24 hours in 100 µL cell culture medium. Higher cell counts and incubation time would oversaturate the essay. As medium a modified Dulbecco-Eagle medium, with 10% heat-inactivated fetal bovine serum, 50 units/mL

penicillin/streptomycin solution added, was used. The wells were pretreated with 0.2 mg/mL polylysin for 20 minutes, washed twice with sterile pure water and dried afterwards. The 12 mM MTT stock solution was prepared by dissolving 5 mg of MTT in 1.0 mL of sterile PBS buffer in a vial and vortexing the mixture until fully dissolved. 10 µL of the stock were used per well. For the treatment 100 µL of test solution was added to the medium for a final volume of 200 µL. As the median concentration in the well 50 mg in 250 mL was chosen, representing the coating of one capsule in a glass of water. Additionally, since Eudragit® L100 contains 0.3 % SDS it was added to P[MA-Gly-*co*-MMA] as well in the respective concentrations. All tested conditions can be found in the supporting information (Table S 1).

At the start of the actual essay, the medium in each well was removed and replaced with 100 µL of fresh cell culture. The MTT stock was added to all wells including the blank (only containing medium and MTT) and gently mixed with the medium. The plates were incubated for four hours at 37 °C in an incubator. Afterwards all medium but 25 µL were removed and 200 µL DMSO were added to dissolve the formed formazane. The wells were homogenized by pipetting up and down and the absorbance was measured at 570 nm using a Flex station 3 plate reader (Molecular Devices, San Jose, USA). To subtract the background an additional measurement at 630 nm was performed, leading to normalized absorbance values.

Statistical Analysis

Student's *t*-tests were performed using the build-in formular of Microsoft Excel. Syntax =TTEST(Array1; Array2;1;3) was used and *p*-values < 0.05 were assumed to be significant.

For the analysis of the MTT-Essay one-way ANOVAs were performed using GraphPad Prism 10.4.2 (633) and *p*-values < 0.05 were assumed to be significant.

Results and discussion

Dissolution pH-threshold

For an initial examination the polymers were dispersed in buffer solutions at room-temperature. At low pH values none of the polymers dissolved. Low solubility at acidic pH is important for enteric polymers, since a release in gastric medium (median pH in fasted

stomach 1.7 [20]) is not desired. The modification of our polymers with L-Lac or Gly did not adversely affect the solubility in acidic pH (and thus the acid resistance (see also Section 3.2)). A striking difference in solubility between the modified polymers and Eudragit® L55 was observed at pH 5 (Table 4). Both modifications of P[MA-*co*-EA] with D,L-Lac and Gly formed a clear solution, while Eudragit® L55 was insoluble at this pH. The lower dissolution pH threshold should increase the dissolution rate of the polymers compared to the commercial product at similar pH. Of course, a more detailed analysis with smaller pH increments is crucial for a final determination of the dissolution pH threshold. Yet, these results already indicate that the modification of the Eudragit backbone with α-hydroxycarboxylic acid decreases the average pK_a of the polymer and thus the dissolution pH threshold. Consequently, faster drug release is expected from formulations using α-hydroxycarboxylic acid modified polymers.

Table 4. Solubility of the tested polymers at different pH values. (-) indicating a turbid dispersion and (+) a clear solution.

Polymer	pH 3	pH 4	pH 5	pH 5.5	pH 6	pH 7
MA-Gly-*co*-MMA	-	-	±	+	+	+
MA-Lac-*co*-MMA	-	-	±	+	+	+
MA-*co*-MMA	-	-	-	-	-	+
Eudragit® L-100	-	-	-	-	-	+
MA-Gly-*co*-EA	-	-	±	+	+	+
MA-Lac-*co*-EA	-	-	±	+	+	+
MA-*co*-EA	-	-	-	-	+	+
Eudragit® L-100-55	-	-	-	±	+	+
MA-Gly-*co*-MMA High MW	-	-	+	+	+	+

Capsule dissolution and acid uptake

After one hour of testing in 0.01 M HCl medium all capsules remained intact and paracetamol release was < 0.5% in all capsules. For effective acid protection of acid labile drugs Missaghi *et al.* proposed a maximum uptake of 10% [21]. The % acid uptake values are depicted in Figure 1A. All polymers tested resulted in adequate resistance to medium uptake, although the unmodified in-house synthesized P[MA-*co*-EA] had an average uptake of 9.05 ± 2.87%. A likely explanation for the higher values of both in-house made polymers (P[MA-*co*-EA] and P[MA-*co*-MMA]) is the lower molecular weight compared to

the commercial products, although more experiments are required to verify this hypothesis.

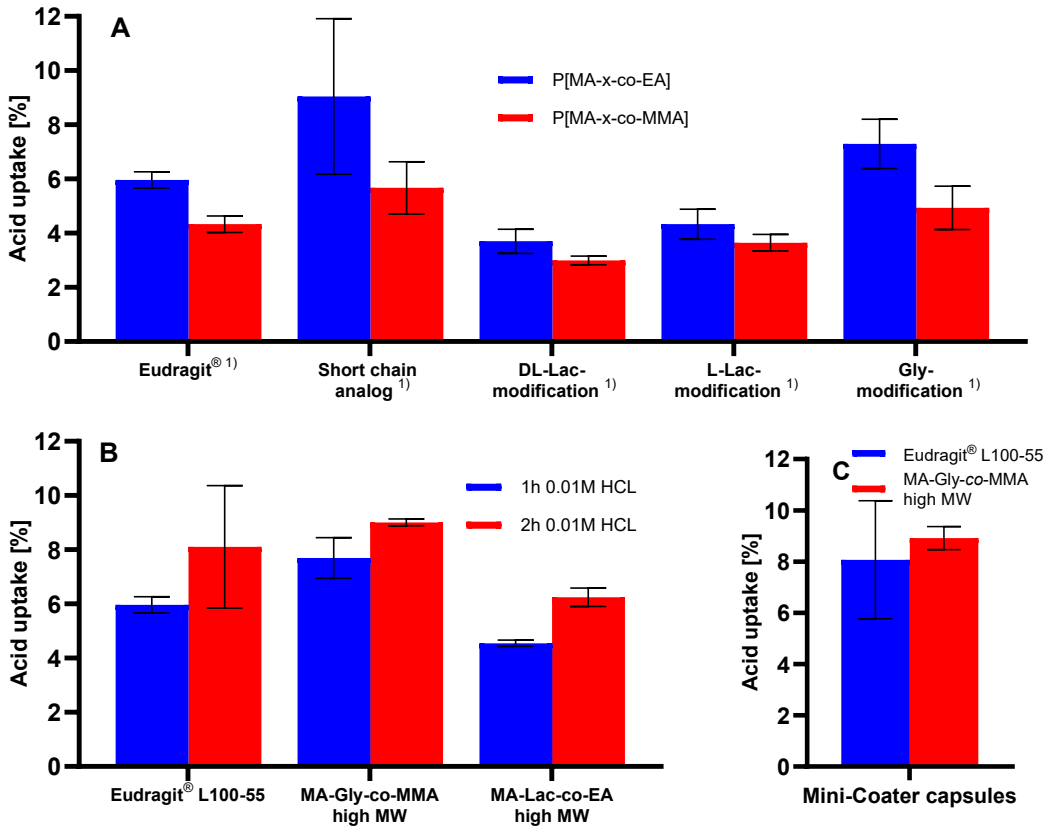

Figure 1. **A** % Acid uptake of enteric-coated capsules (Setup 1) with different coating based on P[MA-co-EA] (blue) and P[MA-co-MMA] (orange) after one hour in 0.01 M HCl. **B** % Acid uptake of enteric-coated capsules (Setup 1,2) after one (blue) and two (orange) hours in 0.01 M HCl. **C** % Acid uptake of enteric-coated capsules (Setup 3,4,5) comparing Eudragit® L100-55 (blue) with P(MA-Gly-co-MMA) high MW (orange) after two hours in 0.01 M HCl. Given are mean values + SD of n=3 or 4 (see Table). [1)] Data already published in chapter 4.

The acid uptake results are also in line with the theoretical predictions made for the monomers (Table 1). The modification with lactic acid resulted in reduced acid uptake values compared to the unmodified polymers.

In Figure 2 the paracetamol release after 45 min in phosphate buffer is depicted. The P[MA-*co*-EA] (-based) polymers released the drug faster than the P[MA-*co*-MMA] (-based) polymers due to the dissolution pH thresholds of Eudragit® L55 and Eudragit® L being 5.5 and 6.0, respectively. Nevertheless, from the Eudragit® L55 and L-coated formulations only 15.60 ± 16.74% and 4.77 ± 7.5% drug release was achieved, respectively. Consequently, the majority of the drug release will probably occur in the more distal parts

of the small intestine. For drugs with an absorption window in the proximal small intestine the bioavailability would be reduced (e.g. iron supplements [5]), thus raising the risk for treatment failure of the enteric-coated dosage form.

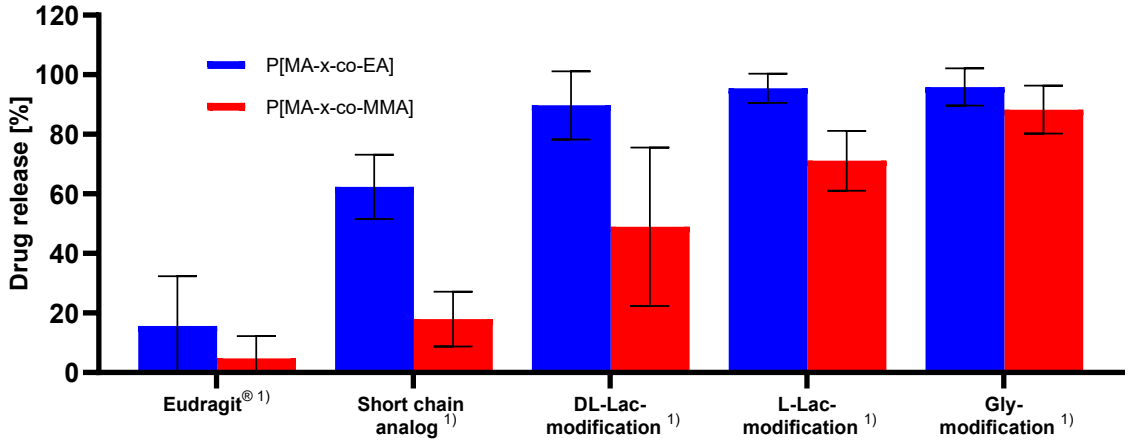

Figure 2. Paracetamol release from enteric-coated capsules at t=45 min after medium change to 15 mM phosphate buffer pH 6.5. Blue and red bars represent the P[MA-co-EA]-based and P[MA-co-MMA]-based polymers, respectively. Given are mean values + SD of n = 3 [1)] Data already published in chapter 4.

The faster release from the in-house synthesized short-chain P[MA-*co*-EA] and P[MA-*co*-MMA] compared to the commercial product can be explained by the lower molecular weight [22]. In addition, the fluid uptake of these capsules was the highest. Consequently, the polymer was already swollen when exposed to the buffered media for the first time which decreases the dissolution time. However, the paracetamol release after 45 min was still incomplete. In contrast, the modification of the P[MA-*co*-EA] and P[MA-*co*-MMA] with lactic and glycolic acid resulted in significant increase in the % drug released after 45 min compared to the release form capsules coated with Eudragit® (p-values < 0.05). Since the release is also faster than from capsules coated with the short chain P[MA-*co*-EA] and P[MA-*co*-MMA], this behavior is attributed to the decreased pK_a values of the modified polymers.

Based on these results P[MA-Lac-*co*-EA] and P[MA-Gly-*co*-MMA] were chosen for further development and Eudragit® L100-55 was used a functional comparator. The scale-up has been described in chapter 4 and succeeded for P[MA-Gly-*co*-MMA] by modifying commercially available Eudragit® L100. To bridge the gap between the screening method (Setup 1) and the later test methods (Setup 3,4,5) additional experiments with dip coated capsules were performed, which showed an increase in acid uptake between one and two

hours in the acid stage (Figure 1B). Additionally, all tested polymers (both commercial and novel) showed a faster drug release after being two hours in acid medium. This could be due to increased swelling and wear at the capsule junction.

The synthesis P[MA-Lac-*co*-EA] based on Eudragit® L100-55 showed technical difficulties, despite being a promising candidate after the screening. The high molecular weight version of the polymer showed great acid resistance as can be seen in Figure 1B, although the drug release lagged behind its comparators. (See Figure S 3).

As a next step both P[MA-Gly-*co*-MMA] and Eudragit® L100-55 were tested according to setup 3. The new Polymer showed an acid uptake 8.92 ± 0.45 g after two hours in 0.01 M HCl while commercially Eudragit® L100-55 showed one of 8.07 ± 2.30 g, which makes them practically indistinguishable (Figure 1C). As for the drug release P[MA-Gly-*co*-MMA] showed a release of 97.63 ± 6.37% while Eudragit® L100-55 showed one of 8.75 ± 15.31% after 45 minutes as can be seen in Figure 3.

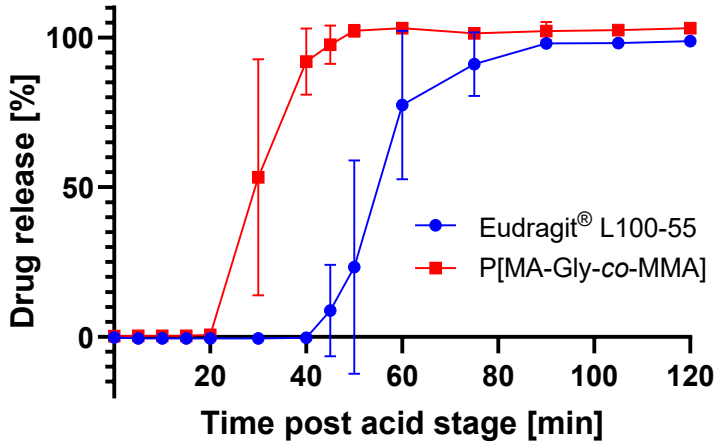

Figure 3 Dissolution profiles of Eudragit® L100-55 (blue) and P(MA-Gly-co-MMA) with high molecular weight (orange) after two hours in 0.01 M HCl in 15 mM phosphate buffer pH 6.5 (Setup 3) Given are mean values + SD of n = 3

Release in physiological bicarbonate buffer

To further confirm the in vivo relevance of those findings, the test conditions were switched from phosphate to bicarbonate buffer, which is the in vivo intestinal buffer (Setup 4). Again the novel P[MA-Gly-*co*-MMA] polymer showed a faster release profile (Figure 4A).

As a final step the conditions were switched again (Setup 5) to further look into gastrointestinal conditions of people with low buffer capacity in their proximal small

intestine. For this purpose, a bicarbonate molarity of 2 mM was selected, for it represents approximately 1.25 standard deviations from the average jejunal bicarbonate molarity (roughly 10th percentile) as reported by Banwell et al. [23] While Eudragit® L100-55 showed no signs of disintegration and almost no release for 2 hours post, the new polymer showed only slight delay compared to 8 mM bicarbonate a practically complete (97.57±1.35%) release at 45 minutes. This is of profound importance, for it shows that the new polymer is capable of achieving much greater robustness vis-à-vis variability in intestinal human composition.

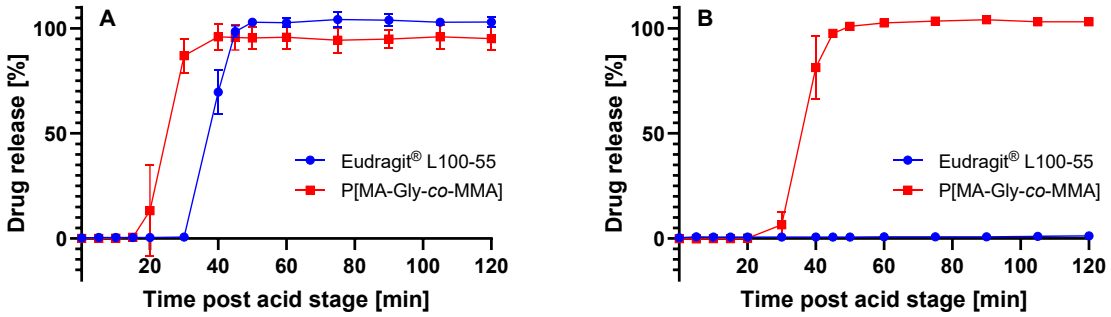

Figure 4 Dissolution profiles of Eudragit® L100-55 (blue) and P(MA-Gly-co-MMA) with high molecular weight (orange) after two hours in 0.01 M HCl in 8 mM bicarbonate buffer pH 6.5 (**A**) and 2 mM bicarbonate buffer pH 5.5 (**B**). (Setup 4 and 5) Given are mean values + SD of n = 3

Stability testing

The newly synthesized P(MA-Gly-co-MMA) showed similar release profiles over the span of twelve months (Figure 5). A slower release would have indicated hydrolysis of the ester modification, returning the polymer back to P(MA-co-MMA).

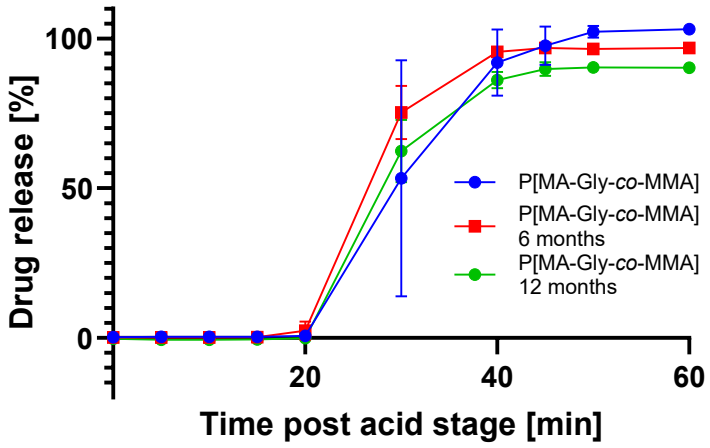

Figure 5 Dissolution profiles of with high molecular weight P(MA-Gly-co-MMA) coated capsules after two hours in 0.01 M HCl in 15 mM phosphate buffer pH 6.5 (Setup 6) Given are mean values + SD of n = 3

MTT-essay

Different concentrations of P(MA-Gly-*co*-MMA) showed no difference in cell activity, measured by the reduction of MTT into formazane, compared to commercial P(MA-co-MMA) (one-way ANOVA, each group against PBS, *p*-value 0.8248). Also incubating the HEK cells for 1, 2 or 4 hours showed no significant differences (one-way ANOVA, each group against each group, *p*-value 0.0606). This was expected, since both Eudragit® L100 and glycolic acid are safe excipients.

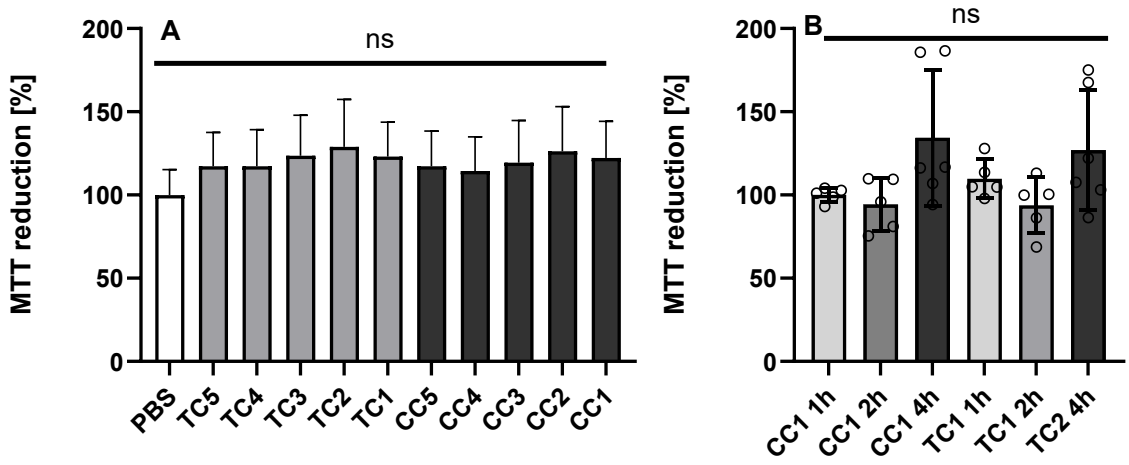

Figure 6 (**A**) MTT reduction [%] of cells treated with different concentrations of P(MA-Gly-co-MMA) and Eudragit® L100 compared to PBS buffer after two hours of treatment (n = 5) (**B**) MTT reduction [%] of cells treated with the same concentrations of P(MA-Gly-co-MMA) and Eudragit® L100 compared to PBS buffer after 1, 2 or 4 hours of treatment (n = 5/5/6)

Conclusion

Drugs from enteric-coated formulations often suffer from poor bioavailability due to slow polymer dissolution. We have shown that a modification of known P[MA-*co*-EA] and P[MA-*co*-MMA] copolymer backbones with α-hydroxycarboxylic acid modified side chains significantly increases the drug release rate, while retaining good acid resistance for the passage through the stomach. This work offers a good starting point for the solution of clinical problems like aspirin treatment failure related to enteric coatings and offers promise for a large variety of drugs, particularly those exhibiting GI-segment dependent bioavailability.

Credit authorship contribution statement

[redacted]: Conceptualization, Methodology, Formal analysis, Investigation, Visualization, Writing – original draft, Writing – review & editing. [redacted] Conceptualization, Methodology, Formal analysis, Investigation, Visualization, Writing – original draft, Writing – review & editing. [redacted]: Conceptualization, Methodology, Writing – review & editing, Supervision. **Dominik Albrecht Hugo Fuchs**: Methodology, Investigation, Writing – review & editing. [redacted] Methodology, Investigation, Writing – review & editing. [redacted]: Conceptualization, Resources, Writing – review & editing, Supervision. [redacted]: Conceptualization, Resources, Writing – review & editing, Supervision

Funding

Part of this work was funded by "WIPANO – Wissens- und Technologietransfer durch Patente und Normen" of the German Federal Ministry of Economic Affairs and Climate Action (Grant number: 03THWRP003).

Conflicts of Interest

[redacted] are inventors of the patent DE 102018129419. The patent had no role in the collection, analyses, or interpretation of data; in the writing of the manuscript, or in the decision to publish the results.

References

1. Agyilirah, G.A.; Banker, G.S. Polymers for enteric coating applications. In Polymers for Controlled Drug Delivery; Tarcha, P.J., Ed.; CRC Press: Boca Raton, FL, USA, 1990; pp 39–66.

2. Breitkreutz, J. Leakage of enteric (Eudragit® L)-coated dosage forms in simulated gastric juice in the presence of poly(ethylene glycol). Journal of controlled release 2000, 67, 79–88, doi:10.1016/S0168-3659(00)00197-8.

3. Evonik Nutrition & Care GmbH: Darmstadt, Germany. Evonik EUDRAGIT®Application Guidelines. Available online: https://idp.evonik.com/nidp/saml2/sso?id=4142&sid=0&option=credential&sid=0 (accessed on 26 March 2020).

4. Al-Gousous, J.; Tsume, Y.; Fu, M.; Salem, I.I.; Langguth, P. Unpredictable Performance of pH-Dependent Coatings Accentuates the Need for Improved Predictive in Vitro Test Systems. Mol. Pharm. 2017, 14, 4209–4219, doi:10.1021/acs.molpharmaceut.6b00877.

5. Rudinskas, L.; Paton, T.W.; Walker, S.E.; Dotten, D.A.; Cowan, D.H. Poor clinical response to enteric-coated iron preparations. Canadian Medical Association journal 1989, 141, 565–566.

6. Mössner, J.; Keim, V. Pancreatic enzyme therapy. Dtsch. Arztebl. Int. 2010, 108, 578–582, doi:10.3238/arztebl.2011.0578.

7. McNeil, J.J.; Wolfe, R.; Woods, R.L.; Tonkin, A.M.; Donnan, G.A.; Nelson, M.R.; Reid, C.M.; Lockery, J.E.; Kirpach, B.; Storey, E.; et al. Effect of Aspirin on Cardiovascular Events and Bleeding in the Healthy Elderly. N. Engl. J. Med. 2018, 379, 1509–1518, doi:10.1056/NEJMoa1805819.

8. Antithrombotic Trialists' Collaboration. Collaborative meta-analysis of randomised trials of antiplatelet therapy for prevention of death, myocardial infarction, and stroke in high risk patients. BMJ 2002, 324, 71–86, doi:10.1136/bmj.324.7329.71.

9. Cox, D.; Maree, A.O.; Dooley, M.; Conroy, R.; Byrne, M.F.; Fitzgerald, D.J. Effect of enteric coating on antiplatelet activity of low-dose aspirin in healthy volunteers. Stroke 2006, 37, 2153–2158, doi:10.1161/01.STR.0000231683.43347.ec.

10. Serebruany, V.L.; Steinhubl, S.R.; Berger, P.B.; Malinin, A.I.; Baggish, J.S.; Bhatt, D.L.; Topol, E.J. Analysis of risk of bleeding complications after different doses of aspirin in 192,036 patients enrolled in 31 randomized controlled trials. Am. J. Cardiol. 2005, 95, 1218–1222, doi:10.1016/j.amjcard.2005.01.049.

11. Liu, F.; Basit, A.W. A paradigm shift in enteric coating: achieving rapid release in the proximal small intestine of man. Journal of controlled release 2010, 147, 242–245, doi:10.1016/j.jconrel.2010.07.105.

12. Liu, F.; Lizio, R.; Meier, C.; Petereit, H.-U.; Blakey, P.; Basit, A.W. A novel concept in enteric coating: a double-coating system providing rapid drug release in the proximal small intestine. Journal of controlled release 2009, 133, 119–124, doi:10.1016/j.jconrel.2008.09.083.

13. Frey, H.; Kersten, E.; Langguth, P.; Blechar, J.A.; Al-Gousous, J. Acrylat-Copolymer für galenische Anwendungen. DE 102018129419, November 22, 2018.

14. Al-Gousous, J.; Salehi, N.; Amidon, G.E.; Ziff, R.M.; Langguth, P.; Amidon, G.L. Mass Transport Analysis of Bicarbonate Buffer: Effect of the CO2-H2CO3 Hydration-Dehydration Kinetics in the Fluid Boundary Layer and the Apparent Effective p Ka Controlling Dissolution of Acids and Bases. Mol. Pharm. 2019, 16, 2626–2635, doi:10.1021/acs.molpharmaceut.9b00187.

15. Mooney, K.G.; Mintun, M.A.; Himmelstein, K.J.; Stella, V.J. Dissolution kinetics of carboxylic acids I: effect of pH under unbuffered conditions. J. Pharm. Sci. 1981, 70, 13–22, doi:10.1002/jps.2600700103.

16. Mooney, K.G.; Mintun, M.A.; Himmelstein, K.J.; Stella, V.J. Dissolution kinetics of carboxylic acids II: effect of buffers. J. Pharm. Sci. 1981, 70, 22–32, doi:10.1002/jps.2600700104.

17. Deutscher Apotheker-Verlag Doktor Roland Schmiedel. Europäisches Arzneibuch 11. Ausgabe, Grundwerk 2023: Amtliche deutsche Ausgabe (Ph. Eur. 11.0), 4 Bände und Registerheft im Schuber; Deutscher Apotheker Verlag: Stuttgart, 2023, ISBN 978-3-7692-8114-9.

18. Al-Gousous, J.; Amidon, G.L.; Langguth, P. Toward Biopredictive Dissolution for Enteric Coated Dosage Forms. Mol. Pharm. 2016, 13, 1927–1936, doi:10.1021/acs.molpharmaceut.6b00077.

19. INTERNATIONAL CONFERENCE ON HARMONISATION OF TECHNICAL. ICH HARMONISED TRIPARTITE GUIDELINE STABILITY TESTING OF NEW DRUG SUBSTANCES AND PRODUCTS Q1A(R2).

20. Mudie, D.M.; Amidon, G.L.; Amidon, G.E. Physiological parameters for oral delivery and in vitro testing. Mol. Pharm. 2010, 7, 1388–1405, doi:10.1021/mp100149j.

21. Missaghi, S.; Young, C.; Fegely, K.; Rajabi-Siahboomi, A.R. Delayed release film coating applications on oral solid dosage forms of proton pump inhibitors: case studies. Drug Dev. Ind. Pharm. 2010, 36, 180–189, doi:10.3109/03639040903468811.

22. Florence, A.T.; Attwood, D. Polymers and macromolecules. In Physicochemical principles of pharmacy: In manufacture, formulation and clinical use, Sixth edition; Florence, A.T., Attwood, D., Eds.; Pharmaceutical Press: London, UK, 2016; pp 301–302, ISBN 9780857111746.

23. Banwell, J.G.; Pierce, N.F.; Mitra, R.C.; Brigham, K.L.; Caranasos, G.J.; Keimowitz, R.I.; Fedson, D.S.; Thomas, J.; Gorbach, S.L.; Sack, R.B.; et al. Intestinal fluid and electrolyte transport in human cholera. J. Clin. Invest. 1970, 49, 183–195, doi:10.1172/JCI106217.

Supporting Information

Evaluation of a novel series of enteric -copolymers for pharmaceutical applications: a-hydroxycarboxylic acid modified polymethacrylates

[redacted] Dominik Albrecht Hugo Fuchs[redacted]XX

[1] Department Pharmaceutical Technology and Biopharmaceutics, Johannes Gutenberg-University Mainz, Staudinger Weg 5, 55128 Mainz, Germany

[2] Department of Pharmaceutical Sciences, University of Michigan, Ann Arbor, MI 48104, USA

[3] Institute of Organic Chemistry, Johannes Gutenberg-University Mainz, Duesbergweg 10-14, 55128 Mainz, Germany

[4] Institute of Pharmaceutical and Biomedical Sciences, Johannes Gutenberg-University Mainz, Staudingerweg 5, 55128, Mainz, Germany.

[*] Correspondence[redacted]

[†] Equal first authors.

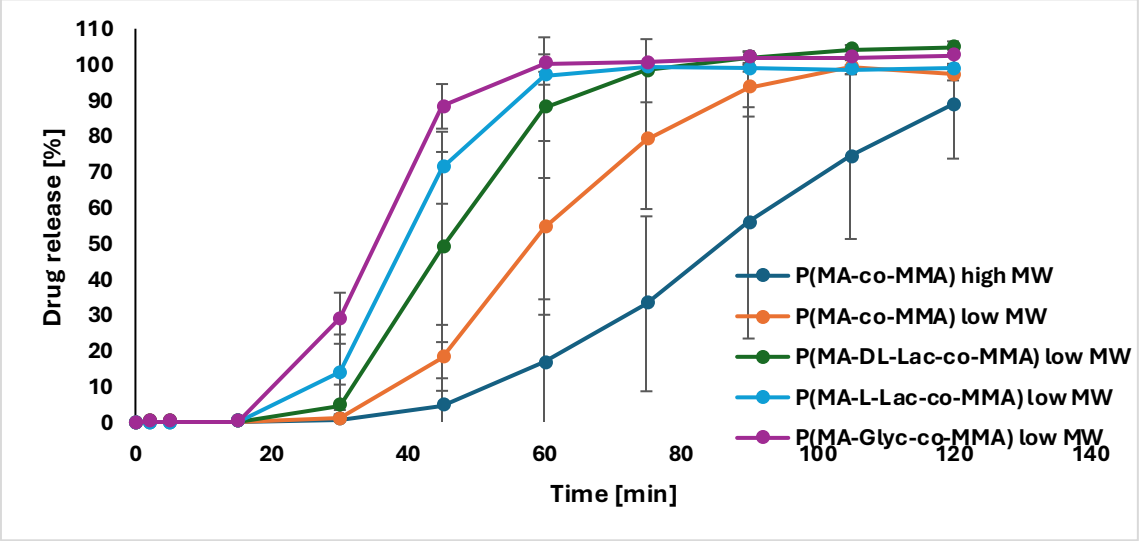

Figure S 1 Paracetamol release profiles form enteric-coated capsules coated with modified P[MA-co-MMA] after medium change to 15 mM phosphate buffer pH 6.5. Given are mean values + SD of n = 3

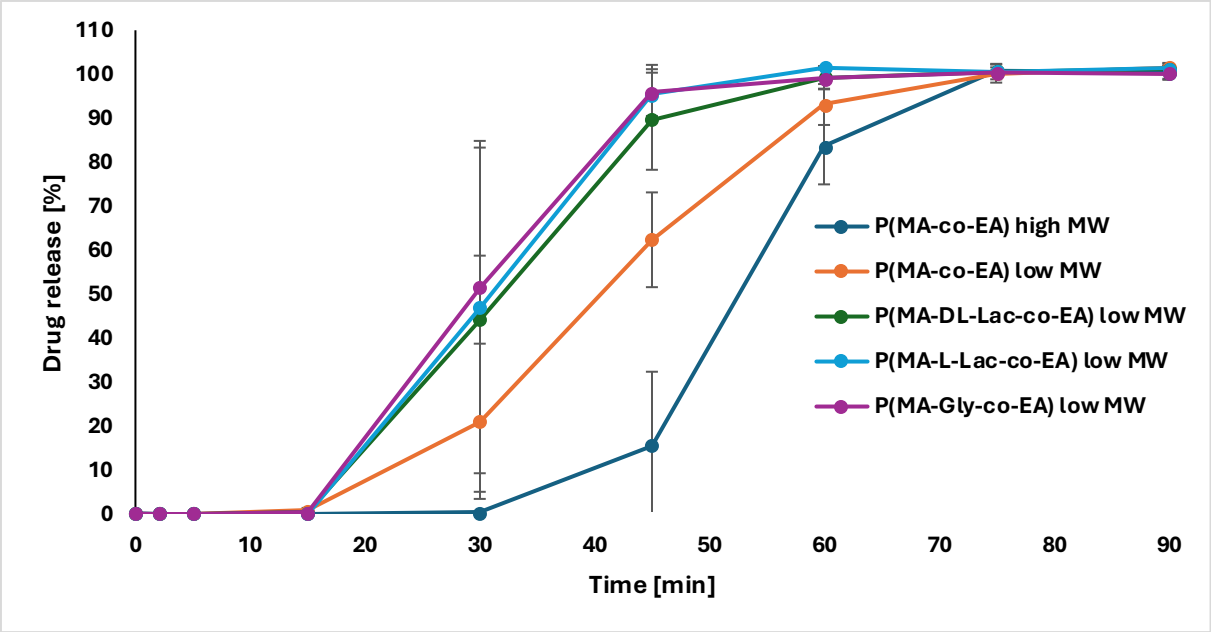

Figure S 2 Paracetamol release profiles form enteric-coated capsules coated with modified P[MA-co-EA] after medium change to 15 mM phosphate buffer pH 6.5. Given are mean values + SD of n = 3

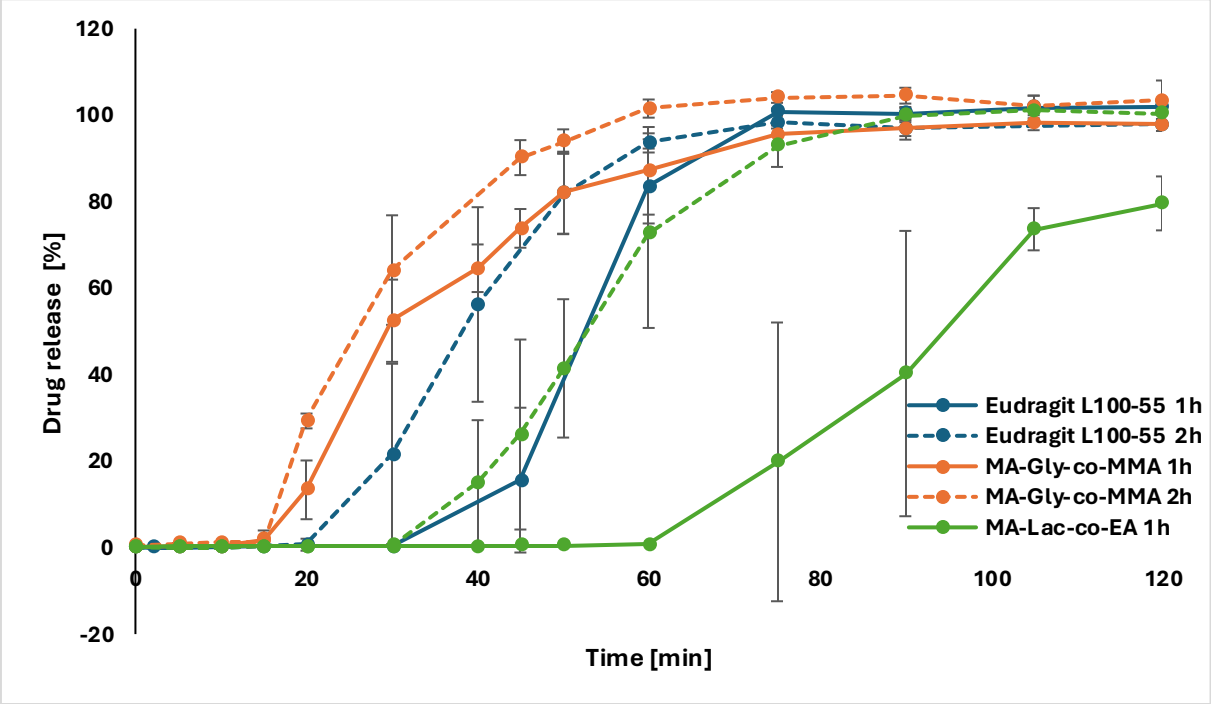

Figure S 3 Paracetamol release profiles form enteric-coated capsules coated with modified polymers after medium change to 15 mM phosphate buffer pH 6.5. Given are mean values + SD of n = 3

Table S 1 Treatment conditions of the MTT essay

Group	Treatment composition	Concentration of the polymer [mg / mL]
CC5	1. Eudragit® L100 2. SDS at 0.3% dry polymer weight 3. Phosphate buffer pH 7.4	0.02
CC4		0.063
CC3		0.2
CC2		0.63
CC1		1.5
CE		10
TC5	1. P(MA-Gly-co-MMA) UMz1b.9 2. SDS at 0.3% dry polymer weight 3. Phosphate buffer pH 7.4	0.02
TC4		0.063
TC3		0.2
TC2		0.63
TC1		1.5
TE		10
TC35	P(MA-Gly-co-MMA) UMz1b.5	0.2
TC36	P(MA-Gly-co-MMA) UMz1b.6	0.2
TC37	P(MA-Gly-co-MMA) UMz1b.7	0.2
TC38	P(MA-Gly-co-MMA) UMz1b.8	0.2
TC39b	P(MA-Gly-co-MMA) UMz1b.9b	0.2
Control	PBS buffer	-
Buffer	Phosphate buffer pH 7.4	-
SDS + PBS	1. PBS buffer 2. SDS at 0.3% dry polymer weight	-
SDS + buffer	1. Phosphate buffer pH 7.4 2. SDS at 0.3% dry polymer weight	-
H_2O_2	Water H_2O_2	-

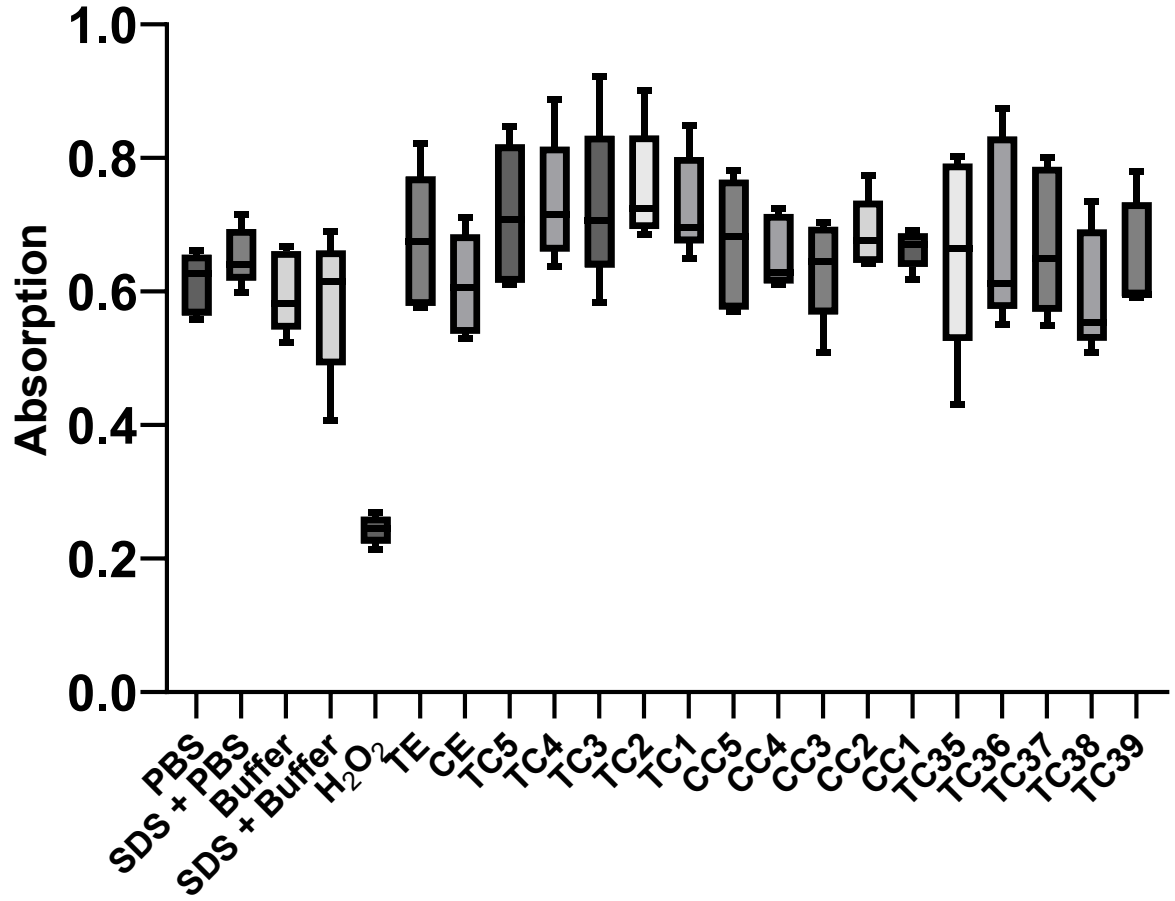

Figure S 4 Absorption of the wells with different treatments during the MTT essay after one hour treatment. (n = 5)

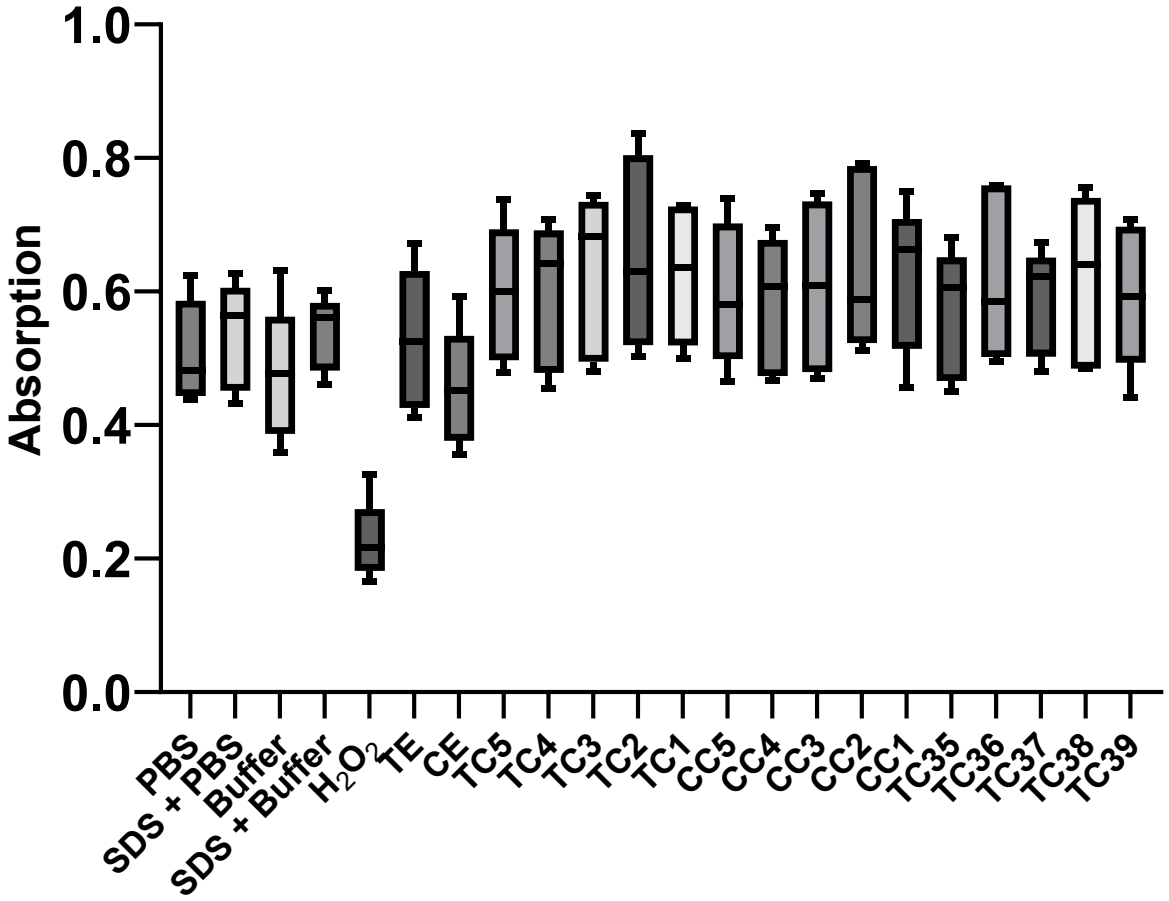

Figure S 5 Absorption of the wells with different treatments during the MTT essay after two hours treatment. (n = 5)

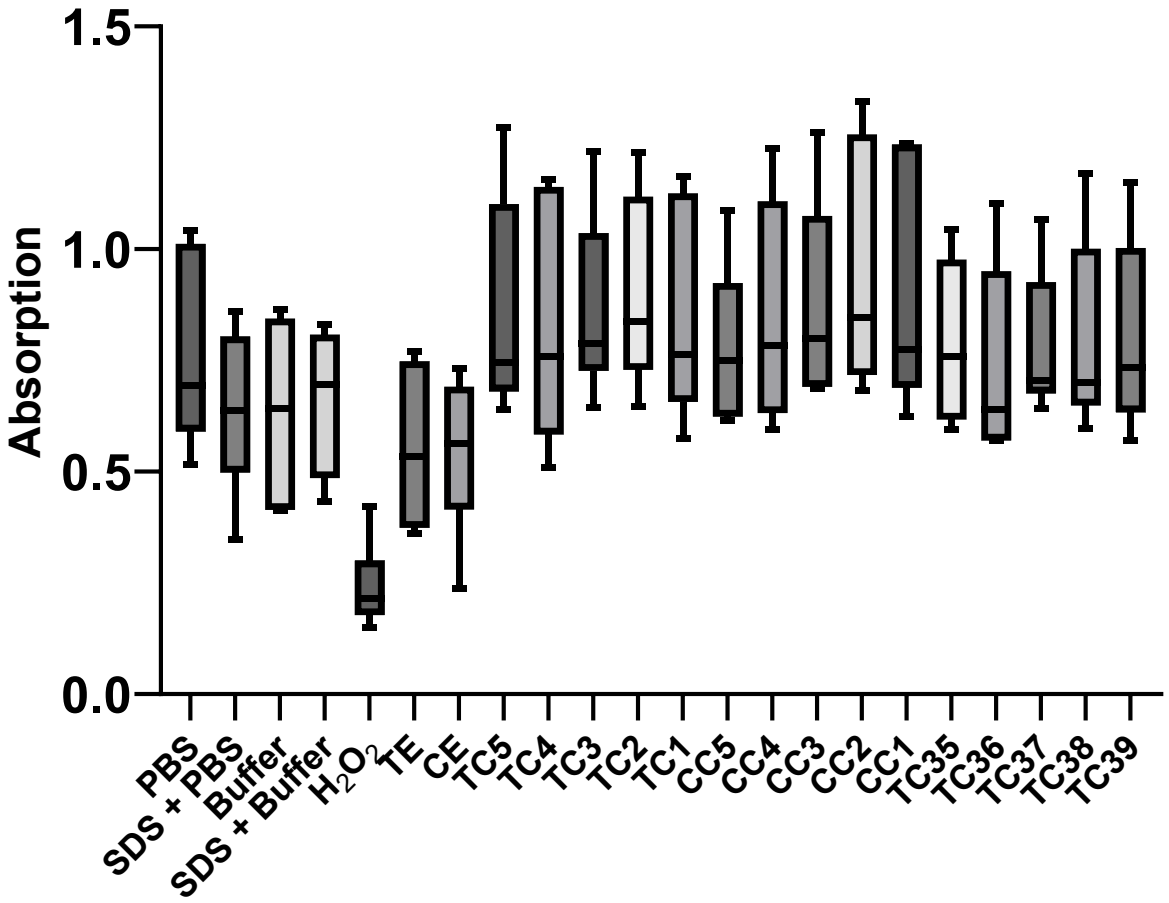

Figure S 6 Absorption of the wells with different treatments during the MTT essay after four hours treatment. (n = 6)

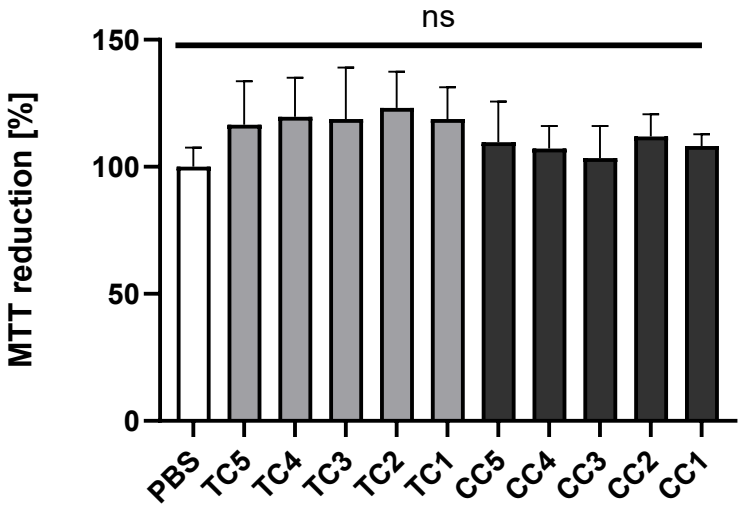

Figure S 7 MTT reduction [%] of cells treated with different concentrations of P(MA-Gly-co-MMA) and Eudragit® L100 compared to PBS buffer after one hour of treatment (n = 5)

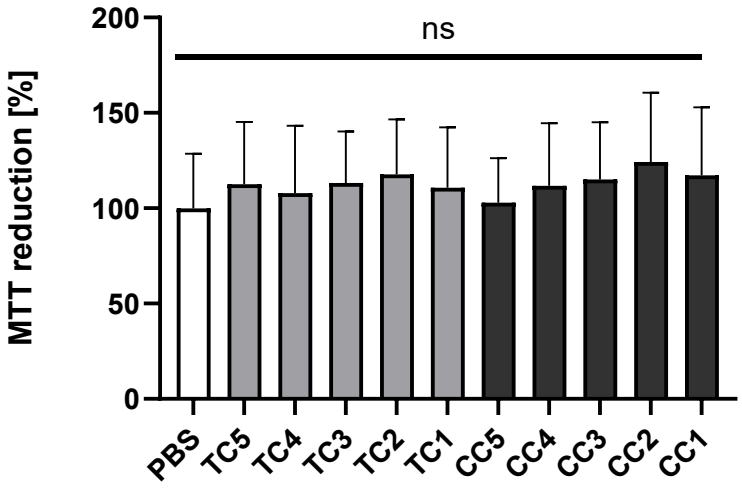

Figure S 8 MTT reduction [%] of cells treated with different concentrations of P(MA-Gly-co-MMA) and Eudragit® L100 compared to PBS buffer after four hours of treatment (n = 5)

Table 2. Enteric polymers used in drug products on the German market [1,2].

Drug	Product	Manufacturer	Enteric polymer
Acetylsalicylic acid	Aspirin protect	Bayer	Methacrylic acid-ethyl acrylate 1:1 copolymer 30 % dispersion
	ASS AbZ protect	AbZ Pharma	Methacrylic acid-ethyl acrylate 1:1 copolymer 30 % dispersion
	ASS-ratiopharm®	ratiopharm	Methacrylic acid-ethyl acrylate 1:1 copolymer 30 % dispersion
Aescin	Reparil®-Dragees	Viatris Healthcare	Methacrylic acid-ethyl acrylate 1:1 copolymer
4-Aminosalicylic acid	GRANUPAS	Eurocept International	Methacrylic acid-ethyl acrylate 1:1 copolymer 30 % dispersion
Bisacodyl	Laxans-ratiopharm®	ratiopharm	Methacrylic acid-ethyl acrylate 1:1 copolymer
	DulcoLax® Dragees	Sanofi	Methacrylic acid-methyl methacrylate 1:1 copolymer, Methacrylic acid-methyl methacrylate 1:2 copolymer
Bromelain	Bromelain-POS®	URSAPHARM Arzneimittel	Methacrylic acid-methyl methacrylate 1:1 copolymer, Methacrylic acid-ethyl acrylate 1:1 copolymer
	Bromelain-tabletten hysan®		
	Phlogenzym®	MUCOS Pharma	Methacrylic acid-methyl methacrylate 1:1 copolymer
	Traumanase®	Cassell-med	Methacrylic acid-methyl methacrylate 1:1 copolymer
Bromelain, Trypsin, Rutoside	Wobenzym®	MUCOS Pharma	Methacrylic acid-methyl methacrylate 1:1 copolymer

Drug	Product	Manufacturer	Enteric polymer
Budesonide	Budenofalk®	Dr. Falk Pharma	Methacrylic acid-methyl methacrylate 1:1 copolymer, Methacrylic acid-methyl methacrylate 1:2 copolymer, Ammonium methacrylate copolymer type A, Ammonium methacrylate copolymer type B
	Entocort	Tillotts Pharma	Methacrylic acid-ethyl acrylate 1:1 copolymer
Calcium amino-ethyle phosphate	Calcium-EAP®	Köhler Pharma	Methacrylic acid-methyl methacrylate 1:1 copolymer,
Diclofenac	Diclofenac AbZ	AbZ Pharma	Methacrylic acid-ethyl acrylate 1:1 copolymer
	Diclofenac-ratiopharm®	ratiopharm	Methacrylic acid-ethyl acrylate 1:1 copolymer
Dimethyl fumarate	Dimethylfumarat-ratiopharm	ratiopharm	Methacrylic acid-ethyl acrylate 1:1 copolymer
	Skilarence	Almirall Hermal	Methacrylic acid-ethyl acrylate 1:1 copolymer
	Tecfidera™	Biogen	Methacrylic acid-methyl methacrylate 1:1 copolymer, Methacrylic acid-ethyl acrylate 1:1 copolymer 30 % dispersion
Dimethyl fumarate, ethyl hydrogen-fumarate	Fumaderm® initial, Fumaderm®	Biogen	Methacrylic acid-methyl methacrylate 1:1 copolymer, Methacrylic acid-ethyl acrylate 1:1 copolymer
Diroximel fumarate	Vumerity™	Biogen	Methacrylic acid-ethyl acrylate 1:1 copolymer
Doxylamine, Pyridoxine	XONVEA	Exeltis	Methacrylic acid-ethyl acrylate 1:1 copolymer
Duloxetine	Cymbalta®, YENTREVE®	Lilly	Hypromellose acetate succinate
	Duloxalta® Duloxetin TAD®	TAD Pahrma	Hypromellose phthalate
	Duloxetin AbZ	AbZ Pharma	Hypromellose phthalate
	Duloxetin Henning	Henning Arzneimittel	Hypromellose acetate succinate
	Duloxetin Mylan	Viatris Healthcare	Hypromellose phthalate
	Duloxetin-neuraxpharm®	neuraxpharm Arzneimittel	Hypromellose phthalate
	Duloxetin-ratiopharm	ratiopharm	Hypromellose phthalate
Escherichia coli	Mutaflor®, Mutaflor® mite	Ardeypharm	Methacrylic acid-methyl methacrylate 1:1 copolymer
Esomeprazole	Esomeprazol AbZ, Esomeprazol-CT	AbZ Pharma	Methacrylic acid-ethyl acrylate 1:1 copolymer 30 % dispersion
	Esomeprazol-ratiopharm®	ratiopharm	Methacrylic acid-ethyl acrylate 1:1 copolymer 30 % dispersion
	Esomeprazol TAD	TAD Pharma	Methacrylic acid-ethyl acrylate 1:1 copolymer 30 % dispersion

Drug	Product	Manufacturer	Enteric polymer
	Nexium® mups	Grünenthal	Methacrylic acid-ethyl acrylate 1:1 copolymer
	Nexium® granulate		Methacrylic acid-ethyl acrylate 1:1 copolymer 30 % dispersion
Herbal medicines	Buscomint®	A. Nattermann & Cie.	Methacrylic acid-ethyl acrylate 1:1 copolymer 30 % dispersion
	Eviprostat N	Pharmazeutische Fabrik Evers	Methacrylic acid-ethyl acrylate 1:1 copolymer 30 % dispersion
	femiLoges®	Dr. Loges	Methacrylic acid-methyl methacrylate 1:1 copolymer
	GeloMyrtol® forte, Myrtol®	G. Pohl-Boskamp	Hypromellose acetate succinate
	Sinolpan	Engelhard Arzneimittel	Methacrylic acid-ethyl acrylate 1:1 copolymer 30 % dispersion
Iron-(II)-salt	ferro sanol® duodenal	UCB pharma	Methacrylic acid-ethyl acrylate 1:1 copolymer
Lansoprazol	Agopton®	Takeda	Methacrylic acid-ethyl acrylate 1:1 copolymer
	Lansoprazol AbZ	AbZ Pharma	Methacrylic acid-ethyl acrylate 1:1 copolymer 30 % dispersion
	Lansoprazol-ratiopharm®	ratiopharm	Methacrylic acid-ethyl acrylate 1:1 copolymer 30 % dispersion
Magnesium citrate, Magnesium hydrogenglutamate	Magnesium Verla® N Dragées	Verla-Pharm Arzneimittel	Methacrylic acid-ethyl acrylate 1:1 copolymer
Mercaptamine	PROCYSBI®	Chiesi	Methacrylic acid-ethyl acrylate 1:1 copolymer
Mesalazine	Asacol®	Tillotts Pharma	Methacrylic acid-methyl methacrylate 1:2 copolymer, Methacrylic acid-methyl methacrylate 1:1 copolymer,
	Claversal®	Recordati Pharma	Methacrylic acid-methyl methacrylate 1:2 copolymer, Methacrylic acid-ethyl acrylate 1:1 copolymer 30 % dispersion
	Mezavant	Takeda	Methacrylic acid-methyl methacrylate 1:2 copolymer, Methacrylic acid-methyl methacrylate 1:1 copolymer
	Salofalk®	Dr. Falk Pharma	Methacrylic acid-methyl methacrylate 1:1 copolymer, Methacrylic acid-methyl methacrylate 1:2 copolymer, Butyl methacrylate-(2-dimethylaminoethyl) methacrylate-methyl methacrylate 1:2.1 copolymer
Mycophenolic acid	Myfortic®	Novartis Pharma	Hypromellose phthalate
Omeprazole	Antra MUPS®	CHEPLAPHARM Arzneimittel	Methacrylic acid-ethyl acrylate 1:1 copolymer 30 % dispersion
	Omeprazol AbZ, Omeprazol-CT	AbZ Pharma	Methacrylic acid-ethyl acrylate 1:1 copolymer

Drug	Product	Manufacturer	Enteric polymer
	Omeprazol dura S®, Omeprazol Mylan	Viatris Healthcare	Methacrylic acid-ethyl acrylate 1:1 copolymer 30 % dispersion
	Omeprazol-ratiopharm® NT	ratiopharm	Methacrylic acid-ethyl acrylate 1:1 copolymer
	Omeprazol-ratiopharm® SK		Hypromellose phthalate
Pancreatic enzymes	Pankreatan®	Nordmark Pharma	Methacrylic acid-ethyl acrylate 1:1 copolymer 30 % dispersion
	Pankreatin Laves®	Laves Arzneimittel	Methacrylic acid-ethyl acrylate 1:1 copolymer 30 % dispersion
	Pankreatin Mikro-ratiopharm®	ratiopharm	Methacrylic acid-ethyl acrylate 1:1 copolymer 30 % dispersion
	Ozym	Trommsdorff	Methacrylic acid-ethyl acrylate 1:1 copolymer 30 % dispersion
	Kreon®	Viatris Healthcare	Hypromellose phthalate
Pantoprazole	Pantoprazol AAA	AAA-Pharma	Methacrylic acid-ethyl acrylate 1:1 copolymer 30 % dispersion
	Pantoprazol AbZ	AbZ Pharma	Methacrylic acid-ethyl acrylate 1:1 copolymer 30 % dispersion
	Pantoprazol auxino	axunio Pharma	Methacrylic acid-ethyl acrylate 1:1 copolymer
	Pantoprazol-CT	AbZ Pharma	Methacrylic acid-ethyl acrylate 1:1 copolymer
	Pantoprazol dura	Mylan	Methacrylic acid-ethyl acrylate 1:1 copolymer 30 % dispersion
	Pantoprazol elac®	Mibe Arzneimittel	Methacrylic acid-ethyl acrylate 1:1 copolymer
	Pantoprazol Hennig®	Henning Arzneimittel	Methacrylic acid-ethyl acrylate 1:1 copolymer 30 % dispersion
	Pantoprazol NYC®, Pantozol®	Takeda	Methacrylic acid-ethyl acrylate 1:1 copolymer
	Pantoprazol-ratiopharm®	ratiopharm	Methacrylic acid-ethyl acrylate 1:1 copolymer
	PANTOZOL control®	DR. KADE Pharmazeutische Fabrik	Methacrylic acid-ethyl acrylate 1:1 copolymer
	Rifun®	Takeda	Methacrylic acid-ethyl acrylate 1:1 copolymer
Pantoprazole, Amoxicillin, Clarithromycin	ZacPac®	Takeda	Methacrylic acid-ethyl acrylate 1:1 copolymer
Penicillamine	Metalcaptase®	Heyl Chem.-pharm. Fabrik	Methacrylic acid-methyl methacrylate 1:1 copolymer, Methacrylic acid-ethyl acrylate 1:1 copolymer
Posaconazole	Noxafil®	MSD Sharp & Dohme	Hypromellose acetate succinate
	Posaconazol Abdi	Abdi Farma	Hypromellose acetate succinate
	Posaconazol-ratiopharm	ratiopharm	Methacrylic acid-ethyl acrylate 1:1 copolymer type B

Drug	Product	Manufacturer	Enteric polymer
Risedronic acid	Actonel	Theramex	Methacrylic acid-ethyl acrylate 1:1 copolymer 30 % dispersion
Rabeprazole	Pariet®	Eisai	Hypromellose phthalate
	Rabeprazol-ratiopharm®	ratiopharm	Hypromellose phthalate
Sodium bicarbonate	bicaNorm®	MEDICE Arzneimittel Pütter	Methacrylic acid-ethyl acrylate 1:1 copolymer
	Nephrotrans®		
Sodium bituminosulfonate	Ichthraletten®	ICHTHYOL-GESELLSCHAFT Cordes, Hermanni & Co.	Methacrylic acid-ethyl acrylate 1:1 copolymer
Sulfasalazine	Azulfidine®	PFIZER PHARMA	Cellulose acetate phthalate
	Sulfasalazin-Heyl®	Heyl Chemisch-pharmazeutische Fabrik	Methacrylic acid-ethyl acrylate 1:1 copolymer
Typhoid vaccine	Typhoral® L	Pharmore	Hypromellose phthalate
Valproate	Ergenyl	Sanofi-Aventis	Methacrylic acid-methyl methacrylate 1:1 copolymer, Cellulose acetate phthalate
	Orfiril	Desitin Arzneimittel	Methacrylic acid-ethyl acrylate 1:1 copolymer
	Valproinsäure-ratiopharm®	ratiopharm	Methacrylic acid-ethyl acrylate 1:1 copolymer
	Valproat-neuraxpharm®	neuraxpharm Arzneimittel	Methacrylic acid-ethyl acrylate 1:1 copolymer
Zink bishydrogen-aspartate	Unizink® 50	Köhler Pharma	Methacrylic acid-methyl methacrylate 1:1 copolymer, Methacrylic acid-ethyl acrylate 1:1 copolymer 30 % dispersion
Zink orotate	Zinkorotat-POS®	URSAPHARM Arzneimittel	Methacrylic acid-methyl methacrylate 1:1 copolymer, Methacrylic acid-ethyl acrylate 1:1 copolymer 30 % dispersion

References

1. ROTE LISTE®. Available online: https://www.rote-liste.de/ (accessed on 26 May 2025).

2. Fachinfo-Service®: Fachinformationsverzeichnis Deutschland. Available online: https://www.fachinfo.de/ (accessed on 26 May 2025).

Curriculum Vitae